

Proceedings of MENU 2007
11th International Conference on
Meson-Nucleon Physics
and the Structure of the Nucleon

IKP, Forschungszentrum Jülich

Germany

September 10-14, 2007

Editors

H. Machner and S. Krewald

Volume II

Contributed Talks and Posters

Foreword

The 11th International Conference on Meson-Nucleon Physics and the Structure of the Nucleon - MENU 2007 - was organized by the Institut für Kernphysik, Forschungszentrum Jülich, Jülich, Germany. It took place from September 10-14, 2007, when approximately 350 participants came together. Conferences in this series take place now in a three year interval. Previous conferences were held in Karlsruhe, Germany (1983), Los Alamos, USA (1987), Gatchina (Leningrad), Russia (1989), Bad Honnef, Germany (1991), Boulder, USA (1993), Blaubeuren, Germany (1995), Vancouver, Canada (1997), Zuz, Switzerland (1999), Washington, DC, USA (2001), and Beijing, China (2004).

The aim of the Conference was to bring together the experts of both meson physics and baryon spectroscopy because of the great overlap of the physics questions in both fields. The progress in symmetry studies and its possible relevance for other fields was discussed. A critical review of the methods for resonance extractions was done and the role of final state interactions in modifying resonance properties has been addressed. Important questions for the future development of the field with regard to common aspects of the charmed quark sector and the light quark sector were worked out.

The aim of the Conference is to bring together the experts of both meson physics and baryon spectroscopy because of the great overlap of the physics questions in both fields. The progress in symmetry studies and its possible relevance for other fields will be discussed. A critical review of the methods for resonance extractions will be done and the role of final state interactions in modifying resonance properties has to be addressed. An important question for the future development of the field is to work out common aspects of the charmed quark sector and the light quark sector. A few overview talks which focus on the basic open questions of the field and possible applications in neighboring fields will be included.

Hadron physics investigates an open frontier of the Standard Model: the strong interaction for large gauge couplings. Experimentally, there two major strategies currently pursued:

- Precision experiments study symmetries and their violations with the aim to extract fundamental quantities of Quantum Chromodynamics, such as the quark masses,
- Studies of the excited states and their decays try to establish the ordering principles of the hadronic spectra in order to shed light on the problem of the confinement of the quarks.

On the theoretical side, the scientific paradigm has shifted within the last two decades to effective field theories. The basic idea is to characterize a physical system by its energy or length scales. Within a given energy range, the important symmetries have to be identified and only the relevant degrees of freedom have to be treated explicitly, while physics at higher energy scales can be summarized by a finite set of low-energy constants. The number of those constants is limited by a systematic counting scheme and depends on the precision one aims for. The effective field theory of Quantum Chromodynamics is called Chiral Perturbation Theory. By now, it is a standard tool for hadron physics in the threshold region. For larger energies, chiral perturbation theory has to be unitarized. Nuclear effective field theory is an extension of chiral perturbation theory based on Weinberg's suggestions. In this field, there has been considerable progress. The two-nucleon potential obtained within nuclear effective field theory has been developed to a precision which is as high as the one of the best phenomenological potentials. Moreover, it allows a systematic inclusion of few-body forces. The few-body forces derived in effective field theory are closely linked to experimental data, such as pion-nucleon scattering and few-body reactions with polarized partners. Since the isospin dependence of those three-body interactions is determined mainly by data, one gains predictive power for theoretical studies of nuclear matter and eventually neutron-rich finite nuclei. These new developments start to bring together previously separated communities which makes them an interesting topic for the MENU conference. Presently, there is a wealth of new data for physics involving the strange quarks. Polarized electron scattering finds that the strangeness content of the nucleon is small. The recent experimental results for exotic atoms obtained by DEAR and at KEK are of high precision and have significantly increased the data base for antikaon-nucleon scattering. These new results start to impact on the discussion concerning the structure of the $\Lambda(1405)$ which is notoriously difficult to obtain in quark models. Kaon production both with the electromagnetic probe and hadronic probes has been investigated and evidence for some new resonances has been claimed.

We hope that the programm achieved these goals. The next conference of this series will be held 2010 when Jefferson Lab. is the host. We wish it great success with exciting new results.

The proceedings consist of two volumes. In Volume I all submitted invited talks are compiled while Volume II contains all submitted contributions, presented orally or as posters.

Siegfried Krewald and Hartmut Machner
Chairpersons, Organizing Committee

Acknowledgements

Many people must be thanked for contributing to the success of the MENU 2007 Conference. There are the members of the International Advisory Committee, the Organizing Committee, the Editorial Committee and the conference secretary Mrs. Y. Abdel-Fattah. The help of a lot of young people, graduate students as well as postdocs, was essential in order to have a smooth running conference. The advice given by the Editorial Committee and the referees is gratefully acknowledged by the editors. Finally we thank the exhibitors and our sponsors for making this meeting possible.

Siegfried Krewald and Hartmut Machner
Chairpersons, Organizing Committee

International Advisory Committee

- Marco Battaglieri (INFN Genoa)
- Veronique Bernard (ULP Strasbourg, France)
- Stan Brodsky (SLAC, Stanford, USA)
- David V. Bugg (Queen Mary, U of London, England)
- Volker Burkert (JLAB, Newport News, VA, USA)
- Avraham Gal (HUJI, Jerusalem, Israel)
- Haiyan Gao (TUNL, Durham, NC, USA)
- Jürg Gasser (University of Bern, Switzerland)
- Carlo Guaraldo (LN Frascati, Italy)
- Hans-Werner Hammer (Univ. Bonn, Germany)
- Muhsin N. Harakeh (KVI, Groningen, The Netherlands)
- Bo Hoistad (TSL, Uppsala, Sweden)
- Bernd Krusche (University of Basel, Switzerland)
- Volker Metag (Univ. Giessen, Germany)
- Takashi Nakano (Osaka U, Japan)
- B.M.K. Nefkens (UCLA, CA, USA)
- Eulogio Oset (University of Valencia, Spain)
- Dan-Olof Riska (University of Helsinki, Finland)
- Craig D. Roberts (ANL, Argonne, IL, USA)
- Andreas Schäfer (Univ. Regensburg, Germany)
- Madeleine Soyeur (DAPHNIA/SPhN-CEA, Saclay, France)
- Ulrike Thoma (Univ. Bonn, Germany)

- Anthony Thomas (JLAB, Newport News, VA, USA)
- Hiroshi Toki (Osaka U, Japan)
- Willem T.H. van Oers (University of Manitoba, Winnipeg, Canada)
- Eberhard Widmann (Austrian Academy of Sciences, Vienna, Austria)
- Frank Wilczek (MIT, Boston, MA, USA)
- Bingsong Zou (Institute of High Energy Physics, Beijing, China)

Organizing Committee

- A. Gillitzer, Jülich
- Detlev Gotta, Jülich
- Christoph Hanhart, Jülich
- Siegfried Krewald, Jülich (Co-Chair)
- Hartmut Machner, Jülich (Co-Chair)
- Rudolf Mayer, Jülich
- Ulf-G. Meißner, Jülich
- James Ritman, Jülich
- Susan Schadmand, Jülich (Scientific Secretary)
- Hans Ströher, Jülich

Editorial Committee

- Albrecht Gillitzer, Jülich
- Detlev Gotta, Jülich
- Christoph Hanhart, Jülich

- Siegfried Krewald, Jülich
- Hartmut Machner, Jülich
- Susan Schadmand, Jülich

Sponsors

- Forschungszentrum Jülich
- Deutsche Forschungsgemeinschaft
- International Union of Pure and Applied Physics
- Jefferson Laboratory
- European Community-Research Infrastructure Activity under the FP6 "Structuring the European Research Area" programme (HadronPhysics, contract number RII3-CT-2004-506078)

Industrial Exhibitors

- CAEN (www.caen-de.com)
- Iseg High Voltage (www.iseg-hv.de)
- CalPlus (www.calplus.de)
- Oerlikon (www.oerlikon.com)
- Pfeiffer-Vacuum (www.pfeiffer-vacuum.de)
- Struck Innovative Systems (www.struck.de)
- Tektronix (www.tek.com)
- Wiener (www.wiener-d.com)

Contents

1	QUASIELASTIC DEUTERON KNOCK OUT AND ITS DEPENDENCE ON NUCLEAR ATOMIC NUMBER	1
	<i>B. M. Abramov et al.</i>	
2	SPONTANEOUS P-PARITY VIOLATION IN DENSE BARYON MATTER	6
	<i>S.S. Afonin et al.</i>	
3	S-WAVE MESON SCATTERING UP TO $\sqrt{s} \lesssim 2$ GeV FROM CHIRAL LAGRANGIANS	11
	<i>M. Albadejo et al.</i>	
4	POINCARÉ INVARIANT COUPLED CHANNEL MODEL FOR THE PION-NUCLEON SYSTEM: INSTANT FORM MODEL	15
	<i>H.H. Alharbi</i>	
5	QCD ANALYSIS FOR NUCLEAR PARTON DISTRIBUTIONS IN THE NEXT TO LEADING ORDER	20
	<i>S. Atashbar Tehrani and Ali N. Khorramian</i>	
6	HOW IS EXOTICS PRODUCED ? WHERE TO SEARCH FOR IT ?	24
	<i>Ya. Azimov et al.</i>	
7	THE PAX EXPERIMENT AT FAIR	28
	<i>L. Barion</i>	
8	DEUTERON SPIN DICHROISM IN CARBON TARGET	32
	<i>V. Baryshevsky and A. Rouba</i>	

9	SYMMETRY TESTS IN NA48 WITH KAONS	36
	<i>M. Behler</i>	
10	THE GOTTFRIED SUM RULE IN AN UNQUENCHED QUARK MODEL	40
	<i>R. Bijker and E. Santopinto</i>	
11	HIGHLIGHTS ON RADIATIVE KAON AND HYPERON DECAYS FROM NA48/2	44
	<i>A. Bizzeti</i>	
12	A HIGH PRECISION MEASUREMENT OF THE PION FORM FACTORS VIA RADIATIVE PION DECAY $\pi^+ \rightarrow e^+ \nu \gamma$	48
	<i>M. Bychkov</i>	
13	COHERENT PHOTOPRODUCTION OF ϕ MESONS FROM DEUTERONS NEAR THRESHOLD	52
	<i>W.C. Chang</i>	
14	MULTICHANNEL CHIRAL APPROACH FOR KAONIC HYDROGEN	57
	<i>A. Cieplý and J. Smekal</i>	
15	FIRST RESULTS ON PION POLARIZABILITIES @ COMPASS	62
	<i>M. Colantoni</i>	
16	STUDIES OF THE η MESON PRODUCTION WITH POLARIZED PROTON BEAM AT COSY-11	66
	<i>R. Czyżykiewicz and P. Moskal</i>	
17	INCLUSIVE DI-ELECTRON PRODUCTION IN C+C COLLISIONS WITH HADES	71
	<i>F. Dohrmann et al.</i>	
18	CHARMONIUM EXCITED STATES FROM LATTICE QCD	76
	<i>J. Dudek, R. G. Edwards, N. Mathur, D. Richards</i>	
19	MESONIC INTERACTIONS AND THEIR CONTRIBUTION TO STRONG PHASES IN FLAVOR PHYSICS	80

<i>B. El-Bennich et al.</i>	
20	IN PURSUIT OF NEW PHYSICS WITH K^+ SCATTERING ON NUCLEI AT INTERMEDIATE ENERGY 85
	<i>S.M. Eliseev</i>
21	LATEST HERMES RESULTS ON TRANSVERSE SPIN IN HADRON STRUCTURE AND FORMATION 89
	<i>R. Fabbri</i>
22	SCALAR MESONS: A CHIRAL LAGRANGIAN FRAMEWORK FOR THEIR MIXING AND SUBSTRUCTURE 93
	<i>A.H. Fariborz</i>
23	NONPERTURBATIVE QUARK-GLUON DYNAMICS 97
	<i>C.S. Fischer et al.</i>
24	THE PANDA DETECTOR AT FAIR 101
	<i>K. Föhl</i>
25	ELEMENTARY COLLISIONS WITH HADES 105
	<i>I. Fröhlich, J. Pietruszko et al.</i>
26	MONTE CARLO SIMULATION OF MESON-NUCLEON AND MESON-NUCLEUS INTERACTIONS AT HIGH ENERGIES 111
	<i>A. Galoyan and V. Uzhinsky</i>
27	MULTIPLICITY FLUCTUATIONS IN INTERACTIONS OF LIGHT NUCLEI WITH CARBON AT MOMENTUM OF $4.2 \text{ GeV}/c$ PER NUCLEON AND THEIR THEORETICAL INTERPRETATION 115
	<i>A. Galoyan et al.</i>
28	MESONS AND GLUEBALLS: A QUANTUM FIELD APPROACH 119
	<i>G. Ganbold</i>
29	DYNAMICS OF \bar{K} AND MULTI-\bar{K} NUCLEI 124
	<i>D. Gazda et al.</i>

30 RECOIL POLARIZATION MEASUREMENTS WITH CB@MAMI	128
<i>D. I. Glazier and D. P. Watts</i>	
31 RESONANCE PHENOMENA IN HEAVY NUCLEI COL- LISIONS AND STRUCTURIZATION OF THE POSITRON SPECTRUM	132
<i>A. V. Glushkov</i>	
32 DISCHARGE OF METASTABLE NUCLEI DURING NEG- ATIVE MUON CAPTURE: ENERGY APPROACH	139
<i>A. V. Glushkov et al.</i>	
33 MULTIPLICITIES IN (ANTI-)NEUTRINO INTERAC- TIONS	144
<i>A. M. Güler and U. Köse</i>	
34 EVALUATION OF THE πN SIGMA TERM USING DIS- PERSION RELATIONS - PRESENT STATUS	149
<i>M. Hadzimehmedovic, H. Osmanovic, J. Stahov</i>	
35 DETERMINATION OF THE POTENTIAL COEFFICIENTS OF THE BARYONS AND THE EFFECT OF SPIN AND ISOSPIN POTENTIAL ON THEIR ENERGY	153
<i>H. Hassanabadi and A. A. Rajabi</i>	
36 $\pi N \rightarrow \eta N$ PROCESS IN A χQM APPROACH	161
<i>J. He et al.</i>	
37 PION PHYSICS FROM LATTICE QCD	165
<i>J. Hu et al.</i>	
38 EXOTIC HADRONS AND $SU(3)$ CHIRAL DYNAMICS	170
<i>T. Hyodo et al.</i>	
39 THREE-BODY RESONANCE POLE OF STRANGE DIBARYON IN THE $\bar{K}NN - \pi YN$ COUPLED SYSTEM	174
<i>Y. Ikeda and T. Sato</i>	
40 PION-NUCLEON P_{33} AND P_{11} SCATTERINGS IN THE LIPPMANN-SCHWINGER APPROACH	178

	<i>T. Inoue et al.</i>	
41	PRECISE DETERMINATION OF KAONIC ^4He X-RAY ENERGY	182
	<i>T. Ishiwatari et al.</i>	
42	APPLICATION OF χPT WITH VECTOR MESONS: KAON ELECTROMAGNETIC FORM FACTORS AND $K\bar{K}$ CONTRIBUTION TO MUON ANOMALOUS MAGNETIC MOMENT	186
	<i>S. Ivashyn and A. Korchin</i>	
43	LIGHT SCALAR MESON DECAYS AND MIXING IN ChPT	190
	<i>S. Ivashyn and A. Korchin</i>	
44	FROM CHARGED TRACKS TO CHPT ANOMALIES	194
	<i>M. Janusz and L. Yurev</i>	
45	η' DECAYS WITH WASA-AT-COSY	198
	<i>B. R. Jany and D. Duniec</i>	
46	SEARCH FOR η-NUCLEUS BOUND STATES	202
	<i>V. Jha et al.</i>	
47	MEASUREMENT OF THE ABC-EFFECT IN THE MOST BASIC DOUBLE-PIONIC FUSION REACTION	207
	<i>O. Khakimova et al.</i>	
48	GENERALIZED MULTICONFIGURATION MODEL OF DECAY OF THE MULTIPOLE GIANT RESONANCES APPLIED TO ANALYSIS OF REACTION $(\mu^- N)$ ON THE NUCLEUS ^{40}Ca	211
	<i>O. Yu. Khetselius et al.</i>	
49	NUCLEAR ELECTRIC QUADRUPOLE MOMENTS AND HYPERFINE STRUCTURE PARAMETERS FOR HEAVY ISOTOPES	217
	<i>O. Yu. Khetselius</i>	
50	ON A POSSIBLE ORIGIN OF A RESONANCE-LIKE STRUCTURE IN THE TWO-PHOTON INVARIANT MASS	

SPECTRUM OF THE REACTION $pp \rightarrow pp\gamma\gamma$.	224
<i>A. S. Khrykin and S. B. Gerasimov</i>	
51 COMPARATIVE STUDY OF THE PROTON-η AND PROTON-η' INTERACTIONS VIA THE PP AND P-MESON INVARIANT MASS DISTRIBUTIONS	229
<i>P. Klaja</i>	
52 PROTON-PROTON CORRELATIONS FOR THE $pp \rightarrow pp\eta$ REACTION MEASURED WITH COSY-11	234
<i>P. Klaja and P. Moskal</i>	
53 MEASUREMENT OF THE SPIN STRUCTURE FUNCTIONS AND LATEST RESULTS ON QUARK HELICITY DISTRIBUTIONS FROM DEEP-INELASTIC SCATTERING AT HERMES	239
<i>P. Kravchenko</i>	
54 $\bar{D}N$ INTERACTION BASED ON MESON-EXCHANGE AND QUARK-GLUON DYNAMICS	244
<i>G. Krein et al.</i>	
55 MEASUREMENTS OF THE GLUON POLARIZATION IN THE NUCLEON AT COMPASS	248
<i>R. Kuhn</i>	
56 MULTIMESON PRODUCTION IN pp INTERACTIONS AS A BACKGROUND FOR η AND η' DECAYS	252
<i>A. Kupsc et al.</i>	
57 RENORMALIZATION GROUP EQUATION FOR NUCLEAR CURRENT OPERATORS	257
<i>A. N. Kvinikhidze et al.</i>	
58 NEUTRON-NEUTRON SCATTERING LENGTH FROM THE REACTION $\gamma d \rightarrow \pi^+ nn$	261
<i>V. Lensky et al.</i>	
59 DECAYS OF NEW HEAVY MESONS CONTAINING STRANGE QUARKS AS HADRONIC MOLECULES	266
<i>V. E. Lyubovitskij et al.</i>	

60 SCREENING IN THE BREMSSTRAHLUNG REACTIONS AND THE MAGNETIC MOMENT OF THE Δ RESO- NANCE.	270
<i>A. I. Machavariani</i>	
61 Dynamically generated resonances in two meson-one baryon systems	275
<i>N. Author</i>	
62 DEVELOPMENT OF A VERSATILE READOUT SYS- TEM FOR HIGH RATE DETECTOR ELECTRONICS	279
<i>M. Mertens et al.</i>	
63 PARTIAL WAVE ANALYSIS OF πN SCATTERING WITH FIXED-t CONSTRAINTS	284
<i>P. Metsä</i>	
64 BRIDGING OVER p-WAVE π-PRODUCTION AND WEAK PROCESSES IN FEW-NUCLEON SYSTEMS WITH CHI- RAL PERTURBATION THEORY	288
<i>S. X. Nakamura</i>	
65 RENORMALIZATION GROUP ANALYSIS OF THE CHI- RAL PION PRODUCTION OPERATOR FOR $NN \rightarrow d\pi$	293
<i>S. X. Nakamura and A. Gårdestig</i>	
66 STRANGENESS PHOTOPRODUCTION WITH CBELSA/TAPS	297
<i>M. Nanova et al.</i>	
67 PRESENT UNDERSTANDING OF SPIN FILTERING EX- PERIMENTS	302
<i>M. Nikipelov</i>	
68 STUDYING PION EFFECTS IN THE QUARK PROPAGA- TOR	306
<i>D. Nickel</i>	
69 NEUTRINO-INDUCED KAON PRODUCTION	310
<i>D. D. van Niekerk and B. I. S. van der Ventel</i>	

70 BOUND KAON APPROACH FOR THE ppK^- SYSTEM IN THE SKYRME MODEL	314
<i>T. Nishikawa and Y. Kondo</i>	
71 ON BARYON-ANTIBARYON CROSS SECTIONS FROM INITIAL STATE RADIATION PROCESSES AT BABAR AND THEIR SURPRISING THRESHOLD BEHAVIOR	318
<i>S. Pacetti</i>	
72 INVESTIGATION OF THE $dp \rightarrow {}^3\text{He} X$ ($X=\eta, \pi^+\pi^-$) REACTIONS AT COSY-ANKE	323
<i>M. Papenbrock et al.</i>	
73 DYNAMICAL COUPLED CHANNEL APPROACH TO OMEGA MESON PRODUCTION	328
<i>M. Paris</i>	
74 $3\pi^0$ FINAL STATES WITH WASA AT CELSIUS AND COSY	332
<i>C. Pauly</i>	
75 HIGH-STATISTICS η PRODUCTION IN PROTON-PROTON COLLISIONS AT $Q=72$ MeV	336
<i>H. Pettersson</i>	
76 CHARM AND CHARMONIUM PHYSICS AT BABAR	340
<i>E. Prencipe</i>	
77 ISOSPIN DEPENDENCE OF THE η' MESON PRODUC- TION IN NUCLEON-NUCLEON COLLISIONS	345
<i>J. Przerwa</i>	
78 IN SEARCH OF THE BOX ANOMALY WITH THE WASA- AT-COSY FACILITY	350
<i>Ch. F. Redmer</i>	
79 PION-NUCLEON SCATTERING IN THE $N^*(1440)$ RES- ONANCE REGION	354
<i>M. E. Sadler et al.</i>	
80 THE GMO SUM RULE REVISITED	358
<i>M. E. Sainio</i>	

81 THE $pd \rightarrow {}^3\text{He}\omega$ REACTION	362
<i>K. Schönning and K. P. Khemchandani</i>	
82 HYPERON PRODUCTION hyperon in the channel $pp \rightarrow K^+\Lambda p$ at COSY-TOF	367
<i>W. Schroeder</i>	
83 IMPROVED STUDY OF A POSSIBLE Θ^+ PRODUCTION IN THE $pp \rightarrow pK^0\Sigma^+$ REACTION WITH THE COSY-TOF SPECTROMETER	371
<i>W. Schroeder</i>	
84 CHIRAL SYMMETRY RESTORATION IN EXCITED MESONS	375
<i>J. Segovia, D. R. Entem, F. Fernández</i>	
85 BOOTSTRAP METHOD FOR THE PHYSICAL VALUES OF πN RESONANCE PARAMETERS	379
<i>K. Semenov-Tian-Shansky, A. Vereshagin, V. Vereshagin</i>	
86 η-MESON PRODUCTION IN THE COUPLED-CHANNEL EFFECTIVE LAGRANGIAN APPROACH	383
<i>V. Shkyar, H. Lenske, U. Mosel</i>	
87 HIGH MASS BARYONS IN PION PHOTOPRODUCTION	387
<i>A. Sibirtsev</i>	
88 ROPER RESONANCE EXCITATION IN NN-COLLISIONS WITH SINGLE- AND DOUBLE-PION PRODUCTION	392
<i>T. Skorodko et al.</i>	
89 PIONIC DEUTERIUM	396
<i>Th. Strauch et al.</i>	
90 PARAMETERS A AND R MEASUREMENTS IN THE RESONANCE REGION OF THE PION-NUCLEON ELASTIC SCATTERING: RECENT RESULTS AND SUBSEQUENT INVESTIGATIONS.	400
<i>V. V. Sumachev et al.</i>	
91 RHO-LIKE-MESON FAMILY IN THE PION-PION SCATTERING	405
<i>Yu. S. Survtsev and P. Bydžovský</i>	

92 ON NATURE OF THE f_0 AND f_2 MESONS	410
<i>Yu. S. Suroutsev and R. Kamiński</i>	
93 RESONANCE POLE BY SPEED PLOT AND TIME DELAY	415
<i>N. Suzuki and T. Sato</i>	
94 EXCLUSIVE PRODUCTION OF QUARKONIA IN pp AND $p\bar{p}$ COLLISIONS FAR FROM THE THRESHOLD	419
<i>A. Szczurek</i>	
95 THE RULE OF OAM AND POLARIZED VALON MODEL	426
<i>F. Taghavi Shahri and F. Arash</i>	
96 Q^2-DEPENDENT OF PPDFS IN VALON MODEL	431
<i>F. Taghavi Shahri and F. Arash</i>	
97 LATTICE QCD STUDY OF $g_A^{N^*N^*}$ WITH TWO FLAVORS OF DYNAMICAL QUARKS	435
<i>T. T. Takahashi and T. Kunihiro</i>	
98 $\Lambda(1405)$ AS A RESONANCE IN THE BARYON-MESON SCATTERING COUPLED TO THE q^3 STATE IN A QUARK MODEL	439
<i>S. Takeuchi and K. Shimizu</i>	
99 THE MASSLESS LINEAR SIGMA MODEL FOR FINITE NUCLEI AND AT FINITE TEMPERATURE	444
<i>S. Tamenaga et al.</i>	
100 PREPARATIONS FOR PELLET TRACKING SYSTEM	448
<i>T. Tolba</i>	
101 D AND \bar{D} MESONS IN HOT AND DENSE MATTER	452
<i>L. Tolós et al.</i>	
102 REACTION DYNAMICS OF ω MESON PRODUCTION IN pp COLLISIONS	457
<i>W. Ullrich et al.</i>	
103 STUDY OF THE $p^6\text{Li} \rightarrow \eta^7\text{Be}$ REACTION	461
<i>N. J. Upadhyay, N. G. Kelkar, K. P. Khemchandani, B. K. Jain</i>	

- 104 SCALING ONSET IN THE REACTIONS $dd \rightarrow p^3H$ AND
 $pd \rightarrow pd$ IN THE GEV REGION 465**
Yu. N. Uzikov
- 105 STUDY OF η -MESON PRODUCTION IN $dd \rightarrow ^4He\eta$ RE-
ACTION 469**
G. Vankova et al.
- 106 SOLITON MODEL APPROACH TO KAON-NUCLEON
SCATTERING IN THE PENTAQUARK CHANNEL 474**
H. Weigel
- 107 SIMULATION OF THE \bar{P} ANDA EXPERIMENT
WITH PANDAROOT 479**
A. Wrońska
- 108 MEASUREMENT OF THE REACTION $dd \rightarrow \alpha K^+ K^-$
WITH ANKE/COSY 484**
X. Yuan et al.
- 109 CASCADE RESONANCE PROPERTIES FROM CHARM
BARYON DECAYS AT BABAR 488**
V. Ziegler
- 110 STUDIES OF THE $\Lambda(1405)$ IN PROTON-PROTON COL-
LISIONS WITH ANKE AT COSY-JÜLICH 492**
I. Zychor

QUASIELASTIC DEUTERON KNOCK OUT AND ITS DEPENDENCE ON NUCLEAR ATOMIC NUMBER

B. M. Abramov, Yu. A. Borodin, S. A. Bulychjov, I. A. Dukhovskoy, A. I. Khanov, A. P. Krutenkova, V. V. Kulikov¹, M. A. Martemianov, M. A. Matsyuk, V. E. Tarasov, E. N. Turdakina

Institute for Theoretical and Experimental Physics, Moscow, Russia

Abstract

The backward quasielastic deuteron knock out has been studied with pion beam in full kinematics on ${}^6\text{Li}$, ${}^7\text{Li}$, ${}^{12}\text{C}$ and ${}^{16}\text{O}$. The experiment was performed at the ITEP Proton Synchrotron with the 3-m magnet spectrometer at an incident pion momentum of 0.72 GeV/c. Momentum and angles of forward going deuteron as well as of the beam and backward scattered pions were measured. The excitation energy spectra, the momentum distributions of the internal motion of the quasideuteron clusters and quasideuteron effective numbers were obtained. A-dependence of quasideuteron effective numbers is practically independent of atomic number in contrast with $A^{0.33}$ dependence observed for inclusive deuteron knock out measured with proton beam. Possible reasons for such a difference are discussed.

Quasielastic deuteron knock out from nuclei is an effective way to study cluster structure, nucleon-nucleon correlations and reaction mechanisms of particle-nucleus interactions. To disentangle the effects of nuclear structure and reaction mechanism it is necessary to have measurements for different projectiles. There are data on quasielastic deuteron knock out taken with proton and electron beams. The aim of our experiment is to widen a variety of projectiles and to obtain the data with pion beam. In [1] pions were used for the first time for a study of quasielastic deuteron knock out from ${}^6\text{Li}$ with identification of ground state of the rest nucleus ${}^4\text{He}$. In the following works [2–4] all spectrum of energy excitation of rest nuclei for ${}^6\text{Li}$, ${}^7\text{Li}$, ${}^{12}\text{C}$, ${}^{16}\text{O}$ has been analysed and also the first data for triton knock out has been

¹E-mail address: kulikov@itep.ru

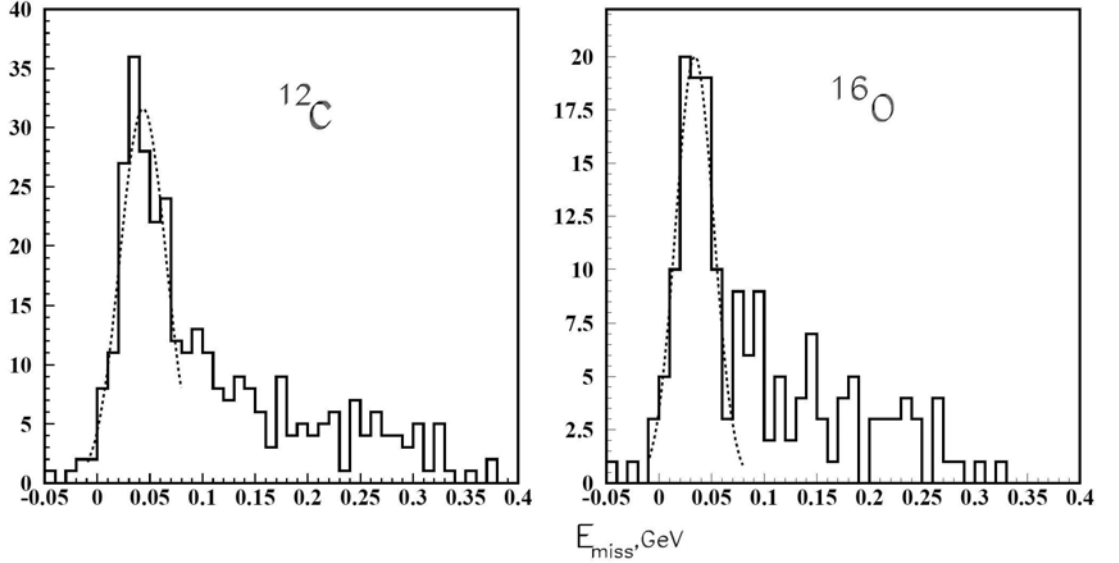


Figure 1: Missing energy distributions for ^{12}C and ^{16}O , fit by gaussian is shown by dotted lines.

obtained. Present work is mainly aimed at an analysis of A-dependence of effective deuteron number in nuclei seen in deuteron knock out.

The experiment has been performed on a negative pion beam of 10 GeV ITEP proton synchrotron at $p_0 = 0.72$ GeV/c. The 3-m magnet spectrometer with spark chambers placed in a magnetic field has been used (see [5] for details). Nuclear targets were placed near the center of a large dipole magnet of $3 \times 1 \times 0.5$ m³ with maximal field 1.66 T. One half of the magnet was used as a forward going deuteron spectrometer. Another half was used as a beam and backward scattered pion spectrometer. An accuracy in an energy excitation of the rest nucleus was ~ 10 MeV. Time-of-flight was used to identify deuterons from the reaction

$$\pi^- + A \rightarrow d + \pi^- + X. \quad (1)$$

A momentum of a quasideuteron intranuclear motion and missing energy (an excitation energy of a rest nucleus) were calculated in plain wave impulse approximation.

Missing energy distributions for the reaction (1) are given for ^{12}C , ^{16}O in Fig.1 as an example. The peaks of quasielastic deuteron knock out are clearly seen. These peaks were fitted by simple gaussians. The mean (r.m.s) is $43 \pm 2(22 \pm 2)$ MeV for ^{12}C and $34 \pm 2(18 \pm 2)$ MeV for ^{16}O . The quasideuteron momentum distributions are given in [3, 4]. An effective number N_d of

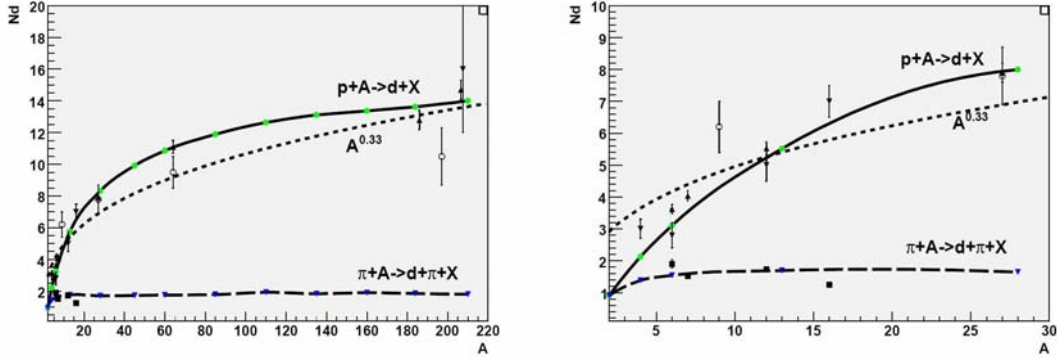


Figure 2: A-dependence of deuteron knock out. Measurements of this experiment - full squares, other data are for inclusive deuteron knock out by protons from compilation [7].

quasideuterons in nucleus participated in the reaction (1) was calculated by integration over the peak area and normalization to backward pion deuteron elastic scattering on free deuteron. These N_d values are shown in Fig.2 by full squares. There is only one measurement of N_d with proton beam in full kinematics on ${}^6\text{Li}$ made at Dubna [6]. It gives $N_d=1.73\pm 0.1$. Our result $N_d=1.90\pm 0.1$ for ${}^6\text{Li}$ is in good agreement with it. Our measurements of N_d are practically independent from atomic number A of a target nucleus. Such a dependence is different from observed in inclusive deuteron knock out measured with proton beam (see compilation of all existing measurements with proton beam in [7]) where A-dependence approximated by $A^{0.33}$ was observed. In contrast to measurement in full kinematics in the inclusive deuteron knock out momentum of backward scattered projectile is not measured. So absorption of the backward scattered projectile in the target nucleus result in smaller N_d value for measurements in full kinematics and possibly in different A-dependence. To try to understand if additional absorption could change an A-dependence so drastically we performed calculations in a simple classic model described below. Our calculation can be treated only as an estimation. In our approach N_d for spherical nucleus is given by

$$N_d = Ck \int_0^{+\infty} b db \int_{-\infty}^{+\infty} \frac{\rho^2(b, x)}{\rho^2(0)} \exp\left(-\int_{-\infty}^x (L_b^{-1} + L_s^{-1}) dx\right) \exp\left(-\int_x^{+\infty} L_d^{-1} dx\right) dx$$

where b - impact parameter, x - coordinate along projectile motion, b and x are equal to zero in the center of a nucleus. It is supposed that projectile, scattered particle and knock out deuteron trajectories are straight lines

parallel to x-direction. It is reasonable for geometry of backward scattering. $\rho(r = \sqrt{b^2 + x^2})$ is Fermi distribution of nuclear density with standard parameters $R_A = r_0 A^{0.33}$, $r_0 = 1.1 \text{Fm}$, $t = 0.5 \text{Fm}$ normalized to atomic number A, $\int_0^{+\infty} \rho(r) \mathbf{dr} = A$. L_{i0} is absorption length where $i=b,s,d$ for beam, scattered projectile and knock out deuteron respectively. $L_i^{-1} = L_i^{-1}(b, x) = L_{i0}^{-1}(1 - 2/A)\rho(b, x)/\rho(0)$. Multiplier $(1 - 2/A)$ effectively corrects the absorption length in such a way that $L_i^{-1}=0$ for deuteron target. $k = 1 + (A - 1)/A$ is of minor importance. It helps to give $N_d = 1$ for free deuteron and it is essential for $A < 5$ only. For inclusive deuteron knock out (where $L_s^{-1} = 0$) we adjusted L_{b0} and L_{d0} to have reasonable description of available experimental data. The result is shown in Fig.2 by full line where $L_{b0} = 0.6 \text{Fm}$ and $L_{d0} = 0.2 \text{Fm}$. Qualitatively it gives much better description of the data on inclusive deuteron knock out by protons than $A^{0.33}$ -dependence drawn by dotted line. For the measurements of N_d in full kinematics we have to introduce non zero L_s^{-1} . An increase of L_s^{-1} results in smaller values of N_d and changes A-dependence from rising to falling one. To have a reasonable description of our measurements (dashed line in Fig.2) we have to take $L_{s0} = 0.1 \text{Fm}$. At a first glance it seems unrealistically small compared to absorption length for projectile. But two arguments make it more realistic. At first the backward scattered pion has a momentum near Δ -resonance that decrease absorption length. And secondly a small angle elastic scattering of all participants on target nucleons are less important for inclusive deuteron knock out than for measurement in full kinematics. This also effectively increases absorption length. Performed estimation shows that larger absorption effects for full kinematics measurements can result in flat A-dependence of deuteron knock out.

The work has been done under support of Federal agency for atomic energy of Russia and RFBR grant 03-0217470.

References

- [1] B.M. Abramov *et al.*, *JETP Letters* **74**, 504(2001).
- [2] B.M. Abramov *et al.*, *JETP Letters* **80**, 214(2004).
- [3] B.M. Abramov *et al.*, *Physics of Atomic Nuclei* **68**, 474(2005).
- [4] B.M. Abramov *et al.*, *Physics of Atomic Nuclei* **70**, 1209(2007).
- [5] B.M. Abramov *et al.*, *Nucl. Phys.* **A723**, 389(2003).
- [6] D. Albrecht *et al.*, *Nucl. Phys.* **A338**, 477(1980).

- [7] A.V. Arefiev *et al.*, *Physics of Atomic Nuclei* **29**, 410(1979).

SPONTANEOUS P -PARITY VIOLATION IN DENSE BARYON MATTER

S.S. Afonin^{*,1}, A.A. Andrianov[§], V.A. Andrianov^{*}, D. Espriu[§]

^{*}St. Petersburg State University, St. Petersburg, Russia

[§]University of Barcelona, Barcelona, Spain

Abstract

We investigate possibilities for dynamical P -parity violation in dense baryon matter in the framework of effective quark models. Dynamical P -parity violation can appear in models with at least two scalar and two pseudoscalar fields, where both scalar fields are condensed at normal conditions. At special configurations of coupling constants, one of pseudoscalar fields can then also condense at some value of baryon density, the phenomenon results in mixing of the scalar and pseudoscalar physical degrees of freedom, hence, giving rise to P -parity violation. We discuss the implications and possible experimental signatures for P -parity violation in strong interactions in future experiments with heavy-ion collisions.

1 Introduction

Presently the issue of dense baryon matter is attracting a lot of interest as long as some striking physical phenomena are expected to occur in certain regimes, such as the phase transition to chirally symmetric hadron matter. The message we would like to convey is that before any phase transition the P -parity in cold dense baryon matter could undergo spontaneous breaking. At zero baryon density (chemical potential) this phenomenon is precluded by the Vafa-Witten theorem [1]. However, the conditions under which this theorem was proven (positivity of the measure of partition function in vector-like theories) do not hold anymore at finite baryon density (see [2] for further discussions).

We shall report some important results of ongoing work along this line. In short, at certain value of quark chemical potential and in the physical range of model parameters, the phenomenon of spontaneous parity breaking (SPB) has been recently observed in extensions of popular low-energy models of

¹E-mail address: afonin24@mail.ru

QCD, namely in a generalized Nambu–Jona-Lasinio model [3] (the so-called Quasilocal Quark Model (QQM)), in extended chiral quark model [4], and in a generalized sigma-model [2]. In all cases, the underlying mechanism turned out to be rather similar, we are going to describe briefly the relevant general features.

2 General analysis

The possibility of SPB arises when two different scalar fields condense with a relative phase between their v.e.v.'s. Let us consider a model with two multiplets of scalar/pseudoscalar fields

$$H_j = \sigma_j \mathbf{I} + i\hat{\pi}_j, \quad j = 1, 2; \quad H_j H_j^\dagger = (\sigma_j^2 + (\pi_j^a)^2), \quad (1)$$

here $\hat{\pi}_j \equiv \pi_j^a \tau^a$ with τ^a being a set of Pauli matrices. We shall deal with scalar systems globally symmetric in respect to $SU(2)_L \times SU(2)_R$ rotations working in the exact chiral limit. We should think of these two chiral multiplets as representing the two lowest-lying radial states for a given J^{PC} . The introduced degrees of freedom possess all the necessary ingredients to study SPB.

The effective potential of the models considered has, in general, the following form at zero quark chemical potential μ (after specifying the v.e.v. $\langle H_1 \rangle = \langle \sigma_1 \rangle$),

$$\begin{aligned} V_{\text{eff}} = \frac{1}{2} \text{tr} \left\{ - \sum_{j,k=1}^2 H_j^\dagger \Delta_{jk} H_k + \lambda_1 (H_1^\dagger H_1)^2 + \lambda_2 (H_2^\dagger H_2)^2 + \lambda_3 H_1^\dagger H_1 H_2^\dagger H_2 \right. \\ \left. + \frac{1}{2} \lambda_4 (H_1^\dagger H_2 H_1^\dagger H_2 + H_2^\dagger H_1 H_2^\dagger H_1) + \frac{1}{2} \lambda_5 (H_1^\dagger H_2 + H_2^\dagger H_1) H_1^\dagger H_1 \right. \\ \left. + \frac{1}{2} \lambda_6 (H_1^\dagger H_2 + H_2^\dagger H_1) H_2^\dagger H_2 \right\} + \mathcal{O} \left(\frac{|H|^6}{\Lambda^2} \right), \quad (2) \end{aligned}$$

with 9 real constants Δ_{jk}, λ_i . QCD bosonization rules indicate that $\Delta_{jk} \sim \lambda_i \sim N_c$. The neglected terms will be suppressed by inverse power of the chiral symmetry breaking scale $\Lambda \simeq 1.2$ GeV. If we assume the v.e.v. of H_j to be of the order of the constituent mass $0.2 \div 0.3$ GeV, it is reasonable to neglect these terms.

To guess the typical values of couplings, it is instructive to consider a specific model. Let us take the QQM [3] as an example. The relevant form of Lagrangian is defined as follows,

$$\mathcal{L}_{\text{QQM}} = \bar{q}(i\cancel{\partial})q + \sum_{k,l=1}^2 a_{kl} [\bar{q}f_k(s)q \bar{q}f_l(s)q - \bar{q}f_k(s)\tau^a \gamma_5 q \bar{q}f_l(s)\tau^a \gamma_5 q]. \quad (3)$$

Here a_{kl} represents a symmetric matrix of real coupling constants and $f_k(s)$, $s \equiv -\partial^2/\Lambda^2$ are the polynomial form factors specifying the quasilocal (in momentum space) interaction. The form factors are orthogonal on the unit interval and the results of calculations do not depend on a concrete choice of form factors in the large-log approximation. A convenient choice is $f_1(s) = 2 - 3s$, $f_2(s) = -\sqrt{3}s$. The values of couplings λ_i in Eq. (2) are then fixed for $i = 2, \dots, 6$: $\lambda_2 = \frac{9N_c}{32\pi^2}$, $\lambda_3 = \frac{3N_c}{8\pi^2}$, $\lambda_4 = \frac{3N_c}{16\pi^2}$, $\lambda_5 = -\frac{5\sqrt{3}N_c}{8\pi^2}$, $\lambda_6 = \frac{\sqrt{3}N_c}{8\pi^2}$.

We shall assume that the scalars under consideration are generated in the quark sector of QCD. The baryon chemical potential is transmitted to the meson sector via a quark-meson coupling. Without loss of generality we can assume that only the first field H_1 has local coupling to quarks; this actually defines the chiral multiplet H_1 . Thus finite density is transmitted to the boson sector via $\Delta\mathcal{L} = -(\bar{q}_R H_1 q_L + \bar{q}_L H_1^\dagger q_R)$, where $q_{L,R}$ are assumed to be constituent quarks. Then the one-loop contribution to V_{eff} is

$$\Delta V_{\text{eff}}(\mu) = \frac{\mathcal{N}}{2} \Theta(\mu - |H_1|) \left[\mu |H_1|^2 \sqrt{\mu^2 - |H_1|^2} - \frac{2\mu}{3} (\mu^2 - |H_1|^2)^{3/2} - |H_1|^4 \ln \frac{\mu + \sqrt{\mu^2 - |H_1|^2}}{|H_1|} \right] \times \left(1 + O\left(\frac{\mu^2}{\Lambda^2}; \frac{|H_1|^2}{\Lambda^2}\right) \right), \quad (4)$$

where $\mathcal{N} \equiv \frac{N_c N_f}{4\pi^2}$ and μ is the chemical potential. The higher-order contributions of chiral expansion in $1/\Lambda^2$ are not considered. This effective potential is normalized to reproduce the baryon density for quark matter $\rho_B = \frac{N_f}{3\pi^2} p_F^3$, where the quark Fermi momentum is $p_F = \sqrt{\mu^2 - |\langle H_1 \rangle|^2}$. Normal nuclear density is $\rho_B \simeq 0.17 \text{ fm}^{-3} \simeq (1.8 \text{ fm})^{-3}$ that corresponds to the average distance 1.8 fm between nucleons in nuclear matter.

Our analysis of the mass-gap equations and mass spectrum based on potential (2) supplemented with the in-medium contribution (4) resulted in a generic picture which is graphically displayed in Fig. 1 and Fig. 2.

3 Discussions

Let us mention several possible signatures of P -parity breaking ensuing from our analysis.

a) Decays of higher-mass meson resonances (radial excitations) into pions. Resonances do not have a definite parity and therefore the same resonance can decay both in two and three pions (in general into even and odd number of pions).

b) At the very point of the phase transition leading to parity breaking one has six massless pion-like states. After crossing the phase transition, in

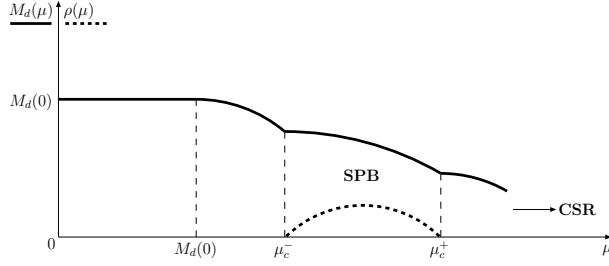


Figure 1: A qualitative dependence of dynamical quark mass M_d and pseudoscalar condensate ρ on quark chemical potential μ (usually $M_d(0) \simeq 300$ MeV). In the points of entering and exiting the phase of spontaneous parity breaking (SPB) the derivatives on μ jump. The region close to the chiral symmetry restoration (CSR) is beyond the range of validity of chiral expansion.

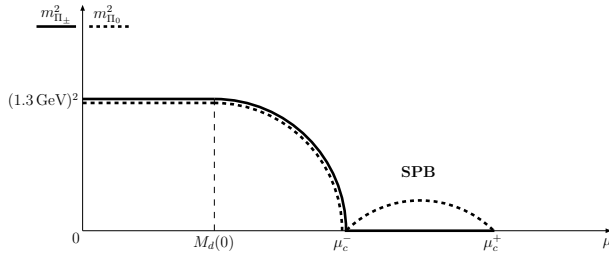


Figure 2: A qualitative behaviour of masses of isospin components for heavy pseudoscalar meson as a function of quark chemical potential μ when the SPB occurs.

the parity broken phase, the massless charged pseudoscalar states remain as Goldstone bosons enhancing charged pion production, whereas the additional neutral pseudoscalar state becomes massive.

c) Reinforcement of long-range correlations in the pseudoscalar channel (this effect could be hunted in lattice simulations).

d) Additional isospin breaking effects in the pion decay constant and substantial modification of the weak decay constant F_{Π^\pm} for massless charged excited pions, giving an enhancement of electroweak decays.

Acknowledgments

This work is supported by research grants FPA2004-04582, SAB2005-0140 and RFBR 05-02-17477 as well as by Programs RNP 2.1.1.1112; LSS-5538.2006.2. The work is also done with support of the EU RTN networks FLAVIANET and ENRAGE.

References

- [1] D. Weingarten, *Phys. Rev. Lett.* **51**, 1830 (1983); C. Vafa and E. Witten, *Phys. Rev. Lett.* **53** 535 (1984); S. Nussinov, *Phys. Rev. Lett.* **52**, 966 (1984); D. Espriu, M. Gross and J.F. Wheeler, *Phys. Lett.* **B146**, 67 (1984); for a review see, S. Nussinov and M. Lambert, *Phys. Rept.* **362**, 193 (2002).
- [2] A.A. Andrianov and D. Espriu, arXiv:0709.0049 [hep-ph].
- [3] A.A. Andrianov and V.A. Andrianov, *Nucl. Phys. Proc. Suppl.* **39BC**, 257 (1995); hep-ph/9911383; A.A. Andrianov, V.A. Andrianov and V.L. Yudichev, *Theor. Math. Phys.* **108**, 1069 (1996); A.A. Andrianov, V.A. Andrianov and S.S. Afonin, hep-ph/0209260; *J. Math. Sci.* **143**, 2697 (2007).
- [4] A.A. Andrianov, D. Espriu and R. Tarrach, *Nucl. Phys.* **B533**, 429 (1998); *Nucl. Phys. Proc. Suppl.* **86**, 275 (2000).

S-WAVE MESON SCATTERING UP TO $\sqrt{s} \lesssim 2 \text{ GeV}$ FROM CHIRAL LAGRANGIANS

M. Albaladejo^{*,1}, J.A. Oller^{*,2}, C. Piqueras[†]

^{*} Departamento de Física, Universidad de Murcia, E-30071, Murcia, Spain

[†] I.E.S. Ribera de los Molinos, E-30170 Murcia, Spain

Abstract

The problem of scalar mesons still remains a challenging puzzle, for which we do not even know which are the right pieces to set up. The proliferation of resonances (some of them are very broad and appear on top of hadronic thresholds) and of coupled channels that interact strongly among each other makes the study of this sector a hard task. Our objective is the study of the strongly interacting mesons in coupled channels with quantum numbers $J^{PC} = 0^{++}$ and $I = 0$ and $I = 1/2$, up to a center of mass energy $\sqrt{s} \lesssim 2 \text{ GeV}$. Our framework is based on Unitary Chiral Perturbation Theory. We include for $I = 0$ the channels: $\pi\pi$, $K\bar{K}$, $\eta\eta$, $\sigma\sigma$, $\eta\eta'$, $\rho\rho$, $\omega\omega$, $\eta'\eta'$, $\omega\phi$, $\phi\phi$, $K^*\bar{K}^*$, $a_1(1260)\pi$ and $\pi^*(1300)\pi$. In addition, and in order to constrain our fits, we also study the $I = 1/2, 3/2$ channels given by $K\pi$, $K\eta$ and $K\eta'$. We finally present the resonant content of our fits with the σ , $f_0(980)$, $f_0(1310)$, $f_0(1500)$, $f_0(1710)$ and $f_0(1790)$.

1 Lagrangians. $U(3)$ symmetry

Due to the spontaneous breakdown of chiral $SU(3)$ symmetry the π , K and η are the octet of pseudo-Goldstone bosons. As it is well known, chiral symmetry strongly constrains the allowed interactions between these pseudoscalars and it is a basic ingredient in any study of strong interactions involving those mesons. If one considers higher energy regions, as it is our case here where we study the $I = 0$ and $1/2$ S-waves up to about 2 GeV, one also needs to take into account the $\eta\eta$, $\eta\eta'$ and $\eta'\eta'$ channels. Interestingly, in the large N_c limit, the η_1 becomes the ninth Goldstone boson. This fact can be used to

¹E-mail address: albaladejo@um.es

²E-mail address: oller@um.es

settle down chiral Lagrangians based on $U(3)$ chiral symmetry and to include the η_1 field. The η_1 - η_8 mixing angle is taken as $\sin \theta = -1/3 \rightarrow \theta \approx -20^\circ$. The channels we include for $I = 0$ are: (1) $\pi\pi$, (2) $K\bar{K}$, (3) $\eta\eta$, (4) $\sigma\sigma$, (5) $\eta\eta'$, (6) $\rho\rho$, (7) $\omega\omega$, (8) $\eta\eta'$, (9) $\omega\phi$, (10) $\phi\phi$, (11) $K^*\bar{K}^*$, (12) $a_1(1260)\pi$ and (13) $\pi^*(1300)\pi$. For $I = 1/2$ and $3/2$ we take the $K\pi$, $K\eta$ and $K\eta'$ ones. For these latter isospin channels we follow ref. [1].

We employ the Chiral Perturbation Theory (ChPT) Lagrangians to lowest order, and the chirally invariant resonance ones [2], with the $J^{PC} = 0^{++}$ singlet and octet multiplets. These Lagrangians also incorporate the r_μ and l_μ external sources by gauging the $U(3)_L \otimes U(3)_R$ chiral symmetry. In our case, as we are interested in the vector resonances, we have $r_\mu = l_\mu = gv_\mu$, where the last term is a matrix of vector fields times a coupling constant, which can be determined through the width of $\rho \rightarrow \pi\pi$, $g = 4.23$.

2 Unitarization. $\sigma\sigma$ channels. Width effects

We want to calculate the amplitudes involving the $\sigma\sigma$ channel from our Lagrangians. As it was shown within UChPT [3], the σ is made up from two pions interacting in $I = 0$ S-wave, which allows us to obtain these amplitudes without any new free parameter. We first consider the amplitudes of a generic channel, say a , to four pions grouped as two $I = 0$ $\pi\pi$ states $((\pi\pi)_0)$. Let us call s_1 and s_2 the total CM energy squared of each of these states. Now, every $(\pi\pi)_0$ state rescatters and gives rise to a σ pole; this is taken into account with the factor $1/D(s_1)D(s_2)$, where $D(s) = (1 + t_2G(s))^{-1}$, t_2 is the elastic $(\pi\pi)_0$ S-wave amplitude at lowest order in ChPT, and $G(s)$ is the two-meson loop function. The transition amplitude is obtained by taking the limits $s_i \rightarrow s_\sigma$, with s_σ the σ pole position. If we denote the $a \rightarrow (\pi\pi)_0(\pi\pi)_0$ amplitude by $T_{a \rightarrow (\pi\pi)_0(\pi\pi)_0}$, and the one deduced from ChPT with resonances by $T_{a \rightarrow (\pi\pi)_0(\pi\pi)_0}^{2+R}$, we have:

$$T_{a \rightarrow (\pi\pi)_0(\pi\pi)_0} = T_{a \rightarrow (\pi\pi)_0(\pi\pi)_0}^{2+R} \frac{1}{D(s_1)D(s_2)}. \quad (1)$$

The $a \rightarrow (\sigma\sigma)_0$ amplitude, $N_{a \rightarrow (\sigma\sigma)_0}$, is obtained from,

$$\lim_{s_i \rightarrow s_\sigma} T_{a \rightarrow (\pi\pi)_0(\pi\pi)_0} = \lim_{s_i \rightarrow s_\sigma} \frac{T_{a \rightarrow (\pi\pi)_0(\pi\pi)_0}^{2+R}}{D_{II}(s_1)D_{II}(s_2)} = N_{a \rightarrow (\sigma\sigma)_0} \frac{g_{\sigma\pi\pi}^2}{(s_1 - s_\sigma)(s_2 - s_\sigma)} \quad (2)$$

The subscript II means that we have to calculate the corresponding function on the second Riemann sheet, where the σ pole appears. Finally, calculating

this limit with an appropriate Laurent expansion around s_σ ,

$$N_{a \rightarrow (\sigma\sigma)_0} = T_{a \rightarrow (\pi\pi)_0(\pi\pi)_0}^{2+R} \left(\frac{\alpha_0}{g_{\sigma\pi\pi}} \right)^2, \quad \left(\frac{\alpha_0}{g_{\sigma\pi\pi}} \right)^2 \simeq 9.1 \cdot 10^{-3} \text{ GeV}^2. \quad (3)$$

Now, the general expression for a coupled channels partial wave amplitude is $T = (I + N(s)g(s))^{-1}N(s)$, where $N(s)$ is a matrix containing our amplitudes between all the channels. Each element of the diagonal matrix $g(s)$ is given by the once subtracted dispersion relation,

$$g_i(s) = g_i(s_0) - \frac{s - s_0}{8\pi^2} \int_{s_{\text{th},i}}^{\infty} ds' \frac{p_i(s')/\sqrt{s'}}{(s' - s_0)(s' - s + i\epsilon)} \quad (4)$$

A remark is in order. These integrals involve the masses of the particles of the scattering states, but some of them, as the σ , ρ , $a_1(1260)$ and $\pi^*(1300)$ have very large widths. To take these effects into account, we consider instead of eq.(4) an integral of this loop function times a mass distribution over a wide range of masses for each of these unstable particles.

3 Results and spectroscopy

With all these amplitudes, one can construct the S -matrix and calculate observables; in our case, these will be phase shifts and amplitude moduli. The curves resulting from our fit are depicted in Fig. 1. We use 13 parameters for about 373 experimental data, and a fair agreement with data is achieved. We have reduced the number of free parameters compared with other approaches in the literature which do not employ (chiral) Lagrangians.

Figure 1: Left panels, from up to down: $\pi\pi \rightarrow \pi\pi$ phase shift, amplitude and the same for $\pi\pi \rightarrow K\bar{K}$. Right panels, from up to down: modulus squared of the S-matrix elements $\pi\pi \rightarrow \eta\eta'$ and $\pi\pi \rightarrow \eta\eta$. The last two figures correspond to the phase and modulus of the $K^-\pi^+ \rightarrow K^-\pi^+$ scattering.

Once the observables are fitted, we can explore the s -complex plane to find the relevant poles of the amplitudes, and discuss their resonance content. We present in Table 1 the masses and widths of the resonances that we find. The agreement with the ones in the PDG is remarkable.

Table 1: Parameters of resonances. On the left columns we have the masses and widths that we find. On the right ones, the values are given by the PDG or the BES Collaboration.

Resonance	Mass (MeV)	Width (MeV)	Mass (MeV)	Width (MeV)
σ	454	475	400-1200	600-1200
$f_0(980)$	980	44	980 ± 10	40-100
$f_0(1370)$	1380	350	1200-1500	200-500
$f_0(1500)$	≈ 1500	100 – 170	1507 ± 5	109 ± 7
$f_0(1710)$	≈ 1680	≈ 160	1718 ± 6	137 ± 8
$f_0(1790)$	≈ 1805	≈ 390	1790^{+40}_{-30}	270^{+60}_{-30}

References

- [1] M. Jamin, J. A. Oller and A. Pich, Nucl. Phys. B **587** (2000) 331; M. Jamin, J. A. Oller and A. Pich, Nucl. Phys. B **622**, 279 (2002)
- [2] J. Gasser and H. Leutwyler, Nucl. Phys. B **250**, 465 (1985); G. Ecker, J. Gasser, A. Pich and E. de Rafael, Nucl. Phys. B **321**, 311 (1989).
- [3] J. A. Oller and E. Oset, Nucl. Phys. A **620**, 438 (1997) [Erratum-ibid. A **652**, 407 (1999)]; J. A. Oller and E. Oset, Phys. Rev. D **60**, 074023 (1999)

POINCARÉ INVARIANT COUPLED CHANNEL MODEL FOR THE PION-NUCLEON SYSTEM: INSTANT FORM MODEL

H. H. Alharbi

National Center for Mathematics and Physics
KACST, P.O. Box 6086
Riyadh, 11442, Saudi Arabia

Abstract

Poincaré invariant instant form model for the pion-nucleon system has been constructed, which describes the coupling between single-baryon and meson-baryon channels. The elastic scattering amplitudes are obtained from three-dimensional Lippmann-Schwinger equations. The S -matrix elements for the various processes transform properly under inhomogeneous Lorentz transformations and moreover are gauge invariant. The mass-operator interactions that describe the processes $\mu B \rightarrow \mu' B'$, where B and B' are baryons and μ is a meson, have been derived. The interactions are assumed to be separable.

1 Introduction

The defining representation of the Poincaré group can be taken to be the set of all inhomogeneous Lorentz transformations. These can be written in the form $x' = ax + b$, where x , and b are four-vectors and a is a 4×4 matrix. This matrix is constrained by the requirement that space-time intervals are invariant, which leads to the relation $\tilde{a}ga = g$, where g is the metric tensor. In quantum mechanics we require the existence of a set of unitary operators that map quantum mechanical state vectors from one inertial frame to another according to $|\psi'\rangle = U(a, b)|\psi\rangle$, and which satisfy the law of combination $U(a', b)U(a, b) = U(a'a, ab + b)$. For the proper subgroup of continuous transformations, these unitary operators can be expressed in terms of 10 real parameters and 10 hermitian generators by means of the expression

$$U(a, b) = \exp(ib^\mu P_\mu) \exp\left(\frac{i}{2}\omega^{\alpha\beta} J_{\alpha\beta}\right) \quad (1)$$

The Hamiltonian H , the three-momentum operator P , the angular momentum operator \mathbf{J} , and the generator of rotationless boosts \mathbf{K} are related to the 10 generators by $P = (P^0, P^1, P^2, P^3) = (H, \mathbf{P})$, $\mathbf{K} = (J_{10}, J_{20}, J_{30})$, and $\mathbf{J} = (J_{23}, J_{31}, J_{12})$. A rotationless boost is a Lorentz transformation that relates two inertial frames moving relative to each other with the corresponding spatial axes parallel. In order for the unitary operators (1) to satisfy the law of combination, the generators must satisfy Poincaré algebra. Poincaré generators can be constructed using Bakamjian-Thomas method [1, 3]. In this approach, the set of Poincaré generators, $\{H, \mathbf{P}, \mathbf{J}, \mathbf{K}\}$, can be expressed in terms of the operators set $\{M, \mathbf{P}, j, \mathbf{X}\}$ according to the relations

$$H = (\mathbf{P}^2 + M^2)^{1/2}, \quad \mathbf{J} = \mathbf{X} \times \mathbf{P} + j, \quad \mathbf{K} = \frac{1}{2}(\mathbf{H}\mathbf{X} + \mathbf{X}\mathbf{H}) - \frac{\mathbf{P} \times j}{M + H} \quad (2)$$

where M is the mass operator, \mathbf{X} is the so-called Newton-Wigner position operator [3, 4], and the spin operator is j .

The virtue of the set $\{M, \mathbf{P}, j, \mathbf{X}\}$ is that these operators satisfy much simpler commutation rules than the generators. In particular the only non-zero commutators are $[X^j, P^k] = i\delta_{jk}$, $[j^j, j^k] = i\varepsilon_{jkl}j^l$, and these commutation relations are familiar from nonrelativistic quantum mechanics. In the Bakamjian-Thomas scheme [1, 3] the operators \mathbf{P} , j , and \mathbf{X} are assumed to be the same as those of the non-interacting system, and an interaction is put into the mass operator M . It follows from these assumptions in (2) that H and \mathbf{K} contain interactions while \mathbf{P} and \mathbf{J} do not. Since the non-interacting operators \mathbf{P} , j , and \mathbf{X} will automatically satisfy the correct commutation relations among themselves, the only commutation relations that have to be enforced are

$$[P, M] = 0, [J, M] = 0, [X, M] = 0 \quad (3)$$

In general we write the mass operator in the form $M = M_0 + U$, where M_0 is the mass operator for the non-interacting system and U contains the interactions. Since M_0 commutes with \mathbf{P} , j , and \mathbf{X} , we only have to ensure that U does.

2 The Model

The model space can be assumed to consists of single-baryon states $|B\rangle$ as well as meson-baryon states $|\mu B\rangle$ [5–8]. Here the possible matrix elements

of the interaction are of the type $\langle B|U|B'\rangle$, $\langle \mu B|U|B'\rangle$, and $\langle \mu B|U|\mu'B'\rangle$. It can be shown that the commutation relations (3) imply that these matrix elements must be of the form

$$\begin{aligned} \langle \mathbf{p}\alpha B|U|\mathbf{p}'\alpha'B'\rangle &= N_B(\mathbf{p})\delta_{\alpha\alpha'}\delta_{BB'} \left[m_B^{(0)} - m_B \right], \\ \langle \mathbf{p}\mathbf{q}\alpha, \mu B|U|\mathbf{p}'\alpha'B'\rangle &= N_{\mu B, B'}(\mathbf{p}, \mathbf{q})\delta^3(\mathbf{p} - \mathbf{p}') \langle \alpha|U_{\mu B, B'}(\mathbf{q})|\alpha'\rangle, \\ \langle \mathbf{p}\mathbf{q}\alpha, \mu B|U|\mathbf{p}'\mathbf{q}'\alpha', \mu'B'\rangle &= N_{\mu B, \mu'B'}(\mathbf{p}, \mathbf{q}, \mathbf{q}')\delta^3(\mathbf{p} - \mathbf{p}') \langle \alpha|U_{\mu B, \mu'B'}(\mathbf{q})|\alpha'\rangle, \end{aligned} \quad (4)$$

Here \mathbf{p} is the total three-momentum of a state, \mathbf{q} is the c.m. three-momentum of the meson, α is the set of spin and isospin quantum numbers, and the N 's are kinematic factors which depend on the normalization of the basis states. Also, m_B is the physical mass of the baryon and $m_B^{(0)}$ is its bare mass. The dynamics appears in the vertex functions $U_{\mu B, B'}(\mathbf{q})$ and the potentials $U_{\mu B, \mu'B'}(\mathbf{q}, \mathbf{q}')$. These are operators in the relevant spin-isospin spaces of the mesons and baryons. In order to ensure that $[j, M] = 0$ they must be rotationally invariant functions of the c.m.-momenta and the spin operators of the mesons and baryons.

The scattering amplitudes can be obtained by solving the Lippmann-Schwinger equations

$$\begin{aligned} T_{\mu B, \mu'B'}(\mathbf{q}', \mathbf{q}; z) &= V_{\mu B, \mu'B'}(\mathbf{q}', \mathbf{q}; z) + \sum_{\mu'' B''} \int V_{\mu B, \mu'' B''}(\mathbf{q}, \mathbf{q}''; z) \\ &\quad \times \frac{d^3 q''}{\Delta_{\mu'' B''}(\mathbf{q}'')} \frac{T_{\mu'' B'', \mu'B'}(\mathbf{q}'', \mathbf{q}'; z)}{2W_{\mu'' B''}(\mathbf{q}'') [z - W_{\mu'' B''}(\mathbf{q}'')]} \end{aligned} \quad (5)$$

where $\Delta_{\mu B}$ is a kinematics' factor that depends on the normalization of the basis states, $W_{\mu B}$ is the c.m.-energy of the μB system, and

$$V_{\mu B, \mu'B'}(\mathbf{q}, \mathbf{q}'; z) = U_{\mu B, \mu'B'}(\mathbf{q}, \mathbf{q}') + \sum_{B''} \frac{U_{\mu B, B''}(\mathbf{q}) U_{B'', \mu'B'}(\mathbf{q}')}{2m_{B''} [z - m_{B''}^{(0)}]}. \quad (6)$$

Equation (6) defines an effective potential which has been obtained by assuming the separable form

$$U_{\mu B, \mu'B'}(q, q') = g_{\mu B}(q) \lambda_{\mu B, \mu'B'} g_{\mu'B'}(q'), \quad (7)$$

$$g_{\mu B}(q) = C_{\mu B} (q/\beta_{\mu B})^l [1 + (q/\beta_{\mu B})^2]^{-K_{\mu B}} \quad (8)$$

For $\mu B \Leftrightarrow B'$ the vertex function expression is

$$U_{\mu B, B'}(q) = C_{\mu B, B'}(q/\beta_{\mu B, B'})^l [1 + (q/\beta_{\mu B, B'})^2]^{-K_{\mu B, B'}} \quad (9)$$

In this formalism, the probabilities of the various processes are Poincaré invariant. In the figure, some of our results are compared with the SAID SM95 phase shifts and elasticity [9].

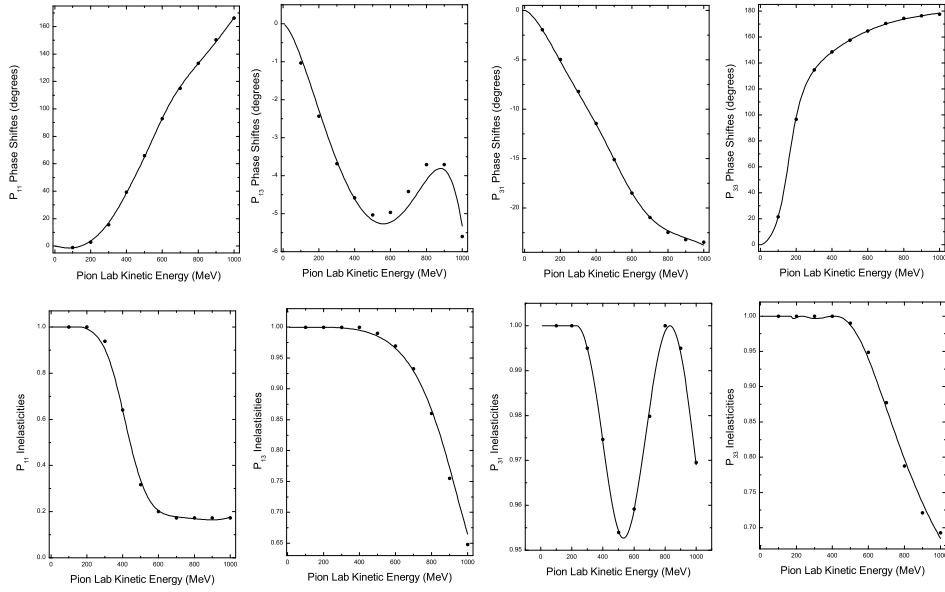


Figure 1: Fits of partial waves P11, P13, P31 and P33 to the SM95 analysis.

References

- [1] B. Bakamjian and L.H. Thomas, *Phys. Rev.* **92**, 1300 (1953).
- [2] J.D. Bjorken and S.D. Drell, *Relativistic Quantum Fields* (McGraw-Hill, New York, 1965)
- [3] B.D. Keister and W.N. Polyzou, *Advances in Nuclear Physics*, edited by J.W. Negele and E. Vogt (Plenum, New York, 1991), Vol. **20**, p. 225.

- [4] T.D. Newton and E.P. Wigner, *Rev. Mod. Phys.* **21**, 400 (1949).
- [5] M.G. Fuda, *Phys. Rev. C* **52**, 2875-2884 (1995).
- [6] Yasser Elmessiri and Michael G. Fuda, *Phys. Rev.* **C57**, 2149-2155 (1998);
M. Doring, E. Oset, M.J. Vicente, *Phys.Rev. C* **70** (2004) 045203.
- [7] M.G. Fuda, *Few-Boody Systems* **23**, 127-148 (1998).
- [8] Yasser Elmessiri and Michael G. Fuda, *Phys. Rev. C* **60**, 044001, 1-16
(1999); A.M.Gasparyan, J.Haidenbauer, C.Hanhart, J.Speth, *Phys.Rev.*
C **68** (2003) 045207.
- [9] SAID online database, http://gwdac.phys.gwu.edu/analysis/pin_analysis.html.

QCD ANALYSIS FOR NUCLEAR PARTON DISTRIBUTIONS IN THE NEXT TO LEADING ORDER

S. Atashbar Tehrani and Ali N. Khorramian
Physics Department, Semnan university, Semnan, Iran;
Institute for Studies in Theoretical Physics and Mathematics (IPM),
P.O.Box 19395-5531, Tehran, Iran

Abstract

A QCD analysis of the nuclear parton distributions and structure functions in the NLO is performed by using the world data. By having bounded parton distributions for a nuclear with atomic number A , we can obtain the nuclear structure function in x space. Our results for nuclear structure function ratio F_2^A/F_2^D for some different values of A , are in good agreement with the experimental data. We compare our results for LO and NLO approximation.

1 Introduction

Parametrization of nuclear parton distributions is investigated in the next-to-leading order (NLO) of α_s . Unpolarized parton distributions in the nucleon are now well determined in the region from very small x to large x by using various experimental data. Initial distributions are assumed at a fixed Q^2 with parameters which are determined by a χ^2 analysis. In this work we used the MRST parametrization [1] as the input parton distributions in the nucleon. In Ref. [2] a LO QCD analysis was performed and authors applied the MRST parton distributions [3] in the nucleon. Until now much efforts have been done to compute the nuclear parton densities and structure functions in the perturbative QCD [2, 4–8]. In this paper after parametrization of nuclear parton distributions in $Q_0^2 = 4 \text{ GeV}^2$, we will obtain the nuclear structure function ratio F_2^A/F_2^D for helium, carbon and calcium nuclei in the LO and NLO.

2 Nuclear Structure Function

Our analysis is done in the next-to-leading order of α_s . According to parton model the nuclear structure function F_2^A in the NLO is given by [9]

$$\begin{aligned} \frac{1}{x} F_2^{eA}(x, Q^2) &= \sum_{q=u,d,s} e_q^2 \left\{ q^A(x, Q^2) + \bar{q}^A(x, Q^2) + \frac{\alpha_s(Q^2)}{2\pi} \right. \\ &\quad \left. \times [c_{q,2} \otimes (q^A + \bar{q}^A) + 2c_{g,2} \otimes g^A] \right\} , \end{aligned} \quad (1)$$

where e_q is the quark charge, and $q^A(\bar{q}^A)$ is the quark (antiquark) distribution in the nucleus A . Here the sum expands over all light quarks $q = u, d, s$ and $c_{q,2}, c_{g,2}$ are as following

$$\begin{aligned} c_{q,2} &= \frac{4}{3} \left[\frac{1+z^2}{1-z} \left(\ln \frac{1-z}{z} - \frac{3}{4} \right) + \frac{1}{4}(9+5z) \right]_+ \\ c_{g,2} &= \frac{1}{2} \left[(z^2 + (1-z)^2) \ln \frac{1-z}{z} - 1 + 8z(1-z) \right] . \end{aligned} \quad (2)$$

The convolutions are defined as

$$c \otimes q = \int_x^1 \frac{dy}{y} c \left(\frac{x}{y} \right) q(y, Q^2) . \quad (3)$$

Notice that

$$\int_x^1 \frac{dy}{y} f \left(\frac{x}{y} \right)_+ g(y) = \int_x^1 \frac{dy}{y} f \left(\frac{x}{y} \right) \left[g(y) - \frac{x}{y} g(x) \right] - g(x) \int_0^x dy f(y) . \quad (4)$$

In this paper we assumed the flavor symmetric antiquark distribution, $\bar{u}^A = \bar{d}^A = \bar{s}^A \equiv \bar{q}^A$. We consider also the nuclear parton distributions as

$$u_v^A = \mathcal{W}_{u_v} \frac{Z u_v + N d_v}{A}, \quad d_v^A = \mathcal{W}_{d_v} \frac{Z d_v + N u_v}{A}, \quad \bar{q}^A = \mathcal{W}_s \bar{q}, \quad g^A = \mathcal{W}_g g, \quad (5)$$

in the above equations, we suppose the functional form for the weight function for all partons as

$$\mathcal{W}_i = 1 + \left(1 - \frac{1}{A^{1/3}} \right) \left(\frac{a_i + b_i x + c_i x^2 + d_i x^3}{(1-x)^{e_i}} \right) . \quad (6)$$

After using the MRST parton distributions in the nucleon at $Q_0^2=4 \text{ GeV}^2$ we can be able to determine some unknown parameters which appear in the

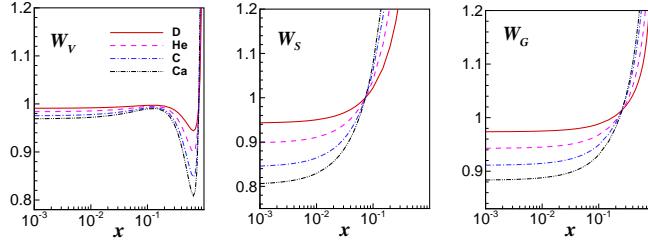


Figure 1: QCD results for weight functions in the NLO for deuteron, helium, carbon and calcium nuclei

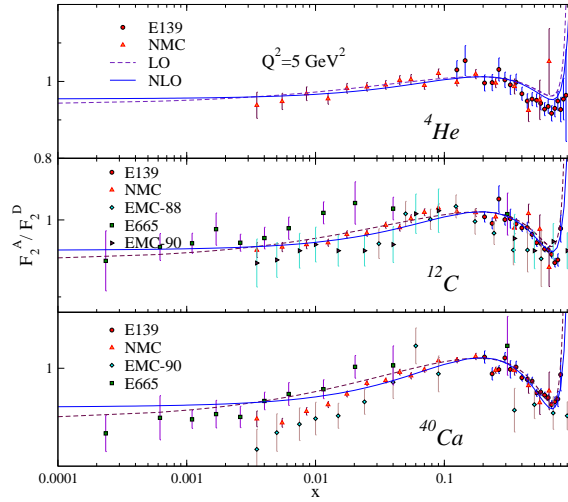


Figure 2: Our QCD results are compared with the experimental data at $Q^2 = 5 \text{ GeV}^2$ for helium, carbon and calcium nuclei in the LO and NLO.

weight functions by a χ^2 analysis of the data on ratio of nuclear structure functions [10–15]. In Fig. 1 we plot our QCD results for weight functions in the NLO, which defined in Eqs. (5, 6) for deuteron, helium, carbon and calcium nuclei. In Fig. 2 our results are compared with the experimental data at $Q^2 = 5 \text{ GeV}^2$ for helium, carbon and calcium nuclei in the LO and NLO.

Acknowledgments

S.A.T. acknowledge the Persian Gulf university for the financial support of this project.

References

- [1] A. D. Martin, W. J. Stirling and R. S. Thorne, *Phys. Lett. B* **636** (2006) 259.
- [2] M. Hirai, S. Kumano and M. Miyama, *Phys. Rev. D* **64** (2001) 034003.
- [3] A. D. Martin, R. G. Roberts, W. J. Stirling and R. S. Thorne, *Eur. Phys. J. C* **14** (2000) 133.
- [4] S. A. Tehrani, A. Mirjalili and A. N. Khorramian, *Nucl. Phys. Proc. Suppl.* **164** (2007) 30.
- [5] S. A. Tehrani, A. N. Khorramian and A. Mirjalili, *Int. J. Mod. Phys. A* **20** (2005) 1927.
- [6] K. J. Eskola, V. J. Kolhinen and C. A. Salgado, *Eur. Phys. J. C* **9** (1999) 61.
- [7] K. J. Eskola, V. J. Kolhinen and P. V. Ruuskanen, *Nucl. Phys. B* **535** (1998) 351.
- [8] D. de Florian and R. Sassot, *Phys. Rev. D* **69** (2004) 074028.
- [9] M. Gluck, E. Reya and A. Vogt, *Z. Phys. C* **48** (1990) 471; M. Gluck, E. Reya and A. Vogt, *Z. Phys. C* **67** (1995) 433.
- [10] J. Ashman *et al.* [EMC], *Phys. Lett. B* **202** (1988) 603.
- [11] M. Arneodo *et al.* [EMC], *Nucl. Phys. B* **333** (1990) 1.
- [12] J. Gomez *et al.*, *Phys. Rev. D* **49** (1994) 4348.
- [13] P. Amaudruz *et al.* [NMC], *Nucl. Phys. B* **441** (1995) 3.
- [14] M. Arneodo *et al.* [NMC.], *Nucl. Phys. B* **441** (1995) 12.
- [15] M. R. Adams *et al.* [E665 Collaboration], *Z. Phys. C* **67** (1995) 403.
- [16] E. G. Floratos, C. Kounnas and R. Lacaze, *Nucl. Phys. B* **192** (1981) 417.
- [17] F. James and M. Roos, *Comput. Phys. Commun.* **10** (1975) 343.

HOW IS EXOTICS PRODUCED ? WHERE TO SEARCH FOR IT ?

Ya. Azimov^{*,1}, K. Goeke[%], and I. Strakovsky[#]

^{*}Petersburg Nuclear Physics Institute, Gatchina, Russia

[%]Ruhr-Universität, Bochum, Germany

[#]George Washington University, Washington, D.C., USA

Abstract

On the basis of existing data, we suggest such a mechanism of production for exotic hadrons that can explain, at least qualitatively, why the Θ^+ -baryon is seen in some experiments and not in others. With our hypothesis, production of exotic hadrons is a new kind of hard processes. We also can propose new experiments to check (and confirm?) existence of exotics and to provide new important information about both exotic and conventional hadrons².

1 Introduction

The problem of exotic hadrons (*i.e.*, non- qqq baryons and/or non- $q\bar{q}$ mesons) stays open. Theoretical studies are uncertain and do not provide any convincing explanation, whether and why such hadrons might/should not exist. But experimental situation is also uncertain in respect to their existence [2].

There are mesons (scalar mesons and some of recently discovered ones) interpreted in the literature as tetraquark ($2q2\bar{q}$) states, but this interpretation is strongly model dependent. Their conventional $q\bar{q}$ interpretation cannot be rejected as well, while rare experimental evidences for explicitly non- $q\bar{q}$ mesons are not sufficiently reliable yet.

The situation may be different for baryons. There are experimental evidences for three explicitly exotic states: $\Theta^+(1530)$, $\Theta_c^0(3100)$, and $\Xi_{3/2}^-(1860)$ (or $\Phi^{--}(1860)$) [2]. However, each of the two latter states was seen by one group only. They have not been found in later dedicated experiments, and we will not discuss them here.

At present, more crucial looks the existence or non-existence of the Θ^+ . The corresponding information is much more copious than for any other

¹E-mail address: azimov@thd.pnpi.spb.ru

²The talk is based on the papers [1].

exotic hadron candidate. But the problem is that there are both positive and negative results, of several groups on each side.

With such data, one can take a viewpoint that all positive results might emerge as statistical fluctuations and not reveal a true physical object. It would be strange, however, to have the same fluctuation in data of more than ten independent groups studying very different processes. Moreover, in such a case we should still live with the open question of what prevents exotic hadrons from being existent and observed.

An opposite viewpoint is that the Θ^+ , as a representative of exotic hadrons, does exist and has properties corresponding to the published positive evidences: rather low mass and unexpectedly narrow width. Then the problem is whether such an unfamiliar production mechanism may exist, with which all the present positive and null data are consistent to each other.

2 Θ^+ Production Mechanism

The ZEUS Collaboration was the first experimental group to study not only existence of the Θ^+ , but also its production properties in Deep Inelastic Scattering (DIS). They compared, in the same kinematical region, characteristics of the three baryons, $\Lambda(1520)$, $\Lambda_c^+(2286)$, and $\Theta^+(1530)$, which could be kinematically similar. However, all three appeared dynamically different [3].

To understand the results, let us first recall the nature of the DIS process. The target hadron (proton at HERA) looks in this process as a set of many partons. At the hard stage of the process, one (or a few number) of the partons is knocked out by the virtual γ/Z . After that, the knocked-out parton(s) and the remnant part of the target hadronize, softly and nearly independently of each other.

The ZEUS results [3] show, that production of the $\Lambda(1520)$ is well described by hadronization of the knocked-out parton-quark, exactly as was expected. Production of the $\Lambda_c^+(2286)$ (or its antiparticle) goes in a different, but also expected way: the virtual γ/Z collides with the parton-gluon, they produce the $c\bar{c}$ -pair, which then hadronizes. Contrary to those, production properties of the $\Theta^+(1530)$ give evidence, quite unexpectedly, that it comes from hadronization of the proton remnant.

Since the remnant is, evidently, a many-parton state, we can generalize this fact as **the Hypothesis**:

- Multiquark (exotic) hadrons are mainly produced through many-parton configurations, which may emerge either as hadron remnants in hard processes or just as virtual short-term fluctuations of the initial hadron(s).

Note that in terms of Quantum Chromodynamics (QCD) any hadron may be described by a Fock column, with different components having different number of partons. In the space-time picture, the short-term fluctuations of a hadron are related with higher Fock components. Hadron picture, as seen in DIS, is also related with higher Fock components. Thus, in framework of our hypothesis, the Θ^+ -production is always due to short-term fluctuations and, at least some stage of this process, should have small characteristic time. This means that the exotics production is, intrinsically, a new kind of hard processes. Of course, it differs from DIS and many other hard processes, that have a continuous parameter to measure the hardness (the photon virtuality Q^2 for DIS). But it is similar to the heavy quark production, having the quark mass as a fixed hardness parameter. For the exotics production, hardness may be related to the fixed minimal number of additional $q\bar{q}$ pairs.

3 Checks for the Production Mechanism

Now we can suggest some immediate checks for the hypothesis.

The more is virtuality Q^2 in DIS, the higher is effective multiplicity of partons in the target. Therefore, we expect that increasing Q^2 should provide some (logarithmically increasing?) enhancement of exotics (say, the Θ^+) production in respect to conventional hadrons. Such expectation does not contradict to the preliminary ZEUS data [4], though present rather large experimental errors do not allow to make a clear conclusion. The situation reminds the case of the Bjorken scaling, which looked exact in early data, while later more exact measurements revealed its violation.

Our hypothesis suggests interesting expectations not only for DIS, but also for exotics production in “soft processes”. If it needs indeed participation of many-parton fluctuations, then the accompanying hadron multiplicity should be higher than in conventional hadron production. Because of kinematical reasons, this should generate energy spectra, which is softer for exotics production than for production of only conventional hadrons. Such expectation appears to be in good correspondence with the recent result of the SVD Collaboration [5], that in NN collisions at $E_{\text{lab}} = 70$ GeV the inclusive spectrum for $\Theta^+(1530)$ is essentially softer than for $\Lambda(1520)$.

Additional, indirect support to our hypothesis comes from calculations of the Θ^+ width [6]. They show that the extremely low experimental value $\Gamma_{\Theta^+} = (0.36 \pm 0.11)$ MeV [7] can be described if the decay $\Theta \rightarrow KN$ goes mainly to higher Fock components of the final nucleon. Our hypothesis applies similar approach to production processes as well.

Analysis of Ref. [1] shows that the hypothesis provides also qualitative

ways to reconcile current positive and null experiments (in particular, CLAS and LEPS data [8]). It allows as well to suggest new experiments (or modification of existing ones) which may confirm and investigate exotic hadrons.

Acknowledgments

The work was partly supported by the Russian Grant RSGSS-1124.2003.2, by the Russian-German Collaboration Treaty (RFBR, DFG), by the COSY-Project Jülich, by Verbundforschung “Hadronen und Kerne” of the BMBF, by Transregio/SFB Bonn, Bochum, Giessen of the DFG, by the U. S. Department of Energy Grant DE-FG02-99ER41110, by the Jefferson Laboratory, and by the Southeastern Universities Research Association under DOE Contract DE-AC05-84ER40150.

References

- [1] Ya. Azimov, K. Goeke, and I. Strakovsky, arXiv:0704.3045.
Ya. Azimov, K. Goeke, and I. Strakovsky, *Phys. Rev.* **D76**, 074013 (2007).
- [2] W.-M. Yao *et al.* [Particle Data Group], *J. Phys.* **G33**, 1 (2006).
- [3] S. Chekanov [H1 and ZEUS Collab.], in *Proc. Int. Europhys. Conf. on High-Energy Physics (July 21-27, 2005) Lisboa, Portugal*; Proc. Sci., HEP2005, 086 (2006); arXiv:hep-ex/0510057.
- [4] U. Karshon [ZEUS Collab.], in *Proc. Int. Workshop PENTAQUARK04, SPring-8, Hyogo, Japan, 2004*, p. 75; arXiv:hep-ex/0410029.
- [5] A. Kubarovsky, V. Popov, and V. Volkov [SVD Collab.], in *Proc. of the 33rd Int. Conf. on High Energy Physics (ICHEP'06), Moscow, Russia, July 26 - August 2, 2006*; arXiv:hep-ex/0610050.
- [6] D. Diakonov and V. Petrov, *Phys. Rev.* **D72**, 074009 (2005).
C. Lorce, *Phys. Rev.* **D74**, 054019 (2006).
C. Lorce, arXiv:0705.1505.
- [7] V. V. Barmin *et al.* [DIANA Collab.], *Yad. Fiz.* **70**, 39 (2007) [*Phys. At. Nucl.* **70**, 35 (2007)].
- [8] T. Nakano [LEPS Collab.], talk at this Conference, (<http://www.fz-juelich.de/ikp/menu2007/Talks/talk-Nakano.pdf>).

THE PAX EXPERIMENT AT FAIR

*L. Barion*¹ (on behalf of PAX collaboration)
Istituto Nazionale di Fisica Nucleare-sezione di Ferrara
and Università di Ferrara
via Saragat 1 - 44100 Ferrara (FE) Italy

Abstract

Polarized antiprotons, by spin filtering with an internal polarized gas target, provide access to a wealth of single- and double-spin observables. This includes a first direct measurement of the transversity distribution of the valence quarks in the proton and a first measurement of the moduli and the relative phase of the time-like Electric and Magnetic Form Factors (EMFF) $G_{E,M}$ of the proton. The PAX (Polarized Antiproton eXperiments) collaboration [1] is developing a viable experimental set-up [2] which can be realized within the FAIR (Facility for Antiproton and Ion Research, GSI - Darmstadt) [3] project for a large european hadron facility, where a low-energy antiproton polarizer ring is used to yield an antiproton beam with sizeable polarization. After acceleration, the polarized antiproton beam can be used to collide with a polarized internal hydrogen target (fixed target mode) or with a beam of polarized protons (collider mode). The detector concept for a large angle apparatus optimized for the detection of lepton pairs of large invariant mass is anticipated.

1 Physics Case

The physics program of the polarized antiproton facility proposed by PAX would extend to a new domain the studies of the nucleon structure performed in unpolarized and polarized Deep Inelastic Scattering (DIS), which have been at the center of high energy physics during the past four decades. The polarized antiproton-proton interactions at HESR (High Energy Storage Ring, GSI - Darmstadt) will allow a unique access to a number of new fundamental physics observables, which can be studied neither at other facilities nor at HESR without transverse polarization of protons and/or antiprotons. In order to exploit all the planned measurements, the physics has been divided into two phases: Phase-I and Phase-II both in the CSR (Cooled Storage Ring, at FAIR).

¹barion AT fe.infn.it

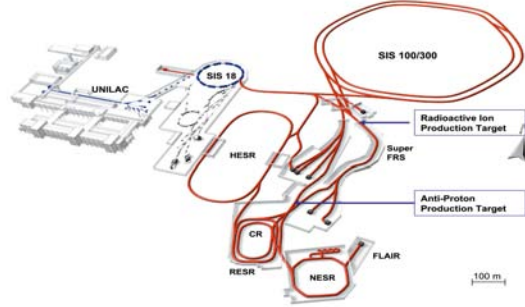


Figure 1: FAIR accelerator layout (future facilities)

1.1 Phase-I

Phase-I (fixed- \hat{A} target) concentrates on the time-like proton form factors and hard elastic scattering measurements. The simple and over-constraint kinematics of these events puts less stringent requirements on the detector performance. The measurements can start even before the detector is completed and can be used to test and optimize each of the sub-systems. In this phase, a polarized/unpolarized p bar beam of momentum up to 4 GeV/c will strike on fixed hydrogen atoms, accumulated in a storage cell. Atomic hydrogen will be produced by a conventional ABS (Atomic Beam Source). This phase is completely independent from HESR, so it does not interfere with the PANDA [4] experiment. At the CSR energies, the outgoing particles have an

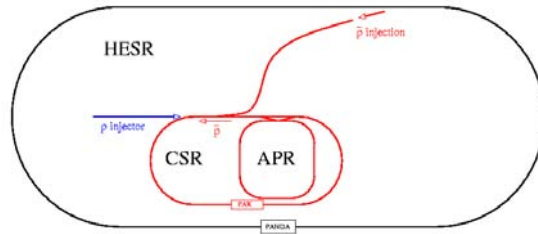


Figure 2: Phase I accelerator setup

almost isotropic distribution and a momentum between 0.5 and 1.5 GeV/c. The expected luminosity is $2.7 \cdot 10^{31} cm^{-2}s^{-1}$. Measurements will take from few hours to few weeks.

1.2 Phase-II

Phase-II (asymmetric \hat{A} -collider mode) concentrates on the h_1 measurement (Transversity Distribution). In this phase a polarized proton beam circulating in HESR ($p=15\text{GeV}/c$) will strike, had-on, on a polarized antiproton beam circulating in CSR ($p=3.5\text{ GeV}/c$). The resulting CM (Center of Mass) energy will be 15 GeV. The inclusive $pp \rightarrow e^+e^- X$ Drell-Yan (DY) process

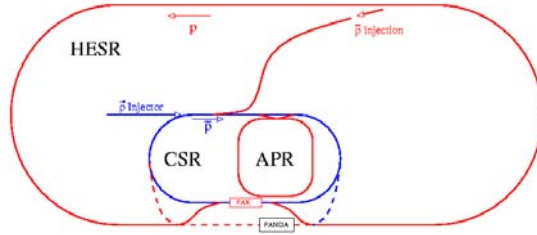


Figure 3: Phase II accelerator setup

has poor kinematic constraints. A rejection factor of 10^3 against background events is required to reduce the rate from few MHz to kHz levels. The trigger asks for two tracks in opposite hemispheres above the Cerenkov threshold. To reduce low-energetic combinatorial background, a cut on the dilepton invariant mass is applied using the deposited energy and the impact point at the calorimeter. The first layer of silicon is used to veto gamma conversions. The expected luminosity [5] is $5 \cdot 10^{31} \text{cm}^{-2} \text{s}^{-1}$. With a polarization of 20%, after one year of datataking, a precision of 10% in the measured h_{1u} in the valence region is expected.

2 Detector

The detector has a barrel geometry (fig. 4) that covers large θ_{lab} angle ($20^\circ - 120^\circ$). It's symmetric in ϕ in order to measure asymmetries of h_1 in ϕ . It has been designed to identify DY events in a large hadronic background (one DY event on 10^7 interactions). It will use five different types of detectors:

- Silicon Tracking Telescopes (two layers @ 5 and 22 cm from the beam axis, inside vacuum)
- Drift chambers (@ 65 and 135 cm from the beam axis)
- Cerenkov (between drift chambers)
- Scintillation odoscopes (in the forward region)

- Electromagnetic calorimeter ($16 \cdot X_0$, up to 5 GeV showers)

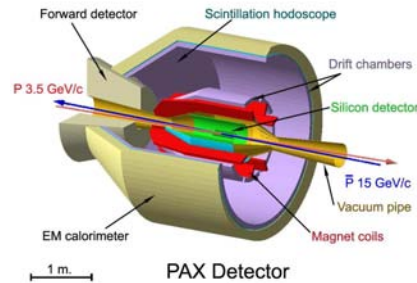


Figure 4: Artists view of PAX detector, produced by GEANT

In order to be compatible (no fringe field) with Cerenkov detector and with transversely polarized target, the chosen magnet design is a superconducting toroid. It's composed of eight separate coils.

3 Summary

PAX project has an innovative spin physics program to explore transversity/SSA (in collider mode) and EMFF/hard p-pbar scatterings (in fixed-target mode). It will open a way to obtain a polarized antiproton beam and will provide at FAIR a flexible second IP (Interaction Point) that really matches the physics items.

References

- [1] <http://www.fz-juelich.de/ikp/pax/>
- [2] PAX Technical Proposal
- [3] <http://www.gsi.de/fair/>
- [4] <http://www-panda.gsi.de/>
- [5] Y. Shatunov et al. (2005)

DEUTERON SPIN DICHROISM IN CARBON TARGET

V. Baryshevsky and A. Rouba

Research Institute for Nuclear Problems¹
Belarusian State University

Abstract

Birefringence phenomenon for unpolarized deuteron with energy up to 20 MeV in carbon target is considered. The estimation for spin dichroism of deuterons is presented. It is shown that magnitude of the phenomenon strongly depends on behavior of the deuteron wave functions on small distance between nucleon in deuteron.

It was shown in [1] that birefringence effect arises for deuterons passing through unpolarized isotropic matter. According to [1] this phenomenon is caused by difference of forward scattering amplitudes for deuterons with spin projection $m = 0$ and $m = \pm 1$ on coordinate axis parallel to deuteron wave vector (m is magnetic quantum number). For unpolarized deuteron beam because of spin dichroism caused by birefringence the tensor polarization appears after target passing. The first experimental study of deuteron spin dichroism in carbon target was carried out at the electrostatic HVEC tandem Van-de-Graaf accelerator with deuterons of up to 20 MeV (Institut für Kernphysik of Universität zu Köln) [2]. As a result spin dichroism of deuteron beam passing through unpolarized carbon target was discovered [2]. Later in 2007 spin dichroism was measured for 5.5 GeV/c deuterons in carbon target on Nuclotron in Dubna [3].

Let us discuss a possible magnitude of the birefringence effect for deuteron with energy up to 20 MeV in carbon target on the base of eikonal approximation. Introducing the deuteron center-of-mass coordinate \mathbf{R} and the relative distance between the proton and neutron in the deuteron $\mathbf{r} = \mathbf{r}_p - \mathbf{r}_n$, the Hamiltonian H can be written as

$$H = -\frac{\hbar^2}{2m_D}\Delta(\mathbf{R}) + H_D(\mathbf{r}) + H_N(\{\xi_i\}) + V_{DN}^N(\mathbf{R}, \mathbf{r}, \{\xi_i\}) + V_{DN}^C(\mathbf{R}, \mathbf{r}, \{\xi_i\}) \quad (1)$$

¹Belarus, 220050, Bobruiskaya Str. 11, Minsk

where H_D and H_N are the deuteron and nuclear Hamiltonian, V_{DN} stands for the energy of deuteron-nucleus nuclear and Coulomb interaction, $\{\xi_i\}$ is a set of coordinates of the nucleons. Let us consider scattering of deuterons with energy above deuterons binding energy ε_d . In that case we can apply the impulse approximation i. e. neglect of $H_D(\mathbf{r})$ in (1). In that approximation r is a parameter, and forward scattering amplitude should be averaged over the that parameter. For fast deuterons the scattering amplitude can be found in the eikonal approximation [4], [5]. The forward scattering amplitude can be written in this approximation as follows

$$f(0) = \frac{k}{2\pi i} \int (e^{i\chi_D(\mathbf{b},\mathbf{r})} - 1) d^2b |\varphi(\mathbf{r})|^2 d^3r \quad (2)$$

where k is the deuteron wave number, \mathbf{b} is the impact parameter, $\varphi(\mathbf{r})$ is deuterons wave function. The phase shift due to the deuteron scattering by a carbon is $\chi_D = \chi_{pN} + \chi_{nN} + \chi_{pN}^C = -\frac{1}{\hbar v} \int_{-\infty}^{+\infty} \{V_{pN} + V_{nN} + V_{pN}^C\} dz'$, where v is the deuteron speed. For deuteron with magnetic quantum number $m = \pm 1$, the wave function is $|\varphi_{\pm 1}(\mathbf{r})|^2$, whereas for $m = 0$, it is $|\varphi_0(\mathbf{r})|^2$. Owing to the additivity of phase shifts, equation (2) can be rewritten as

$$\begin{aligned} f(0) &= F_{pN}(0) + F_{nN}(0) + F_{pN}^C(0) + 2iF_{ppN}^C + \frac{2ik}{\pi} \int t_{nN}\left(\mathbf{b} - \frac{\mathbf{r}_\perp}{2}\right) t_{pN}^C\left(\mathbf{b} + \frac{\mathbf{r}_\perp}{2}\right) \times \\ &\times |\varphi(\mathbf{r}_\perp, z)|^2 d^2bd^2r_\perp dz + \frac{2ik}{\pi} \int t_{pN}\left(\mathbf{b} + \frac{\mathbf{r}_\perp}{2}\right) t_{nN}\left(\mathbf{b} - \frac{\mathbf{r}_\perp}{2}\right) |\varphi(\mathbf{r}_\perp, z)|^2 d^2bd^2r_\perp dz \\ &- \frac{4k}{\pi} \int t_{pN}\left(\mathbf{b} + \frac{\mathbf{r}_\perp}{2}\right) t_{nN}\left(\mathbf{b} - \frac{\mathbf{r}_\perp}{2}\right) t_{pN}^C\left(\mathbf{b} + \frac{\mathbf{r}_\perp}{2}\right) |\varphi(\mathbf{r}_\perp, z)|^2 d^2bd^2r_\perp dz, \end{aligned} \quad (3)$$

where $t_{nN(pN)}^{(C)} = \frac{e^{i\chi_{nN(pN)}^{(C)}} - 1}{2i}$, $F_{nN(pN)}^{(C)}(0) = \frac{k}{\pi} \int t_{nN(pN)}^{(C)}(\xi) d^2\xi = \frac{m_D}{m_{n(p)}} f_{n(p)}^{(C)}(0)$, $F_{ppN}^C(0) = \frac{k}{\pi} \int t_{pN} t_{pN}^C(\xi) d^2\xi$, \mathbf{r}_\perp is the \mathbf{r} component perpendicular to the momentum of incident deuteron, $f_{n(n)}^{(C)}(0)$ is the nuclear and the Coulomb amplitude of the proton (neutron)-carbon zero-angle elastic coherent scattering. So spin dependent part of forward scattering amplitude d_1 is determined by difference of forward scattering amplitudes for deuterons with $m = \pm 1$ and $m = 0$. In accordance with [1], [2] spin dichroism is determined by $Im(d_1)$. At scattering of deuterons on light nucleus the characteristic radius of the deuteron is large comparing with the radius of nucleus. For this reason for estimation of effects, when integrating, we can suppose that the functions t_{pN} and t_{nN} act on φ as δ -function. Then

$$\begin{aligned} Im(d_1) &= -\frac{3}{2\pi} Re \left\{ F_{nN}(0) \int t_{pN}^C(\xi) \left\{ \frac{1}{\sqrt{2}} \frac{u(r)W(r)}{r^2} - \frac{1}{4} \frac{W(r)^2}{r^2} \right\} \frac{\xi^2 - 2z^2}{r^2} d^2\xi dz \right\} \\ &+ \frac{6}{k} Re \{ F_{pN}(0) F_{nN}(0) \} G - \frac{12}{k} Im \{ F_{ppN}^C(0) F_{nN}(0) \} G, \end{aligned} \quad (4)$$

where $G = \int_0^\infty \left\{ \frac{1}{\sqrt{2}} \frac{u(r)W(r)}{r^2} - \frac{1}{4} \frac{W(r)^2}{r^2} \right\} dr$, $r^2 = \xi^2 + z^2$, $u(r)$ and $W(r)$ are the deuteron radial wave functions corresponding to the S-wave and to the D-wave. Now we can evaluate the deuteron spin dichroism. According to [1], [2] spin dichroism A and tensor polarization can be written as $p_{zz} \approx -\frac{4}{3}A$, $p_{xx} = p_{yy} \approx \frac{2}{3}A$, where $A = \frac{I_0 - I_{\pm 1}}{I_0 + I_{\pm 1}} = \frac{N_a z}{2M_r} (\sigma_{\pm 1} - \sigma_0) = \frac{2\pi N_a z}{k M_r} \text{Im}(d_1)$, I_0 and $I_{\pm 1}$ are the occupation numbers for deuterons in spin state $m = 0$ and $m = \pm 1$ after the target, z is thickness of target in g/cm^2 , N_a is Avogadro number, M_r is molar mass for targets matter, $\sigma_{\pm 1}$ and σ_0 are the deuteron total cross-section of scattering for spin state $m = \pm 1$ and $m = 0$ respectively.

For estimation of nucleon-carbon strong interaction in (4) lets consider optical Woods-Saxon potential for 5.25 MeV nucleons $V_{nN}(r) = V_{pN}(r) = \frac{-52.5 - 0.9i}{1 + \exp(2(r - 3.045))}$. For Coulomb p-C interaction in (4) we consider Coulomb screening potential. For calculation of parameter G the deuterons wave functions from [6] was applied. Obtained value G is about 0.05.

In (4) the first item is describe contribution of interference of nuclear n-C and Coulomb p-C interactions (lets denote that as NC), the second item is describe contribution of interference of nuclear p-C and n-C interactions (NN) and the third item is describe contribution of interference of nuclear p-C, n-C and Coulomb p-C interactions (NNC). Dependencies on energy of contributions of every items to $\sigma_{\pm 1} - \sigma_0$ are shown on Fig.1 a).

So for carbon target with $z = 0.1 g/cm^2$ and for energy conditions of experiment (6-13 MeV) [2] dichroism is about 0.01. On the Fig.1 b) is shown dependence of averaged effective difference of total cross-section $\sigma_{\pm 1} - \sigma_0$ on averaged deuteron energy inside carbon targets obtained in experiments.

There are some reasons that can essentially increase birefringence effect. The first is interaction of nucleon with carbon. On the Fig.1 c), d) are shown the estimated total cross-section, calculated by Woods-Saxon potential and eikonal approximation in comparison with experimental total cross-section. Interaction of nucleon with carbon has a lot of resonances in energy region of carried out experiment. Experimental cross-section for some energy interval in 2-2.5 times more than estimated that can result in increasing of effects up to 4-6.25 times for that energy interval. At the second, parameter G is very sensitive to deuterons wave functions at small distances. At the third, the increasing of weight of D-state (in [6] it is 4.85%) is increase birefringence effects. According to Fig.1 a) Coulomb scattering play very important role in birefringence value and behavior. Position of peak, caused by Coulomb interaction is sensitive to Coulomb potential so it can be shifted for realistic interaction. Fig.1 a) and Fig.1 d) give qualitative explanation of experimental results on Fig.1 b): sign of dichroism, strong dependence on energy, non-monotone and non-linear dependence of dichroism on target thickness.

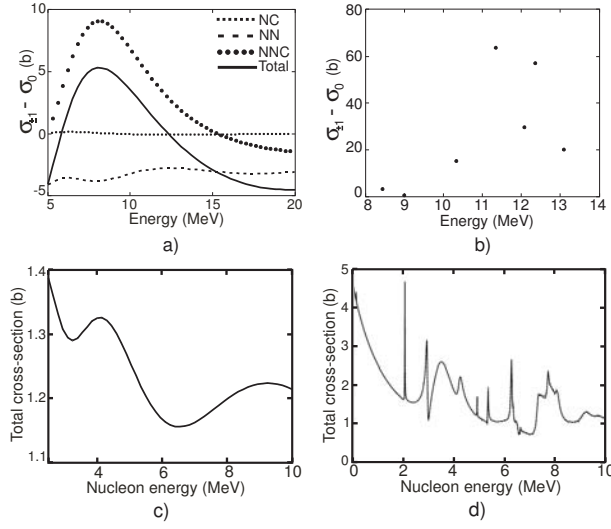


Figure 1: a) Dependencies on deuteron energy of contributions of items NC, NN, NNC and their sum to $\sigma_{\pm 1} - \sigma_0$; b) dependence of averaged effective difference of total cross-section $\sigma_{\pm 1} - \sigma_0$ on averaged deuteron energy inside carbon targets obtained in experiments; c) and d) dependencies on nucleon energy of total nucleon-carbon cross-section calculated by eikonal approximation and from experimental data.

References

- [1] V. Baryshevsky, *Phys. Lett. A* **171**, 431 (1992); *J. Phys. G* **19**, 273 (1993).
- [2] V. Baryshevsky, C. Duweke, R. Emmerich et al., Deuteron Spin Dichroism: From Theory to First Experimental Results, in *Proc. 17th Int. Spin Physics Symp., SPIN2006, Kyoto, Japan*, eds. K. Imai et al. (Melville, New York, 2007), p. 777; LANL e-print arXiv. hep-ex/0501045.
- [3] L.S. Azhgirey, Yu.V. Gurchin, A.Yu. Isupov et al., Observation of tensor polarization of deuteron beam travelling through matter, *XII Workshop on high energy spin physics DSPIN-2007, Dubna, Russia*, [http : //theor.jinr.ru/~spin/Spin-Dubna07/4%2006ThB/4%20Azhgirey/pro10.pdf](http://theor.jinr.ru/~spin/Spin-Dubna07/4%2006ThB/4%20Azhgirey/pro10.pdf)
- [4] W. Cryz, L.C. Maximon, *Ann. Phys.* **52**, 59, (1969).
- [5] *Handbuch der Physik*, Vol. 39 (Springer, Berlin, 1957), p. 112.
- [6] R. Machleidt, *Phys. Rev. C* **63**, 024001 (2001).

SYMMETRY TESTS IN NA48 WITH KAONS

*Matthias Behler*¹

Institut für Physik, Johannes Gutenberg-Universität Mainz
55099 Mainz, Germany
email: Matthias.Behler@uni-mainz.de

Abstract

The main goal of the NA48 experiments at the CERN SPS was the search for direct CP violation (CPV) in kaon decays. Two results of this search will be presented. In the neutral kaon sector the parameter η_{+-} was determined to $|\eta_{+-}| = (2.223 \pm 0.012) \cdot 10^{-3}$ using a sample of about 47000 $K_L \rightarrow \pi^+\pi^-$ and five million $K_L \rightarrow \pi^\pm e^\mp \nu$. In the charged kaon sector NA48/2 measured the asymmetry A_g of the linear slope parameter g in the Dalitz plot of $K^\pm \rightarrow 3\pi$ decays. The results are $A_g^c = (-1.5 \pm 2.1) \cdot 10^{-4}$ using $3.11 \cdot 10^9$ $K^\pm \rightarrow \pi^\pm \pi^+ \pi^-$ decays and $A_g^n = (1.8 \pm 1.8) \cdot 10^{-4}$ using $9.13 \cdot 10^7$ $K^\pm \rightarrow \pi^\pm \pi^0 \pi^0$ decays. Here, no evidence for direct CP violation at the order of 10^{-4} has been found.

1 Experimental set-up

The data for the η_{+-} measurement were taken during a dedicated run in 1999 with a pure K_L beam produced by a 450 GeV primary proton beam impinging on a beryllium target. The neutral beam, after passing the final collimator about 100 m downstream the target, entered the 90 m long decay volume which was followed by the NA48 detector. In 2003 and 2004, two simultaneous focused kaon beams of opposite charge, with a momentum of (60 ± 3) GeV were used to measure the asymmetry of $K^\pm \rightarrow 3\pi$ decays.

The main detector components are a magnetic spectrometer and a Liquid Krypton Calorimeter with tower read-out. The magnetic spectrometer, consisting of four drift chambers and a dipole magnet located between the second and third chamber, has a momentum resolution of about 1% and a spatial resolution of 100 μm . The calorimeter is an almost homogeneous ionization chamber with an active volume of 7 m³ and 27 X_0 thickness. It fully contains electromagnetic showers up to 100 GeV and has an energy resolution of about 1% for 20 GeV photons, and a spatial resolution of about 1 mm. A more detailed description can be found in [1].

¹On behalf of the NA48 and NA48/2 collaborations.

2 CP violation parameter η_{+-}

The observable η_{+-} is related to the parameters of indirect and direct CPV ($\eta_{+-} = \varepsilon + \varepsilon'$) and defined as the amplitude ratio of the neutral kaons decaying into two charged pions: $\eta_{+-} = A(K_L \rightarrow \pi^+\pi^-)/A(K_S \rightarrow \pi^+\pi^-)$. The interest in η_{+-} was aroused by recent KTeV and KLOE measurements [2,3] which disagreed with the previous world average by more than four standard deviations.

The analysis is based on 47000 $K_L \rightarrow \pi^+\pi^-$ and five million $K_L \rightarrow \pi^\pm e^\mp \nu$ decays [4]. The selection requires good 2-track events and additional cuts to suppress the dominant background. The ratio E/p , where E is the energy deposited in the calorimeter and p is the measured track momentum in the spectrometer, is used to separate both decays (Fig 1).

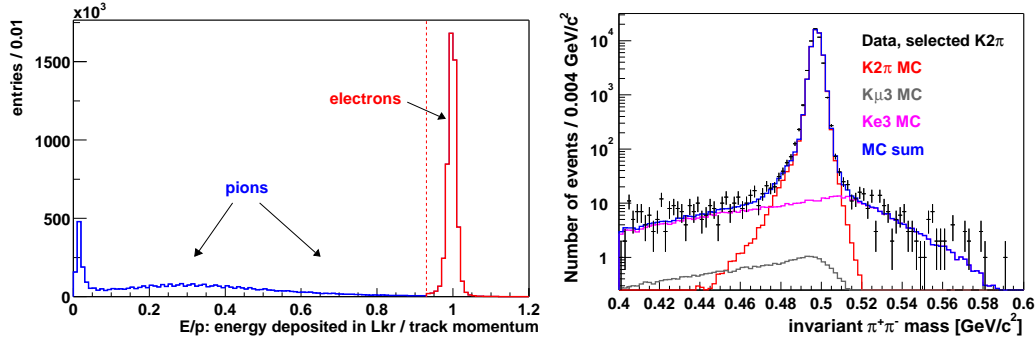


Figure 1: The E/p distribution for K_{e3} events (left) and the invariant $\pi^+\pi^-$ mass for $K_L \rightarrow \pi^+\pi^-$ candidates (right).

The ratio of both decay rates after all corrections is

$$\frac{\Gamma(K_L \rightarrow \pi^+\pi^-)}{\Gamma(K_L \rightarrow \pi^\pm e^\mp \nu)} = (4.835 \pm 0.022_{stat} \pm 0.016_{syst}) \cdot 10^{-3}. \quad (1)$$

Using this ratio and subtracting the contribution of the CP conserving direct emission process $K_L \rightarrow \pi^+\pi^-\gamma$ (DE), while including the CP violating inner bremsstrahlung component $K_L \rightarrow \pi^+\pi^-\gamma$ (IB), we determined the branching ratio of $K_L \rightarrow \pi^+\pi^-$ to

$$\text{BR}(K_L \rightarrow \pi^+\pi^-) = (1.941 \pm 0.019) \cdot 10^{-3}. \quad (2)$$

Finally, we calculated η_{+-} using the kaon lifetimes and the branching ratio of $K_S \rightarrow \pi^+\pi^-$:

$$|\eta_{+-}| = \sqrt{\frac{\text{BR}(K_L \rightarrow \pi^+\pi^-)}{\text{BR}(K_S \rightarrow \pi^+\pi^-)} \cdot \frac{\tau_{K_S}}{\tau_{K_L}}} = (2.223 \pm 0.012) \cdot 10^{-3}. \quad (3)$$

The results are in good agreement with recent measurements by KTeV and KLOE and all three experiments contradict the 2004 PDG value.

3 CP violation in $K \rightarrow 3\pi$ decays

The $K \rightarrow 3\pi$ decays are usually described in terms of two Dalitz variables u and v , depending on the kaon and pion four-momentum P_i and the charged pion mass m_π with $s_i = (P_K - P_i)^2$, $i = 1, 2, 3$ and $s_0 = \frac{1}{3}(s_1 + s_2 + s_3)$:

$$u = (s_3 - s_0)/m_\pi^2, \quad v = (s_1 - s_2)/m_\pi^2. \quad (4)$$

The indices $i = 1, 2$ correspond to the even pions (same charge) and the index $i = 3$ to the odd pion. The matrix element can be expressed as a polynomial expansion of u and v with the Dalitz plot parameters g , h , and k :

$$|\mathcal{M}(u, v)|^2 \propto 1 + gu + hu^2 + kv^2, \quad (5)$$

with $|h|, |k| \ll |g|$. Complementary with ε'/ε , the CP observable in the charged kaon sector is the asymmetry

$$A_g = (g^+ - g^-)/(g^+ + g^-) \approx \Delta g/(2g) \quad (6)$$

of the linear slope parameters g of K^+ and K^- . Since there is no mixing in charged kaon decays, any non-zero value of A_g reflects evidence for direct CPV. SM predictions for the charged asymmetry lay in the range $10^{-6} - 10^{-5}$ [5], while calculations involving processes beyond the SM allow a range of A_g up to 10^{-4} [6].

The measurement is based on the comparison of the u distributions of K^+ and K^- . Due to the regular inversions of the magnetic fields in the beam line and the spectrometer, four ratios $R_{ij}(u)$ of the u distributions can be defined:

$$R_{ij}(u) = \frac{N^+(u)}{N^-(u)} \propto 1 + \frac{\Delta g \cdot u}{1 + gu + hu^2}. \quad (7)$$

The index $i = U (D)$ refers to a configuration in which K^+ runs through the upper (lower) beam path in the achromatic magnet sets, while $j = S (J)$ refers to the spectrometer magnet polarity in which positive particles are deflected to the right (left) (towards the Saleve (Jura) mountain). In each single ratio most detector acceptance effects as well as variations in the response are canceled due to the two charged superimposed beams. However, fake asymmetries caused by the spectrometer magnet or the beam line cancel only in the quadruple ratio

$$R_4(u) = R_{US}(u) \cdot R_{UJ}(u) \cdot R_{DS}(u) \cdot R_{DJ}(u) \propto \left(1 + \frac{\Delta g \cdot u}{1 + gu + hu^2}\right)^4 \quad (8)$$

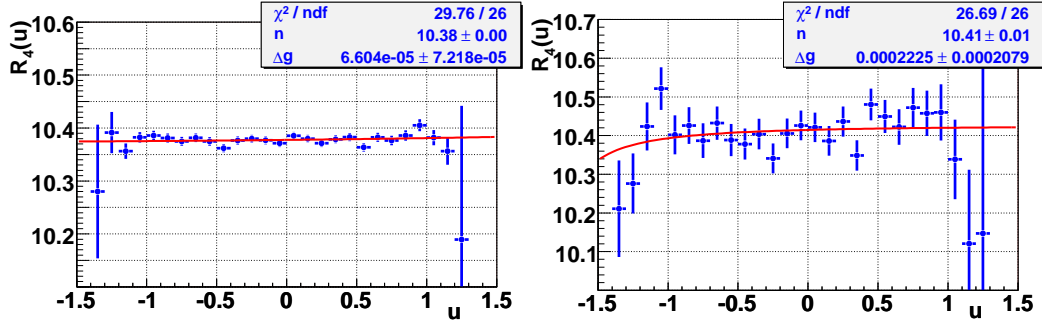


Figure 2: The E/p distribution for K_{e3} events (left) and the invariant $\pi^+\pi^-$ mass for $K_L \rightarrow \pi^+\pi^-$ candidates (right).

which is finally fitted to extract Δg (Fig. 2). The full 2003 and 2004 data contains $3.11 \cdot 10^9 K^\pm \rightarrow \pi^\pm\pi^+\pi^-$ and $9.13 \cdot 10^7 K^\pm \rightarrow \pi^\pm\pi^0\pi^0$ decays. Using the Dalitz plot slope g^c , recently measured by NA48/2 [7], for the charged mode and the PDG value of g^n for the neutral mode the extracted asymmetries from these data sets are

$$\begin{aligned} A_g^c &= (-1.5 \pm 1.5_{\text{stat}} \pm 0.9_{\text{trig}} \pm 1.1_{\text{syst}}) \cdot 10^{-4}, \\ A_g^n &= (1.8 \pm 1.7_{\text{stat}} \pm 0.5_{\text{syst}}) \cdot 10^{-4}. \end{aligned} \quad (9)$$

This is an improvement in accuracy over the previous measurements by more than one order of magnitude. The results are compatible with the SM predictions, i.e. no evidence for direct CP violation at the order of 10^{-4} has been found.

References

- [1] V. Fanti *et al.* [NA48] *Nucl. Inst. Methods* **A574**, 433 (2007).
- [2] T. Alexopoulos *et al.* [KTeV], *Phys. Rev.* **D70**, 092006 (2004).
- [3] F. Ambrosino *et al.* [KLOE], *Phys. Lett.* **B638**, 140 (2006).
- [4] A. Lai *et al.* [NA48], *Phys. Lett.* **B645**, 26 (2007).
- [5] E. Gámiz, J. Prades, I. Scimemi, *JHEP* **10**, 042 (2003);
G. Fäldt, E.P. Shabalín, *Phys. Lett.* **B635**, 295 (2006).
- [6] G. D’Ambrosio, G. Isidori, G. Martimelli, *Phys. Lett.* **B480**, 164 (2000).
- [7] R.J. Batley *et al.* [NA48], *Phys. Lett.* **B649**, 349 (2007).

THE GOTTFRIED SUM RULE IN AN UNQUENCHED QUARK MODEL

R. Bijker^{*,1}, E. Santopinto[%]

^{*}ICN-UNAM, AP 70-543, 04510 Mexico DF, Mexico

[%]INFN and University of Genova, via Dodecaneso 33, 16164 Genova, Italy

Abstract

We present an unquenched quark model for baryons in which the effects of quark-antiquark pairs ($u\bar{u}$, $d\bar{d}$ and $s\bar{s}$) are taken into account in an explicit form. The method is illustrated with an application to the flavor asymmetry of the nucleon sea.

1 Introduction

In the constituent quark model (CQM), the proton is described in terms of a uud three-quark configuration. A direct handle on higher Fock components (such as $uud - q\bar{q}$ configurations) is provided by parity-violating electron scattering (PVES) experiments, which have shown evidence for a nonvanishing strange quark contribution, albeit small, to the charge and magnetization distributions of the proton [1]. The contribution of strange quarks to the nucleon is of special interest because it is exclusively part of the quark-antiquark sea $q\bar{q} = s\bar{s}$. Additional evidence for higher Fock components in the proton wave function comes from measurements of the \bar{d}/\bar{u} asymmetry in the nucleon sea [2] and from CQM studies of baryon spectroscopy.

Theoretically, the role of higher Fock components in the CQM has been studied in [3], while the importance of mesonic contributions to the spin and flavor structure of the nucleon is reviewed in [4]. In another, CQM based, approach the effects of $s\bar{s}$ pairs in the proton were included in a flux-tube breaking model [5].

The aim of the present contribution is to discuss the flavor asymmetry of the nucleon sea in an unquenched quark model in which the effects of quark-antiquark pairs are included in a general and systematic way.

¹E-mail address: bijker@nucleares.unam.mx

2 Unquenched Quark Model

In the flux-tube model for hadrons, the quark potential model arises from an adiabatic approximation to the gluonic degrees of freedom embodied in a flux tube [6]. The impact of quark-antiquark pairs in meson spectroscopy has been studied in a flux-tube breaking model [7] in which the $q\bar{q}$ pair is created with the 3P_0 quantum numbers of the vacuum. Subsequently, it was shown [8] that a *miraculous* set of cancellations between apparently uncorrelated sets of intermediate states occurs in such a way that they compensate each other and do not destroy the good CQM results for the mesons. In particular, the OZI hierarchy is preserved and there is a near immunity of the long-range confining potential, since the change in the linear potential due to the creation of quark-antiquark pairs in the string can be reabsorbed into a new strength of the linear potential, *i.e.* in a new string tension. As a result, the net effect of the mass shifts due to pair creation is much smaller than the naive expectation of the order of the strong decay widths. However, it is necessary to sum over large towers of intermediate states to see that the spectrum of the mesons, after unquenching and renormalizing, is only weakly perturbed. An important conclusion is that no simple truncation of the set of meson loops is able to reproduce such results [8].

The extension of the flux-tube breaking model to baryons requires a proper treatment of the permutation symmetry between identical quarks. As a first step, Geiger and Isgur investigated the importance of $s\bar{s}$ loops in the proton in an unquenched quark model based on an adiabatic treatment of the flux-tube dynamics to which the $s\bar{s}$ pair creation with vacuum quantum numbers is added as a perturbation [5]. In the conclusions, the authors emphasized: *It also seems very worthwhile to extend this calculation to $u\bar{u}$ and $d\bar{d}$ loops. Such an extension could reveal the origin of the observed violations of the Gottfried sum rule and also complete our understanding of the origin of the spin crisis.* In this contribution, we take up the challenge and present a generalization of the formalism of [5] which now makes it possible to study the effects of $q\bar{q}$ pairs in an unquenched quark model (i) for any initial baryon (ground state or resonance), (ii) for any flavor of the quark-antiquark pair, and (iii) for any model of baryons and mesons, as long as their wave functions are expressed in the basis of the harmonic oscillator.

These extensions were made possible by two developments: the solution of the problem of the permutation symmetry between identical quarks by means of group-theoretical techniques, and the construction of an algorithm to generate a complete set of intermediate states for any model of baryons and mesons.

3 Flavor Asymmetry

The first clear evidence for the flavor asymmetry of the nucleon sea was provided by NMC at CERN [9]. The flavor asymmetry is related to the Gottfried integral for the difference of the proton and neutron electromagnetic structure functions

$$S_G = \int_0^1 dx \frac{F_2^p(x) - F_2^n(x)}{x} = \frac{1}{3} - \frac{2}{3} \int_0^1 dx [\bar{d}(x) - \bar{u}(x)] . \quad (1)$$

Under the assumption of a flavor symmetric sea, one obtains the Gottfried sum rule $S_G = 1/3$. The final NMC value is 0.2281 ± 0.0065 at $Q^2 = 4$ $(\text{GeV}/c)^2$ for the Gottfried integral over the range $0.004 \leq x \leq 0.8$ [9], which implies a flavor asymmetric sea. The violation of the Gottfried sum rule has been confirmed by other experimental collaborations [10, 11]. Theoretically, it was shown [12], that the coupling of the nucleon to the pion cloud provides a natural mechanism to produce a flavor asymmetry.

In the present model, the flavor asymmetry can be calculated from the difference of the number of d and u sea quarks in the proton

$$N_{\bar{d}} - N_{\bar{u}} = \int_0^1 dx [\bar{d}(x) - \bar{u}(x)] . \quad (2)$$

Note that, even in absence of explicit information on the (anti)quark distribution functions, the integrated value can be obtained directly from the left-hand side of Eq. (2). The corresponding value for the Gottfried integral is 0.185, in qualitative agreement with the NMC result. It is important to note that in this calculation the parameters were taken from the literature [5, 13], and that no attempt was made to optimize their values. Since the dependence of the Gottfried integral on the value of these parameters and/or different models of baryons and mesons has not yet been investigated in detail, the numerical value quoted here is to be regarded as preliminary.

4 Summary, conclusions and outlook

We discussed an unquenched quark model for baryons which includes, in addition to $s\bar{s}$ loops, the contributions of $u\bar{u}$ and $d\bar{d}$ loops. In an application to the flavor asymmetry of the nucleon sea, it was shown that the $q\bar{q}$ pairs immediately lead to an excess of \bar{d} over \bar{u} quarks in the proton, in agreement with the experimental data.

In our opinion, the result for the flavor asymmetry is very promising and encouraging. We believe that the inclusion of the effects of quark-antiquark

pairs in a general and consistent way, as suggested in [14] and in this contribution, may provide a major improvement to the constituent quark model, increasing considerably its range of applicability.

Acknowledgments

This work was supported in part by a grant from CONACYT, Mexico and in part by INFN, Italy.

References

- [1] A. Acha *et al.*, *Phys. Rev. Lett.* **98**, 032301 (2007).
- [2] G.T. Garvey and J.-C. Peng, *Progr. Part. Nucl. Phys.* **47**, 203 (2001).
- [3] Q.B. Li and D.O. Riska, *Nucl. Phys. A* **791**, 406 (2007), and references therein.
- [4] J. Speth and A.W. Thomas, *Adv. Nucl. Phys.* **24**, 83 (1997).
- [5] P. Geiger and N. Isgur, *Phys. Rev. D* **55**, 299 (1997).
- [6] N. Isgur and J. Paton, *Phys. Lett. B* **124**, 247 (1983); *Phys. Rev. D* **31**, 2910 (1985).
- [7] R. Kokoski and N. Isgur, *Phys. Rev. D* **35**, 907 (1987).
- [8] P. Geiger and N. Isgur, *Phys. Rev. Lett.* **67**, 1066 (1991); *Phys. Rev. D* **44**, 799 (1991); *ibid.* **47**, 5050 (1993).
- [9] P. Amaudruz *et al.*, *Phys. Rev. Lett.* **66**, 2712 (1991); M. Arneodo *et al.*, *Nucl. Phys. B* **487**, 3 (1997).
- [10] K. Ackerstaff *et al.*, *Phys. Rev. Lett.* **81**, 5519 (1998).
- [11] R.S. Towell *et al.*, *Phys. Rev. D* **64**, 052002 (2001).
- [12] A.W. Thomas, *Phys. Lett. B* **126**, 97 (1983).
- [13] S. Capstick and W. Roberts, *Phys. Rev. D* **49**, 4570 (1994).
- [14] E. Santopinto and R. Bijker, arXiv:nucl-th/0701227; R. Bijker and E. Santopinto, arXiv:nucl-th/0703053.

HIGHLIGHTS ON RADIATIVE KAON AND HYPERON DECAYS FROM NA48/2

*A. Bizzeti*¹

Università degli Studi di Modena e Reggio Emilia
I-41100 Modena, Italy
and INFN, Sezione di Firenze
I-50018 Sesto Fiorentino (FI), Italy

Abstract

Recent results on radiative charged Kaon decays from NA48/2 experiment and on Ξ^0 weak radiative decays from NA48/1 experiment are presented. A precise measurement of the Direct Emission contribution in $K^\pm \rightarrow \pi^\pm \pi^0 \gamma$ has been performed, and interference with the dominating Inner Bremsstrahlung has been observed for the first time. The first observations of the very rare decay $K^\pm \rightarrow \pi^\pm e^+ e^- \gamma$ and of the weak radiative decay $\Xi^0 \rightarrow \Lambda e^+ e^-$ are also presented.

1 Beam line and detector

The NA48/2 experiment took data in 2003 and 2004 using two simultaneous beams of (60 ± 3) GeV/c oppositely charged kaons, produced by 400 GeV/c protons from CERN SPS impinging on a beryllium target.

The charged particle reconstruction is provided by a magnetic spectrometer, consisting of a dipole magnet and four drift chambers, with a spatial resolution of 100 μm and a momentum resolution $\Delta p/p = (1.0 \oplus 0.044p[\text{GeV}/c])\%$.

The energy and position of photons and electrons are precisely measured by a Liquid Krypton electromagnetic calorimeter, consisting of a $27X_0$ almost homogeneous ionization chamber with high-granularity tower read-out: its energy resolution is $\Delta E/E = 3.2\%/\sqrt{E[\text{GeV}]} \oplus 9\%/E[\text{GeV}] \oplus 0.42\%$ and its spatial resolution about 1.5 mm.

A scintillator hodoscope for fast triggering and precise time measurement, muon and photon veto counters and an iron-scintillator hadron calorimeter complete the experimental apparatus, a detailed description of which can be found in [1].

¹representing the NA48/1 and NA48/2 collaborations

2 The radiative decay $K^\pm \rightarrow \pi^\pm \pi^0 \gamma$

The $K^\pm \rightarrow \pi^\pm \pi^0 \gamma$ decay amplitude is the sum of two terms: one arises from the inner bremsstrahlung (IB) associated to the decay $K^\pm \rightarrow \pi^\pm \pi^0$ in which the photon is emitted from the outgoing charged pion, the other is due to direct emission (DE) in which the photon is radiated in the intermediate states of the decay.

Although suppressed by the $\Delta I = 1/2$ rule, the IB term dominates the sum. The DE term contains a magnetic amplitude which can be evaluated using Chiral Perturbation Theory (ChPT) and an electric amplitude for which there is no definite theoretical prediction. The latter can be determined by measuring its interference (INT) with the purely electric IB.

In order to kinematically separate (on a statistical basis) IB, DE and INT components in the differential decay width we use the Lorentz invariant variable W , defined as $W^2 = (P_K^* \cdot P_\gamma^*)(P_\pi^* \cdot P_\gamma^*)/(m_K m_\pi)^2$, where P_x^* is the 4-momentum of the particle $x = K^\pm, \pi^\pm, \gamma$.

The differential decay width depends on both W and the charged pion energy T_π^* in the kaon rest frame. Integrating on T_π^* we obtain an expression that splits the different contributions into terms with different powers of W :

$$\frac{d\Gamma^\pm}{dW} \simeq \frac{d\Gamma_{\text{IB}}^\pm}{dW} \left[1 + 2 \frac{m_\pi^2}{m_K^2} W^2 |E| \cos((\delta_1 - \delta_0) \pm \phi) + \frac{m_\pi^4}{m_K^4} W^4 (|E|^2 + |M|^2) \right] \quad (1)$$

where $|E|$ and $|M|$ describe electric and magnetic DE transitions, $(\delta_1 - \delta_0)$ is the $\pi\pi$ phase shift difference, ϕ is an unknown phase responsible for CP violation and the three terms in the sum represent IB, INT and DE contributions respectively. A recent theoretical work by Cappiello and D'Ambrosio [2] suggest the presence of a form factor in the DE term, not yet included in the present analysis, that would modify Eq. (1).

The IB component has been measured by Abrams *et al.* [3] and is in good agreement with QED predictions. Measurements of the DE component have been performed up to now [4–7] ignoring the INT term, in the kinematical region $55 \text{ MeV} < T_\pi^* < 90 \text{ MeV}$ where the dangerous background from $K^\pm \rightarrow \pi^\pm \pi^0$ and $K^\pm \rightarrow \pi^\pm \pi^0 \pi^0$ decays is strongly suppressed.

An almost background-free data sample of $1.24 \cdot 10^5$ $\pi^\pm \pi^0 \gamma$ candidate events with $T_\pi^* < 80 \text{ MeV}$ and $E_\gamma > 5 \text{ GeV}$ has been selected from data taken in 2003. Its W distribution has been fitted to the sum of Monte Carlo simulated W spectra for IB, DE and INT, obtaining the following preliminary values for the fractions of DE and INT with respect to IB:

$$\text{Frac}(DE) \equiv \Gamma(DE)/\Gamma(IB) = (3.35 \pm 0.35_{\text{stat}} \pm 0.25_{\text{syst}})\% \quad (2)$$

$$\text{Frac}(INT) \equiv \Gamma(INT)/\Gamma(IB) = (-2.67 \pm 0.81_{\text{stat}} \pm 0.73_{\text{syst}})\% \quad (3)$$

This is the first measurement of a non vanishing interference term in the $K^\pm \rightarrow \pi^\pm \pi^0 \gamma$ decay. Fig. 1 shows the very high correlation of the DE and INT contributions ($\rho = -0.92$). A substantial reduction in both statistical and systematic errors is foreseen using the full 2003-2004 data set.

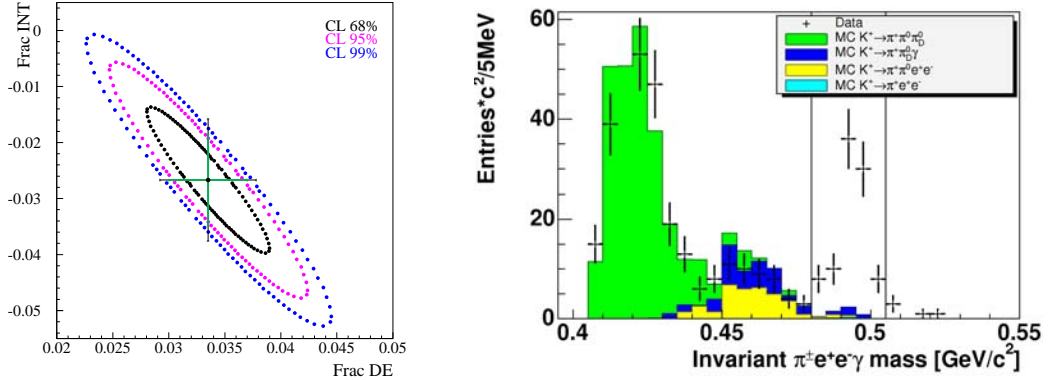


Figure 1 (left): $\Gamma(K^\pm \rightarrow \pi^\pm \pi^0 \gamma)$ DE and INT fractions (normalized to IB). Figure 2 (right): Invariant mass distribution of $\pi^\pm e^+ e^- \gamma$ candidate events.

3 First observation of $K^\pm \rightarrow \pi^\pm e^+ e^- \gamma$

The $K^\pm \rightarrow \pi^\pm e^+ e^- \gamma$ decay kinematics is very similar to that of the $K^\pm \rightarrow \pi^\pm \gamma \gamma$ decay, with one of the photons internally converting into an $e^+ e^-$ pair. A naïf estimate of the branching fraction gives $\text{BR}(K^\pm \rightarrow \pi^\pm e^+ e^- \gamma) \approx \text{BR}(K^\pm \rightarrow \pi^\pm \gamma \gamma) \cdot 2\alpha = 1.6 \cdot 10^{-8}$. Model dependent theoretical estimates based on ChPT [8] predict a BR in the range $(0.9 - 1.6) \cdot 10^{-8}$.

Fig. 2 shows the reconstructed $\pi^\pm e^+ e^- \gamma$ invariant mass of the selected events: the signal region contains 92 events, with a 1 ± 1 accidental background and a 5.1 ± 1.7 misidentification background (mainly $K^\pm \rightarrow \pi^\pm \pi_D^0 \gamma$ events with a lost photon). This is the first observation of the radiative decay $K^\pm \rightarrow \pi^\pm e^+ e^- \gamma$. Using $K^\pm \rightarrow \pi^\pm \pi^0$ as normalization channel we obtain the preliminary result $\text{BR}(K^\pm \rightarrow \pi^\pm e^+ e^- \gamma) = (1.27 \pm 0.14_{\text{stat}} \pm 0.05_{\text{syst}}) \cdot 10^{-8}$.

4 Decay asymmetries in Ξ^0 radiative decays

Radiative decays of the Ξ^0 hyperon have been studied by the NA48/1 experiment. The same detecting apparatus as NA48/2 has been used, with a neutral beam originating from a target close to the beginning of the decay fiducial region.

A sample of 43814 $\Xi^0 \rightarrow \Lambda \gamma$ candidate events has been selected (the Λ being identified through its $p\pi^-$ decay), with a 0.8% background.

The asymmetry parameter $\alpha_{\Xi\Lambda\gamma}$ is extracted from the distribution in the angle $\theta_{\Xi p}$ between the directions of the incoming Ξ^0 and the outgoing proton in the Λ rest frame: $dN/d\cos(\theta_{\Xi p}) = (N/2)[1 - \alpha_{\Xi\Lambda\gamma}\alpha_- \cos(\theta_{\Xi p})]$ (where $\alpha_- = 0.642 \pm 0.013$ [9] is the asymmetry parameter for the decay $\Lambda \rightarrow p\pi^-$), obtaining $\alpha_{\Xi\Lambda\gamma} = -0.68 \pm 0.02_{stat} \pm 0.06_{syst}$. The same method has been used to measure the asymmetry parameter in the $\Xi^0 \rightarrow \Sigma^0\gamma$ decay. From a sample of 13068 events with a $\approx 3\%$ background we obtain $\alpha_{\Xi\Sigma\gamma} = -0.68 \pm 0.03_{stat} \pm 0.07_{syst}$, in excellent agreement with the measured $\alpha_{\Xi\Lambda\gamma}$.

5 First observation of the $\Xi^0 \rightarrow \Lambda e^+e^-$ decay

In 2002 NA48/1 run the $\Xi^0 \rightarrow \Lambda e^+e^-$ decay was observed for the first time. A data sample of 412 candidates has been selected, with an estimated background of 15 events. Using the $\Xi^0 \rightarrow \Lambda\pi^0$, $\pi^0 \rightarrow \gamma e^+e^-$ decay as normalization channel we obtain a branching fraction $\text{BR}(\Xi^0 \rightarrow \Lambda e^+e^-) = (7.7 \pm 0.4_{stat} \pm 0.4_{syst}) \cdot 10^{-6}$. The measured e^+e^- invariant mass spectrum is consistent with an inner conversion-like e^+e^- production mechanism.

The decay asymmetry parameter $\alpha_{\Xi\Lambda ee}$ has been measured from the angular distribution $dN/d\cos(\theta_{\Xi p}) = (N/2)[1 - \alpha_{\Xi\Lambda ee}\alpha_- \cos(\theta_{\Xi p})]$. The obtained value $\alpha_{\Xi\Lambda ee} = -0.8 \pm 0.2$ is in good agreement with the measured $\alpha_{\Xi\Lambda\gamma}$. A detailed description of the data analysis can be found in [10].

References

- [1] V. Fanti *et al.*[NA48 Collab.], *Nucl. Instr. Methods* **A574**, 433 (2007).
- [2] L. Cappiello and G. D'Ambrosio, *Phys. Rev. D* **75**, 094014 (2007).
- [3] R. J. Abrams *et al.*, *Phys. Rev. Lett.* **29**, 1118 (1972).
- [4] S. C. Adler *et al.*[E787 Collab.], *Phys. Rev. Lett.* **85**, 4856 (2000)
- [5] M. A. Aliev *et al.*[KEK-E470 Collab.], *Phys. Lett. B* **554**, 7 (2003)
- [6] M. A. Aliev *et al.*[KEK-E470 Collab.], *Eur. Phys. J. C* **46**, 61 (2006)
- [7] V. A. Uvarov *et al.*, *Phys. Atom. Nucl.* **69**, 26 (2006)
- [8] F. Gabbiani, *Phys. Rev. D* **59**, 094014 (1999)
- [9] W.-M. Yao *et al.*[PDG], *Journal of Physics G* **33**, 1 (2006)
- [10] J. Batley *et al.*[NA48/1 Collab.], *Phys. Lett. B* **650**, 1 (2007)

A HIGH PRECISION MEASUREMENT OF THE PION FORM FACTORS VIA RADIATIVE PION DECAY $\pi^+ \rightarrow e^+ \nu \gamma$

M. Bychkov for the PIBETA collaboration

Department of Physics
University of Virginia
Charlottesville, VA 22903

Abstract

In this paper we present the results of the PIBETA collaboration analysis of the radiative pion decay $\pi^+ \rightarrow e^+ \nu \gamma$. This decay was studied in a broad region of the kinematic phase space allowing for a precise measurement of the pion vector and axial vector form factors F_V and F_A as well as the dependence of the form factors on the invariant mass of the $e\nu$ pair. If known accurately, these parameters impose stringent constraints on the CVC hypothesis and deviations from the $V-A$ form of the weak current.

1 Introduction to Pion Decays

As the lightest mesons, pions present a unique opportunity to study weak interactions of quarks. The ratio of the decay rates of the charged pion $\pi^+ \rightarrow \mu^+ \nu$ ($\pi_{\mu 2}$) to $\pi^+ \rightarrow e^+ \nu$ ($\pi_{e 2}$) is one of the strongest manifestations of the $V-A$ form of the weak interaction. The pion beta, $\pi^+ \rightarrow \pi^0 e^+ \nu$ (π_β), decay rate provides a precise measurement of the V_{ud} element of the CKM matrix [1]. Finally, the radiative pion decay, $\pi^+ \rightarrow e^+ \nu \gamma$ ($\pi_{e 2 \gamma}$), offers a glimpse into the hadronic structure of the charged pion via detection of the real photon associated with the virtual hadronic states of the pion constituents [2].

2 The $\pi_{e 2 \gamma}$ Decay in the Standard Model

The Standard Model description of the $\pi_{e 2 \gamma}$ decay parametrizes the branching ratio of the decay with two *a priori* unknown form factors, i.e., the vector

form factor F_V and axial-vector form factor F_A , such that

$$\begin{aligned} \frac{dB_{\pi e 2\gamma}^{\text{the}}}{dx dy} = & \frac{\alpha}{2\pi} B_{\pi e 2} \left\{ IB + \left(\frac{m_\pi^2}{2f_\pi m_e} \right)^2 [(F_V + F_A)^2 SD^+ + (F_V - F_A)^2 SD^-] \right. \\ & \left. + \left(\frac{m_\pi}{f_\pi} \right) [(F_V + F_A) S_{\text{int}}^+ + (F_V - F_A) S_{\text{int}}^-] \right\} + \text{r.c.}, \end{aligned} \quad (1)$$

where α is the fine structure constant, m_π and m_e are pion and positron masses, and $f_\pi = 130.7 \text{ MeV}$ is the pion decay constant. The $IB(x, y)$, $SD^\pm(x, y)$, and $S_{\text{int}}^\pm(x, y)$ (IB – SD interference) terms depend on the kinematic variables $x = 2E_\gamma/m_\pi$ and $y = 2E_e/m_\pi$ where E_e and E_γ are the particle’s energies, and “r.c.” stands for radiative corrections. The conserved vector current (CVC) hypothesis [3] relates F_V to the π^0 lifetime, yielding $F_V = 0.0259(9)$ [5]. The value of the F_A is model dependent and chiral symmetry calculations (see Ref. [4] and references therein) give a value for F_A in the range 0.010–0.014. In the lowest order of the chiral expansion the ratio of the form factors is related to the pion electric polarizability $\alpha_E = (\alpha/8\pi^2 m_\pi F_\pi^2) \times F_A/F_V$.

3 The $\pi_{e2\gamma}$ Decay in Experiment

Most of the earlier experimental measurements of the $\pi_{e2\gamma}$ decay were conducted in the high- E_γ , high- E_e regions of the phase space and relied on the precise knowledge of the vector form factor from the neutral pion life time, thus looking for the ratio of the F_A/F_V . The world average prior to the PIBETA publications was $F_A = (116 \pm 16) \times 10^{-4}$ [5].

Our measurements were performed at the $\pi E1$ beam line at the Paul Scherrer Institute (PSI), Villigen, Switzerland, using a stopped π^+ beam and the PIBETA detector [6]. For this analysis we used 2.0×10^{13} stopped π^+ ’s and the decay products accumulated in three overlapping regions of the phase space defined as: A : $E_{e^+}, E_\gamma > 50 \text{ MeV}$; B : $E_{e^+} > 10 \text{ MeV}$ and $E_\gamma > 50 \text{ MeV}$; C : $E_{e^+} > 50 \text{ MeV}$ and $E_\gamma > 10 \text{ MeV}$, with relative angle $\theta_{e^+\gamma} > 40^\circ$ for all regions.

In our experiment we have observed positron and photon pairs from the $\pi_{e2\gamma}$ decay in overdetermined kinematics which allowed for a strong suppression of the copious positron background coming from the decays of the muons. The time difference distribution between the positron and the photon arrival to the CsI calorimeter defined our peak signal in the $\Delta t = |t_e - t_\gamma| < 5 \text{ ns}$ region. The sample of the accidental background taken from the sidebands of the same distribution was subtracted from the events in the peak.

In parallel to the $\pi_{e2\gamma}$ events, we have recorded a large sample of the non-radiative π_{e2} decays. In order to reduce the systematic uncertainty associated with the absolute number of pions stopped in the target, we have used these decays for the absolute normalization of the radiative pion decay branching ratio. The π_{e2} absolute branching ratio is a very well known quantity both theoretically and experimentally [5,7,8]. Both types of events were corrected by the detector acceptance. The acceptance calculations were provided by a GEANT3 based rendition of the PIBETA detector. The quality of the data and the simulation is demonstrated in Fig. 1.

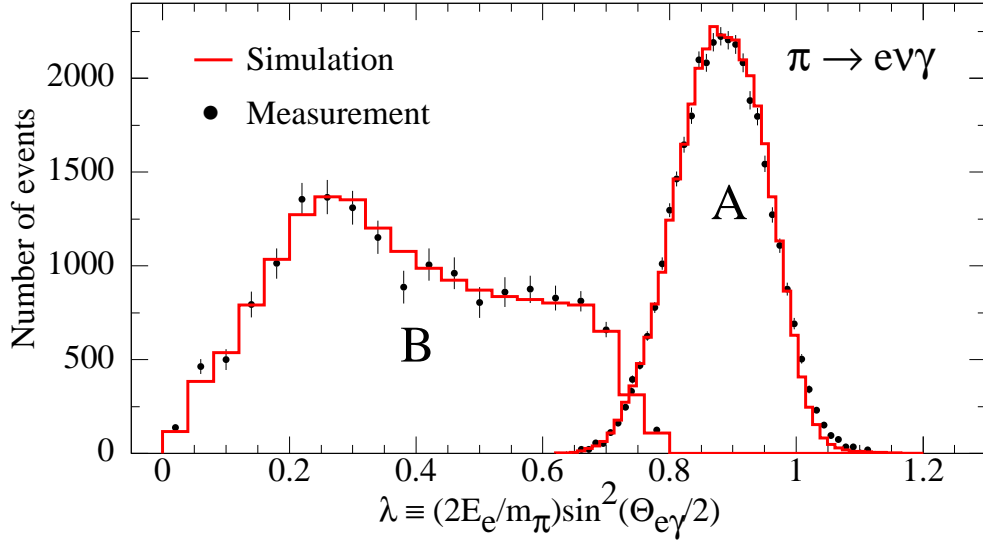


Figure 1: Background-subtracted $\pi^+ \rightarrow e^+\nu\gamma$ distribution of the kinematic variable $\lambda \equiv (2E_e/m_\pi)\sin^2(\theta_{e\gamma}/2)$ for regions B and A .

In order to extract the value of the form factors, experimental and theoretical branching ratios of the $\pi_{e2\gamma}$ decay were combined into the χ^2 function

$$\chi^2 = \sum_{i=A,B,C} \frac{(B_{\pi e2\gamma}^{\text{exp}(i)}(F_A, F_V, a) - B_{\pi e2\gamma}^{\text{the}(i)}(F_A, F_V, a))^2}{\sigma_i^2(F_A, F_V, a)}, \quad (2)$$

where σ_i^2 are the combined uncertainties for each region, and the parameter a signifies the dependence of the form factor on the invariant mass of the $e\nu$ pair q^2 such that $F_V(q^2) = F_V(0)(1 + a \cdot q^2)$ and $F_A(q^2) = F_A(0)$. The χ^2 function was minimized as function of the free parameters F_A , F_V , and a .

4 Results

In this analysis we have reconstructed $35,948 \pm 194$ (0.54%) events in region A , $16,246 \pm 331$ (2.0%) events in region B and $13,263 \pm 161$ (1.2%) events in region C , where numbers in parentheses are fractional statistical uncertainties.

The simplest analysis of our data is in the form of a fit with fixed values of $F_V = 259 \times 10^{-4}$ and $a = 0.041$ [9], leaving only one free parameter, F_A . Under these conditions our data provide $F_A = (119 \pm 1) \times 10^{-4}$. This result represents a sixteenfold improvement in precision over the pre-PIBETA world average. Alternatively, we released all three parameters F_A , F_V , and a simultaneously, and obtained $F_A = (117 \pm 17) \times 10^{-4}$, $F_V = (258 \pm 17) \times 10^{-4}$, and $a = 0.095 \pm 0.058$. These results (i) agree very well with the predictions of the CVC hypothesis for the charged pion form factors, (ii) represent a fourteenfold improvement in the precision of the vector form factor F_V , and (iii) provide the first ever measurement of the charged pion form factor slope parameter a . Finally, fixing $F_V = 0.0259$, $a = 0.041$ (standard model values), and $F_A = 0.0119$ (our best-fit value), we varied the contribution of the putative tensor coupling form factor, F_T , as defined in Ref. [10]. The optimal fit yields $F_T = (-0.6 \pm 2.8) \times 10^{-4}$, or $-5.2 \times 10^{-4} < F_T < 4.0 \times 10^{-4}$ at the 90% confidence limit.

References

- [1] D. Počanić et. al., *PRL* **93**, 181803-1 (2004).
- [2] E. Frlež et. al., *PRL* **93**, 181804-1 (2004).
- [3] V. G. Vaks and B. L. Ioffe, *NC* **10**, 342 (1958).
- [4] J. Bijmens and P. Talavera, *NPB* **489**, 387 (1997).
- [5] S. Eidelman et. al., *Phys. Lett. B* **592**, 1 (2004).
- [6] E. Frlež and others, *NIM* **526**, 300 (2004).
- [7] W. J. Marciano and A. Sirlin, *PRL* **71**, 3629 (1993).
- [8] V. Cirigliano and I. Rosell, *hep-ph/0707.3439v1*, (2007).
- [9] J. Portoles and V. Mateu", *hep-ph/0706.1039v2*, (2007).
- [10] M. V. Chizhov, *hep-ph/0402105*, (2004).

COHERENT PHOTOPRODUCTION OF ϕ MESONS FROM DEUTERONS NEAR THRESHOLD

W.C. Chang
Institute of Physics, Academia Sinica,
Taipei 11529, Taiwan, Republic of China

Abstract

We measured coherent ϕ -meson photo-production from deuterons at forward angles by using linearly polarized photons with $E_\gamma = 1.5\text{-}2.4$ GeV. The decay asymmetries show a dominance of the natural-parity exchange process. The energy dependence of cross sections will explore the behavior of Pomeron exchange at low energies.

1 Introduction

The photoproduction of vector mesons from hadrons has been a valuable tool to study the dynamics of Pomeron exchange at high energies and the resonance channels at low energies [1]. Because of the dominant $s\bar{s}$ quark component in the ϕ meson, quark-exchange (or meson-exchange) mechanisms, and s-channel resonance production are strongly suppressed by the Okubo-Zweig-Iizuka (OZI) rule, compared to the cases of ρ and ω production. This feature makes the photoproduction of ϕ mesons at low energies a unique tool for the study of Pomeron exchange near threshold and multigluon exchange processes other than baryon and meson exchange [2]. Especially the measurement of decay angular distributions of ϕ -meson with the use of linearly-polarized-photon beam can be used to decompose the scattering amplitude into a natural-parity-exchange (Pomeron and glueball) part and an unnatural-parity-exchange (π, η) part.

In the intermediate range of photon energies to the threshold, the coherent vector-meson photoproduction from deuterons filters out the isovector π -meson exchange in t -channel because both the beam and target are isoscalar [3]. The isovector π -meson exchange is the leading component in the unnatural-parity processes because the other channel of η -exchange is

suppressed by the smallness of ηNN coupling and large mass in the exchange propagator. Therefore the study of the coherent ϕ -meson production from deuterons provides the cleanest way to explore the contributions purely from natural-parity processes at low energies.

2 $\gamma d \rightarrow \phi d$

The LEPS experiment measured the ϕ -meson photoproduction from liquid hydrogen and deuterium near threshold in the very forward direction with linearly polarized photons by LEPS experiment [4,5]. Polarized photons were produced by backward Compton scattering with an ultra-violet Ar laser from 8 GeV electrons in the storage ring of SPring-8, Japan. The typical photon flux was about 10^6 s^{-1} . Within the acceptance of the tagger counter, the polarization of the photon beam was 95% at 2.4 GeV and decreased down to 55% at 1.5 GeV. More experimental details are referred to Ref. [6].

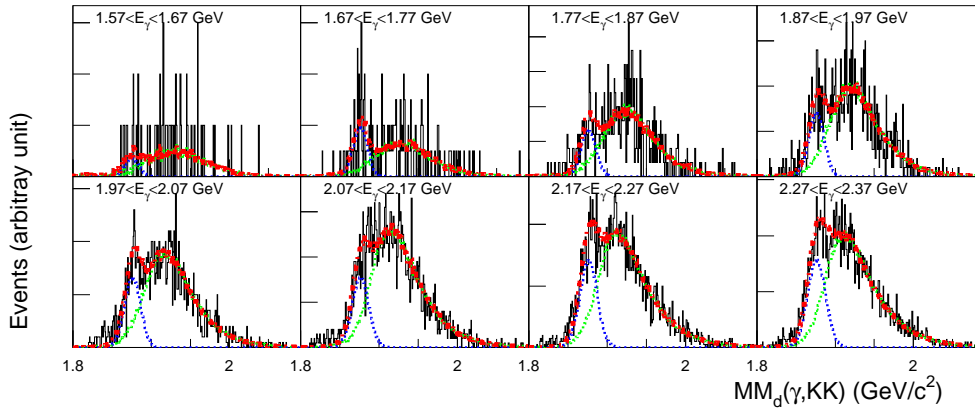


Figure 1: The distributions of missing mass $MM_d(\gamma, KK)$ assuming deuteron target overlapped with the fit (red lines) of MC-simulated coherent (blue lines) and incoherent (green lines) components.

For the interactions with liquid deuterium target [7], we identified the production of ϕ mesons via the charged decay mode with the detection of two tracks K^+ and K^- in the final state. The vertex positions of K^+K^- tracks were required within the target position. A cut on the invariant mass, $|M(KK) - M_\phi| < 0.01 \text{ GeV}/c^2$, was applied to select the ϕ -meson events, either

through coherent or incoherent production. The coherent ϕ production from deuterons, $\gamma d \rightarrow \phi d$, was characterized by the distribution with a peak at the mass of deuterons $1.875 \text{ GeV}/c^2$ in the spectra of missing mass ($\text{MM}_d(\gamma, \text{KK})$) assuming deuteron as the rest target. The $\text{MM}_d(\gamma, \text{KK})$ spectra at various photon energy bins were shown in the Fig. 1.

Our acceptance sat mainly at the very forward direction of $|t - t_{min}^d| < 0.1$ where t_{min}^d is the minimum four-momentum transfer assuming deuteron as the rest target in the reaction. To disentangle the yields of coherent and incoherent interactions, the $\text{MM}_d(\gamma, \text{KK})$ spectra was fitted by the sum of the individual distributions obtained by Monte-Carlo simulation [7]. As seen in Fig. 1 the missing mass spectra of real data were nicely reproduced by MC simulation.

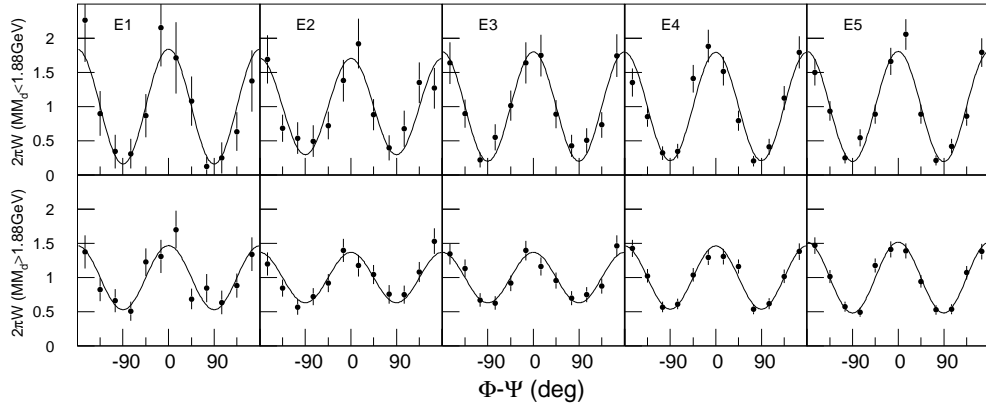


Figure 2: The distributions of $W(\Phi - \Psi)$ in the Gottfried-Jackson frame at the forward angles ($|t - t_{min}^d| < 0.1 \text{ GeV}^2$) for five energy bins of $1.9 < E_\gamma < 2.4 \text{ GeV}$. The E_γ binning starts from E1=(1.87,1.97) GeV and ends at E5=(2.27,2.37) GeV. The top and bottom panel are for the events whose missing-mass values are less than or larger than $1.88 \text{ GeV}/c^2$.

For the measurements of decay asymmetry of coherent and incoherent interactions from the decay angular distributions of $W(\Phi - \Psi)$ in the Gottfried-Jackson frame [8], two sets of distributions of $W(\Phi - \Psi)$ were in five energy regions of $1.9 < E_\gamma < 2.4 \text{ GeV}$. As shown in Fig. 2 with a division at missing mass value of $1.88 \text{ GeV}/c^2$, a larger decay asymmetry was seen for the group of events with smaller missing mass. It was understood in the sce-

nario of different mixing percentage of coherent and incoherent events distributed in the regions of $MM_d(\gamma, KK)$ and their different decay asymmetries. Hence the individual decay asymmetry was disentangled under the assumption of a relationship of linearly weighting from each component. A very large decay asymmetry close to the maximum value corresponding to pure exchange of natural-parity processes was found for the coherent component and this means that the exchange processes for the coherent ϕ production from deuteron are mainly of natural parity, agreeing with the theoretical expectation of an absence of π -exchange together with a small contribution of η -exchange in the sector of unnatural-parity exchanges.

3 Summary

In summary, photoproduction of ϕ mesons from deuterons at forward angles in the low energy region of $E_\gamma=1.5-2.4$ GeV was measured by SPring-8/LEPS experiment with the use of linearly polarized photons. The coherent interactions with deuterons were disentangled from the incoherent ones via the missing mass spectra. A complete dominance of helicity-conserving natural-parity exchange processes were seen from the decay angular distributions of this reaction. The energy dependence of the cross sections to be finalized will be extremely valuable to determine the behavior of Pomeron exchange at low energies and explore the existence of additional significant natural-parity processes beyond the Pomeron exchange.

References

- [1] T.H. Bauer, R.D. Spital, D. R. Yennie and F.M. Pipkin, *Rev. Mod. Phys.* **50**, 261 (1978).
- [2] T. Nakano and H. Toki, *Proceedings of the International Workshop on Exciting Physics and New Accelerators Facilities*, World Scientific, 1997; L.S. Kisslinger and W.-H. Ma, *Phys. Lett. B* **485**, 367 (2000).
- [3] A.I. Titov, M. Fujiwara and T.S.-H. Lee, *Phys. Rev.* **C66**, 022202 (2002).
- [4] T. Nakano *et al.*, *Nucl. Phys.* **A684**, 71 (2001).
- [5] T. Mibe, W.C. Chang *et al.*, *Phys. Rev. Lett.* **95**, 182001 (2005).
- [6] M. Sumihama *et al.*, *Phys. Rev.* **C73**, 035214 (2006).
- [7] W.C. Chang *et al.* (LEPS Collaboration), nucl-ex/0703034.

- [8] A.I. Titov, T.-S.H. Lee, *Phys. Rev. C* **67**, 065205 (2003).

MULTICHANNEL CHIRAL APPROACH FOR KAONIC HYDROGEN

*A. Cieplý*¹

Nuclear Physics Institute
250 68 Řež
Czech Republic

J. Smejkal

Czech Technical University
Institute of Experimental and Applied Physics
Horská 3a/22
128 00 Praha 2
Czech Republic

Abstract

We present an exact solution to the K^- -proton bound state problem formulated in the momentum space. The 1s level characteristics of the kaonic hydrogen are described together with the available low energy $\overline{K}N$ data.

1 Introduction

We developed a precise method of computing the meson-nuclear bound states in momentum space. The method was already applied to pionic atoms and its multichannel version was used to calculate the 1s level characteristics of pionic hydrogen [1]. Here we just remark that our approach is based on the construction of the Jost matrix and involves the solution of the Lippman-Schwinger equation for the transition amplitudes between the various channels. In this work we aim at a simultaneous description of both the 1s level kaonic bound state and the available experimental data for the K^-p initiated processes.

In view of the vastly improved experimental results on the 1s level of kaonic hydrogen [2] the exact solution of the bound state problem should be preferred over the traditional Deser-Trueman formula relating the threshold scattering amplitude to the hadronic energy level characteristics of exotic atoms. Recently, the relation for kaonic hydrogen was modified to include the isospin effects and electromagnetic corrections [3].

¹cieply@ujf.cas.cz

2 Meson-baryon potentials

Unlike the pion-nucleon interaction the $\bar{K}N$ dynamics is strongly influenced by the existence of the $\Lambda(1405)$ resonance, just below the K^-p threshold. This means that the standard chiral perturbation theory is not applicable in this region. Fortunately, one can use non-perturbative coupled channel techniques to deal with the problem and generate the $\Lambda(1405)$ resonance dynamically. Such approach has proven quite useful and several authors have already applied it to various low energy meson-baryon processes [4–6].

Here we follow the approach of Ref. [4] and take the strong interaction part of the potential matrix in a separable form

$$V_{ij}(k, k') = \sqrt{\frac{1}{2E_i} \frac{M_i}{\omega_i}} g_i(k) \frac{C_{ij}}{f^2} g_j(k') \sqrt{\frac{1}{2E_j} \frac{M_j}{\omega_j}}, \quad g_j(k) = \frac{1}{1 + (k/\alpha_j)^2} \quad (1)$$

in which the parameter f stands for the pseudoscalar meson decay constant in the chiral limit. The coupling matrix C_{ij} is determined by chiral SU(3) symmetry and it includes terms up to second order in the meson c.m. kinetic energies. The off shell form factor $g_j(k)$ introduces the inverse range radius α_j that characterizes the radius of interaction in the channel j . In the Born approximation the potentials $V_{ij}(k, k')$ give the same (up to $\mathcal{O}(q^2)$) s-wave scattering lengths as are those derived from the underlying chiral lagrangian. More details on the construction of the effective (chirally motivated) potentials and the specification of the kinematical factors $\sqrt{M_j/(2E_j\omega_j)}$ can be found in Refs. [4, 7]. While the authors of Ref. [4] restricted themselves only to the six channels that are open at the $\bar{K}N$ threshold we have employed all ten coupled meson-baryon channels in our model: K^-p , \bar{K}^0n , $\pi^0\Lambda$, $\pi^+\Sigma^-$, $\pi^0\Sigma^0$, $\pi^-\Sigma^+$, $\eta\Lambda$, $\eta\Sigma^0$, $K^+\Xi^-$, and $K^0\Xi^0$. The potential of Eq. (1) is used not only when solving the bound state problem but we also implement it in the standard Lippman-Schwinger equation and compute the low energy $\bar{K}N$ cross sections and branching ratios from the resulting transition amplitudes.

3 $\bar{K}N$ data fits

The parameters of the chiral lagrangian that enter the coefficients C_{ij} and the inverse range radii α_i determining the off-shell behavior of the potentials are to be fitted to the experimental data. Before performing the fits we reduce the number of the fitted parameters in the following way. First, the axial couplings D and F (concerning the specification of the various chiral couplings we refer the reader to Refs. [4] and [7]) have already been established in the analysis of semileptonic hyperon decays, $D = 0.80$, $F = 0.46$

($g_A = F + D = 1.26$). Then, we fix the couplings b_D and b_F to satisfy the approximate Gell-Mann formulas for the baryon mass splittings, $b_D = 0.064 \text{ GeV}^{-1}$ and $b_F = -0.209 \text{ GeV}^{-1}$. Similarly, we determine the coupling b_0 and the baryon chiral mass M_0 from the relations for the pion-nucleon sigma term $\sigma_{\pi N}$ and for the proton mass (see e.g. [6]). Finally, we reduce the number of the inverse ranges α_i to only five: α_{KN} , $\alpha_{\pi\Lambda}$, $\alpha_{\pi\Sigma}$, $\alpha_{\eta\Lambda/\Sigma}$, $\alpha_{K\Xi}$. This leaves us with 11 free parameters: the five inverse ranges, the pseudoscalar meson decay constant f , and five more couplings from the second order chiral lagrangian denoted by d_D , d_F , d_0 , d_1 , and d_2 .

The fits to low energy $\bar{K}N$ data standardly include the three precisely measured threshold branching ratios γ , R_c and R_n (specified e.g. in Ref. [4]) and the K^-p -initiated total cross sections. For the later ones we consider only the experimental data taken at the kaon laboratory momenta $p_{LAB} = 110 \text{ MeV}$ (for the K^-p , \bar{K}^0n , $\pi^+\Sigma^-$, $\pi^-\Sigma^+$ final states) and at $p_{LAB} = 200 \text{ MeV}$ (for the same four channels plus $\pi^0\Lambda$ and $\pi^0\Sigma^0$). Our results show that the inclusion of more data taken at other kaon momenta is not necessary since the fit at just 1 – 2 points fixes the cross section magnitude and the energy dependence is reproduced nicely by the model. With the inclusion of the DEAR results on the strong interaction shift ΔE_N and the width Γ of the 1s level in kaonic hydrogen we end up with a total of 15 data points in our fits.

Table 1: The fitted $\bar{K}N$ threshold data

$\sigma_{\pi N}$ [MeV]	χ^2/N	ΔE_N [eV]	Γ [eV]	γ	R_c	R_n
20	1.33	232	725	2.366	0.657	0.191
30	1.36	272	683	2.367	0.658	0.190
40	1.38	257	713	2.370	0.658	0.190
50	1.40	266	708	2.370	0.658	0.190
exp	-	193(43)	249(150)	2.36(4)	0.664(11)	0.189(15)

Our results are summarized in Table 1, where the results of our χ^2 fits are compared with the relevant experimental data. Since the value of the pion-nucleon σ -term is not well determined we enforced four different options, which cover the interval of the values considered by various authors. The resulting χ^2 per data point indicate satisfactory fits. It is worth noting that their quality and the computed values do not depend much on the exact value of the $\sigma_{\pi N}$. The low energy cross sections included in the fits are not shown here but we stress that their description is good [7]. The strong interaction energy shift of the 1s level in kaonic hydrogen is reproduced well but we were not able to get a satisfactory fit of the 1s level energy width as our results are significantly larger than the experimental value. However, when considering the interval of three standard deviations and also the older KEK

results [8] (that give less precise but larger width) one cannot conclude that kaonic hydrogen measurements contradict the other low energy $\overline{K}N$ data.

In Table 2 we compare our results (for $\sigma_{\pi N} = 20, 30$ and 50 MeV) for the 1s level characteristics in kaonic hydrogen with the approximate values determined from the K^-p scattering lengths a_{K^-p} that were obtained from the multiple channel calculation that uses the same parametrization of the strong interaction potential (1). The 1s level complex energies are shown for: the standard Deser-Trueman formula (DT), the modified Deser-Trueman formula (MDT) [3] and our “exact” solution of the bound state problem. We have checked that if only the point-like Coulomb potential is considered in the K^-p channel our method reproduces the well known Bohr energy of the 1s level with a precision better than 0.1 eV. This means that the discrepancy between the “MDT” and the “exact” values can be attributed to higher order corrections not considered in the derivation of the MDT. In view of the current level of the experimental precision the use of the MDT formula is sufficient. Though, the situation may change after the coming SIDDHARTA experiment.

Table 2: Precision of the Deser-Trueman formula

a_{K^-p} [fm]	$-0.50 + i 1.01$	$-0.59 + i 0.99$	$-0.60 + i 1.01$
DT: $\Delta E_N - (i/2)\Gamma$ [eV]	$207 - (i/2)832$	$256 - (i/2)806$	$247 - (i/2)830$
MDT: $\Delta E_N - (i/2)\Gamma$ [eV]	$251 - (i/2)714$	$290 - (i/2)664$	$285 - (i/2)689$
exact: $\Delta E_N - (i/2)\Gamma$ [eV]	$232 - (i/2)725$	$262 - (i/2)698$	$266 - (i/2)708$

Acknowledgement: A. C. acknowledges a financial support from the GA AVCR grant A100480617.

References

- [1] A. Cieplý and R. Mach, *Nucl. Phys.* **A609**, 377 (1996)
- [2] G. Beer *et al.* [DEAR Collab.], *Phys. Rev. Lett.* **94**, 212302 (2005).
- [3] U.-G. Meissner, U. Raha, and A. Rusetsky, *Eur. Phys. J.* **C35**, 349 (2004)
- [4] N. Kaiser, P.B. Siegel, and W. Weise, *Nucl. Phys.* **A594**, 325 (1995)
- [5] B. Borasoy, R. Nissler, and W. Weise, *Eur. Phys. J.* **A25**, 79 (2005)
- [6] J.A. Oller, *Eur. Phys. J.* **A28**, 63 (2006)
- [7] A. Cieplý and J. Smejkal. *Eur. Phys. J.* **A34**, 237 (2007)

[8] T. M. Ito et al., Phys. Rev: **C 58**, 2366 (1988)

FIRST RESULTS ON PION POLARIZABILITIES @ COMPASS

*M. Colantoni*¹ on behalf of the COMPASS coll.
Department of Science and Advance Technologies
University of Piemonte Orientale
Via G. Bellini 25, 15100 Alessandria - Italy

Abstract

The COMPASS experiment at SPS/CERN investigates a variety of reactions related to the structure and spectroscopy of hadrons. First data with hadron beams have been collected at the end of 2004. This initial run has been devoted mostly to the measurement of the pion electric ($\overline{\alpha}_\pi$) and magnetic ($\overline{\beta}_\pi$) polarizabilities via the inverse Compton scattering. The preliminary results of $\overline{\alpha}_\pi$ and $\overline{\beta}_\pi$ from the 2004 pion beam data taking are presented.

1 Introduction

The electric ($\overline{\alpha}$) and magnetic ($\overline{\beta}$) polarizabilities characterize the induced dipole moment of hadrons subjected to an external electromagnetic field. They are a measure of the rigidity of the internal structure of a particle. We concentrate here on the π -meson polarizabilities due to the relative simplicity of the $q\bar{q}$ system and its small mass. For this case the Chiral Perturbation Theory (χPT) [1] provides rigorous predictions giving the value:

$$(\overline{\alpha}_\pi - \overline{\beta}_\pi) = (5.7 \pm 1.0) \cdot 10^{-4} fm^3. [2]$$

Other models predict different values for $\overline{\alpha}_\pi$ and $\overline{\beta}_\pi$ (for a review see [3]), but all agree on the fact that $(\overline{\alpha}_\pi + \overline{\beta}_\pi)$ is zero or compatible with zero.

¹colanton@to.infn.it

2 The measurement @ COMPASS

$\bar{\alpha}$ and $\bar{\beta}$ can be obtained from the deviation of the measured Compton cross section from the known behaviour of a point-like particle. The real data can be collected via the Primakoff reaction, i.e. a scattering of a pion beam in the Coulomb field of an heavy nuclear target $\pi + Z \rightarrow \pi + Z + \gamma$.

In 2004, COMPASS took data with a 190 GeV/c beam of both pions and muons. Lead, carbon and copper targets were used. The largest statistics was collected with the lead target. A detailed description of the COMPASS setup can be found elsewhere [4].

In order to select the Primakoff reaction is necessary to reconstruct completely the final state. For this purpose only events with an outgoing pion and a photon detected in the downstream calorimeter were considered. Additional requests were the primary vertex inside the target and a momentum transfer lower than 0.0075 (GeV/c)^2 .

The geometrical acceptance for the data collected with the two beams were found to be similar, the Monte-Carlo simulations are reported in fig. 1a. In fig. 1b the measured Q^2 dependence for pions and muons data is shown. Here, we clearly see the strong diffractive contribution present as background to the pion data that is absent in the muon case. Additional correction were applied in the pion case for the background contributions coming from the K^- (beam contamination) and ρ^- (pion excitation) decay.

The polarizability value was determined under the assumption of $(\bar{\alpha} + \bar{\beta}) = 0$ fitting the ω ($\omega = E_\gamma/E_{beam}$) dependence of the ratio R ($R = \sigma_{measured}/\sigma_{point-like}$).

As a cross-check, from the analysis of the muon data, a value of the muon polarizability compatible with zero was found, as expected. This is illustrated in fig. 2a. The preliminary value (see fig. 2b) for the pion magnetic polarizability $\bar{\beta}_\pi$ was found to be:

$$\bar{\beta}_\pi = (-2.5 \pm 1.7_{stat} \pm 0.6_{syst}) \cdot 10^{-4} fm^3.$$

To obtain this result radiative corrections were applied.

The Z^2 dependence for the cross-section [7] was checked comparing lead data to those of other target C, Cu, as reported in fig. 2a. The cross sections as a function of Q^2 for the three targets are shown in fig. 3b.

The overall statistics considered here correspond to only three days of beam time.

In fig. 4 the current world data on $\bar{\alpha}_\pi = -\bar{\beta}_\pi$ are reported together with the χ_{PT} prediction. The preliminary value measured at COMPASS agrees with the χ_{PT} prediction and is lower than the values measured by the A2 collaboration at MAMI [5] and the previous measurement performed

at Serpukhov [6]. The values given here are still preliminary. In particular MC simulations are running to refine the estimation of the systematic errors from the Q^2 cuts.

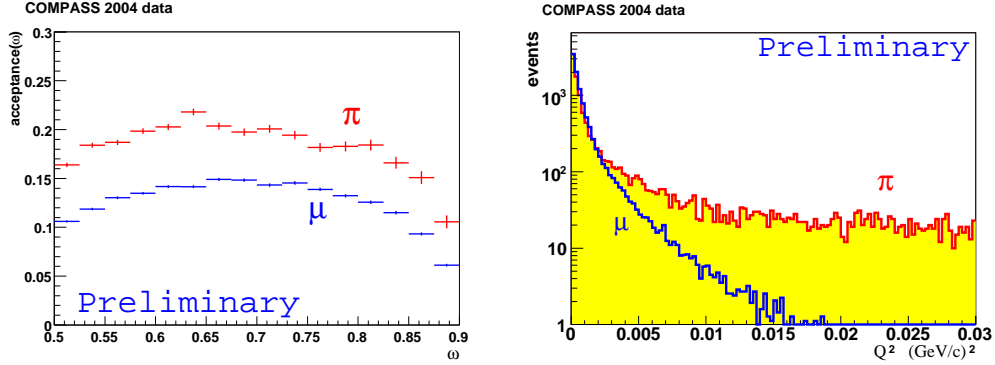


Figure 1: MonteCarlo acceptance for muon and pion as function of $\omega = E_\gamma/E_{beam}$ on the left Q^2 dependence for pion and muon real data on the right.

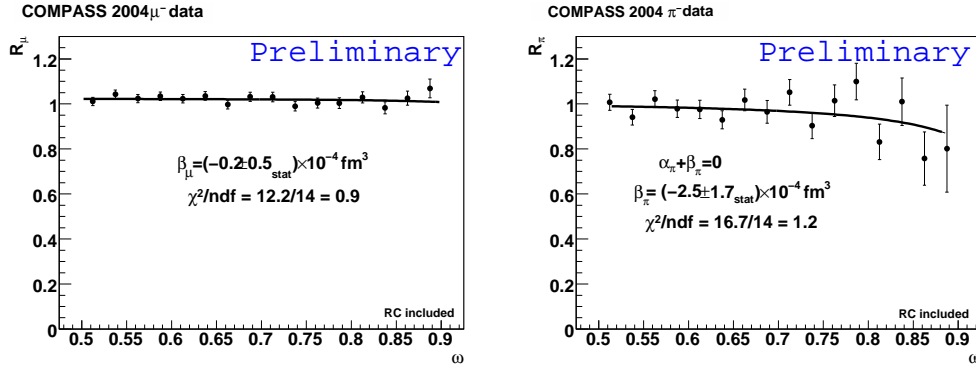


Figure 2: Fitted results for muon (on the left) and pion (on the right) magnetic polarizability.

Acknowledgments

This work has been supported by the University of Piemonte Orientale and Istituto Nazionale di Fisica Nucleare Sezione di Torino (INFN-To)

References

- [1] J. Gasser, H. Leutwyler, *Annals Phys.* **158**, 142 (1984)
 J. Gasser, H. Leutwyler *Nucl.Phys.* **B250**, 465 (1985)
 S. Weinberg, *Physica* **A96**, 327 (1979)

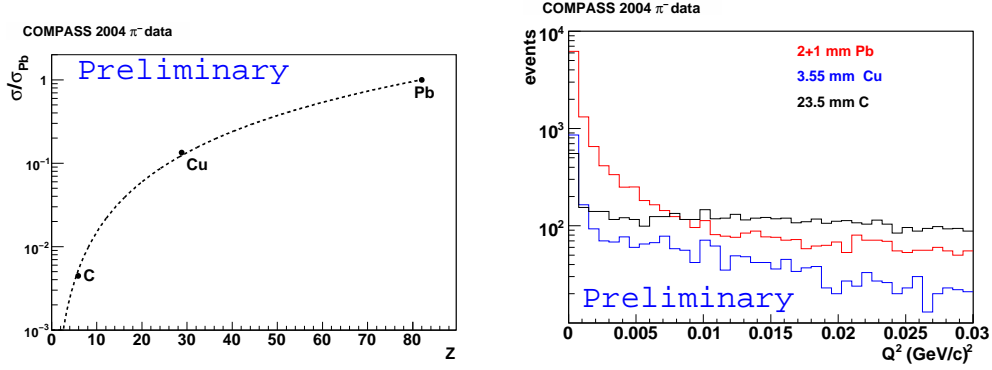


Figure 3: Z^2 -dependence of the cross-section on the left Q^2 -dependence for the C, Cu, Pb target on the right.

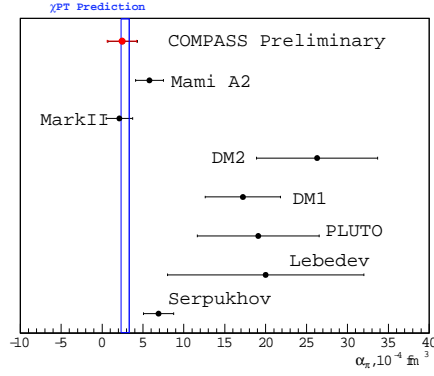


Figure 4: Overview of all pion polarizability measurement together with the χPT prediction. The statistical and systematical errors are summed in quadrature

- [2] J. Gasser *et al.*, Nucl. Phys. Rev **B745**, 84 (2006).
- [3] J. Portoles, M.R. Pennington, *The second DaΦne Physics Handbook v.2*, 579 (1999), hep-ph/9407295
C.A. Wilmot, R.H. Lemmer, Phy. Rev. **C65**, 035206 (2002)
- [4] P. Abbon *et al.*, Nucl. Inst. Meth. **A577**, 455 (2007)
- [5] J. Ahrens *et al.*, Eur. Phys. J. **A23**, 113 (2005)
- [6] Yu.M. Antipov *et al.*, Phys. Lett. **B121**, 445 (1983)
- [7] M. Buenerd, Nucl. Inst. Meth. **A361**, 111 (1997)

STUDIES OF THE η MESON PRODUCTION WITH POLARIZED PROTON BEAM AT COSY-11

R. Czyżykiewicz and P. Moskal

for the COSY-11 collaboration

Institute of Physics, Jagiellonian University, Cracow, PL-30-059, Poland

Abstract

We summarize the COSY-11 measurements of the analyzing power for the $pp \rightarrow pp\eta$ reaction and interpret the results in the framework of the meson exchange models. Determined analyzing power is essentially consistent with zero implying dominance of the s -wave in the η meson production process.

1 Introduction

Investigations of the production and decay of hadrons deliver information needed to deepen our knowledge about the strong interaction in the domain of low energy region, where the application of the perturbative approach of quantum chromodynamics is not possible. Here we briefly present the results concerning the hadronic production of the η meson and interpret them in the framework of meson exchange models. More detailed description has been recently reported in the Proceedings of the Symposium on Meson Physics [1].

From the total and differential cross section measurements for the $pp \rightarrow pp\eta$ reaction [2] it was concluded [4–6] that the production of the η meson proceeds via a two-step process, with the mesonic excitation of a nucleon to the resonance in first stage, and further deexcitation of this state into the N - η system. In fact, any of the π , η , ω , or ρ meson may contribute to the resonance creation. As an intermediate resonance, the $S_{11}(1535)$ is anticipated to be the dominant one, however the other nuclear resonances may give noticeable contribution as well [7].

Studies of the isospin dependence of the η meson production in NN collisions [3] revealed strong isospin dependence of the production process. The production of the η meson with the total isospin $I=0$ exceeds the production with the total isospin $I=1$ by a factor of 12, suggesting that the isovector meson exchange – the π or ρ meson exchange – is the dominant process in the

excitation of the $S_{11}(1535)$ resonance. However, the relative contributions of the pseudoscalar π or vector ρ meson still remained to be determined.

Among the available theoretical models Nakayama et al. postulated [6] a dominance of exchange of the pseudoscalar mesons, while Fäldt and Wilkin [5] found a main contribution originating from the vector meson exchange. Both models are in good agreement with unpolarized observables, however, they differ significantly in the predictions for the analyzing power function.

2 Results

The COSY-11 group has performed measurements of the vector analyzing power A_y for the $\vec{p}p \rightarrow pp\eta$ reaction at the excess energies of $Q=10$ and 37 MeV [8].

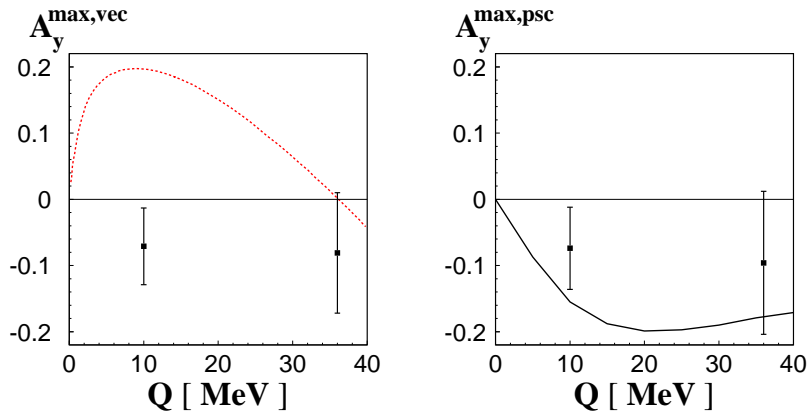


Figure 1: Theoretical predictions for the energy dependence of the amplitude of A_y confronted with the amplitudes determined in the experiments at the excess energies $Q=10$ and 37 MeV for the vector (left) and pseudoscalar meson exchange dominance model (right).

Results, presented in Fig. 1 in the form of the analyzing power amplitude [8], show that the predictions of the model based on the dominance of the π meson exchange [6] are fairly consistent with data (at the level of 1σ), whereas the calculations performed within the frame of the vector meson dominance model, based on the photoproduction data and the assumption of the dominance of the ρ meson exchange [5], differ from the experimental points by more than four standard deviations. This confrontation of the theoretical predictions with the experimental data indicates that the excita-

tion of the nucleon to the $S_{11}(1535)$ resonance is predominantly due to the exchange of the π meson.

The analyzing power values for both excess energies are consistent with zero within one standard deviation. This is in line with the results obtained by the DISTO [9] collaboration in the far-from-threshold energy region. Such a result may indicate that the η meson is predominantly produced in the s -wave.

3 Future perspectives

Recently, the proposal for the measurement of the analyzing power function [10] with the WASA-at-COSY apparatus [11] has been presented and awaits recommendation of the COSY Programme Advisory Committee. Measurements are planned with about 50 times better statistics which, assuming the same background-to-signal ratio in the missing mass spectrum, enables the error bars from Fig. 1 to be reduced of circa 7 times.

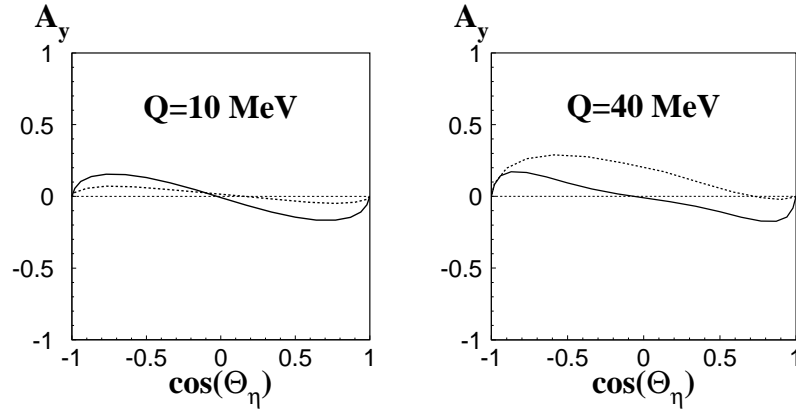


Figure 2: Predictions of the dependence of the analyzing power function on the intermediate resonance type [7].

Fig. 2 presents the dependence of the analyzing power as a function of the cosine of the polar angle of the η meson emission in the center-of-mass system on the intermediate resonance type [7]. Solid lines are the calculations of the pseudoscalar meson exchange model performed under assumption that only $S_{11}(1535)$ resonance contributes to the η meson production amplitude, whereas the dotted lines represent the predictions of the same model, including $D_{13}(1520)$, $S_{11}(1535)$, $S_{11}(1650)$, and $D_{13}(1700)$ resonances. Therefore, the

improvement in the measurement accuracy would enable to investigate the influence of other-than- $S_{11}(1535)$ resonances upon the production amplitude.

4 Acknowledgement

We acknowledge the support of the European Community-Research Infrastructure Activity under the FP6 programme (Hadron Physics, N4:EtaMesonNet, RII3-CT-2004-506078), the support of the Polish Ministry of Science and Higher Education under the grants No. PB1060/P03/2004/26, 3240/H03/2006/31 and 1202/DFG/2007/03, and the support of the German Research Foundation (DFG) under the grant No. GZ: 436 POL 113/117/0-1.

References

- [1] R. Czyżykiewicz et al., arXiv: 0709.4009.
- [2] F. Hibou et al., Phys. Lett. **B 438** (1998) 41; J. Smyrski et al., Phys. Lett. **B 474** (2000) 182; A. M. Bergdolt et al., Phys. Rev. **D 48** (1993) 2969; E. Chiavassa et al., Phys. Lett. **B 322** (1994) 270; H. Calén et al., Phys. Lett. **B 366** (1996) 39; H. Calén et al., Phys. Rev. Lett. **79** (1997) 2642; P. Moskal et al., Phys. Rev. **C 69** (2004) 025203; M. Abdel-Bary et al., Eur. Phys. J. **A 16** (2003) 127.
- [3] H. Calén et al., Phys. Rev. **C 58** (1998) 2667.
- [4] A. Moalem et al., Nucl. Phys. **A 600** (1996) 445. M. Batinić et al., Phys. Scripta **56** (1997) 321. J. F. Germond et al., Nucl. Phys. **A 518** (1990) 308. J. M. Laget et al., Phys. Lett. **B 257** (1991) 254. T. Vetter et al., Phys. Lett. **B 263** (1991) 153. B. L. Alvaredo et al., Phys. Lett. **B 324** (1994) 125. V. Bernard et al., Eur. Phys. J. **A 4** (1999) 259.
- [5] G. Fäldt and C. Wilkin, Phys. Scripta **64** (2001) 427.
- [6] K. Nakayama et al., Phys. Rev. **C 65** (2002) 045210.
- [7] K. Nakayama, private communication (2007).
- [8] R. Czyżykiewicz, P. Moskal et al., Phys. Rev. Lett. **98** (2007) 122003. R. Czyżykiewicz, P. Moskal et al., Int. J. Mod. Phys. **A22** (2007) 518. R. Czyżykiewicz, nucl-ex/0702010, PhD. Dissertation, Jagellonian University (2007).

- [9] F. Balestra et al., Phys. Rev. **C 69** (2004) 064003.
- [10] P. Moskal, M. Hodana et al., COSY Proposal No. 185 (2007).
- [11] H.-H. Adam et al., Proposal for WASA-at-COSY, nucl-ex/0411038.

INCLUSIVE DI-ELECTRON PRODUCTION IN C+C COLLISIONS WITH HADES

F. Dohrmann⁵, G. Agakishiev⁸, C. Agodi¹, A. Balanda^{3,e}, G. Bellia^{1,a},
D. Belver¹⁵, A. Belyaev⁶, A. Blanco², M. Böhmer¹¹, J. L. Boyard¹³,
P. Braun-Munzinger⁴, P. Cabanelas¹⁵, E. Castro¹⁵, S. Chernenko⁶,
T. Christ¹¹, M. Destefanis⁸, J. Díaz¹⁶, A. Dybczak³, T. Eberl¹¹,
L. Fabbietti¹¹, O. Fateev⁶, P. Finocchiaro¹, P. Fonte^{2,b}, J. Friese¹¹,
I. Fröhlich⁷, T. Galatyuk⁴, J. A. Garzón¹⁵, R. Gernhäuser¹¹, C. Gilardi⁸,
M. Golubeva¹⁰, D. González-Díaz⁴, E. Grosse^{5,c}, F. Guber¹⁰, M. Heilmann⁷,
T. Hennino¹³, R. Holzmann⁴, A. Ierusalimov⁶, I. Iori^{9,d}, A. Ivashkin¹⁰,
M. Jurkovic¹¹, B. Kämpfer⁵, K. Kanaki⁵, T. Karavicheva¹⁰, D. Kirschner⁸,
I. Koenig⁴, W. Koenig⁴, B. W. Kolb⁴, R. Kotte⁵, A. Kozuch^{3,e}, F. Krizek¹⁴,
R. Krücken¹¹, W. Kühn⁸, A. Kugler¹⁴, A. Kurepin¹⁰, J. Lamas-Valverde¹⁵,
S. Lang⁴, J. S. Lange⁸, L. Lopes², L. Maier¹¹, A. Mangiarotti², J. Marín¹⁵,
J. Markert⁷, V. Metag⁸, B. Michalska³, D. Mishra⁸, E. Morinière¹³,
J. Mousa¹², C. Müntz⁷, L. Naumann⁵, R. Novotny⁸, J. Otwinowski³,
Y. C. Pachmayer⁷, M. Palka⁴, Y. Parpottas¹², V. Pechenov⁸,
O. Pechenova⁸, T. Pérez Cavalcanti⁸, J. Pietraszko⁴, W. Przygoda^{3,e},
B. Ramstein¹³, A. Reshetin¹⁰, M. Roy-Stephan¹³, A. Rustamov⁴,
A. Sadovsky¹⁰, B. Sailer¹¹, P. Salabura³, A. Schmah⁴, R. Simon⁴,
S. Spataro⁸, B. Spruck⁸, H. Ströbele⁷, J. Stroth^{7,4}, C. Sturm⁷, M. Sudol⁴,
A. Tarantola⁷, K. Teilab⁷, P. Tlusty¹⁴, M. Traxler⁴, R. Trebacz³,
H. Tsertos¹², I. Veretenkin¹⁰, V. Wagner¹⁴, H. Wen⁸, M. Wisniowski³,
T. Wojcik³, J. Wüstenfeld⁵, S. Yurevich⁴, Y. Zanevsky⁶, P. Zumbach⁴

¹Istituto Nazionale di Fisica Nucleare - Laboratori Nazionali del Sud,
95125 Catania, Italy

²LIP-Laboratório de Instrumentação e Física Experimental de Partículas ,
3004-516 Coimbra, Portugal

³Smoluchowski Institute of Physics, Jagiellonian University of Cracow,
30-059 Kraków, Poland

⁴Gesellschaft für Schwerionenforschung mbH, 64291 Darmstadt, Germany

⁵Institut für Strahlenphysik, Forschungszentrum Dresden-Rossendorf,
01314 Dresden, Germany

⁶Joint Institute of Nuclear Research, 141980 Dubna, Russia

⁷Institut für Kernphysik, Johann Wolfgang Goethe-Universität, 60438
Frankfurt, Germany

⁸II.Physikalisches Institut, Justus Liebig Universität Giessen,
35392 Giessen, Germany

⁹Istituto Nazionale di Fisica Nucleare, Sezione di Milano, 20133 Milano,
Italy

¹⁰Institute for Nuclear Research, Russian Academy of Science,
117312 Moscow, Russia

¹¹Physik Department E12, Technische Universität München,
85748 München, Germany

¹²Department of Physics, University of Cyprus, 1678 Nicosia, Cyprus

¹³Institut de Physique Nucléaire d'Orsay, CNRS/IN2P3, 91406 Orsay
Cedex, France

¹⁴Nuclear Physics Institute, Academy of Sciences of Czech Republic,
25068 Rez, Czech Republic

¹⁵Departamento de Física de Partículas, University of Santiago de
Compostela, 15782 Santiago de Compostela, Spain

¹⁶Instituto de Física Corpuscular, Universidad de Valencia-CSIC,
46971 Valencia, Spain

^aAlso at Dipartimento di Fisica e Astronomia, Università di Catania,
95125 Catania, Italy

^bAlso at ISEC Coimbra, Coimbra, Portugal

^cAlso at Technische Universität Dresden, 01062 Dresden, Germany

^dAlso at Dipartimento di Fisica, Università di Milano, 20133 Milano, Italy

^eAlso at Panstwowa Wyzsza Szkola Zawodowa , 33-300 Nowy Sacz, Poland

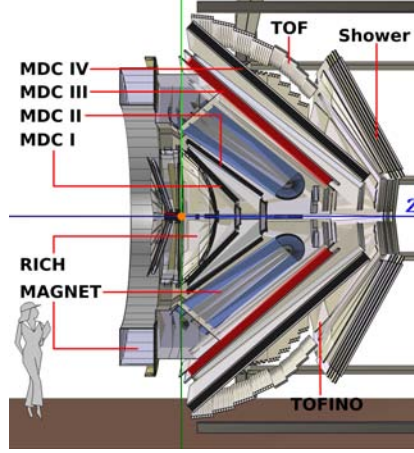
Abstract

Inclusive di-electron production in C+C collisions at 1 and 2 AGeV has recently been measured by the HADES collaboration at GSI. Results are compared to a di-electron cocktail calculated from free hadron (π^0 , η , ω) decays after freeze-out. For the low invariant masses, $M_{e^+e^-} < 0.15$ GeV/ c^2 , the measured distributions are largely explained by the $\pi^0 \rightarrow e^+e^-\gamma$ Dalitz decay but for higher masses experimental yields significantly exceed expectations.

1 HADES

The High-Acceptance DiElectron Spectrometer HADES at GSI, Darmstadt, uses direct probes, i.e. di-electronic decays of light vector mesons, ρ and ω , to investigate hadron properties inside a dense and nuclear medium. These properties are governed by non-perturbative QCD. Models predict,

Figure 1: Cross section of HADES, beam from the left. Detectors: Ring-Imaging Cherenkov (RICH, $\mathcal{O} \sim 1.6$ m) detector, tracking system (2 Mini-Drift Chambers (MDC-I, MDC-II) before, 2 (MDC-III, MDC-IV) behind the magnet), Time-Of-Flight wall (TOF/TOFino) and Pre-SHOWER detectors. A fast diamond start detector located upstream provides a time reference. Solid state targets as well as a liquid hydrogen target may be used [figure from [2]].



that hadron masses and/or lifetimes, depend on the temperature and density of the surrounding nuclear medium, such that a sizeable broadening or shifting of these resonances may be observed. The latter may be related to chiral symmetry restoration (cf. [1]).

HADES consists of a 6-coil toroidal magnet centered on the beam axis and six identical detection sectors located between the coils, covering polar angles between 18° and 85° , see Fig. 1. Details of the data acquisition, trigger, readout etc. as well as details, of the analysis, combinatorial background and systematical uncertainties are in [3].

2 Results on C+C collisions

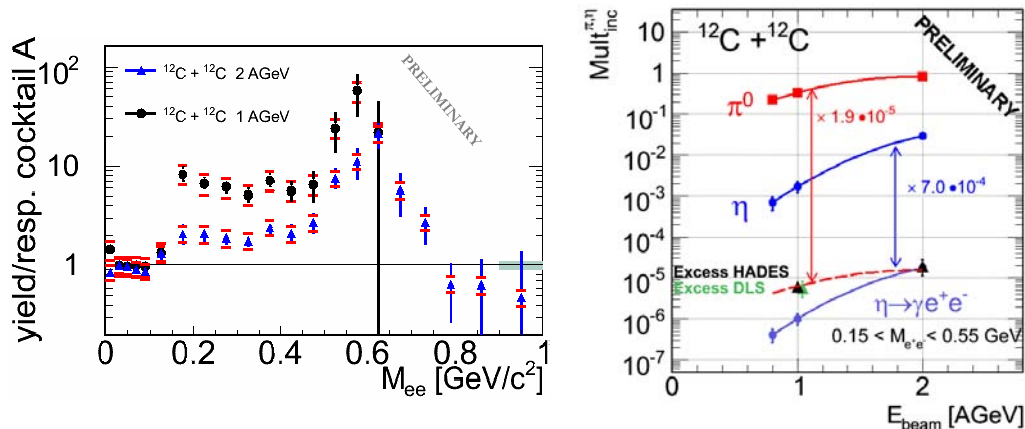


Figure 2: (left) Invariant mass distributions normalized to cocktail A for C+C data at 1 and 2 AGeV. (right) Excitation function of excess in the η region (see text).

The final result on the di-electron invariant mass distributions M_{ee} for 2 AGeV C+C (cf. [3]) included efficiency correction and normalization to the average number of charged pions. The pions were measured within the HADES acceptance and extrapolated to 4π , using measured angular distributions that are also in agreement with UrQMD calculations [4]. The pion multiplicity per number of participating nucleons $M_\pi/A_{part} = 0.137 \pm 0.015$ ($A_{part} = 9.0$) agrees with results from [5] within 11%. The combined systematic uncertainties yield roughly 18%. A pair cocktail (A) was calculated (cf. [3]) from free π^0 , η and ω meson decays, representing all contributions emitted after the chemical freeze-out of the fireball. The π^0 and η sources are constrained by data [5], the ω meson is taken from a m_\perp -scaling ansatz [6].

The HADES event generator PLUTO [7] modeled meson emission from a thermal source with a temperature $T = 80$ MeV, respecting the aforementioned anisotropic angular distributions for pions. While experimental data and the simulated cocktail A are in good agreement in the π^0 region, the cocktail underestimates the data for $M > 0.15$ GeV/ c^2 . Adding decays of short-lived resonances (as ρ , $\Delta(1232)$), excited in the early phase of the collision, will additionally contribute here and slightly improve the situation by populating also the higher-mass regions, but will eventually fail to reproduce the data as well. In Fig. 2 the ratio of the data and cocktail A is shown. In the intermediate mass range of $0.15 - 0.50$ GeV/ c^2 (η region), the enhancement factor above the dominant η contribution is $F(2.0) = 2.1 \pm 0.2(stat) \pm 0.3(sys) \pm 0.4(\eta)$. The third uncertainty (η) reflects the quoted uncertainty of the η multiplicity measured with TAPS [5].

The analysis of the 1 AGeV C+C run was performed on the same footing as for 2 AGeV, and is nearly completed. Compared to the 2 AGeV invariant mass spectrum the excess yield is more pronounced, cf. Fig. 2, the preliminary enhancement factor in the η region is $F(1.0) = 7.0 \pm 0.6(stat) \pm 1.1(sys) \pm 2.0(\eta)$. Here, the corresponding cocktail A (1 AGeV) was generated assuming $T=55$ MeV for freeze-out. Employing the η -yield by TAPS [5] at 1.04 and 2 AGeV the preliminary ratio of the absolute excess yields Y_{exc} in C+C reactions at both energies is: $Y_{exc}^{2AGeV}/Y_{exc}^{1AGeV} = 2.8 \pm 0.2(stat) \pm 1.0(sys) \pm 1.0(\eta)$. Note that the energy scaling of the excess yield follows that of pion production rather than that of η production (cf. [5]).

3 Summary

We discussed a comparison of di-electron invariant mass distributions for C+C 2 AGeV and 1 AGeV, the latter data being preliminary. Both data reveal a significant di-electron excess yield above a thermal pair cocktail from

long-lived mesons. We note that the excess for HADES (1 AGeV) is very similar to the excess reported by DLS for C+C at 1.04 AGeV [10]. The excess energy dependence is similar to that of pions. This hints at the importance of baryonic resonances for the origin of the excess yield, and also demonstrates the need of a systematic investigation of elementary reactions by HADES as input for (cf. [11]). Data on the heavier systems AA system (Ar+KCl) are currently being analyzed.

Acknowledgment

The collaboration gratefully acknowledges support by the following grants: BMBF 06MT238, 06GI146I, 06F-140, and 06DR135 (Germany); DFG cluster of excellence Origin and Structure of the Universe (www.universe-cluster.de); GSI (TM-FR1; GI/ME3,OF/STR), GA CR 202/00/1668 and MSMT LC7050 (Czech Republic); KBN 1P03B 056 29 (Poland); INFN (Italy); CNRS/IN2P3 (France); MCYT FPA2000-2041-C02-02 and XUGA PGID T02PXIC20605PN (Spain); UCY-10.3.11.12 (Cyprus); INTAS grant 03-51-3208, and EU contract RII3-CT-2004-506078.

References

- [1] R. Rapp and J. Wambach, *Adv. Nucl. Phys.* **25**, 1 (2000).
- [2] B. Bannier, Diploma thesis, Technical University Dresden 2007.
- [3] G. Agakichiev et al., *Phys. Rev. Lett.* **98**, 052302 (2007).
- [4] S. A. Bass *et al.*, *Prog. Part. Nucl. Phys.* **41**, 255 (1998).
- [5] R. Auerbeck et al., *Z. Phys. A* **359**, **65** (1997), R. Holzmann et al., *Phys. Rev. C* **56**, R2920 (1997), C. Sturm et al., *Phys. Rev. Lett.* **86**, 39 (2001).
- [6] E. L. Bratkovskaya, W. Cassing, and U. Mosel, *Phys. Lett. B* **424**, 244 (1998).
- [7] I. Fröhlich *et al.*, PoS ACAT:076 (2007), arXiv:0708.2382.
- [8] C. Ernst et al., *Phys. Rev. C* **58**, 447 (1998).
- [9] Y. C. Pachmayer, PhD thesis in preparation, University of Frankfurt.
- [10] R. J. Porter et al., *Phys. Rev. Lett.* **79**, 1229 (1997).
- [11] I. Fröhlich et al., these proceedings.

CHARMONIUM EXCITED STATES FROM LATTICE QCD

J. Dudek^{*,%}, R. G. Edwards[%], N. Mathur^{%¹}, D. Richards^{%²}

^{*}Old Dominion University, Norfolk, VA 23529, USA

[%]Jefferson Laboratory, Newport News, VA 23606, USA

Abstract

We apply the variational method with a large basis of interpolating operators to demonstrate the feasibility of extracting multiple excited states in charmonium from lattice QCD. The calculation is performed in the quenched approximation to QCD, using the clover fermion action on an anisotropic lattice. A crucial element of our approach is a knowledge of the continuum limit of the interpolating operators, providing important additional information on the spin assignment of the states, even at a single value of the lattice spacing. Though we find excited-state masses that are systematically high with respect to the quark potential model, and the experimental masses where known, we attribute this as most likely an artifact of the quenched approximation.

1 Introduction

Interest in the charmonium system has been rekindled by the wealth of new experimental results, with the promise of yet more at future facilities. For the lattice community, the charmonium system is not only fascinating in its own right, but an important theater in which to hone our skills for studies of light-quark systems, such as the search for the photoproduction of exotic mesons by the GlueX Collaboration at the future 12 GeV upgrade of Jefferson Laboratory. These motivations have spurred us to pursue a program of investigations of charmonium [1, 2]. In this talk, I will describe our recent efforts aimed at extracting the resonance spectrum in charmonium, including states with exotic quantum numbers [3], as a precursor to investigating their properties. I will conclude this introduction with a description of how the spectrum is determined from a lattice calculations, before proceeding to our results and discussion.

¹Current address: Dept. of Theoretical Physics, Tata Institute of Fundamental Research, Mumbai 400005, India

²Speaker, E-mail address: dgr@jlab.org

1.1 Excited states and lattice QCD

The spectrum in Euclidean-space lattice QCD is obtained by measuring time-sliced correlation functions between interpolating operators \mathcal{O}_i and \mathcal{O}_j :

$$C_{ij}(t) = \sum_{\mathbf{x}} \langle 0 | \mathcal{O}_i(\mathbf{x}, t) \mathcal{O}_j^\dagger(0) | 0 \rangle \quad (1)$$

We now use the resolution of unity to insert a complete set of states between the two operators. The effect of the time-sliced sum in 1 is to put the intermediate states at rest, and we obtain

$$C_{ij}(t) = \sum_{\alpha} \frac{Z_i^{\alpha*} Z_j^{\alpha}}{2M_{\alpha}} e^{-M_{\alpha} t} \quad (2)$$

where the sum is over all states having non-zero overlap factors $Z_{i,j} = \langle \alpha | \mathcal{O}_{i,j}^\dagger | 0 \rangle$. We delineate the states contributing through the variational method [4,5], by finding the eigenvalues $\lambda_1 > \lambda_2 > \dots$ of $C^{-1/2}(t_0)C(t)C^{-1/2}(t_0)$, which satisfy

$$\lambda_{\alpha}(t, t_0) = e^{-M_{\alpha}(t-t_0)} (1 + \mathcal{O}(e^{-\Delta M_{\alpha}(t-t_0)})),$$

where ΔM_{α} is the minimum absolute energy difference between α and any other state.

The effectiveness of the method depends on a suitable basis of interpolating operators, which must be constructed so as to lay in given irreducible representations of the symmetry group; we use an extension of those in ref. [6]. For states at rest, their symmetry properties on a cubic lattice are classified according to the irreducible representations of the cubic group, with full rotational symmetry recovered only in the continuum limit. The irreps. Λ , their dimension d_{Λ} , and their continuum content, are as follows:

Λ	d_{Λ}	J
A_1	1	0, 4, 6, ...
A_2	1	3, 6, 7, ...
E	2	2, 4, 5, ...
T_1	3	1, 3, 4, ...
T_2	3	2, 3, 4, ...

Each irrep. acquires additional subscripts associated with parity (P) and charge conjugation (C). Within a given irrep., the spectrum contains energies corresponding to each of the continuum angular momenta listed above. Thus, for example, the T_1^{-+} channel contains energies corresponding not only to spin 1, but also to spins 3, 4 and higher.

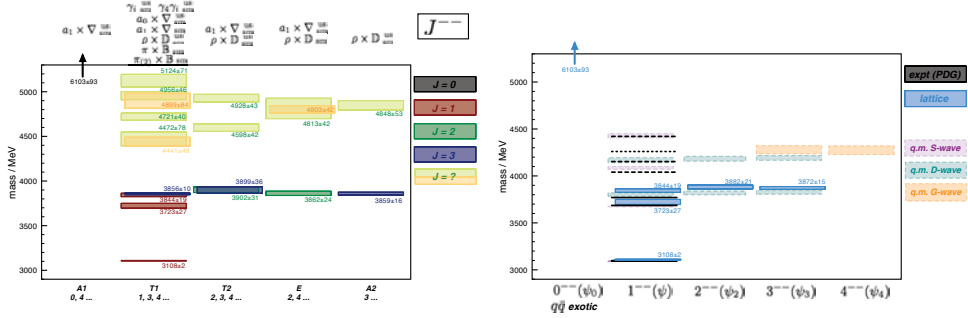


Figure 1: The left-hand figure shows the spectrum according to the lattice irreps., with color coding indicating our spin assignments. The right-hand figure shows the spectrum after the continuum spin assignments, together with quark-model expectations and the experimental values, where known.

The implicit assumption in most calculations is that the lightest state in a given irrep. corresponds to the state of lowest spin. The classical way of identifying a spin is to observe continuum degeneracies between the energies in the different lattice irreps. a procedure requiring the calculation be performed at several lattice spacings; thus a spin-4 state should have degenerate energies in the continuum limit between the E , T_1 and T_2 irreps.. An important realization in ref. [3], which we exploit below, is that a knowledge of the continuum form of the overlaps of operators is an important additional source of information that can aid the identification of the spin.

2 Results

We work in the quenched approximation to QCD, using an anisotropic action with temporal and spatial inverse lattice spacings $a_t^{-1} \simeq 6$ GeV and $a_s^{-1} \simeq 2$ GeV respectively. Beginning with the $J^{PC} = J^{--}$ sector, we show in Figure 1 the spectrum, together with the spin assignments using the methods outlined above. Our ability to perform such a precise extraction of the low-lying excited states is very encouraging, though the masses are high with respect to quark potential model predictions and, where they exist, experiment, which we attribute to the use of the quenched approximation.

Particularly intriguing is the J^{++} channel, where our analysis admits two equally plausible spin assignments, shown in Figure 2. In particular, we cannot assert whether the lowest-lying energy in the T_1^{-+} channel corresponds to the exotic 1^{-+} , or the non-exotic 4^{-+} , and consequently whether the lightest exotic is around 4300 MeV, or around 4700 MeV.

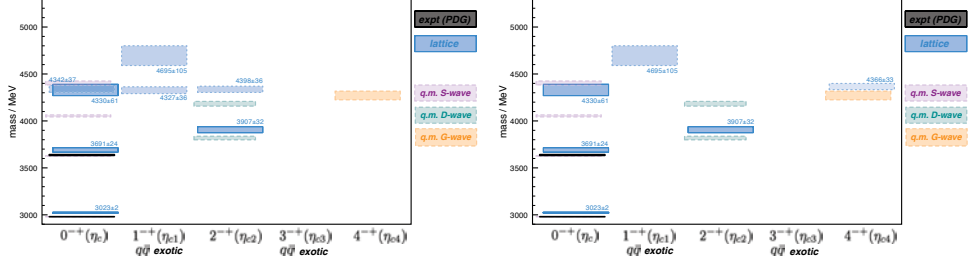


Figure 2: The left- and right-hand panels show the two possible continuum spin assignments in the J^{-+} channel.

We have shown how the variational method, exploiting the continuum behavior of the operators, greatly aids the identification of the continuum spins. Future work will focus on studies at a finer lattice spacing, to better resolve the continuum spin assignments in the T_1^{-+} channel, and on calculations employing 2 and 3 flavors of sea quarks.

Acknowledgments: This work was supported by DOE contract DE-AC05-06OR23177 under which the Jefferson Science Associates, LLC operates the Thomas Jefferson National Accelerator Facility.

References

- [1] J.J. Dudek, R.G. Edwards, D.G. Richards, Phys. Rev. **D73**, 074507 (2006), [hep-ph/0601137](#)
- [2] J.J. Dudek, R.G. Edwards, Phys. Rev. Lett. **97**, 172001 (2006), [hep-ph/0607140](#)
- [3] J.J. Dudek, R.G. Edwards, N. Mathur, D.G. Richards (2007), [arXiv:0707.4162 \[hep-lat\]](#)
- [4] C. Michael, Nucl. Phys. **B259**, 58 (1985)
- [5] M. Luscher, U. Wolff, Nucl. Phys. **B339**, 222 (1990)
- [6] X. Liao, T. Manke (2002), [hep-lat/0210030](#)

MESONIC INTERACTIONS AND THEIR CONTRIBUTION TO STRONG PHASES IN FLAVOR PHYSICS

B. El-Bennich^{*1}, A. Furman[†], R. Kamiński[‡], L. Leśniak[‡], B. Loiseau^{*} and
B. Moussallam[§]

^{*} LPNHE (IN2P3-CNRS, Universités Paris 6 et 7) Énergies, Groupe
Théorie, Université Pierre et Marie Curie, 75252 Paris, France

[†] ul. Bronowicka 85/26, 30-091 Kraków, Poland

[‡] Division of Theoretical Physics, The Henryk Niewodniczański Institute of
Nuclear Physics, Polish Academy of Sciences, 31-342 Kraków, Poland

[§] Institut de Physique Nucléaire, Université Paris-Sud, 91406 Orsay, France

Abstract

We analyze the contributions of hadronic final-state interactions to the strong phases generated in the $B \rightarrow K\pi\pi$ weak decays. To this end, we develop an alternative approach, based upon scalar and vector form factors for $\pi\pi$ and πK interactions, to the commonly employed isobar model.

1 Preliminary remarks

An accurate and unequivocal knowledge of strong phases in weak decay amplitudes is crucial to any precision test of CP -violating observables. Yet, in heavy meson decays, the decay amplitude is still stricken with hadronic uncertainties. This comprises form factors and subleading contributions such as annihilation amplitudes as well as mesonic final-state interactions. Here, we concentrate on the latter hadronic contribution; in particular, we investigate the effects of pion-pion and pion-kaon interactions motivated by recent experimental data on $B \rightarrow K\pi\pi$ decays [1–5]. *Direct CP* violation in $B \rightarrow \rho(770)^0 K, \rho(770)^0 \rightarrow \pi^+\pi^-$ decays was discovered recently [2, 3]. The three-body decays are commonly analyzed within the isobar model. Several resonances are observed in the experimental effective $\pi\pi$ and πK mass distributions. We point out the $f_0(980)$ and $\rho(770)^0$, which we recently treated in detail (as well as their interesting interference effects) [6], and the $K^*(892)$ and $K_0^*(1430)$ which this contribution deals with.

¹E-mail address: bruno.elbennich@lpnhe.in2p3.fr

2 Long-distance form factors in weak decays

We assume that QCD factorization is applicable in the kinematical configuration in which one pion and the kaon form a quasi collinear pair in the B center of mass frame, where their interaction with the second pion emitted in backward direction is suppressed. Thus, we derive weak decay amplitudes for a quasi two-body state following Beneke and Neubert [7]. These amplitudes are given by the product of two factorized currents to which non-factorizable radiative corrections resumable to all orders in $\alpha_s(\mu)$ can be added. The subsequent creation of a two-pion or a pion-kaon pair in an S - or P -wave from vacuum is mediated by one of the currents, namely $\langle(\pi\pi)_{S,P}|\gamma_\mu(1-\gamma_5)|0\rangle$ or $\langle(\pi K)_{S,P}|\gamma_\mu(1-\gamma_5)|0\rangle$, and accordingly described by appropriate scalar or vector form factors which depend on the relative angular momentum and isospin. They can be derived from unitary coupled-channel equations constrained by chiral perturbation theory and experimental data on either $\pi\pi$ or πK phase shifts and inelasticities via dispersion relations.

In the following, we shall concentrate on the case of $(\pi K)_{S,P}$ final-state interactions. In the πK mass range below 2 GeV, the resonances $K^*(892)$ and $K_0^*(1430)$ dominate the πK vector and scalar form factors, respectively. Here, the $B \rightarrow K\pi\pi$ decay amplitudes contain two contributions, one being the QCD factorization amplitudes of weak $b \rightarrow s\bar{d}d$ or $b \rightarrow s\bar{u}u$ transitions previously mentioned, the other a phenomenological long-distance amplitude with either a c - or u -quark in the loop of the corresponding penguin topology² [8]. The S -wave part of the $B^- \rightarrow (K^-\pi^+)_S\pi^-$ decay amplitude reads

$$\begin{aligned}
A_S &= \frac{G_F}{\sqrt{2}}(M_B^2 - m_\pi^2)\frac{m_K^2 - m_\pi^2}{q^2} F_0^{B \rightarrow \pi}(q^2) f_0^{K^-\pi^+}(q^2) \times \\
&\times \left\{ \lambda_u(a_4^u + P_u - a_{10}^u/2) + \lambda_c(a_4^c + P_c - a_{10}^c/2) - \right. \\
&\left. - \frac{2q^2}{(m_b - m_d)(m_s - m_d)} [\lambda_u(a_6^u + S_u - a_8^u/2) + \lambda_c(a_6^c + S_c - a_8^c/2)] \right\}
\end{aligned} \tag{1}$$

while the P -wave amplitude is given by

$$\begin{aligned}
A_P &= 2\sqrt{2}G_F \mathbf{p}_{\pi^-} \cdot \mathbf{p}_{\pi^+} F_1^{B \rightarrow \pi}(q^2) f_1^{K^-\pi^+}(q^2) \times \\
&\times [\lambda_u(a_4^u + P_u - a_{10}^u/2) + \lambda_c(a_4^c + P_c - a_{10}^c/2)].
\end{aligned} \tag{2}$$

Here, q^2 is the effective $K^-\pi^+$ mass squared, $F_{0,1}^{B \rightarrow \pi}(q^2)$ is the scalar/vector $B \rightarrow \pi$ transition form factor and $f_{0,1}^{K^-\pi^+}(q^2)$ denotes the scalar/vector $K^-\pi^+$

² also called charming penguins in the case of long-distance c -loops which, close to on-shell, may be associated with intermediate $D_s^{(*)}D^{(*)}$ states.

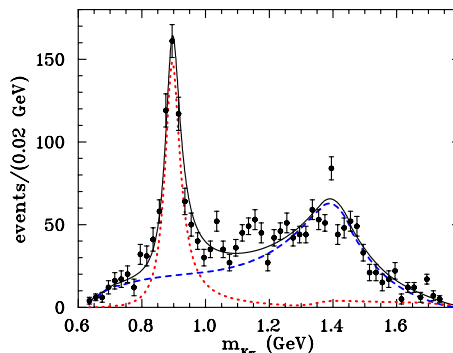


Figure 1: Average $K\pi$ effective mass distributions for $B^\pm \rightarrow K^\pm\pi^\mp\pi^\pm$ decays. The dashed line corresponds to the S -wave, the dotted line to the P -wave and the solid one to the total amplitude. The data are from [3].

form factor. The $a_i^{u,c}$ are combinations of short-distance Wilson coefficients and the λ_i are products of CKM matrix elements (see Ref. [6] for details). The long-distance penguin amplitudes are parameterized by four complex parameters S_u, S_c, P_u and P_c .

3 Results & Conclusions

We are concerned with the four decays $B^\pm \rightarrow K^\pm\pi^\mp\pi^\pm$, $\bar{B}^0 \rightarrow \bar{K}^0\pi^-\pi^+$ and $B^0 \rightarrow K^0\pi^+\pi^-$ and the corresponding experimental data by the Belle and BaBar collaborations [2–5]. The body of available experimental data comprises two-body branching fractions and CP -violating asymmetries as well as 285 data points for the $K\pi$ effective mass and helicity angle distributions. The QCD factorization amplitudes, despite additional strong amplitudes and phases generated by the scalar and vector form factors, do not reproduce the experimental branching fractions. In fact, the theoretical values are too small by a factor spanning from 2.3 to 3.6 if charming penguin amplitudes are not included. This agrees with the recent calculations by Cheng, Chua and Soni [9]. We note that annihilation topologies, for which thus far no complete calculation exists, are not accounted for in this work. Including their contributions introduces a parametrization similar to the charming penguin one, though a different scale sub-leading in Λ_{QCD}/m_b is involved.

In Fig. 1, we present some preliminary results on $K\pi$ effective mass distributions and in Fig. 2 their $\pi\pi$ counterpart obtained previously [6] for comparison's sake. In both cases, charming penguin amplitudes are necessary to reproduce the data. The theoretical curves describe the data structure very well. With the appropriate $\pi\pi$ and πK mass ranges, we may integrate over these distributions and obtain branching fractions for $B \rightarrow f_0(980)K$,

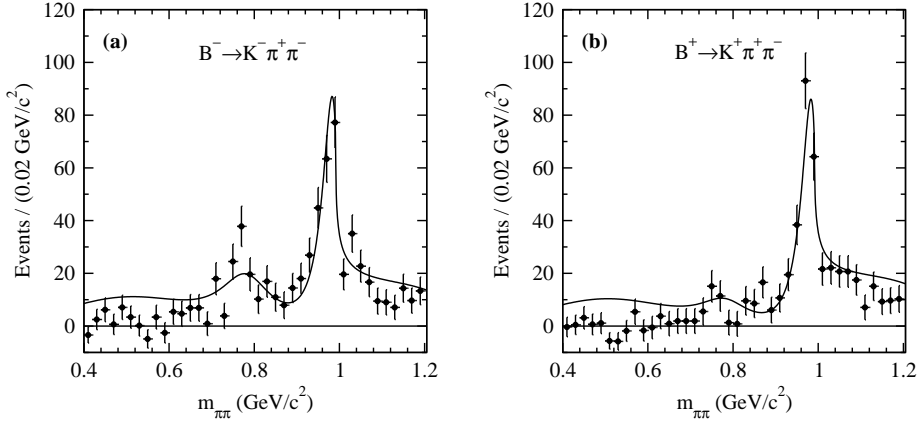


Figure 2: $\pi\pi$ effective mass distributions for $B^- \rightarrow K^- \pi^+ \pi^-$ and $B^+ \rightarrow K^+ \pi^+ \pi^-$ decays; the data are taken from [1]. Note that CP violation is well visible in the $\rho(770)^0$ mass range.

$B \rightarrow \rho(770)^0 K$, $B \rightarrow K^*(892)\pi$ and $B \rightarrow K_0^*(1430)\pi$. However, extracting information on two-body decay rates involving the scalar resonance from these data, requires a careful treatment. In our approach, the final-state interactions are treated using exact relations with well measured scattering phase-shifts. The separation between background and resonance contributions is then performed in a rigorous way, using analyticity properties of the form-factors involved and the fact that a resonance can be associated with a complex pole in the scattering matrix and in the form-factors.

Acknowledgments

This work was supported by the IN2P3-Polish Laboratories Convention (Project No. CSI-12) and the CNRS-Polish Academy of Science agreement (Project No. 19481). B. E. benefitted from the Marie Curie Grant No. 516228.

References

- [1] K. Abe *et al.* [Belle Collaboration], hep-ex/0509001 (2005).
- [2] B. Aubert *et al.* [BaBar Collaboration], *Phys. Rev.* **D72**, 072003 (2005).
- [3] A. Garmash *et al.* [Belle Collaboration], *Phys. Rev. Lett.* **96**, 251803 (2006).
- [4] ÉA. Garmash *et al.* [Belle Collaboration], *Phys. Rev.* **D75** 012006 (2007).

- [5] B. Aubert *et al.* [BaBar Collaboration], *Phys. Rev.* **D73** 031101(R) (2006).
- [6] B. El-Bennich, A. Furman, R. Kamiński, L. Leśniak and B. Loiseau, *Phys. Rev.* **D74**, 114009 (2006).
- [7] M. Beneke and M. Neubert, *Nucl. Phys.* **B675**, 333 (2003).
- [8] M. Ciuchini, E. Franco, G. Martinelli and L. Silvestrini, *Nucl. Phys.* **B501**, 271 (1997).
- [9] H.-Y. Cheng, C.-K. Chua and A. Soni, *Phys. Rev.* **D76**, 094006 (2007).

IN PURSUIT OF NEW PHYSICS WITH K^+ SCATTERING ON NUCLEI AT INTERMEDIATE ENERGY

S.M. Eliseev

Bogoliubov Laboratory of Theoretical Physics,
Joint Institute for Nuclear Research, 141980 Dubna, Russia

Abstract

A new model (*a la* Glauber) for hadron–nuclei interaction at intermediate energy (IE) is proposed. We utilized the principal assumptions as in the approaches of others authors describing (in the framework of the models without QGP) J/Ψ suppression in nuclear collisions at high energy. Yet, a number of new ingredients (noneikonal corrections, correlations of nucleons in the nuclei, *etc.*) are introduced. We show that experimental data on the cross sections of K^+ –nuclei interaction at IE cannot be described by the well-elaborated Glauber model. In comparison with other authors, the model improves the agreement between theory and data but remains the "window" for some "exotics". (These results have been obtained without fitting any new parameters.) The nature of that "exotics" (mass reduction, or "swelling", *etc.*) will be discussed later.

1 Introduction

The contemporary theory of strong interaction-Quantum Chromodynamics (QCD) predicts, that *at high nuclear density* a new state of matter (quark-gluon plasma-QGP) will be formed. One of the principal motivations for the ultrarelativistic heavy ion experiments is the study of the signals of the existence of QGP. In this new stage of matter deconfinement of quark takes place and hadron masses are reduced to zero (restoration of chiral symmetry takes place). However, chiral symmetry is partially restored in medium, for example, in nuclei, *i.e.*, below the critical density. Reduction of hadron masses in medium has been predicted as an effect of partial restoration of chiral symmetry in nuclear matter. In the last years a lot of theoretical and experimental work has been devoted to the search of a signals of such anomalous properties of hadrons in the nuclear environment (in-medium effects) [1–5].

At the same time, the problem of the investigation of the changing of masses of particles is rather complicated. In that situation it is helpful to attack the discussed problem by studying different nuclear reactions, to find others occasions without doubt.

2 The model

Following Glauber [6] the amplitude for a projectile-target elastic scattering, assumes the general form:

$$f(\mathbf{q}) = \frac{ik}{2\pi} \int e^{2i\mathbf{q}\cdot\mathbf{b}} \Gamma(\mathbf{b}) d\mathbf{b}, \quad \Gamma(\mathbf{b}) = 1 - e^{2i\chi(\mathbf{b})} = \frac{1}{2\pi ik} \int e^{-i\mathbf{q}\cdot\mathbf{b}} f(\mathbf{q}) d\mathbf{b} \quad (1)$$

$$\chi_N(\mathbf{b}, \mathbf{r}_1, \dots, \mathbf{r}_A) = \sum_{j=1}^A \chi_j(\mathbf{b} - \mathbf{s}_j), \quad \Gamma_N(\mathbf{b}, \mathbf{r}_1, \dots, \mathbf{r}_A) = 1 - e^{2i\chi_N(\mathbf{b}, \mathbf{r}_1, \dots, \mathbf{r}_A)} \quad (2)$$

where b is the impact parameter, and χ is the corresponding phase shift function. More explicitly, for projectile-nucleus scattering, Eq.(1) can be cast into the form:

$$F(\mathbf{q}) = \frac{ik}{2\pi} \int e^{i\mathbf{q}\cdot\mathbf{b}} \langle |\Gamma_N(\mathbf{b}, \mathbf{r}_1, \dots, \mathbf{r}_A)| \rangle d\mathbf{b}, \quad (3)$$

where \mathbf{s}_j is a component of the radius-vector \mathbf{r}_j of the j^{th} target-nucleon in the direction perpendicular to the incident momentum \mathbf{k} , while the brackets $\langle \rangle$ denote the target ground-state average. The parameters of kaon-nucleon amplitudes were taken from the well-known Martin phase shifts [7].

Further, given the corresponding projectile-target nucleon amplitudes $f(q)$, one can express the above projectile-target nucleus amplitude in the **parameter-free** way. It is then a straightforward matter to determine the total cross section for the case of K^+ -target nucleus scattering according to the optical theorem. The total and reaction cross sections may then be approximated by

$$\sigma_t = 4\pi \int_0^\infty \text{Re}[1 - e^{i\chi(b)}] b db, \quad \sigma_r = 2\pi \int_0^\infty [1 - e^{-2\text{Im}\chi(b)}] b db, \quad (4)$$

where $\chi(b)$ is the nuclear phase shift function. For scattering in the case when the potential is spherically symmetrical, an eikonal expansion of $\chi(b)$ is given by S.J. Wallace [8] in the form:

$$\chi(b) = \sum_n \frac{\mu^{n+1}}{k(n+1)!} \left(\frac{b}{k^2} \frac{\partial}{\partial b} - \frac{\partial}{\partial k} \frac{1}{k} \right)^n \int_{-\infty}^{\infty} V^{n+1}(r) dz, \quad (5)$$

$$V(r) = \frac{2\pi i}{\mu} f(0) \rho(r), \quad (6)$$

where $\rho(r)$ is the nuclear density and $f(0)$ is the average forward scattering amplitude of kaon interaction with moving intranuclear nucleons. The Fermi momentum distribution of nucleons was taken from newly experimental data. The calculation was performed by Monte Carlo method. (For detail see Ref. [9]).

3 Results and outlook

To examine the nuclear interior, the K^+ -meson at IE is regarded as a unique probe due to its long mean free-path in the nuclear matter.

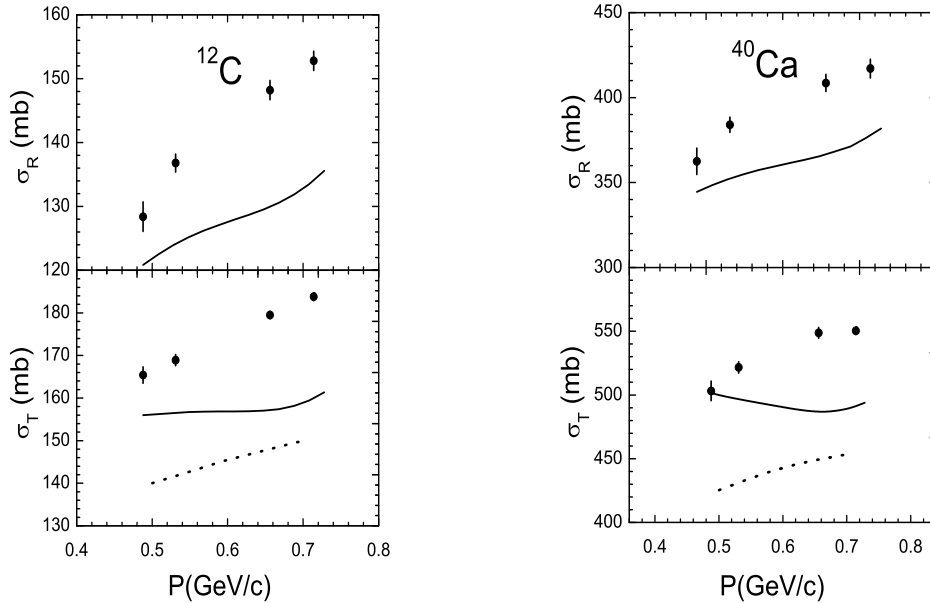


Figure 1: The calculated and experimental total and reaction cross sections for K^+ - meson interaction with nuclei vs. kaon momentum. The solid lines denote the prediction of our model. The experimental data are from Ref. [10] The dotted lines demonstrate the theoretical results of Ref. [11]

A detailed analysis of the cross sections of K^+ - nuclei interactions at IE is presented. We can see that our calculated cross sections for K^+ meson interactions fail to describe the experimental data. It seen an universal discrepancy between the theoretical models and data for particles (K^+ -mesons) interacting in deep regions of the nucleus. (It worth noticing that our results have been obtained without fitting any new parameters.) In comparison with other authors, the model improves the agreement between theory and data but remain the "window" for some "exotics". The nature of that "exotics" (mass reduction, or "swelling", *etc.*) will be discussed latter. The discrepancy between calculations and data on K^+ - nuclei scattering my be regarded as one of more probable signal of new physics in nuclear collisions. (It is just the contrary what was obtained by many authors for J/Ψ suppression in relativistic nuclei collision and color transparency). In conclusion, our model can be used to resolve puzzling discrepancy of theory and data on pion-nuclei collision at IE (see, *e.g.*, Ref. [4]).

References

- [1] G.E. Brown *et al.*, *Phys. Rev. Lett.* **60**, 2723 (1988).
- [2] A. Gal, E. Friedman, *Phys. Rev. Lett.* **94**, 072301 (2005).
- [3] A. Gal, E. Friedman, *Phys. Rev.* **C73**, 015208 (2006).
- [4] E. Friedman and A. Gal, arXiv:nucl-th/0705.3965v2 Aug 07 2007.
- [5] E. Oset *et al.*, arXiv:nucl-th/0702022v1 Feb 07 2007.
- [6] R.J. Glauber, Theory of high-energy scattering, in *Lectures in Theoretical Physics*, ed. W.E. Brittin and L.G. Dunham, (Interscience Publishers, Inc., New York, 1959) p. 315.
- [7] B.R. Martin, *Nucl. Phys.* **B94** 413 (1975).
- [8] S.J. Wallace, *Ann. Phys. (N.Y.)* **78**, 190 (1973).
- [9] S.M. Eliseev and T.H. Rihan, *Phys. of At. Nucl.* **60**, 918 (1997).
- [10] A.Gal, *Nucl. Phys.*, **A639**, 485c (1998).
- [11] M.F. Jiang *et al.*, *Phys. Rev.* **C51**, 857 (1995).

LATEST HERMES RESULTS ON TRANSVERSE SPIN IN HADRON STRUCTURE AND FORMATION

*R. Fabbri*¹,
on behalf of the HERMES Collaboration
DESY, 22607 Hamburg, Germany

Abstract

Preliminary experimental results from measurements of single-spin asymmetries for single pions and kaons, and for pion pairs in deep-inelastic scattering (DIS) with transverse target polarization are presented. These results provide sensitivity to the transverse polarization and orbital angular momentum of quarks in the nucleon.

1 Introduction

At leading twist, neglecting the transverse momentum, the longitudinal momentum and spin of the quarks in the nucleon are described by three parton distribution functions (PDFs): the well-known momentum distribution, the known helicity distribution, and the up-to-now poorly known transversity distribution. These quantities depend only on the Bjorken variable x and on the scale Q^2 . In the helicity basis, transversity is related to the quark-nucleon forward scattering amplitude involving helicity flip of both nucleon and quark. Being chiral-odd, transversity can be investigated only in observables that involve an additional chiral-odd quantity, e.g., in single-spin cross section asymmetries (SSA) in semi-inclusive DIS electroproduction (SIDIS) of single hadrons or hadron pairs on transversely polarized hadrons. Including the transverse momentum of quarks additional PDFs appear. A prominent example is the Sivers function [2] which requires a non-zero quark orbital angular momentum for its existence.

In 2002-05 the HERMES collaboration [1] took data using a gaseous transversely polarized hydrogen target (with an average polarization of $\approx 74\%$) internal to the 27.6 GeV HERA positron or electron beam. The HERMES dual-radiator ring-imaging Čerenkov detector allowed full π^\pm , K^\pm and p identification for particle momenta between 2 and 15 GeV.

¹e-mail: Riccardo.Fabbri@desy.de

2 SSA in single-hadron production

In semi-inclusive electroproduction of hadrons on a transversely polarized nucleon target with an unpolarized lepton beam a single-spin asymmetry A_{UT} in the azimuthal angles around the virtual-photon direction can arise. These angles, measured with respect to the lepton scattering plane, are the azimuthal angle ϕ of detected hadrons and the azimuthal angle ϕ_S of the target transverse polarization direction. The Collins and the Sivers mechanisms [2] have been identified as potential sources of the asymmetry. In the Collins mechanism, the asymmetry arises from the correlation between the transverse polarization of the fragmenting struck quark and the transverse momentum $P_{h\perp}$ of the produced hadron. In the Sivers mechanism, the asymmetry results from an intrinsic transverse momentum asymmetry of the quarks in the target nucleon. A non-zero Sivers function would require a non-zero orbital angular momentum of quarks in the nucleon [2].

In the measured SSA, transversity appears convoluted with the Collins function with the angular modulation $\sin(\phi + \phi_S)$, while the Sivers function appears with the $\sin(\phi - \phi_S)$ modulation. The Collins $2\langle \sin(\phi + \phi_S) \rangle_{UT}^h$ and Sivers $2\langle \sin(\phi - \phi_S) \rangle_{UT}^h$ azimuthal amplitudes are extracted simultaneously through a fit of the measured cross section asymmetry:

$$\begin{aligned} A_{UT}^h(\phi, \phi_S) &= \frac{\sigma_h^\uparrow(\phi, \phi_S) - \sigma_h^\downarrow(\phi, \phi_S)}{\sigma_h^\uparrow(\phi, \phi_S) + \sigma_h^\downarrow(\phi, \phi_S)} \\ &= 2\langle \sin(\phi + \phi_S) \rangle_{UT}^h \sin(\phi + \phi_S) + 2\langle \sin(\phi - \phi_S) \rangle_{UT}^h \sin(\phi - \phi_S), \end{aligned} \quad (1)$$

where h represents the detected hadron, and the symbol \uparrow (\downarrow) is the target spin state. The dependence on x , the fractional hadron energy z , and on $P_{h\perp}$ of the extracted Collins and Sivers amplitudes is shown in Fig. 1 for charged pions and kaons. Compared to the previous publication [1], these results are based on nearly five times more statistics.

The Collins amplitudes are found positive for π^+ and negative for π^- . Assuming u -quark dominance, the large negative π^- amplitude on the proton is rather interesting, suggesting a substantial disfavoured Collins function with a sign opposite to that of the favoured Collins function. For charged kaons no significantly non-zero Collins amplitude is found. The extracted non-zero Collins amplitude for pions implies a non-zero transversity distribution and a non-vanishing Collins function. Recently, using the previously published HERMES data [1] in combination with data from COMPASS and BELLE, the first ever model-dependent extraction of the transversity distributions for up and $down$ quarks has been performed [3].

The Sivers amplitudes are found to be significantly positive for both π^+ and K^+ , implying a non-zero orbital angular momentum for quarks in the

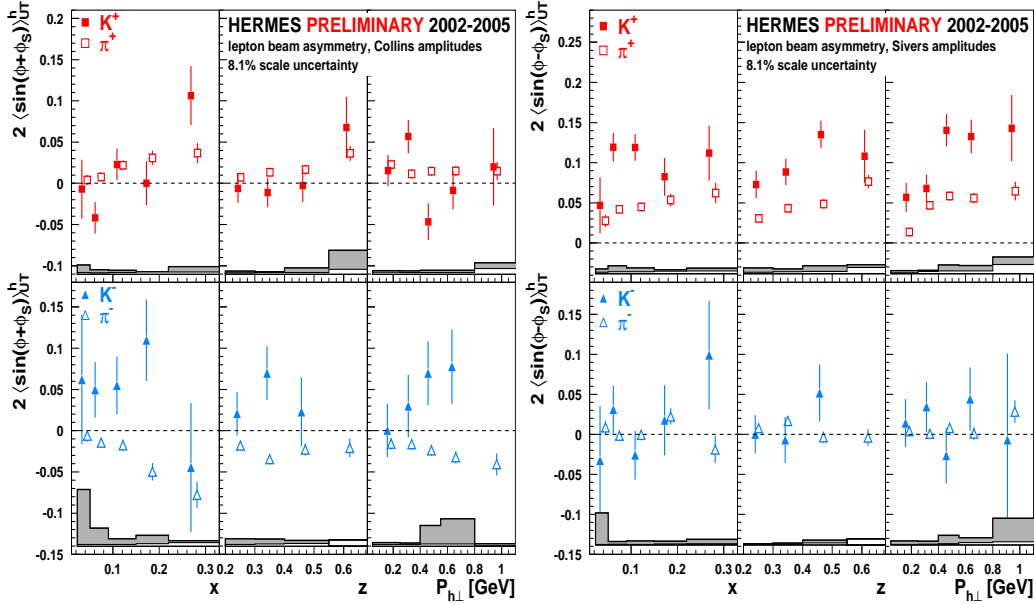


Figure 1: Kinematic dependencies of the extracted Collins (left panels) and Sivers (right panels) amplitudes for single charged pions and kaons on transversely polarized hydrogen target. Systematic uncertainties are shown by shaded bands.

nucleon. The large amplitude for K^+ suggest an important role of sea quarks. For negative pions and kaons the Sivers amplitude is consistent with zero.

3 Transversity in pion-pair production

An independent experimental constraint on transversity could be provided by analysing the SSA in semi-inclusive electroproduction of $\pi^+\pi^-$ pairs on a transversely polarized target [4]. The underlying mechanism is the transfer of the transverse spin of the fragmenting quark to the relative orbital angular momentum of the produced hadron pair. Consequently, this mechanism does not require transverse momentum of the pair. In this process transversity appears with the up-to-now unknown dihadron fragmentation function describing the interference between pion pairs in S - and P -wave.

The amplitude that involves transversity and the above mentioned interference fragmentation function, extracted in the HERMES kinematics, is shown in Fig. 2 versus the invariant mass of the pion pair $M_{\pi\pi}$. The presented data were accumulated during the 2002-04 running period using the positron beam and the transversely polarized hydrogen target. The signal is non-zero in the whole analyzed kinematics implying, for the first time, a non-zero two-pion interference fragmentation function sensitive to transverse

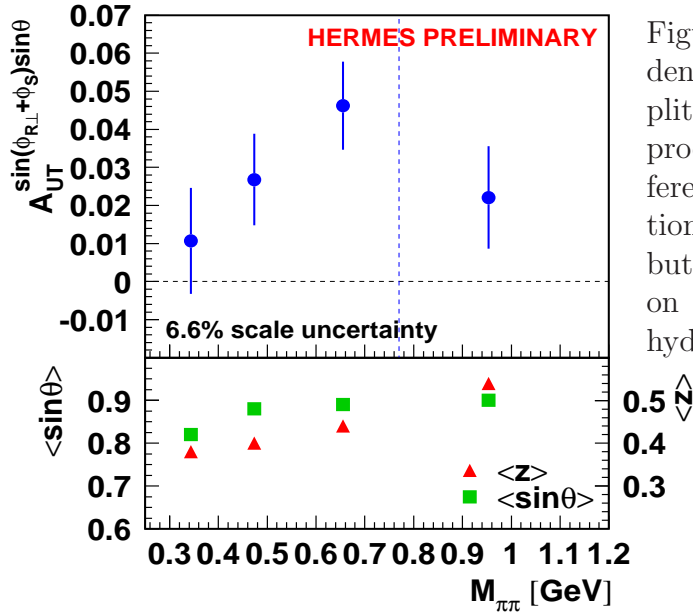


Figure 2: The dependence on $M_{\pi\pi}$ of the amplitude that involves the product of dihadron interference fragmentation function and transversity distribution for SIDIS $\pi^+\pi^-$ pairs on a transversely polarized hydrogen target.

quark polarization in the target nucleon. Furthermore, it is positive in the entire range of $M_{\pi\pi}$, not supporting a predicted sign change of the amplitude around the ρ^0 meson mass. The BELLE collaboration can extract dihadron fragmentation functions from their e^+e^- data. Such results could be combined with the present HERMES dihadron data to extract transversity in the proton, using a channel that is independent from the single-hadron channel. The analysis including the twice larger statistics of 2005 electron data is ongoing, possibly providing a significant constraint on two-pion formation models [4].

References

- [1] HERMES Collaboration, K. Ackerstaff et al., Nucl. Inst. and Methods **A 417** (1998) 230; HERMES Collaboration, A. Airapetian et al., Phys. Rev. Lett. **94**, 012002 (2005).
- [2] J. C. Collins, Phys. Lett. **B 396**, 161 (1993); D. W. Sivers, Phys. Rev. **D 43**, 262 (1991); S. J. Brodsky et al., Phys. Lett. **B 530**, 99 (2002); M. Burkardt, Phys. Rev. **D 66**, 114005 (2002).
- [3] E. S. Ageev et al., COMPASS Collaboration, Nucl. Phys. **B 765**, 31 (2007); R. Seidl et al., Belle Collaboration, Phys. Rev. Lett. **96**, 232002 (2006); M. Anselmino et al., Phys. Rev. **D 75**, 054032 (2007);
- [4] R. L. Jaffe et al., Phys. Rev. Lett. **80**, 1166 (1998); A. Bacchetta and M. Radici, Phys.Rev. **D 74** 114007 (2006).

SCALAR MESONS: A CHIRAL LAGRANGIAN FRAMEWORK FOR THEIR MIXING AND SUBSTRUCTURE

Amir H. Fariborz

Department of Mathematics/Physics
State University of New York Institute of Technology
Utica, NY 13504-3050, U.S.A.

Abstract

The highlights of studies of mixing among scalar mesons below and above 1 GeV within a nonlinear chiral Lagrangian framework is briefly presented. Two scalar meson nonets are introduced to explore the mass spectrum and decay properties of the $I=1/2$ and $I=1$ scalar states. For the $I=0$ states, in addition to these two nonets a scalar glueball component is also taken into account, and together with the constraints from the $I=1/2$ and $I=1$ sectors, their mass spectrum is studied. The fact that an ideally mixed $q\bar{q}$ scalar nonet has a mass ordering which is opposite to that of an ideally mixed four-quark scalar nonet is exploited to gain some insight into the quark substructure of the $I=1/2$, $I=1$ and $I=0$ states below and above 1 GeV. Consequently, numerical estimates of various components of these states (two quark and four quark components of $I=1/2$ and $I=1$ states, and two quark, four quark and glue component of $I=0$ states) are determined.

Scalar states below and above 1 GeV are shown in Fig. 1, and are all listed/discussed in PDG [1]. Not all of these states are well-established: Among these the $f_0(600)$ [or σ] and the $f_0(1370)$ have large uncertainties on their mass and decay widths, as well as the $K_0^*(800)$ [or κ] which has been particularly under a special scrutiny and debate. It is now generally believed that the states below 1 GeV are something other than pure $q\bar{q}$ states, as opposed to those above 1 GeV which have been the favored candidates for a $q\bar{q}$ nonet, even though some of their properties do not quite follow a $q\bar{q}$ assignment. Possible solutions for the status of the lowest-lying scalar states include the MIT bag model, $K\bar{K}$ molecule and unitarized quark model, as well as many recent investigations (see [2] for a selection of refs.). There are reasons to investigate the mixing between the scalar mesons below and above

1 GeV. First, intuitively this is not inconceivable as some of these states [such as $f_0(600)$ and $f_0(1370)$ as well as $K_0^*(800)$] are broad and their masses spread over a wide range, therefore one may expect that some of their properties may overlap. Second, the available experimental data may already be pointing to such mixings. For example, a close look at some of the properties of the $a_0(1450)$ and $K_0^*(1430)$ [which are expected to be two members of the same $q\bar{q}$ scalar meson nonet (see PDG [1])] shows surprising deviations from a $q\bar{q}$ nonet properties. Clearly, their masses are rather puzzling [1]: If these two states belong to the same $q\bar{q}$ nonet, then why should $a_0(1450)$ (which does not contain a strange quark) be heavier than $K_0^*(1430)$ (which does contain a strange quark)? There are also decay properties of these states that cannot be understood based on a pure $q\bar{q}$ picture. As a possible solution, a description of the $I = 1/2$ and $I = 1$ scalar states below and above 1 GeV in terms of two nonets of scalars and within a nonlinear chiral Lagrangian framework was explored in ref. [3]. In that work, it was shown that if an underlying “bare” four-quark nonet N lies beneath an underlying “bare” two-quark nonet N' , then as a result of mixing of N and N' we can easily understand why $a_0(1450)$ becomes heavier than $K_0^*(1430)$ (in addition, the decay properties of these states can be understood in this scenario). Fig. 1 shows how this mechanism works. It was also found in [3] that the $I = 1$ states are close to equal admixtures of two and four-quark states, whereas the $I = 1/2$ states are less mixed, with $K_0^*(800)$ containing close to 75% four-quark and 25% two-quark [and vice versa for $K_0^*(1430)$]. What does this scenario say about the $I = 0$ states? This question was studied in [4] in which the implications of such underlying mixing of nonets N and N' on the $I = 0$ states was investigated. Fig. 1 summarizes the results and shows how the $I = 0$ states originate from the four-quark nonet N , two-quark nonet N' and a scalar glueball G . The mass part of the Lagrangian for N , N' and G is (in the leading order of mixing):

$$\begin{aligned} \mathcal{L}_{mass} = & -a\text{Tr}(NN) - b\text{Tr}(NN\mathcal{M}) - a'\text{Tr}(N'N') - b'\text{Tr}(N'N'\mathcal{M}) \\ & -c\text{Tr}(N)\text{Tr}(N) - d\text{Tr}(N)\text{Tr}(N\mathcal{M}) - c'\text{Tr}(N')\text{Tr}(N') - d'\text{Tr}(N')\text{Tr}(N'\mathcal{M}) \\ & -\gamma\text{Tr}(NN') - \rho\text{Tr}(N)\text{Tr}(N') - gG^2 - eG\text{Tr}(N) - fG\text{Tr}(N') \end{aligned} \quad (1)$$

in which \mathcal{M} is the usual quark mass spurion. The mass of the $I = 1/2$ and $I = 1$ states involve terms a , b , a' , b' and γ only. The mass of $I = 0$ states involve all 13 parameters. The mixing of $I = 0$ states is clearly much more complicated and amounts to 5×5 rotation matrices among N , N' and G . The result of the numerical analysis of [4] for the prediction of the substructure of the $I = 0$ states are given in Fig. 2, in which, in the middle, the dashed lines represent nonet N (that has a mass ordering consistent with an ide-

ally mixed four-quark nonet), the solid lines represent nonet N' (that has a mass ordering consistent with an ideally mixed two-quark nonet) and the box represents the scalar glueball predicted in this model. Identifying the components of the two bare nonets with the corresponding members of an ideally mixed four-quark nonet and ideally mixed two-quark nonet results in conclusion that the bare masses in nonet N are (from bottom to top): $m(\bar{u}\bar{d}ud) = 0.83$ GeV, $m(\bar{d}\bar{s}ud) = 1.06$ GeV, $m[(\bar{s}\bar{d}ds + \bar{s}\bar{u}us)/\sqrt{2}] = 1.24$ GeV; and the bare masses in nonet N' are (from bottom to top): $m[(\bar{u}u + \bar{d}d)/\sqrt{2}] = 1.24$ GeV, $m(\bar{u}s) = 1.31$ GeV and $m(\bar{s}s) = 1.38$ GeV. The uncertainty of the glueball mass (shown by the height of the box, approximately between 1.5 GeV to 1.7 GeV) is due to the uncertainty of the input masses of $f_0(600)$ and $f_0(1370)$. In Fig. 1, on the right, the $I = 0$ physical states are shown, and the height of the two boxes represent the prediction of the present model for the uncertainties of the masses of $f_0(600)$ and $f_0(1370)$, which are (in this model) approximately in ranges $0.4 - 0.7$ GeV and $1.3 - 1.45$ GeV, respectively. On the left, the $I = 1/2$ and $I = 1$ physical states are shown [note the level-crossing that explains the properties of $a_0(1450)$ and $K_0^*(1430)$]. The arrows show the dominant component of each physical state. Finally, the detailed numerical analysis of [4] predicts the substructure of the $I = 0$ scalars (in terms of two quark, four quark and glueball components) which are given in Fig. 2.

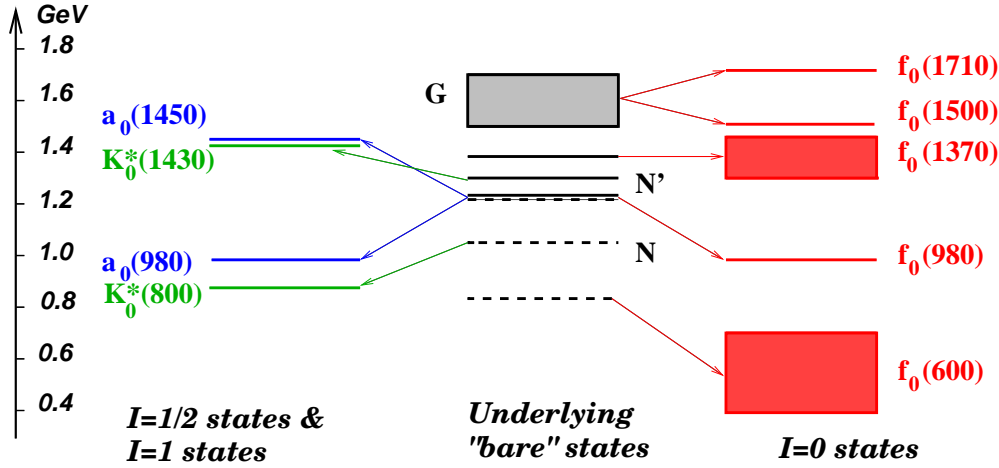


Figure 1: Prediction of the present model for the substructure of the $I = 1/2$, $I = 1$ scalar states below 2 GeV (left) and for the $I = 0$ scalar states below 2 GeV (right) in terms of the underlying “bare” states (middle).

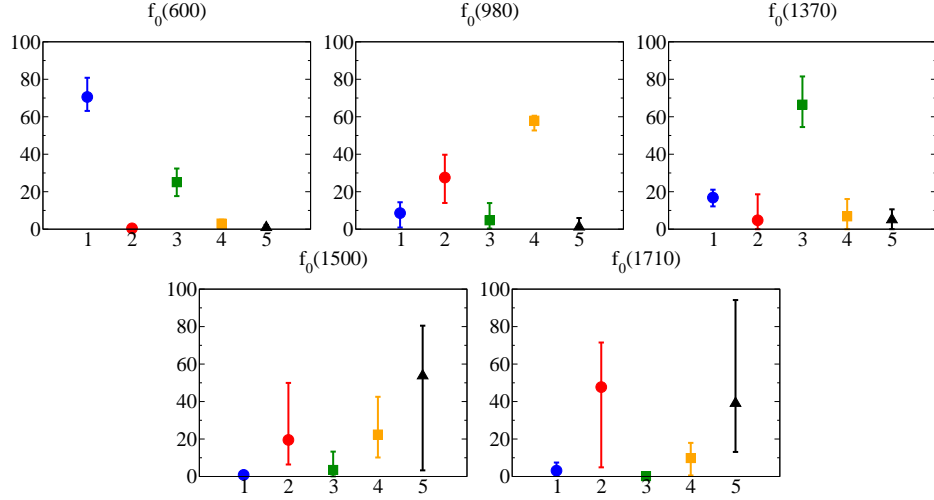


Figure 2: Components 1 to 5 respectively represent $\bar{u}\bar{d}ud$, $(\bar{s}\bar{d}ds + \bar{s}uus)/\sqrt{2}$, $\bar{s}s$, $(\bar{u}u + \bar{d}d)/\sqrt{2}$, and glueball. The symbols represent the averaged values of each component and the error bars reflect the uncertainties of $m^{\text{exp}}[f_0(600)]$ and $m^{\text{exp}}[f_0(1370)]$.

Acknowledgments

The author wishes to thank the organizers of MENU 2007 in particular Dr. S. Schadmand for her help at various stages of the conference. This work has been supported by the NSF Award 0652853.

References

- [1] W-M Yao et al, J. Phys. G: Nucl. Part. Phys. **33**, 1 (2006).
- [2] R.L. Jaffe, Phys. Rev. D **15**, 267 (1977). J. Weinstein, N. Isgur, Phys. Rev. D **41**, 2236 (1990). N.A. Törnqvist, Z. Phys. C **68**, 647 (1995). E. van Beveren et al, Z. Phys. C **30**, 615 (1986). See also: T. Teshima et al, Nucl. Phys. A **759**, 131 (2005). N.N. Achasov, A.V. Kiselev, Phys. Rev. D **73**, 054029 (2006). E. van Beveren et al, Phys. Rev. D **74**, 037501 (2006). J.R. Pelaez, Phys. Rev. Lett. **97**, 242002 (2006).
- [3] D. Black, A.H. Fariborz and J. Schechter, Phys. Rev. D **61**, 074001 (2000).
- [4] A.H. Fariborz, Phys. Rev. D **74**, 054030 (2006). Also see: A.H. Fariborz, Int. J. Mod. Phys. A **19**, 2095 (2004); 5417 (2004).

NONPERTURBATIVE QUARK-GLUON DYNAMICS

Christian S. Fischer^{*1}, Reinhard Alkofer[%], Felipe J. Llanes-Estrada[#],
Kai Schwenzer[%]

^{*}Institut für Kernphysik, Technische Universität Darmstadt, 64289
Darmstadt, Germany

[%]Institut für Physik der Karl-Franzens Universität, A-8010 Graz, Austria

[#]Departamento de Física Teórica I de la Universidad Complutense, 28040
Madrid Spain

Abstract

We summarize recent results on the nonperturbative quark-gluon interaction in Landau gauge QCD. Our analytical analysis of the infrared behaviour of the quark-gluon vertex reveals infrared singularities, which lead to an infrared divergent running coupling and a linear rising quark-antiquark potential when chiral symmetry is broken. In the chirally symmetric case we find an infrared fixed point of the coupling and, correspondingly, a Coulomb potential. These findings provide a new link between dynamical chiral symmetry breaking and confinement.

1 Introduction

The relation between the two fundamental properties of QCD, confinement and dynamical chiral symmetry breaking ($D\chi SB$), is surely a matter of utmost interest. Lattice calculations provide evidence that field configurations with nontrivial topological content may be at the heart of both phenomena [1, 2], but the fine details still remain elusive. Complementary to the strategy of identifying individual confining field configurations is the investigation of the correlation functions of the theory. Certainly, both confinement and $D\chi SB$ manifest themselves in strong, nonperturbative correlations at small momenta. In this talk we discuss these effects and present a novel link between confinement and $D\chi SB$.

¹E-mail address: christian.fischer@physik.tu-darmstadt.de

2 Infrared behaviour of Yang-Mills theory

The infrared behaviour of Landau gauge Yang-Mills theory has been investigated in the past in a number of works in both the Dyson-Schwinger equations (DSE) framework [3–10] and also within the functional renormalisation group (FRG) [11–14]; for reviews see [15–17]. In the deep infrared, i.e. for external momentum scales $p^2 \ll \Lambda_{\text{QCD}}^2$, a general power law behaviour of one-particle irreducible Green functions with $2n$ external ghost legs and m external gluon legs has been derived [9, 10]:

$$\Gamma^{n,m}(p^2) \sim (p^2)^{(n-m)\kappa+(1-n)(d/2-2)}. \quad (1)$$

Here, d is the space-time dimension. One can show that (1) is the only infrared solution in terms of power laws of both the complete hierarchy of DSEs and FRGs [13]. The anomalous dimension κ is known to be positive [4, 5] and is bounded by $\kappa \geq 0.5$ from below [5]. With the (well justified) approximation of a bare ghost-gluon vertex in the infrared one obtains $\kappa = (93 - \sqrt{1201})/98 \simeq 0.595$ [5, 6]. This value corresponds to an infrared vanishing gluon propagator and a strongly infrared enhanced ghost,

$$D_{\mu\nu}(k) = \frac{Z(k^2)}{k^2} \left(\delta_{\mu\nu} - \frac{k_\mu k_\nu}{k^2} \right), \quad D_G(k) = -\frac{G(k^2)}{k^2}, \quad (2)$$

with dressing functions $Z(k^2) \sim (p^2)^{2\kappa}$ and $G(k^2) \sim (p^2)^{-\kappa}$. Such a behavior of the gluon propagator implies positivity violations and therefore may be interpreted as a signal for gluon confinement [3, 8].

An important consequence of (1) is the presence of a nontrivial infrared fixed point in the running couplings related to the primitively divergent vertex functions of Yang-Mills theory:

$$\begin{aligned} \alpha^{gh-gl}(p^2) &= \alpha_\mu G^2(p^2) Z(p^2) \sim \frac{\text{const}_{gh-gl}}{N_c}, \\ \alpha^{3g}(p^2) &= \alpha_\mu [\Gamma^{0,3}(p^2)]^2 Z^3(p^2) \sim \frac{\text{const}_{3g}}{N_c}, \\ \alpha^{4g}(p^2) &= \alpha_\mu \Gamma^{0,4}(p^2) Z^2(p^2) \sim \frac{\text{const}_{4g}}{N_c}, \end{aligned} \quad (3)$$

for $p^2 \rightarrow 0$. The infrared value of the coupling related to the ghost-gluon vertex can be computed [5, 7] and yields $\alpha^{gh-gl}(0) \simeq 2.972$ for $N_c = 3$.

3 Infrared behavior of quenched QCD

Based on the infrared solutions (1), one can also derive the analytical infrared behavior of the quark-gluon vertex [18]. To this end one has to carefully

distinguish the cases of broken or unbroken chiral symmetry. Whereas in the broken case the full quark-gluon vertex Γ_μ can consist of up to twelve linearly independent Dirac tensors, these reduce to a maximum of six when chiral symmetry is realized in the Wigner-Weyl mode. Correspondingly, a broken symmetry induces two tensor structures in the quark propagator, whereas only one is left when chiral symmetry is restored. In a similar way, chiral symmetry breaking reflects itself in every Green's function with quark content.

The presence or absence of the additional tensor structures turns out to be crucial for the infrared behavior of the quark-gluon vertex. When chiral symmetry is broken (either explicitly or dynamically with a valence quark mass $m > \Lambda_{\text{QCD}}$) one obtains a selfconsistent solution of the vertex-DSE which behaves like

$$\lambda^{D\chi SB} \sim (p^2)^{-1/2-\kappa}. \quad (4)$$

Here λ denotes generically any dressing of the twelve tensor structures. If, however, the Wigner-Weyl mode is realized one obtains the weaker singularity

$$\lambda^{\chi S} \sim (p^2)^{-\kappa}. \quad (5)$$

As a consequence the running coupling from the quark-gluon vertex either is infrared divergent ('infrared slavery') or develops a fixed point similar to the Yang-Mills couplings of Eq.(3):

$$\alpha^{qg}(p^2) = \alpha_\mu [\lambda(p^2)]^2 [Z_f(p^2)]^2 Z(p^2) \sim \begin{cases} \frac{1}{p^2} \frac{\text{const}_{qg}^{D\chi SB}}{N_c} & : D\chi SB \\ \frac{\text{const}_{qg}^{\chi S}}{N_c} & : \chi S \end{cases} \quad (6)$$

(Here we use that the quark propagator is constant in the infrared, i.e. $Z_f(p^2) \sim \text{const}$ [19].) Note that in all couplings the irrational anomalous dimensions ($\sim \kappa$) of the individual dressing functions cancel in the RG-invariant products.

Finally, one can analyze the behavior of the quark four-point function $H(p^2)$ which includes the (static) quark potential. With (4) and (5), one obtains $H(p^2) \sim 1/p^4$ in the Nambu-Goldstone and $H(p^2) \sim 1/p^2$ in the Wigner-Weyl realization of chiral symmetry. This leads to a quark-antiquark potential of

$$V(\mathbf{r}) = \frac{1}{(2\pi)^3} \int d^3p e^{i\mathbf{p}\mathbf{r}} H(\mathbf{p}^2) \sim \begin{cases} |r| & : D\chi SB \\ \frac{1}{|r|} & : \chi S \end{cases} \quad (7)$$

which establishes the before mentioned link between dynamical chiral symmetry breaking and confinement.

Acknowledgments

CF thanks the organizers of *Menu07* for all their efforts which made this extraordinary conference possible. This work was supported by the DFG under grant no. Al 279/5-2, by the Helmholtz-University Young Investigator Grant VH-NG-332, by the FWF under contract M979-N16, and by MEC travel grant PR2007-0110, Spain.

References

- [1] J. Greensite, Prog. Part. Nucl. Phys. **51** (2003) 1 [hep-lat/0301023].
- [2] C. Gattringer, Phys. Rev. Lett. **97**, 032003 (2006) [hep-lat/0605018];
- [3] L. von Smekal, A. Hauck and R. Alkofer, Annals Phys. **267** (1998) 1 [Erratum-ibid. **269**, 182 (1998)] [hep-ph/9707327].
- [4] P. Watson and R. Alkofer, PRL **86** (2001) 5239 [hep-ph/0102332].
- [5] C. Lerche and L. von Smekal, PRD **65** (2002) 125006 [hep-ph/0202194].
- [6] D. Zwanziger, Phys. Rev. D **67** (2003) 105001 [arXiv:hep-th/0206053]; Phys. Rev. D **69** (2004) 016002 [arXiv:hep-ph/0303028].
- [7] C. S. Fischer and R. Alkofer, PLB **536** (2002) 177 [hep-ph/0202202];
- [8] R. Alkofer, W. Detmold, C. S. Fischer and P. Maris, Phys. Rev. D **70** (2004) 014014 [hep-ph/0309077];
- [9] R. Alkofer, C. S. Fischer and F. J. Llanes-Estrada, Phys. Lett. B **611** (2005) 279 [arXiv:hep-th/0412330];
- [10] M. Huber, R. Alkofer, C. S. Fischer, K. Schwenzer, 0705.3809[hep-ph].
- [11] J. M. Pawłowski, D. F. Litim, S. Nedelko and L. von Smekal, Phys. Rev. Lett. **93**, 152002 (2004) [arXiv:hep-th/0312324].
- [12] C. S. Fischer and H. Gies, JHEP **0410**, 048 (2004) [hep-ph/0408089].
- [13] C. S. Fischer, J. M. Pawłowski, PRD **75** (2007) 025012 [hep-th/0609009].
- [14] J. Braun, H. Gies and J. M. Pawłowski, 0708.2413[hep-th].
- [15] R. Alkofer and L. von Smekal, Phys. Rept. **353** (2001) 281 [hep-ph/0007355].
- [16] C. S. Fischer, J. Phys. **G32** (2006) R253 [hep-ph/0605173].
- [17] R. Alkofer and J. Greensite, J. Phys. **G34** (2007) S3 [hep-ph/0610365].
- [18] R. Alkofer, C. S. Fischer and F. J. Llanes-Estrada, arXiv:hep-ph/0607293; C. S. Fischer, F. J. Llanes-Estrada, R. Alkofer and K. Schwenzer, in preparation.
- [19] C. S. Fischer and R. Alkofer, PRD **67** (2003) 094020 [hep-ph/0301094].

THE PANDA DETECTOR AT FAIR

K. Föhl ¹

School of Physics, University of Edinburgh,
James Clerk Maxwell Building, The Kings Buildings,
Mayfield Road, Edinburgh EH9 3JZ
United Kingdom

Abstract

The PANDA collaboration plans to study interactions of antiprotons with nucleons and nuclei using a multi-purpose internal target detector system located at the FAIR laboratory in Darmstadt to investigate the physics of strong interactions. With the planned high interaction rates using cooled antiprotons of up to 15 GeV/c the PANDA detector will allow high-precision measurements and the observation of rare reaction channels.

1 Introduction

At the international Facility for Antiproton and Ion Research (FAIR) at Darmstadt, the PANDA (anti-Proton ANnihiliation at DArmstadt) collaboration (see Ref. [1]) prepares to construct a multi-purpose internal target detector system located on the High Energy Storage Ring (HESR) to study interactions of antiprotons with nucleons and nuclei in the mass range of up to $\sqrt{s} = 5.4 \text{ GeV}/c^2$.

The core programme of PANDA comprises charmonium spectroscopy with precision measurements of mass, width and decay branches; the investigation of more exotic configurations like multiquark states, charmed hybrids and glueballs; the search for medium modifications of charmed hadrons in nuclear matter; and the γ -ray spectroscopy of hypernuclei, in particular double λ states.

For the example of charmonium spectroscopy theoretical calculations differ significantly in particular above the $D\bar{D}$ threshold and do not properly predict several recently discovered states. On the experimental side, a fair number of states and their properties at higher energy are not well established.

¹on behalf of the PANDA collaboration

The combination of HESR with cooled antiprotons, and PANDA aims at both high reaction rates and high resolution to be able to study rare production processes and small branching ratios. With up to 10^{11} stored antiprotons for beam momenta 1.5-15 GeV/c and high density targets the experiment anticipates interaction rates of $2 \cdot 10^7 \text{ s}^{-1}$. The stored antiprotons do not have a bunch structure, and with 10% allocated to a barrier bucket, the antiprotons are continuously spread over 90% of the HESR circumference.

Two complementary operating modes are foreseen, high luminosity and high resolution. The high luminosity mode with $\Delta p/p = 10^{-4}$, stochastic cooling and pellet target density of $4 \cdot 10^{15} \text{ cm}^{-2}$ will have a luminosity of $L=10^{32} \text{ cm}^{-2}\text{s}^{-1}$. For the high resolution mode $\Delta p/p = 3 \cdot 10^{-5}$ will be achieved with electron cooling for momenta up to $p = 8.9 \text{ GeV}/c$ and will operate in conjunction with a cluster jet target to limit the energy broadening caused by the target, the luminosity will be $L=10^{31} \text{ cm}^{-2}\text{s}^{-1}$.

The task of the PANDA detector will be to measure $p\bar{p}$ reactions comprehensively and exclusively. This requires simultaneous measurements of leptons as well as charged and neutral hadrons, with potentially high multiplicities. Benchmark channels are simulated to determine the required detector performance from physics parameters. In the example of $p\bar{p} \rightarrow Y(4260) \rightarrow J/\psi\pi^+\pi^-$ with $J/\psi \rightarrow e^+e^-$ one sees that a combined lepton plus hadron detection capability is required, and from further benchmark channels a similar case can be made for charged and neutral particles.

2 The PANDA detector setup

The PANDA detector setup (see Fig. 1) is a fixed target experiment scattering a storage ring antiproton beam off a pellet or cluster jet target. It is divided into two parts, the Target Spectrometer around a solenoid magnet, subdivided into backward endcap, barrel and endcap, and the Forward Spectrometer with an angular acceptance of ± 10 degrees horizontally and ± 5 degrees vertically.

2.1 Magnets

In the Target Spectrometer most of the detectors are housed inside the magnet return yoke, the systems of the barrel part are inside the superconducting solenoid magnet. The Forward Spectrometer starts with a dipole magnet to provide bending power with a B -field perpendicular to the forward tracks. The majority of the detector systems are downstream outside the magnet. Additionally parts of the magnet iron are laminated to allow the insertion of muon detectors into the gaps.

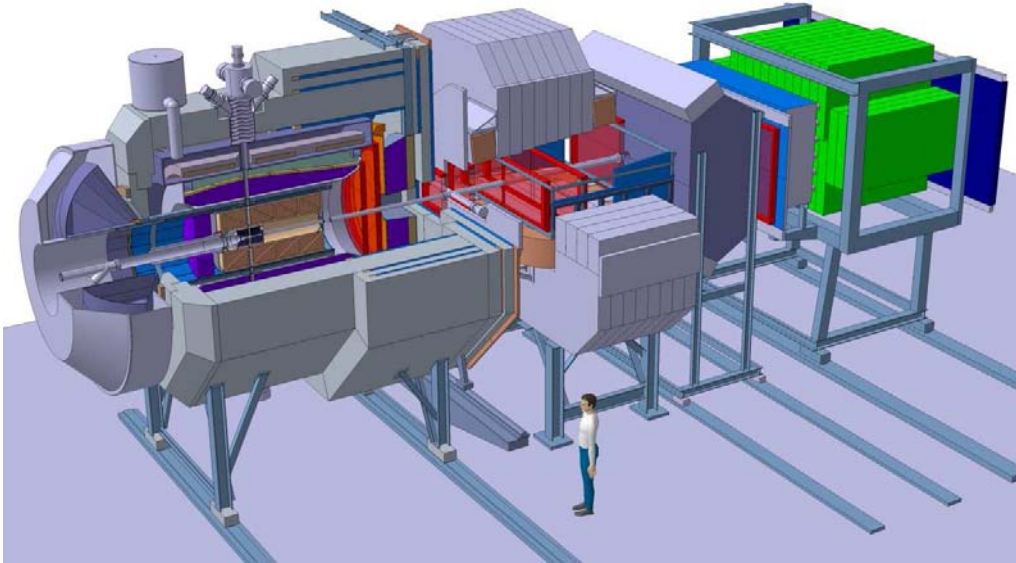


Figure 1: Visualisation of the PANDA detector, the antiproton beam coming from the left. On the left side the Target Spectrometer, on the right side the Forward Spectrometer with individual detectors downstream of the dipole magnet.

2.2 Vertex detectors

Closely surrounding the target area a silicon microvertex detector provides secondary vertex sensitivity for decays of particles with decay lengths in the order of $100 \mu m$.

For the central tracker two technologies are being considered. The more conservative option is a straw tube tracker, a technology known to work for example in the WASA detector. A time projection chamber is the more ambitious option, it must be self-quenching as the requirement is continuous operation in high particle fluxes. Investigation of several technologies for a detector component may continue for a few more years before the choice of one and the freeze of the detector design.

There are several tracking stations in the endcap and forward detector parts. Here the candidate technologies are multiwire drift chambers and gas detectors with GEM readout.

2.3 Calorimetry

For the electromagnetic calorimeters (EMC) inside the Target Spectrometer one foresees lead tungstate (PWO) crystals read out with Avalanche Photo

Diodes (APD). As the crystal light output and the APD performance both improve with lower temperature, the plan is to operate these detectors at $T=-25^{\circ}\text{C}$. In the Forward Spectrometer, a Shashlyk type electromagnetic calorimeter (scintillator fibres in lead matrix) is followed by a scintillator-absorber-sandwich hadron calorimeter.

2.4 Particle identification

Charged particle identification (PID), with a focus on positive kaon identification, is the task of three imaging Cherenkov detectors. Inside the TS a DIRC similar to the BaBar covers the barrel part, in the endcap part a novel design foresees a circular fused silica plate with optical readout elements placed on the rim outside the acceptance. In the FS an aerogel mirror focussing RICH is located after the dipole magnet. Time-of-Flight measurement covers slow particles below the Cherenkov light threshold. Overall PID will also use input from tracking and calorimetry.

2.5 Detector readout

Detector readout has to be self-triggering or continually sampling into a pipeline as there is no beam bunch structure and the triggers software-implemented and configurable using intelligent frontends and powerful compute nodes. The high data rate requires several stages of data selection and reduction with the data logging after an online reconstruction.

3 Conclusions and Outlook

The PANDA detector is designed to be a versatile QCD detector. Novel techniques in detector and readout design are required and are currently being developed. Such Research and Development will continue for a few more years.

4 References

References

- [1] Technical Progress Report for $\bar{\text{P}}\text{ANDA}$, GSI, January 2005.

MENU 2007
11th International Conference
on Meson-Nucleon Physics and
the Structure of the Nucleon
September 10-14, 2007
IKP, Forschungszentrum Jülich, Germany

ELEMENTARY COLLISIONS WITH HADES

I. Fröhlich⁷, J. Pietraszko⁴, G. Agakishiev⁸, C. Agodi¹, A. Balanda^{3,e},
G. Bellia^{1,a}, D. Belver¹⁵, A. Belyaev⁶, A. Blanco², M. Böhmer¹¹,
J. L. Boyard¹³, P. Braun-Munzinger⁴, P. Cabanelas¹⁵, E. Castro¹⁵,
S. Chernenko⁶, T. Christ¹¹, M. Destefanis⁸, J. Díaz¹⁶, F. Dohrmann⁵,
A. Dybczak³, T. Eberl¹¹, L. Fabbietti¹¹, O. Fateev⁶, P. Finocchiaro¹,
P. Fonte^{2,b}, J. Friese¹¹, T. Galatyuk⁴, J. A. Garzón¹⁵, R. Gernhäuser¹¹,
C. Gilardi⁸, M. Golubeva¹⁰, D. González-Díaz⁴, E. Grosse^{5,c}, F. Guber¹⁰,
M. Heilmann⁷, T. Hennino¹³, R. Holzmann⁴, A. Ierusalimov⁶, I. Iori^{9,d},
A. Ivashkin¹⁰, M. Jurkovic¹¹, B. Kämpfer⁵, K. Kanaki⁵, T. Karavicheva¹⁰,
D. Kirschner⁸, I. Koenig⁴, W. Koenig⁴, B. W. Kolb⁴, R. Kotte⁵,
A. Kozuch^{3,e}, F. Krizek¹⁴, R. Krücken¹¹, W. Kühn⁸, A. Kugler¹⁴,
A. Kurepin¹⁰, J. Lamas-Valverde¹⁵, S. Lang⁴, J. S. Lange⁸, L. Lopes²,
L. Maier¹¹, A. Mangiarotti², J. Marín¹⁵, J. Markert⁷, V. Metag⁸,
B. Michalska³, D. Mishra⁸, E. Morinière¹³, J. Mousa¹², C. Müntz⁷,
L. Naumann⁵, R. Novotny⁸, J. Otwinowski³, Y. C. Pachmayer⁷, M. Palka⁴,
Y. Parpottas¹², V. Pechenov⁸, O. Pechenova⁸, T. Pérez Cavalcanti⁸,
W. Przygoda^{3,e}, B. Ramstein¹³, A. Reshetin¹⁰, M. Roy-Stephan¹³,
A. Rustamov⁴, A. Sadovsky¹⁰, B. Sailer¹¹, P. Salabura³, A. Schmah⁴,
R. Simon⁴, S. Spataro⁸, B. Spruck⁸, H. Ströbele⁷, J. Stroth^{7,4}, C. Sturm⁷,
M. Sudol⁴, A. Tarantola⁷, K. Teilab⁷, P. Tlustý¹⁴, M. Traxler⁴, R. Trebacz³,
H. Tsertos¹², I. Veretenkin¹⁰, V. Wagner¹⁴, H. Wen⁸, M. Wisniowski³,
T. Wojcik³, J. Wüstenfeld⁵, S. Yurevich⁴, Y. Zanevsky⁶, P. Zumbach⁴

(HADES collaboration)

¹Istituto Nazionale di Fisica Nucleare - Laboratori Nazionali del Sud,
95125 Catania, Italy

²LIP-Laboratório de Instrumentação e Física Experimental de Partículas,
3004-516 Coimbra, Portugal

³Smoluchowski Institute of Physics, Jagiellonian University of Cracow,
30-059 Kraków, Poland

⁴Gesellschaft für Schwerionenforschung mbH, 64291 Darmstadt, Germany

⁵Institut für Strahlenphysik, Forschungszentrum Dresden-Rossendorf,
01314 Dresden, Germany

⁶Joint Institute of Nuclear Research, 141980 Dubna, Russia

⁷Institut für Kernphysik, Johann Wolfgang Goethe-Universität, 60438
Frankfurt, Germany

⁸II.Physikalisches Institut, Justus Liebig Universität Giessen,
35392 Giessen, Germany

⁹Istituto Nazionale di Fisica Nucleare, Sezione di Milano, 20133 Milano,
Italy

¹⁰Institute for Nuclear Research, Russian Academy of Science,
117312 Moscow, Russia

¹¹Physik Department E12, Technische Universität München,
85748 München, Germany

¹²Department of Physics, University of Cyprus, 1678 Nicosia, Cyprus

¹³Institut de Physique Nucléaire d'Orsay, CNRS/IN2P3, 91406 Orsay
Cedex, France

¹⁴Nuclear Physics Institute, Academy of Sciences of Czech Republic,
25068 Rez, Czech Republic

¹⁵Departamento de Física de Partículas, University of Santiago de
Compostela, 15782 Santiago de Compostela, Spain

¹⁶Instituto de Física Corpuscular, Universidad de Valencia-CSIC,
46971 Valencia, Spain

Abstract

The “High Acceptance DiElectron Spectrometer” (HADES) at GSI, Darmstadt, is investigating the production of e^+e^- pairs in $A + A$, $p + A$ and $N + N$ collisions. The latter program allows for the reconstruction of individual sources. This strategy will be roughly outlined in this contribution and preliminary pp/pn data is shown.

1 Introduction

Recently, the HADES collaboration has reported on the production of dileptons - unique probes to study properties of dense hadronic matter [1] - in the C+C collision at 2 AGeV [2]. In this context, the vector mesons are of particular interest as it has been proposed that their spectral functions change inside the hadronic medium [3]. On the other hand, at these energies measured di-lepton spectra do not contain the vector meson signal only, but also additional lepton pairs from other sources, like $\Delta^{+,0} \rightarrow N\pi^0 \rightarrow N\gamma e^+e^-$ (π -Dalitz), $\Delta \rightarrow Ne^+e^-$ (Δ -Dalitz), $N^*(1535) \rightarrow N\eta \rightarrow N\gamma e^+e^-$ (η -Dalitz) and the decay of baryonic N^* resonances in $N(\omega, \rho)$. This means at beam energies of 1-2 AGeV, corresponding to moderate densities (2-3 ρ_0) and temperatures (60-80 MeV), the production of (vector-)mesons is *always* accompanied by multi-step excitations of a limited number of resonances

and their subsequent decays, a concept which is supported many theoretical models and also corroborated by recent HADES results [4, 5].

One of the most abundant ingredients in this cocktail, the long-lived (i.e. decaying after the freeze-out of the fireball) pseudoscalar mesons $\pi, \eta \rightarrow \gamma\gamma^* \rightarrow \gamma e^+e^-$, have a well described electromagnetic structure [6]. Hence, they can be regarded as “trivial” components that can be subtracted from the measured e^+e^- spectrum. On the other hand, the contribution from short-lived resonances is completely unknown. For example, the Dalitz decay of the Δ resonance has not been measured. In the overall picture, these contributions are additional exchange graphs in the virtual bremsstrahlung process $NN \rightarrow NN\gamma^*$. One of the the questions recently addressed by one-boson exchange models is how the resonance contributions have to be treated among with the bremsstrahlung in coherent calculations, but a debate on this is still ongoing [7, 8]. The general conclusion is, however, that experimentally a strong isospin dependence should be visible in the mass-dependent ratio M_{ee}^{pp}/M_{ee}^{pn} .

To conclude this introduction, for an understanding of di-lepton spectra and resolving medium effects from the vacuum spectral functions it is crucial to fully describe the different sources in the heavy ion cocktail. This means that branching ratios and (spin dependent) form factors have to be known a priori, as well as the features of the different production mechanisms as they serve as input for model calculations since they affect mass and momentum distributions.

2 The elementary collision program

In order to study these different processes, HADES (for a description see [4]) has started a detailed program on the di-lepton production in elementary collisions using a liquid hydrogen target and proton/deuteron beams. The first experimental run using a proton beam with a kinetic beam energy of 2.2 GeV was successfully carried out in the year 2004 with the objective of verifying the lepton pair reconstruction efficiency using the known η production parameters [9]. Moreover, e^+e^- invariant mass results can be compared to the $C + C$ experiment done at a similar kinetic energy per nucleon (2 AGeV) thus providing an important reference.

In the following, two experiments at a lower beam energy were performed: pp at 1.25 GeV and dp at 1.25 AGeV (N.B. the same energy per nucleon). The general idea of these consecutive measurements below the η production threshold was to focus on the low-mass continuum of the di-lepton cocktail. By means of inclusive and exclusive analyses the Δ Dalitz decay can be stud-

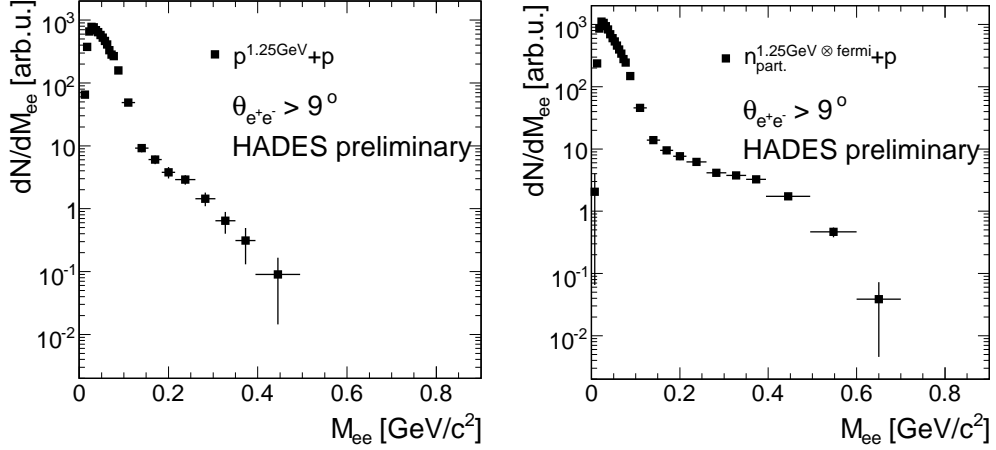


Figure 1: The raw inclusive spectra obtained in the pp reaction at 1.25 GeV (left) and in the np reaction (right, tagged with a proton spectator using the dp reaction at 1.25 AGeV). The spectra are not corrected for efficiency. In addition, for the pn case the fermi motion has to be taken into account. Thus, the spectra cannot be compared directly.

ied in the pp case, as described below, where the bremsstrahlung is negligible. The usage of iso-spin arguments allow for the subtraction of the Δ contribution in the quasi-free pn collision of dp data set and to study the virtual pn -bremsstrahlung. This was made possible by the addition of a forward wall which detected the spectator proton and thus tagged the quasi-free pn reaction. Fig. 1 shows preliminary invariant mass spectra for both the pp as well as the pn reaction, normalized to the same π^0 yield. Here, the pp results was obtained from $2.6 \cdot 10^9$ events, the pn data stems from a preliminary on-line analysis ($2.4 \cdot 10^9$ events, which is 50% of the expected statistics). Isospin effects are clearly visible in the mass region above the π^0 peak, which points to additional sources like pn bremsstrahlung and sub-threshold η production. This has to be discussed using detailed model calculations once the data set has been finally analyzed.

It is clear that before a quantitative conclusion can be drawn a thorough understanding of the Δ Dalitz decay (form factor and branching ratio) is mandatory. The production mechanism and decay of the Δ resonance $\Delta \rightarrow N\pi$ is already known from older measurements [10,11]. This fixes the Δ and π^0 emission angle and momentum, which is modeled in the event generator Pluto [13]. Thus, the “trivial” π^0 component can be subtracted and the Δ

decay can be studied by comparing several theoretical models with our data.

In the most recent experiment, pp collisions at 3.5 GeV have been studied, where ω and ρ are produced with large cross sections. Here, the focus of the analysis is to determine the contribution of vector production mechanisms (partial waves and N^* resonance contributions). The inclusive ω line shape will serve as a reference for future $p + A$ reactions which will be done at the same kinetic beam energy. The preliminary analysis of on-line data suggests a yield of a few hundred ω -mesons in the inclusive pair spectrum. In addition, new precise data on the vector meson production at higher beam energies are absolutely necessary, so the only data on exclusive ρ, ω production come from old bubble chamber experiments [12] with a yield of ω mesons of about 100 counts. No differential cross section distributions have been reported in this energy regime so far, but they are important inputs for the model calculations to be done for the upcoming $p + A$ experiment.

3 Summary and outlook

In summary, HADES has successfully initiated a detailed program using elementary collisions: The pp and pn reactions at 1.25 GeV to study Δ production and decay, and pp collisions at 2.2 GeV and 3.5 GeV. The preliminary analysis of the data suggest a statistics large enough to clarify many open question such as the Δ Dalitz decay, the pn bremsstrahlung and contributions from resonances. In particular, the preliminary analysis of the pp/pn ratio seems to exhibit additional sources, which supports ongoing theoretical work.

Acknowledgments

The collaboration gratefully acknowledges the support by BMBF grants 06MT238, 06GI146I, 06F-140, and 06DR135 (Germany), by the DFG cluster of excellence Origin and Structure of the Universe (www.universe-cluster.de), by GSI (TM-FR1,GI/ME3,OF/STR), by grants GA CR 202/00/1668 and MSMT LC7050 (Czech Republic), by grant KBN 1P03B 056 29 (Poland), by INFN (Italy), by CNRS/IN2P3 (France), by grants MCYT FPA2000-2041-C02-02 and XUGA PGID T02PXIC20605PN (Spain), by grant UCY- 10.3.11.12 (Cyprus), by INTAS grant 03-51-3208 and by EU contract RII3-CT-2004-506078.

References

- [1] J. Stroth, J. Phys. Conf. Ser. **50** (2006) 389.

- [2] G. Agakichiev *et al.*, Phys. Rev. Lett. **98** (2007) 052302.
- [3] G. E. Brown and M. Rho, Phys. Rev. Lett. **66** (1991) 2720.
- [4] F. Dohrmann *et al.*, these proceedings.
- [5] G. Agakichiev *et al.*, Phys. Lett. B, accepted for publication.
- [6] L.G. Landsberg, Phys.Repts. **128**, (1985) 301.
- [7] L. P. Kaptari and B. Kämpfer, Nucl. Phys. A **764** (2006) 338 [arXiv:nucl-th/0504072].
- [8] R. Shyam and U. Mosel, Phys. Rev. **C 67** (2003) 065202.
- [9] I. Fröhlich *et al.*, Eur. Phys. J. A **31** (2007) 831.
- [10] V. Dmitriev, O. Sushkov, and C. Gaarde, Nucl. Phys. **A459** (1986) 503.
- [11] A.B. Wicklund *et al.*, Phys. Rev. **D 35** (1987) 2670.
- [12] A.P. Colleraine and U. Nauenberg, Phys. Rev. **161**, 1387 (1967).
L. Bodini *et al.*, Nuovo Cimento **58A**, 475 (1968).
- [13] I. Fröhlich *et al.*, PoS ACAT:076, 2007 [arXiv:0708.2382].

MONTE CARLO SIMULATION OF MESON-NUCLEON AND MESON-NUCLEUS INTERACTIONS AT HIGH ENERGIES

*A. Galoyan*¹, *V. Uzhinsky*²
Joint Institute for Nuclear Research, Dubna³

Abstract

Simulation of meson-nucleon and meson-nucleus interactions meets various problems. The first one is a connection between the annihilation and non-annihilation channels, or vacuum and non-vacuum exchanges. The second one is the excitation of mesons. The ways to solve these problems are considered. The reggeon theory is applied for solving the first problem. The second one is solved while describing experimental data. As a result a good reproduction of experimental regularities has been reached.

1 Meson-Nucleon Interactions

The meson-nucleus interactions was left out of active theoretical discussions during last decade, though unsolved problems were left. They are annihilation of quark in mesonic interactions, cross section of mesonic diffraction dissociation, reproduction of baryon spectra, transition to the low energies where resonance production is dominated and so on. In various manner they appear in calculations. In Fig. 1 we present a description of π^+p -interactions in the frameworks of the Fritiof [1], UrQMD 1.3 [2] and QGS [3] models⁴.

It is desirable for improvement of the Fritiof and QGS models to take into account resonances in the s -channel and yield of so-called planar diagrams. The planar diagrams are associated with processes of quark annihilation from colliding hadrons. A simulation of the s -channel resonance creation is rather complicated task, thus we omit this interesting question, having in mind that they are important at sufficiently low energies. At high energies the yields of the planar diagrams and pommeron exchanges have to dominate in elastic scattering amplitude according to the Regge phenomenology. They have to

¹Laboratory of Particle Physics, JINR.

²Laboratory of Information Technologies, JINR.

³Dubna, 141980, Moscow region, Russia

⁴We use QGS model implemented in the GEANT-4 package.

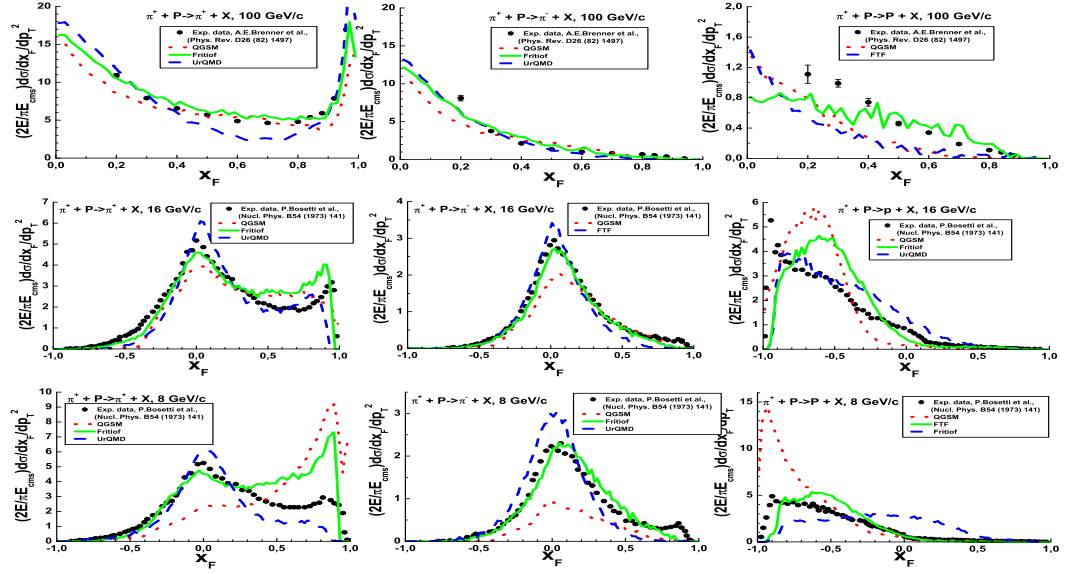


Figure 1: Spectra of π^+ , π^- and protons in π^+p -interactions. Points are experimental data from Durham data base [4]. Lines are calculation results.

be reflected in inelastic processes. The yields of the planar diagrams are not positive defined. This introduces some difficulties in creation of Monte Carlo algorithms. For the Monte Carlo simulation of the meson-nucleon interactions it is desirable to represent total cross section as sum of positive defined terms, $\sigma_{MN}^{tot} = \sigma^{el} + \sigma_M^{dif} + \sigma_N^{dif} + \sigma_{2str} + \sigma_{ann}$. Here σ^{el} is elastic cross section, σ_M^{dif} is cross section of projectile meson dissociation, σ_N^{dif} – cross section of target nucleon dissociation, σ_{ann} is unknown annihilation cross section. In π^+p -interactions it is possible $\bar{d}d$ annihilation. One can expect that the annihilation cross section is proportional to an annihilation probability, w_{ann} . In π^-p -interactions it is possible $\bar{u}u$ annihilation, and the annihilation cross section has to be proportional to $2w_{ann}$, because there is a possibility to annihilate with different u -quarks of a proton. Thus,

$$\sigma_{\pi^+p}^{tot} = \sigma^{el} + \sigma_M^{dif} + \sigma_N^{dif} + \sigma_{2str} + \acute{a} * w_{ann}. \quad (1)$$

$$\sigma_{\pi^-p}^{tot} = \sigma^{el} + \sigma_M^{dif} + \sigma_N^{dif} + \sigma_{2str} + 2 * \acute{a} * w_{ann}.$$

and $c * w_{ann} = \sigma_{\pi^-p}^{tot} - \sigma_{\pi^+p}^{tot}$.

According to our estimations, the annihilation cross sections are not large in π^+p -interactions (10, 9 and 5% at 8, 16 and 100 GeV/c, correspondingly), and can not have a strong influence on calculation results. The main problem in the calculations is connected with 2-string interactions. In Fig. 2 we show yields of the processes in the π^+ -meson spectra at 8 and 16 GeV/c calculated

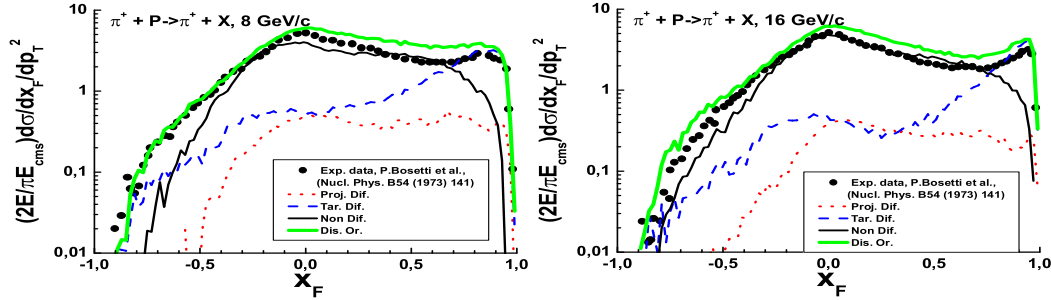


Figure 2: Spectra of π^+ in π^+p -interactions. Points are experimental data. Lines are calculation results.

in the Fritiof model. The dotted curves give the yields of projectile meson diffraction dissociation. The dashed lines are contributions of the target dissociation. The thin solid ones are the yields of 2-string processes. As seen, the 2-string processes are responsible for disagreement of the calculations and the experimental data in the region of $x_F \sim 0.3-1$. It is too difficult to change the calculation results varying model parameters.

After many attempts to improve the results, we accept a hypothesis on string disorientation in the collision process. Usually it is assumed that strings are fragmented along the collision axis. At low energies due to residual interactions a change of the axis can happen. Assuming complete disorientation, randomly rotating events, we obtain promising results presented by thick solid curves in Fig.2. We believe that a good description of experimental data and understanding of the meson-nucleon interaction can be reached on the direction.

2 Meson-Nucleus Interactions

At high energies, the effects considered above are not essential in meson-nucleus interactions, and one can expect a good agreement of the model predictions with experimental data. In Fig. 3 we present such comparison. Points are experimental data [5], solid lines are the Fritiof model calculations, and dotted ones are predictions of the QGS-G model. We have not obtained the UrQMD model results, because the code falls into an infinite loops. We are searching for bugs. As seen, the Fritiof model results are close to the data at large rapidities. In the target fragmentation region, the model underestimates the data due to an absence of formation time and secondary particle interactions in nuclei. All of them are taken into account in the QGS-G model. Thus, good results have been reached. At the same time,

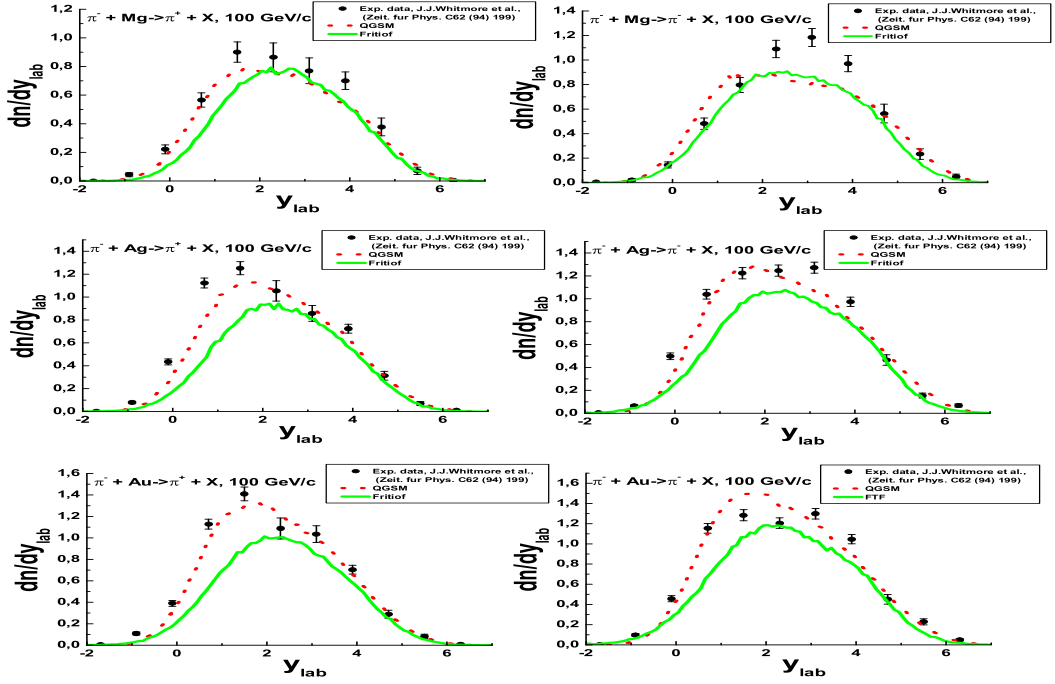


Figure 3: Spectra of π^+ and π^- in π^-A -interactions at 100 GeV/c. Points are experimental data. Lines are calculation results.

as it was shown before, the model works badly for the meson-nucleon interactions. So, a problem of consistence description of the meson-nucleon and meson-nucleus interactions is left.

References

- [1] B. Andersson *et al.* *Nucl. Phys.* **B281**, 289 (1987); B. Nilsson-Almqvist and E. Stenlund, *Comp. Phys. Commun.* **43**, 387 (1987).
- [2] S. A. Bass *et al.* *Prog. Part. Nucl. Phys.* **41**, 225 (1998); M. Bleicher *et al.* *J. Phys.* **G25**, 1859 (1999).
- [3] A. B. Kaidalov and K. A. Ter-Martirosian, *Phys. Lett.* **B117**, 247 (1982); A. B. Kaidalov, *Phys. Lett.* **B116**, 459 (1982); A. Capella, U. Sukhatme, C-I Tan, J. Tran Thanh Van, *Phys. Rept.* **236**, 225 (1994).
- [4] <http://durpdg.dur.ac.uk/HEPDATA/HEPDATA.html>
- [5] J. J. Whitmore *et al.* *Zeit. fur Phys.* **C62**, 199 (1994).

MULTIPLICITY FLUCTUATIONS IN INTERACTIONS OF LIGHT NUCLEI WITH CARBON AT MOMENTUM OF 4.2 GeV/c PER NUCLEON AND THEIR THEORETICAL INTERPRETATION

A. Galoyan^{*,1}, E. N. Kladnickaya[%], V. V. Uzhinsky[#]

^{*}LPP, JINR, Dubna, Russia

[%]LHE, JINR, Dubna, Russia

[#]LIT, JINR, Dubna, Russia

Abstract

New experimental data and their theoretical description are presented on a scaled variance of negative charged particle multiplicity distributions in the interactions of light (p, d, He-4, C-12) nuclei with carbon nuclei at initial momentum of 4.2 GeV/c per nucleon obtained in 4π geometry. Our data show a behavior analogous to one observable by NA49 Collaboration.

A nontrivial dependence of a scaled variance of multiplicity distribution of produced particles in nucleus-nucleus interactions at energy of 158 GeV/nucleon observed by the NA-49 Collaboration [1] (see also [2,3]) has attracted much attention last time. Thus, it is interesting to study the multiplicity fluctuations at lower energies in order to understand the nature of the effect observed by the NA-49 Collaboration.

Below, we present experimental data obtained by a propane bubble chamber collaboration in LHE JINR. The chamber was irradiated by light nuclei with momentum of 4.2 GeV/c per nucleon. π^- -mesons were identified quite well in the propane chamber in 4π -geometry. Protons were identified up to 500 MeV/c. At larger momenta the separation of protons and π^+ -mesons is complicated, but their momenta are defined well. The tracks of positive charged particles with momentum larger than 3 GeV/c and emission angle less than 4° were considered as spectator protons of projectile nuclei. The evaporated protons with momentum less than 300 MeV/c and proton-participants with momentum larger than 300 MeV/c without spectators were selected among protons. A summary charge (Q) of the produced particles (π^+ -, π^- -mesons and proton-participants) has been used as a collision centrality in this paper, $Q = n_+ - n_- - n_{evap} - n_{strp}$.

¹E-mail address: galoyan@cv.jinr.ru

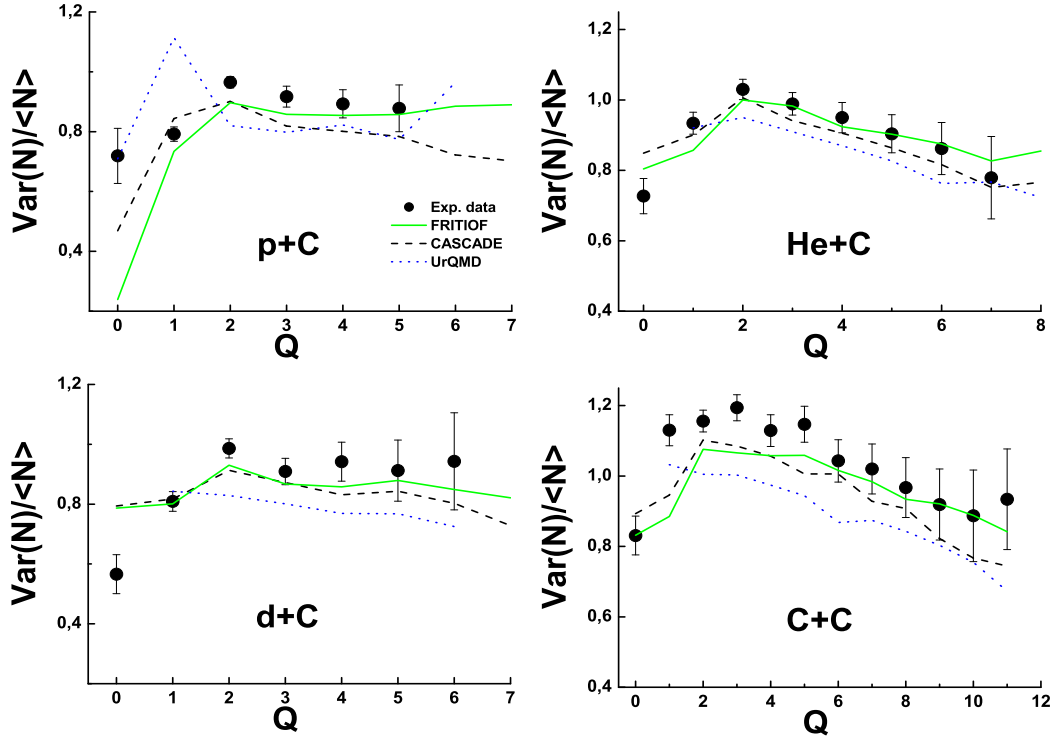


Figure 1: Scaled variances of negative charged particle multiplicity distributions in the light nuclei interactions with carbon nuclei at momentum 4.2 GeV/c/nucleon. Points are experimental data, lines are theoretical calculations. Solid lines are FRITIOF model calculations. Dashed lines are Cascade-Evaporation model calculations. Dotted lines are UrQMD model calculations

In Fig. 1 we present the scaled variances of negative charged particle multiplicity distributions in pC^- , dC^- , αC and CC -interactions. The scaled variance of a distribution is determined as a ratio of the distribution variance to a mean multiplicity of particles. Both the multiplicity fluctuations observed by us and those studied by the NA-49 collaboration [1] show defined dependence on the collision centrality. Scaled variances in peripheral interactions ($Q = 0$) are close to ones in nucleon-nucleon collisions. After that there is a big rise of the fluctuations, and their slowly decrease with increase of collision centrality (increase of Q). The theoretical models applied by us – FRITIOF [4], UrQMD²⁾ [6] and the Cascade-Evaporation model [7] reproduce qualitatively the behaviour of our experimental data in contrast to the

²⁾ The models FRITIOF and UrQMD were enlarged by the Statistical Multi-fragmentation model [5].

situation at higher energies [1]. This allows us to analyze the experimental data.

The FRITIOF model assumes that nucleons of interacting nuclei turn to excited states with continuous mass spectra due to binary collisions. The excited, "wounded" nucleons fragment into observed particles. We have checked that the FRITIOF model predicts slowly decrease of the scaled variance in CC-interactions at fixed multiplicity of "wounded" nucleons and at a consideration of inelastic nucleon-nucleon collisions only (see Fig. 2a dotted line).

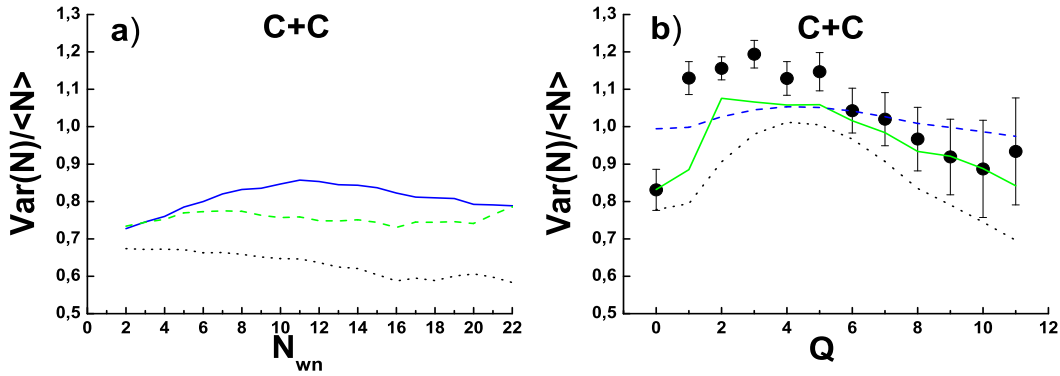


Figure 2: Scaled variances of multiplicity distributions. Points are the experimental data of Fig. 1. The dotted line (Fig. 2a) presents the multiplicity fluctuations of produced particles caused by inelastic NN-collisions only. The dashed line (Fig. 2a) is the calculation of the fluctuations at the elastic and inelastic scattering. The solid line (Fig. 2a) presents the fluctuations at the consideration of ejected nucleons as "wounded" ones. The dotted line (Fig. 2b) is the scaled variance of the multiplicity distribution of the "wounded" and ejected nucleons as a function of the collision centrality. The dashed line (Fig. 2b) – see description in the text. The solid line (Fig. 2b) is the result of complete calculation.

Taking into account elastic scattering of nucleons leads to increase of the scaled variance (a little bit) (see Fig. 2a dashed line). The elastic scattering introduces additional fluctuations into multi-particle production processes. If we consider nucleons ejected at the cascade stage of interactions as "wounded" ones³, then the fluctuations grow up, and their dependence on multiplicity of "wounded" nucleons appears (see Fig. 2a solid line). So, various aspects of multi-particle production do not allow one to understand

³This depends on experimental conditions.

completely the observed dependence of fluctuations on the collision centrality. The scaled variance is also connected with the "wounded" nucleon multiplicity fluctuations. Dotted line in Fig. 2b shows their strong dependence on Q . Let us mark that the quantity Q is nearly equal to the multiplicity of the "wounded" protons. At fixed Q , the multiplicity of the "wounded" neutrons can fluctuate. Thus, the total multiplicity of the "wounded" nucleons also fluctuates at fixed Q . Inserting the calculated "wounded" nucleon multiplicity fluctuations in the expression for the scaled variance of the negative charged particles and using $(\langle n^2 \rangle - \langle n \rangle^2) / \langle n \rangle = 0.8$ and $\langle n \rangle = 0.25$ (see Fig. 2a), we have a result roughly close to the experimental data (see Fig. 2b dashed line). So, we can say that the amplitude of the scaled variance of the negative particle multiplicity distribution is mainly determined by the fluctuations in NN-collisions. The Q dependence of the scaled variance is closely connected with experimental conditions of centrality selection.

References

- [1] C. Alt *et al.* [NA49 Collab.], *Phys. Rev.* **C75**, 064904 (2007).
- [2] M. Gazdzicki *et al.* [NA49 Collab.], *J. of Phys. G* **30**, S701 (2004).
- [3] M. Rybczynski *et al.* [NA49 Collab.], *J. of Phys. Conf. Ser.* **5**, 74 (2005).
- [4] B. Andersson *et al.* *Nucl. Phys.* **B281**, 289 (1987); B. Nilsson-Almqvist and E. Stenlund, *Comp. Phys. Commun.* **43**, 387 (1987).
- [5] J.P. Bondorf, A.S. Botvina, A.S. Ilinov, I.N. Mishustin, K. Sneppen, *Phys. Rept.* **257**, 133 (1995).
- [6] S.A. Bass *et al.* *Prog. Part. Nucl. Phys.* **41**, 225 (1998); M. Bleicher *et al.* *J. Phys.* **G25**, 1859 (1999).
- [7] V.S. Barashenkov and V.D. Toneev, *Interaction of high energy particles and atomic nuclei with nuclei*, Moscow, Atomizadt, 1972; V.S. Barashenkov, F.G. Zheregny and Zh.Zh. Musulmanbekov, Preprint JINR **P2-83-117** (1983).

MESONS AND GLUEBALLS: A QUANTUM FIELD APPROACH

*G. Ganbold*¹

Bogoliubov Laboratory of Theoretical Physics,
Joint Institute for Nuclear Research, Dubna, 141980 Russia

Abstract

Independent and analytic estimates of the masses of the two-quark and two-gluon bound states are provided within a simple relativistic quantum-field model with the analytic confinement. A reasonable framework is provided to compute simultaneously the lowest glueball mass as well as the conventional meson masses by using the ladder Bethe-Salpeter equation.

1 Introduction

The color confinement of the QCD is achieved by taking into account non-perturbative and nonlinear gluon interaction. In the hadron distance the coupling becomes stronger and the correct summation of the higher-order contributions becomes a problem. The structure of the QCD vacuum and the explicit quark and gluon propagator at the confinement scale is not well established yet. However one may suppose that the confinement is not obligatory connected with the strong-coupling regime in QCD. There exists a conception of the *analytic confinement* based on the assumption that the QCD vacuum is realized by a nontrivial homogenous vacuum gluon field [1] which is the classical solution of the Yang-Mills equation. The quark and gluon propagators in the gluon background $\check{B}_\mu(x)$ with constant strength Λ have been calculated [2] and found entire analytic functions on the complex p^2 -plan. However, a direct use of these propagators to the hadron amplitudes is not convenient and leads to long, cumbersome and complicated formulae. In our earlier investigations [3] we used simple Gaussian exponents for the propagators and obtained the mass spectrum of the two-particle bound states in a self-consistent form. Particularly, qualitative Regge behaviors of the excitations [4] were obtained.

¹Institute of Physics and Technology, 210651 Ulaanbaatar, Mongolia

Below we extend the consideration by taking into account the spin, color and flavor degrees of freedom and develop a simple relativistic quantum field model of interacting quarks and gluons.

2 The Model

Assume that the analytic confinement takes place and the quark and gluon propagators S and D are entire analytic functions. The effective QCD Lagrangian may be written as follows [5]:

$$\mathcal{L} = (\bar{q}S^{-1}q) + \frac{1}{2} (AD^{-1}\mathcal{A}) + g \left(\bar{q}_\alpha^a [\Gamma_\mu^C]_{ab}^{\alpha\beta} q_\beta^b \mathcal{A}_\mu^C \right) + \frac{g}{2} f^{ABC} (\mathcal{A}_\alpha^A \mathcal{A}_\beta^B F_{\alpha\beta}^C),$$

where g is the coupling strength, q and \mathcal{A} are the quark and gluon fields, $[\Gamma_\mu^A]_{ab}^{\alpha\beta} = i\gamma_\mu^{\alpha\beta} t_{ab}^A$, $F_{\mu\nu}^C = \partial_\mu \mathcal{A}_\nu^C - \partial_\nu \mathcal{A}_\mu^C$. Consider the generating functional $Z = \int Dq D\bar{q} \int D\mathcal{A} \exp\{-\mathcal{L}\}$. Within the ladder approximation the following terms correspond to the two-quark and two-gluon bound states:

$$\mathcal{L}_M = \frac{g^2}{2} \int \delta\mathcal{A} e^{-\frac{1}{2}(AD^{-1}\mathcal{A})} (\bar{q}\Gamma q D\bar{q}\Gamma q), \quad \mathcal{L}_G = \frac{g^2}{8} \int \delta\mathcal{A} e^{-\frac{1}{2}(AD^{-1}\mathcal{A})} (f\mathcal{A}\mathcal{A}F)^2.$$

The matrix elements of hadron processes at large distance are integrated characteristics of the quark and gluon propagators and the solution of the Bethe-Salpeter equation in a variational approach [5, 7] should not be too sensitive on the details of propagators. Taking into account the correct global symmetry properties and their breaking by introducing additional physical parameters may be more important than the working out in detail (e.g., [6]). We consider the effective quark and gluon propagators:

$$\begin{aligned} \tilde{S}_{\alpha\beta}^{ab}(\hat{p}) &= \delta^{ab} \frac{\{i\hat{p} + m_f [1 + \gamma_5 \omega(m_f)]\}_{\alpha\beta}}{m_f^2} \exp\left\{-\frac{p^2 + m^2}{2\Lambda^2}\right\}, \\ \tilde{D}_{\alpha\beta}^{AB}(p) &= \delta_{\alpha\beta} \delta^{AB} \frac{1}{\Lambda^2} \exp\left\{-\frac{p^2}{\Lambda^2}\right\}, \end{aligned} \quad (1)$$

where $\omega(m_f) = 1/(1 + m_f^2/4)$. These entire analytic functions in Euclidean metric extend our earlier investigations [3, 4] and represent reasonable approximations to the explicit propagators. In doing so, we use a minimal set of physical parameters, the effective coupling constant $\alpha_s = g^2/4\pi$, the scale of confinement Λ and the quark masses $\{m_{ud}, m_s, m_c, m_b\}$.

3 Meson Spectrum and the Glueball

Consider the meson ground states, the pseudoscalar ($P : 0^{-+}$) and vector ($V : 1^{--}$) mesons. Describe shortly the important steps of our approach [3,7]. First, we allocate one-gluon exchange between quark currents and go to the relative co-ordinates in the center of mass system. Then, perform Fierz transformations to obtain colorless bilocal quark currents and diagonalize \mathcal{L}_M on orthonormalized basis functions $\{U_Q(x)\}$. Introduce a Gaussian path-integral representation for the exponentials by using auxiliary meson fields $B_{\mathcal{N}}$. Apply the *Hadronization Ansatz* to identify $B_{\mathcal{N}}(x)$ with meson fields, where $\mathcal{N} = \{J, Q, f_1, f_2\}$ and J - the spin, $Q = n, l, \mu$, -the radial, orbital, magnetic quantum numbers. The diagonalization of the quadratic form in \mathcal{L}_M on $\{U_Q\}$ is nothing else but the solution of the Bethe-Salpeter equation:

$$1 + \lambda_{\mathcal{N}}(-p^2) = \iint dx dy U_Q(x) \left\{ 1 + g^2 \sqrt{D(x)} \int \frac{d^4 k}{(2\pi)^4} e^{-ik(x-y)} \cdot \text{Tr} \left[\Gamma_J \tilde{S}(\hat{k} + \mu_1 \hat{p}) \Gamma_J \tilde{S}(\hat{k} - \mu_2 \hat{p}) \right] \sqrt{D(y)} \right\} U_Q(y), \quad (2)$$

where $\Gamma_P = i\gamma_5$ and $\Gamma_V = i\gamma_\mu$. The meson mass is derived from equation:

$$1 + \lambda_{\mathcal{N}}(M_{\mathcal{N}}^2) = 0. \quad (3)$$

Our estimates for the pseudoscalar and vector meson masses (Fig.1a) compared with experimental data show that the relative error does not exceed $1 \div 3$ percent. The optimal values of model parameters read:

$$\begin{aligned} \alpha_s &= 0.0764, & \Lambda &= 464 \text{ MeV}, & m_{ud} &= 124 \text{ MeV}, \\ m_s &= 156 \text{ MeV}, & m_c &= 1007 \text{ MeV}, & m_b &= 4500 \text{ MeV}. \end{aligned} \quad (4)$$

The existence of glueballs is predicted by the QCD because of the self-interaction of gluons. The lightest glueball is expected to be a scalar particle with mass $1.2 \div 1.8$ GeV. [8–11]. The experimental basis for the glueball parameters is still rather weak and there are predictions expecting the lightest glueball in the mass range $\sim 1.5 \div 1.8$ MeV [12, 13].

The Gaussian character of the gluon propagator (1) allows us to calculate explicitly the equation for the lowest glueball mass:

$$e^{-\frac{M_G^2}{2\Lambda^2}} = \frac{\alpha_s}{96\pi} \max_{0 < b < 1} \left[\frac{b(4-3b)}{2-b} \right]^2 \left(\frac{19}{8} + \frac{b}{2} + \frac{3b^2}{32} + \frac{7-b}{16} \frac{M_G^2}{\Lambda^2} + \frac{1}{64} \frac{M_G^4}{\Lambda^4} \right). \quad (5)$$

Evolution of the lowest-state glueball scaled mass M_G/Λ with α_s is plotted in

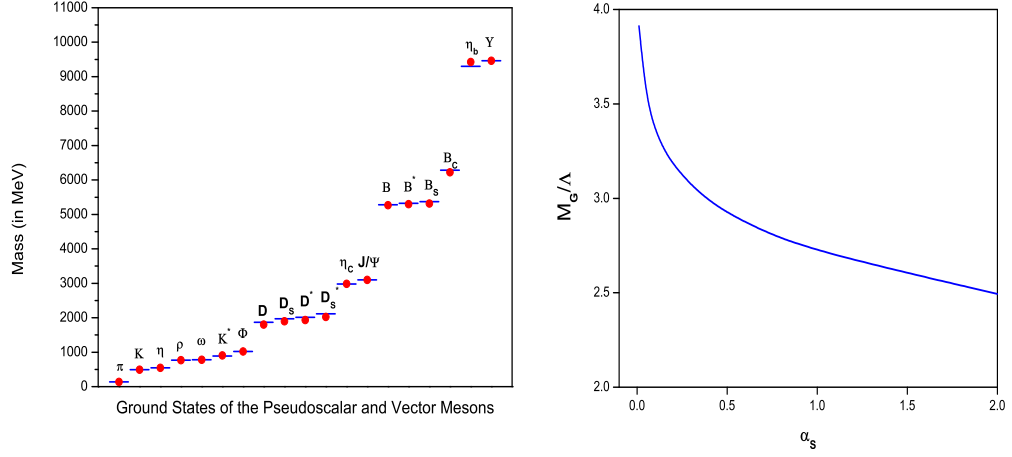


Figure 1: a) The estimated meson masses (dots) compared with experimental data from PDG-2006 (dashes). b) Evolution of the lowest-state glueball mass M_G (scaled to Λ) with the coupling α_s .

Fig.1b. Note, the glueball mass (5) depends on α_s in a nonperturbative way. Particularly, for the parameters $\alpha_s = 0.0764$, $\Lambda = 464$ MeV we estimate

$$M_G = 1592 \text{ MeV} . \quad (6)$$

In conclusion, we have considered a relativistic quantum field model of interacting quarks and gluons under the analytic confinement and estimated the meson ground state spectrum as well as the lowest glueball mass. The merit of our approach is that we describe simultaneously two different sectors of hadron physics by using a minimal set of physical parameters (4).

References

- [1] H. Leutwyler, *Nucl. Phys.* **B179**, 129 (1981).
- [2] Ja.V. Burdanov et al., *Phys. Rev.* **D54**, 4483 (1996).
- [3] G.V. Efimov and G. Ganbold, *Phys. Rev.* **D65**, 054012 (2002).
- [4] G. Ganbold, *AIP Conf. Proc.* **717**, 285 (2004).
- [5] G. Ganbold, arXiv:hep-ph/0610399 (2006).
- [6] T. Feldman, *Int. J. Mod. Phys.* **A15**, 159 (2000).

- [7] G. Ganbold, *AIP Conf. Proc.* **796**, 127 (2005).
- [8] C. Morningstar and M. Peardon, *Phys. Rev.* **D60**, 034509 (1999).
- [9] S. Narison, *Nucl. Phys.* **A675**, 54 (2000).
- [10] H. Forkel, *Phys. Rev.* **D71**, 054008 (2005).
- [11] Y. Chen et. al., *Phys. Rev.* **D73**, 014516 (2006).
- [12] C. Amsler, N.A. Tornqvist, *Phys. Rep.* **389**, 61 (2004).
- [13] D.V. Bugg, *Phys. Lett.* **C397**, 257 (2004).

DYNAMICS OF \bar{K} AND MULTI- \bar{K} NUCLEI

D. Gazda^{*,1}, E. Friedman[%], A. Gal[%], J. Mareš^{*}

^{*}Nuclear Physics Institute, Řež, Czech Republic

[%]Racah Institute of Physics, The Hebrew University, Jerusalem, Israel

Abstract

We report on self-consistent relativistic mean field calculations of single- K^- and multi- \bar{K} nuclear states. In our recent works, we analyzed in detail the interplay between the underlying dynamical processes and the relevant kinematical conditions which determine the decay width of deeply bound \bar{K} -nuclear states. Further, we explored the behavior of the nuclear medium under the influence of increasing strangeness in order to search for \bar{K} condensation precursor phenomena in the multi- \bar{K} nuclei.

1 Model

We studied \bar{K} -nuclear states within the theoretical framework of relativistic mean field theory (RMF) [1,2]. The (anti)kaonic sector was incorporated by adding \mathcal{L}_K to the standard RMF Lagrangian density:

$$\mathcal{L}_K = (\mathcal{D}_\mu)^\dagger (\mathcal{D}^\mu) - m_K^2 K^\dagger K - g_{\sigma K} m_K K^\dagger K \sigma, \quad (1)$$

where $\mathcal{D}_\mu = \partial_\mu + ig_{\omega K}\omega_\mu + ig_{\rho K}\tau \cdot \rho_\mu + ig_{\phi K}\phi_\mu + ie\frac{1}{2}(1 + \tau_3)A_\mu$. This particular choice of interacting scheme induces the following equation of motion for the K^- field:

$$[-\nabla^2 - E_{K^-}^2 + m_K^2 + \text{Re} \Pi_{K^-}]K^- = 0, \quad (2)$$

where the K^- self-energy is given by:

$$\begin{aligned} \text{Re} \Pi_{K^-} = & -g_{\sigma K} m_K \sigma - 2E_{K^-} (g_{\omega K} \omega + g_{\rho K} \rho + g_{\phi K} \phi + eA) \\ & - (g_{\omega K} \omega + g_{\rho K} \rho + g_{\phi K} \phi + eA)^2. \end{aligned} \quad (3)$$

The generalization for nuclear systems containing \bar{K}^0 mesons is straightforward.

¹E-mail address: gazda@ujf.cas.cz

To study the role of p waves in the K^- -nucleus interaction, we included a phenomenological isoscalar p -wave potential:

$$\text{Re } \Pi_{K^-} \rightarrow \text{Re } \Pi_{K^-} + 4\pi (1 + E_{K^-}/m_N)^{-1} c_0 (\nabla \rho_N) \cdot \nabla, \quad (4)$$

where ρ_N is the nuclear density and c_0 is an energy-dependent strength parameter dominated by the contribution of the $\Sigma(1385)$ p -wave resonance [3].

We considered the K^- absorption in the nuclear medium, in order to evaluate the K^- decay width Γ_{K^-} . In our model, this was done by substituting $E_{K^-} \rightarrow E_{K^-} - i\Gamma_{K^-}/2$ and $\text{Re } \Pi_{K^-} \rightarrow \text{Re } \Pi_{K^-} + i\text{Im } \Pi_{K^-}$. Since the imaginary part of the K^- self-energy is not addressed by the traditional RMF model, we adopted the optical model phenomenology by setting:

$$\text{Im } \Pi_{K^-} = (0.7f_{1\Sigma} + 0.1f_{1\Lambda})W_0\rho_N(r) + 0.2f_{2\Sigma}W_0\rho_N^2(r)/\rho_0, \quad (5)$$

with contributions both from (i) single-nucleon absorption processes ($\sim \rho_N$): $\bar{K}N \rightarrow \pi\Sigma, \pi\Lambda$ (70%, 10%) and (ii) conversion processes on two nucleons ($\sim \rho_N^2$): $\bar{K}NN \rightarrow \pi\Sigma$ (20%). The strength of the potential W_0 was fitted to kaonic atom data [1]. We note that the nuclear density $\rho_N(r)$ is a dynamical quantity affected by the presence of a K^- meson. The kinematical suppression factors f_{iY} ($Y = \Sigma, \Lambda$) were introduced to accomplish the reduction of the phase space available for decay products of the K^- deeply bound states.

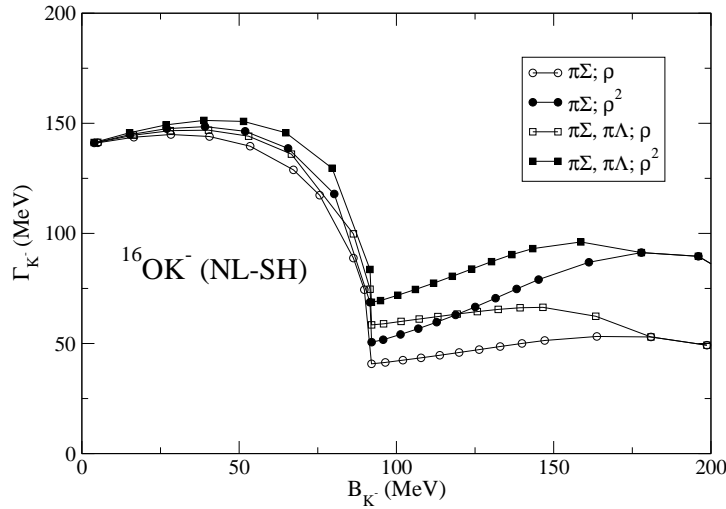


Figure 1: Width of the $1s$ K^- -nuclear state in ^{16}O as function of the K^- binding energy, for absorption through $\bar{K}N \rightarrow \pi\Sigma$, with and without $\bar{K}NN \rightarrow \pi\Lambda$, and assuming ρ or ρ^2 dependence for $\bar{K}NN \rightarrow \Sigma N$.

2 Results and Discussion

We performed fully self-consistent calculations of \bar{K} -nuclear states across the periodic table. Wide range of \bar{K} binding energies was spanned by varying the K^- couplings to the meson fields.

We verified that the interaction of K^- with the ρ -meson mean field affects negligibly the K^- binding energy. For all nuclei and RMF parametrizations considered in our calculations, the ρK^- coupling slightly decreases the K^- binding energy by less than about 5 MeV for $B_{K^-} < 200$ MeV. Similarly, the ϕ -meson contribution in systems with several K^- mesons reduces the K^- binding energy by a few MeV. Calculations involving the p -wave interaction revealed that p waves play a secondary role for deeply bound K^- -nuclear systems where the mean field concept is acceptable. The p -wave interaction enhances the binding energy of a K^- meson, bound initially by 100 MeV due to the purely s -wave interaction, by about 10 MeV and 5 MeV in the case of $^{12}_K\text{-C}$ and $^{40}_K\text{-Ca}$, respectively.

We found that implementation of the $\pi\Lambda$ decay channel in the single-nucleon absorption mode enhances the K^- conversion width for $B_{K^-} \leq 170$ MeV. This enhancement is almost uniform for both linear and non-linear parametrizations and all nuclei under consideration. The most remarkable contribution occurs for binding energies $B_{K^-} \simeq 100 - 160$ MeV where it reaches values of approximately 20 MeV. The assumption of ρ^2 density dependence for the two-nucleon absorption mode adds further conversion width

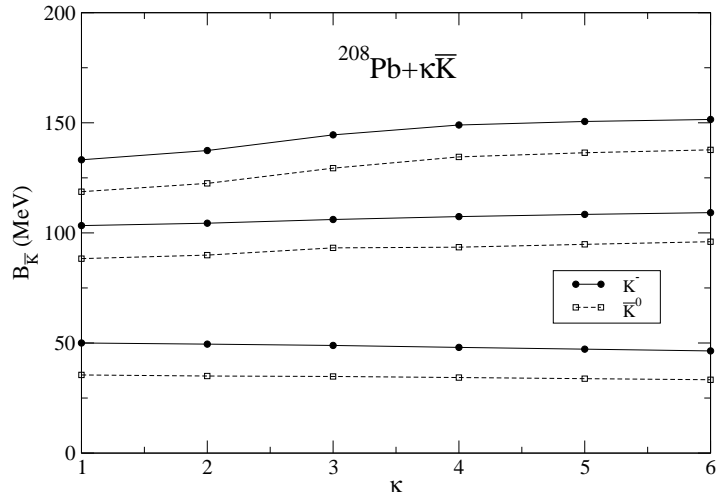


Figure 2: $1s$ \bar{K} binding energy $B_{\bar{K}}$ in $^{208}\text{Pb} + \kappa\bar{K}$ as function of the number κ of antikaons.

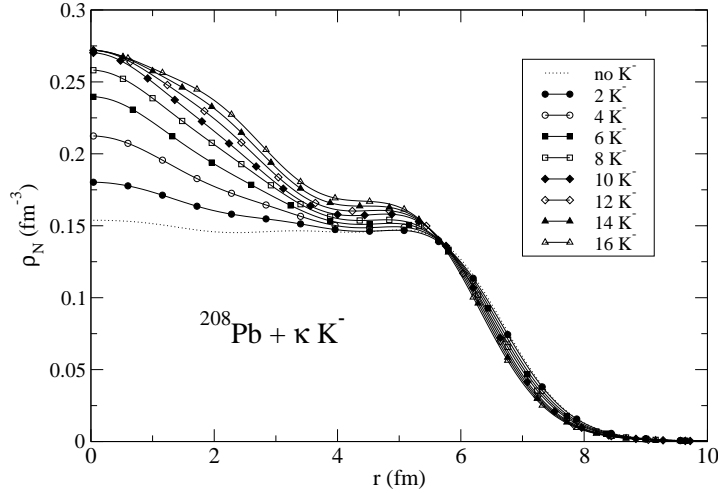


Figure 3: Nuclear density in $^{208}\text{Pb} + \kappa K^-$ for $B_{K^-} = 100$ MeV in $^{208}\text{Pb} + 1K^-$. The dotted curve stands for the ^{208}Pb density in the absence of the K^- meson.

especially for deeply bound K^- -nuclear states ($B_{K^-} > 100$ MeV). Altogether, the results of these comprehensive calculations suggest that K^- total decay widths for deeply bound states are substantial, $\Gamma_{K^-} \sim 50 - 100$ MeV, as illustrated in Fig. 1. total decay widths

e studied also nuclear systems containing several antikaons. The \bar{K} binding energies as well as the nuclear and \bar{K} density distributions were found to increase only moderately or even saturate upon increasing the number of antikaons embedded in the nuclear medium, as shown in Figs. 2 and 3. It is therefore unlikely that multi- \bar{K} nuclei may offer precursor phenomena in nuclear matter towards kaon condensation.

Acknowledgments

This work was supported in part by the GA AVCR grant IAA100480617 and by the Israel Science Foundation grant 757/05.

References

- [1] J. Mareš, E. Friedman, A. Gal, *Nucl. Phys. A* **770**, 84 (2006).
- [2] D. Gazda, E. Friedman, A. Gal, J. Mareš, Dynamics of \bar{K} and multi- \bar{K} nuclei, to appear in *Phys. Rev. C*.
- [3] W. Weise, arXiv:0701035 [nucl-th].

RECOIL POLARIZATION MEASUREMENTS WITH CB@MAMI

D. I. Glazier and D. P. Watts
School of Physics
James Clerk Maxwell Building
University of Edinburgh
Edinburgh, EH9 3JZ,
UK

Abstract

The photoproduction of mesons from a nucleon target is a valuable tool for investigating the underlying structure of the nucleon. Many of the available tagged photon facilities are prioritising the measurement of double polarization observables, in particular experiments with a polarized beam and polarized target. Additionally, measurements of the recoil hadron polarization have been successfully achieved for kaon production, where the weak decay of the produced hyperon contains information on its polarization. For π and η photoproduction the situation is less favourable and a subsequent nuclear scattering interaction is required to deduce the recoiling proton polarization. This talk describes a novel technique to measure recoil polarization using the upgraded Glasgow tagger along with the Crystal Ball detector systems currently in place in the A2 hall at MAMI.

1 Introduction

The last ten years has seen a huge advance in the quantity and quality of photoproduction data from a variety of different labs. Facilities such as MAMI, ELSA, JLAB, GRAAL and LEPS have contributed greatly to this progress utilising high duty factor tagged photon beams and high quality polarized beam and targets. Despite these advances the current experimental situation for recoil polarization observables is much less favourable, due to the requirement of a secondary scattering interaction. However without this crucial information the photoproduction amplitudes and the wealth of information therein, relating to couplings and resonances, cannot be fully constrained in a model independent analysis. Measurement of the recoil polarization in photoproduction reactions is therefore both necessary and timely.

1.1 Pseudoscalar meson photoproduction

The photoproduction of pseudoscalar mesons from a nucleon target, fig. (1), can be described by 16 observables: the differential cross section, 3 single polarization observables (recoil polarization P , target polarization T , beam asymmetry Σ) and a further 12 double polarization observables with combinations of beam, target and recoil polarizations. For these proceedings we will focus on observables that can be measured with a polarized beam and recoil polarization. The differential cross section for such measurements can be written as [1],

$$\rho_f \frac{d\sigma}{d\Omega} = \frac{1}{2} \frac{d\sigma}{d\Omega_{un}} \left\{ 1 - P_\gamma^T \Sigma \cos 2\phi - \sigma_{x'} (P_\gamma^T O_x \sin 2\phi + P_\gamma^C C_x) \right. \\ \left. + \sigma_{y'} (P - P_\gamma^T T \cos 2\phi) - \sigma_{z'} (P_\gamma^T O_z \sin 2\phi + P_\gamma^C C_z) \right\} (1)$$

where O_x , C_x , O_z and C_z are the relevant double polarization observables and P_γ^T and P_γ^C the beam linear and circular polarization respectively. The matrices $\sigma_{i'}$ refer to the hadron quantisation axis of fig. (1) and ρ_f its density matrix. The proposed experiment will potentially allow measurement of 4 observables O_x , C_x , P and T . Together with previous and ongoing measurement of $\frac{d\sigma}{d\Omega}$, Σ , and the beam target observables G and E they will provide the 8 observables necessary to fully constrain the photoproduction amplitudes for the first time [2].

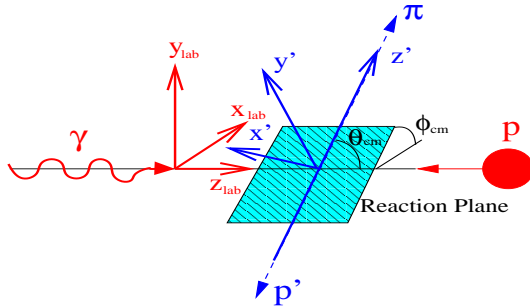


Figure 1: Reference frames in pion photoproduction.

2 Polarimetry with the Crystal Ball/TAPS

2.1 Nucleon Polarimetry

Nucleon polarimeters typically employ nucleon-nucleus scattering interactions which, due to the spin-orbit potential, produce asymmetries proportional to the transverse polarization of the nucleon. This naturally leads to a new reference frame (double primed) with the z-axis along the nucleon momentum direction and y-axis perpendicular to the reaction plane, both in the lab. The resulting azimuthal scattering distribution is then given by,

$$n(\phi_{sc}) = n_o \{1 + A[P_y'' \cos \phi_{sc} - P_x'' \sin \phi_{sc}]\} \quad (2)$$

where ϕ_{sc} is the azimuthal scattering angle and A the analysing power. This allows the polarization components to be extracted from fits to the $n(\phi_{sc})$ distribution after modeling the detector acceptance, or in the case of polarized beam experiments from fits to spin flip asymmetries where the acceptance cancels.

2.2 Polarization Components

Eq. 1 allows us to determine the polarization of the recoiling nucleon in terms of the photoproduction observables. These are found to be for the different beam polarizations,

Circularly Polarized beam

$$P_x = P_\gamma^C C_x, \quad P_y = P, \quad P_z = -P_\gamma^C C_z$$

Linearly Polarized beam

$$P_x = \frac{-P_\gamma^T O_x \sin 2\phi}{(1 - P_\gamma^T \Sigma \cos 2\phi)}, \quad P_y = \frac{P - P_\gamma^T T \cos 2\phi}{(1 - P_\gamma^T \Sigma \cos 2\phi)}, \quad P_z = \frac{-P_\gamma^T O_z \sin 2\phi}{(1 - P_\gamma^T \Sigma \cos 2\phi)}$$

These polarizations must be rotated around the y-axis into the double-primed frame to compare to the polarizations seen by the polarimeter in eqn. (2).

2.3 The Crystal Ball Polarimeter

The Crystal Ball (CB), is an electromagnetic calorimeter comprising 672 NaI crystals arranged spherically and covering 94% of 4π . The forward beam exit hole of the CB is instrumented by the TAPS BaF₂ detector array. Such an arrangement is ideal for detecting the decay photons of neutral mesons such

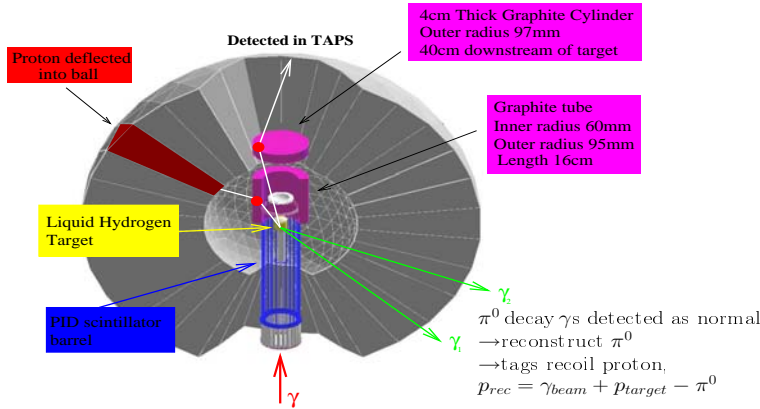


Figure 2: Proposed Crystal Ball polarimeter

as the π^0 and η and the high segmentation allows accurate reconstruction of the meson 4-vectors. In addition as the incident photon 4-vector is accurately determined by the Glasgow photon tagger, the reaction kinematics of meson photoproduction allows accurate reconstruction of the recoil proton 4-vector.

Now, placing a tube of graphite around the proton target at the centre of the ball and a disc of graphite at forward angles shadowing TAPS, as shown in fig. (2), allows the protons to undergo polarized scattering reactions. Subsequent detection of the scattered nucleons in either the CB or TAPS allows reconstruction of the scattered proton direction given its initial momentum from the previous π^0 -tagger analysis. In this way azimuthal scattering asymmetries can be produced and thus the polarizations extracted.

The design illustrated in fig. 2, will be tested in October 2007. The proposed device will allow a full programme of measurements to be undertaken in the coming years on a variety of photoproduction reactions, giving new measurements of polarization observables in π , η and 2π production while taking full advantage of the upgraded MAMI-C facility.

References

- [1] I.S. Barker, A. Donnachie and J.K. Storrow, *Nuc. Phys. B* **95**, 347 (1975).
- [2] Wen-Tai Chiang and Frank Tabakin, *Phys. Rev. C* **55**, 2054 (1975).

MENU 2007
11th International Conference
on Meson-Nucleon Physics and
the Structure of the Nucleon
September 10-14, 2007
IKP, Forschungszentrum Jülich, Germany

RESONANCE PHENOMENA IN HEAVY NUCLEI COLLISIONS AND STRUCTURIZATION OF THE POSITRON SPECTRUM

*A. V. Glushkov*¹
Dept. Nuclear Physics,
Odessa University
Odessa, Ukraine,

Abstract

A consistent unified quantum mechanical and quantum-electrodynamical approach (operator perturbation theory and gauge-invariant quantum-electrodynamical perturbation theory) is used for numerical calculation of the electron-positron pair production cross-section. Resonance phenomena in the nuclear subsystem lead to the structurization of the positron spectrum produced. The positron spectrum narrow peaks are treated as resonance states of the compound superheavy nucleus. Calculation results for the differential cross-sections $d\sigma(\varepsilon s, E_1)/d\varepsilon s$ for U-U collision energies E_1 ($E_1 = 162.0$ keV – the third s -resonance and $E_1 = 247.6$ keV – the fourth s -resonance) are presented.

1 Introduction

Upon collisions of atomic ions or nuclei with energy $E > 1$ MeV the electron-positron pair production is allowed. The cross-section $\sigma(\varepsilon, E)$ of this process depends on the collision energy E and the positron energy ε . It is of a great interest the energy region close to the Coulomb barrier (it corresponds to the energy of several MeV per nucleon). Presently such collisions are under extensive theoretical and experimental study (c.f. refs. [1–12]). Especial attention attract the narrow peaks in the differential cross-section $d\sigma(\varepsilon, E)/d\varepsilon$. The nature of these peaks has not yet any acceptable reasonable interpretation. In principle, the positron spectrum structure can be related with the resonances phenomena of different nature (resonances in the residual electron shell of colliding ions or resonances of the compound nucleus which is created

¹P.O.Box 24a, Odessa-9, 65009, Ukraine, email:glushkov@paco.net

by the colliding nuclei or resonances of new non-identified particles etc.) [3–7]. In general it should be noted that the modern physics of the heavy atoms inner shells deals with the processes which energy and time scales are comparable with those of the low-energy nuclear processes. From this point of view the possibilities of systematic study of the co-operative electron-nuclear processes are appeared. We mean the situation where the interaction of the inner nuclear and electronic degrees of freedom open new reaction channels in both subsystems or leads to appreciable corrections to observable. The correct approach to solution of the related problems must be based on the consistent quantum–mechanical theory of the complicated electron-nuclear system taking into account the quantum–electrodynamics properties of the electron subsystem. The quality of the modelling of inner-nuclear dynamics may have decisive importance. A striking example of such kind presents the electron-positron pair production in the nuclei collision and in strong electromagnetic field (c.f. ref. [3]). The variation of parameters of the inter-nuclear potential within the reasonable limits leads to the qualitative changing of positron spectra [6, 7, 11]. The nuclear subsystem and electron subsystem have been considered on the equal foot as two parts of the complicated system interacting one with another through the model potential. The inner-nuclear dynamics has been treated due to Schrödinger (Dirac equation) with the model potential. The solution of the total electron-nuclear system quantum–mechanical equation is based on the formally exact perturbation theory with the zeroth order Hamiltonian H of the total system being determined by its energy spectrum and the set of the eigenfunctions without specifying analytic form of zero order potential [6–9, 10]. The subsequent corrections of the perturbation theory can be expressed in terms of the matrix elements of total Hamiltonian, calculated between the zeroth order state functions. All the spontaneous decay or the new particle (particles) production processes are excluded in the zero order [6, 7, 11]. The approach treats the widely known distorted waves approximation as the zeroth order approximation in the formally exact quantum–mechanical perturbation theory allowing for successive refinement of calculations [11]. Here we will use a consistent unified quantum mechanical and quantum–electrodynamical approach (operator perturbation theory method and quantum–electrodynamical perturbation theory) [6–8, 10–15] for numeric calculation of the electron–positron pair production cross-section and treat the positron spectrum narrow peaks as resonances states of the compound superheavy nucleus. Resonance phenomena in the nuclear subsystem lead to the structurization of the positron spectrum produced. To calculate the electron-positron pair production cross-section in both cases, we use modified versions of the relativistic energy approach, based on the S -matrix Gell-Mann and Low formalism, and perturbation theory method.

The calculation is carried out for the case of U–U collision (total nuclear system charge being $Z = 184$) with using the two-pocket nuclear potential.

2 Energy approach to calculation of the EPPP cross section

The formulae of EPPP' cross-section can be obtained on the basis of the energy approach [6–11]. As in refs. [6, 7, 11], a one-center model is chosen as a zero-order approximation. Energy approach allows the use of the well developed stationary-state methods to the collisional problem with variable number of particles. In such approximation the calculation of the EPPP' cross-section is reduced to the solution of the ordinary differential equation system. The latter includes: (1) equations for the potentials $V(R)$, $U(r)$ (internuclear potential and electric potential of the compound nucleus), (2) relativistic quantum–mechanical equations for nuclear system– and electron system–state functions, equations for all matrix elements of perturbation theory. The nonstationary feature of our problem manifests itself in the way of the normalization of the nuclear system initial state function and in the principle of the electron system bound state quantization when this state dives into the lower continuum. The motion of nuclear system is described by the Dirac equation whose radial part is represented by

$$\begin{aligned} F' &= -F(\varkappa + |\varkappa|)/T - G(E + 2M\tilde{\alpha}^{-2} - V)\tilde{\alpha}, \\ G' &= G(\varkappa - |\varkappa|)/T + F(E - V)\tilde{\alpha}, \end{aligned} \quad (1)$$

where \varkappa is the Dirac angular quantum number, E is the state energy, F , G being the large and small radial components correspondingly. The two-pocket nuclear potential $V(R)$ is in further used. It is defined by the following differential equation [10]:

$$dV(R) = z \times (R_B/2 - R) \times (3R_B/4 - R) \times (R_B - R) \times R^3(V_B + 8R^8). \quad (2)$$

This potential has the same asymptotics at $R \rightarrow 0$, $R \rightarrow \infty$ as the one-pocket potential used in calculation [6, 7]. Its model parameters are found from the physical conditions: potential generates five S -resonances, the difference $V(R_B) - V(\infty)$ coincide with the experimental energy of the near-barrier collision. It is supposed that $R_B = R_U \approx 6$ fm (radius of compound nucleus charge distribution). It corresponds to the internuclear distance $2R_B \approx 12$ fm. The potential generates the under-barrier s -resonances, whose positions and level widths are listed in the Table 1. The widths of the NS'

Table 1: Energies E and width Γ of s -resonances of the compound U–U nucleus, generated by the potential V

E , keV	25.9	85.8	162.0	247.6	225.2
Γ , eV	0.20×10^{-3}	0.12×10^{-1}	0.86	0.42×10^2	0.16×10^4

states, related to the purely nuclear process, were calculated by the same method as the width of the quasi-stationary state of the electron-positron vacuum with a dived atomic level. The correct procedure was developed earlier and is in the following. In zeroth order of perturbation theory it is used the Hamiltonian generating the same energy spectrum as the potential $V(R)$ but possessing only stationary states. Further note that contrary to the case of the stationary states we use the alternative principle of quantization of the quasi-stationary states [11]. It can be realized by the following procedure: (i) let the trial NS' state energy to be E and preset the function norm by the condition $F(T = 0) = 1$. (ii) Let's integrate the system (1) under this conditions up to asymptotically large T with the simultaneous evaluation of [6, 7]:

$$X(E) = \lim_{T \rightarrow x} T^{2|x|} ((E + 2M\tilde{\alpha}^2 - V)G^2 + (E - V)F^2). \quad (3)$$

This value defines the norm of the state function of the asymptotically free motion [4]. (iii) The value X must be minimized as a function of state energy E . According to our assumption, the stationary points of E correspond to the resonances of the system. The quantization principle for the electron state dived into continuum is described in [4, 7]. The principle is equivalent to the above described principle of the quantization in the case of potential $V(R)$ with a barrier. The main difference is that the role of the potential plays here another function:

$$U_{eff} = (\varepsilon s + 2\tilde{\alpha}^2 - U)(\varepsilon s - U). \quad (4)$$

The effective potential has two turning points T_1, T_2 , dividing the whole integration region into three parts, where $U < \varepsilon s$ ($T < T_1$), $\varepsilon s < U < \varepsilon s + 2\tilde{\alpha}^2$ ($T_1 < T < T_2$), and $U > \varepsilon s + 2\tilde{\alpha}^2$ ($T > T_2$). The quasi-stationary state function must decrease in the second region and oscillate in the third one. The quantization principle implies the minimization of the following function of the trial electron system energy

$$\lim_{T \rightarrow \infty} T^{2|x|} ((\varepsilon s + 2M\tilde{\alpha}^{-2} - U)G^2 + (\varepsilon s - U)F^2). \quad (5)$$

When having found state energy $\varepsilon(1s)$ one must define all the ES' state functions for the zero-order potential U_0 . All the level positions in the potential

U_0 coincide with those in the potential of the compound nucleus electric field U . Functions of all states above the lower continuum are preserved too, the restructuring concerns only the $1s$ -state and the lower continuum states.

The cross-section of the EPPP is connected with the imaginary part of the energy for our system. In the lowest perturbation theory order the second-order diagram describing the polarization of the electron-positron vacuum is calculated as follows [6, 7, 10]:

$$\text{Im}E = -\Gamma/2 = \text{Im}\Sigma(M_{1s,1,F,\varepsilon s})^2/(E_F + \varepsilon(ns) - E_1 - \varepsilon s). \quad (6)$$

The differential cross-section is as follows:

$$d\sigma(\varepsilon, E)/d\varepsilon = \pi(M_{1s,1,F,\varepsilon s})^2(dP_F/dE_F),$$

where P and E are the momentum and energy of the nuclear system final state. The details of numeric procedure are described in refs. [6–13].

3 Results and conclusion

In Ref. [10] we have presented the results of calculation of the differential cross-section for the nuclear subsystem collision energy $E_1 = 352.2$ keV (fifth upper s -resonance). Here we consider calculation results for the differential cross-section $d\sigma(\varepsilon s, E_1)/d\varepsilon s$ (plotted against $\varepsilon(1s) - \varepsilon s$, in B/MeV) for the nuclear subsystem collision energies E_1 : (a) $E_1 = 162.0$ keV (the third s -resonance) and (b) $E_1 = 247.6$ keV (the fourth s -resonance). The main difference of present calculation from analogous calculations [6, 7] is connected with two moments. We use the two-pocket nuclear potential and more correct procedure for account of the perturbation theory higher-order diagrams, describing the additional attraction in the final state of the nuclear subsystem due to the bound electron. The calculation results for $d\sigma(\varepsilon, E_1)/d\varepsilon$ at two different collisional energies $E_1 < V_B$ are presented in Fig.1. It is important to note that the calculation leads to principally the same physical picture as one with one-pocket potential besides appearance of some additional peaks. Naturally, not all processes accompanying the electron-positron pair production are taken into account and considered in this paper. This problem will be considered in the separated paper.

Acknowledgments

The authors are very much thankful to Prof. Dr. Hartmut Machner and also Prof. Dr. S. Krewald, Dr. S. Schadmand for invitation to make

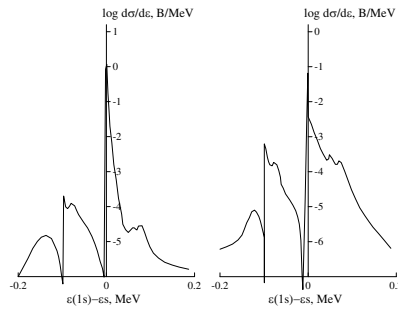


Figure 1: The differential cross-section $d\sigma(\varepsilon s, E_1)/d\varepsilon s$ plotted against $\varepsilon(1s) - \varepsilon s$ (in B/MeV) for the nuclear subsystem collision energies: (a) $E_1 = 162.0$ keV; (b) $E_1 = 247.6$ keV.

contributions on The Eleventh International Conference on Meson-Nucleon Physics and the Structure of the Nucleon-MENU2007 (Juelich, Germany) and support. Authors would like to thank Prof. L. Ivanov, E. Ivanova, V. Letokhov for invaluable advises and Prof. W. Kohn, C. Rothaan, E. Brandas, S.Wilson, C. Maruani, I. Kaplan, A. Theophilou, M. Bonitz, J. Karwowski for useful discussion and comments.

4 References

References

- [1] H.Gould, in: *Photonic, Electronic and Atomic Collisions* eds. F.Aumayr, H.Winter, Singapore: World Scientific, 465 (1997).
- [2] J.C.Wells, B.Segev, in: *Photonic, Electronic and Atomic Collisions* eds. F.Aumayr, H.Winter, Singapore: World Scientific, 487 (1997).
- [3] A.A.Gryb, S.G.Mamaev, V.M.Mostepanenko, *Quantum Effects in Intensive External Fields*, Moscow (1980).
- [4] J.Reinhardt, B.Muller, W.Greiner, *Phys.Rev.A* **24**, 103 (1981).
- [5] J.M.Bang, V.V.Flambaum, J.M.Hansteen, *Z. Phys. A* **330**, 431 (1985).
- [6] L.N.Ivanov, T.V.Zueva, *Phys.Scr.* **43**, 374 (1991).
- [7] L.N.Ivanov, A.V.Glushkov, S.V.Malinovskaya, S.V.Ambrosov, *Preprint of Institute for Spectroscopy AN*, No. AS-5, Troitsk: ISAN, (1991).

- [8] A.V.Glushkov, L.N.Ivanov, *J.Phys.B* **26**, L379 (1993).
- [9] L.N.Ivanov, E.P.Ivanova, L.V.Knight, *Phys.Rev.A* **48**, 4365 (1993).
- [10] A.V.Glushkov., S.V.Ambrosov, A.V.Loboda, in: it New Projects and New Lines of Research in Nuclear Physics eds. G.Fazio, F.Hanappe, Singapore: World Scientific, 126 (2003).
- [11] A.V.Glushkov, in *Low Energy Antiproton Phys.*, AIP Serie. **796**, 206 (2005).
- [12] A.V.Glushkov, S.V.Ambrosov, A.V.Loboda, Yu.G.Chernyakova, O.Yu.Khetselius, A.A.Svinarenko, *Nucl.Phys.A* **734**, e21 (2004).
- [13] A.V.Glushkov, S.V.Ambrosov, A.V.Loboda, Yu.G.Chernyakova, G.P.Prepelitsa, *Int.J.Quant.Chem.* **104**, 562 (2005).
- [14] A.V.Glushkov, L.N.Ivanov, *Phys.Lett.A* **170**, 36 (1992).
- [15] E.P.Ivanova, L.N.Ivanov, A.V.Glushkov, A.E.Kramida, *Phys.Scr.* **32**, 524 (1985).
- [16] A.V.Glushkov, E.P.Ivanova, *J.Quant.Spectr.Rad.Transfer* **36**, 127 (1986).

DISCHARGE OF METASTABLE NUCLEI DURING NEGATIVE MUON CAPTURE: ENERGY APPROACH

A. V. Glushkov^{*%}, ¹, O. Yu. Khetselius^{%#}, A. V. Loboda[%], S. V. Malinovskaya[%]

^{*}Inst. of Spectroscopy (ISAN), Russian Acad.Sci., Troitsk-Moscow, Russia

[%]Odessa University, Odessa, Ukraine

[#]Abdus Salam International Centre for Theoretical Physics, Strada Costiera, Trieste, Italy

Abstract

It is presented a consistent energy approach to the quantum electrodynamics (QED) theory of discharge of a nucleus with emission of γ quantum and further muon conversion, which initiates this discharge. Numerical calculation is carried out for nucleus of ${}_{21}^{49}\text{Sc}_{28}$.

1 Introduction

A negative muon μ captures by a metastable nucleus may accelerate the discharge of the latter by many orders of magnitude (c.f.[1-3]). Principal possibility of storage of significant quantities of the metastable nuclei in processes of the nuclear technology and their concentrating by chemical and laser methods leads to question regarding methods of governing velocity of their decay. It had been considered a possibility of accelerating discharge of a metastable nucleus by means of the angle momentum part to electron shell of atom [3]. A comprehensive QED theory of cooperative laser-electron-nuclear processes is developed in refs. [4-6]. An effect of electron shell is quite small as the parameter r_n/r_a is small (r_n is a radius of nucleus and r_a is a radius of atom). A meso-atomic system differs advantageously of usual atom, as a relation r_n/r_a can vary in the wide limits in dependence upon the nuclear charge. For a certain relation between the energy range of the nuclear and muonic levels the discharge may be followed by the ejection of a muon, which may then participate in the discharge of other nuclei. Here we present a consistent

¹E-mail address:glushkov@paco.net

energy approach in the QED theory of discharge of a nucleus with emission of γ quantum and further muon conversion, which initiates this discharge. Traditional processes of the muon capture are considered in the fundamental papers [7-9] (c.f.[10-13]) and here are not studied. Within energy QED approach (c.f.[4-6, 14-19]), a decay probability is presented as an imaginary part of the energy shift (an energy of excited state of the system).

2 Model and channels of decay for meso-atomic system: Energy approach

We consider a simple one-particle system of nucleus. It is supposed that the system consists off a twice-magic core. A single proton and single muon moves in the core field. The proton and muon interact through the Coulomb potential. This interaction will be accounted for in the first order of the atomic perturbation theory (PT) or second order of the QED PT. Surely a majority of known excited nuclear states have the multi-particle character and it is hardly possible to describe their structure within one-particle model. Nevertheless, the studied effects of muon-proton interaction are not connected with one-particle character of the model. We will calculate probabilities of decay to different channels of the system, which consists of the proton (in an excited state $\Phi_{N_1 J_1}$) and muon (in the ground state Ψ_{1s}^μ). Three channels should be taken into account [3]: i). a radiative purely nuclear 2^j -poled transition (probability P_1); ii). non-radiative decay, when proton transits to the ground state and muon leaves a nucleus with energy: $E = \Delta E_{N_1 J_1}^p - E_\mu^i$; $\Delta E_{N_1 J_1}^p$ is the energy of nuclear transition; E_μ^i is a bond energy of muon in the $1s$ state (P_2); iii). transition of a proton to the ground state with excitation of muon and emission of γ -quantum with energy $h\omega = \Delta E_{N_1 J_1}^p - \Delta E_{nl}^\mu$ (P_3).

A probability of purely radiative nuclear 2^j pole transition is defined as follows ($r_n = 5 \cdot 10^{-13}$ cm):

$$P_1 = 2 \cdot 10^{20} \cdot \frac{j+1}{j[(2j+1)!!]^2} \left(\frac{3}{j+3}\right)^2 \left(\frac{\Delta E [MeV]}{40}\right)^{2j+1} \quad (1)$$

Within the QED PT [5-7], a full probability is divided into the sum of the partial contributions, connected with decay to definite final states of system. These contributions are equal to the corresponding transitions probabilities (P_i). For example, under condition $\Delta E_{N_1 J_1}^p \ll E_\mu^i$ a probability definition reduces to QED calculation of probability of the autoionization decay of the two-particle system. An imaginary part of the energy of excited state of the system in the lowest QED PT order can be written in a standard form (c.f.[14-18]):

$$\begin{aligned}
ImE = e^2 Imi \lim \iint d^4x_1 d^4x_2 e^{\gamma(t_1+t_2)} \bullet \{ & D(r_{c1t1}, r_{c2t2}) \cdot \\
\langle ?_I | (j_{cv}(x_1) j_{cv}(x_2)) | ?_I \rangle + D(r_{p1t1}, r_{p2t2}) \langle ?_I | (j_{pv}(x_1) j_{pv}(x_2)) | ?_I \rangle & (2) \\
+ D(r_{\mu 1t1}, r_{\mu 2t2}) \langle ?_I | (j_{\mu v}(x_1) j_{\mu v}(x_2)) | ?_I \rangle \} &
\end{aligned}$$

Here $D(r_1t_1, r_2t_2)$ is the photon propagator; $j_{cv}, j_{pv}, j_{\mu v}$ are the four-dimensional components for operator of current for particles: core, proton, muon; $? = (r_?, r_?, r_?, t)$ includes the space co-ordinates of three particles and time (equal for all particles); γ adiabatic parameter. After trivial transformations one can get the following expression for imaginary part of the excited state energy of the system as a sum of the corresponding contributions:

$$\begin{aligned}
ImE &= ImEc + ImEp + ImE\mu, \\
ImEa &= -Z_a^2/4\pi \sum_F \iint dr_{c1} dr_{c2} \iint dr_{p1} dr_{p2} \iint dr_{+1\mu 1} dr_{\mu 2} ?_I^*(1) ?_F^*(??) \cdot \\
&\cdot T_a(1, 2) ?_F(1) ?_I(2), \\
T_a(1, 2) &= \exp(w_{IF} r_{a12}) / r_{a12} \{1 - \alpha_1 \alpha_2\},
\end{aligned} \tag{2}$$

Here $r_{a12} = |r_{a1} - r_{aa2}|$; $\hat{O}_c, \hat{O}_p, \hat{O}_e$ are the secondly quantified operators of field of the core particles, the fields of proton and muon. The sum on F designs the summation on the final states of system. Calculation of the probability P_2 can be led to calculation of probability of autoionization decay of the state for two-particle system, i.e. $P_2 = 2ImE/\dot{z}$, where ImE is defined by eq. (2).

3 Calculation for the nucleus ${}_{21}^{49}Sc_{28}$.

The nucleus of ${}_{21}^{49}Sc_{28}$ contains one proton above twice magic core ${}_{20}^{49}Ca_{28}$. The life-time for isolated nucleus in the excited states is of order 10^{-11} . Follow to papers [3,20], let us suppose that a proton moves in an effective field of the core:

$$V - 25 \cdot f(l, j) \cdot V'/r \tag{3}$$

For the self nuclear part of interaction V we accepted the expression from [3,4]. To calculate the corresponding integrals in expression (2), we use the effective Ivanov-Ivanova technique (c.f.[16-19]). The probabilities of the meso- atomic decay (in s^{-1}) for different nuclear transitions are as follows: $P_2(p_{1/2} - p_{3/2}) = 3,93 \cdot 10^{15}$, $P_2(p_{1/2} - f_{7/2}) = 3,15 \cdot 10^{12}$, $P_2(p_{3/2} - -f_{7/2}) =$

$8,83 \cdot 10^{14}$. Let us note that these values are significantly higher than the corresponding non-relativistic estimates [3]. For example, according to [3]: $P_2(p_{1/2} - p_{3/2}) = 3,30 \cdot 10^{15}$. For above indicated transitions the nucleus must give the momentum ΔJ no less than 2,4 and 2 according to the momentum and parity rules. If a meso-atomic system is in the initial state $p_{1/2}$, then the cascade discharge occurs with ejection of the muon on the first stage and the γ quantum emission on the second stage. To consider a case when the second channel is closed and the third one is opened, let us suppose that $E^p(p_{1/2}) - E^p(p_{3/2}) = 0.92$ MeV (fig 2). The energy of the nuclear transition is not sufficient for transition of the muon to the continuum state. However, it is sufficient for excitation to the $2p$ state. It is important to note here that this energy is not lying in the resonant range. The diagram C_1 (fig.1.) describes the proton transition $p_{1/2} - p_{3/2}$ with a virtual excitation of muon to states of series nd and with γ quantum emission of energy:

$$hw = E^p(p_{1/2}) + E^\mu(1s) - E^p(p_{3/2}) - E^\mu(2p).$$

Further the dipole transition $2p - 1s$ can occur. The calculated value for probability of this transition is $P_3 = 1.9 \cdot 10^{13} \text{ s}^{-1}$. This value is significantly more than the corresponding non-relativistic one [3]. It is important also to underline that the value P_3 is more than the probability of the radiation transition $p_{1/2} - p_{3/2}$ and probability of un-radiative transition $p_{1/2} - f_{7/2}$. The next transition $p_{3/2} - f_{7/2}$ occurs without radiation during the time 10^{-15} s with ejection of the muon.

Acknowledgments

The authors are very much thankful to Prof.Dr. Hartmut Machner and also Prof.Dr. S. Krewald, Mrs. S. Schadmand for invitation to make contributions on The Eleventh International Conference on Meson-Nucleon Physics and the Structure of the Nucleon-MENU2007 (Jülich, Germany) and support. Authors would like to thank Prof. L. Ivanov, E. Ivanova, V. Letokhov for invaluable advises.

4 References

References

- [1] V. I. Gol'dansky, V. S. Letokhov, *JETP*. **67**, 513 (1974).
- [2] D. F. Zaretsky, V. Novikov, *Nucl.Phys.* **14**,540 (1960).

- [3] L. N. Ivanov, V. S. Letokhov, *JETP*. **70**, 19 (1976).
- [4] A. V. Glushkov, S. V. Malinovskaya, *In: New projects and new lines of research in nuclear physics*, Eds. G. Fazio and F. Hanappe.- World Sci., Singapore. 242 (2003).
- [5] A. V. Glushkov, S. V. Malinovskaya, Y. G. Chernyakova, A. A. Svinarenko, *Int. Journ. Quant. Chem.* **99**, 889 (2004).
- [6] S. V. Malinovskaya, *Int. Journ. Quant. Chem.* **104**, 531 (2005).
- [7] J. J. Tiomno, J. A. Weller, *Rev.Mod.Phys.* **21**, 153 (1949).
- [8] J. S. Bell, J. Loves, *Nuovo. Cim.* **34**, 433 (1964).
- [9] L. L. Foldi, J. D. Walecka, *Nuovo. Cim.* **34**, 1026 (1964).
- [10] L. I. Ponomarev, G. Fiorentini, *Muon Catal. Fusion.* **1**, 3 (1987).
- [11] S. S. Gerstain, Yu .V. Petrov, L. I. Ponomarev, *Usp. Phys. Nauk* **160**, 3 (1990).
- [12] L. I. Men'shikov, L. N. Somov, *Usp. Phys. Nauk* **160**, 47 (1990).
- [13] A. V. Kravtsov, A. I. Mikhailov, *Phys. Rev. A.* **49**, 3566 (1994).
- [14] A. V. Glushkov, L. N. Ivanov, *Phys.Lett.A.* **170**, 33 (1992).
- [15] A. V. Glushkov, *JETP Lett.* **55**, 97 (1992).
- [16] L. N. Ivanov, E. P. Ivanova, L. N. Knight, *Phys.Rev.A* **48**, 4365 (1993).
- [17] A. V. Glushkov, S. V. Ambrosov, A. V. Loboda, E. P. Gurnitskaya, G. P. Prepelitsa, *Int. Journ. Quant. Chem.* **104**, 537 (2005).
- [18] A. V. Glushkov, S. V. Ambrosov, A. V. Loboda, et al, *Nucl.Phys. A* **734**, e21 (2004).
- [19] A. V. Glushkov, V. D. Rusov, S. V. Ambrosov, A. V. Loboda, *In: New projects and new lines of research in nuclear physics*, Eds. G. Fazio and F. Hanappe.- World Sci., Singapore. 146 (2003).
- [20] J. Bloumkvist, S. Wahlborn, *Ark.Fysic.* **16**, 545 (1960).

MULTIPLICITIES IN (ANTI-)NEUTRINO INTERACTIONS

Ali Murat Güler and Umut Köse

Physics Department of Middle East Technical University
06531-Ankara, Turkey

Abstract

We present an analysis of charged particle multiplicities in charged-current neutrino- and anti-neutrino-nucleus interactions at high energy. Owing to its high spatial resolution and isotropic sensitivity nuclear emulsion is well suited for the investigation of the multiplicity of the production of charged particles. A study of quasi-elastic topologies performed for the first time in nuclear emulsions is also reported. The results of the analysis can be used for tuning Monte Carlo generators of (anti-)neutrino-nucleus interactions.

1 Introduction

The multiplicity of charged particle is an important parameter for investigating particle production mechanism. Therefore, it has been studied in many experiments with different energy and particle beams [1]. The nuclear emulsion with micrometric spatial resolution is very suitable for investigating charged particle multiplicity in (anti-)neutrino interactions. However, only few measurements on neutrino-nucleon interactions in nuclear emulsion are reported. Indeed, there is no measurement on anti-neutrino-nucleus interactions in nuclear emulsion.

A study of charged-particle multiplicities produced in high-energy charged-current (anti-)neutrino interactions in a nuclear emulsion target is performed by the CHORUS collaboration. In this paper, we present the results on the multiplicity of charged particles and a first study of quasi-elastic topologies in ν_μ -A and $\bar{\nu}_\mu$ -A interactions. Such measurements can be useful in order to tune interaction models in Monte Carlo event generators. Further details of the analysis can be found in Ref. [2].

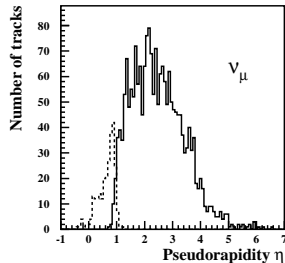


Figure 1: Pseudo-rapidity distributions for tracks classified as shower (full histogram) and grey (dashed histogram) by the scanner.

2 The experimental set-up

The experimental set-up and the characteristics of the CERN wide band neutrino beam are described in more detail in Ref. [3]. The CHORUS detector is a hybrid setup that combines a nuclear emulsion target with several electronic detectors. The target, consisting of *Fuji ET-7B* [4] nuclear emulsions, is segmented into four stacks with overall mass of 770 kg. Each of the stacks consists of eight modules of 36 plates of size 36 cm \times 72 cm. Each plate has a 90 μ m plastic support coated on both sides with a 350 μ m emulsion layer. Each target stack is followed by three interface emulsion sheets with 90 μ m emulsion layers on both sides of an 800 μ m thick plastic base and by a set of scintillating-fibre tracker planes. The emulsion target was exposed perpendicular to the neutrino beam. This allows fast automatic scanning of the emulsion sheets.

3 Analysis

The first step of the event location is to search the tracks reconstructed by the electronic detector in the interface emulsion sheets. Once, a track is found in the interface sheets, it is followed upstream into the emulsion stacks plate by plate. If it is not found in two subsequent plates, the first one is defined as the vertex plate. For this analysis a sample of 1208 events was randomly selected over 150000 located neutrino interactions. These events are scanned visually in order to measure the charged track parameters at the (anti-)neutrino vertex. 627(581) of the selected events contain a leading muon of negative(positive) sign reconstructed by the muon spectrometer.

The sample of events with positive muon has contamination due to ν_μ CC events with the μ^- and punch-through hadrons reconstructed as positive muons in the spectrometer. These contaminations are reduced by applying quality cuts [2] on the muon reconstruction. After the quality selection the sample is reduced to 529 events with positive muon. Finally, We require that square of the invariant mass of the hadronic system, W^2 , of (anti-)neutrino events is greater than $1 \text{ GeV}^2/c^4$. After this selection the number of ν_μ -A ($\bar{\nu}_\mu$ -A) interactions is 496 (369).

The charged tracks are usually classified according to their grain density (number of Ag grains per unit length) as shower, grey and black prongs in the nuclear emulsion as described in Ref. [5]. Since the emulsion sheets were exposed perpendicular to the beam direction in the CHORUS experiment, the track classification based on the grain density is not applied. Instead, ionization features and pseudo-rapidity variable are used for the charged track classification. The black prongs have short path lengths and usually stop within one emulsion plate so that they can be recognized. For the remaining mixture of shower and grey prongs, we measured the particle directions and calculated the pseudo-rapidity variable [6]: $\eta = -\ln \tan \frac{\theta}{2}$ where θ is the emission angle of the prong with respect to the neutrino direction. This has the advantage of being independent of the scanner and of the microscope optics, allowing us to compare in a straightforward manner the multiplicity measurements with the theoretical models. Figure 1 shows the pseudo-rapidity distributions for tracks classified as shower and grey by the scanner, both for neutrino and anti-neutrino interactions. Based on these plots, one can insist that a scanner-independent classification is possible and it is consistent with the traditional one. In the following, all prongs with $\eta \geq 1$ are classified as shower particles. The multiplicities of shower, grey and heavy (grey+black) prongs are denoted by n_{sh} , n_{gr} and n_h , respectively. The total number of charged hadrons classified as shower particles in an event is defined to be $n_{ch} = n_{sh} - 1$, namely the number of shower tracks minus the muon track.

Based on the the pseudo-rapidity selection the average number of shower and heavy prongs in ν_μ -A interactions are $\langle n_{ch}(\nu\text{-A}) \rangle = 3.4 \pm 0.1$ and $\langle n_h(\nu\text{-A}) \rangle = 4.7 \pm 0.2$, respectively. And in the $\bar{\nu}_\mu$ -A induced events are measured to be $\langle n_{ch}(\bar{\nu}\text{-A}) \rangle = 2.8 \pm 0.1$ and $\langle n_h(\bar{\nu}\text{-A}) \rangle = 3.5 \pm 0.2$, respectively. These are the first measurements in nuclear emulsion for anti-neutrino interactions.

The average charged particle multiplicities in $\bar{\nu}$ -A and $\bar{\nu}$ -A interactions have been investigated as a function of W^2 . It is found that the mean multiplicity is in good agreement with a linear dependence of $\ln W^2$ as shown in

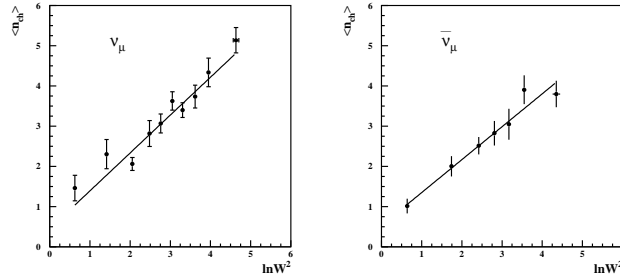


Figure 2: The hadronic shower prong multiplicity distributions as a function of $\ln W^2$ for ν_μ -A, and $\bar{\nu}_\mu$ -A interactions.

Fig. 2. The parameters of the fitted lines were found to be

$$n_{ch}(\bar{\nu}-A) = (0.45 \pm 0.24) + (0.94 \pm 0.08)\ln W^2$$

$$n_{ch}(\nu-A) = (0.53 \pm 0.20) + (0.82 \pm 0.08)\ln W^2.$$

For the first time a sample of (anti-)neutrino events measured in emulsions is large enough to study (QE+RES)-like topologies. In order to have a minimum bias sample of (QE+RES)-like events, the $W^2 \geq 1 \text{ GeV}^2/c^4$ cut was not applied to the located events. Hence, the starting sample of $\nu_\mu - A$ ($\bar{\nu}_\mu - A$) interactions becomes 627 (529). An event is defined as being (QE+RES)-like, if the number of shower prongs is zero or one and the number grey prongs zero or one for for ν -A interactions regardless of the number of black tracks. In order to obtain (QE+RES)-like enriched sample in ν -A interactions, the sum of shower prongs and grey prongs is required to be one or zero regardless of the number of black tracks. After applying the efficiency and background corrections, the fraction of (QE+RES)-like events is found to be $(13.4 \pm 1.0 \pm 2.0)\%$ for ν_μ and $(26.3 \pm 1.4 \pm 3.9)\%$ for $\bar{\nu}_\mu$ interactions, respectively.

References

- [1] C. Berger *et al.* [PLUTO Collab.], Phys. Lett. **B78**, 176 (1978); W. Brandelik *et al.*, [TASSO Collab.], Phys. Lett. **B89**, 418 (1980); K. J. Biehl *et al.*, Fortschr. Phys. **V28**, 124 (1980); G. J. Alner *et al.*, Phys. Reports **154**, 245 (1987); R. E. Ansorge *et al.*, Z. Phys. **C43**, 357, (1989).
- [2] A. Kayis-Topaksu *et al.* [CHORUS Coll.], Eur.Phys.J. **C51**, 775 (2007).
- [3] E. Eskut *et al.* [CHORUS Coll.], Nucl. Inst. Meth. **A401**, 7 (1997).

- [4] S. Aoki *et al.*, [CHORUS Coll.], Nucl. Inst. Meth. **A447**, 361 (2000).
- [5] C. F. Powell, P. H. Fowler and D. H. Perkins, "The Study of Elementary Particles by the Photographic Method", Pergamon Press, London (1959).
- [6] W. M. Yao *et al.*, J. Phys. **G33**, 1 (2006).

EVALUATION OF THE πN SIGMA TERM USING DISPERSION RELATIONS - PRESENT STATUS

M. Hadzimehmedovic, H. Osmanovic, J. Stahov
Faculty of Science
University of Tuzla, Bosnia and Herzegovina

Abstract

The dispersion relations are used to perform an analytical continuation of the πN scattering amplitude \bar{D}^+ to the Cheng-Dashen point and to calculate the πN sigma term. The dispersion relations were evaluated along two different families of dispersion curves passing through different kinematical regions in the s-channel physical region. The obtained results for the sigma term are still within the error bars of the previous Karlsruhe result.

1 Introduction

A low energy theorem [1] relates the πN sigma term to the isoscalar, crossing symmetric scattering amplitude $\bar{D}^+(\nu, t)$ at the Cheng-Dashen point (CD) $\nu = 0, t = 2m_\pi^2$:

$$\Sigma = F_\pi^2 \bar{D}^+(0, 2m_\pi^2), \quad (1)$$

where m_π is a charged pion mass and F_π is the pion decay constant. The bar indicates that a pseudovector Born term is subtracted. For more details about πN kinematics we refer to [2]. To apply the low energy theorem one has to perform analytic continuation of \bar{D}^+ amplitude to the CD point which lies outside of the πN physical region. An analytic continuation may be performed by means of dispersion relations along different curves. In our applications the dispersion curves pass through the regions where the s-channel partial wave expansion converges and the nearby parts of the t-channel cut may be calculated from the t-channel partial waves.

There are two the most frequently used methods of determination of \bar{D}^+ amplitude at the CD point. In the first method [2], \bar{D}^+ amplitude is

represented by the subthreshold expansion:

$$\overline{D}^+(\nu^2, t) = \sum_{m,n} \overline{d}_{mn}^+ \nu^{2m} t^n, \quad \overline{D}^+(0, 2m_\pi^2) = \overline{d}_{00}^+ + \overline{d}_{01}^+ \cdot 2m_\pi^2 + \overline{d}_{02}^+ \cdot (2m_\pi^2)^2 + \dots$$

The validity of expansion is limited by the nearest singularities, s- and u-channel thresholds and the t-channel pseudothreshold $t = 4m_\pi^2$.

In the second approach, the dispersion relations are applied along curves which pass through the CD point [3–6], and \overline{D}^+ amplitude at the CD point is calculated directly.

2 Continuation into the unphysical region

More technical details about our method may be found in [7]. Once subtracted FTDR were performed at 40 t-values $t \in [-3m_\pi^2, 0]$. Using the discrepancy function method, \overline{D}^+ amplitude was extrapolated at 20 equidistant values $\nu^2 \in [0, \nu_{max}^2 = 0.5m_\pi^2]$ inside Mandelstam triangle. An analytic continuation into the part of the Mandelstam triangle $0 < t < 4m_\pi^2$ was performed along hyperbolas in the (s,u) plane [8]:

$$(s - a)(u - a) = b,$$

where a is asymptote and b is a parameter. For $b = (m^2 - a - m_\pi^2) - 4m_\pi^2$ (m is a proton mass) and $a < 0$ hyperbolas remain inside the s-channel physical region and pass through the s-channel threshold (interior hyperbolas). Furthermore, if $a \geq -1 \text{ GeV}^2$ the nearby parts of the t-channel cut ($t \leq 30m_\pi^2$) may be represented by expansion in terms of the $\pi\pi \rightarrow N\overline{N}$ partial waves [9]. If $a = -m^2 + \frac{1}{2}m_\pi^2 \approx -0.871 \text{ GeV}^2$, interior hyperbola passes through the CD point. The interior dispersion relations along this single curve were recently used in [4] to calculate the πN sigma term. In our approach once subtracted IDR for \overline{D}^+ amplitude were evaluated along a set of hyperbolas crossing $\nu = 0$ line at 40 equidistant points $t \in [m_\pi^2, 3m_\pi^2]$. Along each hyperbola \overline{D}^+ amplitude was evaluated at 20 equidistant values $\nu^2 \in [0, \nu_{max}^2 = 0.5m_\pi^2]$. The coefficients $\{\overline{d}_{mn}^+\}$ were determined by fitting of obtained 1600 values of \overline{D}^+ to the subthreshold expansion. In Ref. [5] R. Koch proposed an analytic continuation of the \overline{D}^+ amplitude into the subthreshold region along hyperbolas in a (ν^2, t) plane:

$$(\nu^2 - \nu_0^2)(t - t_0) = \frac{a}{2}.$$

Varying parameters ν_0^2 and t_0 hyperbolas cover a wide angular range in the s-channel physical region, remain within or close to the s-channel physical

region, and pass through the t-channel domain where the t-channel partial wave expansion converge. Hyperbolas in the (ν^2, t) plane are very convenient for calculation of the sigma term because a set of hyperbolas with $a = 2(t - 2m_\pi^2) \cdot \nu_0^2$ passes through the CD point.

3 Results, discussion and conclusions

Partial wave solution GWU06 [10] was used as an input from the s-channel. The nearby parts of the t-channel cut were evaluated using our results for the $\pi\pi \rightarrow N\bar{N}$ s-wave [6] available up to $t = 30m_\pi^2$. Higher energy contribution from the s-channel and the t-channel, and contribution from the d and higher partial waves in the t-channel as well, were included in discrepancy function.

Analytic continuation of \bar{D}^+ amplitude to the CD point was performed along a set of 50 hyperbolas in the (ν^2, t) plane. Parameters ν_0^2 and t_0 assumed values within the range $(-10m_\pi^2, -30m_\pi^2)$. This set of hyperbolas covers the whole of the angular region in the s-channel where new data on πN scattering exist. The following values for \bar{D}^+ amplitude (in m_π units) at CD point and the Σ term were obtained:

$$\bar{D}^+(0, 2m_\pi^2) = 1.185 \pm 0.033; \quad \Sigma = (72 \pm 2)MeV.$$

From our second approach, the following values for the coefficients in the subthreshold expansion (in m_π units) and corresponding value of the Σ term were obtained:

$$\begin{aligned} \bar{d}_{00}^+ &= -1.377 \pm 0.01, & \bar{d}_{01}^+ &= 1.176 \pm 0.01, & \bar{d}_{02}^+ &= 0.039 \pm 0.001, \\ \bar{d}_{03}^+ &= 0.004 \pm 0.001; & \bar{D}^+(0, 2m_\pi^2) &= 1.163 \pm 0.033; & \Sigma &= (71 \pm 2)MeV. \end{aligned}$$

Quoted errors are only due to numerical procedures used in our calculations. Using the same input from the s-channel and taking into account contribution from the nearby parts of the t-channel cut in an implicit way, authors in Ref. [4] obtained significantly higher value for the πN sigma term, $\Sigma = (81 \pm 6)MeV$. We do think that our value obtained by analytic continuation to the unphysical region along many curves is more reliable than the value obtained by continuation along a single curve. It is important to point out that experimental value of the πN sigma term depends on the πN scattering data, especially in the low energy region. The CHAOS collaboration [11] significantly increased the amount of the high quality data at the low energy. These data allow a direct determination of the \bar{D}^+ forward amplitude which makes the analytic continuation of the \bar{D}^+ amplitude into

the unphysical region more reliable. To our knowledge, these data were not included in any of new PWA.

Conclusions: Two methods used in our evaluation of the πN sigma term give mutually consistent values which are still inside the error bars of Karlsruhe value [5]. CHAOS data should be used in forthcoming PWA to get more reliable partial waves close to the threshold.

*Supported by Ministry of Education and Science of Tuzla Kanton.
JS gratefully acknowledges support from FZ Juelich.*

References

- [1] L. S. Brown *et al.*, *Phys. Rev.* **D4**, 2801 (1971).
- [2] G. Höhler, *Pion-Nucleon Scattering, Landolt-Börnstein, Vol.I/9b2* (Springer, 1983).
- [3] D. Moir, R. Jacob, G. E. Hite, *Nucl. Phys.* **B103**, 477 (1976).
- [4] G. E. Hite, W. B. Kaufman, R. J. Jacob, *Phys. Rev.* **C71**, 065201 (2005).
- [5] R. Koch, *Z. Physik* **C15**, 161 (1982).
- [6] M. Hadzimehmedovic, H. Osmanovic, J. Stahov, *Int. J. of Mod. Phys.* **20**, No 8, 9, 1876 (2005).
- [7] J. Stahov, *πN Newsletter*, **15**, 13 (1999).
- [8] G. Hite, F. Steiner, *Nuovo Cim.* **18A**, 237 (1973).
- [9] E. Borie, F. Kaiser, *Nucl. Phys.* **B126**, 173 (1977).
- [10] SAID πN database, <http://gwdac.phys.gwu.edu>.
- [11] H. Denz *et al.*, *Phys. Lett.* **B633**, 209 (2006).
- [12] E. Borie, F. Kaiser, *Nucl. Phys.* **B126**, 173 (1977).

DETERMINATION OF THE POTENTIAL COEFFICIENTS OF THE BARYONS AND THE EFFECT OF SPIN AND ISOSPIN POTENTIAL ON THEIR ENERGY

H. Hassanabadi¹ and A. A. Rajabi

Physics Department, Shahrood University Of Technology
P.O.Box 3619995161-316, Shahrood, Iran

Abstract

Spin-and isospin-dependent terms are of great importance in the study of baryons for several reasons. On the other hand, the relativistic energy spectra has some highly important features which makes it much superior to the nonrelativistic one. The present work investigates the effects of spin-spin, spin-isospin and isospin-isospin interactions on the relativistic energy spectra of baryons. Our study reveals that both confining and non confining terms must be taken into account in order to obtain more exact energy spectra.

1 Introduction

In the relativistic limit, provided that the sizes of the particles under study are in quantum size, we have to use Dirac equation to study a baryonic system with total spin $\frac{1}{2}$ [1-3]. For such a system we represent the total wave function by $\psi_{\nu\gamma} = \begin{pmatrix} \Phi_{\nu\gamma} \\ \chi_{\nu\gamma} \end{pmatrix}$, (γ and ν are introduced after Eqs. (7) and (9) respectively) Just similar to QED, considering non-linear terms in the potential relation in QCD leads to more exact calculations as well [4, 5]. When one single gluon is exchanged in a short distance, as both gluon and photon are massless, the interactions can be taken the same apart from their coupling constants. In many practical applications a harmonic oscillator potential yields spectra not much different from those found from potentials such as columbic plus linear that QCD prejudice would favor [6, 7]. Since harmonic oscillator models have nice mathematical properties, they have often been used as the confining potential [8, 9]. On the other hand, the

¹E-mail address:h.hasanabadi@shahroodut.ac.ir

columbic term alone is not sufficient, because it would allow free quarks to ionize from the system.

By making use of Jacobi coordinates [10]

$$\vec{\rho} = \frac{\vec{r}_1 - \vec{r}_2}{\sqrt{2}}, \vec{\lambda} = \frac{\vec{r}_1 + \vec{r}_2 - 2\vec{r}_3}{\sqrt{6}}, \vec{R} = \frac{\vec{r}_1 + \vec{r}_2 + \vec{r}_3}{3} \quad (1)$$

as well as introducing the hyperradius quantity x , $x = \sqrt{\rho^2 + \lambda^2}$ the potential relation can be written as

$$2U_0(x) = 2V_0(x) = ax^2 + bx - \frac{c}{x}. \quad (2)$$

where a , b and c are constants. Note that in writing the potential relation in the above form we have neglected the center of mass motion. In terminology, the potentials $V_0(x)$ and $U_0(x)$ are respectively called vector and scalar potentials [11, 12]. The reason is that the so-called scalar potential is bracketed with the mass and the so-called vector potential goes with the energy in Dirac equation. We have considered the case $U_0(x) = V_0(x)$ since the potential relation has in general the form $U(x) = \frac{1}{2}(1 + e\gamma_0)A(x)$, where $A(x) = ax^2 + bx - \frac{c}{x}$. For e we use the typical values $e = 0$ and $e = 1$. The latter is most important since it implied by $SU(2)$ symmetry as well as duality of angular momentum studied by Bell and Ruegg [13, 14]. It should be noted that the value $e = 0$ results in a scalar potential.

2 Exact analytical solution of Dirac equation

By representing the mass and energy of one quark respectively by m_1 and ε_1 , the corresponding Dirac equation is written as

$$[\vec{\alpha} \cdot \vec{p} + \beta(m_1 + U_0(x))]\psi_{\nu\gamma}(x) = (E_{\nu\gamma} - V_0(x))\psi_{\nu\gamma}(x), \quad (3)$$

where $m = 3m_1$, $E_{\nu\gamma} = 3\varepsilon_{\nu\gamma}$. Note that in obtaining the above equation the three quarks have been assumed to be of both equal rest mass and energy. For the up component of the wave function, we have

$$(p_1^2 + p_2^2 + p_3^2)\Phi_{\nu\gamma} = \sum_{i=1}^3 (\varepsilon_i^2 - m_i^2)\Phi_{\nu\gamma} - 2U_{01}(x) \sum_{i=1}^3 (\varepsilon_i + m_i)\Phi_{\nu\gamma}. \quad (4)$$

By using the above equation as well as the relation [15–17]

$$\nabla^2 = \nabla_\rho^2 + \nabla_\lambda^2 = -\left[\frac{d^2}{dx^2} + \frac{5}{x} \frac{d}{dx} - \frac{L^2(\Omega_\rho, \Omega_\lambda, \xi)}{x^2}\right], \quad (5)$$

where L is the total angular momentum operator, one can find that

$$\begin{aligned} & -\left[\frac{d^2}{dx^2} + \frac{5}{x} \frac{d}{dx} - \frac{L^2(\Omega_\rho, \Omega_\lambda, \xi)}{x^2}\right] \Phi_{\nu\gamma} \\ & = \frac{1}{3}(E_{\nu\gamma}^2 - 9m_1^2)\Phi_{\nu\gamma} - (ax^2 + bx - \frac{c}{x})(E_{\nu\gamma} + 3m_1)\Phi_{\nu\gamma}. \end{aligned} \quad (6)$$

It should be noted that [18]

$$\Phi_{\nu\gamma} = \phi_{\nu\gamma}(x)Y_{\gamma, l_\rho, l_\lambda}(\Omega_\rho, \Omega_\lambda, \xi), \quad (7)$$

where $\Omega_\rho = (\theta_\rho, \phi_\rho)$ and $\Omega_\lambda = (\theta_\lambda, \phi_\lambda)$ are solid angles corresponding to and coordinates respectively, $\xi = \text{Arctg}\frac{\rho}{\lambda}$ is called the hyperangle and γ is the grand angular quantum number given by $\gamma = 2n + l_\rho + l_\lambda$, where n is a non negative integer, l_ρ and l_λ are the angular momentum corresponding to the coordinates ρ and λ respectively. On the other hand, as [15–17]

$$L^2(\Omega_\rho, \Omega_\lambda, \xi)Y_{\gamma, l_\rho, l_\lambda}(\Omega_\rho, \Omega_\lambda, \xi) = \gamma(\gamma + 4)Y_{\gamma, l_\rho, l_\lambda}(\Omega_\rho, \Omega_\lambda, \xi). \quad (8)$$

By choosing $\phi_{\nu\gamma}(x)$ (see equation 7) as

$$\phi_{\nu\gamma}(x) = x^{-\frac{5}{2}}\varphi_{\nu\gamma}(x), \quad (9)$$

where ν determines the number of nodes the wave function and in fact represents the distinct solutions corresponding to a particular grand angular quantum number, and $\varphi_{\nu\gamma}(x)$ as

$$\varphi_{\nu\gamma}(x) = f_\nu(x)e^{g_\nu(x)}. \quad (10)$$

After considering appropriate ansatzs for $f_\nu(x)$ and $g_\nu(x)$ [19–21] and taking $a = (E_{\nu\gamma} + 3m_1)\omega^2$, it can be proved that, for the case $\nu = 0$, is given by [26]

$$E_{0\gamma} = \frac{3(2\gamma + 5)^2[m_1 + \omega(2\gamma + 6)] - 9m_1c^2}{(2\gamma + 5)^2 + 3c^2}. \quad (11)$$

In the energy spectra obtained from Schrödinger equation two important points are not taken into account: first, the spin of the particles and second, their rest mass energy. On the contrary, in the energy spectra obtained from Dirac equation both spin and rest mass are taken in to account. Finally it is proved that the total wave function in the ground state and in the case $\gamma = 0$ is [26]

$$\psi_{00} = N_{00} \left(\frac{1}{\frac{i\vec{\sigma}\cdot\hat{x}}{E_{00}+3m_1}(\alpha x + \beta)} \right) \exp\left[-\frac{1}{2}(E_{00} + 3m_1)\omega x^2 - \frac{b}{2\omega}x\right] Y_{[0],0,0}(\Omega_\rho, \Omega_\lambda, \xi), \quad (12)$$

Table 1:

<i>Baryon</i>	$I(J^p)$	$a(fm^{-3})$	$b(fm^{-1})$	c
$N(938)$	$\frac{1}{2}(\frac{1}{2})^+$	0.7182	1.5294	2.0757
$\Lambda(1115)$	$0(\frac{1}{2})^+$	0.7024	1.5118	2.0831
$\Sigma(1189)$	$1(\frac{1}{2})^+$	0.6935	1.4781	2.0894
$\Sigma(1192)$	$1(\frac{1}{2})^+$	0.6927	1.4706	2.0907
$\Sigma(1197)$	$1(\frac{1}{2})^+$	0.6919	1.4693	2.0913
$\Xi(1314)$	$\frac{1}{2}(\frac{1}{2})^+$	0.5856	1.3852	2.1014
$\Xi(1321)$	$\frac{1}{2}(\frac{1}{2})^+$	0.5819	1.3809	2.1032
$N(1440)$	$\frac{1}{2}(\frac{1}{2})^+$	0.5226	1.3771	2.1085

where \hat{x} is the unit vector in the hypersphere space and N_{00} is the normalization constant. On the other hand, the charge radius of each baryon is defined as [22]

$$\langle x^2 \rangle^{\frac{1}{2}} = \frac{\int_0^\infty [1 + \frac{((E_{0\gamma} + 3m_1)\omega x + \frac{b}{2\omega})^2}{E_{0\gamma}^2(1 + \frac{3m_1}{E_{0\gamma}})^2}] \exp(-(E_{0\gamma} + 3m_1)\omega x^2 - 2\frac{b}{2\omega}x)x^7 dx}{\int_0^\infty [1 + \frac{((E_{0\gamma} + 3m_1)\omega x + \frac{b}{2\omega})^2}{E_{0\gamma}^2(1 + \frac{3m_1}{E_{0\gamma}})^2}] \exp(-(E_{0\gamma} + 3m_1)\omega x^2 - 2\frac{b}{2\omega}x)x^5 dx}, \quad (13)$$

where the parameters b and ω are not yet determined. By using the Eq. (11) as well as substituting the corresponding value of the charge radius of each baryon in Eq. (13) we have calculated the parameters b , ω and thereby the parameters a , c in each case, and have listed them in Table 1.

Now, by knowing the values of parameters a , b and c , the wave function is a function of the hyperradius quantity x only.

3 Spin and isospin effects

Within the algebraic approach, the quark energy is written in terms of symmetry groups to introduce an isospin-dependent terms, which turns out to be important for the description of spectrum [23,24]. Furthermore, the splittings within the multiplets are not all adequately described by the hyperfine interaction. One should remind that the form often assumed for the hyperfine interaction contains a δ -like term, which is troublesome from the theoretical point of view. On the other hand, the splitting can be originated also by other terms, for instance isospin dependent ones. The standard hyperfine interaction is used to reproduce the splitting with in the SU(6)-multiplets.

As this interaction contains a term it is modified by introducing a smearing factor given by a Gaussian factor of the hyper radius x

$$H_S = A_S \left(\frac{1}{\sqrt{2}\sigma_S} \right)^3 \exp\left(-\frac{x^2}{\sigma_S^2}\right) \sum (S_i \cdot S_j), \quad (14)$$

Where $A_S = 67.4(fm^2)$ and $\sigma_S = 2.87(fm)$ and

$$\sum (S_i \cdot S_j) = \frac{1}{2}(S^2 - \frac{9}{4}). \quad (15)$$

There are different multiples for the introduction of a flavour dependent term in the three-quark interaction. The well known Gueresey-Radicati mass formula contains flavour dependent terms, which is essential for the description of the strange baryon spectrum [24]. For the non strange baryons this formula implies isospin dependence [24]. It has also been pointed recently that an isospin dependence of the quark potential can be obtained by means of quark exchange [25]. More generally, one can expect that the quark-quark pair production can lead to an effective quark interaction containing an isospin dependent term. With these motivations in mind, we have calculated the effects of two isospin terms as well as the introduced spin dependent one. The first one depends on the isospin only and has the form

$$H_I = A_I \left(\frac{1}{\sqrt{2}\sigma_I} \right)^3 \exp\left(-\frac{x^2}{\sigma_I^2}\right) \sum (I_i \cdot I_j), \quad (16)$$

Where $A_I = 51.7(fm^2)$ and $\sigma_I = 3.45(fm)$. The second one is a spin-isospin interaction, Given by:

$$H_{SI} = A_{SI} \left(\frac{1}{\sqrt{2}\sigma_{SI}} \right)^3 \exp\left(-\frac{x^2}{\sigma_{SI}^2}\right) \sum (S_i \cdot S_j)(I_i \cdot I_j), \quad (17)$$

Where $A_{SI} = -106.2(fm^2)$ and $\sigma_{SI} = 2.31(fm)$. Finally, by using the first order time-independent perturbation theory we have calculated the obtained results and have listed them in table-2. A look at table-2 reveals that the first-order energy shift due to spin-spin interaction has the greatest value in comparison with the two other mentioned perturbations. It also shows that the heavier the baryon, the less the energy shifts due to spin-isospin and isospin-isospin perturbations. The reason is that the heavier the baryon, the less u and d quarks there are in its quark content.

Table -2 .

<i>Baryon</i>	$I(J^p)$	$\Delta_S^{(1)}(MeV)$	$\Delta_I^{(1)}(MeV)$	$\Delta_{SI}^{(1)}(MeV)$
$N(938)$	$\frac{1}{2}(\frac{1}{2})^+$	-30.15	-20.73	-12.07
$\Lambda(1115)$	$0(\frac{1}{2})^+$	-23.17	-18.59	-11.83
$\Sigma(1189)$	$1(\frac{1}{2})^+$	-22.85	-18.06	11.13
$\Sigma(1192)$	$1(\frac{1}{2})^+$	-21.13	-17.76	11.05
$\Sigma(1197)$	$1(\frac{1}{2})^+$	-20.72	-17.64	10.85
$\Xi(1314)$	$\frac{1}{2}(\frac{1}{2})^+$	-17.38	-13.29	9.31
$\Xi(1321)$	$\frac{1}{2}(\frac{1}{2})^+$	-17.19	-12.47	8.65
$N(1440)$	$\frac{1}{2}(\frac{1}{2})^+$	-15.42	-19.04	11.36

4 Conclusion

By using the energy spectra obtained from the exact analytical solution for the three-body baryonic system we calculated the potential coefficients for each baryon and thereby the effects of spin-spin, spin-isospin and isospin-isospin interactions by considering the corresponding potentials as perturbations. Our study reveals that the first-order energy shift due to spin-spin interaction has the greatest value in comparison with the two other mentioned perturbations. We also found that the heavier the baryon, the less the energy shift due to spin-isospin and isospin-isospin perturbations. The reason is that the heavier the baryon, the less u and d quarks there are in its quark content. Also, one can see that the shift due to spin-spin term has the greatest value among the three considered terms.

References

- [1] F. Halzen. and D. Martin, Quarks and leptons, John Wiley (1984) 168-169.
- [2] F. E. Close, (1979). An Introduction to quarks and partons, New York, Academic press.
- [3] M. M. Giannini, E. Santopinto, F. Iachello, in symmetries in Science VII, edited by B. Gruber (plenum Press, New York, 1995)p. 445.
- [4] Gunnar S. Bali et al., Phys. Rev D 62, 054503 (2000); Gunnar S. Bali, Phys. Rep 343, 1 (2001).
- [5] A. A. Rajabi, Indian Journal of pure and applied physics vol41, pp. 89-94 February (2003).

-
- [6] M. Znojil, *J.Math Phys* .31, (1990).
- [7] M. Fabre de la Ripelle, *Ann. Phys (N.Y)*.147, 281-320 (1983).
- [8] M. Ferraris, M. M. Giannini, M. Pizzo, E. Santopinto, L. Tiator, *Phys. Lett. B* 364, 231 (1995).
- [9] M. Campostrini, K. Moriarty, C. Rebbi, *Phys, Rev. D* 36, 3450 (1987); L.Heller, in *quarks and Nuclear Forces*, edited by D.C. Vries, B. Zeitnitz, *Springer Tracts Mod. phys. Vol. 100* (Speringer, Berlin, p. 145 1982).
- [10] M. M. Giannini, E. Santopinto and A. Vassallo, *Nuclear Physics A*699, 308 -311 (2002)., *Nuclear Physics. A*623, 100c-109c (1997).
- [11] K. Gottfried, *Hadronic Spectroscopy*, in: *Proc Int Euro: phys conf on High energy Physics*, Brighton, (1983).
- [12] G. B. Smith and J. Tassie, *J Phys*, 65 (1971) 352.
- [13] L. J. Reinders, H. R. Rubinstein and S. Yazaki, *Nucl Phys B*, 186 (1981) 109.
- [14] J. S. Bell and H. Rueggm *Nucl Phys*, 98 B (1975) 151.
- [15] M. Fabre De la Ripelle, " *Proceeding of the International School on Nuclear Theoretical Physics (Predeal 1969)*" (A. Corciovei, Ed), *Inst. Atom. Phys.*, Bucarest, 1969; *Rev. Roum. Phys.* 14 (1969) 1215.
- [16] V. Aquilanti, S. Tonzanu, *J.chem. Phys* 126,4066(2004).
- [17] O. I. Tolstikhin and H. Nakamura, *J. Chem. Phys.* 108, 8899 (1998).
- [18] O. I. Tolstikhin, V. N. Ostrovsky, and H. Nakamura, *Phys. Rev. Lett.* 80, 41 (1998).
- [19] R. S. Kaushal, *Ann Phys Ny* 206, 90 (1991).
- [20] S. Oezelik, and M. Simek, *Phys Lett. A* 152, 145 (1991).
- [21] M. M. Giannini, E. Santopinto, and A. Vassallo *Eur Phys.J.A.* 12, 447-452 (2001).
- [22] A. A. Rajabi, *Few-Body systems* 37, 197-213(2005).
- [23] R. Bijker, F. Iachello and A. Leviatan, *Ann. Phys (N.Y.)* 236, 69 (1994).
- [24] F. Guersey and L. A. Radicati, *Phys. Rev. Lett.* 13, 173 (1964).

- [25] M. M. Giannini, E. Santopinto and A. Vassalo, Progress in particle and Nuclear physics 50,263-270 (2003).
- [26] H. Hassanabadi, and A. A. Rajabi, Few-Body systems, Vol 41, 1 (2007).

$\pi N \rightarrow \eta N$ PROCESS IN A χ QM APPROACH

Jun He*, Xianhui Zhong⁺, Bijan Saghai*, Qiang Zhao⁺

*Laboratoire de recherche sur les lois fondamentales de l'Univers,
DSM/DAPNIA/SPhN, CEA/Saclay, 91191 Gif-sur-Yvette, France

⁺Institute of High Energy Physics, Chinese Academy of Sciences, Beijing,
100049, P.R. China

Abstract

A chiral quark model approach is used to investigate the $\pi^- p \rightarrow \eta n$ process at low energies. The roles of the most relevant nucleon resonances in $n \leq 2$ shells are briefly discussed.

1 Introduction

The $\pi^- p \rightarrow \eta n$ reaction provides a suitable probe to investigate the structure of low-lying nucleon resonances as well as the ηN interaction.

Recent high precision data released by the BNL Crystal Ball Collaboration [1] has revived the interest in that process. The impact of those data on the meson-baryon interactions has been emphasized by the SAID Group [2]. Extensive theoretical efforts are also being deployed *via* coupled-channel formalisms, such as the K-matrix approach [3], meson-exchange model [4], chiral model [5], T-matrix [6], and dynamical formalism [7].

We have extended to the $\pi N \rightarrow \eta N$ process a comprehensive and unified approach [8] to the meson photoproduction, based on the low energy QCD Lagrangian in terms of quarks degrees of freedom. This latter formalism has been developed and proven [9] to be successful in investigating $\gamma p \rightarrow \eta p$, $K^+ \Lambda$ and $\gamma N \rightarrow \pi N$ reactions. In this approach, only a few parameters are required. In particular, only one parameter is needed for the nucleon resonances to be coupled to the pseudoscalar mesons. All the resonances can be treated consistently in the quark model.

2 Theoretical frame

In the chiral quark model, the low energy quark-meson interactions are described by the effective Lagrangian

$$\mathcal{L} = \bar{\psi}[\gamma_\mu(i\partial^\mu + V^\mu + \gamma_5 A^\mu) - m]\psi + \dots, \quad (1)$$

where vector (V^μ) and axial (A^μ) currents read

$$V^\mu = \frac{1}{2}(\xi \partial^\mu \xi^\dagger + \xi^\dagger \partial^\mu \xi), \quad A^\mu = \frac{1}{2i}(\xi \partial^\mu \xi^\dagger - \xi^\dagger \partial^\mu \xi), \quad (2)$$

with $\xi = \exp(i\phi_m/f_m)$, where f_m is the meson decay constant. ψ and ϕ_m are the pion and quark fields, respectively.

The η meson production amplitude can be expressed in terms of Mandelstam variables, $\mathcal{M} = \mathcal{M}_s + \mathcal{M}_u + \mathcal{M}_t$.

The s - and u -channel transitions are given by:

$$\mathcal{M}_s = \sum_j \langle N_f | H_\eta | N_j \rangle \langle N_j | \frac{1}{E_i + \omega_\pi - E_j} H_\pi | N_i \rangle, \quad (3)$$

$$\mathcal{M}_u = \sum_j \langle N_f | H_\pi \frac{1}{E_i - \omega_\eta - E_j} | N_j \rangle \langle N_j | H_\eta | N_i \rangle, \quad (4)$$

where ω_π and ω_η are the energies of the incoming π -meson and outgoing η -meson, respectively. H_π and H_η are the standard quark-meson couplings at tree level. $|N_i\rangle$, $|N_j\rangle$, and $|N_f\rangle$ stand for the initial, intermediate, and final state baryons, respectively, and their corresponding kinetic energies are E_i , E_j , and E_f .

Given that the a_0 meson decay is dominated by $\pi\eta$ channel [11], we consider the a_0 exchange as the prominent contribution to the t -channel,

$$\mathcal{M}_t = \sum_j \frac{g_{a_0\pi\eta} g_{a_0qq} m_\pi^2}{t^2 - m_{a_0}^2} \langle N_f | \bar{\psi}_j \psi_j \mathbf{a}_0 | N_i \rangle. \quad (5)$$

where m_{a_0} is the mass of the a_0 meson.

With above effective Lagrangian and following the procedures used in Ref. [8], we obtain the amplitude in the harmonic oscillator basis [10].

3 Results and discussion

Using the formalism sketched above, we have investigated the cross-section for the $\pi^- p \rightarrow \eta n$ process. In our model, non-resonant components include nucleon pole term, u -channel contributions (treated as degenerate to the harmonic oscillator shell n), and t -channel contributions due to the a_0 -exchange.

The resonant part embodies the following $n=1,2$ shell nucleon resonances:

- $n=1$: $S_{11}(1535)$, $S_{11}(1650)$, $D_{13}(1520)$, $D_{13}(1700)$, and $D_{15}(1675)$,
- $n=2$: $P_{11}(1440)$, $P_{11}(1710)$, $P_{13}(1720)$, $P_{13}(1900)$, $F_{15}(1680)$, and $F_{15}(2000)$.

Here we use the Breit-Wigner masses and widths given in the PDG [11]. For meson-nucleon-nucleon couplings we adopt $g_{\pi NN}=13.48$ and $g_{\eta NN}=0.81$.

Our results for the differential cross-section are depicted in Fig. [1] for pion incident momenta $P_{\pi}^{lab} = 0.718, 0.850, \text{ and } 1.005$ GeV, corresponding to the total centre-of-mass energies $W = 1.507, 1.576, \text{ and } 1.674$ GeV, respectively.

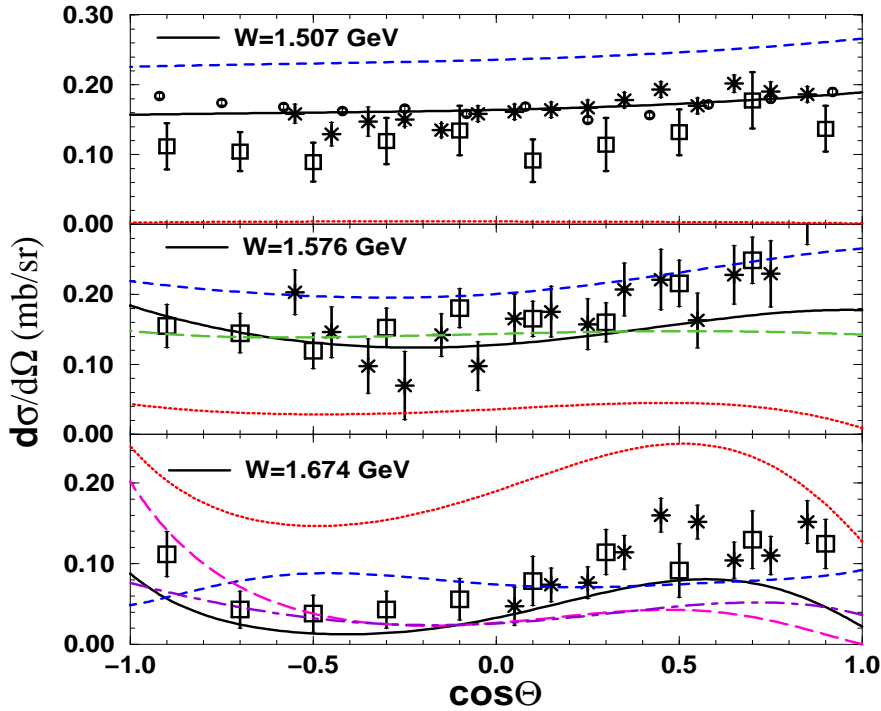


Figure 1: Differential cross-section for $\pi^-p \rightarrow \eta n$. The curves appearing in all the three boxes are: full model (solid black), the $S_{11}(1535)$ switched off (dotted red), and the $S_{11}(1650)$ switched off (dashed blue). In the middle box: the $D_{13}(1520)$ switched off (long dashed green). In the lower box: the $P_{11}(1710)$ switched off (long dashed magenta) and without the $n=2$ shell contributions (dot-dashed violet). Data are from Prakhov *et al.* [1] (circles), Richards *et al.* [12] (squares), and Deinet *et al.* [13] (stars).

We get a good agreement with the data at those energies (full curves). In order to single out the importance of various resonances, at each energy we show results while one *significant* resonance is switched off. The $S_{11}(1535)$

plays a crucial role in this energy range. At the lowest energies it has a constructive effect, while at the highest one its contribution becomes destructive. The $S_{11}(1650)$ has a (much) smaller and destructive effect. The role of the $D_{13}(1520)$, shown at $W=1.576$ GeV, is merely to produce the right curvature. At the highest energy, although the overall contribution from $n=2$ shell is rather small, the $P_{11}(1710)$ produces significant effects. This point was emphasized in our recent work [10], and led us to adopt here a reversed sign for that resonance *from the beginning*. That sign change for the $P_{11}(1710)$ could be an indication, e.g. for the breakdown of the non-relativistic constituent quark model or for unconventional configurations inside that resonance. More investigation is needed to underpin the origins of this novelty.

References

- [1] S. Prakhov *et al.*, *Phys. Rev. C* **72**, 015203 (2005).
- [2] R. A. Arndt, W. J. Briscoe, I. I. Strakovsky, R. L. Workman, *Phys. Rev. C* **74**, 045205 (2006).
- [3] G. Penner and U. Mosel, *Phys. Rev. C* **66**, 055211 (2002); V. Shklyar, H. Lenske, U. Mosel, *Phys. Lett. B* **650**, 172 (2007).
- [4] A. M. Gasparyan, J. Haidenbauer, C. Hanhart, J. Speth, *Phys. Rev. C* **68**, 045207 (2003).
- [5] T. Inoue, E. Oset, M. J. Vicente-Vacas, *Phys. Rev. C* **65**, 035204(2002).
- [6] S. Ceci, A. Svarc, B. Zauner, *Phys. Rev. Lett.* **97**, 062002 (2006).
- [7] A. Matsuyama, T. Sato, T.-S.H. Lee, *Phys. Rept.* **439**, 193 (2007).
- [8] Z. Li, H. Ye, M. Lu, *Phys. Rev. C* **56**, 1099 (1997).
- [9] B. Saghai and Z. Li, *Eur. Phys. J.* **A11**, 217 (2001); B. Saghai, nucl-th/0408054; B. Saghai *et al.* *Eur. Phys. J. A* **31**, 512 (2007); Q. Zhao *et al.*, *Phys. Rev. C* **65**, 065204 (2002).
- [10] Xian-Hui Zhong, Qiang Zhao, Jun He, Bijan Saghai, nucl-th/0706.3543.
- [11] W. M. Yao *et al.*, *J. Phys. G* **33**, 1 (2006).
- [12] W. B. Richards *et al.*, *Phys. Rev. D* **1**, 10 (1970).
- [13] W. Deinet *et al.*, *Nucl. Phys. B* **11**, 495 (1969).

PION PHYSICS FROM LATTICE QCD

Jie Hu^{*,1}, Fu-Jiun Jiang^{%,2}, Brian C. Tiburzi^{#,3}

^{*}Department of Physics, Duke University, Box 90305, Durham, NC 27708-0305, USA

[%]Institute for Theoretical Physics, Bern University, Sidlerstrasse 5, CH-3012 Bern, Switzerland

[#]Maryland Center for Fundamental Physics, Department of Physics, University of Maryland, College Park, MD 20742-4111, USA

Abstract

We use chiral perturbation theory coupled to electromagnetism in a periodic box to study the impact of volume corrections on pion physics in lattice QCD. We demonstrate that conserved currents can be additively renormalized by infrared effects and construct gauge invariant single particle effective theories to explain these results. In such theories, current renormalization arises from operators involving the zero mode of the gauge field. No contradictions with Ward identities, or low-energy theorems are encountered. We also investigate finite volume corrections to the Compton scattering tensor to study the extraction of pion electromagnetic polarizabilities from lattice QCD. We argue, however, that such results cannot be used to ascertain volume corrections to polarizabilities determined in lattice QCD with background field methods. Connection is lacking because momentum expansions are not permitted in finite volume. Our argument also applies to form factors.

1 Introduction

Today lattice gauge theory [1] is a mature field. Lattice QCD can be employed to determine QCD observables from first principles using non-perturbative numerical techniques. The finite spacetime volume of the lattice is one source of systematic errors in these numerical simulations. To address the systematic errors the study of field theories in finite volume is of practical utility. We focus our research on pions.

¹E-mail address: hujie@phy.duke.edu

²E-mail address: fjjiang@itp.unibe.ch

³E-mail address: bctiburz@umd.edu

Recent work [2] suggests that electromagnetically gauge invariant amplitudes at finite volume may differ from their infinite volume form. Specifically investigated was the finite-size scaling of nucleon electromagnetic and spin polarizabilities that arise in nucleon Compton scattering (see, e.g., [3, 4]). In infinite volume, the zero-frequency Compton amplitude is fixed by gauge invariance to be proportional to the total charge squared. However in finite volume, we find modifications for pion Compton scattering [5] at zero frequencies which suggest a finite volume renormalization of the basic interaction between the photon and the hadron's charge.

Electromagnetic polarizabilities encode fundamental properties of bound states. Pion polarizabilities can be calculated from chiral perturbation theory (χ PT) [6] in terms of a few low-energy constants [7]. However, the predictions from χ PT do not agree with experimental results. It is unclear whether the disagreement has its roots in the experimental analysis, or in the behavior of the chiral expansion. As a first principles method, lattice QCD can be employed to determine pion polarizabilities. To this end, we perform a one-loop analysis of the quenching and partial quenching effects, as well as the volume dependence of pion Compton scattering [8]. As polarizabilities are the coefficients at second order in an expansion in photon momentum ω , one would naively expect that finite volume corrections to polarizabilities can be determined from momentum expanding the finite volume Compton tensor. We find this is not the case.

2 χ PT, $Q\chi$ PT and $PQ\chi$ PT for Pions

Chiral perturbation theory provides an effective theory of low-energy QCD and is written in terms of a coset field $\Sigma = \exp(2i\Phi/f)$ which parametrizes the Goldstone manifold. At leading order in p^2 the Lagrangian is

$$\mathcal{L} = \frac{f^2}{8} \text{tr} (D_\mu \Sigma^\dagger D^\mu \Sigma) + \lambda \frac{f^2}{4} \text{tr} (m_Q^\dagger \Sigma + \Sigma^\dagger m_Q) \quad (1)$$

The $U(1)$ gauge field, A_μ , appears in the action of the covariant derivative, $D_\mu \Sigma = \partial_\mu \Sigma + ieA_\mu [\mathcal{Q}, \Sigma]$. We work in the isospin limit, $m_u = m_d$, for simplicity.

In current lattice calculations, valence and sea quarks are often treated differently. In the rather extreme approximation known as quenched QCD (QQCD), the sea quarks are completely absent. Less extreme is partially quenched QCD (PQQCD), where sea quarks are retained but have different masses than their valence counterparts. While both approximations are certainly contrary to nature, the latter retains QCD as a limit. $PQ\chi$ PT

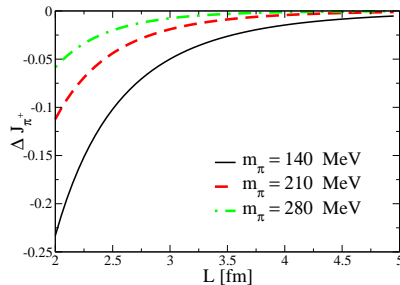


Figure 1: Finite volume screening of the charged pion current.

and $Q\chi$ PT describes the low-energy dynamics of PQQCD and QQCD, respectively. Our calculations address both quenching and partial quenching theories.

3 Current Renormalization in Finite Volume

In the limit of zero frequency and infinite volume, the current matrix element between charged pion states is required by gauge and Lorentz invariance to be

$$\langle \pi^\pm(P) | J_\mu | \pi^\pm(P) \rangle = \pm 2eP_\mu, \quad (2)$$

where $2m_\pi$ in the right hand side is a renormalization factor. In finite volume, because of $SO(4)$ breaking, the spacial component of current is not simply the charge times the velocity. Instead, the current is screened by finite volume effects, $\mathbf{J} = (\pm e)[1 - \mathcal{Q}(L)]\mathbf{P}$. In Fig. 1, we plot this finite volume modification [5] as a function of the box size L .

In the limit of zero frequency and infinite volume, the Compton tensor is sensitive only to the longest ranged electromagnetic interaction

$$T_{\mu\nu} = 2(Qe)^2 g_{\mu\nu}, \quad (3)$$

For neutral pion, the Compton tensor is naively expected to be zero, but in finite volume it has nonzero contributions. In Fig. 2 we plot the neutral pion finite volume amplitude. In both figures the finite volume effect is exponentially suppressed in asymptotic volume.

These finite volume results are not anticipated from infinite volume gauge invariance. In our paper [5], however, we construct gauge invariant single particle effective theories which couple to zero mode of the gauge field and demonstrate that such finite volume results are completely consistent with Ward-Takahashi identities valid in finite volume.

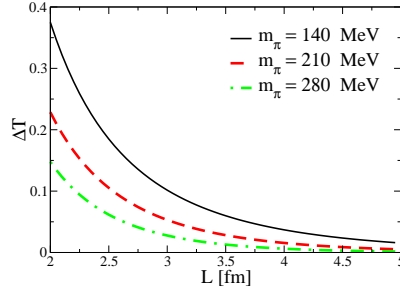


Figure 2: Finite volume zero frequency neutral pion Compton amplitude.

4 Pion Polarizabilities and Volume Effects in Lattice QCD

In infinite volume Compton scattering amplitude for a real photon to scatter off a pion can be parametrized as

$$\begin{aligned}
 T_{\gamma\pi} = & 2m_\pi \left[\left(-\frac{e^2 Q_\pi^2}{m_\pi} + 4\pi \alpha_E \omega^2 \right) \boldsymbol{\epsilon}'^* \cdot \boldsymbol{\epsilon} + 4\pi \beta_M \omega^2 (\boldsymbol{\epsilon}'^* \times \hat{\mathbf{k}}') \cdot (\boldsymbol{\epsilon} \times \hat{\mathbf{k}}) \right] \\
 & + \frac{e^2 Q_\pi^2}{2m_\pi^2} \omega^2 (\boldsymbol{\epsilon}'^* \cdot \hat{\mathbf{k}}) (\boldsymbol{\epsilon} \cdot \hat{\mathbf{k}}') (1 - \cos\theta) + \dots, \quad (4)
 \end{aligned}$$

where in the center-of-momentum frame the photon momenta are $k_\mu = (\omega, \omega \hat{\mathbf{k}})$ for the initial state, $k'_\mu = (\omega, \omega \hat{\mathbf{k}}')$ for the final state and $\cos\theta = \hat{\mathbf{k}}' \cdot \hat{\mathbf{k}}$. The electric and magnetic polarizabilities are the first structure dependent terms in the low-energy expansion of the Compton scattering amplitude. We determine α and β at one loop order in χ PT, PQ χ PT and Q χ PT at infinite volume [8].

We deduce the Compton scattering amplitude in a finite box for both charged and neutral pions for the process $\gamma\pi \rightarrow \gamma\pi$ to one loop order in our paper [8] for both partially quenched QCD and quenched QCD simulations. In finite volume, however, the decomposition of the Compton tensor in Eq. (4) is no longer valid. $SO(4)$ breaking makes the results frame dependent. Moreover, we find there are many terms in the finite volume Compton tensor not anticipated by infinite volume gauge invariance. All terms are form factors in ωL , where L is the spatial size of the lattice. Because of momentum quantization ($\omega = 2\pi \mathbf{n}/L$), these form factors cannot be expanded in ωL . Thus the connection between the frequency expansion and the polarizabilities is lost. As polarizabilities are typically calculated in lattice QCD using background field methods [2, 9–11], this means we cannot use the finite volume Compton tensor to deduce finite volume corrections to polarizabilities

extracted from background field correlation functions. The same problem exists for electromagnetic moments. Their volume effects cannot be deduced from series expanding finite volume electromagnetic form factors about zero momentum transfer.

5 Acknowledgments

This work is supported in part by the U.S. Dept. of Energy, Grant Nos. DE-FG02-05ER-41368-0 (J.H. and B.C.T.), DE-FG02-93ER-40762 (B.C.T), and by the Schweizerischer Nationalfonds (F.-J.J.).

References

- [1] T. DeGrand and C. DeTar, *Lattice Methods for Quantum Chromodynamics* (World Scientific, 2006)
- [2] W. Detmold, B. C. Tiburzi, and A. Walker-Loud, Phys. Rev. **D73**, 114505 (2006), hep-lat/0603026
- [3] C. E. Hyde-Wright and K. de Jager, Ann. Rev. Nucl. Part. Sci. **54**, 217 (2004), nucl-ex/0507001
- [4] M. Schumacher, Prog. Part. Nucl. Phys. **55**, 567 (2005), hep-ph/0501167
- [5] J. Hu, F.-J. Jiang and B. C. Tiburzi, Phys. Lett. **B653**, 350(2007), arXiv:0706.3408[hep-lat]
- [6] J. Gasser and H. Leutwyler, Ann. Phys. **158**, 142 (1984)
- [7] B. R. Holstein, Comments Nucl. Part. Phys. **A19**, 221 (1990)
- [8] J. Hu, F.-J. Jiang and B. C. Tiburzi, to appear in Phys. Rev. D
- [9] F. Fucito, G. Parisi, and S. Petrarca, Phys. Lett. **B115**, 148 (1982)
- [10] G. Martinelli, G. Parisi, R. Petronzio, and F. Rapuano, Phys. Lett. **B116**, 434 (1982)
- [11] C. W. Bernard, T. Draper, K. Olynyk, and M. Rushton, Phys. Rev. Lett. **49**, 1076 (1982)

EXOTIC HADRONS AND SU(3) CHIRAL DYNAMICS

Tetsuo Hyodo^{*,%,1}, Daisuke Jido[%], Atsushi Hosaka[#]

^{*}Physik-Department, Technische Universität München, D-85747 Garching, Germany

[%]Yukawa Institute for Theoretical Physics (YITP), Kyoto University, Kyoto, 606-8502, Japan

[#]Research Center for Nuclear Physics (RCNP), Ibaraki, 567-0047 Japan

Abstract

We explore a possibility to generate exotic hadrons dynamically in the scattering of hadrons. The s -wave scattering amplitude of an arbitrary hadron with the Nambu-Goldstone boson is constructed so as to satisfy the unitarity condition and the chiral low energy theorem. We find that the chiral interaction for the exotic channels is in most cases repulsive, and that the strength of the possible attractive interaction is uniquely determined. We show that the attractive interaction in exotic channels is not strong enough to generate a bound state, while the interaction in nonexotic channel generate bound states which are considered to be the origin of some resonances observed in nature.

Strong interaction of QCD exhibits rich spectra of hadrons in the non-perturbative vacuum at low energy, where about 300 hadronic states have been observed [1]. It is important to investigate the properties of hadrons to understand the low energy dynamics of QCD. Chiral symmetry provides us a way to study hadron properties in connection with the fundamental theory of QCD.

Dynamical models based on chiral symmetry, known as chiral unitary approach, successfully describe the two-body scattering of hadrons with the Nambu-Goldstone (NG) bosons in coupled channels, dynamically generating some s -wave resonances in the scattering [2–5]. These studies are along the same line with the coupled-channel dynamical models for the meson-baryon scattering studied in 60's, where the vector meson exchange interaction was adopted. This phenomenological interaction is now identified as the

¹E-mail address: thyodo@ph.tum.de

Weinberg-Tomozawa (WT) term, which is the leading order term in chiral perturbation theory. In this respect, one can introduce higher order corrections into the interaction systematically. The WT interaction was originally derived in current algebra. Since current algebra tells us about the interaction for arbitrary target hadrons, it is possible to apply the chiral unitary approach to the system with spin 3/2 baryons with the decuplet baryons as target, to the heavy quark sectors, and to the axial vector mesons. In the series of studies, the properties of the generated resonances are in fair agreement with experimental data.

On the other hand, the hadrons observed so far can be classified by their flavor quantum numbers. *Empirically*, there is a regularity in the quantum numbers of the observed hadrons: the states with the valence quark contents of $\bar{q}q$ or qqq were observed, while no state was well established with larger number of valence quarks (4, 5, 6, . . . quarks). The latter states, called exotic hadrons, were intensively studied recently after the report on the Θ^+ by LEPS collaboration [6]. In spite of the large amount of theoretical works, it is not clear why the exotic hadrons are difficult to observe.

In order to clarify this issue, we have recently performed an analysis of exotic hadrons in s -wave chiral dynamics [7–10]. We utilize the framework of the chiral unitary approach, since it is naively expected that the resonances produced in the dynamical model should have large component of the multi-quark configuration, which is the flavor partner of the exotic hadrons in the s -wave scattering.

We construct the scattering amplitude of an arbitrary hadron with the Nambu-Goldstone boson $t(\sqrt{s})$ as

$$t(\sqrt{s}) \rightarrow V^{\text{chiral}}(\sqrt{s}) \quad \text{at low energy,} \quad (1)$$

$$\text{Im}t^{-1}(\sqrt{s}) = \frac{\rho(\sqrt{s})}{2}, \quad (2)$$

where $V^{\text{chiral}}(\sqrt{s})$ is the low energy interaction based on chiral symmetry and $\rho(\sqrt{s})$ is the phase space of the two-body scattering. Eq. (1) is the constraint from the chiral low energy theorem, whereas Eq. (2) guarantees the unitarity of the S-matrix. Utilizing this approach, we would like to study what chiral dynamics tells us about the existence of the exotic hadrons.

The low energy s -wave interaction of a target hadron (T) with the NG boson in a channel α is given by

$$V_\alpha = -\frac{\omega}{2f^2}C_{\alpha,T}, \quad (3)$$

where ω and f are the energy and the decay constant of the NG boson, and the expression for the group theoretical factor $C_{\alpha,T}$ is given in Refs. [7–10].

By examining the coupling strength $C_{\alpha,T}$ for exotic channels, we find that the interaction for exotic channels is in most cases repulsive, and the strength of the possible attractive interaction is uniquely determined as

$$C_{\text{exotic}} = 1. \quad (4)$$

Eqs. (3) and (4) determines the low energy interaction V_{chiral} in Eq. (1) for exotic channels.

Next we construct the scattering amplitude consistent with Eq. (2). Based on the N/D method [4], the general form of the scattering amplitude $t_{\alpha}(\sqrt{s})$ can be written down with one subtraction constant, which is determined by the requirement (1) at the scale $\sqrt{s} = M_T$ [8]. Thus we obtain the scattering amplitude $t_{\alpha}(\sqrt{s})$ which satisfies both Eqs. (1) and (2). We then search for poles of bound states in the amplitude $t_{\alpha}(\sqrt{s})$. From the energy dependence of the interaction and the loop function, we find the critical value for the attractive interaction strength which is enough to make a bound state as

$$C_{\text{crit}} = \frac{2f^2}{m[-G(M_T + m)]}, \quad (5)$$

where $G(\sqrt{s})$ is defined as once-subtracted dispersion integral [8]. If the interaction strength $C_{\alpha,T}$ is larger than this critical value, a bound state is generated in the amplitude. Comparing C_{crit} with the attractive interaction in the exotic channel (4), we show that the interaction is not strong enough to generate a bound state for the mass of the target hadron smaller than 6 GeV.

In this way, we have studied the exotic states in the NG boson-hadron scattering. We construct the scattering amplitude which satisfies the chiral low energy theorem and unitarity condition. Considering an arbitrary target hadron, we find that the interaction in the exotic channels are in most cases repulsive, and possible attractive interaction is uniquely given as $C_{\text{exotic}} = 1$. We show that the strength of the attractive interaction is not sufficient to generate a bound state for the physically known masses of the target hadrons.

In order to draw a general and model-independent conclusion, we have simplified the framework of the chiral unitary approach. Our basic assumptions are 1) flavor SU(3) symmetry and 2) dominance of the leading order interaction. Once we accept these conditions, the subsequent arguments are straightforward. In practice, however, the SU(3) symmetry is broken and the higher order terms of the chiral expansion would play a substantial role, especially for the NG boson with larger masses. These effects could be included in the kernel interaction based on chiral perturbation theory, but we need experimental data to determine the low energy constants. It should

be noted that the exotic hadrons constructed by other mechanisms than the present analysis, such as by quark dynamics, are not excluded.

In this study, we stress that the WT term is the leading order term of the chiral expansion and the strength is only determined by the group theoretical factor. We can therefore argue that the leading order term does not provide bound states in exotic channel, without performing experiments. Given the success of the chiral unitary approach in the nonexotic sectors which our arguments are based on, our result may partly explain the difficulty to observe exotic hadrons in nature.

Acknowledgements

T.H. appreciates Prof. W. Weise for the discussion about the convergence of chiral expansion. T. H. thanks the Japan Society for the Promotion of Science (JSPS) for financial support. This work is supported in part by the Grant for Scientific Research (No. 17959600, No. 19853500, No. 18042001, and No. 16540252) and by Grant-in-Aid for the 21st Century COE "Center for Diversity and Universality in Physics" from the Ministry of Education, Culture, Sports, Science and Technology (MEXT) of Japan.

References

- [1] Particle Data Group, W. M. Yao *et al.*, J. Phys. **G33**, 1 (2006).
- [2] N. Kaiser, P. B. Siegel, and W. Weise, Nucl. Phys. **A594**, 325 (1995).
- [3] E. Oset and A. Ramos, Nucl. Phys. **A635**, 99 (1998).
- [4] J. A. Oller and U. G. Meissner, Phys. Lett. B **500**, 263 (2001).
- [5] M. F. M. Lutz and E. E. Kolomeitsev, Nucl. Phys. **A700**, 193 (2002).
- [6] T. Nakano *et al.*, [LEPS Collab.], Phys. Rev. Lett. **91**, 012002 (2003).
- [7] T. Hyodo, D. Jido, and A. Hosaka, Phys. Rev. Lett. **97**, 192002 (2006).
- [8] T. Hyodo, D. Jido, and A. Hosaka, Phys. Rev. D **75**, 034002 (2007)
- [9] T. Hyodo, D. Jido and A. Hosaka, hep-ph/0612333.
- [10] T. Hyodo, D. Jido and A. Hosaka, Prog. Theor. Phys. Suppl. **168**, 32 (2007).

MENU 2007
11th International Conference
on Meson-Nucleon Physics and
the Structure of the Nucleon
September 10-14, 2007
IKP, Forschungszentrum Jülich, Germany

THREE-BODY RESONANCE POLE OF STRANGE DIBARYON IN THE $\bar{K}NN - \pi YN$ COUPLED SYSTEM

*Y. Ikeda and T. Sato*¹

Department of Physics, Graduate School of Science, Osaka University, Toyonaka, Osaka, 560-0043, Japan

Abstract

$\bar{K}NN$ three body resonance has been studied by $\bar{K}NN - \pi YN$ coupled channel Faddeev equation. The S-matrix pole has been investigated using the scattering amplitude on the unphysical Riemann sheet. As a result we found a three-body resonance of strange dibaryon system with the binding energy $B \sim 79\text{MeV}$ and the width $\Gamma \sim 74\text{MeV}$.

1 Introduction

The meson-nucleus bound state has been an important tool to study the meson properties inside the nuclear medium. The \bar{K} -nuclear system is particularly interesting because of the $I = 0$ resonance $\Lambda(1405)$ below the $\bar{K}N$ threshold. The attractive nature of the kaon-nucleus interaction obtained from the analysis of the kaonic atom [1] might be largely related to the $\Lambda(1405)$. In a few nucleon system, where one hopes to learn about the kaon-nucleon interaction with less ambiguity on nuclear many body dynamics, possible deeply bound states of the kaon in nuclei have been proposed by Akaishi and Yamazaki [2]. The predicted binding energy B and width Γ of the smallest nuclear system K^-pp is $(B, \Gamma) = (48, 61)\text{MeV}$. FINUDA collaboration reported a signal of the K^-pp bound state from the analysis of the invariant mass distribution of $\Lambda - p$ in the K^- absorption reaction on nuclei [3]. The reported central value of the binding energy is $(B, \Gamma) = (115, 67)\text{MeV}$.

The binding energy of K^-pp resonance will be strongly influenced by the dynamics of the $\Lambda(1405)$ resonance. For the resonance interaction in a few body system, it will be very important to take into account fully

¹ikeda@kern.phys.sci.osaka-u.ac.jp, tsato@phys.sci.osaka-u.ac.jp

the kaon-nucleon dynamics in the $\overline{K}NN$ system including the decay of the $\Lambda(1405)$ into the $\pi\Sigma$ state. The purpose of this work is to study the strange dibaryon system by taking into account the three-body dynamics using the $\overline{K}NN - \pi YN$ coupled channel Faddeev equation with the relativistic kinematics. The resonance can be studied from the pole of the S-matrix or scattering amplitude [4]. We briefly explain our procedure to search the three-body resonance in Sec. 2. The structure of the $\Lambda(1405)$ has been a long standing issue. The chiral Lagrangian [5] approach is able to describe well the low energy $\overline{K}N$ reaction. In this work, we describe a $\overline{K}N - \pi\Sigma$ state using the s-wave meson-baryon potentials guided from the lowest order chiral Lagrangian. The model of the two-body meson-baryon interaction used in this work is explained in Sec. 3. We report our result on the $\overline{K}NN$ dibaryon resonance in Sec. 4. This work is based on our previous works(see Refs. [6]).

2 AGS equation and resonance pole

Our starting point is the Alt-Grassberger-Sandhas(AGS) equation [7] for the three-body scattering problem. It is possible because all of our two-body interactions are separable forms. The AGS equation for the three-body scattering amplitude $X_{i,j}$ is given as

$$X_{i,j} = (1 - \delta_{i,j})Z_{i,j} + \sum_{n \neq i} \int d\mathbf{p}_n Z_{i,n} \tau_n X_{n,j}. \quad (1)$$

Here we represent the spectator particle $i = 1, 2, 3$ and the interacting particles j, k . Scattering t-matrix for particle j, k is denoted as an isobar propagator τ_i and a driving term $Z_{i,j}$ denotes the particle exchange interaction. After anti-symmetrizing the amplitude for two nucleons [8] and the partial wave expansion of the amplitude restricting s-wave, the AGS-equation reduces into the following coupled integral equation,

$$X_{l,m}(p_l, p_m) = Z_{l,m}(p_l, p_m) + \sum_n \int dp_n p_n^2 K_{l,n}(p_l, p_n) X_{n,m}(p_n, p_m). \quad (2)$$

Here we used simplified notation for the kernel $K = Z\tau$. The AGS-equation of Eq. (2) is the Fredholm type integral equation with the kernel $K = Z\tau$. Using the eigenvalue $\eta_a(W)$ and the eigenfunction $|\phi_a(W)\rangle$ of the kernel for given energy W , the scattering amplitude X can be written as

$$X = \sum_a \frac{|\phi_a(W)\rangle \langle \phi_a(W)| Z}{1 - \eta_a(W)}. \quad (3)$$

At the energy $W = W_p$ where $\eta_a(W_p) = 1$, the amplitude has a pole and therefore W_p gives the bound state or resonance energy.

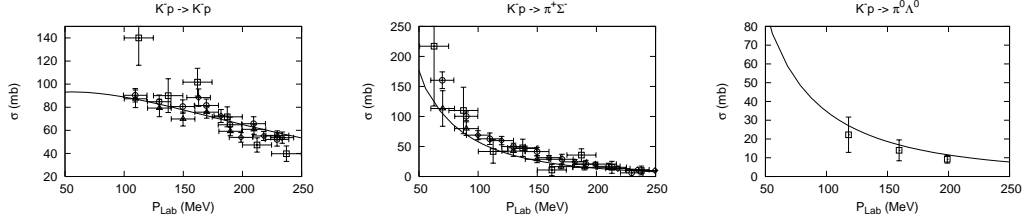


Figure 1: The total cross section of K^-p reaction together with data [10].

3 Two-body ingredients

In this section, we explain our model of the most important $\bar{K}N$ interaction. We start from the leading order chiral effective Lagrangian, and the meson-baryon potential can be written as

$$\langle \mathbf{p}', \alpha | V_{BM} | \mathbf{p}, \beta \rangle = -C_{\alpha,\beta} \frac{1}{(2\pi)^3 8 F_\pi^2} \frac{E_{M'}(\mathbf{p}') + E_M(\mathbf{p})}{\sqrt{4E_{M'}(\mathbf{p}')E_M(\mathbf{p})}} \times v_\alpha(\mathbf{p}')v_\beta(\mathbf{p}). \quad (4)$$

Here \mathbf{p} and \mathbf{p}' are the momentum of the meson in the initial state β and the final state α . The strength of the potential at zero momentum is determined by the pion decay constant F_π . The relative strength among the meson-baryon states is given by the constants $C_{\alpha,\beta}$, which are $C_{\bar{K}N-\bar{K}N} = 6, C_{\bar{K}N-\pi\Sigma} = \sqrt{6}$ and $C_{\pi\Sigma-\pi\Sigma} = 8$. The only parameter of our model is cut off Λ of the phenomenologically introduced vertex function $v_\alpha(\mathbf{p}) = \Lambda_\alpha^4 / (\mathbf{p}^2 + \Lambda_\alpha^2)^2$. The cut off Λ is determined so as to reproduce the scattering length of $\bar{K}N$ given by Martin [9], which is summarized in Refs. [6]. In $I = 0$ channel, our model has a resonance. Our model predicts that the pole energy of the $\Lambda(1405)$ is $1420 - i30\text{MeV}$. Our model give satisfactory description of the total cross section of K^-p reaction at low energy shown in Fig. 1.

4 Result and Discussion

We have searched the resonance pole of the strange dibaryon ($J^\pi = 0^-, I = 1/2$) using the method described in Sec. 2 and the $\bar{K}N$ interaction explained in Sec. 3. NN interaction for 1S_0 channel and πN interaction are included in the AGS-equation. However YN interaction is not included in this work.

Our result of the $\bar{K}NN - \pi YN$ resonance pole energy is $W = M - i\Gamma/2 = 2m_N + m_K - 79.3 - i37.1\text{MeV}$. Our resonance has deeper binding energy and similar width compared with the prediction of Ref. [2]. Recently Shevchenko *et al.* [11] studied K^-pp system using coupled channel Faddeev equation with nonrelativistic kinematics. Their result is almost consistent with ours.

Acknowledgments

This work is supported by a Grant-in-Aid for Scientific Research on Priority Areas(MEXT),Japan with No. 18042003.

References

- [1] J. Mares, E. Friedman, and A. Gal, Nucl. Phys. **A770**, (2006) 84. L. Tolós, A. Ramos, and E. Oset, Phys. Rev. C **74**, (2006) 015203.
- [2] Y. Akaishi and T. Yamazaki, Phys. Rev. C **65**, (2002) 044005. T. Yamazaki and Y. Akaishi, Phys. Lett. **B535**, (2002) 70. A. Dote *et al.*, Phys. Rev. C **70**, (2004) 044313.
- [3] M. Agnello *et al.*, Phys. Rev. Lett. **94**, (2005) 212303.
- [4] W. Glöckle, Phys. Rev. C **18**, (1978) 564. A. Matsuyama and K. Yazaki, Nucl. Phys. **A534**, (1991) 620. A. Matsuyama, Phys. Lett. **B408**, (1997) 25. B. C. Pearce and I. R. Afnan, Phys. Rev. C **30**, (1984) 2022. I. R. Afnan and B. F. Gibson, Phys. Rev. C **47**, (1993) 1000.
- [5] D. Jido *et al.*, Nucl. Phys. **A725**, (2003) 181. B. Borasoy, R. Nißler, and W. Weise, Eur. Phys. J. **A25**, (2005) 79.
- [6] Y. Ikeda and T. Sato, Phys. Rev. C **76**, (2007) 035203. arXiv:nucl-th/0701001.
- [7] E. O. Alt, P. Grassberger, and W. Sandhas, Nucl. Phys. **B2**, (1967) 167.
- [8] I.R. Afnan and A.W. Thomas, Phys. Rev. C **10**, (1974) 109.
- [9] A.D. Martin, Nucl. Phys. **B179**, (1981) 33.
- [10] W. E. Humphrey and R. R. Ross, Phys. Rev. **127**, (1962) 1305. M. Sakitt *et al.*, Phys. Rev. **139**, (1965) B719. J. K. Kim, Phys. Rev. Lett. **14**, (1965) 29. W. Kittel, G. Otter, and I. Wacek, Phys. Lett. **21**, (1966) 349. D. Evans *et al.*, J. Phys. **G9**, (1983) 885.
- [11] N. V. Shevchenko, A. Gal and J. Mares, Phys. Rev. Lett. **98**, (2007) 082301. N. V. Shevchenko *et al.*, arXiv:0706.4393[nucl-th].

PION-NUCLEON P_{33} AND P_{11} SCATTERINGS IN THE LIPPMANN-SCHWINGER APPROACH

*Takashi Inoue*¹

Department of Physics, Sophia University
7-1 Kioi-cho, Chiyoda-ku, Tokyo 102-8554, Japan

Abstract

We study the pion-nucleon P_{33} and P_{11} scattering, where the Delta and the Roper resonances are seen, respectively. We use the Lippmann-Schwinger equation extended to couple to a one-body state, and investigate nature of these resonances by taking and omitting a one-baryon state into account. We see validity and puzzle of the standard quark model interpretation, for the Delta and the Roper resonances, respectively.

1 Introduction

Nowadays, the Delta resonance is well recognized as an appearance of a three-constituent-quark(3Q) ground state in the (10,4) representation of the flavor SU(3) and spin SU(2). While, before the quark model, the resonance was explained as a temporal bound state of pion and nucleon produced by attraction due to cross diagram and the centrifugal repulsion. The physical resonance in experimental data could be contributed from the both.

Nature of the Roper resonance is interested for many years. Naive quark model doesn't account for the resonance for the level reverse puzzle, where the Roper is lighter than the negative parity nucleon $N^*(1535)$. Graz group claim that the short range part of one-pion-exchange in 3Q system is enough strong to reverse two masses [1]. While, Jülich group argue that the Roper is a temporal bound state of nucleon and correlated two pions [2].

Then, the purpose of this paper is that we study the pion-nucleon P_{33} and P_{11} scattering in the Lippmann-Schwinger approach with and without including a one-baryon(3Q) state, and see these interpretations.

¹takash-i@sophia.ac.jp

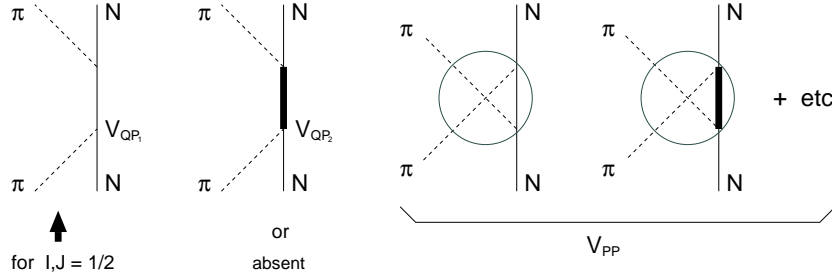


Figure 1: Elementary processes taken into account.

2 Formulation

We solve the Lippmann-Schwinger equation and then T matrix is given by

$$T_{PP} = M^{-1}V_{PP} + M^{-1}V_{PQ}G_QV_{QP}M^{-1t} \quad M = 1 - V_{PP}G_P^{(0)} \quad (1)$$

$$G_Q = (G_Q^{(0)-1} - \Sigma_Q)^{-1} \quad \Sigma_Q = V_{QP}G_P^{(0)}M^{-1}V_{PQ} \quad (2)$$

here the Hilbert space is divided in two with projections P and $Q = 1 - P$ where the P-space is spanned by meson-baryon states, while the Q-space is the one-baryon state. The first term is the T-matrix solved in the P-space only and is the solution of the ordinary Lippmann-Schwinger equation. The second term is the effect of the Q-space *i.e.* baryon state, and is the most important part in this study. This term is composed of the full propagator of the baryon including a self-energy due to coupling to pion-nucleon states.

We consider the elementary processes shown in Fig.1. For the P_{11} partial wave, we take the nucleon pole diagram. The baryon pole diagram, we try both taking and omitting it, as explained. We include the rest of processes *i.e.* the cross-diagram and so on, as an effective potential in the P-space, V_{PP} . We parametrize the matrix elements of these interactions as

$$\langle Q | V_{QP} | \mathbf{k} \rangle = b^{5/2} V_{QP} \mathbf{k} \cdot \boldsymbol{\Sigma} e^{-\frac{b^2}{2}k^2} \quad (3)$$

$$\langle \mathbf{k}' | V_{PP} | \mathbf{k} \rangle = a^5 V_{PP} \mathbf{k} \cdot \mathbf{k}' e^{-\frac{a^2}{4}k^2} e^{-\frac{a^2}{4}k'^2} \quad (4)$$

where $\boldsymbol{\Sigma}$ is the so called transition spin operator which is nothing but the spin operator for πNN interaction. Note the (bi-)linear momentum dependence due to P-wave interaction. The sum over intermediate states is taken by using the Gauss integral method. We include Gaussian form-factors for simplicity so that the integral converges. We apply the semi-relativistic prescription.

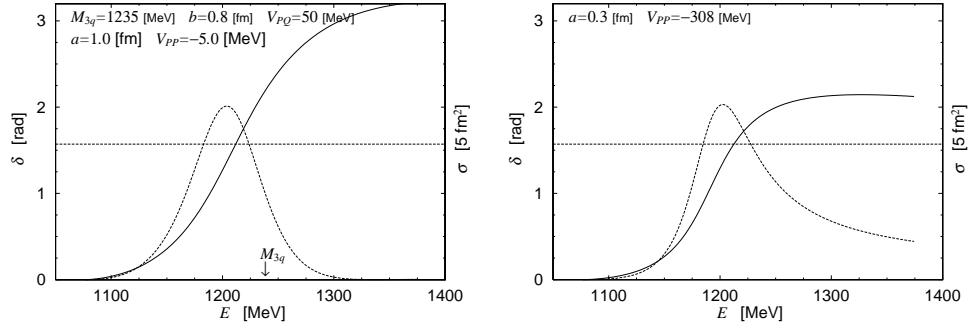


Figure 2: Phase-shift and cross-section of P_{33} scattering v.s. the total energy, obtained in the model with(left) and without(right) baryon pole.

3 Result and Discussion

We start with P_{33} partial wave scattering. Fig.2 left shows the phase-shift and cross-section obtained in the model with a baryon pole, as a function of the total energy. Entire feature of data is well reproduced by putting a baryon state around 1235[MeV]. Essentially the potential V_{PP} is not needed but a weakly attractive and soft one is added to improved the threshold behavior. The resonance appears at the almost bare energy of the baryon(slightly below). This supports the standard quark model scenario.

The right figure of Fig.2 shows the results obtained in the model without a baryon pole. By assuming a potential with a particular combinations of range and depth, *e.g.* $a = 0.3$ [fm] and $V_{PP} = -308$ [MeV], a resonance occur at the right energy. However, within the present energy independent potential, the result differ from data at energy above the resonance. This demonstrate the necessity of a baryon couple to πN in P_{33} state. The above V_{PP} should be regarded as an effective potential including the baryon.

We turn to P_{11} partial wave scattering. Fig.3 left shows the result in the model with a baryon pole in addition to nucleon one. Entire feature of data is well reproduced by putting two baryons at 939[MeV] and 1410[MeV]. Again, no need of V_{PP} essentially. Note that the bare energy of the baryon is 1410[MeV], and the resonance appears at energy slightly above. This means that the baryon is shifted to upward. This result doesn't help the conventional quark model at all. We know that the model does not predict a positive parity excited nucleon around the energy, but around 1550[MeV]. Hence, it must be shifted to downward largely in order to reproduce data. However, the present result shows that a baryon state will be shifted to upward by coupling to πN scattering state. After all, the puzzle of Roper resonance in the model, still remains.

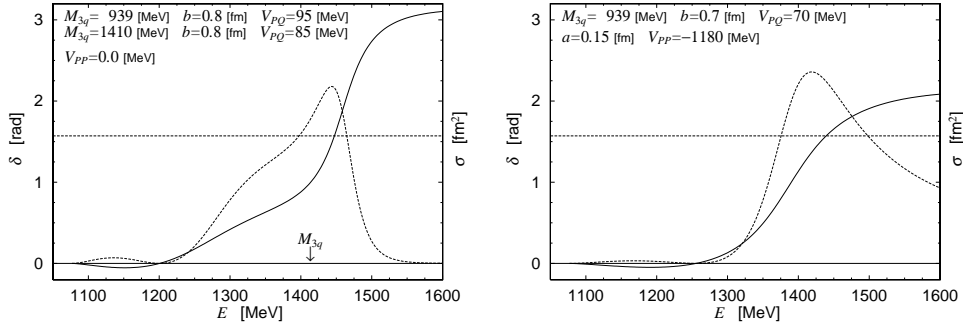


Figure 3: Phase-shift and cross-section of P_{11} scattering v.s. the total energy, obtained in the model with(left) and without(right) baryon pole.

Then, we try to reproduce P_{11} data in absence of a baryon corresponding to the resonance. The right figure of Fig.3 shows the result obtained with the nucleon pole and an effective potential. Again, by assuming a potential with a particular combinations of range and depth, a resonance occur at the right energy. This may indicate hadron dynamical origin of the Roper resonance. In this case, we need a very short range and deep potential, *e.g.* $a = 0.15[\text{fm}]$ and $V_{PP} = -1180[\text{MeV}]$. We do not have explicit $\pi\pi N$ channel in the present study, and the process $\pi N \rightarrow \pi\pi N \rightarrow \pi N$ is regarded as a part of V_{PP} . The above deep potential may be originated from the process, *e.g.* with the strong $\pi\pi$ correlation in the paper by Jülich group [2]. This is interesting and must be studied into more details.

Acknowledgments

This work is supported by the Grant for Scientific Research No.18042006 from the Ministry of Education, Culture, Science and Technology, Japan.

References

- [1] L. Y. Glozman and D. O. Riska, Phys. Rept. **268**, 263 (1996) [arXiv:hep-ph/9505422].
- [2] O. Krehl, C. Hanhart, S. Krewald and J. Speth, Phys. Rev. C **62**, 025207 (2000) [arXiv:nucl-th/9911080].

PRECISE DETERMINATION OF KAONIC ^4He X-RAY ENERGY

T. Ishiwatari^{*,1}, G. Beer[%], H. Bhang[#], M. Cargnelli^{*}, J. Chiba[§], S. Choi[#],
C. Curceanu[&], Y. Fukuda⁺, T. Hanaki[§], R. S. Hayano[±], M. Iio[∓],
T. Ishikawa[±], S. Ishimoto[×], K. Itahashi[∓], M. Iwai[×], M. Iwasaki[∓],
B. Juhász^{*}, P. Kienle^{*,⊗}, J. Marton^{*}, Y. Matsuda[∓], H. Ohnishi[∓],
S. Okada[∓], H. Ota[∓], M. Sato[∓], P. Schmid^{*}, S. Suzuki[×], T. Suzuki[∓],
H. Tatsuno[±], D. Tomono[∓], E. Widmann^{*}, T. Yamazaki^{±,∓}, H. Yim[#],
J. Zmeskal^{*}

^{*}Stefan Meyer Institut für subatomare Physik, Vienna, Austria

[%]Department of Physics and Astronomy, University of Victoria, BC,
Canada

[#]Department of Physics, Seoul National University, Seoul, South Korea

[§]Department of Physics, Tokyo University of Science, Chiba, Japan

[&]Laboratori Nazionali di Frascati dell' INFN, Frascati, Italy

⁺Department of Physics, Tokyo Institute of Technology, Tokyo, Japan

[±]Department of Physics, University of Tokyo, Tokyo, Japan

[∓]Nishina Center for Accelerator-based Science, RIKEN, Saitama, Japan

[×]High Energy Accelerator Research Organization (KEK), Ibaraki, Japan

[⊗]Physik Department, Technische Universität München, Garching, Germany

Abstract

The E570 experiment determined the strong-interaction shift of the kaonic ^4He $2p$ state by measuring the kaonic ^4He X-ray energy using Silicon Drift Detectors (SDDs). The obtained shift is 2 ± 2 (stat.) ± 2 (syst.) eV. This value is in agreement with the theoretical calculations using the optical-potential models or the model predicting deeply-bound kaonic nuclear states, while it disagrees with the experimentally determined values in the past three experiments. Therefore, a long-standing discrepancy between the theories and experiments on the kaonic ^4He $2p$ state (kaonic helium puzzle) was eliminated for the first time.

¹E-mail address: tomoichi.ishiwatari@assoc.oeaw.ac.at

1 Introduction

The strong-interaction shift and width of the kaonic ${}^4\text{He}$ $2p$ state were measured in the three experiments from 1970's to 1980's [1]. The average of the shift is -43 ± 8 eV, while the analysis of the kaonic atom X-ray data with $Z > 2$ using the optical-potential model gives about 0 eV [2]. The recent calculation predicting deeply bound kaonic nuclear states shows that the shift can be possible within ± 10 eV [3]. This discrepancy between the experiments and theories is known as “kaonic helium puzzle”.

Using a new technique to detect X-rays with high resolution in both energy and timing, we determined the most accurate value of the strong-interaction shift of the kaonic ${}^4\text{He}$ $2p$ state [4]. Here, the experimental results will be given briefly.

2 Experiment

The E570 experiment measured the energy of the kaonic ${}^4\text{He}$ X-ray transitions to the $2p$ state (Balmer lines) at the KEK-PS K5 beamline in Oct. 2005 and Dec. 2005. For this experiment, 8 Silicon Drift Detectors (SDDs), as well as pure Ti and Ni calibration foils, are installed in the E549 experimental setup [5].

As a target, super fluid liquid ${}^4\text{He}$ (0.145 g/cm 3) was used, and the target cell is cylindrical in shape (15 cm long and 20 cm in diameter). Each SDD has an effective area of 1 cm 2 and an active layer of 260 micron. The SDDs were cooled down to 83 K. Typical resolution of energy and time is about 185 eV (FWHM) at 6.4 keV and about 160 ns (rms).

The production points of the kaonic atoms were determined by detecting the secondary charged particles produced by the kaon reactions using the vertex chambers. The stopped kaon events inside the target cell were selected with the data of the vertex chambers and T0 counter [5].

Precise calibration of the X-ray energy spectra needs X-ray data with high statistics. The kaon beam contains a large number of high-energy pions ($\pi : K = 200 : 1$), which passed through the target cell and hit on the Ti and Ni foils. The pion-induced Ti/Ni X-ray lines detected by the SDDs with the self trigger were used as the calibration lines.

3 Data Analysis

Studies of the X-ray fit function are a key point to obtain the X-ray peak position with a precision of a few eV. The fit function for the pileup events

was obtained using the Flash ADC data, in which a SDD signal shape was recorded. The fit function for the low-energy tails due to the incomplete charge collection was obtained by the fit to the Ti/Ni X-ray peaks. The effects of the incoherent (Compton) scattering on the He target were studied by simulating the X-ray data with GEANT4 including an extension package for the Low-Energy Compton Scattering (LECS) [6].

Table 1: Measured and calculated values [7] EM of the kaonic ${}^4\text{He}$ x-ray energy. The quoted error is statistical only.

Transition	$3d \rightarrow 2p$	$4d \rightarrow 2p$	$5d \rightarrow 2p$
Measured energy E_{exp} (eV)	6466.7 ± 2.5	8723.3 ± 4.6	9760.1 ± 7.7
EM calc. energy E_{calc} (eV)	6463.5	8721.7	9766.8

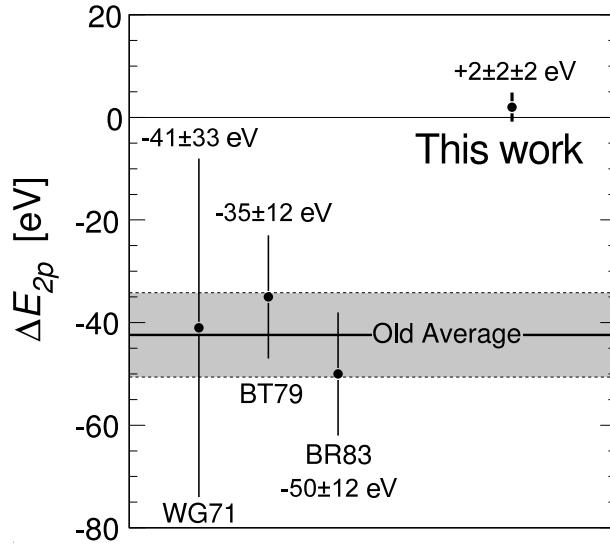


Figure 1: Comparison of experimental results for the hadronic shift ΔE_{2p} of the kaonic ${}^4\text{He}$ 2p state

The measured values of the kaonic helium X-ray energy is given in Table 1, as well as the calculated values with the QED effects only [7]. The strong-interaction shift is obtained from the difference of the measured and calculated values: $\Delta E_{2p} = E_{exp} - E_{calc}$. Taking the average of the shifts of the three lines, we obtained the shift as $2 \pm 2 \pm 2$ eV. The comparison with the previous experiments is shown in Fig. 1.

Acknowledgments

This research was supported by KEK, RIKEN, SMI and Grant-in-Aid for Scientific Research from the Ministry of Education of Japan, No. 17340087, No. 14102005 and No. 17070007.

References

- [1] C. E. Wiegand *et al.*, Phys. Rev. Lett. **27** 1410 (1971); C. J. Batty *et al.*, Nucl. Phys. **A 326** (1979) 455; S. Baird *et al.*, Nucl. Phys. **A 392** (1983) 297.
- [2] C. J. Batty, Nucl. Phys. **A 508** (1990) 89c; S. Hirenzaki *et al.*, Phys. Rev. **C 61** (2000) 055205; E. Friedman, private communication.
- [3] Y. Akaishi, proceedings for *International Conference on Exotic Atoms (EXA05)*, Austrian Academy of Sciences Press, Vienna, 2005, p. 45.
- [4] S. Okada *et al.*, Phys. Lett. B **653** (2007) 387.
- [5] M. Sato *et al.*, submitted to Phys. Lett. B.
- [6] R. M. Kippen, New Astron. Rev. **48** (2004) 221.
- [7] T. Koike, in preparation.
- [8] R. S. Hayano *et al.*, Proposal of J-PARC 50-GeV PS “Precision spectroscopy of Kaonic Helium $3\ 3d \rightarrow 2p$ X-rays” (J-PARC E17) (2006).

APPLICATION OF χ PT WITH VECTOR MESONS: KAON ELECTROMAGNETIC FORM FACTORS AND $K\bar{K}$ CONTRIBUTION TO MUON ANOMALOUS MAGNETIC MOMENT

S. Ivashyn and A. Korchin

Institute for Theoretical Physics,
NSC “Kharkiv Institute for Physics and Technology”,
Akademichna 1, Kharkiv 61108, Ukraine

Abstract

In framework of Chiral Perturbation Theory with vector and axial-vector mesons we develop a model for charged and neutral kaon electromagnetic form factors. Regions of time-like and space-like photon momentum are considered. Beyond the tree level the model includes certain loop corrections, such as self-energy operators in vector-meson (ρ , ω , ϕ) propagators and “dressed” photon-meson vertices. The contribution of $\rho' = \rho(1450)$, $\omega' = \omega(1420)$ and $\phi' = \phi(1680)$ resonances is included. Results are compared with experimental data on form factors and good agreement is achieved without making a fit. We evaluate $K\bar{K}$ -channel contribution to the muon anomalous magnetic moment as well.

1 Introduction

We review here results of our recent paper [1] devoted to application of Chiral Perturbation Theory [2] (ChPT) to calculation of kaon electromagnetic (EM) form factors (FF)s. The particles of interest are K^0 and K^\pm . Quark composition of mass eigenstates reads: $K^+ = u\bar{s}$, $K^0 = d\bar{s}$ (strangeness = +1) and $K^- = \bar{K}^+ = \bar{u}s$, $\bar{K}^0 = \bar{d}s$ (strangeness = -1), and the corresponding masses are $m_{K^+} = 493.7$ MeV and $m_{K^0} = 497.6$ MeV.

FFs $F_K(q^2)$ for the time-like momentum $q^2 > 0$ enter the matrix element of EM current operator between vacuum and kaon-antikaon states: $\langle K(p_1)\bar{K}(p_2)|j_{em}^\mu(x=0)|0\rangle \equiv (p_1 - p_2)^\mu F_K(q^2)$. Here p_1 and p_2 are kaon momenta, photon invariant mass q^2 is equal to kaon pair invariant mass $q^2 = (p_1 + p_2)^2 \equiv s$, and quark EM current is $j_{em}^\mu(x) = \frac{2}{3}\bar{u}(x)\gamma^\mu u(x) - \frac{1}{3}\bar{d}(x)\gamma^\mu d(x) - \frac{1}{3}\bar{s}(x)\gamma^\mu s(x)$.



Figure 1: Illustration of the form factor.

We mainly focus on the region above the $K\bar{K}$ threshold $(2 m_K)^2 < s < 4 \text{ GeV}^2$. It covers the set of low-lying vector ($J^P = 1^-$) resonances V : $\rho(770)$, $\omega(782)$, $\phi(1020)$, and their excitations V' : $\rho' = \rho(1450)$, $\omega' = \omega(1420)$, $\phi' = \phi(1680)$, which directly couple to the $K\bar{K}$ pair. The extension to the space-like region is straightforward through analyticity properties of $F_K(q^2)$. We limit our consideration in the space-like region to the interval $-0.16 \text{ GeV}^2 < s < 0$, where data are available.

The approach [2] is appropriate for this problem, it gives rise to an effective hadronic model with coupling structures guided by the chiral symmetry. Among interesting features of the model let us note vector-meson dominance of the EM interaction. At the same time vector mesons ρ, ω, ϕ are not considered as gauge bosons of local chiral symmetry. In addition Wess-Zumino-Witten Lagrangian and some odd-intrinsic-parity interactions are incorporated in the model in order to describe EM vertex dressing and vector meson self energies.

Our results for FFs allow also for calculation of the $K\bar{K}$ contribution to the muon anomalous magnetic moment (AMM). This contribution and other hadronic contributions are presently the main source of uncertainty in theoretical prediction for muon AMM [3].

2 Model

Starting from χPT with vector mesons [2] one can obtain general expression for the charged and neutral kaon FFs:

$$F_{K^+}(s) = 1 - \sum_{V=\rho,\omega,\phi} \frac{g_{VK^+K^-}}{f_V(s)} A_V(s), \quad F_{K^0}(s) = - \sum_{V=\rho,\omega,\phi} \frac{g_{VK^0\bar{K}^0}}{f_V(s)} A_V(s),$$

where $A_V(s) \equiv \frac{s}{s - m_V^2 - \Pi_V(s)}$, m_V is the mass of V , and $\Pi_V(s)$ is self-energy. g_{VKK} is the constant of strong coupling of vector meson V to kaon pair, it can be found from data on strong decays of V (using $SU(3)_f$ symmetry if necessary). $f_V(s)$ is the EM coupling of V to photon, and its dependence on energy accounts for loop modification of electromagnetic vertex. The normalization of $f_V(s)$ at $s = m_V^2$ follows from decay widths of $V \rightarrow e^+e^-$ (for details see [1]). The FF is illustrated in Fig. 1.

Analogously, for inclusion of higher resonances we add the terms:

$$\Delta F_{K^+}(s) = -\sum_{V'} \frac{g_{V'K^+K^-}}{f_{V'}} A_{V'}(s), \quad \Delta F_{K^0}(s) = -\sum_{V'} \frac{g_{V'K^0\bar{K}^0}}{f_{V'}} A_{V'}(s).$$

For these resonances one may assume constant (and imaginary) self-energy: $\Pi_{V'} = -i m_{V'} \Gamma_{V'}$, as it is difficult to unambiguously find and test the energy dependence of $\Pi_{V'}$. We impose $SU(3)_f$ relations for ratios of the strong and EM couplings for the ‘‘primed’’ resonances, similarly to those for ρ , ω and ϕ , and use available data on branching ratios from [4]. This leads to: $g_{\rho'K^+K^-}/f_{\rho'} = -0.063$, $g_{\omega'K^+K^-}/f_{\omega'} = -0.021$, and $g_{\phi'K^+K^-}/f_{\phi'} = -0.036$.

The normalization conditions $F_{K^+}(0) = 1$ and $F_{K^0}(0) = 0$ are fulfilled automatically in the present model.

3 Results and conclusion

Fig. 2a and Fig. 2b show comparison of our results for kaon FFs with experiments at $2 m_K < \sqrt{s} < 1.75$ GeV. Small deviations from the data at $\sqrt{s} > 2$ GeV may be addressed to $\rho(1700)$ and $\omega(1650)$ resonances which are not included. Experimental information in the time-like region comes from measurements (CMD-2, SND, KLOE) of electron-positron annihilation $e^+e^- \rightarrow K\bar{K}$ cross section $\sigma(e^+e^- \rightarrow K\bar{K}) = \frac{\pi\alpha^2}{3q^2} \left(1 - \frac{4m_K^2}{q^2}\right)^{3/2} |F_K(q^2)|^2$.

FF also agrees with the data at $-q^2 < 0.16$ GeV² (Fig. 2c). Available information¹ comes from kaon scattering on atomic electrons (SPS). Theoretical error corridors (hatched) shown in Fig. 2 are caused by uncertainties in the model parameters.

The $K\bar{K}$ channel contribution to muon AMM [5] can be calculated via the dispersion integral [10] technique: $a_\mu^{\text{had},K\bar{K}} = \frac{\alpha^2}{3\pi^2} \int_{4m_K^2}^{\infty} W(s)R(s) \frac{ds}{s}$, where $\alpha = 1/137$, $R(s) = \frac{\sigma(e^+e^- \rightarrow K\bar{K})}{\sigma(e^+e^- \rightarrow \mu^+\mu^-)}$, $W(s) = \int_0^1 \frac{x^2(1-x)}{x^2 + (1-x)s/m_\mu^2} dx$. Our estimate is

$$\begin{aligned} a_\mu^{\text{had},K^+K^-} &= (19.06 \pm 0.57) \times 10^{-10}, \\ a_\mu^{\text{had},K^0\bar{K}^0} &= (15.64 \pm 0.44) \times 10^{-10}, \end{aligned}$$

resulting in $a_\mu^{\text{had,total}K\bar{K}} = (34.70 \pm 1.01) \times 10^{-10}$. This value agrees with result [11] obtained from e^+e^- annihilation.

¹Data analysis at large momentum transfer up to $-s \sim 3$ GeV² from $ep \rightarrow e\Lambda K^+$ and $ep \rightarrow e\Sigma^0 K^+$ (JLab experiment E98) is not completed yet.

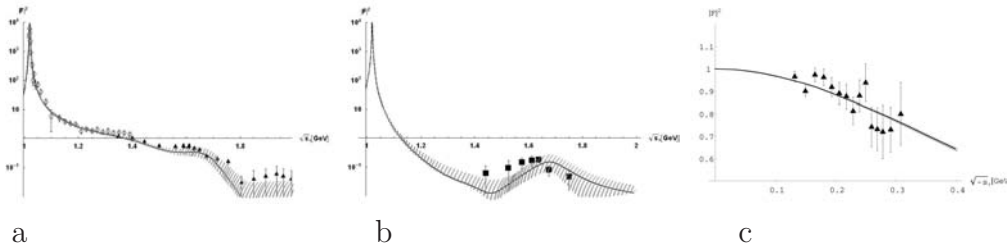


Figure 2: a: Charged kaon FF and b: neutral kaon FF in the time-like region; c: charged kaon FF in the space-like region. Data for a: diamonds from [6], triangles from [7]; for b: boxes from [8]; and for c: triangles from [9].

Acknowledgement

The authors are grateful to the Organizers of MENU 2007 for invitation and support. S.I. also acknowledges the hospitality of A. Salam ICTP in Trieste, where this paper was prepared. A.K. acknowledges support by the INTAS grant 05-1000008-8328. We thank N.P. Merenkov for useful discussions.

References

- [1] S. Ivashyn and A.Yu Korchin, *Eur. Phys. Jour. C* **49**, 697 (2007).
- [2] G. Ecker, J. Gasser, A. Pich, E. de Rafael, *Nucl. Phys. B* **321**, 311 (1989).
- [3] M. Passera, *Nucl. Phys. Proc. Suppl.* **169**, 213 (2007).
- [4] Particle Data Group, W-M Yao *et al.*, *J. Phys. G Nucl. Part. Phys.* **33**, 1 (2006) (URL: <http://pdg.lbl.gov>).
- [5] J. P. Miller, E. de Rafael and B. L. Roberts, *Rept. Prog. Phys.* **70** (2007) 795.
- [6] P.M. Ivanov *et al.*, *Phys. Lett. B* **107**, 297 (1981).
- [7] D. Bisello *et al.* [DM2 Collaboration], *Z. Phys. C* **39**, 13 (1988).
- [8] F. Mane *et al.* [DM1 Collaboration], *Phys. Lett. B* **99**, 261 (1980).
- [9] S.R. Amendolia *et al.* [NA7 Collaboration], *Phys. Lett. B* **178**, 435 (1986).
- [10] S.J. Brodsky and E. de Rafael, *Phys. Rev.* **168**, 1620 (1968).
- [11] M. Davier, S. Eidelman, A. Höcker, and Z. Zhang, *Eur. Phys. J. C* **31**, 503 (2003).

LIGHT SCALAR MESON DECAYS AND MIXING IN ChPT

S. Ivashyn and A. Korchin
Institute for Theoretical Physics,
NSC “Kharkiv Institute for Physics and Technology”,
Akademichna 1, Kharkiv 61108, Ukraine

Abstract

We propose description of light scalar meson interactions in framework of Chiral Perturbation Theory (ChPT), where scalar and vector mesons are explicitly present. Currently the scalar mesons are of great interest in view of their poorly known structure and properties. Radiative decays with scalar mesons may give information on their properties. We calculate various radiative decays within a consistent approach.

1 Introduction

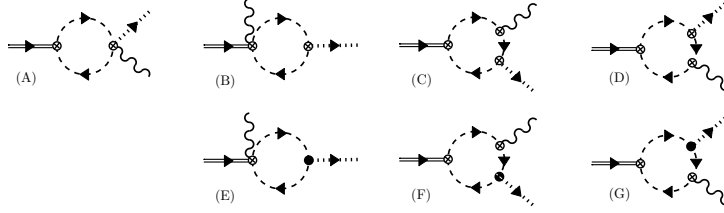
We focus on $a_0(980)$ ($I^G(J^{PC}) = 1^-(0^{++})$) and $f_0(980)$ ($0^+(0^{++})$) mesons. The aim is to build a ChPT-based framework for unified description of $\phi(1020) \rightarrow \gamma a_0(980)$, $\phi(1020) \rightarrow \gamma f_0(980)$, $a_0(980) \rightarrow \gamma\gamma$, $f_0(980) \rightarrow \gamma\gamma$, and $f_0(980)/a_0(980) \rightarrow \gamma \rho(770)/\omega(782)$ radiative decays, where scalar mesons are in the initial or final states. These decays were studied previously within different approaches in Refs. [1–4]. Apparently the underlying dynamics of all these decays has much in common. We assume the dominance of the pseudoscalar-loop mechanism.

2 Application of ChPT for light scalars

We choose ChPT Lagrangian of Ecker et al. [5] which explicitly incorporates $SU(3)$ flavor scalar singlet, octet and their interactions¹ with pseudoscalar mesons

$$L = c_d \langle S^{oct} u_\mu u^\mu \rangle + c_m \langle S^{oct} \chi_+ \rangle + \tilde{c}_d S^{sing} \langle u_\mu u^\mu \rangle + \tilde{c}_m S^{sing} \langle \chi_+ \rangle. \quad (1)$$

¹The author [6] adds point-like $S\gamma\gamma$ vertex. It seems also possible to employ vector meson dominance [7] along that. We do not introduce direct coupling of scalars to photons or vector mesons.


 Figure 1: $\phi \rightarrow \gamma a_0/f_0$ lowest order diagrams.

Both derivative and non-derivative couplings of scalar mesons to pseudoscalar ones appear naturally in Lagrangian. The parts for scalar singlet and scalar octet interactions are written separately. One has to assume a multiplet decomposition for scalars in order to relate “singlet” and “octet” pieces of Lagrangian to physical states, which are observed. We choose

$$\begin{cases} a_0 = S_3^{oct}, \\ f_0 = S^s \cos \theta - S_8^{oct} \sin \theta, \end{cases}$$

where S_3 , S_8 are the octet components and θ is the octet-singlet mixing angle. We suppose isovector a_0 and isoscalar f_0 do not mix and possible violation of isospin conservation [8] is not considered.

For the singlet couplings (\tilde{c}_d, \tilde{c}_m) and the octet ones (c_d, c_m) we employ the large N_c relations [9]. This allows one to reduce the number of free parameters. Although applicability of these relations to scalar meson radiative decays gives rise to some doubts (see Refs. [10, 11] for instance).

Following this approach one naturally comes to pseudoscalar meson-loop picture for decay mechanisms. The lowest-order diagrams are shown in Ref. [12] (see Fig. 1 for $\phi \rightarrow \gamma a_0/f_0$). A simple chiral counting tells us that these diagrams are of order $\mathcal{O}(p^4)$. Some vertices for interacting photons, vectors and pseudoscalars are calculated in Ref. [13]. Gauge invariance of the decay amplitudes and cancellation of divergences arising due to loop integrals is demonstrated in [12]. The relation $F_V = 2 G_V$ for vector-mesons chiral couplings appears crucial for cancellation of divergences. The loop integrals are calculated numerically².

3 Main results

We take $M_{a_0} = 984.7 \pm 1.2 \text{ MeV}$ and $M_{f_0} = 980 \pm 10 \text{ MeV}$. Couplings c_d , c_m and parameter θ are fixed from fitting $\Gamma_{a_0 \rightarrow \gamma\gamma}$, $\Gamma_{f_0 \rightarrow \gamma\gamma}$ and $\Gamma_{\phi \rightarrow \gamma f_0}$. This

²Our results agree with analytical expressions of Close, Isgur and Kumano [2].

allows us to calculate miscellaneous widths, shown in Table 1³. The results of calculation are also compared with experiment and predictions of $K\bar{K}$ -molecule model of Ref. [4].

In addition, in the present model, for any values of coupling constants we obtain the ratios: $\frac{\Gamma_{a_0 \rightarrow \gamma\gamma}}{\Gamma_{\phi \rightarrow \gamma a_0}} \approx 0.4$, $\frac{\Gamma_{a_0 \rightarrow \gamma\rho}}{\Gamma_{a_0 \rightarrow \gamma\omega}} \approx 1$ and $\frac{\Gamma_{a_0 \rightarrow \gamma\rho(\omega)}}{\Gamma_{\phi \rightarrow \gamma a_0}} \approx 12$. Only the first ratio can be extracted from available data [14] (≈ 0.927). From results of Ref. [4] one can infer approximately 0.4, 1 and 5.7 respectively for the same ratios, thus there is a satisfactory agreement with [4].

We estimate pseudoscalar loop contribution ratio for decays with f_0 . Ratio of ($K\bar{K}$ only) to ($K\bar{K}$ and $\pi\pi$) contribution is approximately 1, 1.64 and 1.91 for $\phi \rightarrow \gamma f_0$, $f_0 \rightarrow \gamma\rho$ and $f_0 \rightarrow \gamma\gamma$ decay widths respectively. Thus the $f_0 \rightarrow \gamma\rho$ and $f_0 \rightarrow \gamma\gamma$ decays turn out to be sensitive to *pion loop mechanism* in addition to the kaon loops.

Table 1: Estimates for decay widths of scalar mesons.

Observable	Our estimate	Kaon loop model [4]	PDG [14]
$\frac{\Gamma_{\phi \rightarrow \gamma a_0}}{\Gamma_{\phi}}$	1.7×10^{-4}	1.4×10^{-4}	$(7.6 \pm 0.6) \times 10^{-5}$
$\frac{\Gamma_{\phi \rightarrow \gamma f_0}}{\Gamma_{\phi}}$	$4.4 \times 10^{-4*}$	1.4×10^{-4}	$(4.40 \pm 0.21) \times 10^{-4}$
$\frac{\Gamma_{\phi \rightarrow \gamma f_0}}{\Gamma_{\phi \rightarrow \gamma a_0}}$	2.6	1	6.1 ± 0.6
$\Gamma_{a_0 \rightarrow \pi\eta}$	14.2 MeV	—	—
$\Gamma_{f_0 \rightarrow \pi\pi}$	41.8 MeV	—	$34.2^{+22.7}_{-14.3}$ MeV
$\Gamma_{a_0}(tot)$	17.8 MeV	—	50 – 100 MeV
$\Gamma_{a_0 \rightarrow \gamma\gamma}$	0.30 keV*	0.24 keV	0.30 ± 0.10 keV
$\Gamma_{f_0 \rightarrow \gamma\gamma}$	0.31 keV*	0.24 keV	$0.31^{+0.08}_{-0.11}$ keV
$\Gamma_{a_0 \rightarrow \gamma\rho}$	9.1 keV	3.4 keV	—
$\Gamma_{f_0 \rightarrow \gamma\rho}$	9.6 keV	3.4 keV	—
$\Gamma_{a_0 \rightarrow \gamma\omega}$	8.7 keV	3.4 keV	—
$\Gamma_{f_0 \rightarrow \gamma\omega}$	15.0 keV	3.4 keV	—

4 Summary

Within ChPT with vector and scalar mesons we calculated the radiative decay widths of $a_0 \rightarrow \gamma\gamma$, $f_0 \rightarrow \gamma\gamma$, $a_0 \rightarrow \gamma\rho(\omega)$, $f_0 \rightarrow \gamma\rho(\omega)$, $\phi \rightarrow \gamma a_0$ and $\phi \rightarrow \gamma f_0$. The calculation is carried out in one-loop approximation, and we employed the large N_c assumption and relation $F_V = 2G_V$ between

³Asterisk * marks the experimental values used as inputs for extraction of couplings.

electromagnetic and strong couplings for vector mesons. Comparison of calculations with available data and predictions of $K\bar{K}$ model of Ref. [4] shows a satisfactory agreement.

The present approach may also be useful for further studies of scalar mesons, not only the lightest ones.

Acknowledgments

We thank Nikolai Merenkov, Simon Eidelman and Christoph Hanhart for useful remarks, comments and suggestions. S.I. is very grateful to the Organizers of MENU 2007 for inviting him for a talk and providing with financial support. A.K. acknowledges support by the INTAS grant 05-1000008-8328.

References

- [1] N.N. Achasov, V.N. Ivanchenko, *Nucl. Phys. B* **315**, 465 (1989).
- [2] F. Close, N. Isgur, S. Kumano, *Nucl. Phys. B* **389**, 513 (1993).
- [3] D. Black, M. Harada, J. Schechter, *Phys. Rev. D* **73**, 054017 (2006).
- [4] Yu. Kalashnikova, A. Kudryavtsev *et al.*, *Phys. Rev. C* **73**, 045203 (2006).
- [5] G. Ecker, J. Gasser, A. Pich, E. de Rafael, *Nucl. Phys. B* **321**, 311 (1989).
- [6] S. Fajfer, *Phys. Rev. D* **51**, 1101 (1995).
- [7] D. Black, M. Harada and J. Schechter, *Phys. Rev. Lett.* **88**, 181603 (2002).
- [8] C. Hanhart, *AIP Conf. Proc.* **688**, 61 (2004).
- [9] G. Ecker, J. Gasser, H. Leutwyler, A. Pich, *Phys. Lett. B* **223**, 425 (1989).
- [10] J.R. Pelaez, *Phys. Rev. Lett.* **92**, 102001 (2004).
- [11] R.L. Jaffe, *arXiv:hep-ph/0701038* (2007).
- [12] S. Ivashyn and A.Yu Korchin, *arXiv:0707.2700 (hep-ph)* (2007).
- [13] S. Ivashyn and A.Yu Korchin, *Eur. Phys. Jour. C* **49**, 697 (2007).
- [14] Particle Data Group, W-M Yao *et al.*, *J. Phys. G Nucl. Part. Phys.* **33**, 1 (2006) (URL: <http://pdg.lbl.gov>).

FROM CHARGED TRACKS TO CHPT ANOMALIES

M. Janusz^{*,#,1} and L. Yurev^{%,#,2}
for the WASA-at-COSY collaboration

* Institute of Physics, Jagellonian University, PL30059, Cracow, Poland

% Dzhelapov Laboratory of Nuclear Problems, JINR, RU141980 Dubna,
Russia

IKP-2 Forschungszentrum Juelich, D52428 Juelich, Germany

Abstract

Invariant mass distributions of the $\pi^+\pi^-e^+e^-$ and $e^+e^-e^+e^-$ decay channel of the η -meson have been predicted by chiral unitary approach calculation [1,2] and the experimental tests have been started using the WASA-at-COSY facility. Leptonic decays of η mesons provide information about the dynamics of these processes; it is also experimental preparation for studies of charged η' decays.

In this work we present the tracking detectors of the WASA-at-COSY [3] experiment, consisting of straw chambers which are crucial for the analysis of charged decays. We describe the first steps of the analysis performed so far. The chambers are equipped with newly designed fast electronics to improve the performance of these detectors.

1 Front-end electronics and data readout

There are two straw chamber detectors in the WASA detector setup [3]: the Mini Drift Chamber (MDC) and the Forward Proportional Chamber (FPC). The MDC, as a vertex detector, is placed in the central part of the setup and delivers timing information, as well as track coordinates and the momentum for charged particles. The FPC is placed in the forward part and provides track coordinates and angular information for particles leaving from the interaction point between 3° - 18° with respect to the beam axis.

Straw chambers are connected to the DAQ (Data Acquisition System) via the

¹E-mail address: m.janusz@fz-juelich.de

²E-mail address: l.yurev@fz-juelich.de

amplifier-discriminator chip CMP-16 [4,5]. The panels with CMP-16 were designed for the MDC and FPC according to the geometry of the chambers and their location in the WASA setup. CMP-16 panels for the FPC are mounted directly on the support structure for the FPC straws. The CMP-16 board is based on the analog-digital converter chip with 16 channels which transforms analog signals to LVDS standard. It can run at very high speed at reduced electromagnetic noise. The transfer characteristics of the amplification and discrimination are presented in [5]. For the readout electronics, 64 channel time-to-digital converter based on the F1 TDC chip from ACAM [4,6] is used. Presently, the WASA DAQ system is able to read out typically 10 k events per second [7].

2 Event identification technique

Tagging of the $pp \rightarrow pp\eta$ reaction in the WASA-at-COSY setup is realized in the forward detector by requiring two protons from the same event. The FPC delivers precise information for the proton tracks. Events are selected by requiring the missing mass of the two protons close to the η meson mass. The identification of electrons and pions is accomplished by using a correlation plot of deposited energy in PSB (ΔE) or in the electromagnetic calorimeter (E) and the momentum of the reconstructed tracks from MDC (P). The reconstruction of the track vertices of e^+e^- and $\pi^+\pi^-$ - pairs efficiently suppresses background which originates mainly from $\pi^+\pi^-\pi^0 \rightarrow \pi^+\pi^-\gamma$ and γ conversion on the 1.2 mm thin beam pipe. The $(\Delta E - P)$ method will be used as a main criteria to find $\pi^+\pi^-e^+e^-$ and $e^+e^-e^+e^-$ candidates. Fig. 1 documents the application of the method to data. Pions and electrons have been separated successfully.

3 Physics background

Decays of the η and η' mesons are good tools to investigate symmetries and anomalies in nature [?,8]. In this work we restrict ourselves to the $\pi^+\pi^-e^+e^-$ decay and double-Dalitz $e^+e^-e^+e^-$ decay which are driven by the box and triangle anomalies of QCD, respectively. They probe the transition form factor of the η as a dynamical property of the decaying η meson. One goal in the study of the $\pi^+\pi^-e^+e^-$ η decay channel is to investigate the invariant mass distributions of e^+e^- and $\pi^+\pi^-$, respectively, which can test predictions obtained within the Unitary Chiral Perturbation Theory approach [2]. The decay $\eta \rightarrow e^+e^-e^+e^-$ will probe Double Vector Meson Dominance by

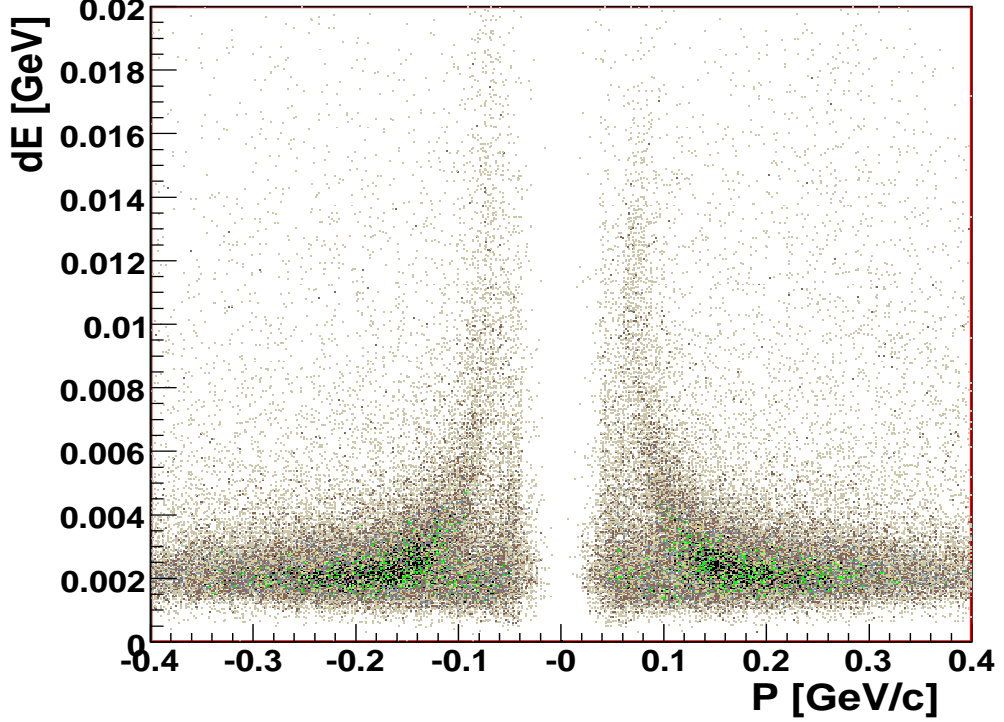


Figure 1: Sign-momentum and $(\Delta E - P)$ applied to the April 2007 data sample; 10 percent of data have been evaluated for this plot.

extracting the transition form factor as a function of the invariant mass squared of the two virtual photons $-F(q_1^2, q_2^2)$. Such a measurement is important for understanding the anomalous magnetic moment of the muon and kaon decays [8].

4 Summary and outlook

The first WASA-at-COSY production run has been carried out in April 2007 using a proton beam with a kinetic energy of 1400 MeV and the hydrogen pellet target. A total 10^7 eta mesons have been registered and, according the Monte Carlo studies of about 10^3 $\pi^+\pi^-e^+e^-$ and 10^2 $e^+e^-e^+e^-$ events are expected.

Acknowledgments

Essential help and explanations from B. Borasoy and R. Nissler are gratefully acknowledged. We are grateful to M. Wolke, A. Kupsc for their valuable advice. Great thanks to M. Jacewicz for his fruitful help in the calibration of the straw chambers. Many thanks to H. Ohm for hundred hours spent in laboratory who was very patient with us. Many thanks to V. Serdyuk for immediate help concerning drift chamber construction and electronics. We acknowledge the support of the German Research Foundation and the Polish Ministry of Science and Higher Education under grants No. 3240/H03/2006/31 and 1202/DFG/2007/03.

References

- [1] B. Borasoy, R. Nissler, *Eur. Phys. J.*, **A319**, 367-382, (2004).
- [2] B. Borasoy, R. Nissler, *Eur. Phys. J.*, **A33**, 95, (2007).
- [3] H-H. Adam et al., e-Print: **nucl-ex/0411038**, (2004).
- [4] H. Kleines et al., *IEEE Trans. Nucl. Sci* **53**, 893 (2006).
- [5] <http://www-hep.phys.cmu.edu/cms/DOCUMENTATION/>
- [6] <http://www.acam.de/fileadmin/Download/pdf/English/>
- [7] V. Hejny, *Performance issues of the new DAQ system for WASA at COSY*, 15th IEEE Real Time Conference 2007 (RT 07), Batavia, Illinois, 29 Apr - 4 May 2007.
- [8] J. Bijnens, *Goldstone boson production and decay*, **hep-ph/9710341** (1997).
- [9] B. M. K. Nefkens, *Rare and not-so-rare decays of light mesons* Workshop On Meson Production, Interaction And Decay, 6-11 May 1991. proc. ed. by A. Magiera, W. Oelert, E. Grosse. World Scientific, River Edge, NJ (1991), p. 40-64.

η' DECAYS WITH WASA-AT-COSY

Benedykt R. Jany^{∞*1} and David Duniec^{#2}
for the WASA-at-COSY Collaboration

[∞]Nuclear Physics Division, Jagiellonian University, 30059 Cracow, Poland

*IKP-2, Forschungszentrum-Jülich, 52428 Jülich, Germany

#Department of Nuclear and Particle Physics, Uppsala University, 75121 Uppsala, Sweden

Abstract

This article describes the physics of the $\eta' \rightarrow \eta\pi\pi$ decays. Predictions of the Chiral Unitary Approach for these decays are discussed. The first look into high energy data of a commissioning of WASA-at-COSY are presented.

1 Theory overview and predictions

The strong, isospin conserving decays of the η' into three mesons, $\eta' \rightarrow \pi\pi\eta$ are responsible for most (65.3% [1]) of the total decay width of the η' . There are some data available for these decays [2–5], with at most about ten thousand events. Another very interesting decay is $\eta' \rightarrow \pi^+\pi^-\pi^0$ which violates the Isospin Symmetry and was never measured. These decays allow to study fundamental symmetries of QCD, for example, by means of Chiral Unitary Approach framework [6]. One uses the low energy expansion of QCD – Chiral Perturbation Theory together with relativistic coupled channels, via Bethe-Salpeter Equation (BSE). Based on the framework and on the available data one can predict distributions of the decay products of hadronic η' decays. In Fig. 1, the expected shape of the Dalitz plot for $\eta' \rightarrow \pi\pi\eta$ is shown. The influence of $a_0(980)$ ($I = 1$) Fig. 1a or $f_0(980)/\sigma$ ($I = 0$) Fig. 1b in the final state can be observed by different populations in the Dalitz plot. The limited statistics of the existing experimental data does not allow to distinguish between the two possible scenarios since the difference is small (the total variation of the Dalitz plot densities is only 20%). The Branching Ratio (1.8%) and Dalitz plot for the yet unobserved $\eta' \rightarrow \pi^+\pi^-\pi^0$ decay is predicted in Fig. 2.

¹E-mail address: b.jany@fz-juelich.de, jany@if.uj.edu.pl

²deceased

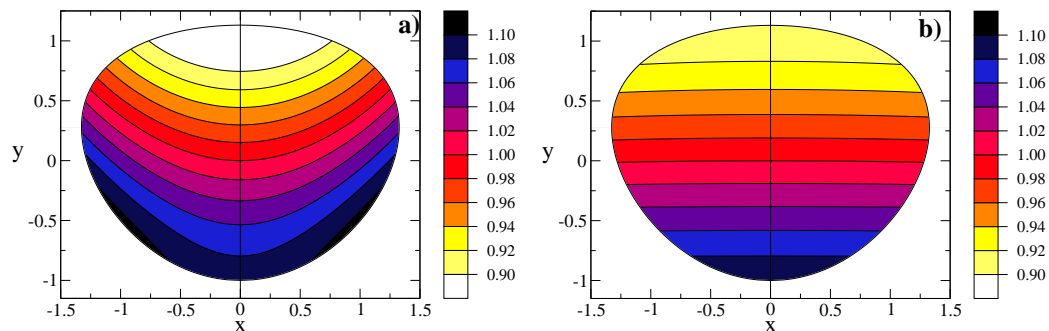


Figure 1: Predicted Dalitz Plot for the $\eta' \rightarrow \pi\pi\eta$ decay: a) with $a_0(980)$ dominance, b) with $f_0(980)/\sigma$ dominance [8].

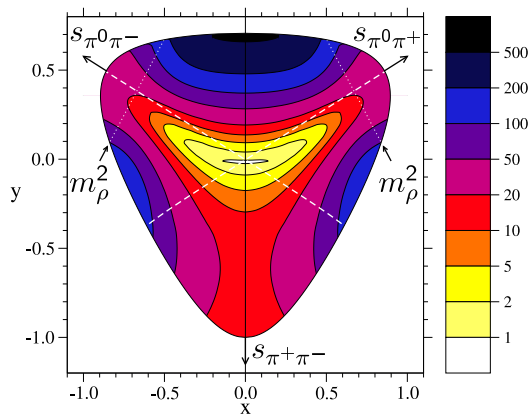


Figure 2: Predicted Dalitz Plot for the $\eta' \rightarrow \pi^+\pi^-\pi^0$, one sees $\rho^\pm(770)$ dominance [7].

2 Data First Look

The recently commissioned WASA-at-COSY detector [9] at the COSY accelerator in Jülich is well suited to study decays of the η' meson. It has a large acceptance with nearly 4π sr coverage and both charged and neutral decay products can be measured. During commissioning a total of about 45 hours of data was taken at the proposed η' production proton beam momentum $3.35\text{GeV}/c$ for the $pp \rightarrow ppX$ reaction. The analysis of this data has focused on the experimentally clean $\eta' \rightarrow \pi^0\pi^0\eta \rightarrow 5\pi^0 \rightarrow 10\gamma$ reaction channel. One finds events consistent with the η' signal in the plot of the invariant mass of the 10 reconstructed photons versus the missing mass of the two protons, as shown on Fig. 3a. If one looks at the projection onto the invariant mass and missing mass axis Fig. 3b, Fig. 3b, one observes about 20 η' candidates. This is consistent with luminosity estimates based on the monitoring reaction $pp \rightarrow pp(\eta \rightarrow \gamma\gamma)$ collected simultaneously.

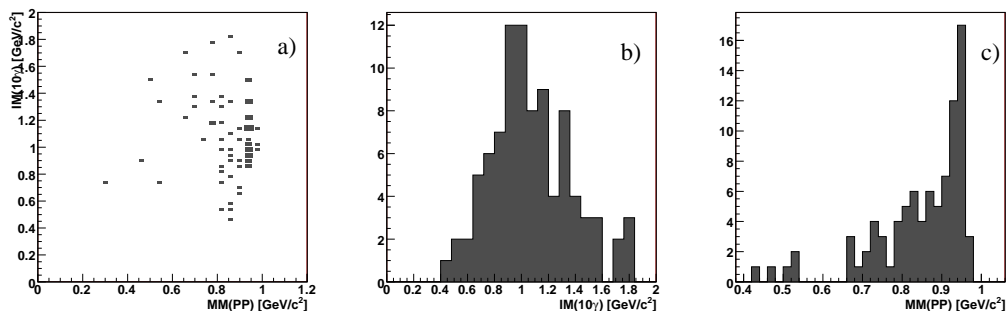


Figure 3: Results of a first Look onto Data: a) Invariant Mass of 10 reconstructed photons versus Missing Mass of 2 charged tracks, b) Projection to the Invariant Mass axis, c) Projection to the Missing Mass axis.

3 Summary

The hadronic decays of η' are well suited to study symmetries in nature and to provide experimental verifications of the Chiral Unitary Approach predictions. The first results gives confidence that the WASA-at-COSY detector can contribute with precise data.

References

- [1] W. M. Yao, et al., *J. Phys.* **G33**, 1–1232 (2006).
- [2] G. R. Kalbfleisch, *Phys. Rev.* **D10**, 916 (1974).
- [3] D. Alde, et al., *Z. Phys.* **C36**, 603–609 (1987).
- [4] R. A. Briere, et al., *Phys. Rev. Lett.* **84**, 26–30 (2000).
- [5] V. Dorofeev, et al. (2006), [hep-ph/0607044](#).
- [6] B. Borasoy, U.-G. Meissner, and R. Nissler, *Phys. Lett.* **B643**, 41–45 (2006), [hep-ph/0609010](#).
- [7] B. Borasoy and R. Nissler, *Eur. Phys. J.* **A26**, 383–398 (2005), [hep-ph/0510384](#).
- [8] B. Borasoy and R. Nissler, private communication (2007), borasoy@itkp.uni-bonn.de, rnissler@itkp.uni-bonn.de.
- [9] H. H. Adam, et al. (2004), [nucl-ex/0411038](#).

SEARCH FOR η -NUCLEUS BOUND STATES

V. Jha^{*,1}, A. Budzanowski[%], A. Chatterjee^{*}, P. Hawranek[±], R. Jahn[⊥], S. Kailas^{*}, K. Kilian[§], S. Kliczewski[%], Da. Kirillov[§], Di. Kirillov[&], D. Kolev⁺, M. Kravcikova[#], T. Kutsarova[°], M. Lesiak[±], J. Lieb[×], L. C. Liu[⊐], H. Machner[§], A. Magiera[±], R. Maier[§], G. Martinska[⊕], S. Nedev[‡], N. Piskunov[&], D. Protić[§], J. Ritman[§], P. von Rossen[§], B. J. Roy^{*}, P. Shukla^{*}, I. Sitnik[&], R. Siudak[%], R. Tsenov⁺, J. Urban[⊕], G. Vankova⁺

*Nuclear Physics Division, BARC, Mumbai-400 085, India

%Institute of Nuclear Physics, Polish Academy of Sciences, Krakow, Poland

⊥Helmholtz-Institut für Strahlen- und Kernphysik der Universität Bonn

±Institute of Physics, Jagellonian University, Krakow, Poland

§Institut für Kernphysik, Forschungszentrum Jülich, Jülich, Germany

&Laboratory for High Energies, JINR Dubna, Russia

+Physics Faculty, University of Sofia, Sofia, Bulgaria

#Technical University, Kosice, Kosice, Slovakia

°Institute of Nuclear Physics and Nuclear Energy, Sofia, Bulgaria

×Physics Department, George Mason University, Fairfax, Virginia, USA

⊕J. Safarik University, Kosice, Slovakia

‡University of Chemical Technology and Metallurgy, Sofia, Bulgaria

⊐Theoretical Division, Los Alamos National Laboratory, New Mexico 87545

Abstract

We have performed an experiment to search for the formation of η -mesic nuclear states using recoil-free ($p, {}^3\text{He}$) transfer reactions on ${}^{27}\text{Al}$ nuclei. The decay of such states is expected to proceed through $N^*(1535)$ resonance which would lead to the proton- π^- pair emitted in opposite direction. A coincidence measurement of ${}^3\text{He}$ particles with the η -mesic decay particles shows a low statistics enhancement in the excitation energy spectra of the residual system below the free η production threshold.

¹E-mail address: vjha@magnum.barc.gov.in

1 Introduction

The possible existence of a bound state of η -meson and a nucleus, the so-called η -mesic nuclei, was first proposed by Haider and Liu two decades ago [1]. This came out as a result of their theoretical findings that the low energy η -nucleon interaction is attractive and it can bind η in nuclei. This attraction arises because the η -nucleon (ηN) interaction at low energies is strongly influenced by the presence of the S-wave nucleon resonance $N^*(1535)$ which lies close to the η -nucleon production threshold. Since then a large number of theoretical calculations have been performed and almost all of them predict the possibility of η -nucleus bound state formation. However, depending on the value of η -nucleon scattering length $a_{\eta N}$ that is used in the calculations, different limits for mass numbers A are predicted for which a η -bound state can exist. The detailed calculations of C. Garcia-Recio et al however, suggest that it is only in the region of mass region $A = 24$ that the bound state peaks with widths comparable to binding energy can be experimentally observed [2].

Initial experimental measurements for search of bound η -meson states with the (π^+, p) reaction at Brookhaven AGS [3] couldn't confirm their existence. Recent data on photoproduction of η meson on ^3He and ^{12}C [4] nuclei have been interpreted to provide signatures of η -mesic nucleus formation. More direct measurements with better statistics are required however for any conclusive evidence. In this contribution, we describe an experiment to search for the η -nucleus bound state formation that has been performed at COSY using the $(p, ^3\text{He})$ reaction on ^{27}Al target at recoilless kinematic conditions.

2 Experiment

The experimental search employs the reaction $p + ^{27}\text{Al} \rightarrow ^3\text{He} + ^{25}\text{Mg} \otimes \eta$ at the recoil-free conditions ($p_{beam} = 1745 \text{ MeV}/c$) in which the bound state formation and decay takes place via $\eta + N \rightarrow N^* \rightarrow \pi^- + p$. The outgoing ^3He particles have been measured under zero degree by the 3D2Q magnetic spectrometer BigKarl(BK) along with its focal plane detectors. Tracks of ^3He particles were measured in the focal plane of the spectrometer with two stacks of multi-wire drift chambers (MWDC) followed by two layers of scintillator hodoscopes to measure energy loss and time of flight of particles. Two momenta settings of spectrometer at $859 \text{ MeV}/c$ and $897 \text{ MeV}/c$ were used to measure ^3He particles, which cover $\sim 80 \text{ MeV}$ range each in the missing mass spectrum. To enhance the sensitivity of measurement the decay products of

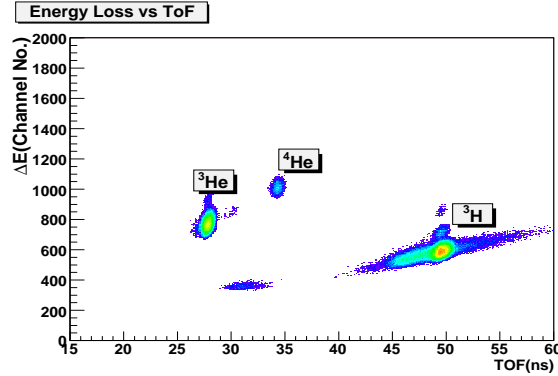


Figure 1: **Left:** Energy loss versus the Time of Flight spectra from the focal plane hodoscopes. ${}^3\text{He}$ particles can be clearly identified.

the η mesic nuclei are measured in a large acceptance plastic scintillator detector ENSTAR [5] in coincidence with ${}^3\text{He}$ particles. The signature for the η -bound formation in this experiment is a peak in the missing mass spectrum of residual nuclear system at the excitation energies corresponding to the production of negative energy η 's in two-body kinematics.

3 Data Analysis and Results

The energy loss in the first hodoscope layer is shown in Fig. 1 as a function of time of flight of the different particle groups. Clearly the ${}^3\text{He}$ ions can be identified by from the spectra. The inclusive missing mass spectra of the residual reaction products in $p^{27}\text{Al} \rightarrow {}^3\text{He}X$ reaction is a uniform distribution which show mainly the acceptance of the spectrograph. To suppress the background and select signal corresponding to η bound state formation coincidence conditions from ENSTAR detector were used. Events corresponding to the coincidence peak in the time spectrum of the ENSTAR detectors have been selected and background has been estimated. Missing mass spectra for selected events corresponding to two decay particles emitted back-to-back measured in ENSTAR shows a low statistics enhancement at almost similar range of values in both momentum setting of spectrograph as shown in Fig. 2. Based on the estimates of detection efficiency due to detector geometry and analysis cuts of 0.7 we obtain $\frac{d\sigma}{d\Omega_{3\text{He}}}(\theta_{3\text{He}} = 0^\circ, (p\pi^-)) = 0.2 \pm 0.08$ nb/sr. If this structure corresponds to the decay of a bound η decaying via $N^* \rightarrow \pi^- + p$ an upper limit of ~ 0.5 nb/sr on the formation cross section

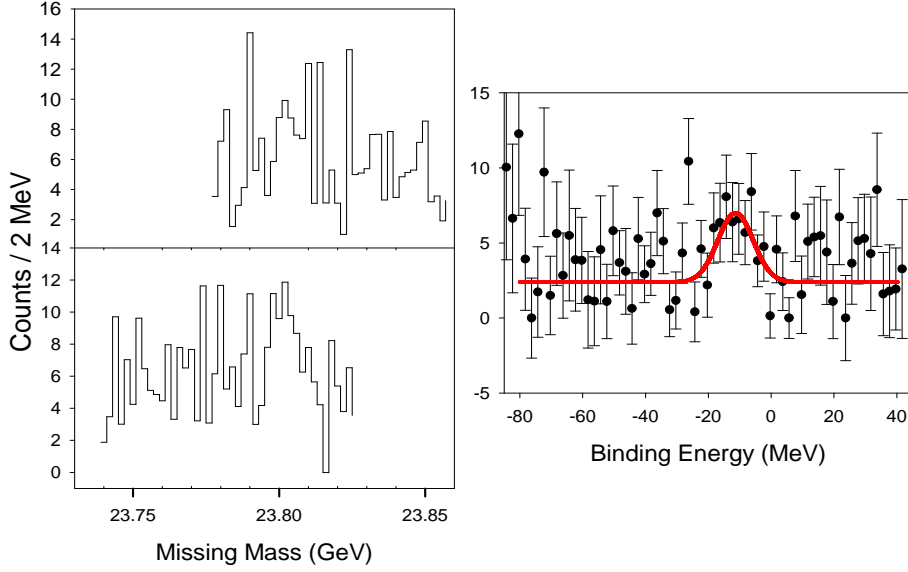


Figure 2: **a**: Missing mass spectra of residual nuclear products in coincidence with ENSTAR cuts at two Big Karl settings. **b**: Summed binding energy spectra at two settings fitted with the background plus a gaussian.

of η -bound state can be estimated.

4 Summary

In summary, we have performed a dedicated experiment to search for the signals of formation of eta-,mesic nuclei using the reaction $p^{27}\text{Al} \rightarrow {}^3\text{He} + \pi^- + p + X$. In two missing mass spectra taken at independent spectrograph settings, we observe an enhancement for negative binding energies. An upper bound of ~ 0.5 nb for the formation cross section of η -nucleus bound state has been estimated.

References

- [1] L.C. Liu, Q. Haider Phys. Rev. C**34**, 1845 (1986).
- [2] C. Garcia-Recio *et al.* Phys. Lett.**B550**, 47 (2002).
- [3] R.E. Cherien *et al.* Phys. Rev. Lett.**60**, 865 (1988).

- [4] G.A. Sokol *et al.* Fisika **B8**, 81 (1999), M. Pfeiffer *et al.* Phys. Rev. Lett.**92**, 252001 (2004).
- [5] M.G.Betigeri *et al.* Nuclear Instruments and Methods **A578**, 198 (2006).

MEASUREMENT OF THE ABC-EFFECT IN THE MOST BASIC DOUBLE-PIONIC FUSION REACTION

O. Khakimova^{*,1}, C. Bargholtz[%], M. Bashkanov^{*}, D. Bogoslawsky[#], H. Calen[⊥], F. Cappellaro[§], H. Clement^{*}, L. Demiroers⁺, E. Doroshkevich^{*}, D. Duniec[§], C. Ekström[⊥], K. Franssen[⊥], L. Geren[%], L. Gustafsson[§], B. Höistad[§], G. Ivanov[#], M. Jacewicz[§], E. Jiganov[#], T. Johansson[§], M. Kaskulov^{*}, S. Keleta[§], I. Koch[§], F. Kren^{*}, S. Kullander[§], A. Kupść[⊥], A. Kuznetsov[#], K. Lindberg[%], P. Marciniowski[⊥], R. Meier^{*}, B. Morosov[#], C. Pauly[‡], H. Pettersson[§], Y. Petukhov[#], A. Povtorejko[#], A. Pricking^{*}, K. Schönning[§], W. Scobel⁺, B. Schwartz[±], T. Skorodko^{*}, V. Sopov[‡], J. Stepeniak[◊], P.-E. Tegner[%], P. Thörngren-Engblom[§], V. Tikhomirov[#], G. J. Wagner^{*}, M. Wolke[‡], A. Yamamoto[□], J. Zabierowski[▷], I. Zartova[%], J. Złomanczuk[§]

^{*}Physikalisches Institut der Universität Tübingen, D-72076 Tübingen, Germany

[%]Department of Physics, Stockholm University, Stockholm, Sweden

[#]Joint Institute for Nuclear Research, Dubna, Russia

[⊥]The Svedberg Laboratory, Uppsala, Sweden

[§]Uppsala University, Uppsala, Sweden

⁺Hamburg University, Hamburg, Germany

[±]Budker Institute of Nuclear Physics, Novosibirsk, Russia

[‡]Institute of Theoretical and Experimental Physics, Moscow, Russia

[‡]Forschungszentrum Jülich, Germany

[□]High Energy Accelerator Research Organization, Tsukuba, Japan

[◊]Soltan Institute of Nuclear Studies, Warsaw, Poland

[▷]Soltan Institute of Nuclear Studies, Lodz, Poland

¹E-mail address: khakimov@pit.physik.uni-tuebingen.de

Abstract

The ABC effect - a puzzling low-mass enhancement in the $\pi\pi$ invariant mass spectrum - is known from inclusive measurements of two-pion production in nuclear fusion reactions. The first exclusive measurements carried out at CELSIUS-WASA for the most basic fusion reaction in this context - the $pn \rightarrow d\pi^0\pi^0$ reaction - reveal this effect to be a σ channel phenomenon associated with the formation of a $\Delta\Delta$ system in the intermediate state. The total cross section exhibits a resonance-like energy dependence with a width of 100 MeV or less. Both the ABC effect and the intriguing energy dependence can be accommodated by a quasibound state in the $\Delta\Delta$ system leading to a resonance in the pn and $d\pi^0\pi^0$ systems.

1 Introduction

The ABC effect - first observed by Abashian, Booth and Crowe [1] - in the double pionic fusion of deuterons and protons to ${}^3\text{He}$, stands for an unexpected enhancement at low masses in the $M_{\pi\pi}$ spectrum. Follow-up experiments [2] revealed this effect to be of isoscalar nature and to show up in cases, when the two-pion production process leads to a bound nuclear system.

Initially the low-mass enhancement had been interpreted by an unusually large $\pi\pi$ scattering length and evidence for the σ meson, respectively [1]. Since the effect showed up particularly clearly at beam energies corresponding to the excitation of two Δ s in the nuclear system, the ABC effect was interpreted later on by a $\Delta\Delta$ excitation in the course of the reaction process leading to both a low-mass and a high-mass enhancement in isoscalar $M_{\pi\pi}$ spectra [3–5]. In fact, the missing momentum spectra from inclusive measurements have been in support of such predictions. It has been shown [6] that these structures can be enhanced considerably in theoretical calculations by including ρ exchange and short-range correlations.

2 Experiment and Results

In order to shed more light on this issue, first exclusive measurements of the $pd \rightarrow pd\pi^0\pi^0$ reaction ($T_p = 1.03$ and 1.35 GeV) have been carried out at $T_p = 1.03$ and 1.35 GeV at CELSIUS using the 4π WASA detector setup including the deuterium pellet target system [2]. The $pd \rightarrow pd\pi^0\pi^0$ reaction is observed as quasifree $pn \rightarrow d\pi^0\pi^0$ reaction with a low-energetic spectator proton. Since all ejectiles except of the spectator have been measured, the

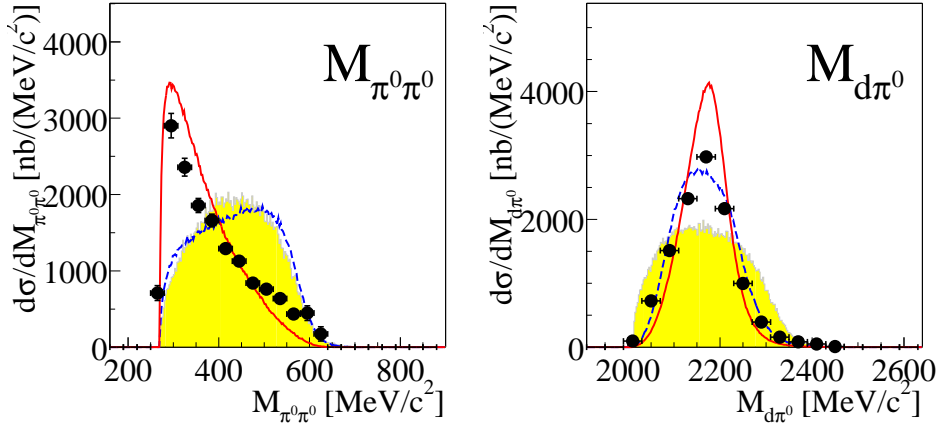


Figure 1: Distributions of the invariant masses $M_{\pi^0\pi^0}$ and $M_{d\pi^0}$ from the exclusive measurement of the quasifree $pn \rightarrow d\pi^0\pi^0$ reaction at a beam energy $T_p = 1.35$ GeV. The shaded areas show the pure phase space distributions. Solid and dashed curves give $\Delta\Delta$ calculations with and without the assumption of a quasibound state in the $\Delta\Delta$ system leading to a resonance in the pn and $d\pi^0\pi^0$ systems.

spectator momentum has been reconstructed by kinematical fits with three overconstraints.

Results of our measurements are shown in Fig. 1. Note that due to Fermi motion of the nucleons in the target deuteron the quasifree reaction process proceeds over a range of effective collision energies with according kinematical smearing in the differential distributions. This smearing may be reduced strongly by dividing the data into narrow bins of effective collision energy at the cost of statistics.

Fig. 1 depicts the spectra of the invariant masses $M_{\pi^0\pi^0}$ and $M_{d\pi^0}$ for the quasifree $pn \rightarrow d\pi^0\pi^0$ reaction at the beam energy $T_p = 1.35$ GeV. The $\pi^0\pi^0$ channel, which is free of any isospin $I=1$ contributions, exhibits a pronounced low-mass enhancement (ABC effect) in the $M_{\pi^0\pi^0}$ spectrum similar to the situation in the fusion process leading to ${}^3\text{He}$ [2]. The $M_{d\pi^0}$ spectrum shows clearly the excitation of the Δ resonance. The data are only consistently described, if two Δ states are excited simultaneously in this reaction. The spectra shown in Fig. 1 are very similar to the ones obtained at the lower energy [2], i.e. do not change with energy as predicted in previous $\Delta\Delta$ calculations.

Also the $\pi\pi$ low-mass enhancements observed in the exclusive data for the $\pi^0\pi^0$ channels turn out to be much larger than predicted in previous $\Delta\Delta$

calculations [3, 5, 6]. As an example we show by the dashed lines in Figs.1 model ansatz of Ref. [3], where we additionally included the pion angular distribution in Δ decay and the Fermi smearing of the nucleons bound in the final nucleus. Contrary to these predictions the data also do not exhibit any high-mass enhancement.

A clue to the real nature of the ABC effect is provided by the intriguing energy dependence [2] of the double-pionic fusion in the isoscalar channel, which exhibits a pronounced resonance-like excitation with a width of roughly 100 MeV or possibly even below, i.e. much smaller than twice the Δ width expected from usual $\Delta\Delta$ calculations. Both the energy dependence of the total cross section and the differential cross section data can be accommodated by the assumption of a quasibound state in the $\Delta\Delta$ system (solid lines in Fig. 1), which decays into this system to proceed via relative s-waves between the two Δ s and which couples to the initial pn system.

Acknowledgments

We acknowledge valuable discussions with E. Oset, C. Wilkin, Ch. Hanhart, A. Sibirtsev, L. Alvarez-Ruso, A. Kaidalov, L. Dakhno and V. Anisovitch on this issue. This work has been supported by BMBF (06TU201, 06TU261), COSY-FFE, DFG (Europ. Graduiertenkolleg 683), Landesforschungsschwerpunkt Baden-Württemberg and the Swedish Research Council. We also acknowledge the support from the European Community-Research Infrastructure Activity under FP6 "Structuring the European Research Area" programme (Hadron Physics, contract number RII3-CT-2004-506078).

References

- [1] N. E. Booth, A. Abashian, K. M. Crowe, *Phys. Rev. Lett.* **7**, 35 (1961) ; **6** (1960) 258; *Phys. Rev.* **C132**, 2296ff (1963)
- [2] see M. Bashkanov et al. *et al.*, contribution to this conference
- [3] T. Risser and M. D. Shuster, *Phys. Lett.* **43B**, 68 (1973)
- [4] I. Bar-Nir, T. Risser, M. D. Shuster, *Nucl. Phys.* **B87**, 109 (1975)
- [5] C. A. Mosbacher, F. Osterfeld, nucl-th/990364
- [6] L. Alvarez-Ruso, *Phys. Lett.* **B452**, 207(1999); PhD thesis, Univ. Valencia 1999

GENERALIZED MULTICONFIGURATION MODEL OF DECAY OF THE MULTIPOLE GIANT RESONANCES APPLIED TO ANALYSIS OF REACTION (μ^-N) ON THE NUCLEUS ^{40}Ca

O. Yu. Khetselius^{# 1}, A. V. Glushkov^{*%}, A. V. Loboda[%],
E.P.Gurnitskaya[%]

^{*}Inst. of Spectroscopy (ISAN), Russian Acad.Sci., Troitsk-Moscow, Russia

[%]Odessa University, Odessa, Ukraine

[#]Abdus Salam International Centre for Theoretical Physics, Strada
Costiera, Trieste, Italy

Abstract

It is presented the generalized multiconfiguration model to describe a decay of high-excited states (the multipole giant resonances), which is based on the mutual using the shell models (with limited basis) and microscopic model of pre-equilibrium decay with statistical account for complex configurations 2p2h, 3p3h etc. The model is applied to analysis of reaction (μ^-n) on the nucleus ^{40}Ca .

1 Introduction

As it is well known, the multipole giant resonances (MGR) are the highly excited states of nuclei, which are interpreted as the collective coherent vibrations with participation of large number of nucleons [1-5]. Two theoretical approaches to the description of MGR are usually used. In the phenomenological theories it is supposed that the strong collectivization of states allows to apply the hydrodynamical models to the description of vibrations of the nuclear form and volume. The microscopic theory is based on the shell model of a nucleus. In the simple interpretation an excitation of the MGR is result of transition of the nucleons from one closed shell to another one, i.e. the MGR is an result of coherent summation of many particle-hole (p-h) transitions with necessary momentum and parity. Here we present generalized

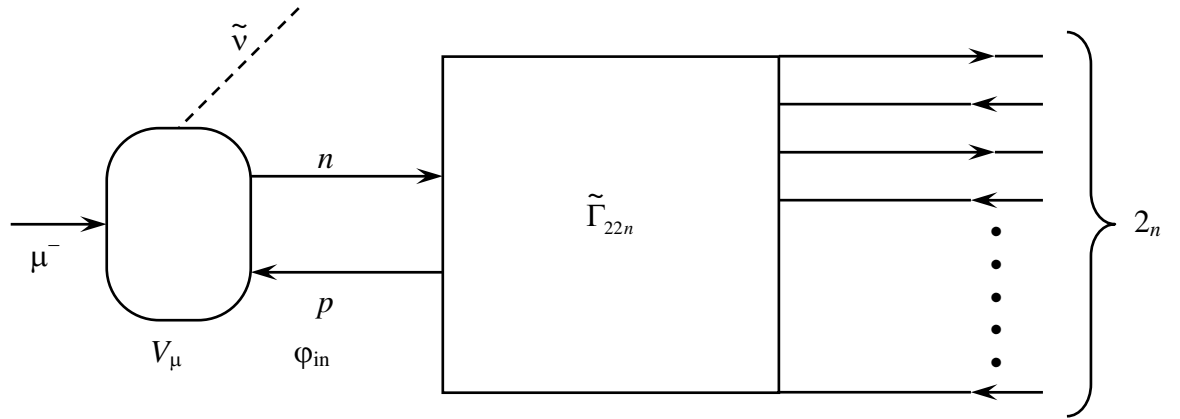
¹E-mail address:glushkov@paco.net

multiconfiguration model to describe a decay of high-excited states, which is based on the mutual using the shell models (with limited basis) and microscopic Zhivopistsev-Slivnov model of pre-equilibrium decay with statistical account for complex configurations 2p2h, 3p3h etc. The model is applied to analysis of reaction (μ^-n) on the nucleus ^{40}Ca . The comparison with experimental and other theoretical data is presented.

2 Generalized multiconfiguration model of the MGR decay

The MGR is treated on the basis of the multiparticle shell model. Process of arising a collective state of MGR and an emission process of nucleons are described by the diagram in fig.1.

Figure 1: Diagram of process for production of the collective state MGR and emission of nucleons (or more complex particles).



Here V_μ is effective hamiltonian of interaction, resulted in capture of muon by nucleus with transformation of proton to neutron and emission by antineutrino. Isobaric analogs of isospin and spin-isospin resonances of finite nucleus are excited. The diagrams for photonuclear reactions look to be analogous; $\tilde{\Gamma}_{22}^n$ is the full vertex part (full amplitude of interaction, which transfers the interacting p-h pair to the finite npnh state. The full vertex $\Gamma \tilde{\Gamma}_{22}^n$ is defined by the system of equations within quantum Green function modified approach [3,11].

All possible configurations are divided on two groups: i). group of complicated configurations “n₁”, which must be considered within shell model with account for residual interaction; ii). statistical group “n₂” of complex configurations with large state density $p(n, E)$ and strong overlapping the states $G_n D_{n-1} D_n$ (D_n is an averaged distance between states with $2n$ exciton; G_n is an averaged width). Matrix elements of bond $|n|V|n'\rangle$ are small and characterized by a little dispersion. To take into account a collectivity of separated complex configurations for input state a diagonalization of residual interaction on the increased basis (ph, ph+phonon, ph+2 phonon) is used. All complex configurations are considered within the pre-equilibrium decay model by Feschbach-Zhivopistsev et al [5,6] with additional account of “n₁” group configurations. The input wave functions of MGR for nuclei with closed or almost closed shells are found from diagonalization of residual interaction on the effective 1p1h basis.

Statistical multistep negative muon capture through scalar intermediate states of compound nucleus is important. Intensities of nucleon spectra are defined by standard way [6].

The intensity of nucleonic spectra is defined as follows:

$$\frac{dI}{d\varepsilon_f}(E_\mu, l, \varepsilon_f, J\pi) = \sum_{\substack{n=1, \\ \Delta n=1}} \frac{\Gamma_n^\uparrow(l, \varepsilon_f, J\pi)}{\Gamma_n(J\pi)} \cdot \left[\prod_{k=1}^{n-1} \frac{\Gamma_k^\downarrow(J\pi)}{\Gamma_k(J\pi)} \right] \cdot \Lambda_\mu(E_\mu, J\pi) \quad (1)$$

where

$$\Gamma_n^\uparrow(l, \varepsilon_f, J\pi) = 2\pi \cdot \left| \langle \varphi_{N_n}(J\pi) | I_{N_n, N_B+1} \right| \cdot \left| [\varphi^{(+)}(l, \varepsilon_f) \varphi_{N_B}(U_B, I_B)]_{J\pi} \right|^2 > \rho(l, \varepsilon_f) \rho^{(b)}(N_B, U_B, I_B)$$

$$\Gamma_k^\uparrow(J\pi) = \sum_{l,f} \int d\varepsilon_f \Gamma_k^\uparrow(l, \varepsilon_f, J\pi)$$

$$\Gamma_k(J\pi) = \Gamma_k^\uparrow(J\pi) + \Gamma_k^\downarrow(J\pi)$$

$$\Gamma_k^\downarrow(J\pi) = 2\pi \cdot \left| \langle \varphi_{N_k}(J\pi) | I_{N_k, N_{k+1}} | \varphi_{N_{k+1}}(J\pi) \right|^2 > \rho^{(b)}(N_{k+1}, J\pi, E_\mu)$$

$$E_\mu = \varepsilon_f + U_B + B_N$$

Here l is the orbital moment of the emission nucleon, ε_f is its energy; B_N is the bond energy of nucleon in the compound nucleus; $\Lambda_\mu(E_\mu, J\pi)$ is probability of μ -capture with excitation of the state $\varphi_{in}(E_\mu, J\pi)$ with energy E_μ , spin J and parity π . As in ref.[5,6], we neglect the interference between contributions of separated “dangerous” configurations. The above indicated features of the statistical group of configurations are not fulfilled for the “dangerous” configurations (c.f.[5]). However, the value $\Gamma_n^\downarrow(n_1)$ for some dangerous configuration is weakly dependent upon the energy. Indeed, configuration n_1 is the superposition of the large number of configurations, i.e. [5,13]

$$\Gamma_n^\downarrow(n_1) = \sum_{n+1} \frac{|\langle n_1 | I_{n_1, n+1} | n+1 \rangle|^2}{(E_\mu - E_{n+1})^2 + \Gamma_{n+1}^2/4}$$

The other details of model can be found in refs. [5-7,11-14].

3 Results and conclusion

The wave functions of the input state $\{\varphi_{in}\}$ in the reaction $^{40}\text{Ca}(\mu^-n)$ are calculated within the shell model [12,13]. As one could wait for that a collectivity of initial input state leads to significant decreasing Γ_1^\downarrow . The separation into groups n_1 and n_2 is naturally accounted for the 2p2h configuration space [5] and the contribution of configurations “ph+phonon” and weakly correlated 2p2h states was revealed [15]. A probability of transition to the “dangerous” configurations 2p2h is defined by the value of matrix element:

$$|\langle \varphi_{in}(ph, J\pi, E) | I_{ph, 2p2h} | \varphi(2p2h, J\pi, E) \rangle|^2$$

and additionally by density $\rho(2p2h, J\pi, E)$ for statistical group n_2 . The contribution of weakly correlated 2p2h configurations is defined by expression [5]:

$$\Gamma_{2p2h}^\downarrow = 2\pi \cdot \langle | \langle I_{ph, 2p2h} \rangle |^2 \rangle \rho_{2p2h}$$

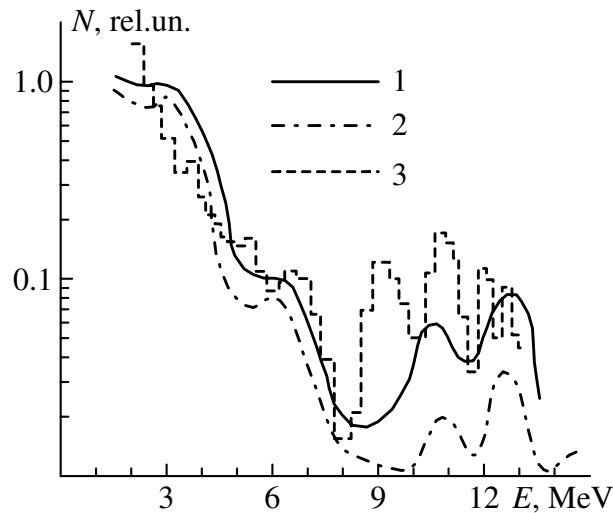
The residual interaction has been chosen in the form of Soper forces:

$$V = g_0(1 - \alpha + \alpha \cdot \sigma_1 \sigma_2) \cdot \delta(\mathbf{r}_1 - \mathbf{r}_2),$$

where $g_0/(4\pi r_o^3) = -3$ MeV, $\alpha = 0,135$. The phonons have been considered in the collective model and calculation parameters in the collective model and generalized RPA are chosen according to ref.[13]. The phonons contribution is distributed as follows: 2^+ ($E=3,9$ MeV; $\beta=0,075$) $\sim 42\%$, 3^- ($E=3,736$

MeV; $\beta=0,345$) $\sim 8\%$, 5^- ($E=4,491$ MeV; $\beta=0,216$) $\sim 3\%$ etc. with growth of the phonon moment. Our theoretical results are compared with experimental data and other calculation results [2] in fig.2. In the range of 5-13MeV the experiment gives the intensity $\sim 10\%$ from the equilibrium one. As it has been shown earlier (c.f.[5,6], the 1^- , 2^- states do not the significant contribution. However, they exhaust $\sim 80\%$ of the intensity of μ^- -capture.

Figure 2: The comparison of calculated spectra (curve 2) with experimental data (dotted line)[8] and theoretical data by Zhivopistsev-Slivnov (curve 1)[5].



4 Index

Acknowledgments

The authors are very much thankful to Prof. Dr. Hartmut Machner and also Prof.Dr. S. Krewald , Mrs. S. Schadmand for invitation to make contributions on The Eleventh International Conference on Meson-Nucleon Physics and the Structure of the Nucleon-MENU2007 (Juelich, Germany) and support.

5 References

References

- [1] O. Bohr, B. Mottelsson, *Structure of Atomic Nucleus*, N.-Y., (1975).
- [2] I. Izenberg, B. Grainer, *Models of Nuclei. Collective and One-body Phenomena*, N.-Y., (1975).
- [3] A. V. Glushkov., S. V. Ambrosov, A. V. Loboda, in: *New Projects and New Lines of Research in Nuclear Physics* eds. G. Fazio, F. Hanappe, Singapore: World Scientific, 242 (2003).
- [4] H. Feschbach *et al.*, *Ann. Phys.* **125**, 429 (1980).
- [5] F. A. Zhivopistsev, A. M. Slivnov, *Izv. AN USSR. Ser. Phys.* **48**, 821 (1984).
- [6] F. A. Zhivopistsev *et al.*, *Izv. AN USSR. Ser. Phys.* **45**, 1935 (1981).
- [7] F. A. Zhivopistsev, A. V. Lukashev, V. A. Eltekov, *Vestnik MGU. Ser. Phys.* **2**, 201 (1973).
- [8] I. Vaytkowska, *Nucl. Phys.* **15**, 1154 (1972).
- [9] A. V. Glushkov, in *Low Energy Antiproton Phys.*, AIP Serie. **796**, 206 (2005).
- [10] A. V. Glushkov *et al.*, *Nucl. Phys. A* **734**, e21 (2004).
- [11] A. V. Glushkov, S. V. Malinovskaya, A. V. Loboda, in *Proc. III Int. Workshop on Non-equilibrium Green's Functions*, Univ. Kiel (Germany), (2005).
- [12] S. V. Malinovskaya, in *Low Energy Antiproton Phys.*, AIP Serie. **796**, 211 (2005).
- [13] A. V. Glushkov, S. V. Ambrosov, A. V. Loboda, E. P. Gurnitskaya, O. Yu. Khetselius, *Recent Advances in Theor. Phys. and Chem. Systems* **15**, 301 (2006).
- [14] S. V. Malinovskaya, A. V. Glushkov, Yu. V. Dubrovskaya, L. A. Vitavetskaya, *Recent Advances in Theor. Phys. and Chem. Systems* **15**, 285 (2006).
- [15] R. A. Broglia *et al.*, *Nucl. Phys. A* **371**, 413 (1981).

MENU 2007
11th International Conference
on Meson-Nucleon Physics and
the Structure of the Nucleon
September 10-14, 2007
IKP, Forschungszentrum Jülich, Germany

NUCLEAR ELECTRIC QUADRUPOLE MOMENTS AND HYPERFINE STRUCTURE PARAMETERS FOR HEAVY ISOTOPES

*O. Yu. Khetselius*¹
Dept. Nuclear Physics,
Odessa University
Odessa, Ukraine,

Abstract

Consistent calculation of the nuclear electric quadrupole moments and hyperfine structure parameters for heavy elements is carried out within the gauge-invariant QED perturbation theory with using the optimized one-quasiparticle representation with account of relativistic, correlation, nuclear, QED effects. The charge distribution in a nucleus is modelled within the Gauss model. Nuclear electric quadrupole moments Q , the hyperfine structure constants for a number valent states of ^{201}Hg , ^{223}Ra are defined.

1 Introduction

In last years a studying the spectra of heavy elements isotopes is of a great interest for further development as atomic and as nuclear theories (c.f.[1-8]). Well known multi-configuration Dirac-Fock (MCDF) approach is the most reliable version of calculation for atomic systems, but, as a rule, detailed description of the method for studying role of the nucleus finite size effect (NFSE) is lacking. As alternative approach one can consider the PT on parameters $1/Z$, αZ (α is a fine structure constant). It permits evaluations of the relative contributions of different expansion energy terms: non-relativistic, relativistic ones, as the functions of Z . But, the serious problems are connected with correct definition of the QED corrections: the Lamb shift (LS), the LS self-energy (SE) part, vacuum polarization (VP), the nuclear finite size correction etc. Here we present the results of calculation of the nuclear electric quadrupole moments and hyperfine structure parameters for

¹P.O.Box 24a, Odessa-9, 65009, Ukraine, email:glushkov@paco.net

heavy elements (Hg, Ra) within the gauge-invariant QED perturbation theory with using the optimized one-quasiparticle representation and correct account of relativistic, correlation, nuclear, QED effects [9-14].

2 QED perturbation theory approach with account of the nuclear corrections

The wave functions zeroth basis is found from the Dirac equation solution with potential, which includes the core ab initio potential, electric, polarization potentials of nucleus (the gaussian form for charge distribution in the nucleus is used). We set the charge distribution in the nucleus by the Gaussian function:

$$\rho(r|R) = (4\gamma^{3/2}/\sqrt{\pi}) \exp(-\gamma r^2)$$

Here $\gamma = 4/\pi R^2$; R is an effective nucleus radius, defined as: $R = 1.60 \times 10^{-13} z^{1/3}$ (cm).

The Coulomb potential for spherically symmetric density $\rho(r|R)$ is:

$$V_{nuc}(r|R) = -((1/r) \int_0^r dr' r'^2 \rho(r'|R) + \int_r^\infty dr' r' \rho(r'|R))$$

One can write the DF-like equations for a N-electron system. Formally they fall into one-electron Dirac equations for the corresponding orbitals with potential: which includes the electrical and polarization potentials of the nucleus. The correlation corrections are taken into account within the Green functions method (with the use of the Feynman diagram technique). There have taken into account all correlation corrections of the second order and dominated classes of the higher orders diagrams (electrons screening, particle-hole interaction, mass operator iterations) [9-14]. The part V_{ex} accounts for exchange inter-electron interaction. The main exchange effect will be taken into account. The rest of the exchange-correlation effects are accounted for in the first two PT orders by the total inter-electron interaction [12]. The core electron density is defined by iteration algorithm within gauge invariant QED procedure [10]. The magnetic inter-electron interaction is accounted in the lowest (on α^2 parameter), the LS polarization part - in the Uehling-Serber approximation, self-energy part of the LS is accounted effectively within the Ivanov-Ivanova non-perturbative procedure [15].

Table 1: Presented values of nuclear electric quadrupole moment $Q(\text{mb})$ of ^{201}Hg [3]

$Q(\text{mb})$
380 387 (6) 347 (43,0) 385 (40) 485 (68) 386 (49) 267 (37) 390 (20) 455 (40) 420 500 (50) 600 500

3 Hyperfine structure constants and nuclear quadrupole moment for ^{201}Hg isotope.

We carried out the calculation of the hyperfine structure constants and nuclear quadrupole moment for ^{201}Hg isotope. Mercury has one stable isotope ^{201}Hg ($I = 3/2$) with relative abundance 13,2%. The isotope ^{199}Hg with relative abundance 16,9% has two excited states at 158 and 208 keV. Values of the quadrupole moments for several radioactive isotopes with masses from 185 to 203 were reported by Ulm et al. (c.f.[3]). A comprehensive compilation of the quadrupole moments for the isotopes in the mass range 185-206 was included in the tables of Raghavan. Most of these data are based on the primary $Q(^{201}\text{Hg})$ value, combined with measured isotopic ratios. A number of available experimental values of the quadrupole moment $Q(^{201}\text{Hg})$ are quoted in table 1. The "muonic 3d" value of 386(49)mb was used in a recent "year-2001" summary of nuclear quadrupole moments [3]. In table 2 we present our calculated values of the nuclear electric quadrupole moment $Q(\text{mb})$ of ^{201}Hg and magnetic dipole hyperfine structure constants A (MHz) of the 3P_1 state of neutral mercury, compared with the uncorrelated DF, MCDF (with account Breit and QED corrections) [3]. Our final result fits between the latest values obtained by the group of Ulm. Regarding an error bar, preliminary analysis gives an estimate $\Delta Q \sim 7\text{mb}$.

Note: ^a standard value of Raghavan [3]; ^b combines the ^{199}Hg ($I=5/2$) value with the 201/199 ratio;

^c direct muonic measurement on ^{201}Hg ; ^d solid HgCl_2 plus ^{199}Hg nuclear primary value;

4 Hyperfine structure constants and nuclear quadrupole moment for ^{223}Ra isotope

Further we present the experimental data and our theoretical results (QEDPT with the gauss model of charge distribution in a nucleus) calculating the energies and constants of the hyperfine structure, nuclear moments Q for atom of radium $^{223}_{88}\text{Ra}$. It has the external valent shell $7s^2$ and can be treated as

Table 2: Calculated values of the nuclear electric quadrupole moment Q (mb) of ^{201}Hg and magnetic dipole hyperfine structure constants A (MHz) of the $^3\text{P}_1$ state of ^{201}Hg , compared with the uncorrelated DF, MCDF (with account Breit and QED corrections) [3].

Method	Q (mb)	A (MHz)	B (MHz)
Uncorelated DF	478,13	-4368,266	—
MCDF (Breit+QED)	386,626	-5470,810	—
This work	380, 518	-5464, 324	-286,512
Experiment	See table 1	-5454,569 (0,003)	-280,107 (0,005)

Table 3: Experimental and theoretical data on magnetic dipole constant of the hyperfine structure A (in MHz) for the states: $7s7p\ ^1\text{P}_1$, $^3\text{P}_1$ and $^3\text{P}_2$ of radium (calculation by different methods: DF, MCDF with accounting for the Breit and QED corrections, relativistic method of configuration interaction with accounting for correlation corrections within random phase approximation (RCI-RPA) and QED perturbation theory method) [4].

Method/State	$^1\text{P}_1$	$^3\text{P}_1$	$^3\text{P}_2$
DF	-226,59	803,97	567,22
MCDF (Brait+KED)	-330,3	1251,9	737,1
RCI-RPA	-242,4	-	-
QEDPT	-339,1	1209	704,5
Experiment	-344,5(0,9)	1201,1(0,6)	699,6(3,3)

the two-quasiparticle system. In table 10 we present the experimental and theoretical data on magnetic dipole constant of the hyperfine structure A (in MHz) for the states: $7s7p\ ^1\text{P}_1$, $^3\text{P}_1$ and $^3\text{P}_2$ of radium $^{223}_{88}\text{Ra}$. In table 3 we present also the results of calculation by other methods, namely: standard uncorrelated Dirac-Fock (DF) method, multiconfiguration DF method (MCDF) with accounting for the Breit and QED corrections, relativistic method of configuration interaction with accounting for correlation corrections within random phase approximation (RCI-RPA) [4].

In table 4 we present the values of electric quadrupole moment Q (in barn) for isotope of ^{223}Ra [3], which are experimentally obtained by the ISOLDE Collaboration (CERN) within different methodics and theoretically on the basis of calculations by MCDF (with account of the QED and Breit corrections), relativistic multi-body perturbation theory (RMBPT) and our QED perturbation theory (QEDPT).

The key factor of agreement between theory and experiment is connected with a correct accounting for interelectron correlation effects, corrections

Table 4: Values of electric quadrupole moment Q (in barn) for isotope of ^{223}Ra

Method	Q (barn)
MCDF (Breit plus QED)	1,21 (0,03)
ISOLDE Collaboration fs RaII	1,254 (0,003) {0,066}
Wendt et al, fs RaI	1,19 (0,12)
RMBPT	1,28
ISOLDE Collaboration fs RaI	1,190 (0,007) {0,126}
ISOLDE Collaboration B(E2)	1,2
QEDPT	1,22 (0,03)

due to the finite size of nucleus, the Breit and radiative QED corrections. The key difference between calculation results by MCDF, RMBT, QEDPT methods is connected with different schemes of accounting for interelectron correlations. The well-known MCDF [1-4] method is not gauge-invariant one and an accounting of multi-electron correlations is not fully fulfilled. From the other side, contributions of the high orders QED PT corrections, nuclear contributions may reach dozens of MHz and must be correctly accounted for. It is necessary also to take into account more correctly the spatial distribution of magnetic moment inside a nucleus (the Bohr-Weisskopf effect), the nuclear-polarization corrections that can be done within solving the corresponding nuclear task, for example with using the shell model with Woods-Saxon and spin-orbit potentials [12-14].

Acknowledgments

The author is very much thankful to Prof.Dr.Hartmut Machner and also Prof.Dr. S. Krewald , Mrs. S. Schadmand for invitation to make contributions on The Eleventh International Conference on Meson-Nucleon Physics and the Structure of the Nucleon-MENU2007 (Juelich, Germany) and support . Author acknowledges the support of the Abdus Salam ICTP Centre (Trieste, Italy), University of Dresden (Germany).

5 References

References

- [1] Cheng K., Kim Y and Desclaux J *Atom.Data Nucl .Data Tabl.* 24 11 (1979)
- [2] Johnson WR, Sapirstein J and Blundell SA *Phys. Scripta* 46 184 (1993)
- [3] Bieron J , Pyykko P and Jonsson P *Phys.Rev. A* 71 012502 (2005)
- [4] Bieron J and Pyykko P *Phys.Rev.A* 71 032502 (2005)
- [5] Shabaev VM , Tomaselli M , Kuhl T , Yerokhin VA, Artemyev AN *Phys.Rev.A* 56 252 (1997)
- [6] Nagasawa T , Naga A and Nakano M *Phys.Rev.C* 69 034322 (2004)
- [7] Tomaselli M , Schneider SM , Kankleit E and Kuhl T *Phys.Rev.C* 51 2989 (1995)
- [8] Labzowsky LN, Johnson WR , Soff G and Schneider SM *Phys.Rev.A* 51 4597 (1995)
- [9] Glushkov AV *JETP Lett.* 55 97 (1992)
- [10] Glushkov AV and Ivanov LN *Phys.Lett.A* 170 33 (1992)
- [11] Glushkov AV, Khetselius OY, Ambrosov SV, Loboda AV, Chernyakova YuG and Svinarenko AA *Nucl.Phys.A* 734 21 (2004)
- [12] Glushkov AV , Khetselius OY, Ambrosov SV , Loboda AV and Gurnitskaya EP *Recent Advances in the Theory of Chemical and Physical Systems, Eds*
- [13] Julien P , Maruani J , Mayou D, Wilson S ,Delgado-Barrio G. Ser. *Progress in Theoretical Chemistry and Physics* 15 285. (2006)
- [14] Glushkov AV, Rusov VD, Ambrosov SV and Loboda AV *New Projects and New Lines of Research in Nuclear Physics* ed G Fazio and F Hanappe (Singapore: World Scientific) 126. (2003)
- [15] Glushkov A.V., Gurnitskaya E.P., Loboda A.V., *Low Energy Antiproton Physics.*

- [16] Eds. Grzonka D., Czyzykiewicz R., Oelert Walter, Rozek T., Winter P.,
AIP Serie. 796 217.
- [17] Ivanov L.N., Ivanova E.P., Aglitsky EV *Phys.Rep.* 164 315. (1988)

ON A POSSIBLE ORIGIN OF A RESONANCE-LIKE STRUCTURE IN THE TWO-PHOTON INVARIANT MASS SPECTRUM OF THE REACTION

$pp \rightarrow pp\gamma\gamma$.

A. S. Khrykin^{*,1}, and S. B. Gerasimov[#]

^{*}Dzelepov Laboratory of Nuclear problems, Joint Institute for Nuclear
Problems, 141980 Dubna, Moscow Region, Russia

[#]Bogolubov Laboratory of Theoretical Physics, Joint Institute for Nuclear
Problems, 141980 Dubna, Moscow Region, Russia

Abstract

We show that the resonance-like structure found by the *CELSIUS-WASA Collaboration* in the two-photon invariant mass spectrum of the reaction $pp \rightarrow pp\gamma\gamma$ is rather a signature of the NN -decoupled dibaryon resonance $d_1^*(1956)$ that is produced in the radiative process $pp \rightarrow \gamma d_1^*$ and then undergoes radiative decay into two protons $d_1^* \rightarrow pp\gamma$. It is found that a contribution of the dibaryon mechanism $pp \rightarrow \gamma d_1^* \rightarrow pp\gamma\gamma$ of the reaction $pp \rightarrow pp\gamma\gamma$ to the invariant mass spectrum of its photon pairs can reasonably well reproduce the experimentally observed spectrum in the vicinity of the resonance-like structure.

1 Introduction

The resonance-like structure found by the *CELSIUS-WASA Collaboration* in the two-photon invariant mass spectrum of the exclusive reaction $pp \rightarrow pp\gamma\gamma$ at 1.2 and 1.36 GeV has been taken by the authors of Ref. [1] as evidence for dynamical formation of the S-wave dipion resonance σ [2] in the pp collision process. It was assumed [1] that this structure might result from interference between the process $pp \rightarrow pp\sigma \rightarrow pp\gamma\gamma$ and one of the double pp -bremsstrahlung. However, such an interpretation is at least questionable merely because the amplitude of the double pp -bremsstrahlung is unknown in the energy range considered in Ref. [1] where this process, to our knowledge,

¹khrykin@nusun.jinr.ru

has not been investigated yet either experimentally or theoretically. The aim of this paper is to propose an alternative interpretation of a possible origin of this structure which is based on the dibaryon mechanism of the two-photon emission in NN collisions [3, 4].

2 The dibaryon mechanism of two-photon emission in NN collisions

The dibaryon mechanism of two-photon emission in NN collisions $NN \rightarrow \gamma d_1^* \rightarrow NN\gamma\gamma$ governs the electromagnetic transition between the initial and final NN states by a sequential emission of two photons, one of which is caused by production of the NN decoupled dibaryon resonance d_1^* and other by its subsequent decay. In the overall center-of-mass system the energy of the photons E_γ^F associated with the d_1^* production is determined by the dibaryon mass M_R and the energy of colliding nucleons $W = \sqrt{s}$ as $E_\gamma^F = (W^2 - M_R^2)/2W$. The energy of photons E_γ^D emerging as a result of the d_1^* decay in the resonance rest frame is given by $E_\gamma^D = (M_R^2 - M_{NN}^2)/2M_R$, where M_{NN} is the invariant mass of the final NN state. The matrix element for the $NN \rightarrow NN\gamma\gamma$ transition will in general be a function of the four-momenta of the incoming and outgoing particles together with the mass and quantum numbers of the resonance d_1^* which are still not established. It can be written in the form $\mathcal{M} = \mathcal{M}_F \cdot \mathcal{D}(p_R) \cdot \mathcal{M}_D$, where \mathcal{M}_F and \mathcal{M}_D are the matrix elements for the dibaryon formation and decay, $\mathcal{D}(p_R) = 1/(p_R^2 - M_R^2 + iM_R\Gamma_R)$ is the propagator of the dibaryon with the four-momentum p_R and Γ_R is its decay width. In this work the $pp \rightarrow pp\gamma\gamma$ transition has been treated within the assumption that at large distances the NN -decoupled six-quark d_1^* state is a bound $p\Delta(1232)$ state with the spin-parity $J^P = 0^-$ and the isospin $I = 2$ [5]. Owing to a relatively small energy ~ 80 MeV released in the d_1^* decay, the matrix element \mathcal{M}_D was derived in terms of a simple picture in which the decay $(p\Delta)_{bound} \rightarrow pp\gamma$ proceeds via the virtual $\Delta^+ \rightarrow p\gamma$ $M1$ -transition. As a radial wave function for the bound $p\Delta$ -state we have considered two functional forms: the Gaussian $R_G(r) = N_G \cdot r \exp(-b_G^2 r^2)$ and the Fermi-type (or Woods-Saxon) distribution $R_F(r) = N_F \cdot (1 - j_0(\kappa_F r))$ for $r < R_0$ and $R_F(r) = N_F \cdot C_F \cdot [1 + \exp[a \cdot (r - R_0)]]^{-1}$ for $r \geq R_0$, where $r = |\mathbf{r}_\Delta - \mathbf{r}_p|$, $a = \sqrt{2m_{red}E_b(d_1^*)}$, m_{red} is the reduced mass of the $(p\Delta)$ -system, $E_b = M_\Delta + m_N - M_R$ is the binding energy of this system, $N_{F(G)}$ are the normalization constants, the parameters C_F , R_0 and κ_F are defined from the continuity requirements for $R_F(r)$ and its first and second derivatives at $r = R_0$. The specific form of the correlation function $f(r) = 1 - j_0(\kappa_F r)$

($j_0(z)$ is the spherical Bessel function of 0^{th} order), describing effects of the soft core in the $N\Delta$ -interaction potential is taken in accordance with the Ref. [6]. The parameter b_G^2 is chosen such that the rms radius of the ($p\Delta$)-state is the same for both versions of the wave function.

Unlike the decay process, the d_1^* formation one takes place at relatively high energies of colliding protons. Therefore, its mechanism may be more involved. The lack of an explicit theory of such a process forced us to resort to the phenomenology. Namely, we adopt $|\mathcal{M}_F|^2_{c.m.} \simeq A \cdot \exp(-k_\perp/b)$, where A is the normalized constant, k_\perp is the transverse momentum of a photon and b is a parameter. This formula was shown [7] to give a good fit for the reaction $pp \rightarrow \pi^+d$ for incident proton momenta in the range 3.4 – 12.3 GeV/c with $k_\perp \rightarrow p_\perp(\pi^+)$. According to [8], it is equal to 0.26 GeV/c at $E_{c.m.} = 3.0$ GeV. In our calculation we used $b = 0.6$ CeV/c. This value follows from the assumption that $b(pp \rightarrow \gamma d_1^*)/b(pp \rightarrow \pi^+d) = \text{rms radius}(d)/\text{rms radius}(d_1^*)$. The effects of the final state interactions between decay protons in the 3P_1 -state were included with the help of the phenomenological correlation function $f_{phen}(r) = 1 - j_0(\kappa r)$, $\kappa = 3.93 \text{ fm}^{-1}$ by multiplying the $L = 1$ radial wave function of free motion by this function. The approximate relevance of this procedure is demonstrated numerically in [9].

3 The method of calculations and results

The calculations of the invariant mass spectra of photon pairs from the dibaryon mechanism of the reaction $pp \rightarrow pp\gamma\gamma$ at 1.36 GeV for the geometry and kinematics of the experiment [1] were done using the Monte Carlo method. A computer program for the MC calculations was made on the basis of the GENBOD event generator [11] which was used to randomly generate four-momenta of particles for the process $pp \rightarrow \gamma + d_1^* \rightarrow \gamma + \gamma + pp$. A probability of any event was given by its weight $WT = \langle \sum_{\sigma_{1,2,3,4}} \sum_{\lambda_{1,2}} |\mathcal{M}|^2 \rangle$, where σ_i are the spin projections of the protons and λ_i stand for the polarizations of the photons. The calculated spectra for both forms of the radial wave function for the bound $p\Delta$ -state are presented in Fig.1. Both spectra are seen to reproduce reasonably well the experimentally observed spectrum [1] in the vicinity of the resonance-like structure. The spectrum calculated with the matrix element from Ref. [10], which was obtained for the case of point-like dibaryon, is also shown in the same figure for comparison. In this calculation the effects of the final state interactions were ignored.

Our results show that the structure observed in the two-photon invariant mass spectrum of the reaction $pp \rightarrow pp\gamma\gamma$ by the CELSIUS-WASA collaboration is very likely to be due to the dibaryon mechanism of the reaction

$pp \rightarrow pp\gamma\gamma$ [3, 4]. They can thus be considered as one more confirmation of the existence of this two-photon production mechanism in NN collisions and, hence, the existence of the dibaryon d_1^* itself. In this connection we note that more experimental and theoretical studies are needed to completely clarify the situation with the existence of the dibaryon resonance d_1^* .

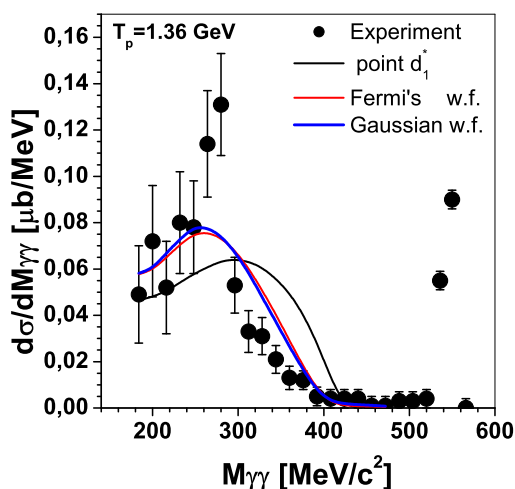


Figure 1: Experimentally observed two-photon invariant mass spectrum of the reaction $pp\gamma\gamma$ and those for the process $pp \rightarrow \gamma d_1^* \rightarrow \gamma\gamma pp$ calculated with two different types of radial wave function of the bound $p\Delta$ -state, Fermi's and Gaussian. The spectrum calculated with the matrix element from [10] is given by the black solid line.

References

- [1] M. Bashkanov, H. Clement, E. Doroshkevich, M. Kaskulov, R. Meier, T. Skorodko and G.J. Wagner, Int. Jour of Mod. Phys. **A20**, 554(2005);hep-ex/0406081.
- [2] L. M. Brown and P. Singer, Phys. Rev. Letters **8**, 460 (1962).
- [3] A. S. Khrykin et al., Phys. Rev. C **64**, 034002(2001).
- [4] A. S. Khrykin, Nucl.Phys. **A721**, 625c(2003).
- [5] A. Matsuyama, Phys. Lett. **B 408**, 25 (1997).
- [6] W. Weise, Nucl.Phys. **A278**, 402 (1977).
- [7] H. L. Anderson, et al., Phys. Rev. D **3**, 1536 (1971).
- [8] J. V. Allaby et al., Phys. Lett. **B 29**, 198 (1969).
- [9] A. Parreno and A. Ramos, Phys. Rev. C **65**, 015204(2002), arXiv:nucl-th/0104080

- [10] O. Scholten, J. G. O. Ojwang, and S. Tamenaga, Phys. Rev. C **71**, 034005(2005).
- [11] F. James, *Monte Carlo Phase Space*, CERN 68-15. 1968.
- [12] O. Scholten, J. G. O. Ojwang, and S. Tamenaga, Phys. Rev. C **71**, 034005(2005).

COMPARATIVE STUDY OF THE PROTON- η AND PROTON- η' INTERACTIONS VIA THE PP AND P-MESON INVARIANT MASS DISTRIBUTIONS

*P. Klaja*¹ for the COSY-11 collaboration

Nuclear Physics Department
Jagellonian University
30-059 Cracow, Poland

Institut für Kernphysik
Forschungszentrum Jülich
52425 Jülich, Germany

Abstract

The determined pp and $p - meson$ invariant mass distributions for $pp \rightarrow pp\eta$ and $pp \rightarrow pp\eta'$ reactions are used for comparative study of the interaction within $proton - meson$ system. The elaboration of the measurement of the $pp\eta$ system has been completed and results were published in reference [1]. In this contribution we present preliminary invariant mass distributions determined for the $pp \rightarrow pp\eta'$ reaction and compare them to the theoretical predictions.

The COSY-11 collaboration continues the comparative study of interaction of the η and η' mesons with protons. To perform that studies the $pp \rightarrow pp\eta$ and $pp \rightarrow pp\eta'$ reactions were measured at the same excess energy ($Q = 15.5$ MeV) corresponding to the beam momentum of 2.0259 GeV/c and 3.257 GeV/c, respectively.

First part of investigations, namely the evaluation of the high-statistics measurement of the $pp \rightarrow pp\eta$ reaction is completed and the results are published in reference [1]. The $pp \rightarrow pp\eta'$ reaction has also been measured, the data has been analysed and at present the results are being interpreted.

The interaction between particles in close-to-threshold collisions determines strongly the dependence of the total cross section as a function of the centre-of-mass excess energy. The excitation functions for the $pp \rightarrow pp\eta'$ [2, 3] and $pp \rightarrow pp\eta$ [3–7] reactions compared to the arbitrarily normalized phase-space integral reveal that proton-proton FSI enhances the total cross section by

¹p.klaja@fz-juelich.de

more than one order of magnitude for low energies. In the case of the η' meson production the data are described well assuming that the on-shell proton-proton amplitude exclusively determines the phase-space population. This indicates that the proton- η' interaction is too small to manifest itself in the excitation function within the presently achieved statistical uncertainty [8].

The interaction between particles depends on their relative momenta or equivalently on the invariant masses of the two-particles subsystems [1]. It should manifest itself as modification of the phase-space abundance in kinematical regions where particles have small relative velocities. Only two invariant masses of three subsystems are independent and therefore the whole accessible information about the final state interaction can be showed in the Dalitz plot. One can also use the projection of the phase-space distribution onto the invariant masses of proton-proton or proton-meson subsystems [1]. Qualitative phenomenological analysis of the determined differential invariant proton-proton and proton- η mass distributions for the $pp \rightarrow pp\eta$ reaction revealed an enhancement of the population density at the kinematical region corresponding to the small proton- η momentum [1, 9]. That effect occurs to be unexpectedly large and is not yet understood. The deviations at the small proton- η relative momenta can not be described by the on-shell inclusion of the proton-proton and proton- η FSI. Better description is achieved when contributions based on calculations under assumption of ${}^3P_0 \rightarrow {}^1S_0s$ as those proposed in references [10,11] and ${}^1S_0 \rightarrow {}^3P_0s$ transition [10], are taken into account. Also three-body calculations presented in references [12,13] describe data well in mentioned proton- η momentum region. In fact, for the simultaneous description of excitation function and invariant mass distributions a rigorous three-body approach with inclusion of higher partial waves is needed [1].

Using the COSY-11 detection system, utilizing a stochastically cooled proton beam and the hydrogen cluster target, The COSY-11 collaboration performed a high statistics measurement of the $pp \rightarrow pp\eta'$ reaction at the beam momentum of 3.257 GeV/c. The experiment was based on registration of the four-momenta of outgoing particles, whereas the η' meson was identified via the missing mass technique. We selected only these events with two reconstructed tracks ($pp \rightarrow ppX$). The missing mass resolution depends on the accuracy of the registered protons momentum determination which in case of the reconstruction used by COSY-11 group relies on the knowledge of the position of the center of the interaction region. The possible changes of the position where beam crosses target could have significantly influenced the momentum reconstruction and in consequence could worsen the determination of the mass of undetected particle but shifts of the center of interactions

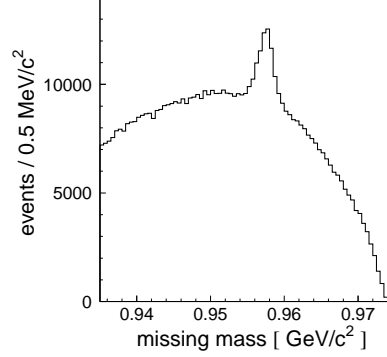


Figure 1: Experimental missing mass spectrum, determined from the whole data set, for the $pp \rightarrow ppX$ reaction measured at the beam momentum of 3.257 GeV/c.

were found to be at the negligible level of 0.01 mm [14]. In the figure 1 we present the preliminary missing mass spectrum, determined for the whole data set, for the $pp \rightarrow ppX$ reaction measured at the beam momentum of 3.257 GeV/c. In the figure a clear signal corresponding to the $pp \rightarrow pp\eta'$ reaction is visible with around 17000 events of the η' meson creation.

Now after introducing the reaction identification, in order to determine the differential cross sections, the luminosity integrated during the measurement time has been established by the comparison of the angular distributions of the elastically scattered protons with the results of the EDDA collaboration [15]. The achieved value of the integrated luminosity amounts to $L = (5.842 \pm 0.072)pb^{-1}$ [14].

The achieved luminosity value allowed for the overall normalization of the derived from data differential cross section as functions of s_{pp} and $s_{p\eta'}$ invariant masses. The preliminary distributions of invariant proton-proton and proton- η' masses are presented in the figure 2. The experimental differential distributions are compared with theoretical calculations. The dotted lines depict calculations where only proton-proton interaction is taken into account and solid lines correspond to homogenous phase-space distribution. The homogenous phase-space distribution deviates strongly from the experimental determined spectra. It is also easily seen that, theoretical calculations including proton-proton on-shell interaction do not fit the experimental data at large values of s_{pp} , similar as it was in case of the $pp \rightarrow pp\eta$ reaction. The interpretation of the results is in progress.

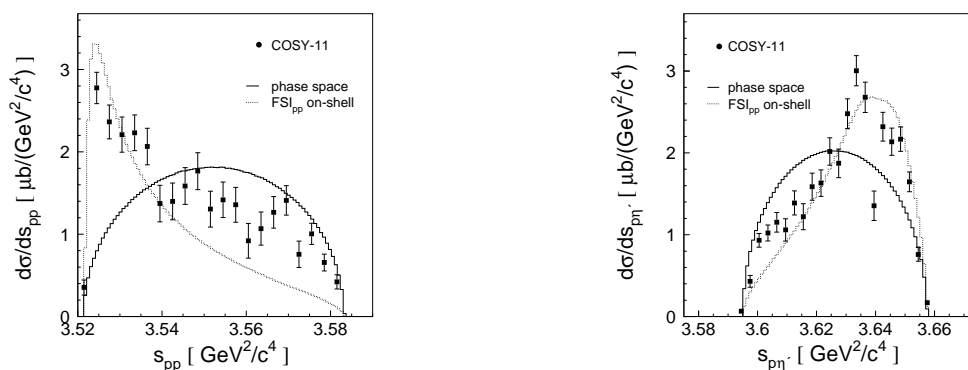


Figure 2: Distributions of the square of the proton-proton (s_{pp}) (left) and proton- η' ($s_{pn'}$) (right) invariant masses determined experimentally for the $pp \rightarrow pp\eta'$ reaction (full circles). The integrals of the phase space weighted by a square of the proton-proton on-shell scattering amplitude (dotted lines)- FSI_{pp} , have been normalized arbitrarily at small values of s_{pp} . The expectation under the assumption of the homogeneously populated phase space are shown as thick solid lines.

Acknowledgments

We acknowledge the support of the European Community-Research Infrastructure Activity under the FP6 programme (Hadron Physics, N4:EtaMesonNet, RII3-CT-2004-506078), the support of the Polish Ministry of Science and Higher Education under the grants No. PB1060/P03/2004/26, 3240/H03/2006/31 and 1202/DFG/2007/03, and the support of the German Research Foundation (DFG).

References

- [1] P. Moskal et al., *Phys. Rev. C* **69**, (2004) 025203.
- [2] F. Balestra et al., *Phys. Lett. B* **491** (2000) 29;
R. Wurzinger et al., *Phys. Lett. B* **374** (1996) 283;
P. Moskal et al., *Phys. Rev. Lett.* **80** (1998) 3202;
P. Moskal et al., *Phys. Lett. B* **474** (2000) 416;
A. Khoukaz et al., *Eur. Phys. J. A* **20** (2004) 345.
- [3] F. Hibou et al., *Phys. Lett. B* **438** (1998) 41.
- [4] E. Chiavassa et al., *Phys. Lett. B* **322** (1994) 270;
H. Calén et al., *Phys. Rev. Lett.* **79** (1997) 2642.

-
- [5] A. M. Bergdolt et al., *Phys. Rev. D* **48**, (1993) R2969.
 - [6] J. Smyrski et al., *Phys. Lett. B* **474** (2000) 182.
 - [7] H. Calén et al., *Phys. Lett. B* **366** (1996) 39.
 - [8] P. Moskal et al., *Phys. Lett. B* **482** (2000) 356.
 - [9] M. Abdel-Bary et al., *Eur. Phys. J. A* **16** (2003) 127.
 - [10] K. Nakayama et al., *Phys. Rev. C* **68** (2003) 045201.
 - [11] V. Baru et al. , *Phys. Rev. C* **67** (2003) 024002.
 - [12] A. Fix, H. Arenhövel, *Phys. Rev. C* **69** (2004) 014001.
 - [13] A. Fix, H. Arenhövel, *Nucl. Phys. A* **697** (2002) 277.
 - [14] P. Klaja, et al., AIP, in print.
 - [15] D. Albers et al., *Phys. Rev. Lett.* **78** (1997) 1652.

PROTON-PROTON CORRELATIONS FOR THE $pp \rightarrow pp\eta$ REACTION MEASURED WITH COSY-11

*P. Klaja*¹ and *P. Moskal*² for the COSY-11 collaboration

Nuclear Physics Department
Jagellonian University
30-059 Cracow, Poland

Institut für Kernphysik
Forschungszentrum Jülich
52425 Jülich, Germany

Abstract

Based on the high statistics data for the $pp \rightarrow ppX$ reaction measured by the COSY-11 collaboration [1] we have derived a two-proton correlation function for the production of the $pp\eta$ and $pp + pions$ systems. The measured correlation function normalized to the value simulated for a point-like source was compared with a theoretical prediction in order to estimate the size of the reaction volume. The presented poster comprises summary of results recently reported in the proceedings of the Symposium on Meson Physics of the COSY-11 and WASA-at-COSY [2].

The momentum correlations of particles at small relative velocities are widely used to study the spatio-temporal characteristics of the production processes in the relativistic heavy ion collisions [3]. This technique, called after Lednicky *a correlation femtoscopy* [4], was initiated in intensity interferometry by Hanbury-Brown and Twiss [5]. Implemented into nuclear physics [4, 6, 7] it permits to determine the duration of the emission process and the sizes of the source from which the particles are emitted [4]. It is based on the correlation function [4]. The importance of the correlation femtoscopy has been well established in heavy ion collisions with high multiplicity. However, as pointed out by Chajecski [8], in the case of low-multiplicity collisions the interpretation of the correlation function measurements is still not fully satisfactory, especially in view of the surprising STAR collaboration observation indicating universality of the resulting femtoscopic radii for both, the hadronic (proton-proton), and heavy ion collisions [9]. The understanding

¹p.klaja@fz-juelich.de

²p.moskal@fz-juelich.de

of the contributions from the non-femtoscopic correlations which may be induced by the decays of resonances, global conservations laws [8], or by other unaccounted for interactions, is one of major goals. In particle physics the best place to study two-proton correlations are exclusive measurements of meson production in the collisions of hadrons conducted close to the kinematical threshold where the fraction of the available phase-space associated with low relative momenta between ejectiles is large [10]. Here, we report on measurements of the two-proton correlation function for the η meson and multi-pion production, in which the mesons were generated in the collisions of protons at the beam momentum close to the kinematical threshold for the $pp \rightarrow pp\eta$ reaction. The experiment was conducted using the proton beam of the cooler synchrotron COSY [11] and the internal hydrogen cluster target [12]. Momentum vectors of outgoing protons from the $pp \rightarrow ppX$ reaction were measured by means of the COSY-11 facility [13]. The two-proton correlation function $R(q)$ ³ was determined for the $pp\eta$ and $pp(m\pi)$ systems, respectively. It was calculated as a ratio of the reaction yield $Y(q)$ to the uncorrelated yield $Y^*(q)$ according to the formula (c.f. [15])

$$R(q) + 1 = C^* \frac{Y(q)}{Y^*(q)}, \quad (1)$$

where C^* denotes an appropriate normalization constant. $Y^*(q)$ was derived from the uncorrelated reference sample obtained by using the event mixing technique [7]. In the discussed experiment, only four-momenta of two protons were measured and the unobserved meson was identified via the missing mass technique [1, 16]. It is impossible to know whether in a given event the η meson or a few pions have been created. However, statistically, one can separate these groups of events on the basis of the missing mass spectra, for each chosen region of the phase-space. As a next step, we calculated the acceptances and efficiencies of the COSY-11 system for the registration and reconstruction of the $pp \rightarrow pp\eta$ and $pp \rightarrow pp(m\pi)$ reactions as functions of the relative momentum of the outgoing protons. For details of analysis the interested reader is referred to [17] and [2]. In order to estimate the influence of the shape induced by the kinematical bounds we have reconstructed the correlation functions from the data for both, the $pp \rightarrow pp\eta$ and $pp \rightarrow pp + pions$ reaction assuming a point-like source and using a Monte-Carlo simulation. The shape of the correlation function free from the influence of the energy

³Here, $R(q)$ denotes a projection of the correlation function onto the relative momentum of emitted particles $q = |\mathbf{p}_1 - \mathbf{p}_2|$. Note, that some authors instead of q take as the independent variable the proton-proton center-of-mass momentum $k = q/2$ (c.f. reference [14]).

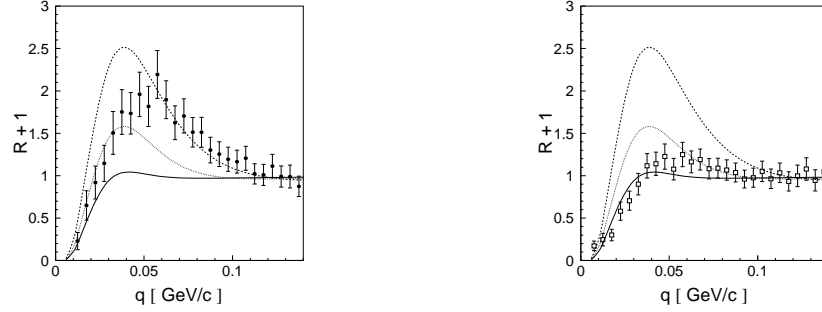


Figure 1: The two-proton correlation functions corrected for acceptance and normalized to the corresponding correlation function simulated for the point-like source. Full dots and open squares represent experimental points for the $pp \rightarrow pp\eta$ and $pp \rightarrow pp + \text{pions}$ reaction, respectively. The superimposed lines show the result of calculations [14] for the reaction volume parametrized by a Gaussian with radius $r_0 = 2.0$ fm (dashed line), $r_0 = 3.0$ fm (dotted line) and $r_0 = 5.0$ fm (solid line), respectively.

and momentum conservation was extracted from the experimental data by constructing a double ratio:

$$R(q) + 1 = C_{exp/MC} \left(\frac{Y_{exp}(q)}{Y_{exp}^*(q)} / \frac{Y_{MC}(q)}{Y_{MC}^*(q)} \right), \quad (2)$$

where $C_{exp/MC}$ denotes the normalization constant, the indices 'exp' and 'MC' refer to the experimental and simulated samples, respectively. The determined double ratios are presented in figure 1. Such procedure is used e.g. by the ALEPH collaboration for the studies of correlations in the Z decays [18] or W-pairs decays [19]. In order to estimate the size of the emission source the results are compared with theoretical predictions, obtained by assuming a simultaneous emission of the two protons and derived under the assumption that the final-state interaction between the two detected particles dominates, while other interactions are negligible. The source density was taken to be a Gaussian specified by a radius parameter r_0 and further particulars of the calculations are presented in reference [14]. A rough comparison between the theoretical correlation function and the experimental points indicates that the effective size of the emission source amounts to about 2.4 fm for the $pp\eta$ system and about 4 fm for the $pp + \text{pions}$ system. Extended calculations including the production of the η meson [20] and a detailed comparison and interpretation of results is in progress.

Acknowledgments

We acknowledge the support of the European Community-Research Infrastructure Activity under the FP6 programme (Hadron Physics, N4:EtaMesonNet, RII3-CT-2004-506078), the support of the Polish Ministry of Science and Higher Education under the grants No. PB1060/P03/2004/26, 3240/H03/2006/31 and 1202/DFG/2007/03, and the support of the German Research Foundation (DFG).

References

- [1] P. Moskal *et al.*, Phys. Rev. C **69**, (2004) 025203.
- [2] P. Klaja, P. Moskal and A. Deloff, e-Print Archive: ArXiv:0709.4566.
- [3] M. A. Lisa *et al.*, Ann. Rev. Nucl. Part. Sci. **55**, (2005) 357.
- [4] R. Lednický, Nukleonika **49 (Sup. 2)**, (2004) S3.
- [5] R. Hanbury-Brown, R. G. Twiss, Phil. Mag. **45**, (1954) 663.
- [6] S. E. Koonin, Phys. Lett. B **70**, (1977) 43.
- [7] G. I. Kopylov, M. I. Podgoretsky, Sov. J. Nucl. Phys. **15**, (1972) 219.
- [8] Z. Chajecki, Eur. Phys. J. C **49**, (2007) 81.
- [9] Z. Chajecki, M. Lisa, e-Print Archive: nucl-th/0612080.
- [10] P. Moskal, M. Wolke, A. Khoukaz, W. Oelert, Prog. Part. Nucl. Phys. **49**, (2002) 1.
- [11] D. Prasuhn *et al.*, Nucl. Instr. & Meth. A **441**, (2000) 167.
- [12] H. Dombrowski *et al.*, Nucl. Instr. & Meth. A **386**, (1997) 228.
- [13] S. Brauksiepe *et al.*, Nucl. Instr. & Meth. A **376**, (1996) 397.
- [14] A. Deloff, e-Print Archive: ArXiv:0709.4354.
- [15] D. H. Boal *et al.*, Rev. Mod. Phys. **62**, (1990) 553.
- [16] P. Moskal, e-Print Archive: hep-ph/0408162.
- [17] P. Klaja *et al.*, Acta Phys. Slovaca **56**, (2006) 251.

- [18] R. Barate *et al.*, Phys. Lett. B **475**, (2000) 395.
- [19] R. Barate *et al.*, Phys. Lett. B **478**, (2000) 50.
- [20] A. Deloff, Private communication (2007).

MEASUREMENT OF THE SPIN STRUCTURE FUNCTIONS AND LATEST RESULTS ON QUARK HELICITY DISTRIBUTIONS FROM DEEP-INELASTIC SCATTERING AT HERMES

*P. Kravchenko*¹ for the HERMES Collaboration
Petersburg Nuclear Physics Institute,
High Energy Physics Division, Gatchina, St Petersburg

Abstract

The HERMES experiment at DESY is a second generation experiment to provide a precise measurement of the nucleon spin structure in deep-inelastic lepton scattering. Using the 27.5 GeV longitudinal polarised lepton beam at HERA and longitudinally polarized hydrogen and deuterium gaseous targets, the HERMES experiment can probe the longitudinal spin structure functions $g_1^{p,d,n}$ and the quark helicity distributions. An overview of most recent results is given.

1 Introduction

The spin structure of the nucleon has been one of the most important subjects in Quantum Chromodynamics (QCD) since the European Muon Collaboration [1] reported that the quark spin contribution to the proton spin is small, an observation which is commonly referred to as *Proton Spin Puzzle*. The nucleon spin can be decomposed conceptually into the angular momentum contributions of its constituents according to equation

$$S^N = \frac{1}{2} = \frac{1}{2}\Delta\Sigma + L_g + J_g, \quad (1)$$

¹E-mail: polina@mail.desy.de

where the three terms give the contributions to the nucleon spin from the quark spins, the quark orbital angular momentum, and the total angular momentum of the gluons, respectively. The objective of these studies is to determine the fraction of the nucleon spin which is carried by the quarks. Detailed information on $\Delta\Sigma$ and its flavor decomposition can be obtained from various sources. The HERMES experiment at DESY uses the 27.5 GeV polarized lepton beam of the HERA collider and pure polarized gaseous targets (hydrogen or deuterium). With a large forward acceptance of the HERMES spectrometer and its reliable particle identification [2] it is possible to measure not only inclusive reactions in deep-inelastic scattering, where only the scattered lepton is detected, but also semi-inclusive DIS events where hadrons are detected in coincidence with the lepton. For the hydrogen data set, pions could be identified using the information from a threshold Cherenkov counter (1996-1997 years). For the deuterium data a Ring-Imaging Cherenkov (RICH, 1998-2000 years) detector provided identification of pions and kaons over the kinematic range of 2-15 GeV/c.

2 Spin Structure Function g_1

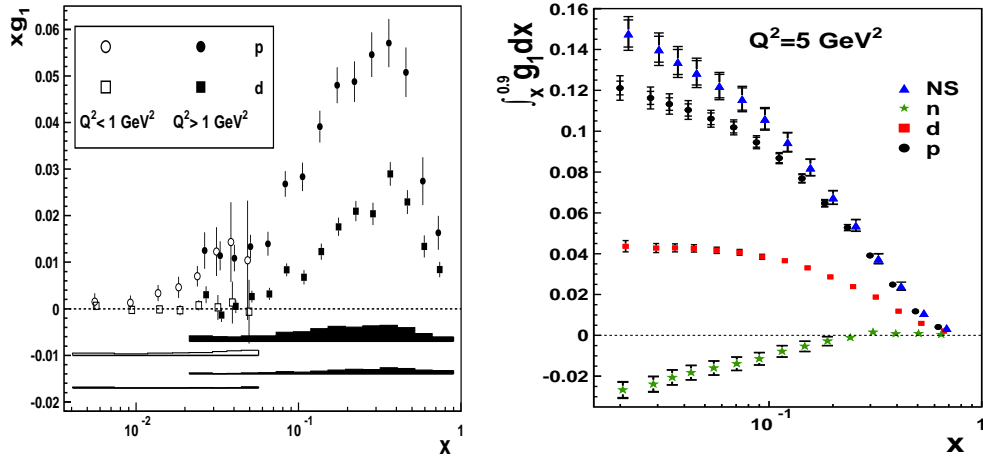


Fig.1. HERMES result for xg_1 vs x for the proton and the deuteron Fig.2. Integrals of $g_1^{p,d,n,NS}$ over the range $0.021 \leq x \leq 0.9$.

The polarized structure functions $g_1^{p,d}$ can be extracted from double-spin asymmetries $A_{\parallel}^{p,d}$ in inclusive deep-inelastic scattering (DIS) using

$$g_1(x, Q^2) = \frac{1}{1 - \frac{y}{2} - \frac{y^2}{4}\gamma^2} \times \left[\frac{Q^4}{8\pi\alpha^2 y} \frac{d^2\sigma_{UU}(x, Q^2)}{dx dQ^2} A_{\parallel}(x, Q^2) + \frac{y}{2}\gamma^2 g_2(x, Q^2) \right] \quad (2)$$

The final HERMES results for the polarized structure function g_1 [3] from all data taken with longitudinally polarized hydrogen and deuterium targets are presented in Fig. 1. The statistical precision of the HERMES proton data is comparable to that of the hitherto most precise data from CERN and SLAC in the same x range. The HERMES deuteron data provide the most precise determination of the spin structure function $g_1^d(x, Q^2)$. In the region $x < 0.03$ the SMC data favor negative values, while the HERMES deuteron data are compatible with zero, as are the recent COMPASS data. As shown in Fig.2, integrals of the spin structure function g_1 of proton, deuteron and neutron were evaluated. The HERMES deuteron integral appears to saturate at $x < 0.04$. Based on saturation of the integral of g_1^d and using the assumption of SU(3) flavor symmetry in the hyperon decays in the spin- $\frac{1}{2}$ baryon octet, the flavor-singlet axial charge a_0 has been determined:

$$a_0(Q^2 = 5\text{GeV}^2) = 0.330 \pm 0.011(\text{theo.}) \pm 0.025(\text{exp.}) \pm 0.028(\text{evol.}). \quad (3)$$

In the \overline{MS} scheme which was used in this analysis, a_0 can be interpreted as the contribution of quark helicities to the nucleon helicity. A value of 1/3 acquires still major contribution from gluons and/or orbital angular momenta of quarks and gluons.

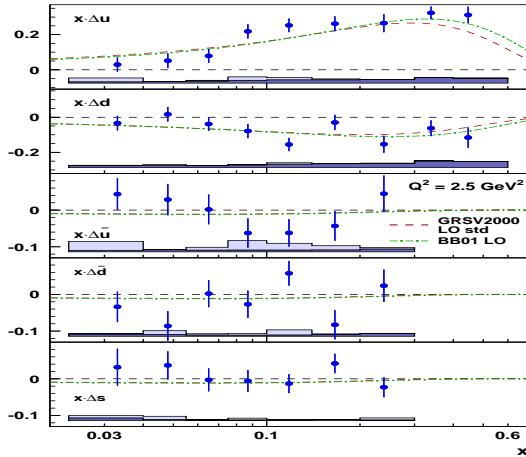


Fig.3. Quark helicity distributions $x\Delta q(x, Q_0^2)$ at $Q_0^2 = 2.5 \text{ GeV}^2$. The curves show LO QCD global analysis [6].

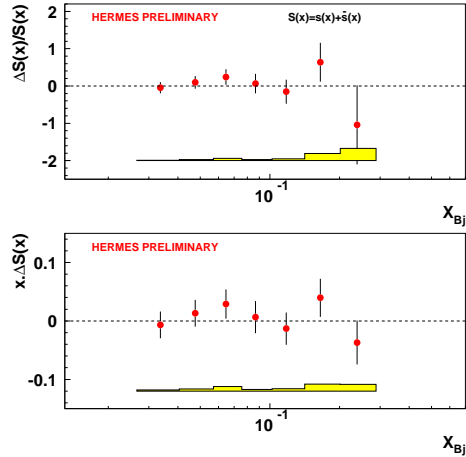


Fig.4. Strange quark helicity distributions at $Q^2 = 2.5 \text{ GeV}^2$ as a function of x .

3 Quark helicity distribution

Semi-inclusive DIS (SIDIS) is a powerful tool to determine the separate contributions $\Delta q_f(x)$ of the quarks and antiquarks of flavor f to the total spin of the nucleon. The hadron asymmetries $A_1^h(x)$ are related to the quark polarization distributions $\Delta q_f(x)$ through the so-called purity matrix P_f^h . A combined analysis of the inclusive and semi-inclusive spin asymmetries for π^+ , π^- , K^+ and K^- has been carried out for the longitudinally polarized hydrogen and deuterium targets [4]. Figure 3 shows the results for the x -weighted distributions $x\Delta q(x)$. Note that in contrast to the LO QCD fits to inclusive data overlaid in Fig.4, in the HERMES analysis no assumptions were made on the symmetry of the sea quark polarizations, except $\Delta\bar{s}/\bar{s}$ is assumed to be zero. The systematic error bands include uncertainties in addition to the experimental error of the asymmetries (used pdf's, tune for extracting purities). For $x > 0.3$, the polarization of the sea flavors was set to zero, the small uncertainties for the non-sea flavors arising from this as well as from setting $\Delta\bar{s}/\bar{s} \equiv 0$ were also included in the systematic error. As expected the helicity density of the u quark is found to be positive and large at $x > 0.1$, and that of the d quark is negative and rather flat in x . The helicity densities of the light sea quarks are all found to be compatible with zero. For sea quarks, within the experimental uncertainties, there is no disagreement with the QCD fits.

4 Isoscalar method

An alternative analysis was performed on the extractions of $\Delta s(x) + \Delta\bar{s}(x)$ [5]. Because the strange quark helicity $\Delta s(x) + \Delta\bar{s}(x)$ has no isospin, it can be extracted from the isoscalar deuteron target alone. A simple purity matrix can be computed extracting the needed purities for kaons from the measured HERMES multiplicities. The strange helicity distributions obtained in the HERMES leading-order analysis are presented in Fig.4. The integral over the measured region of x is consistent with zero.

References

- [1] J. Ashman *et al.* *Phys. Lett.* B**206**, 364 (1988).
- [2] K. Ackerstaff *et al.* *Nucl. Instrum. Meth.* A **417**, 230 (1998);
N. Akopov *et al.* *Nucl. Instrum. Meth.* A **479**, 511 (2002).

- [3] A. Airapetian *et al.* *Phys. Rev D* **75**, 012007 (2007).
- [4] A. Airapetian *et al.* *Phys. Rev D* **71**,012003 (2005).
- [5] H. E. Jackson, in these proceeding (2006)
- [6] J. Blümlein *et al.* *Nucl.Phys. B* **636** 225 (2002);
M. Glück *et al.* *Phys.Rev. D* **63** 094005 (2001)

$\bar{D}N$ INTERACTION BASED ON MESON-EXCHANGE AND QUARK-GLUON DYNAMICS

G. Krein^{%,1}, J. Haidenbauer^{*}, U.-G. Meißner^{#,*}, A. Sibirtsev[#]

[%]Instituto de Física Teórica, UNESP, São Paulo, Brazil

^{*}Forschungszentrum Jülich, Institut für Kernphysik, Jülich, Germany

[#]HISKP (Theorie), Universität Bonn, Bonn, Germany

Abstract

We introduce a meson exchange model, supplemented with short-distance contributions from one-gluon-exchange, to investigate the $\bar{D}N$ interaction at low energies. The main ingredients are provided by vector meson (ρ , ω) exchange and higher-order box diagrams involving \bar{D}^*N , $\bar{D}\Delta$, and $\bar{D}^*\Delta$ intermediate states. The short range part is assumed to receive additional contributions from genuine quark-gluon processes. It is found that the ω -exchange plays a very important role. Its interference pattern with the ρ -exchange clearly determines the qualitative features of the interaction.

1 Introduction and Motivation

In the present communication we report selected results from our recent investigation of the $\bar{D}N$ interaction within a meson-exchange model and a quark model utilizing one-gluon-exchange (OGE) [1]. There are several reasons for studying the interactions of D mesons with nucleons. One reason is that D mesons can provide important clues on mechanisms of chiral symmetry restoration in a hot and/or dense medium. This is so because the properties of the light quarks in a D meson are sensitive to temperature and density, and thus D -meson properties like masses and sizes are expected to change in medium, and likewise their interactions with ordinary hadrons can be expected to change in medium. However, a reasonable understanding of the interaction in free space is required before one can infer in-medium changes of the interaction. There are planned experiments by the \bar{P} ANDA collaboration at FAIR (GSI) to measure such interactions and estimates for the magnitude of such cross sections are urgently required.

¹E-mail address: gkrein@ift.unesp.br

2 The model

Our model for the $\bar{D}N$ interaction is an extension of the KN meson-exchange model of the Jülich group [2–5], generalized by assuming SU(4) symmetry. Not only single-meson (and baryon) exchanges are taken into account, but also higher-order box diagrams involving \bar{D}^*N , $\bar{D}^*\Delta$, and $\bar{D}\Delta$ intermediate states. All meson-meson-meson and baryon-baryon-meson vertices are furnished with form factors, which are taken over from Ref. [3]. The rationale for this is based on the notion that those form factors parameterize predominantly the off-mass-shell behavior of the exchanged particles, which are the same for the $\bar{D}N$ and KN systems. With respect to the contributions in the scalar sector we consider them as being due to correlated $\pi\pi$ exchange, analogous to the KN system [3]. But we investigate also a scenario assuming genuine scalar-meson exchange.

The short-distance quark contribution is based on a quark-interchange process [6], as for KN system in Ref. [4]. We use the dominant contributions of the OGE exchange, namely the Coulomb and spin-spin parts. Since the mass of the c quark is much heavier than the mass of the s quark, the size parameter of the D and K mesons wave functions are different and, therefore, the $\bar{D}N$ interaction due to the quark-interchange process differs from the one for KN .

The explicit expressions for the interaction Lagrangians, SU(4) symmetry relations for the coupling constants, the quark model expressions for the effective $\bar{D}N$ interaction, and the values of parameters are given in great detail in Ref. [1].

3 Results and Conclusions

Fig. 1 presents the different meson-exchange contributions to the total cross-section, starting with ρ exchange (dashed), then adding ω (dash-dotted) and so on. The most remarkable result is that for $I = 0$ there is a destructive interference between ρ and ω exchanges. On the other hand, for $I = 1$ both contributions add up. Also seen is that the addition of the scalar contributions and of baryon ($\Lambda_c(2285)$, $\Sigma_c(2455)$) exchange influences the results for $\bar{D}N$ very little. The cross sections in both isospin channels are of comparable magnitude.

Fig. 2 presents results when adding the short-ranged quark contribution, and for treating the scalar contribution as being either due to correlated $\pi\pi$ or genuine scalar-meson exchange. The main conclusion is that the (repulsive) quark-gluon contribution strongly affects the threshold behavior, and their

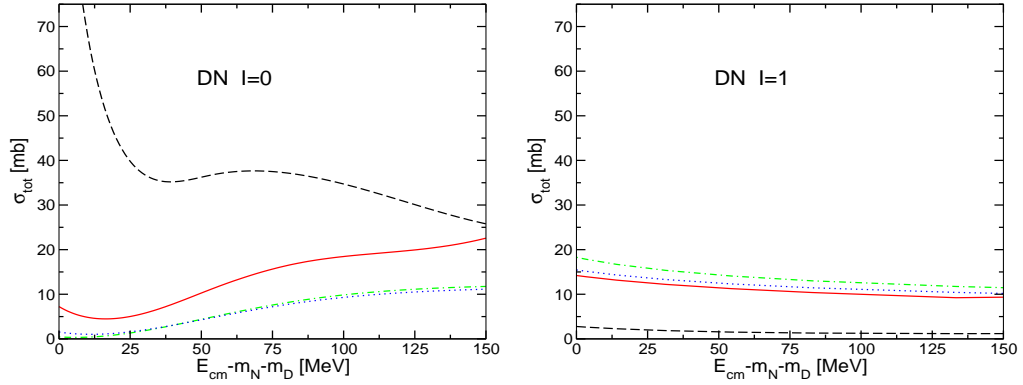


Figure 1: $\bar{D}N$ cross sections in the isospin channels $I=0$ (left panel) and $I = 1$ (right panel) including consecutively ρ (dashed curve), ω (dash-dotted), scalar mesons and baryon-exchange diagrams (dotted), and box diagrams (solid).

effect is stronger in the $I = 1$ channel. Also, as seen in the figure, the different assumptions about the nature of the scalar contribution lead to very different results for the $I = 1$ channel.

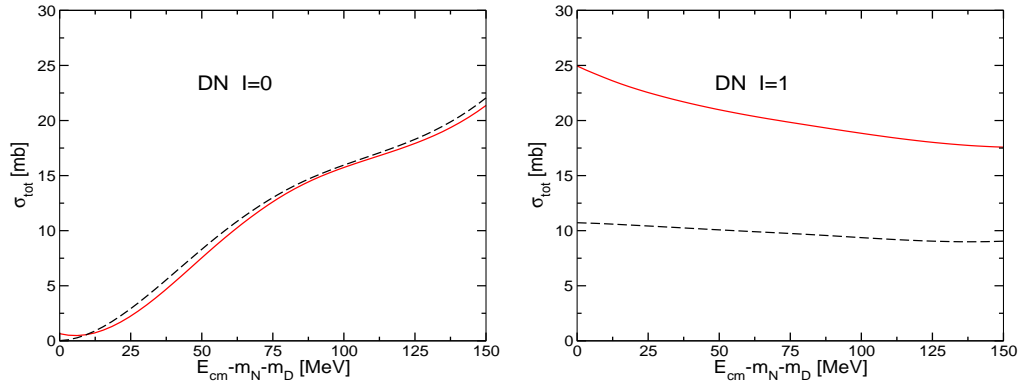


Figure 2: Full model, including meson-exchange and OGE. Solid lines are for scalar contributions due to correlated $\pi\pi$ exchange, and dashed lines are for genuine scalar-meson exchange.

We have also calculated scattering lengths, finding $a^{I=0} = -0.13$ fm, $a^{I=1} = -0.29$ fm, for the quark-gluon interaction alone and $a^{I=0} = 0.07$ fm, $a^{I=1} = -0.45$ fm, for the full model. The former results are close to the values found by Lutz and Korpa [7] while the latter are qualitatively very similar to the results obtained for the KN interaction [3]. They are also in good agreement with the results presented by Laura Tolos at this meeting [8].

In conclusion, the most interesting finding of our study is the important role played by the ω -exchange contribution. Its interference pattern with the ρ -exchange, which is basically fixed by the assumed SU(4) symmetry, clearly determines the qualitative features of the $\bar{D}N$ interaction. Predictions for $\bar{D}N$ where only ρ -exchange are taken into account differ drastically and should be regarded with caution in view of our results.

Acknowledgments

Work partially supported by the DFG (Project no. 444 BRA-113/14) and the Brazilian agencies CAPES, CNPq and FAPESP, by the EU I3HP under contract number RII3-CT-2004-506078, by the DFG through funds provided to the SFB/TR 16, by the EU Contract No. MRTN-CT-2006-035482, and by BMBF (grant 06BN411). A.S. acknowledges support by the JLab grant SURA-06-C0452 and the COSY FFE grant No. 41760632 (COSY-085).

References

- [1] J. Haidenbauer, G. Krein, U. G. Meißner and A. Sibirtsev, *Eur. Phys. J.* **A33**, 107 (2007).
- [2] R. Büttgen, K. Holinde, A. Müller–Groeling, J. Speth and P. Wyborny, *Nucl. Phys.* **A506**, 586 (1990).
- [3] M. Hoffmann, J.W. Durso, K. Holinde, B.C. Pearce and J. Speth, *Nucl. Phys.* **A593**, 341 (1995).
- [4] D. Hadjimichef, J. Haidenbauer and G. Krein, *Phys. Rev. C* **66**, 055214 (2002).
- [5] J. Haidenbauer and G. Krein, *Phys. Rev. C* **68**, 052201 (2003).
- [6] D. Hadjimichef, G. Krein, S. Szpigel and J. S. da Veiga, *Annals Phys.* **268**, 105 (1998).
- [7] M. F. M. Lutz and C. L. Korpa, *Phys. Lett.* **B633**, 43 (2006).
- [8] L. Tolos, Open-charm mesons in hot and dense nuclear matter, *contribution to these proceedings*.

MEASUREMENTS OF THE GLUON POLARIZATION IN THE NUCLEON AT COMPASS

R. Kuhn

Technische Universität München
Physik-Department E18
James-Franck-Straße
85748 Garching b. München
Germany

Abstract

One of the main goals of the COMPASS experiment at CERN is the determination of the gluon polarization in the nucleon, $\Delta G/G$, from double spin asymmetries in deep inelastic scattering of polarized muons on a polarized ${}^6\text{LiD}$ target. The gluon polarization is accessible in photon–gluon fusion (PGF) events, either tagging them by open charm production or enriching them in the inclusive production of hadron pairs with high transverse momentum. The analysis method is outlined and results from the data taking periods of 2002–2004 are shown.

1 Introduction

In the framework of QCD, the spin of the nucleon is composed of the contributions from quark and gluon spins, $\Delta\Sigma$ and ΔG , and their orbital angular momenta, L_q and L_g .

$$J_N = \frac{1}{2} = \frac{1}{2}\Delta\Sigma + \Delta G + L_q + L_g$$

With $\Delta\Sigma$ of the order of $\frac{1}{3}$ [1], and because QCD fits only weakly constrain ΔG , direct measurements of the gluon polarization are necessary. The method of high p_T hadron pairs outlined below has been used by the HERMES [2] and SMC [3] collaborations. In addition to improving the accuracy of the data set, COMPASS [4] provides a qualitatively new measurement in the form of the open charm method.

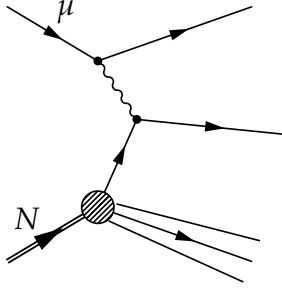


Figure 1: Leading process in deep inelastic scattering.

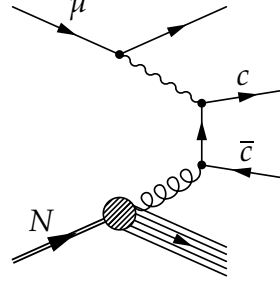


Figure 2: The photon–gluon fusion process in leading order.

2 High p_T

The leading process in deep inelastic scattering is depicted in fig. 1. Transverse momentum is either generated in the fragmentation process or stems from intrinsic k_T of the quark in the nucleon. Since both of these effects amount to $\lesssim 1\text{GeV}/c$, requiring the hadron in the final state to have high transverse momentum reduces the contribution of the leading process in favor of the photon–gluon fusion shown in fig. 2. Using the fact that the latter process produces two outgoing quarks, COMPASS requires two hadrons, each with $p_{T,i} > 0.7\text{GeV}/c$ and in total $\sum_i p_{T,i}^2 > 2.5\text{GeV}^2/c^2$. Contributions from resonances are suppressed by restricting the invariant mass of the 2-hadron system to be larger than $1.5\text{GeV}/c^2$. The target fragmentation region is excluded by $x_F > 0.1$, and hadrons are positively identified using the hadron calorimeters.

The analysis is done in two kinematic regimes. For $Q^2 > 1\text{GeV}^2/c^2$, resolved photon processes can be neglected, leaving at leading order only the QCD compton scattering besides the already discussed processes. Using the LEPTO generator, the fraction of photon–gluon fusion in this sample has been determined to $R_{PGF} = 0.34 \pm 0.07$. Given the smallness of A_1 for $x_B < 0.05$, the other processes can be regarded as unpolarized background, leading to

$$A^{\gamma^*N \rightarrow hh} = R_{PGF} a_{LL}^{PGF} \frac{\Delta G}{G}$$

with the virtual photon–nucleon asymmetry $A^{\gamma^*N \rightarrow hh}$ and the analyzing power a_{LL}^{PGF} . From the data of 2002 and 2003 the preliminary value

$$\left. \frac{\Delta G}{G} \right|_{\langle x_g \rangle \approx 0.13, \mu^2 = 3\text{GeV}^2/c^2} = 0.06 \pm 0.31_{\text{stat}} \pm 0.06_{\text{sys}}$$

The statistical uncertainty estimated for the full sample 2002–2006 is 0.14.

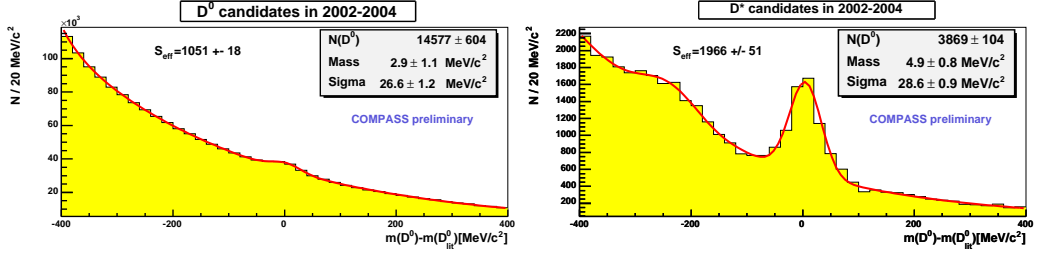


Figure 3: D mesons reconstructed from deep inelastic scattering events in 2002–2004. The left plot shows the untagged $D^0 \rightarrow \pi^\pm K^\mp$ channel while the right plot shows the events tagged with $D^{*\pm} \rightarrow D^0 \pi^\pm$.

In the quasi-real regime $Q^2 < 1\text{GeV}^2/c^2$, the statistics are about a factor 10 higher, but the sample also includes resolved photon processes. These have been taken into account using a PYTHIA simulation, see [5] for details on the analysis method. With $R_{PGF} = 0.32$, the analysis of the data from 2002–2004 yields the preliminary result

$$\left. \frac{\Delta G}{G} \right|_{\langle x_g \rangle \approx 0.085, \mu^2 = 3\text{GeV}^2/c^2} = 0.016 \pm 0.058_{\text{stat}} \pm 0.55_{\text{syst}}$$

3 Open Charm

The photon–gluon fusion process can be selected rather cleanly by D mesons in the final state, since the intrinsic charm content of the nucleon is extremely short-lived and therefore strongly correlated with the gluonic structure. The decay channels investigated so far are $D^0 \rightarrow \pi^+ K^- + c.c.$ as well as the same decay preceded by $D^{*+} \rightarrow D^0 \pi^+$. The signals obtained from these channels are shown in fig. 3. The higher purity of the D^* tagged sample outweighs its lower statistics, leading to slightly lower statistical uncertainties. Possible background asymmetries are much smaller than the statistical uncertainty achieved so far, as has been checked using sideband samples, thus the connection between the measured asymmetry and the gluon polarization is

$$A^{\gamma^* N \rightarrow D} = \frac{S}{S+B} a_{LL}^{\text{opencharm}} \frac{\Delta G}{G}$$

The polarization transfer from the incoming muon to the virtual photon as well as the analyzing power $a_{LL}^{\text{opencharm}}$ strongly vary between events depending on the kinematics, wherefore the analysis is made in bins of a_{LL} . The preliminary result from 2002–2004 is

$$\frac{\Delta G}{G} = -0.57 \pm 0.41_{\text{stat}} \pm 0.17_{\text{syst}}$$

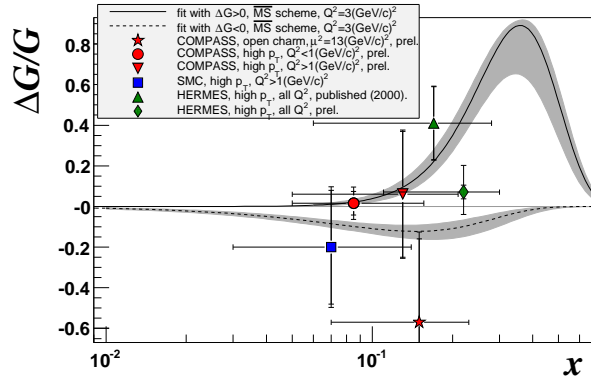


Figure 4: Gluon polarization measurements of COMPASS in comparison to measurements by HERMES and SMC. The curves are the result of a QCD fit by COMPASS [1].

at a scale $\mu^2 = 13\text{GeV}^2/c^2$ and $x_B \approx 0.15$. The statistical uncertainty estimated for the full sample 2002–2006 is 0.28.

4 Conclusion

COMPASS has investigated the polarized gluon structure of the nucleon using three complementary methods, all of which exclude a very large positive gluon polarization. On the other hand, they are consistent with QCD fits to the world data, which indicate an absolute value of $0.2 \div 0.3$ for the contribution of the gluons' spin to the spin of the nucleon.

References

- [1] COMPASS, *Phys. Lett.* **B647**, 8 (2007)
- [2] HERMES, *Phys. Rev. Lett.* **84**, 2584 (2000)
- [3] SMC, *Phys. Rev.* **D70**, 012002 (2004)
- [4] COMPASS, *Nucl. Instr. Meth.* (A577), 455 (2007)
- [5] COMPASS, *Phys. Lett.* **B633**, 25 (2006)

MULTIMESON PRODUCTION IN pp INTERACTIONS AS A BACKGROUND FOR η AND η' DECAYS

A. Kupsc[†], P. Moska[§] and M. Zieliński[§]

[†]Uppsala University, Uppsala, Sweden

[§]Jagiellonian University, Cracow, Poland

Abstract

Multimeson production in pp interactions comprises important background for η , ω and η' mesons production experiments and for the studies of their decays planned with WASA detector at COSY. The available information about the reactions is summarized and the need for efforts to describe the processes is stressed.

1 Multimeson production

Direct production of three or more pions in proton-proton interactions, has not received proper attention, neither experimentally nor theoretically, despite the fact that it comprises the main background for η , η' and ω production experiments. With a 4π facility such as WASA, aiming for measurements of decays of η and η' produced in pp interactions [1], the understanding of the $pp \rightarrow pp\pi\pi\pi$ reactions becomes very important as they constitute a severe background for studies of η and η' decays into three pions. Those decays provide key ingredients for determination of the ratios of light quark masses [2,3], since the partial decay widths are proportional to d and u quark mass difference squared. In addition precise studies of η' decays require knowledge of $pp \rightarrow pp\pi\pi\pi\pi$, $pp \rightarrow pp\pi\pi\pi\pi\pi$, $pp \rightarrow pp\pi\eta$ and $pp \rightarrow pp\pi\pi\eta$ reactions for beam energies around η' production threshold. For more than forty years there were only three experimental points available for the cross section of $pp \rightarrow pp\pi^+\pi^-\pi^0$ and $pp \rightarrow pn\pi^+\pi^+\pi^-$ reactions, all coming from bubble chamber experiments [4-6]. Only recently the data base has been extended by the measurements of $pp \rightarrow pp\pi^+\pi^-\pi^0$ and $pp \rightarrow pp\pi^0\pi^0\pi^0$ reactions cross sections near the threshold by the CELSIUS/WASA collaboration [7]. For the remaining reactions there is no data in that energy region.

The direct production should proceed by an excitation of one or two baryon resonances followed by the subsequent decays [8]. For example in

the case of three pion production the low energy region a mechanism with simultaneous excitation of N^* and $\Delta(1232)P_{33}$ resonances is expected to dominate. The N^* involved has to decay into $N\pi\pi$ and therefore the lowest lying Roper ($N(1440)P_{11}$) and $N(1520)D_{13}$ resonances could be considered.

The influence of the resonances can be studied in the invariant mass distributions of the subsystems of the outgoing protons and pions. Such studies were done for the $pp \rightarrow pp\pi^+\pi^-\pi^0$ and $pp \rightarrow pn\pi^+\pi^+\pi^-$ reactions in bubble chamber experiments performed at higher energies (beam kinetic energies of 4.15 GeV and 9.11 GeV) with up to thousand events [9–11]. However, close to the threshold the analysis is not conclusive since the widths of the involved resonances are comparable with the available excess energy (Q). Therefore, in this case one expects that phase space distribution and the final state interaction among the outgoing nucleons provide a reasonable description of the observed cross sections. The near threshold cross sections for the single meson production via the nucleon-nucleon interaction can indeed be quite satisfactory described by such ansatz. For the productions of multiple mesons the assumption should hold even for higher excess energies since on average the energy available to the pairs of the outgoing particles will be lower. That is consistent with CELSIUS/WASA results on $pp \rightarrow pp\pi^+\pi^-\pi^0$ and $pp \rightarrow pp\pi^0\pi^0\pi^0$ reactions studied at $Q \approx 100$ MeV.

The production mechanism could be studied instead by measuring ratios of the cross sections for the different charge states. With the lack of information the simplest assumption is Fermi model [12], where amplitudes for all isospin states are put to be equal. The assumption leads to definite predictions for ratios between different charge states of the reactions. For example $\sigma(pp \rightarrow pp\pi^+\pi^-\pi^0) : \sigma(pp \rightarrow pp\pi^0\pi^0\pi^0) : \sigma(pp \rightarrow pn\pi^+\pi^+\pi^-) \equiv \sigma_1 : \sigma_2 : \sigma_3 = 8 : 1 : 10$. Resonances in the intermediate state will modify the ratios. The effect can be illustrated in the Isobar Model [8] where the ratio $\sigma_1 : \sigma_2 : \sigma_3$ is $7 : 1 : 25$ (assuming ΔN^* intermediate state) or $5 : 2 : 10$ (assuming $N_1^* N_2^*$). Experimentally: $\sigma_1 : \sigma_3$ at beam kinetic energy 2.0 GeV ($1:2.53 \pm 0.46$) [4] and at 2.85 GeV ($1:1.59 \pm 0.27$) [5]. The ratio $\sigma_1 : \sigma_2 = 5.2 \pm 0.8 : 1$ was measured at lower energy – 1.36 GeV in recent CELSIUS/WASA experiment [7]. One trivial modification to the predicted ratios close to threshold comes from difference between volumes of the phase spaces due to $m_{\pi^+} \neq m_{\pi^0}$ and it amounts to 18% at 1.36 GeV.

Due to lack of microscopic model calculations, of the same kind as those for single meson or for double pion production the semiclassical Isobar Model is at present the only option to describe more complicated reactions below $\sqrt{s} \approx 5$ GeV. The modern version of the isobar model is used as input to relativistic ions calculations using transport equations [13, 14]. Reliability of the calculations can be tested in simpler cases by comparison with exist-

ing calculations for the double pion production [15]. The implementation of the resonances in the Isobar Model, their production cross sections and decay branching ratios can be evaluated by studying exclusive meson production reactions. Multimeson production in proton-proton interactions provides very sensitive test of the parameters. The existing calculations within the framework have focused so far on production of dileptons in proton-proton interactions with the aim to understand the background for high density nuclear matter probes [16]. The byproduct of such studies were calculations of the background for η and η' decays involving dileptons (see for example ref. [17]). There is a need to extend the calculations to obtain predictions also for multimeson processes.

2 Background for η , η' decays

A feature of $\eta(\eta')$ detection from $pp \rightarrow pp\eta(\eta')$ in the WASA detector is the precise tagging by missing mass technique with a resolution of a few MeV/c². The resolution of the invariant mass of the decay system is typically considerably worse. Therefore a figure of merit to describe background from direct production process, leading to the identical final state as for an $\eta(\eta')$ decay, is given by $\rho_B \equiv d\sigma_B/d\mu|_{\mu=m_{\eta(\eta')}} -$ the differential cross section for the background at the $\eta(\eta')$ peak in the pp missing mass μ . Figure 1 shows inclusive ρ_B values for η' derived from the COSY-11 measurements [18–20]. When estimating the background for a given decay channel, quantity $\rho_B\Delta\mu$ (where $\Delta\mu$ is the resolution in the missing mass) should be compared to $\sigma_{\eta(\eta')}BR_i$ (production cross section times branching ratio for the decay mode). The ρ_B value depends on the total cross section and on the reaction mechanism. For $\eta(\eta')$ production close to threshold the background distributions at the edge of the phase space are relevant. For both signal and the multimeson production this region of the phase space is strongly influenced by pp final state. When approaching the threshold the ρ_B decreases quickly and in addition missing mass resolution improves (since it is constrained more by the beam momentum resolution) increasing signal to background ratio. The price is however a lower production cross section $\sigma_{\eta(\eta')}$.

Detailed studies of $\eta \rightarrow \pi\pi\pi$ decays in $pp \rightarrow pp\eta$ reaction at beam energy 1.36 GeV by CELSIUS/WASA collaboration shows that background from direct three pion production is 10–20% for the $\pi^0\pi^+\pi^-$ and 5% for the $\pi^0\pi^0\pi^0$ channel in the final data sample [7, 22]. This allows for precise study of the η decays providing large number of events is collected. For η' decays the situation is quite different: the three pion decays have branching ratios at percent or permil level [23]. In comparison to the η meson the η' production

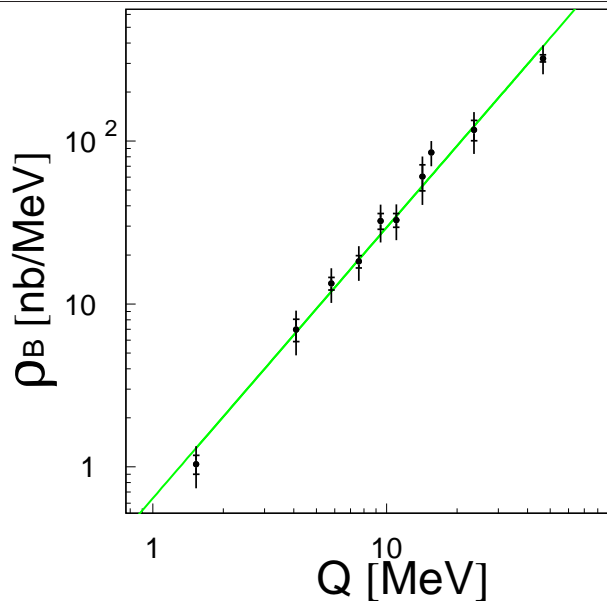


Figure 1: Inclusive differential cross section ρ_B for multipion production derived from the COSY-11 data [18–20]. The line is the parametrization $\rho_B = \alpha(Q/(1 \text{ MeV}))^\beta$ fitted to the data: $\alpha = 0.64 \pm 0.14$ [nb/MeV] and $\beta = 1.66 \pm 0.08$ [21].

cross section at similar excess energies is about 30 times lower [18–20, 24–26]. Finally the total cross section for multipion reactions increases strongly when going from η to η' production threshold region, e.g. for $pp \rightarrow pp\pi\pi\pi$ reaction 50–100 times. In conclusion embarking on the η' decay program in pp interactions requires much better understanding of multimeson production reactions.

References

- [1] H. H. Adam *et al.* [WASA-at-COSY Collab.], arXiv:nucl-ex/0411038.
- [2] D. J. Gross, S. B. Treiman, F. Wilczek, *Phys. Rev.* **D19**, 2188 (1979).
- [3] H. Leutwyler, *Phys. Lett.* **B378**, 313 (1996).
- [4] E. Pickup, D. K. Robinson, E. O. Salant, *Phys. Rev.* **125**, 2091 (1962).
- [5] E. L. Hart *et al.*, *Phys. Rev.* **126**, 747 (1962).
- [6] A. M. Eisner *et al.*, *Phys. Rev.* **138**, B670 (1965).

-
- [7] C. Pauly *et al.*, *Phys. Lett.* **B649**, 122 (2007).
- [8] R. M. Sternheimer, S. J. Lindenbaum, *Phys. Rev.* **123**, 333 (1961).
- [9] G. Alexander *et al.*, *Phys. Rev.* **154**, 1284 (1967).
- [10] A. P. Colleraine, U. Nauenberg, *Phys. Rev.* **161**, 1387 (1967).
- [11] S. P. Almeida *et al.*, *Phys. Rev.* **174**, 1638 (1968).
- [12] E. Fermi, *Prog. Theor. Phys.* **5**, 570 (1950).
- [13] S. Teis *et al.*, *Z. Phys.* **A356**, 421 (1997).
- [14] S. A. Bass *et al.*, *Prog. Part. Nucl. Phys.* **41**, 255 (1998).
- [15] L. Alvarez-Ruso, E. Oset, E. Hernandez, *Nucl. Phys.* **A633**, 519 (1998).
- [16] A. Faessler *et al.*, *J. Phys.* **G29**, 603 (2003).
- [17] A. Faessler *et al.*, *Phys. Rev.* **C69**, 037001 (2004).
- [18] P. Moskal *et al.*, *Phys. Rev. Lett.* **80**, 3202 (1998);
- [19] P. Moskal *et al.*, *Phys. Lett.* **B474**, 416 (2000);
- [20] A. Khoukaz *et al.*, *Eur. Phys. J.* **A20**, 345 (2004).
- [21] M. Zieliński, Diploma thesis, Jagellonian University, in preparation.
- [22] M. Bashkanov *et al.*, *Phys. Rev.* **C76**, 048201 (2007).
- [23] W. M. Yao, *et al.*, *J. Phys.* **G33**, 1 (2006).
- [24] A. M. Bergdolt *et al.*, *Phys. Rev.* **D48**, R2969 (1993); E. Chiavasa *et al.*, *Phys. Lett.* **B322**, 270 (1994); H. Calen *et al.*, *Phys. Lett.* **B366**, 39 (1996); H. Calen *et al.*, *Phys. Rev. Lett.* **79**, 2642 (1997); J. Smyrski *et al.*, *Phys. Lett.* **B474**, 182 (2000).
- [25] F. Hibou *et al.*, *Phys. Lett.* **B438**, 41 (1998);
- [26] F. Balestra *et al.*, *Phys. Lett.* **B491**, 29 (2000).

RENORMALIZATION GROUP EQUATION FOR NUCLEAR CURRENT OPERATORS

*A. N. Kvinikhidze*¹ and *B. Blankleider*

Department of Physics
 Flinders University
 Bedford Park, SA 5042, Australia

Abstract

In order to eliminate the present ambiguity in the renormalization group equation for nuclear current operators, we introduce a new condition specifying the cutoff independence of the five point Green function corresponding to the two-body propagator with current operator insertion. The resulting effective current operator is then shown to obey a modified Ward-Takahashi identity which differs from the usual one, but that nevertheless leads to current conservation.

1 Current Operator RG Equation

The use of the Wilsonian renormalization group (RG) method [1] to impose a cutoff Λ on the momenta of virtual states is an important tool for studying various aspects of nuclear effective field theory (EFT) [2]. In this context, our main goal here is to provide an unambiguous derivation of the recently proposed RG equation for nuclear current operators [3]. At the same time we examine the questions of current conservation and application to EFT.

Defining projection operators [3]

$$\eta = \int \frac{d^3\mathbf{k}}{(2\pi)^3} |\mathbf{k}\rangle \langle \mathbf{k}| \theta(\Lambda - k), \quad (1)$$

$$\lambda = \int \frac{d^3\mathbf{k}}{(2\pi)^3} |\mathbf{k}\rangle \langle \mathbf{k}| \theta(\bar{\Lambda} - k) \theta(k - \Lambda), \quad (2)$$

where $\bar{\Lambda} > \Lambda$, the RG equation for the reduced space effective potential V_Λ can then be written as [2]

$$\frac{\partial V_\Lambda}{\partial \Lambda} = V_\Lambda G_0 \frac{\partial \lambda}{\partial \Lambda} V_\Lambda \quad (3)$$

¹Permanent address: A. Razmadze Mathematical Institute, Georgian Academy of Sciences, Aleksidze Str.1, Tbilisi 0193, Georgia

where $G_0 = (E - H_0)^{-1}$ is the two-body free propagator. Eq. (3) can be derived from the reduced space Lippmann-Schwinger equation

$$T = V_\Lambda + V_\Lambda \eta G_0 T \quad (4)$$

by requiring the off-shell scattering amplitude, T , not to depend on Λ . Recently NA have derived the corresponding RG equation for the reduced space effective current operator O_Λ^μ [3]. Writing this current operator as

$$O_\Lambda^\mu = \eta \Gamma_\Lambda^\mu \eta, \quad (5)$$

the RG equation derived by NA can be expressed as

$$\frac{\partial \Gamma_\Lambda^\mu}{\partial \Lambda} = V_\Lambda G_0 \frac{\partial \lambda}{\partial \Lambda} \Gamma_\Lambda^\mu + \Gamma_\Lambda^\mu \frac{\partial \lambda}{\partial \Lambda} G_0 V_\Lambda. \quad (6)$$

However, Eq. (6) was derived as only a sufficient condition for the Λ invariance of the physical matrix element of O_Λ^μ :

$$\frac{\partial \langle O_\Lambda^\mu \rangle}{\partial \Lambda} = \frac{\partial}{\partial \Lambda} \bar{\psi}_\beta \eta \Gamma_\Lambda^\mu(E_\beta, E_\alpha) \eta \psi_\alpha = 0. \quad (7)$$

That is, the equation used to define Γ_Λ^μ was chosen to be²

$$\langle O_\Lambda^\mu \rangle \equiv \bar{\psi}_\beta \eta \Gamma_\Lambda^\mu(E_\beta, E_\alpha) \eta \psi_\alpha = \bar{\psi}_\beta \Gamma^\mu(E_\beta, E_\alpha) \psi_\alpha \quad (8)$$

where

$$\Gamma^\mu(E_\beta, E_\alpha) \equiv O_{\bar{\Lambda}}^\mu(E_\beta, E_\alpha) = \eta \Gamma_\Lambda^\mu(E_\beta, E_\alpha) \eta|_{\Lambda=\bar{\Lambda}} \quad (9)$$

can be identified with the current vertex function of the full space [4] in the limit $\bar{\Lambda} \rightarrow \infty$. The sandwiching two-body wave functions $\bar{\psi}_\beta$ and ψ_α include bound states, and scattering states whose relative momenta, p' and p , respectively, are smaller than the cutoff parameter: $p', p < \Lambda$.

We have eliminated the ambiguity in the validity of Eq. (6) by showing that this RG equation is a sufficient and *necessary* condition for Λ independence of the five-point function $\eta G \eta \Gamma_\Lambda^\mu \eta G \eta$ [5]. Specifically we chose Γ_Λ^μ to be defined by

$$\eta G(E') \eta \Gamma_\Lambda^\mu(E', E) \eta G(E) \eta = \eta G^\mu(E', E) \eta \quad (10)$$

for all $\Lambda < \bar{\Lambda}$, where G^μ is the five-point function defined as

$$G^\mu(E', E) = G(E') \eta \Gamma_\Lambda^\mu(E', E) \eta G(E)|_{\bar{\Lambda}=\Lambda} = G(E') \Gamma^\mu(E', E) G(E). \quad (11)$$

²To save on notation we suppress total momentum variables from the argument of Γ_Λ^μ .

We note that G^μ corresponds to the two-body Green function G with all possible insertions of a current [4]. In the five-point function $\eta G^\mu \eta$, neither the incoming nor outgoing two-body states are on the energy shell; by contrast, both these states are on the energy shell in $\bar{\psi} \Gamma^\mu \psi$. At the same time, such five-point Green functions are necessary ingredients for three-body currents where two-body subsystems are off shell. In this sense the use of $\eta G^\mu \eta$ for the RG approach to the current operator, is naturally related to the RG approach to the two-body interaction, where the cutoff independence of the fully off-shell two-body scattering amplitude is used [2].

1.1 Solution of the Current Operator RG Equation

We find, unambiguously, that the solution to Eq. (6) is given by³

$$\begin{aligned} O_\Lambda^\mu &= \eta(1 - V_\Lambda G_0 \lambda)^{-1} O_\Lambda^\mu (1 - \lambda G_0 V_\Lambda)^{-1} \eta \\ &= \eta [1 + V_\Lambda \lambda (E' - H_0 - V_\Lambda \lambda)^{-1}] O_\Lambda^\mu [1 + (E - H_0 - \lambda V_\Lambda)^{-1} \lambda V_\Lambda] \eta \end{aligned} \quad (12)$$

Unfortunately Eq. (12) cannot be used as a basis of a perturbation theory for O^μ because V , V_Λ and O^μ enter Eq. (12) not only at low momenta; moreover, only high momentum intermediate states are involved due to projectors λ . Nevertheless, Eq. (12) is useful for a range analysis of O_Λ^μ , showing that the long range part of O_Λ^μ is not affected by cutoff Λ - only the short range part is different from the one of O_Λ^μ .

2 Current Conservation

In order to avoid the well known problems of current conservation in theories with a finite cutoff, we consider the simple case where the starting cutoff is taken to infinity, $\bar{\Lambda} = \infty$. Then in the best case we will have the usual two-body Ward-Takahashi (WT) identities [9]

$$q_\mu G^\mu(E', E) = \Gamma_0^0 G(E) - G(E') \Gamma_0^0, \quad (13a)$$

$$q_\mu \Gamma^\mu(E', E) = G^{-1}(E') \Gamma_0^0 - \Gamma_0^0 G^{-1}(E) \quad (13b)$$

where Γ_0^0 is the zero'th component of the current operator Γ_0^μ of two non-interacting particles, and is specified for initial (final) total four-momentum $P = p_1 + p_2$ ($P' = p'_1 + p'_2$) and relative momentum \mathbf{p} (\mathbf{p}') as

$$\begin{aligned} \langle \mathbf{p}' | \Gamma_0^0(P', P) | \mathbf{p} \rangle &= i(2\pi)^3 [e_1 \delta(\mathbf{p}'_2 - \mathbf{p}_2) + e_2 \delta(\mathbf{p}'_1 - \mathbf{p}_1)] \\ &= i(2\pi)^3 [e_1 \delta(\mathbf{p}' - \mathbf{p} - \mathbf{q}/2) + e_2 \delta(\mathbf{p}' - \mathbf{p} + \mathbf{q}/2)] \end{aligned} \quad (14)$$

³The solutions in Refs. [3, 6, 7] are misquoted; however, the calculations are correct [8].

The WT identities of Eqs. (13) are damaged after the introduction of a finite momentum cutoff Λ : introducing the cutoff into Eq. (13b) gives [5]

$$q_\mu \eta \Gamma_\Lambda^\mu(E', E) \eta = \eta [G_0^{-1}(E') - V_\Lambda(E')] \eta \Gamma_0^0 [1 + \lambda G_0(E) V_\Lambda(E)] \eta - \eta [1 + V_\Lambda(E') G_0(E') \lambda] \Gamma_0^0 \eta [G_0^{-1}(E) - V_\Lambda(E)] \eta. \quad (15)$$

Although Eq. (15) is not a usual WT identity, it still leads to a conserved current:

$$q_\mu \bar{\psi}_{\mathbf{p}'} \eta \Gamma_\Lambda^\mu(E', E) \eta \psi_{\mathbf{p}} = 0. \quad (16)$$

It is important to note that the modified WT identity, Eq. (15), relates the reduced space effective current vertex Γ_Λ^μ , only to the corresponding effective potential V_Λ (the initial potential V is not involved), and that it enters the WT identity only with relative momenta below Λ for all physically interesting low energy transitions. These properties are indispensable for constructing a self-contained effective field theory (EFT) in the reduced momentum space [10]. The longitudinal part of the effective current operator is fully determined by just the effective potential. This is exactly the situation one has from the beginning, on the level of the EFT Lagrangian. The predictive power of the EFT with cutoff is the same as of the underlying EFT, i.e. as it would be had one used the EFT Lagrangian in the renormalization scheme.

References

- [1] K. G. Wilson and J. B. Kogut, *Phys. Rept.* **12**, 75 (1974).
- [2] M. C. Birse, J. A. McGovern, and K. G. Richardson, *Phys. Lett.* **B464**, 169 (1999).
- [3] S. X. Nakamura and S.-i. Ando, *Phys. Rev. C* **74**, 034004 (2006).
- [4] A. N. Kvinikhidze and B. Blankleider, *Phys. Rev. C* **60**, 044003 (1999).
- [5] A. N. Kvinikhidze and B. Blankleider, (2007), arXiv:0706.4277 [nucl-th].
- [6] S. X. Nakamura and S.-i. Ando, (2006), nucl-th/0611052.
- [7] S. X. Nakamura and A. Gärdestig, (2007), arXiv:0704.3757 [nucl-th].
- [8] S. X. Nakamura, Private communication.
- [9] W. Bentz, *Nucl. Phys.* **A446**, 678 (1985).
- [10] In preparation.

NEUTRON-NEUTRON SCATTERING LENGTH FROM THE REACTION

$$\gamma d \rightarrow \pi^+ nn$$

V. Lensky^{*,%,1}, V. Baru[%], E. Epelbaum^{*,#}, J. Haidenbauer^{*}, C. Hanhart^{*},
A. Kudryavtsev[%], U.-G. Meißner^{#,*}

^{*}Institut für Kernphysik, Forschungszentrum Jülich GmbH, D-52425 Jülich,
Germany

[%]Institute for Theoretical and Experimental Physics, 117259

B. Cheremushkinskaya 25 Moscow, Russia

[#]Helmholtz-Institut für Strahlen- und Kernphysik (Theorie), Universität
Bonn, Nußallee 14-16, D-53115 Bonn, Germany

Abstract

We discuss the possibility to extract the value of the neutron-neutron scattering length a_{nn} from experimental data on the reaction $\gamma d \rightarrow \pi^+ nn$. We provide a high accuracy calculation of the differential cross sections for this reaction within chiral perturbation theory. We argue that for properly chosen kinematics, the theoretical uncertainty of the method can be as low as 0.1 fm.

A precise determination of the neutron-neutron scattering length a_{nn} is important for an understanding of the effects of charge symmetry breaking in nucleon-nucleon forces. However, a direct measurement of a_{nn} in a scattering experiment is practically impossible at the moment due to the absence of a free neutron target, and the commonly used value for a_{nn} is obtained as a result of analysis of reactions where there are three particles in the final state, *e.g.* $\pi^- d \rightarrow \gamma nn$ or $nd \rightarrow pnn$. There is a large spread in the results for a_{nn} obtained by various groups. For instance, analyses of the reaction $nd \rightarrow pnn$ give significantly different values for a_{nn} : $a_{nn} = -16.1 \pm 0.4$ fm [1] and $a_{nn} = -18.7 \pm 0.6$ fm [2], whereas the value obtained from the reaction $\pi^- d \rightarrow \gamma nn$ is $a_{nn} = -18.5 \pm 0.3$ fm [3]. For the proton-proton scattering

¹E-mail address: v.lensky@fz-juelich.de

length, which is directly measured, the analysis gives $a_{pp} = -17.3 \pm 0.4$ fm [4] after correction for electromagnetic effects, which means that even the sign of $\Delta_a = a_{pp} - a_{nn}$ is not fixed.

Here we discuss a possibility to determine a_{nn} from differential cross sections in the reaction $\gamma d \rightarrow \pi^+ nn$. Our calculation is based on the recent work of Ref. [5], where the transition operator for the reaction $\gamma d \rightarrow \pi^+ nn$ was calculated in chiral perturbation theory (ChPT) up to order $\chi^{5/2}$ with $\chi = m_\pi/M_N$, and $m_\pi(M_N)$ being the pion (nucleon) mass. Half-integer powers of χ in the expansion arise from three-nucleon cuts. The results of Ref. [5] are in a good agreement with the experimental data for the total cross section. The main theoretical error is due to the uncertainty in the leading photoproduction multipole E_{0+} , which was fixed from the ChPT calculation [6], and is the only input parameter in the calculation. In order to estimate the theoretical uncertainty that arises from the nucleon-nucleon (NN) wave functions, we use NN wave functions constructed within the same ChPT framework—this is what a consistent field theory calls for. In our present analysis [7] we used next-to-next-to-leading order NN wave functions constructed in Ref. [8].

To examine the theoretical uncertainty for the extraction of a_{nn} , we employ our leading order calculation as a baseline result and quantify the uncertainty from the effects of the higher orders that we calculated completely.

We use in what follows the function F proportional to the five-fold differential cross section for unpolarized particles

$$F(p_r, \theta_r, \phi_r, \theta_\pi, \phi_\pi) = C \frac{d^5 \sigma(p_r, \theta_r, \phi_r, \theta_\pi, \phi_\pi)}{d\Omega_{\mathbf{p}_r} d\Omega_{\mathbf{k}_\pi} dp_r^2}, \quad (1)$$

where \mathbf{p}_r (\mathbf{k}_π) is the relative momentum of the two final neutrons (momentum of the final pion) in the center-of-mass frame, θ_r , ϕ_r (θ_π , ϕ_π) are the corresponding polar and azimuthal angles, respectively. We consider only shapes of cross sections and therefore the value of the dimensionful constant C is not important for our analysis. For the differential cross section F there are two characteristic regions that are important for our considerations: the region of quasi-free production (QF peak) at large p_r , where those production diagrams dominate that do not contain the NN interaction in the final or intermediate states, and the region with prominence of the strong NN final-state interaction (FSI peak) at small p_r .

The subject of our interest, a_{nn} , is a low-energy characteristic of neutron-neutron scattering and manifests itself in the momentum dependence of the cross section at small p_r . Therefore the influence of different values of a_{nn} is significant in the FSI peak and marginal in the QF peak. On the other

hand, we have shown [7] that the relative height of the QF and the FSI peaks changes if the effects of higher orders are included, whereas the individual shapes of these peaks change marginally. Therefore those angular configurations are to be preferred, where the quasi-free production is suppressed and thus the shape of the whole spectrum is only marginally influenced by higher orders. This takes place when \mathbf{p}_r is perpendicular to the initial photon momentum \mathbf{q}_γ .

To quantify the theoretical uncertainty, we use the function \mathcal{S} , defined as

$$\mathcal{S}(a_{nn}, \Phi) = \int_0^{p_{\max}} dp_r \left(F(p_r | a_{nn}^{(0)}, \Phi^{(0)}) - N(a_{nn}, \Phi) F(p_r | a_{nn}, \Phi) \right)^2 w(p_r), \quad (2)$$

where p_{\max} is the maximal value of p_r , and $F(p_r | a_{nn}, \Phi)$ is defined in Eq. (1). In the latter we refrained from showing the angular dependence in favor of the parametric dependence of F on a_{nn} as well as the multi-index Φ , which symbolizes the dependence of F on the chosen chiral order and the wave functions used. The weight function $w(p_r)$ allows us to suppress particular regions of momenta in the analysis. We may assume \mathcal{S} to be dimensionless; all dimensions can be absorbed into the constant C defined in Eq. (1).

The value $a_{nn}^{(0)}$ denotes the central value of a_{nn} (−18.9 fm) for which we estimate the theoretical uncertainty, whereas $\Phi^{(0)}$ corresponds to the baseline calculation, namely leading order with a certain choice of chiral wave functions (see Ref. [7]). The relative normalization $N(a_{nn}, \Phi)$ is fixed by demanding that \mathcal{S} gets minimized for any given pair of parameters a_{nn}, Φ ($\partial\mathcal{S}/\partial N = 0$). Thus, \mathcal{S} characterizes the mean-square deviation of the shape of the cross section from the baseline cross section $F(p_r | a_{nn}^{(0)}, \Phi^{(0)})$. This way to determine the theoretical uncertainty is in full analogy to the standard method of data analysis.

To quantify the theoretical uncertainty, we define Φ_{\max} as that chiral order and choice of wave function, where $\mathcal{S}(a_{nn}^{(0)}, \Phi_{\max})$ gets maximal:

$$\mathcal{S}(a_{nn}^{(0)}, \Phi_{\max}) = \max_{\Phi} \{ \mathcal{S}(a_{nn}^{(0)}, \Phi) \} . \quad (3)$$

Therefore $\mathcal{S}(a_{nn}^{(0)}, \Phi_{\max})$ provides an integral measure of the theoretical uncertainty of the differential cross section. Demanding that the effect of a change in the scattering length by the amount Δa_{nn} matches that by the inclusion of higher orders *etc.*, we identify Δa_{nn} as an uncertainty in a_{nn} . In terms of \mathcal{S} , Δa_{nn} is defined via

$$\mathcal{S}(a_{nn}^{(0)} + \Delta a_{nn}, \Phi^{(0)}) = \mathcal{S}(a_{nn}^{(0)}, \Phi_{\max}) . \quad (4)$$

Since the signal region is located at low p_r and, on the other hand, the theoretical uncertainty of the differential cross section is largest for large values of p_r , we use such weight functions $w(p_r)$ that suppress the contribution of large momenta. For instance, for $w(p_r) = \Theta(p^{\text{cut}} - p_r)$, and $p^{\text{cut}} = 30$ MeV, the value Δa_{nn} reduces to 0.07 fm. This is due to the fact that the signal changes only very little when a restriction to small values of p_r is applied. At the same time this procedure significantly reduces the value of the uncertainty $\mathcal{S}(a_{nn}^{(0)}, \Phi_{\text{max}})$. We found that the ideal value for p^{cut} is between 25 and 40 MeV. This translates into values of Δa_{nn} between 0.05 and 0.1 fm. The value of θ_π also has some impact on the theoretical uncertainty, however, in its whole parameter range the estimated uncertainty stays below 0.1 fm for $p^{\text{cut}} = 30$ MeV. We therefore argue that the reaction $\gamma d \rightarrow \pi^+ nn$ appears to be a good tool for the extraction of a_{nn} (perhaps as a complementary way to the reaction $\pi^- d \rightarrow \gamma nn$ [9]).

Acknowledgments

This work is part of the EU Integrated Infrastructure Initiative Hadron Physics Project under contract no. RII3-CT-2004-506078, and was supported by the DFG-RFBR grant no. 05-02-04012 (436 RUS 113/820/0-1(R)) and the DFG SFB/TR 16 "Subnuclear Structure of Matter". A. K. and V. B. acknowledge the support of the Federal Program of the Russian Ministry of Industry, Science, and Technology (grant no. 02.434.11.7091). E. E. acknowledges the support of the Helmholtz Association (contract no. VH-NG-222).

References

- [1] V. Huhn *et al.*, *Phys. Rev. Lett.* **85**, 1190 (2000); *Phys. Rev. C* **63**, 014003 (2000)
- [2] D. E. Gonzales Trotter *et al.*, *Phys. Rev. C* **73**, 034001 (2006)
- [3] C. R. Howell *et al.*, *Phys. Lett. B* **444**, 252 (1998)
- [4] R. B. Wiringa, V. G. J. Stoks, and R. Schiavilla, *Phys. Rev. C* **51**, 38 (1995)
- [5] V. Lensky, V. Baru, J. Haidenbauer, C. Hanhart, A. Kudryavtsev, and U.-G. Meißner, *Eur. Phys. J. A* **26**, 107 (2005)
- [6] V. Bernard, N. Kaiser and U.-G. Meißner, *Phys. Lett. B* **383**, 116 (1996)

- [7] V. Lensky, V. Baru, E. Epelbaum, C. Hanhart, J. Haidenbauer, A. Kudryavtsev and U.-G. Meißner, *Eur. Phys. J. A* **33**, 339 (2007)
- [8] E. Epelbaum, W. Glöckle and U.-G. Meißner, *Nucl. Phys. A* **747**, 362 (2005)
- [9] A. Gårdestig, D. R. Phillips, *Phys. Rev. C* **73**, 014002 (2006), and these proceedings

DECAYS OF NEW HEAVY MESONS CONTAINING STRANGE QUARKS AS HADRONIC MOLECULES

Valery E. Lyubovitskij, Amand Faessler, Thomas Gutsche
Institut für Theoretische Physik, Universität Tübingen,
Auf der Morgenstelle 14, D-72076 Tübingen, Germany

Abstract

We discuss a possible interpretation of $D_{s0}^*(2317)$, $D_{s1}(2460)$, $B_{s0}^*(5725)$ and $B_{s1}(5778)$ mesons as hadronic molecules. Using a phenomenological Lagrangian approach we calculate their strong, radiative and weak decays.

1 Introduction

Nowadays there is strong interest to study newly observed mesons and baryons in the context of a hadronic molecule interpretation [1]. As stressed for example in Ref. [2] the scalar $D_{s0}^*(2317)$ and axial $D_{s1}(2460)$ mesons could be candidates for a scalar DK and a axial D^*K molecule because of a relatively small binding energy of ~ 50 MeV. These states were discovered and confirmed just a few years ago by the Collaborations BABAR at SLAC, CLEO at CESR and Belle at KEKB [3]. In the interpretation of these experiments it was suggested that the $D_{s0}^*(2317)$ and $D_{s1}(2460)$ mesons are the P -wave charm-strange quark states with spin-parity quantum numbers $J^P = 0^+$ and $J^P = 1^+$, respectively. It is worth noting that the existing experimental information on the properties of the $D_{s0}^*(2317)$ and $D_{s1}(2460)$ mesons leaves quite a significant uncertainty in their possible assignment of $J^P = 0^+$ and $J^P = 1^+$ quark-antiquark states.

A new feature related to the molecular $D^{(*)}K$ structure of the $D_{s0}^*(2317)$ and $D_{s1}(2460)$ mesons is that the presence of $u(d)$ quarks in the $D^{(*)}$ and K mesons gives rise to a direct strong isospin-violating transitions $D_{s0}^* \rightarrow D_s \pi^0$ and $D_{s1} \rightarrow D_s^* \pi^0$ in addition to the decay mechanism induced by $\eta - \pi^0$ mixing as considered previously. In this paper we present the calculation of the strong, radiative and weak decays of $D_{s0}^*(2317)$ and $D_{s1}(2460)$ mesons in the the context of a hadronic molecule interpretation using a phenomenological Lagrangian approach [4]. Also we extend our formalism to the bottom sector: $B_{s0}^*(5725)$ and $B_{s1}(5778)$ states.

2 Approach: basic notions and results

In this section we briefly discuss the formalism for the study of the hadronic molecules. As example, we consider $D_{s_0}^{*\pm}(2317)$ mesons as a bound state of D and K mesons. Extension to other states is straightforward. First of all we specify the quantum numbers of the $D_{s_0}^{*\pm}(2317)$ mesons. We use the current results for the quantum numbers of isospin, spin and parity: $I(J^P) = 0(0^+)$ and mass $m_{D_{s_0}^*} = 2.3173$ GeV [3]. Our framework is based on an effective interaction Lagrangian describing the coupling between the $D_{s_0}^*(2317)$ meson and their constituents - D and K mesons:

$$\mathcal{L}_{D_{s_0}^*}(x) = g_{D_{s_0}^*} D_{s_0}^{*-}(x) \int dy \Phi_{D_{s_0}^*}(y^2) D(x + w_{KD}y) K(x - w_{DK}y) + \text{H.c.} \quad (1)$$

where D and K are the corresponding meson doublets, $w_{ij} = m_i/(m_i + m_j)$ is the kinematical variable, m_D and m_K are the masses of D and K mesons. The correlation function $\Phi_{D_{s_0}^*}$ characterizes the finite size of the $D_{s_0}^*(2317)$ meson as a $D K$ bound state and depends on the relative Jacobi coordinate y with x being the center of mass (CM) coordinate. In numerical calculations we employ the Gaussian form of $\Phi_{D_{s_0}^*}$. Its Fourier transform reads as $\tilde{\Phi}_{D_{s_0}^*}(p_E^2) = \exp(-p_E^2/\Lambda_{D_{s_0}^*}^2)$, where p_E is the Euclidean Jacobi momentum. Here $\Lambda_{D_{s_0}^*}$ is a size parameter, which parametrizes the distribution of D and K mesons inside the $D_{s_0}^*$ molecule. The coupling constant $g_{D_{s_0}^*}$ is determined by the compositeness condition [5, 6], which implies that the renormalization constant of the hadron wave function is set equal to zero: $Z_{D_{s_0}^*} = 1 - \Sigma'_{D_{s_0}^*}(m_{D_{s_0}^*}^2) = 0$, where $\Sigma'_{D_{s_0}^*}$ is the derivative of the $D_{s_0}^*$ meson mass operator. This condition was originally applied to the study of the deuteron as a bound state of proton and neutron [5]. Then it was extensively used in low-energy hadron phenomenology as the master equation for the treatment of mesons and baryons as bound states of light and heavy constituent quarks [6, 7].

Effective Lagrangian (1) is the starting point for the study of the decays of hadronic molecules. It defines the transition of the molecule into their constituents. Then we should specify the Lagrangian which describes the interaction of the constituents with external fields (hadrons and gauge bosons) and the diagrams which contribute to the matrix elements of physical processes. All further details can be found in Refs. [4]. Below in Tables 1 – 4 we display our results for the strong and radiative decay widths and their ratios $R_{D_{s_0}^*} = \Gamma(D_{s_0}^* \rightarrow D_s^* \gamma) / \Gamma(D_{s_0}^* \rightarrow D_s \pi)$ and $R_{D_{s_1}} = \Gamma(D_{s_1} \rightarrow D_s \gamma) / \Gamma(D_{s_1} \rightarrow D_s^* \pi)$, including extension to bottom sector, and compare them with the predictions of other approaches. Also we present our results for the leptonic decay constants: $f_{D_{s_0}^*} = 67.1$ MeV and $f_{D_{s_1}} = 144.5$ MeV.

Table 1: Strong decay widths in keV.

Approach	$\Gamma(D_{s0}^* \rightarrow D_s \pi)$	$\Gamma(D_{s1} \rightarrow D_s^* \pi)$
Nielsen 2005	6 ± 2	
Colangelo 2003	7 ± 1	7 ± 1
Guo 2006	8.69	11.41
Godfrey 2003	10	10
Fayyazuddin 2003	16	32
Bardeen 2003	21.5	21.5
Lu 2006	32	35
Wei 2005	39 ± 5	43 ± 8
Cheng 2003	10 – 100	
Ishida 2003	155 ± 70	155 ± 70
Azimov 2004	129 ± 43	187 ± 73
Lutz 2007	140	140
Our results	46.7 – 75	50.1 – 79.2

Table 2: Radiative decay widths in keV.

Approach	$\Gamma(D_{s0}^* \rightarrow D_s^* \gamma)$	$\Gamma(D_{s1} \rightarrow D_s \gamma)$
Fayyazuddin 2003	0.2	
Oset 2007	0.49	
Colangelo 2003	0.85 ± 0.05	
Close 2005	1	≤ 7.3
Lu 2006	≈ 1.1	0.6 – 2.9
Wang 2006	1.3 – 9.9	5.5 – 31.2
Azimov 2004	≤ 1.4	≈ 2
Bardeen 2003	1.74	5.08
Godfrey 2003	1.9	6.2
Colangelo 2005	4 – 6	19 – 29
Lutz 2007	< 7	$\simeq 43.6$
Ishida 2003	21	93
Our results	0.47 – 0.63	2.37 – 3.73

Table 3: Ratios

Approach	$R_{D_{s0}^*}$	$R_{D_{s1}}$
Fayyazuddin 2003	0.01	
Azimov 2004	≤ 0.02	0.01 - 0.02
Lutz 2007	< 0.05	$\simeq 0.31$
Bardeen 2003	0.08	0.24
Colangelo 2003	0.11 – 0.14	
Godfrey 2003	0.19	0.62
Ishida 2003	0.09 - 0.25	0.41 - 1.09
PDG 2007	≤ 0.059	0.44 ± 0.09
Our results	$\simeq 0.01$	$\simeq 0.05$

Table 4: Decay widths of $B_{s0}^*(5725)$ and $B_{s1}(5778)$ in keV.

Approach	$\Gamma(B_{s0}^* \rightarrow B_s \pi)$	$\Gamma(B_{s1} \rightarrow B_s^* \pi)$	$\Gamma(B_{s0}^* \rightarrow B_s^* \gamma)$	$\Gamma(B_{s1} \rightarrow B_s \gamma)$
Guo 2006	7.92	10.36		
Our results	52.9 – 87.1	53.5 – 87.3	1.54 – 2.04	1.04 – 1.22

Acknowledgments

This work was supported by the DFG (contracts FA67/31-1 and GRK683). This research is also the part of the EU Integrated Infrastructure Initiative Hadronphysics project under contract number RII3-CT-2004-506078 and President grant of Russia "Scientific Schools" No. 5103.2006.2.

References

- [1] J. L. Rosner, *Phys. Rev.* **D74**, 076006 (2006).
- [2] T. Barnes, F. E. Close and H. J. Lipkin, *Phys. Rev.* **D68**, 054006 (2003).
- [3] W. M. Yao *et al.* [Particle Data Group], *J. Phys.* **G33**, 1 (2006).
- [4] A. Faessler, T. Gutsche, V. E. Lyubovitskij and Y. L. Ma, *Phys. Rev.* **D76**, 014005 (2007); A. Faessler, T. Gutsche, S. Kovalenko and V. E. Lyubovitskij, *Phys. Rev.* **D76**, 014003 (2007); A. Faessler, T. Gutsche, V. E. Lyubovitskij and Y. L. Ma, arXiv:0709.3946 [hep-ph]; A. Faessler, T. Gutsche and V. E. Lyubovitskij, in progress.
- [5] S. Weinberg, *Phys. Rev.* **130**, 776 (1963); A. Salam, *Nuovo Cim.* **25**, 224 (1962).
- [6] G. V. Efimov and M. A. Ivanov, *The Quark Confinement Model of Hadrons*, (IOP Publishing, Bristol & Philadelphia, 1993).
- [7] M. A. Ivanov, M. P. Locher and V. E. Lyubovitskij, *Few Body Syst.* **21**, 131 (1996); M. A. Ivanov, V. E. Lyubovitskij, J. G. Körner and P. Kroll, *Phys. Rev.* **S56**, 348 (1997); A. Faessler, T. Gutsche, M. A. Ivanov, V. E. Lyubovitskij and P. Wang, *Phys. Rev.* **D68**, 014011 (2003); A. Faessler, T. Gutsche, M. A. Ivanov, J. G. Korner, V. E. Lyubovitskij, D. Nicmorus and K. Pumsa-ard, *Phys. Rev.* **D73**, 094013 (2006); A. Faessler, T. Gutsche, B. R. Holstein, V. E. Lyubovitskij, D. Nicmorus and K. Pumsa-ard, *Phys. Rev.* **D74**, 074010 (2006).

MENU 2007
11th International Conference
on Meson-Nucleon Physics and
the Structure of the Nucleon
September 10-14, 2007
IKP, Forschungszentrum Jülich, Germany

SCREENING IN THE BREMSSTRAHLUNG REACTIONS AND THE MAGNETIC MOMENT OF THE Δ RESONANCE.

A. I. Machavariani^{a,b,c}

^a Institut für Theoretische Physik der Universität Tübingen,
Tübingen D-72076, Germany

^b Joint Institute for Nuclear Research, Dubna, Moscow region 141980,
Russia

^c Tbilisi State University, University Str. 9, Tbilisi, Georgia

Abstract

Starting from the modified Ward-Takahashi identity for the on shell radiative πN scattering amplitude a generalization of the soft photon theorem approach is obtained for an arbitrary energy of an emitted photon [1]. The external particle radiation part of the $\pi N \rightarrow \gamma' \pi' N'$ amplitude is analytically reduced to the double Δ exchange amplitude with the intermediate $\Delta \rightarrow \gamma' \Delta'$ vertex. We have shown, that the double Δ exchange amplitudes with the intermediate Δ radiation is connected by current conservation with the corresponding part of the external particle radiation terms. Moreover according to current conservation the internal and external particle radiation terms with the $\Delta - \gamma' \Delta'$ vertex have a opposite sign i.e. they must cancel each other. Therefore we have a screening of the internal double Δ exchange diagram with the $\Delta - \gamma' \Delta'$ vertex by the external particle radiation. This enables to obtain a model independent estimation of the dipole magnetic moment of Δ^+ and Δ^{++} resonances μ_Δ through the anomalous magnetic moment of the proton μ_p as $\mu_{\Delta^+} = \frac{M_\Delta}{m_p} \mu_p$ and $\mu_{\Delta^{++}} = \frac{3}{2} \mu_{\Delta^+}$ in agreement with the values obtained from the fit of the experimental cross section of the $\pi^+ p \rightarrow \gamma' \pi^+ p$ reaction.

Considering pions and nucleons as bound systems of quarks in the conventional quantum field theory a generalized Ward-Takahashi identity for the on shell πN radiation amplitude is derived. This identity presents a general scheme of the current conservation which allows to obtain the model independent relations between the external and internal particle radiation amplitudes. The resulting equations for the external and internal particle

radiation amplitudes of the πN bremsstrahlung reaction have the same form as in formulation without the quark degrees of freedom [2]. Therefore current conservation and the Δ resonance pole position of the πN scattering amplitude determines analytically the dipole magnetic moment of the Δ resonances μ_Δ through the anomalous magnetic moment of the proton μ_p .

Present investigation of the πN radiation reaction based on the Ward-Takahashi identity for the on shell amplitudes. It generates the following model-independent relations:

(i) An amplitude of an arbitrary $a + b \longrightarrow \gamma' + f_1 + \dots + f_n$ ($n = 1, 2, \dots$) reaction fulfills the generalized current conservations

$$k'_\mu \langle out; f_1, \dots, f_n | \mathcal{J}^\mu(0) | a, b; in \rangle = \left[\mathcal{B}_{f_1 \dots f_n - ab} + k'_\mu \mathcal{E}_{\gamma' f_1 \dots f_n - ab}^\mu \right]_{on \text{ mass shell } f_1, \dots, f_n; a, b} = 0, \quad (I)$$

where $\mathcal{E}_{\gamma' f_1 \dots f_n - ab}^\mu$ corresponds to the complete set of Feynman (or three-dimensional time-ordered) diagrams with the photo-emission from each external particles and

$$\mathcal{B}_{f_1 \dots f_n - ab} = \sum_{m=1}^n (I_1 \tilde{\chi}_m^0 \dots I_{n-1} \tilde{\chi}_m^0) e_m \langle out; f_1 \dots f_{I_{n-1}} | J_m(0) | a, b; in \rangle - e_a \langle out; f_1 \dots f_n | J_a(0) | b; in \rangle - e_b \langle out; f_1 \dots f_n | J_b(0) | a; in \rangle \quad (II)$$

stands for amplitudes of the $a + b \longrightarrow f_1 + \dots + f_n$ reaction without γ' emission.

A special case of relation (I) is the external particle radiation terms.

Equation (I) and (II) are also valid for an arbitrary number of external photons. For instance, these equations can be used as current conservation for the pion photo-production reaction $\gamma A \rightarrow \pi' A'$, for Compton scattering $\gamma A \rightarrow \gamma' A'$ etc.

(ii) Current conservation (I) requires the existence of the internal particle radiation amplitude $\mathcal{I}_{\gamma' f_1 \dots f_n - ab}^\mu$ which ensures the validity of this condition

$$k'_\mu \mathcal{I}_{\gamma' f_1 \dots f_n - ab}^\mu = \mathcal{B}_{f_1 \dots f_n - ab}, \text{ or } k'_\mu \mathcal{E}_{\gamma' f_1 \dots f_n - ab}^\mu + k'_\mu \mathcal{I}_{\gamma' f_1 \dots f_n - ab}^\mu = 0. \quad (III)$$

This means that $\mathcal{E}_{\gamma' f_1 \dots f_n - ab}^\mu$ and $\mathcal{I}_{\gamma' f_1 \dots f_n - ab}^\mu$ have a different sign and they must be subtracted from each other. Thus we have a screening of the internal particle radiation amplitudes by the external one-particle radiation terms.

(iii) For the soft emitted photons $k' \rightarrow 0$ our approach immediately reproduces the low energy theorems for the bremsstrahlung reactions.

(iv) The external particle radiation part of the bremsstrahlung amplitude \mathcal{E}^μ contains the electromagnetic form factors of the external particles only in the tree approximation. This follows from the equal-time commutators which are a result of charge conservation. Thus we must modify the equal-time commutators between the Heisenberg operators of the external particles in order to apply the full electromagnetic form factors of pions and nucleons in the current conservation condition (I) or (III).

The above screening mechanism has been applied to the πN bremsstrahlung reaction with the leading double Δ exchange term. We have shown, that in the low energy region, where the electric quadrupole and the magnetic octupole momenta of Δ can be neglected, the intermediate Δ radiation radiation term is completely cancelled against the corresponding part of the external particle radiation amplitude. From this cancellation follows the normalization condition for the Coulomb monopole part of the $\Delta - \gamma'\Delta'$ vertex which allows to extract the Δ^+ and Δ^{++} dipole magnetic momenta $\mu_{\Delta^+} = G_{M1}(0) = \frac{M_\Delta}{m_N} \mu_p$ and $\mu_{\Delta^{++}} = \frac{3}{2} \mu_{\Delta^+} = 5.46e/2m_p$ or $\mu_{\Delta^{++}}/\mu_p \sim 1.95$. Our result for $\mu_{\Delta^{++}}$, based on the model independent current conservation condition, is in agreement with the prediction of the naive $SU(6)$ quark model for $\mu_{\Delta^{++}} = 2\mu_p = 5.58e/2m_p$ [3, 4], with the nonrelativistic potential model [11] $\mu_{\Delta^{++}} = 4.6 \pm 0.3$. and with extraction of $\mu_{\Delta^{++}}$ from the $\pi^+p \rightarrow \gamma\pi^+p$ experimental cross section in the framework of the low energy photon approach $\mu_{\Delta^{++}} = 3.6 \pm 2.0$ [6], $\mu_{\Delta^{++}} = 5.6 \pm 2.1$ [7] and $\mu_{\Delta^{++}} = 4.7 - 6.9$ [9]. Our result is larger as the predictions in the modified $SU(6)$ models [5, 12] and in the soft-photon approximation $\mu_{\Delta^{++}} = 3.7 \sim 4.9e/2m_p$ [8]. On the other hand our result is smaller as the values obtained in the framework of the effective meson-nucleon Lagrangian $\mu_{\Delta^{++}} = 6.1 \pm 0.5e/2m_p$ [15], in the effective quark model $\mu_{\Delta^{++}} = 6.17e/2m_p$ [16] and in the modified bag model $\mu_{\Delta^{++}} = 6.54$ [13].

The summary of the numerical estimations of the magnetic moments of Δ^+ and Δ^{++} resonances is given in table 1. In a number of approaches the magnetic moment of Δ is treated as an adjustable parameter in the radiative πN scattering which is determined using the most sensitive configurations to the $\Delta - \gamma\Delta$ vertex in the slow photon regime. Corresponding results obtained from the experimental cross sections of the $\pi^+p \rightarrow \gamma\pi^+p$ reaction are indicated in the table 1 with the index f . It must be emphasized, that only our approach and naive $SU(6)$ quark model gives an analytical form for μ_{Δ^+} and $\mu_{\Delta^{++}}$. But our result for μ_{Δ^+} is $M_\Delta/m_p \sim 1.31$ -times larger as $\mu_{\Delta^+} = \mu_p = 2.79e/2m_p$ in refs. [3, 16].

This screening mechanism can be observed in the cross sections of the πN bremsstrahlung reaction or in the $\gamma p \rightarrow \gamma\pi^0 p$ reaction by comparison of the

Table 1: Magnetic moments of Δ^+ and Δ^{++} in units of the nuclear magneton $\mu_N = e/2m_N$. The ref. in front of the index f indicates the theoretical model which is used to fit of the experimental data and to extract the magnetic moment μ_Δ .

MODELS	<i>This work</i>	<i>SU(6)</i>	<i>Potential and K-matrix appr.</i>	<i>Modified Bag</i>	<i>Soft photon theorem</i>	<i>Eff. πN Lagran.</i>	<i>Eff. quark</i>
μ_{Δ^+}	3.64	2.79 [3, 4]					2.79 [16]
$\mu_{\Delta^{++}}$	5.46	5.58 [3, 4] 4.25 [5] 4.41-4.89 [12]	6.9-9.7 [10]f 4.6 \pm 0.3 [11]f 5.6-7.5 [14]f	6.54 [13]	3.6 \pm 2.0 [6]f 5.6 \pm 2.1 [7]f 4.7-6.9 [9]f 3.7-4.9 [8]f	6.1 \pm 0.5 [15]f	6.17 [16]

cross sections in and outside the Δ resonance region. Due to the importance of the double Δ exchange diagram (Fig. 2B) one must have a different $1/k'$ behavior of the bremsstrahlung amplitude in and outside the Δ resonance region.

Next we have extended our work [1] of the analytic extraction of the dipole magnetic moments of the Δ resonances on the base of the modified Ward-Takahashi identities for the on shell πN bremsstrahlung amplitude [2]. This extension is done in the framework of the general field-theoretical approach, where particles are constructed as the bound (composite) states of quarks and gluons. The creation and annihilation operators of the composite pions and nucleons enables to construct the pion-nucleon radiation amplitude $\langle out; \mathbf{p}'_N \mathbf{p}'_\pi | J^\mu(0) | \mathbf{p}_\pi \mathbf{p}_N; in \rangle$ with on mass shell pions and nucleons in the asymptotic "in" and "out" states and $J^\mu(0)$ current operator of photon. Afterwards the Ward-Takahashi identity follows from the current conservation $k'_\mu \langle out; \mathbf{p}'_N \mathbf{p}'_\pi | J^\mu(0) | \mathbf{p}_\pi \mathbf{p}_N; in \rangle = 0$. Besides we have used the charge conservation which determines the equal-time commutation rules for the photon current operator and quark field operators. A model-independent connection between the external \mathcal{E}^μ and internal \mathcal{I}^μ particle radiation terms follows from the corresponding Ward-Takahashi identity which has the same form as in the formulation without quark-gluon degrees of freedom. In particular, \mathcal{E}^μ and \mathcal{I}^μ have the opposite sign because they satisfy the condition $k'_\mu \langle out; \mathbf{p}'_N \mathbf{p}'_\pi | J^\mu(0) | \mathbf{p}_\pi \mathbf{p}_N; in \rangle = k'_\mu \mathcal{E}^\mu + k'_\mu \mathcal{I}^\mu = 0$. Therefore after the same transformations as in [1] one obtains $\mathbf{D}^\mu(\Delta\Delta) = -\mathcal{I}^\mu(\Delta\Delta)$ Thus the internal particle radiation part $\mathcal{I}^\mu(\Delta\Delta)$ and the corresponding double Δ exchange part of the external particle radiation amplitude \mathcal{E}_2^μ cancel. In other words the same screening of the internal particle radiation terms by the external particle radiation diagrams must be observed in the bremsstrahlung

reactions in the formulations with and without quark degrees of freedom. This screening mechanism allows us determine the dipole magnetic moments of the Δ resonances via the magnetic moments of the external nucleons in the same way as it was done in our previous paper without quark degrees of freedom [1].

The general current conservation for the bremsstrahlung reactions with and without quarks were studied in the framework of the 3D time-ordered field theoretical approach.

References

- [1] A. I. Machavariani and A. Faessler. Preprint arXiv:nucl-th/0703080v2 23Mar 2007.
- [2] A. I. Machavariani and A. Faessler. (in preparation)
- [3] M. A.B. Beg, B.W. Lee and A. Pais, Phys. Rev. Lett. **13** (1964) 514,
- [4] H. Georgi. Lie Algebras in Particle Physics (Reading) 1982.
- [5] M. A.B. Beg, and A. Pais, Phys. Rev. **137** (1965) B1514,
- [6] M. M. Musakhanov, Sov. J. Nucl. Phys. **19** (1974) 319.
- [7] P. Pascual, and R. Tarrach, Nucl. Phys. **B134** (1978) 133.
- [8] D. Lin and M. K. Liou, Phys. Rev. **C43** (1991) R930
- [9] B. M. K. Nefkens at al., Phys. Rev. **D18** (1978) 3911.
- [10] L. Heller, S. Kumano, J. C. Martinez, and E. J. Moniz, Phys. Rev. **C35** (1987) 718.
- [11] A. M. Bosshard at al., Phys. Rev. **D44** (1991) 1962; C. A. Meyer at al., Phys. Rev. **D38** (1988) 754.
- [12] G. E. Brown, M. Rho, and V. Vento, Phys. Lett. **B97** (1980) 423.
- [13] M. I. Krivoruchenko, Sov. J. Nucl. Phys. **45** (1987) 109.
- [14] R. Wittman, Phys. Rev. **C37** (1988) 2075.
- [15] G. Lopez Castro and I. A. Marino, Nucl. Phys. **697** (2002) 440.
- [16] J. Franklin, Phys. Rev. **D66** (2002) 033010.

Dynamically generated resonances in two meson-one baryon systems

A. Martínez Torres¹, K. P. Khemchandani, E. Oset

Departamento de Física Teórica and IFIC, Institutos de Investigación de Paterna, Aptd. 22085, 46071 Valencia, Spain

Abstract

We study the systems of two mesons and one baryon with total strangeness $S = -1$ ($\pi\bar{K}N$, $\pi\pi\Sigma$, etc.) by solving Faddeev equations in the coupled channel approach. The calculations have been carried out for $L = 0$, leading to total spin parity $1/2^+$ for the three body system. The study resulted into dynamical generation of many low-lying Σ and Λ resonances which can be associated to those in the Particle Data Book.

1 Introduction

After the finding of a narrow peak in the invariant mass of the K^+n system [1], which was associated to a strangeness +1 pentaquark state, i.e., the θ^+ , a series of experimental groups reported findings of the same state but in the pK_S invariant mass (see discussion in [2] for example). Since the K_s is a mixed state of K^0 and \bar{K}^0 , the pK_S system can possess strangeness +1 or -1. Therefore, the narrow state found in the pK_S system could be, for example, a Σ^{*+} instead of a θ^+ . A search for a Σ or Λ resonance in this mass region is thus interesting.

In fact, there exist Λ and Σ resonances in this energy region but with poor or controversial status [3]. Also some of them seem to remain unexplained in terms of two-body dynamics, e.g., a study of the $K^-p \rightarrow \pi^0\pi^0\Lambda$ reaction in [4], where the $\Lambda(1520)$ gets dynamically generated and which explains the bulk of the data [5], fails to explain a bump in the $\Lambda(1600)$ region. Additionally, in [6] the excitation of the $\Sigma(1660)$ has been indicated in the data on the $K^-p \rightarrow \pi^0\pi^0\Sigma^0$ reaction. These findings naturally demand a study of three-body system(s) such as $\pi\pi\Sigma$, $\pi\pi\Lambda$, $\pi\bar{K}N$, etc.

¹E-mail address: Alberto.Martinez@ific.uv.es

2 Formalism

The first striking thought is that adding a π to the $\Lambda(1405)$, which is a resonance in the $\pi\Sigma$ system, one obtains a total mass ~ 1542 MeV. This is exactly the energy region where the narrow state in the pK_S system was found and where the $S=-1$ resonances are not well understood. The $\Lambda(1405)$ has been studied extensively using chiral dynamics [7–9] where it gets dynamically generated in the $\bar{K}N$ system and its coupled channels and its properties are well reproduced. The idea, thus, is to exploit this knowledge and extend it to a study of the three-body systems formed by adding a pion to all the combinations of 0^- mesons and $1/2^+$ baryons which couple to strangeness -1 . For the net charge zero, we end up with 22 coupled channels [10].

The input two-body t -matrices required to solve the Faddeev equations

$$T^i = t^i + t^i G [T^j + T^k], \quad i \neq j \neq k = 1, 3$$

have been calculated by solving the Bethe-Salpeter equation using the potentials obtained from chiral Lagrangians as in [7, 9]. The form of the potentials in this approach is such that it can be divided into an on-shell part, which depends only on the center of mass (C.M) energy of the interacting particles, and an off-shell part, which is inversely proportional to the propagator of the particle. This gives rise to three body forces [10] which have been found, in some approximations, to cancel with those originating directly from the chiral Lagrangian [10]. For a realistic case, the total contribution of three-body forces from all the sources has been found to be about 5% of the total on-shell contribution [10]. Hence, the calculations have been done using on-shell two body t -matrices. In this case, the terms with two successive interaction can be expressed as $t^i g^{ij} t^j$, with

$$g^{ij} = \left(\prod_{r=1}^D \frac{N_r}{2E_r} \right) \frac{1}{\sqrt{s} - E_i(\mathbf{k}_i) - E_j(\mathbf{k}_j) - E_k(\mathbf{k}_i + \mathbf{k}_j) + i\epsilon}$$

where \sqrt{s} is the total energy in the global CM system, $E_l = \sqrt{\mathbf{k}_l^2 + m_l^2}$ is the energy of the particle l , N_l is a normalization constant and D is the number of particles propagating between two interactions [10]. These terms correspond to the situation where there are no loops and hence the g^{ij} propagators depend on the on-shell variables only. The terms with three t -matrices involve a loop function of three particle propagators, e.g.

$$\int \frac{d^3q}{(2\pi)^3} t^1(s_{23}) g^{13}(\mathbf{q}) t^3(s_{12}(q)) g^{32}(\mathbf{q}) t^2(s_{13}) \quad (1)$$

where s_{13} , s_{23} are defined in terms of on-shell variables and $s_{12}(q)$ denotes the dependence of the t^3 -matrix on the loop variable. Therefore, t^1 and t^2 can be extracted out of the integral, but not t^3 . However, if we re-arrange the expression (1) as

$$t^1(s_{23}) \left[\int \frac{d^3q}{(2\pi)^3} g^{13}(\mathbf{q}) t^3(s_{12}(q)) g^{32}(\mathbf{q}) [g^{32}]^{-1} [t^3(s_{12})]^{-1} \right] t^3(s_{12}) g^{32} t^2(s_{13}) \quad (2)$$

where an identity expression depending on the on-shell variables, i.e., $[g^{32}]^{-1} [t^3(s_{12})]^{-1} t^3(s_{12}) g^{32}$, has been introduced, and define

$$G^{132} = \int \frac{d^3q}{(2\pi)^3} g^{13}(\mathbf{q}) t^3(s_{12}(q)) g^{32}(\mathbf{q}) [g^{32}]^{-1} [t^3(s_{12})]^{-1} \quad (3)$$

the equation (1) can be expressed as $t^1(s_{23}) G^{132} t^3(s_{12}) g^{32} t^2(s_{13})$. Now the $t^3(s_{12}) g^{32} t^2(s_{13})$ term depends only on the on-shell variables, the dependence of t^3 and g^{32} on the running variable has been taken care of when defining the G function. With this, the Faddeev equations can be written as [10]

$$T_R^{ij} = t^i g^{ij} t^j + t^i \left[G^{iji} T_R^{ji} + G^{ijk} T_R^{jk} \right] \quad i \neq j, j \neq k = 1, 3, \quad (4)$$

which are algebraic equations.

3 Results and discussion

We plot the squared \tilde{T}_R -matrix as a function of \sqrt{s} and $\sqrt{s_{23}}$ after subtracting the $t^i g^{ij} t^j$ terms ($\tilde{T}_R = \sum_{ij} T_R^{ij}$), which evidently do not have a resonance structure and just provide a background to the amplitudes.

In order to identify the nature of the resulting states, the T -matrix has been projected on the isospin base defined in terms of the total isospin of the three particles, I , and the total isospin of the two mesons, I_m .

In Fig.1 we show our results for the total isospin one, obtained by keeping the two pions in the isospin 2 configuration. We see two peaks: one at $\sqrt{s} = 1656$ MeV with a width of 30 MeV, which we correlate with the well-established $\Sigma(1660)$ [3], and another at 1630 MeV with a width of 39 MeV [10]. This is the first time when an evidence for the three body structure (two mesons and one baryon) of the $\Sigma(1660)$ has been found. We associate the peak at $\sqrt{s} = 1630$ MeV with the $\Sigma(1620)$, for which the experimental and partial wave analyzes results are listed separately, with a note saying that its not clear if there are one or more resonances in this energy region.

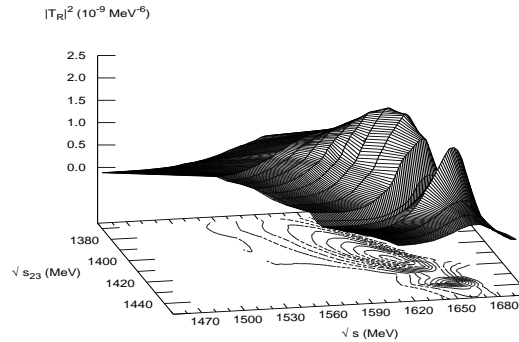


Figure 1: Two resonances in the $\pi\pi\Sigma$ amplitude in $I = 1$, $I_\pi = 2$ configuration.

Our calculations resulted also into dynamical generation of more strangeness $= -1$ resonances which are not well-understood, for example, $\Sigma(1560)$ with J^π unknown [3] and for which our results predict $J^\pi = 1/2^+$, $\Sigma(1770)$, which is listed as a one star resonance in [3]. Finally, in the isospin zero sector we find evidence for two peaks in $\Lambda(1600)$ region and one corresponding to $\Lambda(1810)$ [10].

References

- [1] T. Nakano *et al.*, *Phys. Rev. Lett.* **91**, 012002 (2003).
- [2] Q. Zhao and F. E. Close, *J. Phys.* **G31**, L1 (2005).
- [3] W.-M. Yao *et al.*, *J. Phys.* **G33**, 1 (2006).
- [4] L. Roca *et al.*, *Phys. Rev.* **C73**, 045208 (2006).
- [5] S. Prakhov *et al.*, *Phys. Rev.* **C69**, 042202 (2004).
- [6] S. Prakhov *et al.*, *Phys. Rev.* **C70**, 034605 (2004).
- [7] E. Oset and A. Ramos, *Nucl. Phys.* **A635**, 99 (1998).
- [8] D. Jido *et al.*, *Nucl. Phys.* **A725**, 181 (2003).
- [9] J. A. Oller and U. G. Meissner, *Phys. Lett.* **B500**, 263 (2001).
- [10] A. Martínez Torres, K. P. Khemchandani, E. Oset, arXiv:0706.2330 [nucl-th].

DEVELOPMENT OF A VERSATILE READOUT SYSTEM FOR HIGH RATE DETECTOR ELECTRONICS

M.C. Mertens^{*,1}, F. Hügging^{*}, J. Ritman^{*}, T. Stockmanns^{*}

^{*}Institut für Kernphysik, Forschungszentrum Jülich, D-52425 Jülich,
Germany

Abstract

During the research and design phase of new detector electronics, the development of a suitable test environment takes significant amount of time. Most existing systems are specifically designed for certain frontend electronics and cannot be reused for future developments.

Thus, our approach is to build a flexible test environment with state-of-the-art hardware, which can be reconfigured to support various frontend electronics. This is achieved by deploying a modular design concept, which is followed in both hardware and software. A key feature of the hardware platform is the modern FPGA (Virtex 4) and consequent separation of analog and digital parts of the readout. This is accompanied by a modular software framework written in C++ which declares different communication layers for easy hardware access. These levels of abstraction make it easy to add support for changed or completely new devices.

The system is presented and its key features are explained in detail.

1 Introduction

The availability of a suitable readout system for debugging is mandatory during the research and design of new detectors. The setup of such a readout system is required for all new detector developments. Due to the lack of a generic, easy to use readout solution, a custom system is usually designed specific to the projected needs.

Since no suitable readout system already existed for our purpose, this task also came up during development of the *Micro Vertex Detector* (MVD) for the upcoming $\overline{\text{P}}\text{ANDA}$ experiment (See Ref. [1]).

¹E-mail address: m.mertens@fz-juelich.de

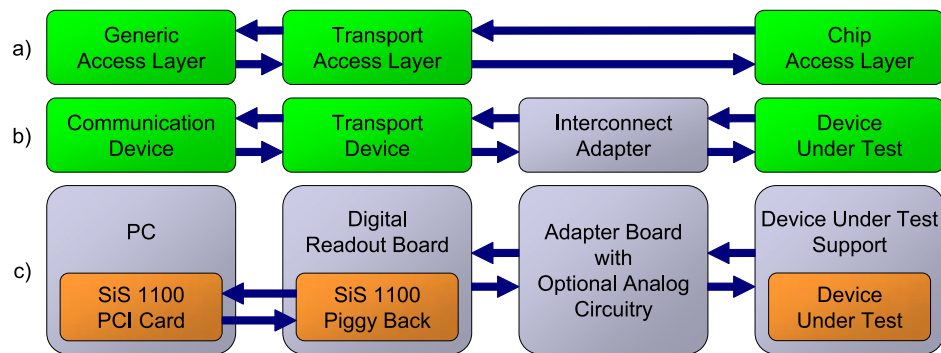


Figure 1: Readout chain. a) shows the abstract model of the software modules, b) the abstract model of the hardware devices and c) shows the actual setup.

One of our main goals is to design the readout system in a way which is generic enough to make it easily reusable, yet simple enough to be easy to use.

2 System Overview

The complete readout system features a modular design of hardware with a corresponding software framework which comprises the following parts (normal text indicates generic parts of the system, while *italics* denote application specific parts):

- Hardware
 - SiS 1100 PCI card (gbps optical link).
 - Digital readout board featuring Xilinx Virtex 4 LX60.
 - *Pinout adapter board.*
 - *Device under test support.*
- Software
 - SiS 1100 device driver (for Linux kernels 2.4 and 2.6).
 - C++ communication layer declarations and base definitions.
 - *Device specific communication protocol.*

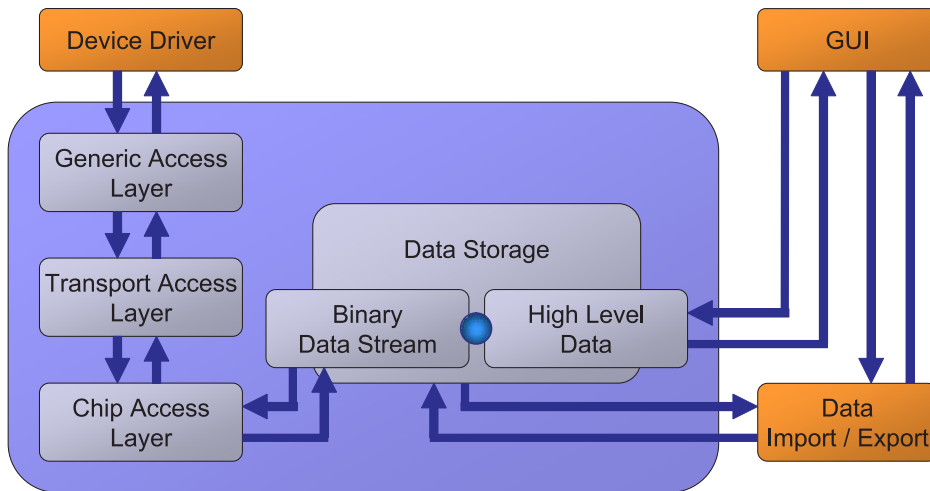


Figure 2: MVD readout framework.

The readout hardware strictly separates analog and digital parts of the readout. While the digital readout board itself contains purely digital components, any (optional) analog circuitry is implemented on an additional adapter board which connects the frontend support with the digital readout board. Its embedded FPGA can be reconfigured to support arbitrary communication protocols and I/O pinouts. The connection to the PC is realized via two SiS 1100 optical gigabit links, one is installed as PCI card in the PC, the other integrated as piggy back on the readout board. The interconnects of the actual setup are shown in Fig. 1c.

2.1 Software Environment

The software framework, in the following referred to as MRF², follows a modular design approach by implementing an abstract communication model which defines a hierarchy of communication layers, each layer corresponding to a single module in the software framework (compare Fig. 1a) respectively a single hardware device within the readout chain (Fig. 1b).

In addition to the definition of an abstract model, the MRF implements the base functionality for each communication layer where possible, so only device specific code has to be added. Another module of the MRF is a special data storage class which provides a common interface for transfer, storage

²MVD Readout Framework. This name originates from the initial motivation of building a generic readout system which is primarily intended to be used during development of the PANDA MVD.

and display of both configuration data and data returned by the device. Fig. 2 shows the interaction of individual MRF modules.

The MRF's communication model defines a hierarchy of three communication layers. Direct interaction is only allowed between adjacent layers, thus each layer uses only the functions provided by its direct lower layer for communication. This, in combination with the definition of the minimum functionality each layer has to provide, ensures that the specific implementations of all three layers are independent from each other and can be exchanged in a modular way.

The three modules implementing the communication layers are complemented by an additional module for data storage. All modules along with a functional description are summarized below.

- Generic Access Layer (GAL)
 - Lowest level communication layer.
 - Directly interacts with the communication device installed in the PC.
 - Provides register based read and write access.
- Transport Access Layer (TAL)
 - Uses GAL to communicate with the transport device.
 - Provides access to transport device features (*e.g.*, raw data transfer to the device under test (DUT), built-in diagnostic routines).
- Chip Access Layer (CAL)
 - Provides access to the connected device under test.
 - Functions in this layer implement DUT related commands (*e.g.*, configuration, initialization of data transfer).
 - Uses TAL to implement data transfer between control software and DUT.
- Data Storage Class
 - Display and configuration of device parameters as well as retrieval and display of data returned by the device.
 - Conversion between logical data entities (*e.g.*, integral values) and a device specific data stream.
 - Common interface to store data in a standard format for transmission via MRF functions.

2.2 Hardware Platform

The central component of the readout system is the *digital readout board* featuring a Xilinx XC4VLX60 Virtex 4 FPGA, DMA enabled data transfer at a rate of one gigabit per second to the PC via a SiS 1100 optical link, 32 LVDS I/O lines, four separately adjustable voltage lines and three differential clock lines. Its flexibility, resulting from the powerful FPGA, the freely configurable output lines, clock sources and supply voltages, allows to easily adapt this board for a wide variety of readout tasks.

Next part within the chain is the *pinout adapter board*. Its main purpose is to interface between the connectors of the digital readout board and those on the DUT support, but it can also be used for placing possibly needed analog circuitry (*e.g.* in order to connect to frontend chips with analog output lines). This board has to be designed specific to the actual application.

The *device under test* (typically a frontend chip) is then mounted on a corresponding support board (*DUT support*) which connects it to the pinout adapter board.

Compare Fig. 1c for an overview on the setup of the readout chain.

3 Conclusion

We have introduced a versatile readout system comprising reconfigurable hardware and a modular software framework. This approach makes it possible to deploy the readout system in various environments by reconfiguring the FPGA based hardware and adding the necessary application specific code to the generic software framework.

4 Acknowledgments

We would like to thank:

H. Kleines, P. Kämmerling, M. Ramm, P. Wüstner *et al.* (ZEL, FZ Jülich) for development and production of the digital readout board hardware and Linux kernel module driver for the SiS 1100 PCI card.

The $\bar{\text{P}}$ ANDA MVD subgroup at TU Dresden (K.-T. Brinkmann, R. Kliemt, T. Würschig, H.-G. Zaunick *et al.*) for fruitful discussions.

References

- [1] $\bar{\text{P}}$ ANDA Collab., *Technical Progress Report*, www-panda.gsi.de.

PARTIAL WAVE ANALYSIS OF πN SCATTERING WITH FIXED- t CONSTRAINTS

P. Metsä

Department of Physical Sciences
P.O. Box 64
FIN-00014 University of Helsinki
Finland

Abstract

We have finished the forward analysis of πN scattering and are proceeding with non-zero angles to achieve a full fixed- t constrained partial wave analysis. The outcome of the forward analysis is a set of coefficients of Pietarinen's expansion together with a full covariance matrix, which can be used for calculating some forward observables with proper error bars. As an illustration, we calculated some of the subthreshold expansion coefficients c_{n0}^{\pm} and their errors.

1 Introduction

As is well known, the experimental data alone is not enough to give a unique partial wave solution [1, 2], and some theoretical constraints are required. Besides the standard constraints of unitarity, crossing symmetry and isospin symmetry, we are incorporating the fixed- t analyticity constraint in the form of Pietarinen's expansions [3]

$$C^{\pm}(\nu, t) = C_N^{\pm}(\nu, t) + H^{\pm}(Z, t) \sum_{k=1}^N c_k^{\pm} \left[\frac{\alpha - \sqrt{\nu_T^2 - \nu^2}}{\alpha + \sqrt{\nu_T^2 - \nu^2}} \right]^k. \quad (1)$$

Here α is controlling the distribution of the experimental data along the unit circle of the conformal mapping and at $t = 0$ the threshold value $\nu_T = \mu$ (mass of the charged pion). The functions $H^{\pm}(Z, t)$ are taking care of the assumed asymptotic behaviour of the amplitudes and the nucleon pole terms $C_N^{\pm}(\nu, t)$ are treated separately. The coefficients c_k^{\pm} of Eq. (1) are fixed by fitting to the experimental data and to a partial wave solution of the earlier

iteration step. The simple form (1) of the expansion is valid for t -values from 0 to -0.52 GeV^2 , below that the s - and u -channel cuts are overlapping and they should be treated separately.

2 Input data

For forward analysis, we used all πN forward scattering data available on the Particle Data Group data bases [4] except a few data sets, which are listed in ref. [5]. In addition, we used the scattering lengths from pionic hydrogen experiments [6] and from a discrete phase shift analysis [7]. For the partial wave analysis, all elastic πN data available at the Durham HEP database [8] have been used. Before the analysis, the electromagnetic effects and delta splitting were removed from the data as described in [?, 5], and the corrected data were assumed to be purely hadronic and isospin invariant.

3 Forward Analysis

Our forward analysis is described in ref. [5]. As the end result of the analysis, the coefficients of the expansion (1) for $t = 0$ were obtained together with the full correlation matrix. These can be used to calculate any desired forward scattering observable with proper statistical errors, and as illustration, we give some of the subthreshold expansion coefficients c_{n0}^\pm in [5]. The shape of the solution is much better known than the overall normalization, and respectively the c_{00}^\pm coefficients can not be pinned down with the same accuracy as the higher ones. The coefficients c_{nm}^\pm with non-zero m are not accessible in a forward analysis. The asymptotic behaviour of the total cross sections, calculated from our solution, is presented in Figs. 1 and 2.

4 Upcoming PWA

After fixing the coefficients c_k of Eq. (1) for all desired t -values, the partial waves are found by fitting both to the expansions (1) and to the experimental data. In fitting, the χ^2 -function includes terms taking care of the unitarity constraint as well as a term measuring the deviation from the old solution. The latter is essential, because in order to smooth out the statistical fluctuations in the experimental data, the iteration should be carried out almost in "adiabatic" manner, *i.e.*, the iteration step size should be as small as the CPU time allows. For the same reason, the data are renormalized to the earlier iteration solution in every iteration step. The procedure is continued

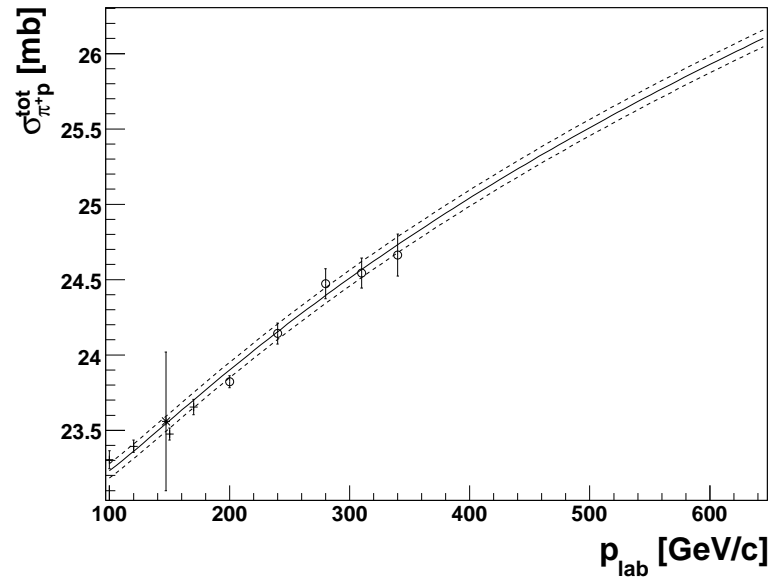


Figure 1: The asymptotic behaviour of $\sigma_{\pi+p}^{\text{Tot}}$. The Carroll 1976 data are marked with dashes, Brick 1982 data with asterisks and Carroll 1979 data with circles. All data points are available at PDG web site [4].

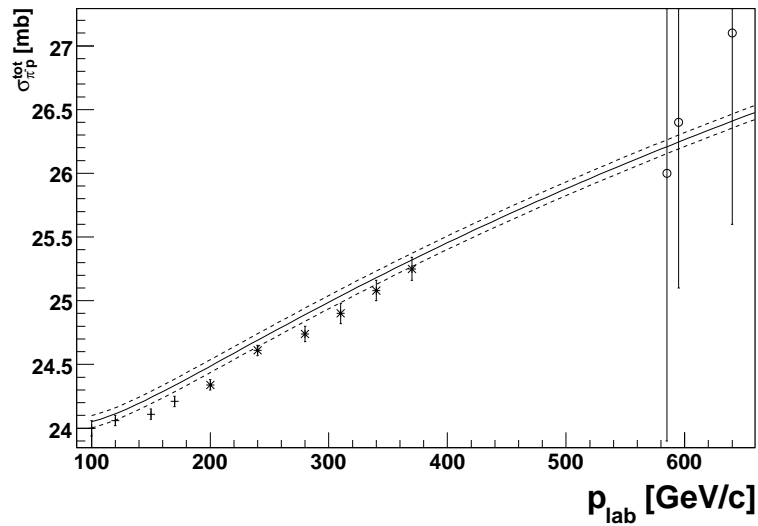


Figure 2: The asymptotic behaviour of $\sigma_{\pi-p}^{\text{Tot}}$. The Carroll 1976 data are marked with dashes, Carroll 1979 data with asterisks and Dersch 1999 data with circles. All data points are available at PDG web site [4].

iteratively until all parts will agree within a few percent. This kind of fitting procedure should be able to fix the phase shifts at least up to f -waves.

Acknowledgments

I gratefully acknowledge the financial support of the Magnus Ehrnrooth Foundation and the Waldemar von Frenckell Foundation. This work was supported in part by the EU Contract MRTN-CT-2006-035482, FLAVIANet.

References

- [1] G. Höhler, *Pion-Nucleon Scattering*, Landolt-Börnstein, edited by H. Schopper, Vol.I/9b2 (Springer, Berlin 1983).
- [2] A. Švarc, these proceedings.
- [3] E. Pietarinen, *Nuovo Cim.* **A12**, 522 (1972).
- [4] W.-M. Yao *et al.*, *J. of Phys.* **G33**, 1 (2006)
(<http://pdg.lbl.gov/2006/hadronic-xsections/hadron.html>).
- [5] P. Metsä, *Eur. Phys. J.* **A33**, 349 (2007) (arXiv:0705.4528 [hep-ph]).
- [6] H.-Ch. Schröder *et al.*, *Eur. Phys. J.* **C21**, 473 (2001).
- [7] V.V. Abaev, P. Metsä and M.E. Sainio, *Eur. Phys. J.* **A32**, 321 (2007)
(arXiv:0704.3167 [hep-ph]).
- [8] <http://durpdg.dur.ac.uk/HEPDATA/> .
- [9] B. Tromborg, S. Waldenstrøm and I. Overbø, *Phys. Rev.* **D15**, 725 (1977).

BRIDGING OVER p -WAVE π -PRODUCTION AND WEAK PROCESSES IN FEW-NUCLEON SYSTEMS WITH CHIRAL PERTURBATION THEORY

*S. X. Nakamura*¹

Theory Group, TRIUMF, 4004 Wesbrook Mall, Vancouver, BC V6T 2A3,
Canada

Abstract

We focus on a powerful aspect of chiral perturbation theory (χ PT) which provides us with a “bridge” over different reactions. For this purpose, we study a contact operator which contributes p -wave π -production and several weak processes. We fix the unknown coupling of the contact operator using a matrix element of a low-energy weak process ($pp \rightarrow de^+\nu_e$), and then calculate a partial wave amplitude (a_0) for the p -wave π -production ($pp \rightarrow pn\pi^+$). We find that the chiral operator including the contact term does not reproduce a_0 extracted from data, showing that the bridging over reactions with significantly different kinematics is not necessarily successful. We argue the importance of a specific higher order calculation. In order to gain an insight into a higher order calculation, we consider a higher order counter term, and find that the energy dependence of a_0 is then consistent with the data.

1 Introduction

Since the beginning of 1990’s, chiral perturbation theory (χ PT) has been extensively applied to few-nucleon system. An advantageous point inherent in χ PT is that it bridges over different reactions in a model-independent manner. Once couplings (the so-called low-energy constant, LEC) included in a chiral operator are fixed using data for one of the reactions, then the other reactions are predicted using the same operator. An interesting interaction in this context is, $\mathcal{L} = \tilde{d}N^\dagger S \cdot u N N^\dagger N$, with $f_\pi u_\mu = -\tau_a \partial_\mu \pi_a - \epsilon_{3ab} V_\mu \pi_a \tau_b + f_\pi A_\mu + \dots$. The spin operator is S , and the external vector (axial) current is

¹snakamura@triumf.ca

$V_\mu(A_\mu)$. The constant \tilde{d} is a LEC. This contact interaction contributes to the three-nucleon force, and several processes such as the p -wave π -production ($pp \rightarrow pn\pi^+$ [1]), and weak processes (tritium β -decay, $pp \rightarrow de^+\nu_e$ [2]). We can fix \tilde{d} using one of the above reactions, and predict the others.

Such a ‘‘bridging program’’ has been done in several works. One of them was done by Park *et al.* [2], where they fixed \tilde{d} using the experimental tritium β -decay rate, and performed a parameter-free calculation of the weak proton capture by a proton (or ^3He). Another work was due to Hanhart *et al.* [1]. The authors calculated a partial wave amplitude (a_0) for the p -wave π -production ($pp \rightarrow pn\pi^+$). Even though this work was not a fully consistent bridging program, they showed that the use of \tilde{d} fixed by three-nucleon observables consistently reproduces a_0 extracted from data [3].

In this work (see Ref. [4] for a full account), we investigate more seriously how reliably the bridging program, an important aspect of χPT , works. We believe that our investigation is important because we have sometimes seen an argument which supposes, without a serious test, that the bridging program works. For this purpose, we calculate a partial wave amplitude (a_0) for the p -wave π -production ($pp \rightarrow pn\pi^+$), with \tilde{d} fixed by a low-energy weak process. This obviously provides a stringent test of χPT , because the two reactions are strong and weak processes, and are quite different in kinematics.

2 Chiral p -wave π -production operator

We use the following π -production operators by referring to Ref. [1] in which the operators were derived using a counting rule based on an expansion parameter, $\sqrt{m_\pi/m_N}$; the nucleon (pion) mass is denoted by m_N (m_π). The leading order (LO, $\mathcal{O}(1)$) operator is the one-body direct production of the pion off the nucleon. Another LO mechanism we consider is the Δ -excitation followed by the π emission. In Ref. [1], the authors used the wave function which explicitly includes the Δ component, and considered the one-body operator which produces the pion with the Δ deexcited to the nucleon. Because we use nuclear wave functions with only the nucleonic degrees of freedom, we alternatively use a two-body operator in which the Δ is excited either by the π -exchange or by a contact interaction. Next we discuss next-to-leading order (NLO, $\mathcal{O}(m_\pi/m_N)$) terms: the recoil correction to the LO terms; a pion rescattering through the vertices whose strength are c_3 and c_4 , or through the Weinberg-Tomozawa term or its Galilean correction; a pion emission from the contact term whose coupling constant is \tilde{d} . The unknown coupling, \tilde{d} , will be determined in the next paragraph.

We start with a benchmark calculation. We employ the same axial current

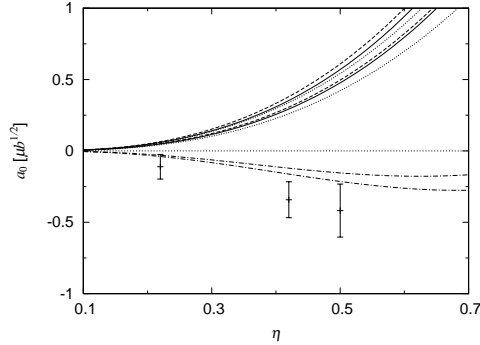


Figure 1: The amplitude a_0 for $pp \rightarrow pn\pi^+$. The upper (lower) solid, dashed and dotted curves correspond to $\Lambda = 500, 600$ and 800 MeV, respectively, $h_A = 2.10$ (2.68). The lower (upper) dash-dotted curve is obtained with $\tilde{d} = 0$, $\Lambda = 800$ MeV, $h_A = 2.10$ (2.68). Data are from Ref. [3].

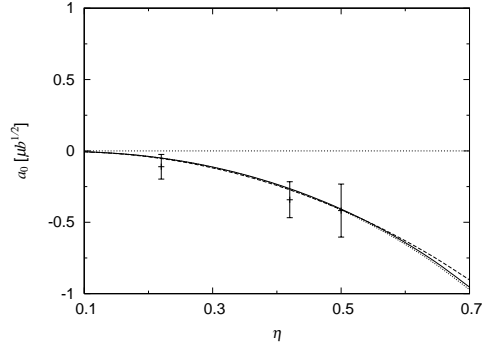


Figure 2: The amplitude a_0 for $pp \rightarrow pn\pi^+$. The chiral NLO π production operator plus the \tilde{e} -term is used. The solid, dashed and dotted curves correspond to $\Lambda = 500, 600$ and 800 MeV, respectively, and $h_A = 2.10$. The other features are the same as Fig. 1.

operator used in Ref. [2]. The \tilde{d} value in this operator has been fixed using the tritium β -decay rate. We calculate the Gamow-Teller matrix element for the low-energy $pp \rightarrow de^+\nu_e$ reaction and regard it as the benchmark. Our axial current is different from Ref. [2] in that we consider the Δ explicitly. We calculate the matrix element using our operator and fit \tilde{d} to the benchmark result. We use several combinations of the $\pi N\Delta$ coupling (h_A), the NN potential and the cutoff (Λ), and obtain the corresponding \tilde{d} values with a natural strength.

3 Result

With the chiral operator fixed in the previous section, we calculate a_0 for $pp \rightarrow pn\pi^+$. In Fig. 1, we present a_0 as a function of $\eta \equiv q_\pi^{max}/m_\pi$, where q_π^{max} is the maximum pion momentum. We used the CD-Bonn NN potential and two (three) choices of h_A (Λ). Our result is rather different from the data. For comparison, we show a_0 obtained without the \tilde{d} term. The inclusion of the \tilde{d} term makes the disagreement worse; even the sign of \tilde{d} fixed by the low-energy weak process is inconsistent with the data. We change the values of Λ , h_A and the NN potential, however, the situation of the disagreement does not change. This result shows that the bridging program among reactions with significantly different kinematics is not necessarily successful.

The failure of the bridging program is understandable if we recall the success of the chiral nuclear force which describes the NN scattering in a wide energy region. This is partly because the LECs have been fitted to data from the same energy region. In order to accurately describe the two reactions in different energy regions, data from the both energy region are necessary to fix the LECs. It is also expected that higher order terms are necessary to accurately reproduce the data from the wide energy region.

To explore, even roughly, a higher order calculation, we perform a simple extension of the previous calculation by adding $\mathcal{L}_{\text{CT}}^{(2)} = \tilde{e}N^\dagger \boldsymbol{\tau} \sigma \cdot \nabla \boldsymbol{\pi} N (N^\dagger \nabla^2 N + \text{h.c.})$ to the NLO operator. Now we have the two independent LECs: \tilde{d} and \tilde{e} . We fix these two LECs to reproduce two quantities: the benchmark result for the matrix element of $pp \rightarrow de^+\nu_e$; a_0 for $pp \rightarrow pn\pi^+$ at $\eta = 0.5$ from data. We obtain a set of \tilde{d} and \tilde{e} with a natural strength in this way. We calculate a_0 with the extended operator and show the result in Fig. 2. By construction, the calculated a_0 goes through the central value of the data at $\eta = 0.5$. We examined the dependence of a_0 on h_A , Λ and the NN potential, and found that the η dependence of a_0 is consistent with the data.

4 Summary

We determined \tilde{d} , the LEC of the contact term, using the weak process and then used it to predict a_0 for $pp \rightarrow pn\pi^+$. Through this work, we tried to explore the power of χ PT that enables us to bridge different reactions. Our prediction of a_0 with the NLO operator does not agree with the data. The result indicates that the bridging program between reactions with significantly different kinematics is not always successful.

Acknowledgments

The Natural Sciences and Engineering Research Council of Canada is thanked for financial support. TRIUMF receives federal funding via a contribution agreement through the National Research Council of Canada.

References

- [1] C. Hanhart *et al.*, *Phys. Rev. Lett.* **85**, 2905 (2000).
- [2] T.-S. Park *et al.*, *Phys. Rev. C* **67**, 055206 (2003).
- [3] R. W. Flammang *et al.*, *Phys. Rev. C* **58**, 916 (1998).

- [4] S. X. Nakamura, arXiv:0709.1239.

RENORMALIZATION GROUP ANALYSIS OF THE CHIRAL PION PRODUCTION OPERATOR FOR $NN \rightarrow d\pi$

S. X. Nakamura

Theory Group, TRIUMF
4004 Wesbrook Mall, Vancouver, BC
V6T 2A3, Canada

A. Gårdestig

Department of Physics and Astronomy
University of South Carolina
Columbia, SC 29208
U.S.A.

Abstract

We are interested in the consistency between the cutoff, chiral symmetry, and the power counting. For this purpose, we apply the Wilsonian renormalization group (RG) to an operator and then decrease the Wilsonian cutoff. As an example, we study the s -wave pion production operator for $NN \rightarrow d\pi$, derived in chiral perturbation theory. We find that the renormalized part of the RG effective operator is accurately absorbed by chiral counter terms of higher order with natural coefficients. Thus, the use of the (sharp) cutoff regularization does not require us to introduce chiral-symmetry-breaking counter terms, at least in the case of the $NN \rightarrow d\pi$ reaction.

1 Introduction

Chiral symmetry and its spontaneous breaking are important low-energy properties of QCD, and therefore it is natural to hope to incorporate them into the description of nuclear systems. A promising solution is to employ the chiral perturbation theory (χ PT), which has been successfully used in nucleonic systems since the beginning of the 1990's. The nuclear operators are derived from a chiral Lagrangian following a counting rule. The transition matrix element is evaluated by convoluting the operator with nuclear wave functions. In the evaluation, a cutoff is usually applied to the operator, suppressing high momentum modes. The question then arises whether

this regulated operator is still consistent with chiral symmetry. If not, we may need to introduce a chiral-symmetry-violating operator to recover the symmetry, or find another regularization scheme, which is consistent with the symmetry. Although it is conventionally supposed that effects of the high momentum modes are captured by higher order chiral counter terms, it is important to confirm this. We consider a renormalization group (RG) analysis to be useful for this purpose.

In this work, we apply the Wilsonian Renormalization group (WRG) equation to the s -wave pion production in $NN \rightarrow d\pi$ as described by χ PT [1]. The cutoff is reduced using the WRG equation, and the operator runs as a result. In the next step, we try to reproduce the RG low-momentum operator using the starting operator plus chiral counter terms of higher order. If the chiral symmetry is not violated by the cutoff, the renormalized part of the operator should be accurately captured by the chiral counter terms.

2 Wilsonian RG equation for operator

At first, we discuss why we use the WRG equation to reduce the cutoff. This is based on a consistency with the construction of an effective Lagrangian. An effective Lagrangian can be obtained formally via a path integral formulation based on the Lagrangian of the underlying, more fundamental theory. One then integrates out the high energy degrees of freedom. When integrating out the high momentum states of the nucleon in the heavy-baryon χ PT Lagrangian, we can also use the path integral. This procedure is equivalent to solving the WRG equation derived below. One of the present authors derived the WRG equation for the NN interaction in this way in Ref. [2]. The WRG equation for a transition operator (π production operator in our case) can also be derived in essentially the same way.

Here we outline a simpler derivation of the WRG equation following Ref. [3] in which a detailed account is given (Appendix A). We start with a matrix element in which the transition operator is defined in a model space spanned by plane wave states of the two-nucleon system. The maximum magnitude of the relative momentum in this model space is given by the cutoff Λ . We differentiate the matrix element with respect to Λ and impose the renormalization condition that the matrix element is invariant under cutoff changes. This gives the WRG equation for the low-momentum transition operator. (For explicit expressions, see Refs. [3,4].) This differential equation is solved, and the solution in integral form is actually the same as the effective operator in the Bloch-Horowitz formalism.

3 Results

We start with the chiral NLO s -wave pion production operator for the $NN \rightarrow d\pi$ reaction [1]. Using the integral form of the WRG equation, we calculate the RG low-momentum operator for $\Lambda = 500$ MeV, using the CD-Bonn NN -potential. We employ near threshold kinematics, *i.e.*, $\eta = 0.1$, where $\eta = q/m_\pi$ is the emitted pion momentum divided by the pion mass. We use the chiral counter terms of higher order {see Eq. (7) of Ref. [4] for expressions} to simulate the renormalized part of the low-momentum operator; the lowest chiral counter terms are NNLO.

The running of the radial part of the ${}^3P_1 \rightarrow {}^3S_1$ transition operator (diagonal matrix elements) is shown in Fig. 1. The solid line is the starting NLO chiral operator (before RG running). After the RG running, we obtain the RG low-momentum operator shown by the dashed line ($\Lambda = 1000$ MeV), dotted line ($\Lambda = 750$ MeV), and dash-dotted line ($\Lambda = 500$ MeV). We parameterize this low-momentum operator using the NLO operator plus the counter terms, omitting the kink part when fitting the counter terms. In Fig. 2 we show the simulation of the low-momentum operator using the NLO operator plus the counter terms. The dash-dotted line is the starting NLO chiral operator. The dashed line contains the NLO operator plus the lowest counter term. The dotted line contains the additional terms of one higher order. The renormalized part (the difference between the solid and dash-dotted lines) is thus accurately captured by the higher order counter terms of natural strength. As for the off-diagonal matrix elements, we find a similar trend in the simulation using the counter terms. Our result allows us to conclude that, to the level of precision (and order) we are working, the $NN \rightarrow d\pi$ calculation is renormalized without including a chiral-symmetry-violating counter term. However, this outcome does not necessarily mean that the (sharp) cutoff regularization does not generate *any* chiral-symmetry-violating operator. Nevertheless, we could still claim that there is no *practical* ground for introducing a chiral-symmetry-violating operator for this process.

4 Summary

We have studied what happens to the pion production operator when a cutoff is reduced. In particular, we are interested in the possibility that the running with cutoff requires us to introduce a chiral-symmetry-violating interaction. We started with the chiral NLO operator [1] for s -wave pion production in $NN \rightarrow d\pi$ and reduced a cutoff by using the WRG equation. After the RG running, we parameterized the RG low-momentum operator by a

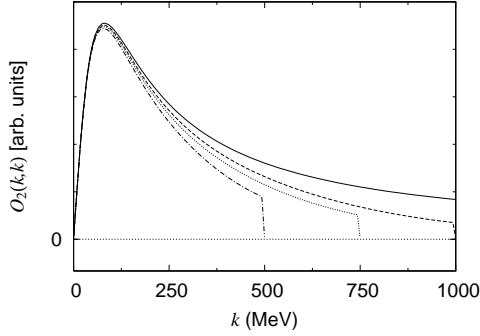


Figure 1: Running of the π production operator for $NN \rightarrow d\pi$ ($\eta = 0.1$, ${}^3P_1 \rightarrow {}^3S_1$). Solid line indicates the starting chiral NLO operator. RG running results in the low-momentum operators for $\Lambda = 1000$ MeV (dashed line), 750 MeV (dotted line), and 500 MeV (dash-dotted line).

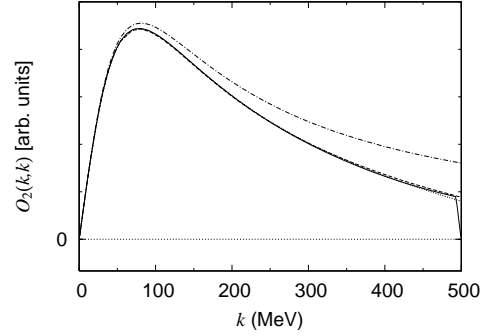


Figure 2: The RG low-momentum pion production operator ($\Lambda = 500$ MeV, $\eta = 0.1$, solid line) is simulated by the original NLO operator (dash-dotted line) plus a contact term with one nucleon derivative (dashed line). The dotted line has additional contact terms with three derivatives.

chiral expansion including higher-order counter terms, which are expected to absorb contributions from the high momentum states that were integrated out. We found that the expansion is indeed accurate, with the LECs of natural strength. Therefore, we see no evidence that the running with the cutoff reduction generates chiral-symmetry-violating interactions.

Acknowledgments

This work was supported by the Natural Sciences and Engineering Research Council of Canada and the U. S. National Science Foundation through grant PHY-0457014.

References

- [1] V. Lensky *et al.*, *Eur. Phys. J.* **A27**, 37 (2006).
- [2] S. X. Nakamura, *Prog. Theor. Phys.* **114**, 77 (2005).
- [3] S. X. Nakamura *et al.*, *Phys. Rev. C* **74**, 034004 (2006).
- [4] S. X. Nakamura *et al.*, arXiv:0704.3757.

STRANGENESS PHOTOPRODUCTION WITH CBELSA/TAPS

M. Nanova^{*1}, J. C. S. Bacelar⁸, B. Bantes², O. Bartholomy³,
D. Bayadilov^{3, 4}, R. Beck³, Y.A. Beloglazov⁴, R. Castelijns^{8, a},
V. Crede⁵, H. Dutz², A. Ehmans³, D. Elsner², K. Essig³, R. Ewald²,
I. Fabry³, H. Flemming^{6, b}, K. Fernet-Ponse², M. Fuchs³, Ch. Funke³,
R. Gothe^{2, c}, A.B. Gridnev⁴, R. Gregor¹, E. Gutz³, S. Höffgen²,
P. Hoffmeister³, I. Horn³, I. Jaegle⁷, J. Junkersfeld³, H. Kalinowsky³,
S. Kammer², V. Kleber², Frank Klein², Friedrich Klein², E. Klempt³,
H. Koch⁶, M. Konrad², B. Kopf⁶, M. Kotulla¹, B. Krusche⁷, M. Lang³,
J. Langheinrich^{2, 6}, H. Löhner⁸, I.V. Lopatin⁴, J. Lotz³, S. Lugert¹,
H. Matthäy⁶, D. Menze², T. Mertens⁷, V. Metag¹, C. Morales²,
D.V. Novinski⁴, R. Novotny¹, M. Ostrick^{2, e}, L. M. Pant^{1, f}, H. van
Pee³, M. Pfeiffer¹, A. Roy^{1, g}, A. Radkov⁴, S. Schadmand^{1, a},
Ch. Schmidt³, H. Schmieden², B. Schoch², S. Shende⁸, V. Sokhoyan³,
A. Süle², V. V. Sumachev⁴, T. Szczepanek³, U. Thoma^{3,1}, D. Trnka¹,
R. Varma^{1, g}, D. Walther^{2,3}, Ch. Weinheimer^{3, h}, Ch. Wendel³
(The CBELSA/TAPS Collaboration)

¹II. Physikalisches Institut, Universität Gießen, Germany

²Physikalisches Institut, Universität Bonn, Germany

³Helmholtz-Institut für Strahlen- u. Kernphysik, Universität Bonn, Germany

⁴Petersburg Nuclear Physics Institute, Gatchina, Russia

⁵Department of Physics, Florida State University, Tallahassee, FL, USA

⁶Institut für Experimentalphysik I, Universität Bochum, Germany

⁷Physikalisches Institut, Universität Basel, Switzerland

⁸Kernfysisch Versneller Instituut, Groningen, The Netherlands

^aPresent address: Forschungszentrum Jülich, Germany

^bPresent address: GSI, Darmstadt, Germany

^cPresent address: University of South Carolina, Columbia, SC, USA

^dPresent address: KVI, Groningen, The Netherlands

^ePresent address: Universität Mainz, Germany

^f Present address: BARC, Mumbai, India

^g Present address: I.I.T. Powai, Mumbai, India

^hPresent address: Universität Münster, Germany

^{1*}E-mail address: Mariana.Nanova@physik.uni-giessen.de

Abstract

The exclusive measurement of the reactions $\gamma p \rightarrow K^0 \pi^0 \Sigma^+(1189)$ and $\gamma p \rightarrow K^{*0} \Sigma^+(1189)$ with $p 4\pi^0$ final states is presented. The experiment has been performed at the tagged photon facility ELSA (Bonn) in the beam energy range up to 2.5 GeV. The Crystal Barrel and the photon spectrometer TAPS were combined to a detector system providing an almost 4π coverage of the geometrical solid angle, very well suited for studying photoproduction with multi-photon final states. Differential and total cross sections are reported and discussed. In addition, our analysis provides information about two higher lying Σ^* states with masses 1385 MeV and 1660 MeV, respectively.

1 Introduction

The internal structure of the nucleon appears in the rich pattern of baryon resonances. The number of known, experimentally observed resonances is much smaller than predicted from theory. This is often referred to as the so-called 'missing' resonance problem. Some of the resonances are predicted to decay into final states containing strange particle pairs [1]. Moreover, higher mass nucleon resonances could favor decay into $K^* \Sigma$. Therefore K^* vector meson photoproduction can be used to search for nucleon resonances which couple strongly to the $K^* Y$ channel, where Y denotes a hyperon [2]. The photoproduction of K^* shares elements in common with other strangeness production reactions, such as $\gamma p \rightarrow K \Lambda$ and $\gamma p \rightarrow K \Sigma$ or $\gamma p \rightarrow \pi K \Sigma$, which proceed via to N^* and/or Δ^* resonance excitations with different couplings [3]. The investigation of higher lying hyperon Σ^* resonances will provide more information about baryon resonances in meson-hyperon decay channels.

2 Experiment and Analysis

The reactions $\gamma p \rightarrow K^0 \pi^0 \Sigma^+$ and $\gamma p \rightarrow K^{*0} \Sigma^+$ have been measured from threshold up to $E_\gamma = 2.5$ GeV with the CB/TAPS setup at ELSA in Bonn. The K^0 has been detected by the decay $K^0 \rightarrow K_{short}^0 \rightarrow \pi^0 \pi^0$, the K^{*0} by $K^{*0} \rightarrow \pi^0 K^0$, the Σ^+ by $\Sigma^+ \rightarrow p \pi^0$. For both reactions we have a proton and eight photons in the final state; all particles have been detected. Because of the insufficient proton energy information a kinematic fit with missing proton and 4 pions as constraints has been applied. An important competing channel, leading to the same final state is $\gamma p \rightarrow p \pi^0 \eta \rightarrow p 4\pi^0$. Those events in which three π^0 's are produced via the decay of an η meson

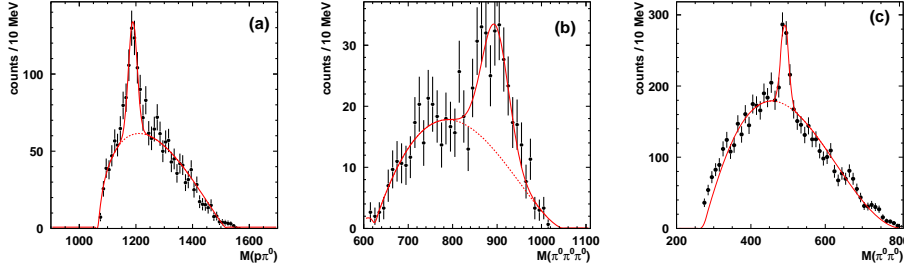


Figure 1: Invariant mass distribution $p\pi^0$ (a) with a peak at 1189 MeV, the $\pi^0\pi^0\pi^0$ invariant mass (b), with a peak at 896 MeV and the $\pi^0\pi^0$ invariant mass spectrum (c), with a peak at 496 MeV.

with an additional π^0 have been selected and removed from the data sample. Subsequently, all invariant mass combinations of $p\pi^0$ versus $\pi^0\pi^0\pi^0$ have been filled in a two dimensional histogram. The spectra show clear peaks at 1189 MeV and 892 MeV, corresponding to Σ^+ and K^{*0} (Fig. 1a,b). The $\pi^0\pi^0$ invariant mass from six different combinations is shown in Fig. 1c. All combinations have been taken into account, and a cut on the $p\pi^0$ invariant mass between 1160 and 1220 MeV is used to reduce the background. The peak at 496 MeV corresponds to K^0 mesons from the K^{*0} decay emitted in the reaction $\gamma p \rightarrow K^{*0}\Sigma^+$ and also in other reactions with the same final states. The higher lying hyperon states Σ^* contribute to K^0 production via: $\gamma p \rightarrow K^0\Sigma^* \rightarrow K^0\pi^0\Sigma^+ \rightarrow (\pi^0\pi^0)(\pi^0 p\pi^0)$ with the same final states, where Σ^* could be $\Sigma^*(1385)$ or $\Sigma^*(1660)$ decaying into $\pi^0\Sigma^+$. The reactions on the proton with neutral final states like $\gamma p \rightarrow K^0\pi^0\Sigma^+$ exclude Λ 's. Requiring the invariant mass $M(p\pi^0)$ to be close to the $\Sigma^+(1189)$ mass, namely between 1160-1220 MeV, figure 2 shows a plot of $M(p\pi^0\pi^0)$ versus $M(\pi^0\pi^0)$ for incident photon energies of 2000-2300 MeV. The verticle line around 500 MeV on the x-axis is due to K^0 mesons (figure 1c). The projection on the y-axis, with a cut on $M(\pi^0\pi^0)$ between 470 and 520 MeV, which is $\mp 2.5\sigma$ cut on the K^0 invariant mass, is fitted by a combination of polynomial background and two Gaussian functions. Two peaks at 1385 MeV and at 1630 MeV are observed.

3 Results and Conclusions

In the energy range 1500-1850 MeV where the Σ^+ production occurs through the channel $\gamma p \rightarrow K^0\pi^0\Sigma^+$ the differential cross section is very flat. These measurements are in good agreement with the theoretical prediction of [9]

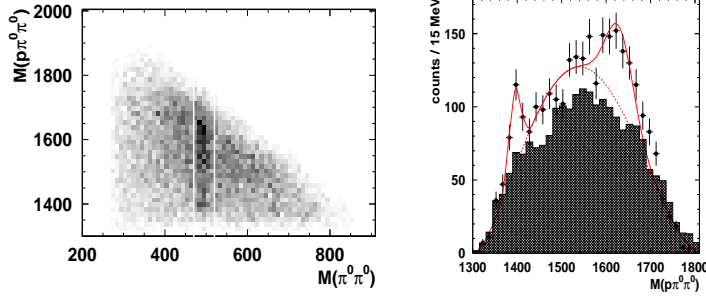


Figure 2: (left) The invariant mass $M(p\pi^0\pi^0)$ versus the invariant mass $M(\pi^0\pi^0)$. (right) The projection onto $M(p\pi^0\pi^0)$ axis with the two peaks at 1385 MeV and at 1630 MeV. The fit function is composed of a polynomial background with two Gaussian functions. The width (σ) is 13 MeV and 40 MeV, respectively. The shadow area represents the background in the sideband region of K^0 .

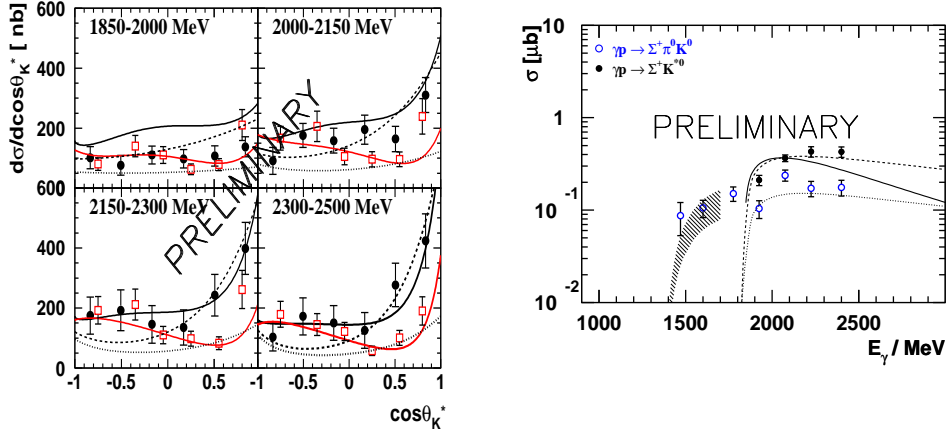


Figure 3: left: Differential cross section for $\gamma p \rightarrow K^{*0}\Sigma^+$ (full circles). The solid curves represent the theoretical calculations for the $\gamma p \rightarrow K^{*0}\Sigma^+$ reaction in [4, 5]. The dashed and dotted curves denote the calculations in [6] with κ meson exchange in the t -channel. The empty squares are the CLAS experimental data [7], corrected in [8], and the theoretical curves as published in [5]. right: Total cross sections for $\gamma p \rightarrow K^0\pi^0\Sigma^+$ (empty circles) and $\gamma p \rightarrow K^{*0}\Sigma^+$ (filled circles). The shadow area represents a band for the predicted values from the theoretical calculations in [9]. The solid curve denotes the calculations in [4]. The dashed and dotted curves are from the theoretical calculations in [6] with κ meson exchange in the t -channel

based on the model of [3], which is a genuine prediction of a chiral dynamical calculation based on the dominance of the $\Delta(1700)$ in the entrance channel, plus the coupling of this resonance to $K\Sigma^*(1385)$. The differential cross section for the reaction $\gamma \rightarrow K^{*0}\Sigma^+$ shows a rise in the forward direction when plotted vs the K^{*0} production angle (fig. 3). Production of K^{*0} meson via t -channel exchange seems to play an important role in the reaction dynamics. These results are consistent with the theoretical prediction of [4]. $\Sigma^*(1385)$ and $\Sigma^*(1660)$ have been observed in the $\Sigma^+\pi^0$ decay channel. On the basis of existing data we estimate the production cross section of these states to be of the order of few hundred nanobars. Further experiments are required to study the higher lying Σ^* states.

Acknowledgments

This work is supported by the Deutsche Forschungsgemeinschaft (DFG) within the SFB/TR16.

References

- [1] S. Capstick and W. Roberts, *Prog. Part. Nucl. Phys.* **45**, 241 (2000).
- [2] S. Capstick and W. Roberts, *Phys. Rev. D* **57**, 4301 (1998).
- [3] M. Döring, E. Oset, D. Strottman, *Phys. Rev. C* **73**, 045209 (2006).
- [4] Q. Zhao, J. S. Al-Khalili, C. Bennhold, *Phys. Rev. C* **64**, 052201 (2001).
- [5] Q. Zhao, updated quark model predictions for K^* photoproduction, *private communication*.
- [6] Y. Oh and H. Kim, *Phys. Rev. C* **74**, 015208 (2006).
- [7] I. Hleiqawi et al., CLAS Collaboration, *Phys. Rev. C* **75**, 042201 (2007).
- [8] I. Hleiqawi et al., CLAS Collaboration: *arXiv*: nucl-ex/0701036v3.
- [9] M. Döring, E. Oset, D. Strottman, *Phys. Lett. B* **639**, 59-67 (2006).

PRESENT UNDERSTANDING OF SPIN FILTERING EXPERIMENTS

M. Nekipelov for the PAX collaboration

Institut für Kernphysik
Forschungszentrum Jülich
Jülich, D 52428, Germany

Abstract

An overview on the present understanding of the spin filtering methods is given, and the planned measurements on spin filtering at the COSY ring with protons are described.

1 Introduction

Polarized antiprotons provide access to a wealth of single- and double-spin observables, from which outstanding physics questions like “What is the transversity distribution of the valence quarks in the proton?” may be answered. Interest in the polarization of antiprotons has recently been stimulated by a proposal to build a High Energy Storage Ring (HESR) for antiprotons at the new Facility for Antiproton and Ion Research (FAIR) at the Gesellschaft für Schwerionenforschung (GSI) [1]. A Letter-of-Intent for spin-physics experiments has been submitted by the PAX collaboration [2] to employ a polarized antiproton beam incident on a polarized internal storage cell target.

Although a number of different approaches were investigated in the past and new ideas have been put forward recently, the only viable way for producing polarized antiprotons for FAIR at present is via spin filtering [3]. This method exploits the spin-dependent scattering of an unpolarized beam of antiprotons on a polarized hydrogen target. Technically this will have to be done by repeatedly sending the stored beam in a cooler cyclotron through a storage cell of the polarized target. In fact, such an experiment (FILTEX) has been performed some time ago with protons at the TSR [4], proving the feasibility of the method. One of the (many) still open questions is, however, how spin filtering actually works, since two different interpretations of the FILTEX-result have been put forward, one with substantial spin-filtering of

(anti)protons by polarized electrons [5, 6], while the second one suggests a self-cancellation of the electron contribution to spin-filtering [7] leaving only the hadronic contribution.

2 Polarization Buildup Mechanisms

All the possible methods to polarize (anti)protons are based on two mechanisms: selective loss or/and selective flip (see Fig. 1) [8]. In case of the selective loss one spin state is discarded more than the other one, while in the flip scenario one of the two states is reversed more intensively. The flip mecha-

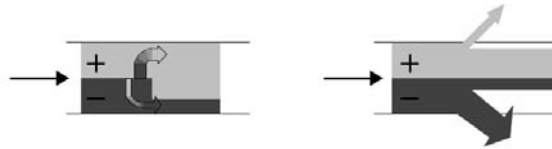


Figure 1: Two principles to polarize (anti)proton beam. The left figure depicts selective flip mechanism, while the right one illustrates selective loss.

nism includes spin transfer by co-moving polarized electrons or positrons [6]. Another method is a dynamic nuclear polarization in flight with co-moving polarized electrons or positrons. The loss mechanism includes polarization of an antiproton beam via Stern-Gerlach separation. Theoretically this seems to be impossible due to averaging effects in a stored beam [9]. Another method is polarization by channeling through bent crystals [10]. The only successfully tested method is spin filtering [4].

3 Spin Filtering and Depolarization Experiments at COSY

Spin filtering at COSY has two main objectives, understanding of the spin filtering mechanism and disentangling of the electromagnetic and hadronic contributions to the polarizing cross section. The latter can be reached with help of experiments using pure electron and nuclear polarized targets. This in turn requires strong holding fields applied longitudinally followed by a necessity of having a Siberian snake in the ring. Such massive hardware modifications can be avoided in case simpler experiments are possible that could reveal the role of electrons.

It is natural to assume that if polarized electrons polarize an initially unpolarized beam, then unpolarized electrons should depolarize an initially polarized beam. Therefore, using deuterium as an effective electron target we would like to distinguish the electron effect from the depolarization in COSY without target. Prerequisites for these studies however are large beam and polarization lifetimes of the proton beam, and this is currently being tested at COSY. Provided, both lifetimes are large enough, a 4-5 σ target effect can result from a 4 week data taking period.

A different approach is to use co-moving electrons in the electron cooler of COSY instead of the target electron to observe depolarization. This idea is motivated by the recent Walcher-Arenhövel estimation of electron-to-proton spin transfer at low-relative energy [6]. It is predicted that the corresponding

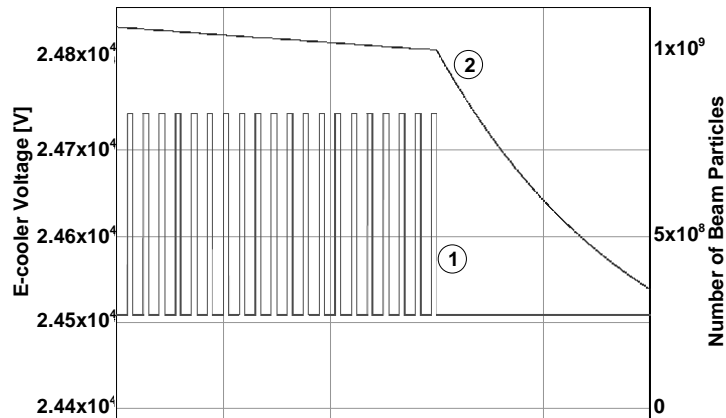


Figure 2: An example of COSY cycle structure for depolarization studies. E-cooler voltage (1) and the number of beam particles (2) are shown. The kink in the particle number is when the target is switched on.

cross section is very large at a proton kinetic energy of about 1 keV in the electron rest frame. The necessary experimental conditions are fulfilled by detuning the electron cooler in such a way that one can reach the required energy difference. The energy resolution of the detuned beam decreases rapidly, therefore only a limited time can be spent at these conditions. This leads to a periodically alternating structure of the cycle (see Fig. 2). After some time a target has to be switched on, and polarization of the beam must be measured. The polarization decrease is then directly related to the depolarizing cross section. This experiment is currently being prepared [11] and shall be performed in early 2008 provided the COSY Program Advisory Committee approves the investigation.

4 Spin Filtering: Status

Spin filtering is expected to be an effective way to polarize antiprotons. But a lack of experimental data leaves space for a controversy in explaining how spin filtering really works. The conclusion is that there are further experimental tests necessary to disentangle the effects of electrons and nucleons for the polarization buildup process. Depolarization as well as spin-filtering experiments will be carried out at COSY (Jülich) with protons, followed by spin-filtering experiments with antiprotons at the Antiproton Decelerator Ring (AD/CERN) [12].

References

- [1] Conceptual Design Report for *An International Facility for Antiproton and Ion Research*. Available from www.gsi.de/GSI-Future/cdr.
- [2] Letter-of-Intent for the HESR at FAIR, Jülich (2004), and references therein. Available from www.fz-juelich.de/ikp/pax.
- [3] F. Rathmann *et al.*, Phys. Rev. Lett. **94**, 014801 (2005).
- [4] F. Rathmann *et al.*, Phys. Rev. Lett. **71**, 1379 (1993).
- [5] C. J. Horowitz and H. O. Meyer, Phys. Rev. Lett. **72**, 3981 (1994).
- [6] Th. Walcher *et al.*, ePrint: arXiv 0706.3765 [physics.acc-ph] (2007).
- [7] A. I. Milstein and V. M. Strakhovenko, Phys. Rev. E **94**, 014801 (2005); N. N. Nikolaev and F. F. Pavlov, ePrint: arXiv hep-ex/0601184.
- [8] H. O. Meyer, Workshop summary of *Polarized Antiprotons - How?*, Daresbury, UK, August 29-31 2007; to be published.
- [9] D. Barber, Talk at Workshop *Polarized Antiprotons - How?*, Daresbury, UK, August 29-31 2007; to be published.
- [10] M. Ukhonov, AIP Proc. 17th Int. Spin Physics Symposium, Kyoto 2006, 940 (2007).
- [11] COSY Proposal #181, Jülich (2007). Available from www.fz-juelich.de/ikp/pax.
- [12] Letter-of-Intent for the AD, Jülich (2005). Available from www.fz-juelich.de/ikp/pax.

STUDYING PION EFFECTS IN THE QUARK PROPAGATOR

D. Nickel^{*,1}, C. S. Fischer^{*}, J. Wambach^{*}

^{*}Institut für Kernphysik, Technische Universität Darmstadt, Germany

Abstract

Within the framework of Schwinger-Dyson and Bethe-Salpeter equations we investigate the importance of pions for the quark-gluon interaction. To this end we choose a truncation for the quark-gluon vertex that includes intermediate pion degrees of freedom and adjust the interaction such that unquenched lattice results for various current quark masses are reproduced. The corresponding Bethe-Salpeter kernel is constructed from constraints by chiral symmetry. After extrapolation to the physical point we find a considerable contribution of the pion back reaction to the quark mass function as well as to the chiral condensate. The quark wave function is less affected.

1 Introduction and framework

Dynamical chiral symmetry breaking is one of the most striking properties of low-energy QCD. The resulting appearance of massless pions in the chiral limit is the basis of a systematic expansion for hadronic observables in terms of chiral perturbation theory. The difference between quenched and unquenched simulations in lattice QCD is also attributed to the importance of the pions' dynamics. Here we study the pion contribution and back reaction on the quark degrees of freedom in the Green's function approach to Landau gauge QCD using Schwinger-Dyson and Bethe-Salpeter equations (SDE/BSE) [?, 1]. We consider this as an extension of previous NJL-model studies [3] to full QCD and to be complementary to previous studies within the SDE/BSE approach neglecting the back reaction of pions [4, 19].

Our starting point is the SDE of the quark propagator

$$S^{-1}(p) = Z_2 S_0^{-1}(p) + \Sigma(p), \quad (1)$$

¹E-mail address: dominik.nickel@physik.tu-darmstadt.de

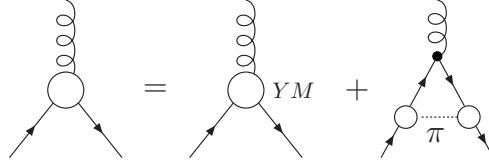


Figure 1: The approximated Schwinger-Dyson equation for the quark-gluon vertex. All internal propagators are fully dressed.

where $S_0^{-1}(p) = ip \cdot \gamma + m$ denotes the inverse bare quark-propagator, while $S^{-1}(p) = (ip \cdot \gamma + M(p^2))/Z_f(p^2)$ is the dressed propagator being parameterized by the quark mass $M(p^2)$ and the quark wave function $Z_f(p^2)$. Z_2 is the renormalization factor of the quark field. The quark self energy in Landau gauge is given by

$$\Sigma(p) = g^2 C_F Z_{1F} \int \frac{d^4 q}{(2\pi)^4} \gamma_\mu S(q) \Gamma_\nu(q, k) \frac{Z(k^2)}{k^2} \left(\delta_{\mu\nu} - \frac{k_\mu k_\nu}{k^2} \right), \quad (2)$$

with $k = p - q$, the Casimir $C_F = (N_c^2 - 1)/(2N_c)$ and the renormalization factor Z_{1F} of the quark gluon vertex. The self energy depends on the fully dressed quark-gluon vertex $\Gamma_\nu(q, k)$ and the gluon dressing function $Z(k^2)$.

The widely used rainbow-ladder approximation amounts to the replacement

$$\gamma_\mu Z(k^2) \Gamma_\nu(q, k) \rightarrow \gamma_\mu \Gamma(k^2) \gamma_\nu, \quad (3)$$

where $\Gamma(k^2)$ can be viewed as a combination of the gluon dressing function and a purely k^2 -dependent dressing of the γ_ν -part of the quark-gluon vertex. Aiming at an extension of this approximation which includes explicit pion degrees of freedom, we can motivate the quark-gluon vertex diagrammatically shown in Fig. 1 by its SDE (see Ref. [6] for details). The main idea is to single out the leading contribution involving pions and approximate the remaining part as the vertex used in the rainbow-ladder approximation. Using this ansatz in the SDE of the quark propagator we can motivate - after intermediate steps - the truncation diagrammatically shown in Fig. 2. Guided by chiral symmetry constraints we construct a Bethe-Salpeter kernel that guarantees the pion to be massless in the chiral limit (see again Ref. [6] for details).

2 Results

Given the unquenched lattice QCD results for the quark propagator in Landau gauge at relatively large quark masses [7] and a parameterization for the

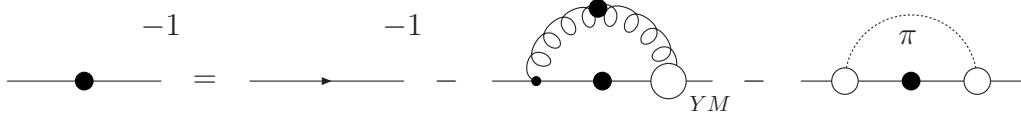


Figure 2: The approximated Schwinger-Dyson equation for the quark propagator with effective one-gluon exchange and one-pion exchange.

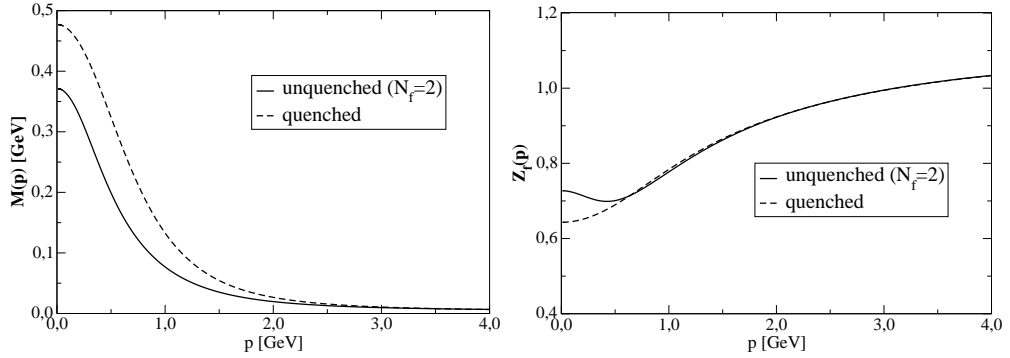


Figure 3: The quenched and unquenched ($N_f=2$) quark mass (left) and wave function (right) for physical up/down quarks with $M(2.9 \text{ GeV}) = 10 \text{ MeV}$.

dressings of the quark-gluon vertex in rainbow-ladder approximation adopted from similar investigations of quenched lattice QCD results [8], we can adjust the parameters of the rainbow-ladder contribution to our truncation of the quark-gluon vertex. We get nice agreement with the lattice QCD results for the quark mass function as well as for the wave function (see Ref. [6]). Switching off the pion contribution to the quark self-energy and furthermore comparing to unquenched lattice QCD results, we find the pion contribution to be overestimated. This may be due to a further numerical approximation and is detailed in Ref. [6].

The general tendency is however in line with the lattice QCD results and we can perform an extrapolation to physical value of the pion mass, *i.e.* current quark mass, and to the chiral limit. In Fig. 3 we also show the quark mass function and the wave function at the physical point. At small momenta the current quark mass dependence is most pronounced for the wave function, whereas the dependence of the mass function is strongest at intermediate momenta. To illustrate this we present the chiral extrapolation of the mass function at some momenta accessed in the lattice QCD simulations in Fig. 4. In contrast to the rainbow-ladder truncation, which gives an almost linear extrapolation, we find a sizeable non-linear behavior at small quark masses and momenta due to the pion contribution.

This work has been supported by the Helmholtz-University Young Inves-

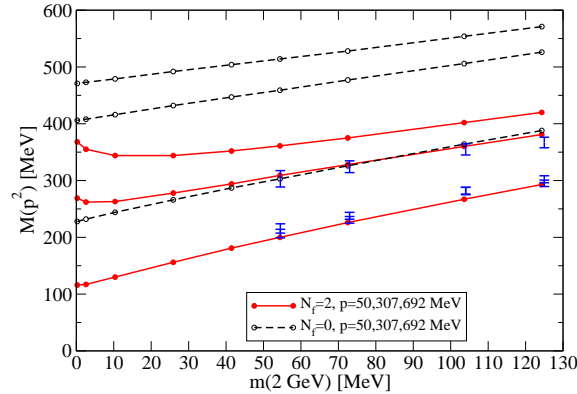


Figure 4: Chiral extrapolation of the mass function at stated momenta from bottom to top including the pion effects in the quark-gluon vertex (red) and neglecting it (black). Also given are lattice QCD results for the momenta corresponding to the touching red lines.

tigator Grant VH-NG-332.

References

- [1] P. Maris, C. D. Roberts and P. C. Tandy, *Phys. Lett. B* **420** (1998) 267.
- [2] R. Alkofer and L. von Smekal, *Phys. Rept.* **353** (2001) 281; P. Maris and C. D. Roberts, *Int. J. Mod. Phys. E* **12** (2003) 297; C. S. Fischer, *J. Phys. G* **32**, R253 (2006).
- [3] V. Dmitrasinovic, H. J. Schulze, R. Tegen and R. H. Lemmer, *Annals Phys.* **238**, 332 (1995); E. N. Nikolov, W. Broniowski, C. V. Christov, G. Ripka and K. Goetze, *Nucl. Phys. A* **608**, 411 (1996); M. Oertel, M. Buballa and J. Wambach, *Phys. Atom. Nucl.* **64**, 698 (2001).
- [4] P. Watson and W. Cassing, *Few Body Syst.* **35** (2004) 99.
- [5] C. S. Fischer and R. Alkofer, *Phys. Rev. D* **67** (2003) 094020; C. S. Fischer, P. Watson and W. Cassing, *Phys. Rev. D* **72**, 094025 (2005).
- [6] C. S. Fischer, D. Nickel and J. Wambach, arXiv:0705.4407 [hep-ph].
- [7] P. O. Bowman, U. M. Heller, D. B. Leinweber, M. B. Parappilly, A. G. Williams and J. b. Zhang, *Phys. Rev. D* **71** (2005) 054507.
- [8] M. S. Bhagwat, M. A. Pichowsky, C. D. Roberts and P. C. Tandy, *Phys. Rev. C* **68**, 015203 (2003); C. S. Fischer and M. R. Pennington, *Phys. Rev. D* **73** (2006) 034029; and arXiv:hep-ph/0701123.

NEUTRINO-INDUCED KAON PRODUCTION

*D. D. van Niekerk*¹ and *B. I. S. van der Ventel*²

Department of Physics
Stellenbosch University
Matieland, 7602
South Africa

Abstract

A formalism is presented for the description of neutrino-induced kaon and associated hypernucleus production. It is shown that the cross section can be written as the contraction of a leptonic and hadronic tensor if the interaction is modelled as a quasifree process. The hadronic tensor is written in a model-independent way in terms of thirteen nuclear structure functions. A Born-term model is used to describe the underlying elementary hyperon and kaon production process. The bound state wave functions of the hyperon and nucleon are calculated within a relativistic mean field approximation. Preliminary results are discussed.

1 Introduction

The main motivation for this work is the realization that kaons and hypernuclei are likely products of weak neutrino-nucleus reactions. The role of neutrinos and strange hadrons in the behaviour of supernovae is also a contemporary research topic. Other phenomena that can be illuminated by the study of weak strangeness production is neutrino oscillations (a spontaneous change in neutrino flavour). Currently experiments to detect these events are underway at Fermilab (BooNe) and JPARC. Neutrino-induced kaon production is especially important since kaons produced by the interactions of atmospheric neutrinos with nuclei can mimic the signals of kaons arising from proton-decay predicted by supersymmetric theories (see Ref. [1]).

Our model is the first attempt at describing the weak production of hypernuclei and kaons. It is a fully relativistic treatment of this problem since

¹ddvniekerk@sun.ac.za

²bventel@sun.ac.za

both relativistic kinematics and dynamics are used. Refs. [2] and [3] give descriptions of the elementary neutrino-nucleon scattering process in terms of Born s , t and u channels and Ref. [4] discusses a formalism for the description of neutrino-induced associated production. Our work is based on a general scattering formalism developed in Refs. [5] and [6].

2 Our Model

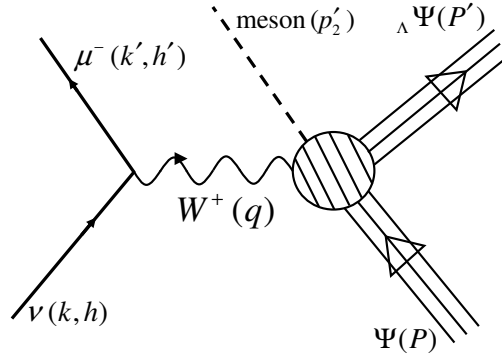


Figure 1: General charged current neutrino scattering process resulting in production of a hypernucleus and a kaon.

Figure 1 shows the general type of scattering process we describe. A more complete discussion of the model can be found in Ref. [7]. The cross section is written as

$$d\sigma = \frac{1}{2(2\pi)^5 E_{p'_2}} \delta^4(k + P - k' - p'_2 - P') d^3\mathbf{k}' d^3\mathbf{p}'_2 d^3\mathbf{P}' |\mathcal{M}|^2. \quad (1)$$

The invariant matrix element squared is written as the contraction of a leptonic and a hadronic tensor

$$|\mathcal{M}|^2 = \frac{G_F^2}{2} \cos^2 \theta_C \ell_{\mu\nu} W^{\mu\nu}, \quad (2)$$

where θ_C is the Cabibbo angle and G_F is the Fermi-constant for beta-decay. These tensors describe the relativistic dynamics of the projectile and the nucleus. The leptonic tensor is derived using a conventional relativistic approach of Dirac planewave spinors and the weak leptonic current operator.

The hadronic tensor is parametrised in a model-independent basis using 13 structure functions. Eq. (2) then gives

$$\begin{aligned} \ell_{\mu\nu} W^{\mu\nu} = & \frac{4}{E_k E_{k'}} [(-W_1(k \cdot K') + W_2 f_1(q) + W_3 f_1(P) + W_4 f_1(p'_2)) \\ & + W_5 f_2(P, q) + W_6 f_2(q, p'_2) + W_7 f_2(P, p'_2)) + i (W_{10} \epsilon_{\mu\nu\alpha\beta} P^\mu p'_2{}^\nu k^\alpha K'^\beta \\ & + W_{11} f_3(q, P) + W_{12} f_3(q, p'_2) + W_{13} f_3(P, p'_2))] , \end{aligned} \quad (3)$$

where

$$\begin{aligned} f_1(x) &= (k \cdot x)(K' \cdot x) - x^2/2(k \cdot K'), \\ f_2(x, y) &= (k \cdot x)(K' \cdot y) + (k \cdot y)(K' \cdot x) - (x \cdot y)(k \cdot K'), \\ f_3(x, y) &= (k \cdot y)(K' \cdot x) - (k \cdot x)(K' \cdot y), \end{aligned} \quad (4)$$

and

$$K' \equiv \frac{1}{2}(k' - h' m_{k'} s) \xrightarrow{m=0} k' \delta_{h', -1}, \quad (5)$$

$$s^\mu(\mathbf{k}') \equiv \frac{1}{m} \left(|\mathbf{k}'|, E_{k'} \hat{\mathbf{k}}' \right). \quad (6)$$

2.1 Model-dependent evaluation of the hadronic vertex

We make use of the quasifree approximation for the hadronic vertex. A Born-term model (s , t and u -channels) is used to construct the current of the elementary hadronic process (see Ref. [2]). The form of the elementary currents is extended to the quasifree case by integrating over the momentum of the bound nucleon

$$h^\mu = \int d^3 \mathbf{p}_1 \bar{\mathcal{U}}_Y(\mathbf{q} + \mathbf{p}_1 - \mathbf{p}'_2) J^\mu \mathcal{U}(\mathbf{p}_1). \quad (7)$$

The bound state wave functions we use are calculated using a relativistic mean-field formalism (FSUGold for neutron and NLSH for hyperon). The model-dependent hadronic tensor is then given by

$$(W^{\mu\nu})_{\text{model}} = \sum_{m_N, m_Y} h^\mu (h^\nu)^*, \quad (8)$$

where m_N and m_Y refer to the projections of the total angular momentum of the nucleon and hyperon. The structure functions are extracted from the model-dependent hadronic tensor as described in Ref. [7] and inserted into Eq. (3).

3 Results

An example calculation was done for a 3 GeV neutrino projectile and a 1.5 GeV ejectile muon for the reaction $\nu + {}^{12}\text{C} \rightarrow \mu^- + K^+ + {}^{12}_\Lambda\text{C}$ (elementary process: $\nu + n \rightarrow \mu^- + K^+ + \Lambda$). Fig. 2 (a) shows that the largest channel-contributions to the differential cross section come from the s and t -channels

for which exact phenomenological form factors were used. The u -channel, for which we assumed an exact SU(3) symmetry which lead to approximate form factors in the baryon octet, delivers only a small contribution.

Fig. 2 (b) shows the contribution of the different helicity states of the ejectile muon to the total differential cross section. The contribution of the negative helicity muon clearly far exceeds that of the positive helicity one. This can be ascribed to the fact the muon mass is so small in comparison to its energy that the helicity of the neutrino ($h = -1$) is largely conserved in the reaction.

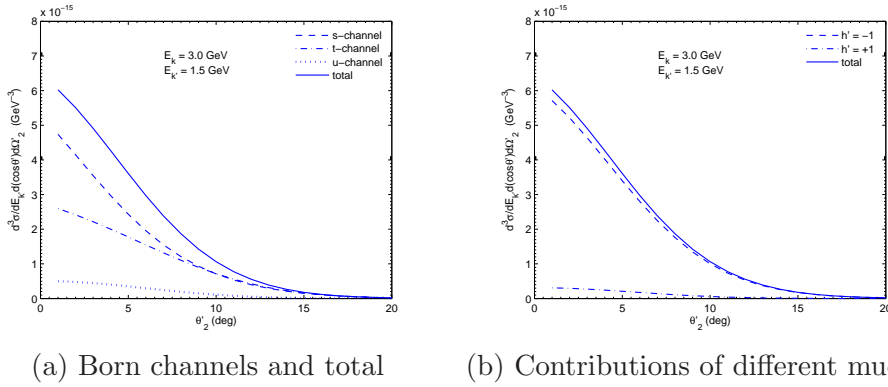


Figure 2: Differential cross section of the $1p^{3/2}$ neutron to $1s^{1/2}$ hyperon transition.

References

- [1] K. Datchev, *APS Meeting Abstracts*, 2002.
- [2] R.E. Shrock, *Phys. Rev. D* **12**, 2049 (1975).
- [3] H.K. Dewan, *Phys. Rev. D* **24**, 2369 (1981).
- [4] W. Mecklenburg, *Acta Physica Austriaca* **48**, 293 (1978).
- [5] B.I.S. van der Ventel and J. Piekarewicz, *Phys. Rev. C* **69**, 35501 (2004).
- [6] B.I.S. van der Ventel and J. Piekarewicz, *Phys. Rev. C* **73**, 25501 (2006).
- [7] D.D. van Niekerk and B.I.S. van der Ventel, *Eur. Phys. J. A* **33**, 273 (2007).

BOUND KAON APPROACH FOR THE ppK^- SYSTEM IN THE SKYRME MODEL

T. Nishikawa

Department of Physics, Tokyo Institute of Technology, 2-12-1,
Oh-Okayama, Meguro, Tokyo 152-8551, Japan

Y. Kondo

Kokugakuin University, Higashi, Shibuya, Tokyo 150-8440, Japan

Abstract

The lightest nuclear \bar{K} bound state, ppK^- , is investigated in the Skyrme model. We describe the ppK^- system as two-Skyrmion around which a kaon field fluctuates. The two-Skyrmion is projected onto $(pp)_{S=0}$ state using the collective coordinate quantization method. We find that the energy of K^- can be considerably small, and that ppK^- is a molecular state. The binding energy of the ppK^- is estimated in the Born-Oppenheimer approximation to be $B.E. = 104 - 126$ MeV. The mean pp distance is $\sqrt{\langle r_{pp}^2 \rangle} = 1.6 - 1.8$ fm.

1 Introduction

For recent years, lots of theoretical or experimental efforts to explore the possibility of nuclear \bar{K} -bound states [1] have been made. No firm evidences to show their existence are known up to now, although there is one result reported by FINUDA collaboration [2] suggesting the existence of the lightest \bar{K} -nucleus, ppK^- . On the other hand, theoretical studies of ppK^- have also been done by several groups [1, 3]. In the present work, we investigate the issue of the kaonic nuclei from completely different point of view, the topological soliton model of baryons. The topological soliton of the pion field, which is called “Skyrmion”, behaves like a nucleon [4]. Hyperons can be well described as bound states of \bar{K} and a Skyrmion [5].

We describe the ppK^- system as two-Skyrmion around which a kaon field fluctuates [6]. The two-Skyrmion is projected onto spin-singlet proton-proton state using the method of collective coordinate quantization. We derive the kaon’s equation of motion for the Skyrmions at fixed positions. Then we obtain the energy of kaon as a function of the pp relative distance. Next, we solve the dynamics of the pp radial motion to estimate the binding energy of the ppK^- . The possible structure of the ppK^- state is also discussed.

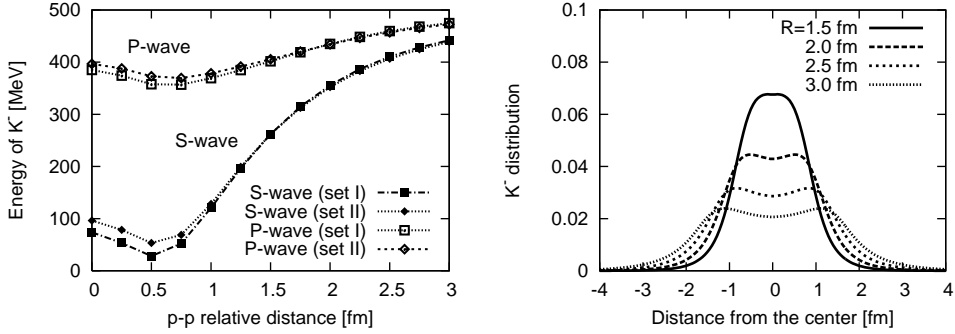


Figure 1: Left: Energy of S - and P -wave K^- as functions of the proton-proton relative distance, R . Right: Distribution of K^- in unit of eF_π .

2 Behavior of K^- coupled to pp

First, we derive the equation of motion for K^- coupled to pp . We assume the following ansatz for the chiral field, $U = U(1)U_K U(2)$, where $U(1)$ and $U(2)$ are the fields of the baryon number $B = 1$ $SU(2)$ Skyrmions whose relative distance is R . U_K is the field carrying strangeness. By substituting the ansatz into the action of the Skyrme model, we obtain the Lagrangian for the kaon field under the background of $B = 2$ Skyrmion. KNN interaction is unambiguously determined once the ansatz for U is given. By applying the collective coordinate quantization method, we project the two-Skyrmion onto the spin-singlet pp state. The direction of the line joining the two Skyrmions is averaged. Then the background field becomes spherical, which allows us to perform the spherical partial wave analysis.

We solve the kaon's equation of motion numerically. We take $m_\pi = 0$, $m_K = 495$ MeV, $F_K/F_\pi = 1.23$. For F_π and the Skyrme parameter, e , we examine two choices (i) Set I: fitted to N and Δ masses, $F_\pi = 129.0$ MeV and $e = 5.45$, (ii) Set II: fitted to Δ and $\Lambda(1405)$ masses, $F_\pi = 129.7$ MeV and $e = 5.0$.

The left panel of Figure.1 shows the energy of K^- , ω , as a function of the pp relative distance, R . We can see the dependence on the choice of the parameter is weak. Looking at the S -wave channel, the binding of the kaon is extremely strong for smaller distance, *i.e.* $R \lesssim 1.0$ fm. As R is increased, the binding becomes looser. However, at $R = 2.0$ fm, for instance, which is close to the average inter NN distance in normal nuclei, the binding is still deep: the binding energy is about 140 MeV.

In the right panel of Figure 1, we plot the distribution of K^- in S -wave. The distribution for relatively larger separation, $R \gtrsim 2.0$ fm, is characteristic

parameter set	$\langle T_{NN} \rangle$	$\langle V_{NN} \rangle$	$\langle \omega_{L=0} - m_K \rangle$	total	$\sqrt{\langle r_{NN}^2 \rangle}$
set I	42.0	74.5	-239.2	-125.5	1.63
set II	36.2	73.7	-211.3	-104.0	1.80

Table 1: Energy (MeV) of the ppK^- bound state relative to $2M_N + m_K$ and its decomposition. The mean pp distance (fm), $\sqrt{\langle r_{NN}^2 \rangle}$, is also shown.

to molecular orbital states [6]. This is expected from the fact that the potential acting on the kaon is a double-well potential which is most attractive at the proton's respective position. Then K^- experiences the strong attraction from pp without increase of the kinetic energy. In this sense, it is quite natural that the binding of K^- to two-proton is stronger than to one proton.

3 pp radial motion

We assume that the pp radial motion is governed by the Hamiltonian, $H = T_{NN}(R) + V_{NN}(R) + \omega_{L=0}(R) - m_K$, where T_{NN} is the kinetic energy and the nucleon is regarded as a non relativistic point like particle with the mass $M_N = 939$ MeV. $V_{NN}(R)$ is the state-independent part of the NN potential obtained from the product of $B = 1$ Skyrmion. $\omega_{L=0}(R)$ is the S -wave kaon's energy. $V_{NN}(R) + \omega_{L=0}(R) - m_K$ can be regarded the effective pp potential in the ppK^- system. In Figure 2, we show the behavior of the potential terms. The attractive potential generated by bound kaon (lower curve), $\omega_{L=0}(R) - m_K$, is so strong that it overcomes the strongly repulsive $V_{NN}(R)$ (upper curve). As a result, the effective pp potential in the ppK^- system (middle curve) is strongly attractive in the medium range.

The energy of the ppK^- state is obtained by solving the Schrödinger equation. In Table 1, we display the energy of the ppK^- bound state relative to $2M_N + m_K$, its decomposition, and the mean pp distance. Our result of the ppK^- binding energy is 104 – 126 MeV. The smallness of the NN kinetic energy may imply that the Born-Oppenheimer approximation is not so poor. The mean pp distance is 1.6 – 1.8 fm, which is smaller than or comparable with the average NN distance in normal nuclei.

4 Conclusion

We have applied the Skyrme model to a study of the lightest \bar{K} -nuclear bound state, ppK^- . The ppK^- state can be realized as a very deeply bound

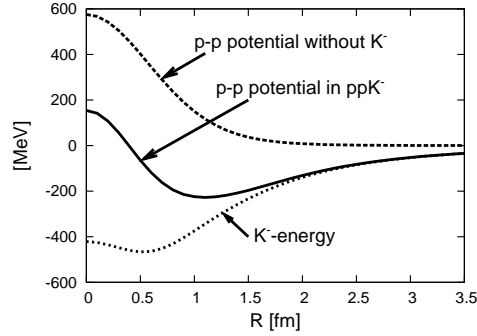


Figure 2: The upper curve is the pp potential in the absence of K^- , $V_{NN}(R)$. The lower one is the energy of K^- ($\omega_{L=0}(R) - m_K$). The middle one corresponds to their sum, the effective pp potential in the ppK^- system.

and compact state, whose binding energy is $B_{ppK^-} = 104 - 126$ MeV and the mean pp distance is $\sqrt{\langle r_{NN}^2 \rangle} \simeq 1.6 - 1.8$ fm.

5 Acknowledgment

This work was supported in part by the 21st Century COE Program at Tokyo Institute of Technology “Nanometer-Scale Quantum Physics” from the Ministry of Education, Culture, Sports, Science and Technology, Japan.

References

- [1] Y. Akaishi and T. Yamazaki, Phys. Rev. **C65**, 044005 (2002).
- [2] M. Agnello *et al.*, Phys. Rev. Lett. **94**, 212303 (2005).
- [3] N.V. Shevchenko, A. Gal and J. Mares, Phys. Rev. Lett. **98**, 082301 (2007); Y. Ikeda and T. Sato, arXiv:0704.1978; A. Arai, M. Oka and S. Yasui, arXiv:0705.3936.
- [4] T.H.R. Skyrme, Proc. Roy. Soc. **A260**, 127 (1961); G.S. Adkins, C.R. Nappi and E. Witten, Nucl. Phys. **B233**, 109 (1984).
- [5] C.G. Callan, K. Hornbostel and I. Klebanov, Phys. Lett. **B202**, 269 (1988); M. Rho, D.O. Riska and N.N. Scoccola, Z. Phys. **A341**, 343 (1992).
- [6] T. Nishikawa and Y. Kondo, hep-ph/0703100; arXiv:0710.0948.

ON BARYON-ANTIBARYON CROSS SECTIONS FROM INITIAL STATE RADIATION PROCESSES AT *BABAR* AND THEIR SURPRISING THRESHOLD BEHAVIOR

*Simone Pacetti*¹

representing the *BABAR* Collaboration

Enrico Fermi Center, Rome, Italy²

INFN, Laboratori Nazionali di Frascati, Frascati, Italy³

Abstract

BABAR has measured with unprecedented accuracy the $e^+e^- \rightarrow p\bar{p}$ and $e^+e^- \rightarrow \Lambda\bar{\Lambda}$ cross sections by means of the initial state radiation technique, which has the advantages of good efficiency and energy resolution, and full angular acceptance in the threshold region. A striking feature of these cross sections is their non-vanishing values at threshold. In the case of charged baryons, the phenomenon is well understood in terms of the Coulomb interaction between the outgoing baryon and antibaryon. However, such an effect is not expected for neutral baryons. We suggest a simple explanation for both charged and neutral baryon pairs based on Coulomb interactions at the valence quark level.

1 Introduction

Unexpected features [1] in recent measurements of the $e^+e^- \rightarrow p\bar{p}$ and $e^+e^- \rightarrow \Lambda\bar{\Lambda}$ cross sections in the near threshold region are pointed out in the following. *BABAR* has measured these processes [2, 3] (Fig. 1), with unprecedented accuracy, from their thresholds up to $W_{p\bar{p}(\Lambda\bar{\Lambda})} \approx 4(3)$ GeV by means of the initial state radiation (ISR) technique ($W_{\mathcal{B}\bar{\mathcal{B}}}$ is the invariant mass of the baryon-antibaryon system and \mathcal{B} stands for baryon). The main advantages in measuring a two body process via ISR are: a threshold efficiency quite high,

¹simone.pacetti@lnf.infn.it

²Via E. Fermi, 40 – I-00044 Frascati (Rome), Italy

³Compendio Viminale – I-00184 Rome, Italy

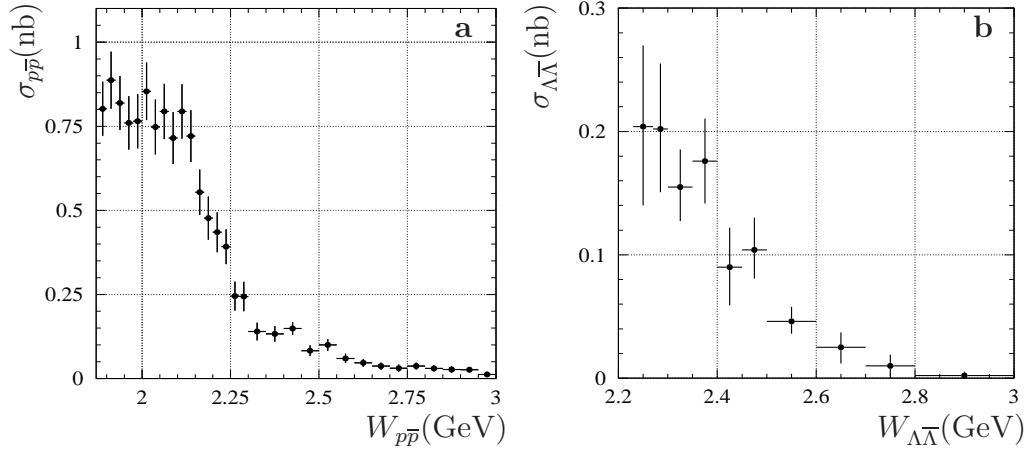


Figure 1: The $e^+e^- \rightarrow p\bar{p}$ (a) and $e^+e^- \rightarrow \Lambda\bar{\Lambda}$ (b) total cross sections [2,3].

a good invariant mass resolution (≈ 1 MeV), and a full angular acceptance when the radiated photon is detected.

In Born approximation the $e^+e^- \rightarrow \mathcal{B}\bar{\mathcal{B}}$ differential cross section is

$$\frac{d\sigma_{\mathcal{B}\bar{\mathcal{B}}}}{d\Omega}(W_{\mathcal{B}\bar{\mathcal{B}}}^2) = \frac{\alpha^2\beta C}{4W_{\mathcal{B}\bar{\mathcal{B}}}^2} \left[(1 + \cos^2\theta)|G_M^{\mathcal{B}}|^2 + 4M_{\mathcal{B}}^2/W_{\mathcal{B}\bar{\mathcal{B}}}^2 \sin^2\theta|G_E^{\mathcal{B}}|^2 \right], \quad (1)$$

where β is the baryon velocity, C is a Coulomb correction that will be discussed in the following, θ is the scattering angle in the center of mass frame, and $G_M^{\mathcal{B}}$ and $G_E^{\mathcal{B}}$ are the magnetic and electric Sachs form factors (FF).

In the case of the $e^+e^- \rightarrow p\bar{p}$ cross section $\sigma_{p\bar{p}}$ [2], Fig. 1a, we observe that: it is suddenly different from zero at threshold, being constant and ≈ 0.85 nb up to about 200 MeV above the threshold, then it drops. Similar features have been observed by *BABAR* in the $\Lambda\bar{\Lambda}$ channel [3] (Fig. 1b). In particular the cross section $\sigma_{\Lambda\bar{\Lambda}}$ is non-zero at threshold, being ≈ 0.2 nb.

In principle, due to the finite energy-bin width, experiments can not exclude vanishing cross sections at threshold with extremely sharp rises, in that case the relationship between data and predictions, reported in the following, could be accidental.

It is well known that Coulomb corrections to the Born cross section have to be accounted for in the case of production of pointlike charged fermions [4]. This correction, C in Eq. (1), is $C = 1$ (no effect) for neutral baryons, and $C(W_{\mathcal{B}\bar{\mathcal{B}}}) = (\pi\alpha/\beta)/(1 - e^{-\pi\alpha/\beta})$ for charged baryons. Very near threshold the Coulomb factor behaves like $\pi\alpha/\beta$ and cancels out the phase-space β , making the cross section finite and non-zero even at $\beta = 0$. However, as it is shown in Fig. 2, as soon as the baryon velocity is no more vanishing,

only few MeV above the threshold, it is $C \approx 1$ and Coulomb effects become negligible. In the case of $e^+e^- \rightarrow p\bar{p}$ the expected Coulomb-corrected cross

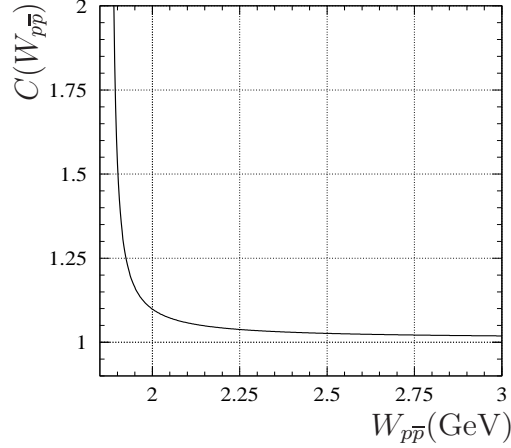


Figure 2: Coulomb enhancement factor for the $p\bar{p}$ channel.

section at threshold is

$$\sigma_{p\bar{p}}(4M_p^2) = (\pi^2 \alpha^3 / 2M_p^2) \cdot |G^p(4M_p^2)|^2 = 0.85 \cdot |G^p(4M_p^2)|^2 \text{ nb},$$

where $G^p = G_E^p = G_M^p$ is expected at threshold from unitarity. This is in striking similarity with the measured values just above threshold if $|G^p(4M_p^2)| \approx 1$. Hence the interpretation of the FF as the static overlap of baryon and antibaryon wavefunctions, plus a dominant contribution from the Coulomb effect explains the data.

In the case of the Λ , Coulomb effects should not be taken into account because of the neutral electric charge. It follows that, contrary to the data, Fig. 1b, the $e^+e^- \rightarrow \Lambda\bar{\Lambda}$ cross section is expected to vanish at threshold.

Some authors (e.g. Ref. [5]) emphasize that similar threshold effects, due to strong interaction, are forecast in the case of heavy quark pair production.

2 A simple interpretation at quark level

Assuming that the Coulomb dominance is not a mere coincidence, we investigate what is expected at the valence-quark level. Once quark pairs are produced they experience an attractive Coulomb interaction. For each pair there is a Coulomb amplitude with a phase to account for the displacement inside the baryon. The interference terms are suppressed by various factors

(e.g.: displacement and velocity spread). In addition, the Coulomb correction for charges of the same sign vanishes at threshold (same formula for C but with negative α), then it should be a safe approximation to neglect interference terms. In the proton case we have

$$\sigma_{p\bar{p}}(4M_p^2) = (\pi^2\alpha^3/2M_p^2)(2Q_u^2 + Q_d^2) \cdot |G^p(4M_p^2)|^2 = 0.85 \cdot |G^p(4M_p^2)|^2 \text{ nb},$$

the pointlike result is recovered. In the case of the $e^+e^- \rightarrow \Lambda\bar{\Lambda}$ cross section, at quark level, with no interference at all (upper limit):

$$\sigma_{\Lambda\bar{\Lambda}}(4M_\Lambda^2) = (\pi^2\alpha^3/2M_\Lambda^2)(Q_u^2 + Q_d^2 + Q_s^2) \cdot |G^\Lambda(4M_\Lambda^2)|^2 = 0.4 \cdot |G^\Lambda(4M_\Lambda^2)|^2 \text{ nb},$$

while at hadron level: $\sigma_{\Lambda\bar{\Lambda}}(4M_\Lambda^2) = 0$. Hence the expectation range for $\sigma_{\Lambda\bar{\Lambda}}$ at threshold, still assuming $|G^\Lambda(4M_\Lambda^2)| \approx 1$, is $(0 \div 0.4)$ nb in **agreement with the experimental value** shown in Fig. 1b.

3 Conclusions

Data on cross sections for the processes $e^+e^- \rightarrow p\bar{p}$, $\Lambda\bar{\Lambda}$ have been discussed.

The most surprising feature is their non-zero cross section at threshold. Indeed, in Born approximation, Eq. (1), the cross section $\sigma_{B\bar{B}}$ is proportional to the velocity β of the baryon and, assuming analytic FF's, it must be zero at threshold. The pointlike Coulomb correction gives a factor $1/\beta$ that cancels out the phase space velocity only when charged baryons are involved. This correction is very large at threshold and just above, and can describe the data with the reasonable value $|G^p(4M_p^2)| \approx 1$. For neutral baryons there is no pointlike Coulomb interaction, hence the cross section should vanish at threshold, in contrast with what we observe, within the errors, in the case of $\sigma_{\Lambda\bar{\Lambda}}$, Fig. 1b.

We can explain this threshold behavior by considering Coulomb interactions among the constituent quarks. In such a way, in both $p\bar{p}$ and $\Lambda\bar{\Lambda}$ channels, we obtain that the cross section data, at threshold, are fully described by the Coulomb correction and are compatible with $|G^{p,\Lambda}(4M_{p,\Lambda}^2)| \approx 1$.

References

- [1] R. Baldini, S. Pacetti and A. Zallo, arXiv:0711.1725 [hep-ph].
- [2] B. Aubert *et al.* [*BABAR* Collaboration], Phys. Rev. D **73**, 012005 (2006).
- [3] B. Aubert *et al.* [*BABAR* Collaboration], arXiv:0709.1988 [hep-ex].

- [4] A.D. Sakharov, Zh. Eksp. Teor. Fiz. **18**, 631 (1948); [Sov. Phys. Usp. **34**, 375 (1991)]. A. Sommerfeld, *Atombau und Spektrallinien* (Vieweg, Braunschweig, 1944); J. Schwinger, *Particles, Sources, and Fields*.
- [5] S.J. Brodsky *et al.* Phys. Lett. B **359**, 355 (1995) [arXiv:hep-ph/9508274]; G. Castellani *et al.* arXiv:hep-ph/0509089 and references therein.

INVESTIGATION OF THE $dp \rightarrow {}^3\text{He} X$ ($X=\eta, \pi^+\pi^-$) REACTIONS AT COSY-ANKE

M. Papenbrock^{*,1}, A. Khoukaz^{*}, P. Goslawski^{*}, T. Mersmann^{*},
M. Mielke^{*}, T. Rausmann^{*}, A. Täschner^{*} for the ANKE collaboration

^{*}Institut für Kernphysik, Westfälische Wilhelms-Universität Münster,
Wilhelm-Klemm-Straße 9, 48149 Münster, Germany

Abstract

Differential and total cross sections for the $dp \rightarrow {}^3\text{He}\eta$ reaction have been measured in a high precision, high statistics COSY-ANKE experiment near threshold using a continuous beam energy ramp up to an excess energy Q of 11.3 MeV. The very rapid rise of the total cross section to its maximum value within 0.5 MeV of threshold implies a very large η - ${}^3\text{He}$ scattering length and hence the presence of a quasi-bound state extremely close to threshold. Simultaneously, data on the reaction $dp \rightarrow {}^3\text{He}\pi^+\pi^-$ have been measured which are investigated with respect to the still poorly understood ABC effect.

1 The reaction $dp \rightarrow {}^3\text{He}\eta$

The anomalous energy dependence found at low excess energies in the η - ${}^3\text{He}$ system suggests that the strong η - ${}^3\text{He}$ final state interaction (*fsi*) might lead to the formation of an η - ${}^3\text{He}$ quasi-bound state [1] for nuclei much lighter than originally postulated [2]. However, this question is far from being settled and further high quality data are required. Therefore, the reaction $dp \rightarrow {}^3\text{He}\eta$ has been investigated using the ANKE spectrometer situated at an internal position of the COoler SYnchrotron COSY-Jülich [3]. During each of the beam cycles of 277 seconds, the deuteron beam energy was ramped slowly and linearly in time, from an excess energy of $Q = -5.05$ MeV to $Q = +11.33$ MeV. The produced ${}^3\text{He}$ nuclei were detected in the ANKE forward detection system, which consists of two multi-wire proportional chambers, one drift chamber and three layers of scintillation hodoscopes. The η meson production was subsequently identified using the missing-mass technique. The geometrical acceptance for the ${}^3\text{He}$ nuclei of interest was $\sim 100\%$,

¹E-mail address: michaelp@uni-muenster.de

so that systematic uncertainties from acceptance corrections are negligible. The η center of mass (c.m.) momentum p_η was derived from the radius of the ${}^3\text{He}$ momentum locus in the c.m. frame for each of the one second time bins during the COSY ramp. It was found that the value of $Q = p_\eta^2/2m_{red}$ (m_{red} is the $\eta{}^3\text{He}$ reduced mass) increases perfectly linear with ramp time. From this distribution the uncertainty in the determination of the mean value of the excess energy itself was derived and found to be ± 9 keV for each time bin. This method is described in more detail in [4].

The total cross sections for $dp \rightarrow {}^3\text{He}\eta$ obtained at 195 bins in excess energy are compatible with those of SPESII [5] and COSY-11 [6], though the other data sets do not define firmly the energy dependence in the near threshold region. At ANKE it was found that the total cross section reaches its maximum within 0.5 MeV of threshold and hardly decreases for higher energies. This is in complete contrast to phase space expectations and indicates a strong final state interaction.

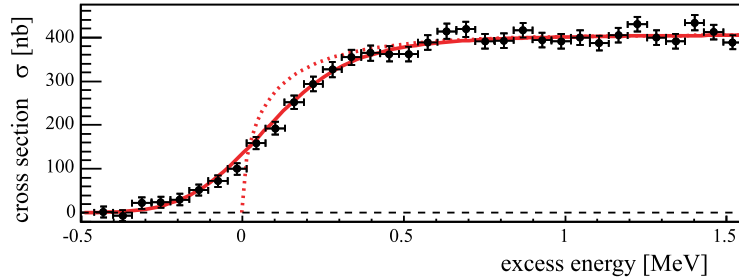


Figure 1: Total cross section data extracted in the vicinity of the threshold.

With p_d as the initial c.m. momentum the angular average of the amplitude-squared is derived from the total cross section σ_{tot} through

$$|\overline{f}|^2 = \frac{p_d}{p_\eta} \cdot \frac{\sigma_{tot}}{4\pi}. \quad (1)$$

We parametrize the s-wave component f_s in the form

$$f_s = \frac{f_B}{(1 - p_\eta/p_1)(1 - p_\eta/p_2)}. \quad (2)$$

In the presence of a strongly attractive final state interaction there should be a pole of f_s where $|p_1|$ is very small, while the second singularity has no direct physical meaning.

The shape of the η production below the nominal threshold as shown in Fig. 1 is a very sensitive measure of the momentum width of the COSY

beam. This resolution has to be taken into account in any phenomenological analysis [3]. The effect of the beam smearing can easily be seen in Fig. 1, where the unsmearred parameterization is shown as the dotted curve. The fit to the whole energy range up to $Q = 11$ MeV provided

$$\begin{aligned} p_1 &= [(-5 \pm 7_{-1}^{+2}) \pm i(19 \pm 2 \pm 1)] \text{ MeV}/c \\ p_2 &= [(106 \pm 5) \pm i(76 \pm 13_{-2}^{+1})] \text{ MeV}/c \end{aligned} \quad (3)$$

and this results in a scattering length of

$$\begin{aligned} a &= -i(p_1 + p_2)/p_1 p_2 \\ &= [\pm(10.7 \pm 0.8_{-0.5}^{+0.1}) + i(1.5 \pm 2.6_{-0.9}^{+1.0})] \text{ fm}, \end{aligned} \quad (4)$$

where the first errors are statistical and the second (where given) systematic, including effects associated with the fitting range assumed.

The results show that a is dominantly real with large errors on the imaginary part. The value of $|a|$ is much larger than that found in earlier work [5, 7] or in the later COSY-11 experiment [6]. This is due, in part, to the treatment of energy-smearing effects, whose need is very evident in our data with the fine energy steps near threshold.

In order to affect the cross section variation over a scale of less than 1 MeV, there must be a pole of the production amplitude in the complex plane that is typically only 1 MeV away from $Q = 0$. From our fit values we found a stable pole at $Q_0 = p_1^2/2m_{\text{red}} = [(-0.30 \pm 0.15 \pm 0.04) \pm i(0.21 \pm 0.29 \pm 0.06)]$ MeV.

Additionally, differential cross sections have been extracted from the data. The observed asymmetry implies contributions of higher partial waves in the near threshold region [3]. Defining an asymmetry parameter α through $(d\sigma/d\Omega)_{c.m.} = \sigma_{tot}(1 + \alpha \cos \theta_{c.m.})/4\pi$, this is seen to become positive above $p_\eta = 40$ MeV/c ($Q = 1.7$ MeV) and increase monotonically with p_η much faster than observed at SPESII [5]. This effect could originate from a rapid variation of the phase of the near-threshold s-wave amplitude and might be connected to a possible η - ${}^3\text{He}$ quasi-bound state [8].

2 The reaction $dp \rightarrow {}^3\text{He} \pi^+ \pi^-$

Simultaneously to the η production, data on the pion pair production in the reaction $dp \rightarrow {}^3\text{He} \pi^+ \pi^-$ have been recorded in order to investigate the still poorly understood ABC-effect, which shows up as a strong enhancement at low $\pi^+ \pi^-$ invariant masses. The identification of this reaction channel was performed by detecting the ${}^3\text{He}$ nuclei in the forward detector and the π^-

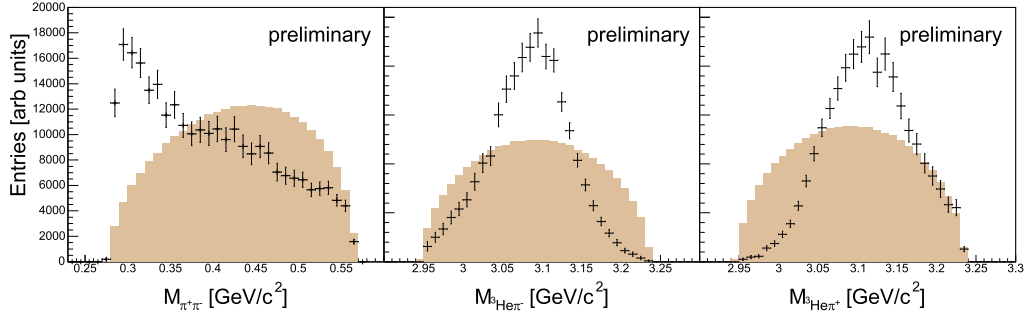


Figure 2: Invariant mass distributions of the $\pi^+\pi^-$ and ${}^3\text{He}\pi^\pm$ systems

meson in the negative system of the ANKE spectrometer. The undetected π^+ meson was identified using the missing-mass technique.

In Fig. 2 the obtained invariant mass distributions of the $\pi^+\pi^-$ and ${}^3\text{He}\pi^\pm$ systems are displayed and compared with phase space Monte-Carlo simulations. The observed deviations from phase space are in good agreement with recent results from the CELSIUS/WASA experiment [9]. Currently, the data are under final evaluation and will be investigated with respect to possible production mechanism, such as the double pion production via a double Δ resonance production ($\Delta\Delta \rightarrow N\pi N\pi$) or the excitation of an N^* resonance ($N^* \rightarrow \Delta\pi \rightarrow N\pi\pi$) [10].

References

- [1] C. Wilkin, *Phys. Rev. C*, 47(R938), 1993.
- [2] R.S. Bhalearo and L.C. Liu., *Phys. Rev. Lett.*, 54(865), 1985.
- [3] T. Mersmann et al., *Phys. Rev. Lett.*, 98(242301), 2007.
- [4] T. Mersmann, *PhD thesis, University Münster*, 2007
- [5] B. Mayer et al., *Phys. Rev. C*, 53(2068), 1996.
- [6] J. Smyrski et al., *Phys. Lett. B*, 649(258), 2007.
- [7] H.-H. Adam et al., *Phys. Rev. C*, 75(014004), 2007.
- [8] C. Wilkin et al, *Phys. Lett. B*, 654(92), 2007.
- [9] M. Bashkanov et al., *Phys. Lett. B*, 637(223), 2006.

- [10] M. Mielke, *diploma thesis (in preparation)*, University Münster, 2007.

DYNAMICAL COUPLED CHANNEL APPROACH TO OMEGA MESON PRODUCTION

M. Paris
Excited Baryon Analysis Center
Theory Group
Thomas Jefferson National Accelerator Facility
12000 Jefferson Avenue MS 12H2
Newport News, Virginia 23606

Abstract

The dynamical coupled channel approach of Matsuyama, Sato, and Lee is used to study the ω -meson production induced by pions and photons scattering from the proton. The parameters of the model are fixed in a two-channel ($\omega N, \pi N$) calculation for the non-resonant and resonant contributions to the T matrix by fitting the available unpolarized differential cross section data. The polarized photon beam asymmetry is predicted and compared to existing data.

1 Introduction

Nucleon resonances are thought to play a decisive role in reactions of strong, electromagnetic and weak probes on nucleons. The extent to which nucleon resonances determine both unpolarized and polarized observables remains an open question in the second and third resonance regions from center-of-mass (COM) energies, E in the range $1.4 \text{ GeV} \leq E \leq 2.0 \text{ GeV}$. A model determination of the T matrix consistent with the observed meson production data in this kinematic regime seeks to resolve the resonance structure of the nucleon. The determination of the resonance spectrum will yield insight into fundamental aspects of quantum chromodynamics, such as confinement.

In the second and third resonance regions, channels such as ηN , $\pi\Delta$, ρN , σN , ωN and $\pi\pi N$ become important. Matsuyama, Sato, and Lee (MSL) [1] have developed a dynamical coupled channel formalism to handle any number of channels with up to three particles in intermediate and final states. In this exploratory study, we consider the ω meson production reactions, $\pi^- p \rightarrow \omega n$

and $\gamma p \rightarrow \omega p$, in a two-coupled channel $\pi N, \omega N$ formalism. A full calculation incorporating the effect of stable ηN and unstable channels $\pi\Delta, \rho N, \sigma N$ is being pursued presently.

In this study our objective is to show that it is possible (when the ω production is extended to include the four additional channels $\eta N, \pi\Delta, \rho N, \sigma N$) to predict polarized observables from the model resulting from fits to the unpolarized differential cross section data.

We will briefly describe the MSL model theory for the two-channel model for πN and ωN and present results of the fit.

2 Model reaction theory

The T matrix for $\gamma N \rightarrow \omega N$ and $\pi N \rightarrow \omega N$ is separated into non-resonant, t and resonant, t^R terms

$$T(E) = t(E) + t^R(E), \quad (1)$$

where E is the scattering energy of the particles in the center-of-mass frame. The non-resonant contribution is a smooth, regular operator function of the energy while the resonant term is meromorphic in the energy. No additional assumption is made about the relative size of the contributions of these terms.

The non-resonant contribution, $t(E)$ to the full transition matrix satisfies the (relativistic) Lippmann-Schwinger (LS) equation

$$t(E) = [1 + t(E)G_0(E)]v \quad (2)$$

At leading order in the coupling constants of the Lagrangian the kernel, v is given by the Born amplitudes for pion production and photoproduction amplitudes. We neglect the contribution of the η, a_0 , and f_2 in the non-resonant terms.

The kernel depends on coupling and cutoff parameters which are varied (along with the resonance parameters, see below) to fit the observed data. The varied parameters are

$$v = v(g_{\rho NN}, \kappa_\rho, g_{\rho\pi\pi}, g_{\omega NN}, \kappa_\omega, g_{\omega\pi\rho}, \Lambda_{\pi NN}, \Lambda_{\rho NN}, \Lambda_{\rho\pi\pi}, \Lambda_{\omega NN}, \Lambda_{\omega\pi\rho}). \quad (3)$$

The remaining parameters are fixed at the SL [2] values. Form factors are assumed at each vertex. The gauge invariance is ensured only at the Born amplitude level. Inclusion of coupled channel and rescattering effects violates the gauge invariance. This is obviously an unsatisfactory aspect of the model which is hoped to nevertheless be useful in analyzing meson production reactions.

All particles, except the resonances N^* , are assumed to be stable. In particular, we neglect the width of the ω meson $\Gamma_\omega = 8.5(1)$ MeV.

The resonant contribution, $t^R(E)$ to the scattering matrix is given as

$$t^R(E) = \bar{\Gamma}(E) \frac{1}{E - H_0 - \Sigma(E)} \bar{\Gamma}(E), \quad (4)$$

where $H_0 |N^*\rangle = M_{N^*}^{(0)} |N^*\rangle$ and $\bar{\Gamma}(E)$ is the dressed vertex operator and $\Sigma(E)$ the resonance self-energy.

The resonance parameters which can be tuned to fit the experimental data are the bare masses $M_{N^*}^{(0)}$, the amplitudes G_{LSMB}^{JT} , $A_{\lambda, TN, z}^{JT}$, and the cutoffs Λ_{LS}^{JT} , Λ_λ^{JT} . In practice we only use two cutoffs. One for all the strong vertices, $\Lambda_{LS}^{JT} = \Lambda_M$ and one for the electromagnetic vertices $\Lambda_\lambda^{JT} = \Lambda_\gamma$.

3 Results and discussion

The fit to the $\gamma p \rightarrow \omega p$ data is shown in Fig.(1). The simultaneous fit (not shown here) to the $\pi^- p \rightarrow \omega n$ data is of similar quality. In particular, this fit near threshold is consistent with data. The behavior near threshold appears to be described well in the current coupled channel approach [3]. The prediction for the linearly polarized photon beam asymmetry $\Sigma(\theta; E)$ is shown for $E = 1.743$ GeV in Fig.(2). Although the predicted $\Sigma(\theta; E)$ is not consistent with the data, the size and sign are correct. It is hoped that the effect of other channels such as $\pi\Delta, \rho N$, etc. and possibly other resonances will help to improve the agreement.

This work is supported by the U.S. Department of Energy, Office of Nuclear Physics Division under contract No. DE-AC02-06CH11357, and contract No. DE-AC05-06OR23177 under which Jefferson Science Associates operates Jefferson Lab, and by the Japan Society for the Promotion of Science, Grant-in-Aid for Scientific Research©15540275.

References

- [1] A. Matsuyama, T. Sato and T.-S.H. Lee, *Phys. Rept.* **439**, 193 (2007)
- [2] T. Sato and T.-S.H. Lee, *Phys. Rev.* **C63**, 2660 (1996)
- [3] G. Penner and U. Mosel, arXiv:nucl-th/0111024.
- [4] J. Barth *et. al.*, *Phys. Lett.* **B572**, 127 (2003)
- [5] J. Ajaka *et. al.*, *Phys. Rev. Lett.* **96**, 132003 (2006)

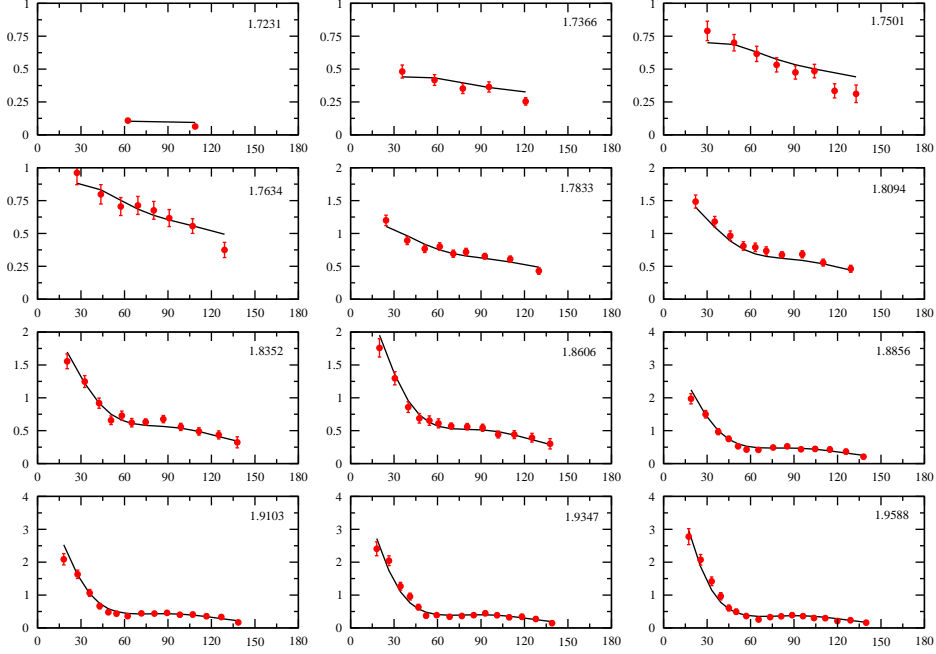


Figure 1: Observed unpolarized differential cross section [4] (circles) for $\gamma p \rightarrow \omega p$ compared to calculated values. The differential cross section, $\frac{d\sigma}{d\Omega}$ in $\mu\text{b}/\text{sr}$ is plotted against the ω emission angle, θ in the center-of-mass frame. Each panel shows the cross section for given center-of-mass energy, E in GeV in the upper-right corner.

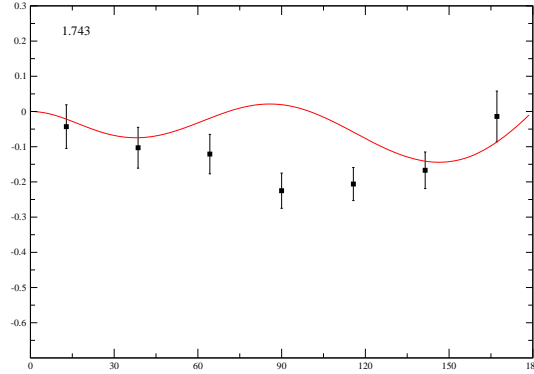


Figure 2: Photon beam asymmetry compared to data from GRAAL [5] for values of COM energy shown in the lower left-hand corner of each panel. Solid curves are for the full calculation. At energy $E = 1.743$ GeV the sensitivity to the resonance contribution is studied (see text).

$3\pi^0$ FINAL STATES WITH WASA AT CELSIUS AND COSY

C. Pauly¹, P. Vlasov for the CELSIUS/WASA and WASA-at-COSY coll.
Institut fuer Kernphysik, Forschungszentrum Juelich
52425 Juelich
Germany

Abstract

High statistic samples of $3\pi^0$ final states in pp scattering at different energies have been measured using the WASA detector. Cross sections for prompt $3\pi^0$ production were determined, η -production dynamics are studied by means of pp and p η invariant mass distributions, and the $\eta \rightarrow 3\pi^0$ Dalitz plot density distribution was measured.

1 Introduction

Hadronic $3\pi^0$ production in pp scattering opens up a wide and interesting field of research and allows to study multi pion production mechanisms, η -production dynamics, and gives the possibility of precise tests of QCD model calculations and predictions. In this text, we summarize on measurements which were done using the WASA 4II detector installed at the CELSIUS accelerator in Sweden. The analysed data were measured during several production beam periods in 2002 and 2003 using a proton beam with kinetic energy of 1300 MeV to 1450 MeV ($Q=17$ MeV to $Q=74$ MeV above the η -threshold), impinging on frozen hydrogen pellets from the unique WASA pellet target system.

In this energy range, two basic mechanisms for $3\pi^0$ production seem to be important: Direct, *prompt* production ($pp \rightarrow pp3\pi^0$, here also including possible excitation of intermediate N^* or Δ resonances) and the *resonant* process via production and decay of an η -meson, $pp \rightarrow pp(\eta \rightarrow 3\pi^0)$. The cross section for prompt $3\pi^0$ production in this energy range has never been measured before, and the obtained results provide first hints on the reaction dynamics in the production mechanism. Further more, the prompt multi-pion production is an important background channel in the analysis of other, rare η decay channels as proposed with WASA-at-COSY, thus a precise knowledge of the

¹c.pauly@fz-juelich.de

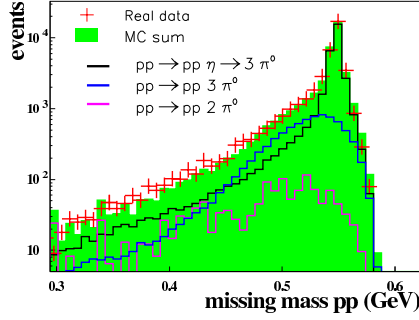


Figure 1: Experimental pp missing mass distribution for $pp\pi^0\pi^0\pi^0$ final states at beam energy $T=1360$ MeV with fit of the Monte Carlo distributions for $2\pi^0$, $3\pi^0$ and η production.

cross section is essential for their analysis.

Analysis of the resonant process allows to study η -production dynamics in the range from $Q=17$ MeV to $Q=74$ MeV above production threshold by means of invariant mass distributions and Dalitz plots of particle subsystems. A precise measurement of the $3\pi^0$ Dalitz plot density distribution for the $\eta \rightarrow 3\pi^0$ decay poses an important test of QCD calculations.

2 Event reconstruction

The analysis is based only on completely reconstructed events with both protons measured in the WASA Forward detector (3° to 17°), and all 6 gammas being detected in the CsI(Na) calorimeter (20° to 140°). Additional cuts on energy thresholds (20 MeV for gammas), overall energy and momentum conservation, and time cuts are used to further suppress background and event overlap. The most probable combinations of the 6 gammas to form 3 pions are selected and used in a final kinematical fit of the full event, based on 8 overconstraints. Separation between prompt and resonant contribution is obtained by applying a narrow cut on the pp missing mass distribution, the remaining prompt background below the η peak is in the order of 5-10 %. The good agreement between Monte Carlo and real data is demonstrated in fig. 1 showing a fit of Monte Carlo simulated distributions for prompt and resonant $3\pi^0$ production to data.

3 Cross section for prompt $3\pi^0$ production

The ratio of prompt and resonant contribution obtained by the fit of the pp missing mass distribution can be directly converted into cross sections for prompt $3\pi^0$ production by using the well known $pp \rightarrow pp(\eta \rightarrow 3\pi^0)$ cross section for normalization. As a cross check, the resonant η -production cross sections were calculated using the luminosity obtained from pp elastic

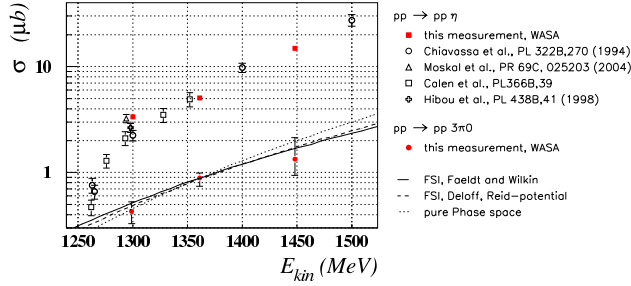


Figure 2: Cross section overview for η production $pp \rightarrow pp\eta$ and prompt 3 pion production, $pp \rightarrow pp3\pi^0$ as function of beam energy.

scattering and applying a complete acceptance correction. The results are summarized in fig. 2. The deduced $pp \rightarrow pp3\pi^0$ excitation function is consistent with the increase of phase space volume, which allows for a first rough extrapolation also to higher energies available now with WASA-at-COSY. The obtained η production cross sections are in good agreement with results from other experiments. Further discussion of the results can be found in [2].

4 Eta production dynamics

In Fig. 3 the obtained invariant mass distributions for the pp and $p\eta$ subsystems are shown. The obtained results nicely combine with results from previous measurements by COSY11 [4] and COSY-TOF [5], and expand these studies to a higher energy range. One can clearly see how the spectra at lowest excess energy, $Q=17$ MeV, are dominated by pp final state interaction leading to an enhancement for low pp invariant mass. The pp FSI effect fades out for the higher excess energies and is replaced by a prominent dip in the $p\eta$ invariant mass distribution, which is the dominant deviation from phase space at $Q=74$ MeV. This dip lacks a theoretical description yet, a possible explanation might be higher partial wave contributions.

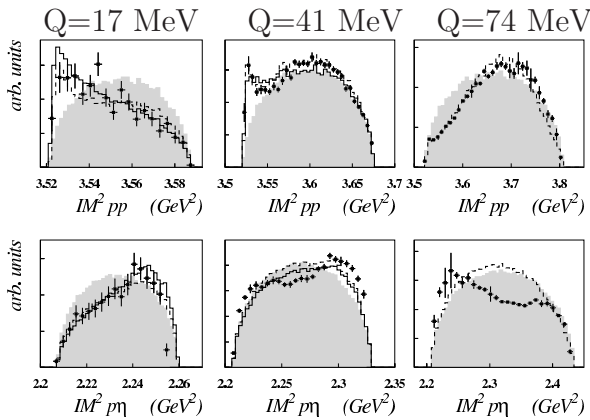


Figure 3: Invariant mass of the pp and $p\eta$ system for events of type $pp \rightarrow pp \eta$ from $Q=17$ MeV to $Q=74$ MeV above the η production threshold. Solid line shows the calculation from [?]

5 $\eta \rightarrow 3\pi^0$ Dalitz plot density distribution

The distribution of events in a symmetrized Dalitz plot of the 3 pions in the $\eta \rightarrow 3\pi^0$ decay is a sensitive probe for the interaction of pions in the final state. Without any pion rescattering, the Dalitz plot population would be flat due to the three identical final state particles. A linear fit to the one dimensional density distribution (expressed as function of the radial parameter z) yields the slope parameter α . Different approaches on the theory side exist to include this pion rescattering, a precise measurement of α is a crucial test of these QCD calculations. Two high precision measurements of α were performed by KLOE [6] and Crystal Ball [7], each based on $> 10^6$ events in the Dalitz plot. The CELSIUS/WASA result for α , shown in fig 4, is based on 75000 events and in agreement within stated errors but limited by statistics. More details can be found in [3].

These studies are now continued with WASA-at-COSY, data taken during a first production run in April 2007 will significantly increase the present statistic and hopefully allow for a more accurate determination of α .

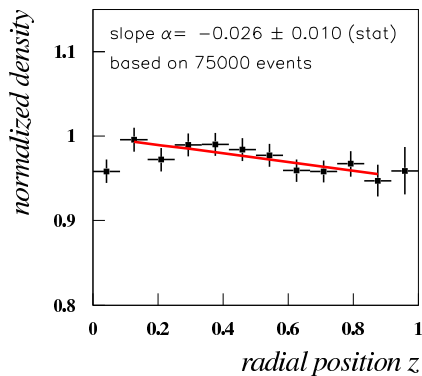


Figure 4: Efficiency corrected Dalitz plot density distribution as function of radial variable z , together with the fitted result for slope α . Only statistical errors are shown.

References

- [1] A. Deloff, *Phys. Rev. C* **69**, 035206 (2004).
- [2] C. Pauly et al., *Phys. Lett. B* **649**, 122 (2007).
- [3] M. Bashkanov et al., *Phys. Rev. C* **76**, 048201 (2007)
- [4] P. Moskal et al., *Phys. Rev. C* **69**, 025203 (2004).
- [5] M. Abdel-Bary et al., *Eur. Phys. J. A* **16**, 127 (2003).
- [6] F. Ambrosino et al., *arXiv:0707.4137[hep-ex]*.
- [7] W. B. Tippens et al., *Phys. Rev. Lett.* **87**, 192001 (2001).

HIGH-STATISTICS η PRODUCTION IN PROTON-PROTON COLLISIONS AT Q=72 MeV

*H. Pettersson*¹ for the CELSIUS/WASA collaboration
Department of Nuclear and Particle Physics²
Uppsala University
Uppsala, Sweden

Abstract

The production of η mesons at an excess energy of Q=72 MeV has been studied in the reaction $pp \rightarrow pp(\eta)\gamma\gamma$. Preliminary angular distributions and projections of invariant masses are presented. Deviations from phase space behavior is observed, indicating the presence of different partial waves.

1 Introduction

Meson production experiments give us the possibility to study the interaction between nucleons and short-lived mesons. The interactions between the final state particles are expected to show up as a non-homogeneous population in some regions of the Dalitz plots. The large mass of the mesons produced and the corresponding large momentum transfer make meson production experiments a way of probing the short-range part of the nucleon-nucleon interaction. An additional motivation for η production experiments is the strong coupling of the η to the $N^*(1535)$ resonance close to threshold. Successful modelling of the production mechanism of η could therefore lead to information on this resonance.

There are previous near-threshold measurements of η production in proton-proton collisions at CM excess energies of Q=15 MeV [1], 15.5 MeV [2], 16 and 37.6 MeV [3] and 41 MeV [1]. The measurement at 37.6 MeV, performed at CELSIUS, showed some anisotropy in the scattering angle of the η in the CM system, whereas the measurement at 41 MeV, performed at COSY using a detector with higher acceptance, is consistent with isotropy.

¹Dept. of Nuclear and Particle Physics, Uppsala University

²Box 535, 751 21 Uppsala, Sweden

We would like to investigate the presence of higher partial waves in the $pp \rightarrow pp\eta$ reaction. Thanks to an energy upgrade of the CELSIUS storage ring, WASA can add one data point in the region where the onset of higher partial waves is expected [4]. The WASA detector also has much higher acceptance than the one used in Ref. [3].

In this context, it is interesting to consider the results from the DISTO collaboration, who have measured differential cross sections at higher excess energies [5]. At their lowest excess energy (324 MeV) they observe an isotropy where the η is produced preferentially perpendicular to the beam. The isotropy weakens with energy and vanishes at their highest energy (554 MeV). In their studies of the momentum differential cross sections, the authors see the influence of the $N^*(1535)$, but no need for other partial waves than s-wave to explain their data.

2 Analysis

The data was taken in December 2003 with the WASA detector [6] and the η was detected through its decay into 2γ . This decay was chosen because of its high branching ratio and clear signature and as a means to cross-check the study of the $\eta \rightarrow 3\pi^0$ decay (the same trigger was used). The trigger required at least two charged particles in the forward detector, and no charged particles in the central detector. Furthermore, the deposited energy in the calorimeter had to exceed a certain threshold. A veto on hits in the forward veto hodoscope [6] was applied in order to cut down background from pion production.

To select the $\eta \rightarrow 2\gamma$ events in the off-line analysis, we required two tracks with precise angular information in the forward detector and exactly two hit clusters from photons in the calorimeter. The invariant mass of the two photons was required to be above 450 MeV, and the missing mass of the two protons was required to be between 525 and 575 MeV. The geometric acceptance of the WASA setup for this four-particle final state is about 43%, and the reconstruction efficiency for the signal reaction as determined from a Monte Carlo simulation of the detectors is around 10 %. While no kinematical fitting was used, momentum balance was imposed by the requirement that the η momenta as reconstructed from the two photons and from the two protons be within 28 degrees of each other, and that the invariant mass squared of the difference between the four-vectors be less than 0.02 GeV^2 . From comparison with signal and background (assumed to consist of non-resonant $2\pi^0$ -production) Monte Carlo, the fraction of background in the data is estimated to 15-30 %.

3 Results

The preliminary distributions shown are based on a sample of $167 \cdot 10^3$ events. The acceptance has been determined by passing generated events with phase space weights through a GEANT3 [7] simulation of the detector. Only statistical errors are shown as the magnitude of the systematical errors has not yet been determined.

The CM η scattering angle shown in figure 1 is non-isotropic, which implies the presence of higher partial waves, as does the distribution in $\cos \theta_p^{pp}$ seen in figure 2. In the invariant mass squared of the two protons (figure 3)

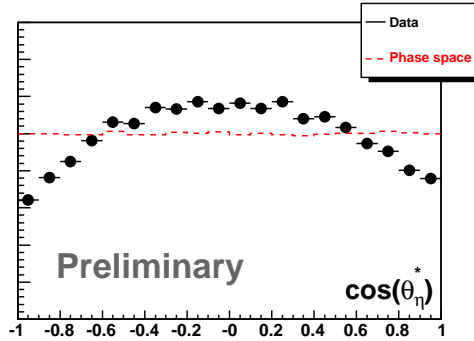


Figure 1: Differential cross section (in arbitrary units) as a function of the η scattering angle in the CM system.

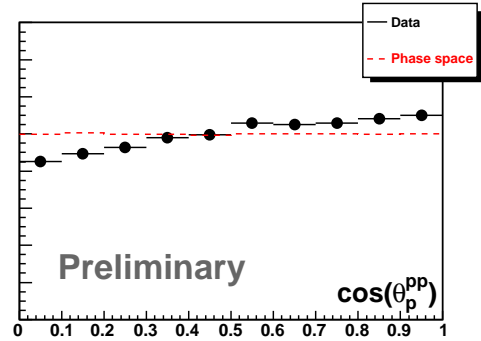


Figure 2: Differential cross section (in arbitrary units) as a function of the proton scattering angle in the proton-proton system.

a small effect of the proton-proton final state interaction (FSI) is barely visible around 3.54 GeV^2 . The enhancement over phase space around 3.7 GeV^2 has also been observed at COSY [1], and could be explained by proton-proton P wave [8]. Isolating any effect of the proton- η FSI from the effect of higher partial waves in the invariant mass squared of one proton and the η (figure 4) requires further analysis.

4 Conclusions

Differential cross section of the $pp \rightarrow pp\eta$ reaction have been measured at $Q=72$ MeV. The $\cos \theta_\eta^*$ -distribution and the $\cos \theta_p^{pp}$ -distribution both show deviations from isotropy, indicating the presence of higher partial waves. To separate the contributions from higher waves from proton- η FSI, further measurements with polarized protons are desirable *e.g.* by WASA at COSY.

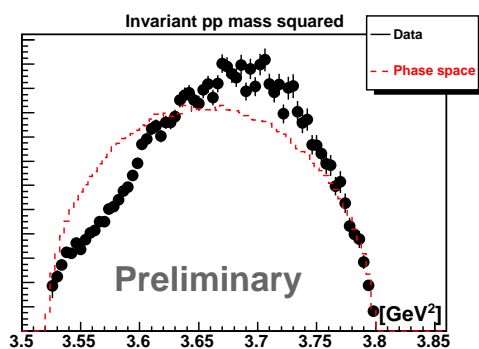


Figure 3: Differential cross section (in arbitrary units) as a function of the pp invariant mass squared.

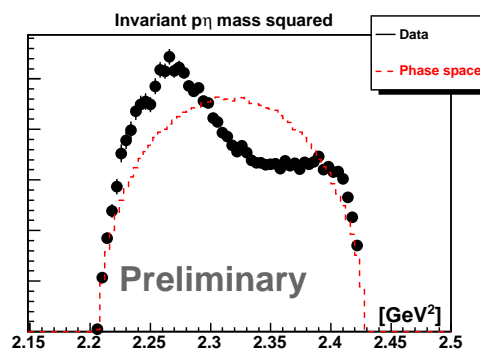


Figure 4: Differential cross section (in arbitrary units) as a function of the $p\eta$ invariant mass squared.

Acknowledgments

This contribution is dedicated to the memory of David Duniec.

References

- [1] M. Abdel-Bary *et al.* [COSY-TOF Collab.], *Eur. Phys. J. A* **16**, 127 (2003).
- [2] P. Moskal *et al.*, *Phys. Rev. C* **69**, 025203 (2004).
- [3] H. Calén *et al.*, *Phys. Lett. B* **458**, 190 (1999).
- [4] P. Moskal, *Hadronic interaction of η and η' mesons with protons* (Wydawnictwo uniwersytetu Jagiellońskiego, Cracow, 2004).
- [5] F. Balestra *et al.* [DISTO Collab.], *Phys. Rev. C* **69**, 064003 (2004)
- [6] J. Zabierowski *et al.*, The CELSIUS/WASA Detector Facility, in *Eta Physics Handbook (Physica Scripta T99 2002)*.
- [7] R. Brun *et al.*, GEANT. CERN DD/EE/84-1
- [8] K. Nakayama *et al.*, *Phys. Rev. C* **68**, 045201 (2003)

CHARM AND CHARMONIUM PHYSICS AT *BABAR*

Elisabetta Prencipe
prencipe@slac.stanford.edu
University of Ferrara & INFN
via Saragat, 1 - 44100 Ferrara (IT)

Abstract

The *BaBar* experiment, located in SLAC at the PEP-II asymmetric storage ring, achieved the luminosity of 477 fb^{-1} , so Spectroscopy studies are possible. The *B-Factory BaBar* offers an excellent opportunity in searching new states and their decay modes to understand their nature. Here below the states recently observed at *BaBar* are briefly presented.

1 Charm Spectroscopy

Only 4 $c\bar{s}$ quarks bound states were observed before *B-factories* started to work in this field, in perfect agreement with the theoretical models.

BaBar observed $D^*(2317)^+$ and $D_{sj}(2460)^+$ in the decay modes $D_s^+\pi^0$ and $D_s^{*+}\pi^0$ respectively, at energies where the theory has not done predictions. New non-expected states were observed, making more rich the mass spectrum, most of them decaying to channels where D_s got involved: $D_{sj}^*(2317)^+$ and $D_{s1}(2536)^+$. For these analyses, high precision measurements and high statistics were required [1]. These very narrow states were detected in inclusive decays of the *B* meson.

A very interesting contribution of *Babar* was given in the measurement of the mass difference of D_{s1} and D^* . In the PDG06 [2] the value was: $(525.0 \pm 0.6 \pm 0.1) \text{ MeV}/c^2$; *BaBar* obtained: $m(D_{s1} - m(D^*)) = (525.85 \pm 0.02 \pm 0.04) \text{ MeV}/c^2$ [3, 4], a large improvement in the error measurement. By searching in the inclusive modes: $e^+e^- \rightarrow D^{0,\pm}K^{0,\pm}X$, *BaBar* observed on 240 fb^{-1} the values reported in the table below.

A new state in the mass spectrum was added: Ω_c^{*0} [5]. On 232 fb^{-1} *BaBar* searched this $c\bar{s}s$ state, $J^P = \frac{3}{2}^+$, decaying to $\Omega_c^0\gamma$, with Ω_c^0 decaying in 4 different modes. By combining them, the mass difference of Ω_c^{*0} and Ω_c^0 was

measured: $(70.8 \pm 1.0 \pm 1.1) \text{ MeV}/c^2$. In addition, we report the measured value: $\frac{\sigma(e^+e^- \rightarrow \Omega_c^{*0})}{\sigma(e^+e^- \rightarrow \Omega_c^0)} = (1.01 \pm 0.23 \pm 0.11)$.

Another interesting contribution of *BaBar* was given in the analysis of the invariant mass of $D - \text{proton}$: a known state was confirmed, $\Lambda_c(2880)^+$, and a new state was observed: $\Lambda_c(2940)^+$ [6].

Evidence of excited charmed baryons was found: $\Xi_c(2980)^+$, $\Xi_c(3077)^+$, $\Xi_c(3077)^0$, and the recent observations for $\Xi_c(3055)^+$ and $\Xi_c(3125)^+$ make this study more interesting [7]. They are in agreement with the corresponding values published by the *Belle* collaboration, even if the measurements done in *Belle* show to be slightly overestimated from the corresponding ones measured in *BaBar*, the smaller values of mass and width in some cases due to the treatment of proximity to the threshold.

<i>Decay mode</i>	<i>State</i>	<i>Mass(MeV/c²)</i>	$\Gamma(\text{MeV})$
$D^0 \rightarrow K^- \pi^+$	$D_{s2}^*(2573)$	$2572.2 \pm 0.3 \pm 1.0$	$27.1 \pm 0.6 \pm 5.6$
$D^0 \rightarrow K^- \pi^+$	$X(2690)$	$2688 \pm 4 \pm 3$	$112 \pm 7 \pm 36$
$D^0 \rightarrow K^- \pi^+$	$D_{sj}^*(2860)$	$2856.6 \pm 1.5 \pm 5.0$	$47 \pm 7 \pm 10$
<i>D proton</i>	$\Lambda_c(2880)^+$	$2881.9 \pm 0.1 \pm 0.5$	$5.8 \pm 1.5 \pm 1.1$
<i>D proton</i>	$\Lambda_c(2940)^+$	$2939.8 \pm 1.3 \pm 1.0$	$17.5 \pm 5.2 \pm 5.9$

2 Charmonium Spectroscopy

The $c\bar{c}$ mass spectrum is not completely understood, and not full-filled yet. In fact, states below the $D\bar{D}$ threshold are well known, and some 1^{--} states above; moreover they fit well theoretical models. Recently, some other states were observed but they do not fit well theoretical predictions. More than one prediction was done from theorists [11]. Here below are presented the results of the more recent *charmonium-like* states observed in *Babar*.

BaBar searched for the narrow state $X(3872)$ [8] ($\Gamma < 2.3 \text{ MeV}$ and $M = (3782.4 \pm 0.6) \text{ MeV}/c^2$, world average) in $B \rightarrow XK$, $X \rightarrow J/\psi \pi^+ \pi^-$, and also in the decay $B \rightarrow J/\psi \gamma K$, on 260 fb^{-1} . Thanks to this decay mode observed, we could establish that the parity C of this state is positive [9].

An important implication concerning the decay modes of $X \rightarrow J/\psi \pi^+ \pi^-$ is that the invariant mass of $\pi^+ \pi^-$ is compatible with the ρ mass, so we should look at the charged partners of X ($I = 1$). But the search for X^+ or X^- gave no evidence of signal [10]. So we can conclude that the resonance X is a isospin violating state ($I = 0$). That is the reason why we observed such a

narrow width.

Recently, *BaBar* searched for the decay: $B \rightarrow \bar{D}^0 D^{*0} K$ [12]. By studying the invariant mass of $\bar{D}^0 D^{*0}$, with $D^{*0} \rightarrow D^0 \pi^0$ and $D^{*0} \rightarrow D^0 \gamma$, we observed an excess of events at $(3875.1 \pm 0.7 \pm 0.5) \text{ MeV}/c^2$. This important result confirms the measurement that *Belle* performed in $B \rightarrow \bar{D}^0 D^0 \pi^0 K$, even if this mass value is 4.5σ above the world average of $X \rightarrow J/\psi \pi^+ \pi^-$.

The X(3872) is probably not a charmonium state. But we cannot exclude other interpretations, yet [11].

Searching in the decay $B \rightarrow J/\psi \omega K$ *BaBar* confirmed another important result: the discovery of the X(3940) [13].

BaBar analyzed the invariant mass of $J/\psi \omega$, where $\omega \rightarrow \pi^+ \pi^- \pi^0$, and $J/\psi \rightarrow l^+ l^-$, $\pi^0 \rightarrow \gamma \gamma$, $K_s \rightarrow \pi^+ \pi^-$. In order to check the purity of the signal sample *BaBar* weighted each event with the appropriate function (Legendre polynomial of the second order $\times \cos \theta$, where θ is the ω Dalitz-plot helicity angle), so we can be sure that no contribution of non-resonant $\pi^+ \pi^- \pi^0$ can create a peak in the $J/\psi \omega$ invariant mass.

By combining the charged and the neutral modes, *BaBar* found with 350 fb^{-1} the mass value $M = (3914.3_{-3.4}^{+3.8}(\text{stat}) \pm 1.6(\text{sys})) \text{ MeV}/c^2$ and a width: $\Gamma = (33 \pm 0.7_{-8}^{+12}(\text{stat}) \pm 0.6(\text{sys})) \text{ MeV}$.

The B.R. of the $B \rightarrow J/\psi \omega K$ was measured, too. It is in good agreement with the *Belle* measurements, while the measurements of mass and width of the state X(3940) done in *Belle* are overestimated compared to what we observed in *BaBar*, because we obtained the measurement of a more narrow state and a mass value being $30 \text{ MeV}/c^2$ smaller.

The discovery of the state called Y(4260) [14] came from ISR events, and *Belle* confirmed by *CLEO*. The mass value is $(4258 \pm 8_{-4}^{+6}) \text{ MeV}/c^2$ and the width is $(88 \pm 23_{-4}^{+6}) \text{ MeV}$.

As it comes from ISR events, its quantum numbers are $J^{PC} = 1^{--}$. But in the plot of the ratio R (the ratio between the cross section of $e^+ e^- \rightarrow \text{hadrons}$ to the cross section of $e^+ e^- \rightarrow \mu^+ \mu^-$) we expected to look at a maximum corresponding to the energy in the center of mass of 4.26 GeV. Indeed, we looked at a local minimum there, that is a very peculiar behaviour. So, in order to reject some possibilities, we searched for the decay modes: $Y(4260) \rightarrow \pi^+ \pi^- \phi$, $Y(4260) \rightarrow D \bar{D}$ and $Y(4269) \rightarrow p \bar{p}$: we observed no yields, so probably it is not a glueball or charmonium state. There is also an evidence of this new state in the charged B decay: the measurement of this B.R. ($B \rightarrow Y(J/\psi \pi^+ \pi^-) K$) is $(2.0 \pm 0.7 \pm 0.2) 10^{-5}$.

The search for the Y(4260) decay modes, and other searches in the inclusive

$J\psi\pi^+\pi^-$ led to the discovery of another resonance, whose mass is (4324 ± 24) MeV/ c^2 [15] and whose width is (172 ± 33) MeV. It is not compatible with the above mentioned Y(4260), neither with Y(4415) or S-waves-three-body-phase space. That is a new peak, confirmed now also from the *Belle* Collaboration.

Acknowledgments

We are grateful for the excellent luminosity and machine conditions provided by our PEP-II colleagues, and for the substantial dedicated effort from the computing organizations that support *BaBar*.

References

- [1] BABAR Collaboration, B. Aubert *et al.* Phys. Rev. Lett. **74** 032007;
- [2] D. E. Groom *et al.* [Particle Data Group Coll.], “ *Review of particle physics,*” Eur. Phys. J. C **15**;
- [3] BABAR Collaboration, B. Aubert *et al.* hep-ex/0607084 ;
- [4] BABAR Collaboration, B. Aubert *et al.* Phys. Rev. Lett. **97** 222001;
- [5] BABAR Collaboration, B. Aubert *et al.* Phys. Rev. Lett. **97** 232001;
- [6] BABAR Collaboration, B. Aubert *et al.* Phys. Rev. Lett. **98** 012001;
- [7] BABAR Collaboration, B. Aubert *et al.* hep-ex/0607042;
- [8] Belle Collaboration, Phys. Rev. Lett. **91** 262003; BABAR Collaboration, B. Aubert *et al.* Phys. Rev. Lett. **73** 011101; Phys. Rev. Lett. **74** 071101;
- [9] BABAR Collaboration, B. Aubert *et al.* Phys. Rev. Lett. **71** 031501;
- [10] BABAR Collaboration, B. Aubert *et al.* hep-ex. arXiv:0708.1565;
- [11] Phys. Rev. D. **71** 074005; Phys. Rev. D. **71** 014028;
- [12] BABAR Collaboration, B. Aubert *et al.* arXiv: hep-ex/0708.1565
- [13] BABAR Collaboration, B. Aubert *et al.* Phys. Rev. Lett. **95** 142001;
- [14] BABAR Collaboration, B. Aubert *et al.* Phys. Rev. Lett. **73** 011101; Phys. Rev. Lett. **73** 012005;

- [15] BABAR Collaboration, B. Aubert *et al.* Phys. Rev. Lett. **98** 212001;

ISOSPIN DEPENDENCE OF THE η' MESON PRODUCTION IN NUCLEON-NUCLEON COLLISIONS

Joanna Przerwa for the COSY-11 collaboration

Institute of Physics
Jagiellonian University
Cracow, PL-30-059

Abstract

Using the COSY-11 detection setup we intend to determine the excitation function of the total cross section for the $pn \rightarrow pn\eta'$ reaction near the kinematical threshold. The comparison of the $pp \rightarrow pp\eta'$ and $pn \rightarrow pn\eta'$ total cross sections will allow to learn about the production mechanism of the eta-prime meson in nucleon-nucleon collisions and to investigate aspects of the gluonium component of the η' meson. A method of the measurement and preliminary results are presented in this report.

1 Introduction

Despite the fact that the η' meson was observed forty years ago, there is not much known about the relative contribution of the possible reaction mechanisms of the production of this meson. It is expected that the η' meson can be created through heavy meson exchange, through the excitation of an intermediate resonance or via emission from the virtual meson [1]. It is also possible that η' meson is produced from excited glue in the interaction region of the colliding nucleons, which couple to the η' meson directly via its gluonic component or through its SU(3)-flavour-singlet admixture [2, 3]. As suggested in reference [4], η' production via the colour-singlet object does not depend on the total isospin of the colliding nucleons and should lead to the same production amplitude for the η' in the $pn \rightarrow pn\eta'$ and $pp \rightarrow pp\eta'$ reactions. In case of the η meson, the ratio of the total cross sections for the reactions $pn \rightarrow pn\eta$ and $pp \rightarrow pp\eta$ was determined to be $R_\eta = 6.5$ [5], what suggest the dominance of isovector meson exchange in the η production in nucleon-nucleon collisions. Since the quark structure of η and η' mesons is very similar, in case of the dominant isovector meson exchange – by the

analogy to the η meson production – we can expect that the ratio $R_{\eta'}$ should also be about 6.5. If however η' meson is produced via its flavour-blind gluonium component from the colour-singlet glue excited in the interaction region the ratio should approach unity after corrections for the initial and final state interactions. The close-to-threshold excitation function for the $pp \rightarrow pp\eta'$ reaction has already been determined [6–10], whereas the total cross section for the η' meson production in the proton-neutron interaction is still unknown.

2 Measurement of the $pn \rightarrow pn\eta'$ reaction

In August 2004 –for the first time– using the COSY–11 facility [?, 12] we have conducted a measurement of the η' meson production in the proton-neutron collision. A quasi-free proton-neutron reactions were induced by a proton beam impinging on a deuteron target. The experiment is based on the reg-

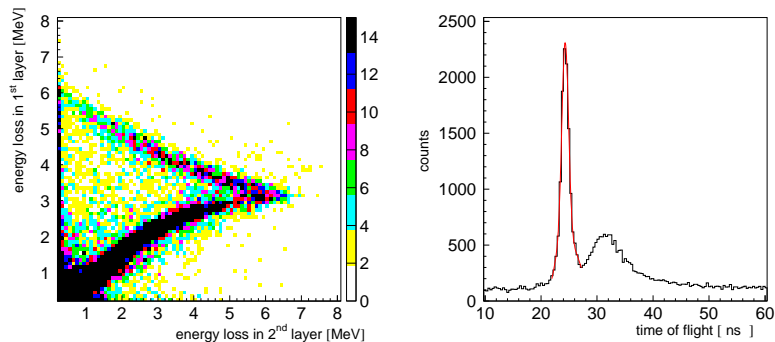


Figure 1: Energy losses in the first layer versus the second layer as measured at COSY–11 with a deuteron target and a proton beam with momentum of 3.35 GeV/c (left). Time-of-flight determined between the target and the neutron detector (right).

istration of all outgoing nucleons from the $pd \rightarrow p_{sp}pnX$ reaction. Protons are measured in two drift chambers and scintillator detectors [13], neutrons are registered in the neutral particle detector [14]. Protons considered as spectators are measured by the dedicated silicon-pad detector [15, 16]. Figure 1 (left) shows energy losses in the 1th layer of the spectator detector versus 2nd layer. Slow spectator protons are stopped in the first layer of the detector whereas fast particles cross both detection layers. The total

energy available for the quasi-free proton-neutron reaction can be calculated for each event from the vector of the momenta of the spectator and beam protons, assuming that the spectator does not take part in the reactions and escapes untouched carrying the Fermi momentum possessed at the time of the reaction. The absolute momentum of neutrons is determined from the time-of-flight between the target and the neutron detector. Figure 1(right) presents the time-of-flight distribution – for neutral particles – measured between the target and the neutral particle detector. A clear signal originating from the gamma rays is seen over a broad enhancement from neutrons. This histogram shows that discrimination between signals originating from neutrons and gamma quanta can be done by a cut on the time of flight. Application of the missing mass technique allows to identify events with the creation of the meson under investigation. However, due to the smaller efficiency and lower resolution for the registration of the quasi-free $pn \rightarrow pn$ meson reaction in comparison to the measurements of the proton-proton reactions, the elaboration of the data encounters problems of low statistic. However one can determine the number of registered $pn \rightarrow pn\eta'$ events from the multi-pion background by comparison of the missing mass distributions for the negative values of Q , when only pions may be created, and for Q values larger than 0 [17]. The evaluation of the background is in progress.

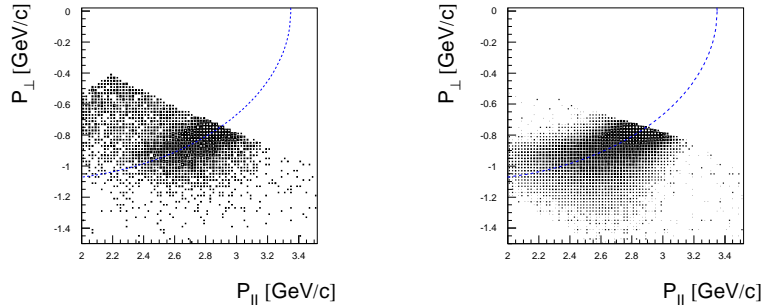


Figure 2: Parallel versus transversal momentum component of the reconstructed fast proton momentum as obtained in the experiment (left) and in the simulation (right).

The luminosity will be established from the number of the quasi-free proton-proton elastic scattering events employing the method described in

the [18]. Figure 2 shows parallel versus transversal component of the reconstructed momentum of the forward scattered proton. Events corresponding to the elastic scattered protons are seen near the kinematical ellipse, which is marked as a solid line. The comparison of the experimental and simulated distributions will enable to determine the value of the integrated luminosity [18].

Acknowledgments

We acknowledge the support of the European Community-Research Infrastructure Activity under the FP6 programme (Hadron Physics, N4:EtaMesonNet, RII3-CT- 2004-506078), the support of the Polish Ministry of Science and Higher Education under the grants No. PB1060/P03/2004/26, 3240/H03/2006/31 and 1202/DFG/2007/03, and the support of the German Research Foundation (DFG).

References

- [1] K. Nakayama *et al.*, *Phys. Rev. C* **61** 024001 (2000).
- [2] S. D. Bass, A. W. Thomas, *Phys. Lett. B* **634** 368 (2006).
- [3] S. D. Bass, *Acta Phys. Slov* **56** 245 (2005).
- [4] S. D. Bass, *Phys. Lett. B* **463** 286 (1999).
- [5] H. Calen *et al.*, *Phys. Rev. C* **58** 2667 (1998).
- [6] P. Moskal, ArXiv: hep-ph/0408162 (2004).
- [7] P. Moskal *et al.*, *Phys. Lett. B* **474** 416 (2000).
- [8] A. Khoukaz *et al.*, *Eur. Phys. J. A* **20** 345 (2004).
- [9] F. Balestra *et al.*, *Phys. Lett. B* **491** 29 (2000).
- [10] P. Moskal *et al.*, *Phys. Rev. Lett.* **80** 3202 (1998).
- [11] S. Brauksiepe *et al.*, *Nucl. Instr. & Meth. A* **376** 397 (1996).
- [12] P. Klaja *et al.*, *AIP Conf.Proc.* **796** 160 (2005).
- [13] J. Smyrski *et al.*, *Nucl. Instr. & Meth. A* **541** 574 (2005).

- [14] J. Przerwa *et al.*, *Int. J. of Mod. Phys. A* **20** 625 (2005).
- [15] R. Bilger *et al.*, *Nucl. Instr. & Meth. A* **457** 64 (2001).
- [16] M. Janusz, diploma thesis, Jagellonian University, Cracow (2004).
- [17] P. Moskal *et al.*, *J. Phys. G* **32** 629 (2006).
- [18] P. Moskal and R. Czyżykiewicz, ArXiv:0709.4021 (2007).

IN SEARCH OF THE BOX ANOMALY WITH THE WASA-AT-COSY FACILITY

*Christoph Florian Redmer*¹
 for the WASA-at-COSY Collaboration
 Institut für Kernphysik
 Forschungszentrum Jülich
 52425 Jülich, Germany

Abstract

The decays $\eta, \eta' \longrightarrow \pi^+\pi^-\gamma$ provide a good tool to study the box anomaly but so far the available statistics is rather poor. Additionally, the measurements with highest statistics yield contradictory results.

The WASA-at-COSY facility provides a unique opportunity to study decays of η and η' with highest statistics. This presentation intends to show the feasibility of the measurement of $\eta, \eta' \longrightarrow \pi^+\pi^-\gamma$.

1 Theoretical Aspects

The box anomaly is a higher order term of the Wess-Zumino-Witten Lagrangian (WZW) [1, 2], which describes the direct coupling of three pseudoscalar mesons and a photon. Its name results from the shape of the Feynman diagrams representing the WZW as can be seen in Fig. 1.

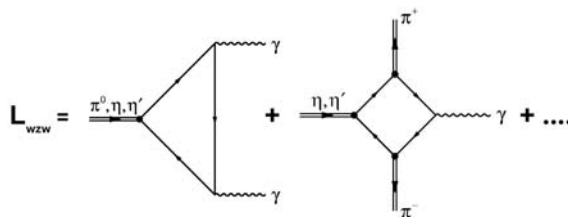


Figure 1: Lower orders of the Wess-Zumino-Witten Lagrangian illustrated by Feynman diagrams

Predestined for experimental studies are the decays of η and η' into two pions and a single photon. Since the box anomaly describes a non-resonant coupling, the invariant mass of the pions is a good observable to disentangle possible resonant contributions, e.g. from the ρ -meson.

¹e-mail: c.redmer@fz-juelich.de

Unfortunately the WZW is only valid at the chiral limit whereas the kinematic range of the decays of η and η' is well above it. In case of the η' even the mass of the ρ -meson is covered. Therefore, efforts have been made to describe the contributions of the anomalies to these decays correctly, mainly by implementing unitarity effects via final state interactions. The latest approaches are:

- N/D-structure matching the one loop corrections, realized by an Omnès-function [3].
- Evaluation of the WZW in the context of hidden local symmetries [4].
- Chiral unitarity approach using a Bethe-Salpeter-equation with coupled channels [5].

2 Results of other facilities

A number of experiments have already measured the decays $\eta, \eta' \longrightarrow \pi^+\pi^-\gamma$. This section will concentrate on the samples with highest statistics.

Already in the 1970s the η decay had been measured by Gormley [6] and Layter [7] yielding 7257 ± 180 events and 18150 events, respectively, after background subtraction. An analysis of these data sets according to the approaches described above showed that they are either in contradiction to each other [4], or that they show some inconsistency when trying to handle the data sets in a combined way [8].

The largest published data sample on the η' decay is the one of the Crystal Barrel Collaboration [9], containing 7369 events after background subtraction. In addition to the resonant contribution of the ρ -meson a non-resonant term was needed to fit the invariant mass spectrum of the two pions, which was interpreted as clear evidence of the box anomaly. This was also affirmed by all theoretical approaches applied on these data [3–5].

The L3 collaboration published another data sample of this η' decay of 2786 events [10]. In contrast to the result of Crystal Barrel, the resonant contribution of the ρ -meson was sufficient to describe the invariant mass spectrum. A test to use the parameterization of the Crystal Barrel results was only possible at a confidence level of 3%.

Consequently, there is a variety of theoretical calculations, but only few experimental data sets are available. In addition, the experiments with the largest statistics are not consistent. This is the situation where WASA-at-COSY [11] will come into play.

3 Investigations with WASA-at-COSY

η and η' mesons will be produced in proton-proton collisions at beam momenta of 2.14 GeV/c and 3.35 GeV/c, respectively. The close to 4π sr coverage of the WASA detector setup allows for exclusive measurements. In the Forward Detector (FD) the two outgoing protons from the $pp \rightarrow pp\eta^{(\prime)}$ reaction will be measured, providing the missing mass information necessary to tag the meson production. The decay products will be measured in the Central Detector (CD). As an example Fig. 2 shows the simulated distribution of the kinetic energy as a function of the θ -angle for protons, π 's and γ 's for produced η 's decaying to $\pi^+\pi^-\gamma$. The dashed lines indicate the range covered by the FD in case of the protons and by the CD in case of pions and gammas. By that mean a geometric acceptance of approximately 46% can be extracted. In case of the η' decay it is approximately 34%.

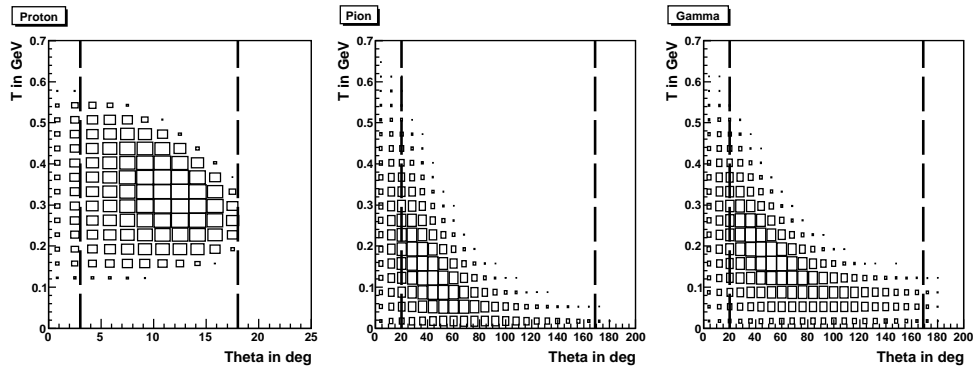


Figure 2: Distribution of energies as a function of θ -angle for p, π and γ . Simulation of $\eta \rightarrow \pi^+\pi^-\gamma$ assuming homogeneous phase space population. The dashed lines delimit the angular coverage of the detector.

Assuming the design luminosity of $10^{32} \text{cm}^{-2} \text{s}^{-1}$ rates of 22 (η) and 3 (η') $\pi^+\pi^-\gamma$ events in acceptance can be expected per second. This will allow to take within few weeks data samples which are orders of magnitudes higher than the presently available world statistics.

Tab. 1 shows some of the possible background channels taken into account for initial studies. The major contribution is assumed to originate from wrongly reconstructed reactions, where one of the decay products was lost due to the geometrical acceptance of the detector. Unfortunately, even the main hadronic decays of η and η' themselves contribute. Another class of background results from the secondary interactions of pions in the calorimeter. Due to pion decays or hadronic absorption an additional neutral cluster

may appear in the reconstructed event.

$pp \longrightarrow ppX$	2.14 GeV/c	$pp \longrightarrow ppX$	3.35 GeV/c
$\eta \longrightarrow \pi^+\pi^-\pi^0$	28.7%	$\eta' \longrightarrow \pi^+\pi^-\eta$	14%
$\pi^+\pi^-\pi^0$	17.3%	$\omega \longrightarrow \pi^+\pi^-\pi^0$	6%
$\pi^+\pi^-$	34.2%	$\rho \longrightarrow \pi^+\pi^-$	38.7%
		$\eta \longrightarrow \pi^+\pi^-\pi^0$	2.5%
		$\pi^+\pi^-\pi^0$	5.5%
		$\pi^+\pi^-$	12%

Table 1: Possible background channels and the geometric acceptance to detect them with only a single photon.

The cross sections of the background channels shown in Tab. 1 is of the same or even higher orders of magnitude. One of the most promising methods to suppress background is to explicitly demand the conservation of energy and momentum in the reconstructed events. The development of these methods has just started and extensive Monte Carlo studies will follow. Early tests on data of the first WASA-at-COSY production run were already able to extract an η signal in the missing mass spectrum.

References

- [1] J. Wess and B. Zumino, *Phys. Lett.* **B37**, 95 (1971).
- [2] E. Witten, *Nucl. Phys.*, **B223**, 422-432 (1983).
- [3] B. R. Holstein, *Phys. Scripta*, **T99**, 55-67 (2002).
- [4] M. Benayoun *et al*, *Eur. Phys. J.*, **C31**, 525-547 (2003).
- [5] B. Borasoy and R. Nissler, *Nucl. Phys.*, **A740**, 362-382 (2004).
- [6] M.Gormley *et al*, *Phys. Rev.*, **D2**, 501 (1970).
- [7] J. D. Layter *et al*, *Phys. Rev.*, **D7**, 2565 (1973).
- [8] B. Borasoy and R. Nissler, *arXiv:0705.0954 [hep-ph]* (2007).
- [9] A. Abele *et al*. [Crystal Barrel Collab.], *Phys. Lett.* **B402**, 195-206 (1997).
- [10] M. Acciarri *et al*. [L3 Collab.], *Phys. Lett.* **B418**, 399-410 (1998).
- [11] H.-H. Adam *et al*. [WASA-at-COSY Collab.], *nucl-ex/0411038* (2004).

PION-NUCLEON SCATTERING IN THE N*(1440) RESONANCE REGION

M. E. Sadler, J. Stahov¹, and S. Watson

Department of Physics
Abilene Christian University
Abilene, TX 79699 USA

Abstract

Complete sets of measurements for pion-nucleon scattering in the N*(1440) resonance region have been made since 1980, when the landmark Karlsruhe-Helsinki (KH) and Carnegie Mellon-Berkeley (CMB) partial wave analyses (PWA) were completed. These measurements consist of differential cross sections and analyzing powers for elastic scattering and charge exchange and spin rotation parameters for elastic scattering in the momentum interval 0.4–0.7 GeV/c. The program culminated with measurements of $\pi^-p \rightarrow$ Neutrals (charge exchange, multiple π^0 final states, η production, and inverse photoproduction) by the Crystal Ball Collaboration at Brookhaven National Laboratory. Resonance parameters for the N*(1440) in the Review of Particle Physics by the Particle Data Group have been obtained from the KH and CMB analyses. The 2006 edition also includes the analysis by George Washington University (GWU), but the parameters were unchanged. An example of the data is presented along with comparisons to PWA.

1 Introduction

The P₁₁(1440) resonance, often called the Roper, has been a curiosity since its discovery in pion-nucleon (π N) partial wave analysis (PWA) [1]. It has the same spin, isospin and parity as the nucleon. It does not appear as a bump in the π^-p total cross section. The Breit-Wigner mass and width are more poorly determined than the overlapping D₁₃(1520) and S₁₁(1535) and other N* resonances at higher excitation. The Particle Data Group (PDG) [2] has traditionally used the analyses of Karlsruhe-Helsinki (KH) [3–5], Carnegie Mellon University and Lawrence Berkeley Laboratory (CMB) [6–8] and Kent

¹Also University of Tuzla, 75000 Tuzla, Bosnia and Herzegovina.

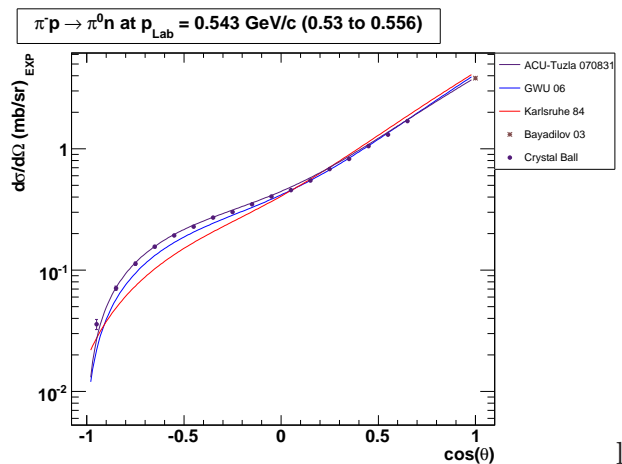


Figure 1: Fit to data for $\pi^-p \rightarrow \pi^0n$ at 543 MeV/ c by the ACU-Tuzla PWA. Also shown are the KH84 and GWU (SP06) analyses.

State University (KSU) [9] for their averages and fits. The mass determinations (in MeV) vary from 1410 ± 12 [3] to 1462 ± 10 [9] and the widths from 135 ± 10 [3] to 545 ± 170 [8]. It is classified as a four-star resonance.

The recent PWA (SP06) from the George Washington University (GWU) group [10] incorporates constraints from dispersion relations and a fit to $\pi^-p \rightarrow \eta n$ data. This analysis was included by the PDG in the 2006 edition [11] for “averages, fits, limits, etc” but the estimated values for the mass and width were unchanged. They obtain a mass of 1485.0 ± 1.2 and a full width of 284 ± 18 MeV. The VPI/GWU analyses have reported two poles on the Riemann surface for the P_{11} amplitude in their recent analyses [12, 13]. Cutkosky and Wang [8] addressed this issue, concluding that poles on different Riemann sheets were expected above inelastic thresholds, in this case the $\pi\Delta$ threshold.

2 Analysis

A new PWA effort of the Karlsruhe-Helsinki type has been undertaken by the authors. The goal is to analyze the post-1980 data [14–21] with the same dispersion relation constraints as in Ref. [3–5]. Preliminary results have been obtained and a fit to charge exchange data [22] at 543 MeV/ c is shown in Fig. 1. Also shown are the KH84 and GWU (SP06) analyses.

Comparisons of the three PWAs for the S_{11} and P_{11} partial wave amplitudes are shown in Fig. 2. The ACU-Tuzla results are still very preliminary.

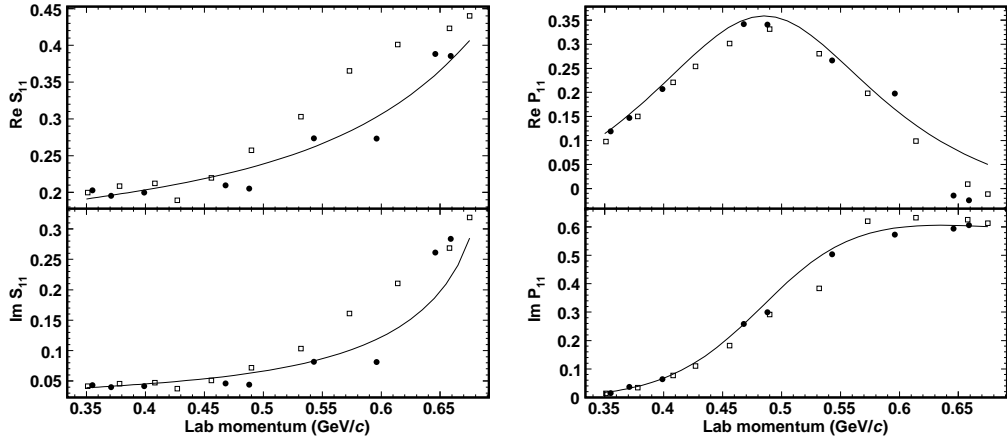


Figure 2: Comparison of the S_{11} and P_{11} partial wave amplitudes from the energy-dependent GWU06 analysis (solid curve) with KA84 (open squares) and ACU-Tuzla (filled circles).

It is hoped eventually to include this analysis in a coupled channel formalism. The $\pi^-p \rightarrow \pi^0\pi^0n$ reaction is a particularly promising channel to elucidate the resonance parameters for the $N^*(1440)$ since the total cross sections exhibit a bump near 1440 MeV [23].

Acknowledgments

This research was funded by USDOE grant DE-FG03-94ER40860.

References

- [1] L. D. Roper, *Phys. Rev. Lett.* **12**, 340 (1964).
- [2] S. Eidelman *et al.* (Particle Data Group) Review of Particle Physics, *Phys. Lett.* **B 592**, 1 (2004).
- [3] G. Hoehler, F. Kaiser, R. Koch, and E. Pietarinen, *Handbook of Pion-Nucleon Scattering* Fachinformationszentrum, Karlsruhe (1979).
- [4] R. Koch in *Proc. of IV International Conference on Baryon Resonances*, ed. N. Isgur (University of Toronto, Canada, 1980), p. 3.
- [5] G. Hoehler, *Pion-Nucleon Scattering*, Springer, Berlin (1983).

-
- [6] R. E. Cutkosky *et al.* Phys. Rev. **D20** 2804 (1979).
- [7] R. E. Cutkosky *Proc. of IV International Conference on Baryon Resonances*, ed. N. Isgur (University of Toronto, Canada, 1980), p. 19.
- [8] R. E. Cutkosky and S. Wang, Phys. Rev. **D42** 235 (1990).
- [9] D. M. Manley and E. M. Saleski, Phys. Rev. **D45** 4002 (1992).
- [10] R. A. Arndt, W. J. Briscoe, I. I. Strakovsky and R. L. Workman, Phys. Rev. **C74** 045205 (2006).
- [11] W.-M. Yao *et al.* (Particle Data Group) J. Phys. **G 33**, 1 (2006).
- [12] R. A. Arndt, J. M. Ford, and L. D. Roper, Phys. Rev. D **32**, 1085 (1985).
- [13] R. A. Arndt, W. J. Briscoe, I. I. Strakovsky, R. L. Workman, and M. M. Pavan, Phys. Rev. C **69**, 035213 (2004).
- [14] M. E. Sadler, W. J. Briscoe, D. H. Fitzgerald, B. M. K. Nefkens and C. J. Seftor, Phys. Rev. **D35** 2718 (1987).
- [15] A. Mokhtari, A. D. Eichon, G. J. Kim, B. M. K. Nefkens, J. A. Wightman, D. H. Fitzgerald, W. J. Briscoe, and M. E. Sadler, Phys. Rev. **D35**, 810 (1987).
- [16] J. A. Wightman *et al.* Phys. Rev. **D38** 3365 (1988).
- [17] C. J. Seftor *et al.* Phys. Rev. **D39** 2457 (1989).
- [18] G. J. Kim *et al.* Phys. Rev. **D41** 733 (1990).
- [19] I. Supek *et al.* Phys. Rev. **D47** 1762 (1993).
- [20] M. Sadler *et al.* Phys. Rev. **C69** 055206 (2004).
- [21] A. Starostin *et al.* Phys. Rev. **C72** 015205 (2005).
- [22] M. Sadler in *NSTAR 2005, Proc. of the Workshop on the Physics of Excited Nucleons* eds. S. Capstick, V. Crede and P. Eugenio, Florida State University, (World Scientific, 2005) p. 286.
- [23] S. Prakhov *et al.* Phys. Rev. **C69** 045202 (2004).

THE GMO SUM RULE REVISITED

M. E. Sainio
Helsinki Institute of Physics
P.O. Box 64
FI-00014 University of Helsinki
Finland

Abstract

A brief introduction is given for the analysis of pion-nucleon data with the Goldberger-Miyazawa-Oehme sum rule. With information on pionic hydrogen, low-energy π^+p scattering and total cross sections, a value $f^2 = 0.075 \pm 0.002$ for the coupling constant is deduced.

1 Introduction

The Goldberger-Miyazawa-Oehme sum rule [1] provides a simple relation connecting four different quantities:

- the s -wave π^-p scattering length a_{π^-p} ,
- the s -wave π^+p scattering length a_{π^+p} ,
- the πN coupling constant f^2 ,
- the weighted integral, J^- , of the difference of the π^-p and π^+p total cross sections.

By evaluating the forward dispersion relations at the physical threshold one obtains [2]

$$(1 + \mu/m)(a_{\pi^-p} - a_{\pi^+p})/\mu = 4f^2/(\mu^2 - \omega_B^2) + 2J^-, \quad (1)$$

where μ is the (charged) pion mass, m is the proton mass, $\omega_B = -\mu^2/2m$ and

$$J^- = 1/(4\pi^2) \int_0^\infty (\sigma_{\pi^-p}^{\text{Tot}} - \sigma_{\pi^+p}^{\text{Tot}})/\omega dk. \quad (2)$$

Here I'll present the results of an evaluation [3] of three of these quantities, a_{π^-p} , a_{π^+p} and J^- , and give a value for the resulting coupling constant, f^2 .

2 Pionic Hydrogen

The strong interaction shift of the $1s$ level of the pionic hydrogen provides a handle to the scattering length a_{π^-p} . The connection is the Deser-type formula [4]

$$\epsilon_{1s} = -2\alpha^3 \mu_c^2 a_{\pi^-p} (1 + \delta_\epsilon), \quad (3)$$

where μ_c is the reduced mass of the π^-p system and $\alpha \simeq 1/137.036$ is the fine structure constant. In Eq. (3) the identification $a_{0+}^+ + a_{0+}^- = a_{\pi^-p}$ of the sum of the isoscalar and isovector s -wave πN scattering lengths has been made. The quantity δ_ϵ evaluated next-to-leading order in isospin breaking and in the low-energy expansion has the value [4]

$$\delta_\epsilon = (-7.2 \pm 2.9) \times 10^{-2}. \quad (4)$$

The pionic hydrogen level shift has been measured [5, 6] to the precision of about 0.2 %

$$\epsilon_{1s} = -7.120 \pm 0.008 \pm 0.009 \text{ eV}, \quad (5)$$

where the first error is due to statistics and the second due to systematics. The measured level shift, Eq. (5), gives then for the scattering length

$$a_{\pi^-p} = 0.0933 \pm 0.0029 \text{ } 1/\mu, \quad (6)$$

if errors are added linearly.

3 The π^+p S-wave Scattering Length

Information on angular distributions of the π^+p scattering observables has been used as input for a discrete phase shift analysis in the laboratory momentum range $k = 0.077 - 0.725 \text{ GeV}/c$. The Tromborg corrections [7] were applied to extract the hadronic amplitudes from the experimental data. Constraints from forward dispersion relations [8] were also implemented. The resulting s -wave scattering length for π^+p is

$$a_{\pi^+p} = -0.0764 \pm 0.0014 \text{ } 1/\mu \quad (7)$$

in rather close agreement with the Matsinos *et al.* result [9]

$$a_{\pi^+p} = -0.0751 \pm 0.0039 \text{ } 1/\mu \quad (8)$$

based on a fit with a low-energy model.

4 Integral J^-

The integral J^- , given in Eq. (2), has been evaluated with the total cross section input from the forward dispersion relation analysis of Ref. [8], where corrections for the electromagnetic interaction [7] and the P_{33} splitting of π^-p [10] were applied. The result of the evaluation [3] is displayed in the Table together with some earlier determinations. An important issue is the question

Table 1: The values of the integral J^- (mb).

Reference	J^- (mb)
Höhler-Kaiser [11]	-1.06
Koch [12]	-1.077 ± 0.047
Gibbs <i>et al.</i> [13]	-1.051 ± 0.005^a
Ericson <i>et al.</i> [14]	-1.083 ± 0.032
Abaev <i>et al.</i> [3]	-1.060 ± 0.030

^a Statistical error only.

of the uncertainty to be attached to the value of the integral J^- . Abaev *et al.* [3] combine linearly errors related to statistics (0.007 mb), discrepant data sets (0.012 mb), electromagnetic corrections beyond the Tromborg range (0.006 mb) and the asymptotic behavior (0.004 mb).

5 Results and Conclusions

With the values for a_{π^-p} , a_{π^+p} and J^- one can solve f^2 from Eq. (1). The outcome is $f^2 = 0.075 \pm 0.002$. The result depends on the techniques used to extract the hadronic scattering length from the level shift measurement, potential model calculations tend to produce larger values for f^2 .

In the present analysis the largest uncertainty in f^2 is due to the uncertainty in a_{π^-p} which, in turn, is a consequence of the largely unknown low-energy constant f_1 needed to fix δ_ϵ . Assuming isospin invariance, a precise value for Γ_{1s} , the width of the pionic hydrogen $1s$ state, would avoid this problem.

Acknowledgments

A travel grant from the Magnus Ehrnrooth Foundation is gratefully acknowledged. This work was supported in part by the EU Contract MRTN-CT-2006-035482, FLAVIANet.

References

- [1] M.L. Goldberger, H. Miyazawa and R. Oehme, *Phys. Rev.* **99**, 986 (1955).
- [2] J. Hamilton and W.S. Woolcock, *Rev. Mod. Phys.* **35**, 737 (1963).
- [3] V.V. Abaev, P. Metsä and M.E. Sainio, *Eur. Phys. J.* **A32**, 321 (2007).
- [4] J. Gasser, M.A. Ivanov, E. Lipartia, M. Mojžiš and A. Rusetsky, *Eur. Phys. J.* **C26**, 13 (2002).
- [5] H.-Ch. Schröder *et al.*, *Eur. Phys. J.* **C21**, 473 (2001).
- [6] L.M. Simons, *Int. J. Mod. Phys.* **A20**, 1644 (2005).
- [7] B. Tromborg, S. Waldenstrøm and I. Overbø, *Phys. Rev.* **D15**, 725 (1977).
- [8] P. Metsä, *Eur. Phys. J.* **A33**, 349 (2007).
- [9] E. Matsinos, W.S. Woolcock, G.C. Oades, G. Rasche and A. Gashi, *Nucl. Phys.* **A778**, 95 (2006).
- [10] V.V. Abaev and S.P. Kruglov, *Z. Phys.* **A3553**, 85 (1995).
- [11] G. Höhler and F. Kaiser, Karlsruhe report, KfK 3027, 1980, unpublished.
- [12] R. Koch, Karlsruhe TKP 85-5, 1985, unpublished.
- [13] W.R. Gibbs, Li Ai and W.B. Kaufmann, *Phys. Rev.* **C57**, 784 (1998).
- [14] T.E.O. Ericson, B. Loiseau and A.W. Thomas, *Phys. Rev.* **C66**, 014005 (2002).

THE $pd \rightarrow {}^3\text{He}\omega$ REACTION

K. Schönning^{*,1} for the CELSIUS/WASA collaboration,
K. P. Khemchandani[%]

^{*}Dept. of Nucl. and Part. Phys., Uppsala Universitet, Uppsala, Sweden
[%]Dept. de Física Teórica and IFIC, Centro Mixto Univ. de Valencia, Spain

Abstract

ω production in $pd \rightarrow {}^3\text{He}\omega$ has been studied with the WASA detector at two beam energies, $T_p = 1360$ MeV and $T_p = 1450$ MeV. Angular distributions have been reconstructed and compared with results from calculations using a two-step model. There is a qualitative agreement between data and theory at $T_p = 1360$ MeV but a disagreement at extreme angles at $T_p = 1450$ MeV.

1 Introduction

A study of the $pd \rightarrow {}^3\text{He}\omega$ reaction, with focus on the full angular distribution, is currently being carried out by the CELSIUS/WASA collaboration. Data were taken at two beam energies, $T_p = 1360$ MeV and $T_p = 1450$ MeV, corresponding to excess energies of 17 MeV and 64 MeV, respectively. This reaction has been studied near the kinematic threshold before [1-3], but [1] only lead to preliminary results, [2] remains unpublished and the correctness of the data interpretation in [3] has been questioned [4].

On the theoretical side, production of η , ω , ϕ and η' in $pd \rightarrow {}^3\text{He}X$ were studied in, e.g., [5] and [6]. However, no attempts to calculate the full angular distribution have been made until now, when the ongoing experimental investigation has raised an interest for the reaction.

2 Analysis of the WASA data

The data in this work were taken with the WASA detector [7] in Uppsala, Sweden, using a proton beam impinging on a deuterium pellet target [8]. The ${}^3\text{He}$'s were identified by the $\Delta E/E$ -method as described in [9] and [10]. We focus on the $\omega \rightarrow \pi^+\pi^-\pi^0$ decay channel ($BR = 89.1\%$). The selection

¹E-mail address: karin.schonning@tsl.uu.se

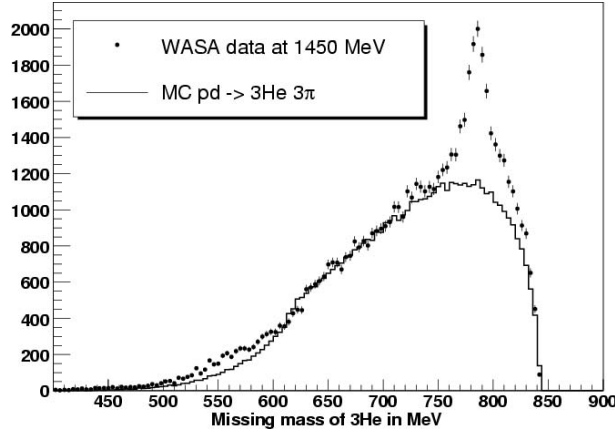


Figure 1: 1450 MeV data (dots) with cuts optimized for $\omega \rightarrow \pi^+\pi^-\pi^0$ and simulated $\pi^+\pi^-\pi^0$ data (line).

criteria are described in [10]. The constraints given there give an acceptance of 39% at $T_p = 1450$ MeV while it is 36% at $T_p = 1360$ MeV. In Fig. 1 and 2, the ${}^3\text{He}$ missing mass distributions at both energies are shown. The major part of the background comes from pion production in $pd \rightarrow {}^3\text{He}\pi^+\pi^-\pi^0$, but also from overlapping events and beam halo interacting with either rest gas or the beam pipe.

The aim of this work is to reconstruct the differential cross section as a function of $\cos\theta_\omega^*$. The procedure is described in [10] and [11]. At $T_p = 1450$ MeV, the normalization is performed using the SPES3 point at $\cos\theta_\omega^* = -0.65$ [2]. The resulting angular distribution is shown in Fig 3.

The analysis of the 1360 MeV data is more difficult. Firstly, ω has a finite width ($\Gamma = 8.44$ MeV), which close to threshold means that ω 's with high mass cannot be produced, giving an asymmetric ω peak. Secondly, the background fitting is more difficult since the background continuum ends under the ω peak (see Fig 2). Thirdly, the signal-to-background ratio is small. The statistical and systematical uncertainties are thus significantly larger at 1360 MeV, which is clear from Fig 4. The angular distribution at $T_p = 1360$ MeV is very preliminary and the normalization arbitrary.

3 Model calculations

A theoretical study of this reaction has been carried out using a two-step model (see diagram and details in [12]). The T -matrix for this mechanism, which favors sharing of the large momentum transfer (~ 1 GeV at both

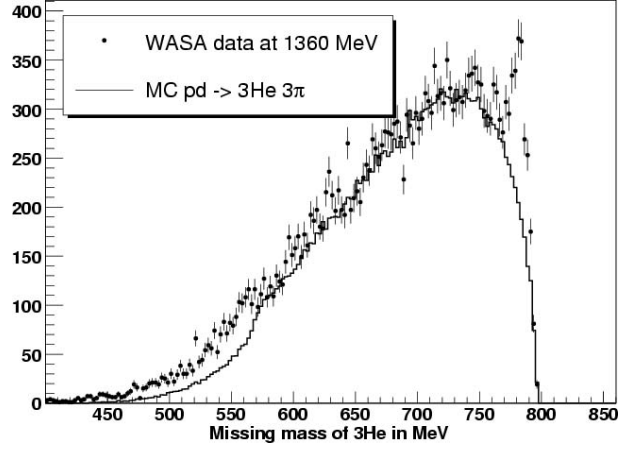


Figure 2: 1360 MeV data (dots) with cuts optimized for $\omega \rightarrow \pi^+\pi^-\pi^0$ and simulated $\pi^+\pi^-\pi^0$ data (line).

energies), can be written as

$$\langle |T_{pd \rightarrow {}^3\text{He}\omega}| \rangle = i \frac{3}{2} \frac{d\mathbf{P}_1}{(2\pi)^3} \frac{d\mathbf{P}_2}{(2\pi)^3} \sum_{int m's} \langle pn|d \rangle \frac{\langle |T_{pp \rightarrow \pi d}| \rangle}{K_\pi^2 - m_\pi^2 + i\epsilon} \langle |T_{\pi n \rightarrow \omega p}| \rangle \langle {}^3\text{He}|pd \rangle.$$

All the inputs for these calculations except the $\pi N \rightarrow \omega N$ T -matrix have been taken as in [13]. The $\pi N \rightarrow \omega N$ sub-process has been written in terms of the Giessen model [14], where it was shown that the reaction cross section could be explained well including up to $l=3$ partial waves, hinting towards importance of multiple resonances also in ω production in pd collisions. Hence, the calculations in this work also include all partial waves up to $l=3$. The result of the calculations performed in the plane wave approach, at $T_p = 1450$ MeV and 1360 MeV, is shown in Fig 3 (with the preliminary data from [10]) and 4, respectively. The figures also show the contribution of various partial waves to the cross sections. The results from the two-step model and the data at $T_p = 1450$ MeV clearly disagree at extreme angles. The addition of higher partial waves does not seem to change the shape of the distribution drastically though it does seem to be essential to reproduce the magnitude of the cross section. The result of the calculations at $T_p = 1360$ MeV looks, qualitatively, in agreement with the behavior of the – yet very preliminary – data. On the theoretical front, adding the $\omega - {}^3\text{He}$ final state interaction to this model and further exploration of this reaction using different models for the production mechanism is in progress.

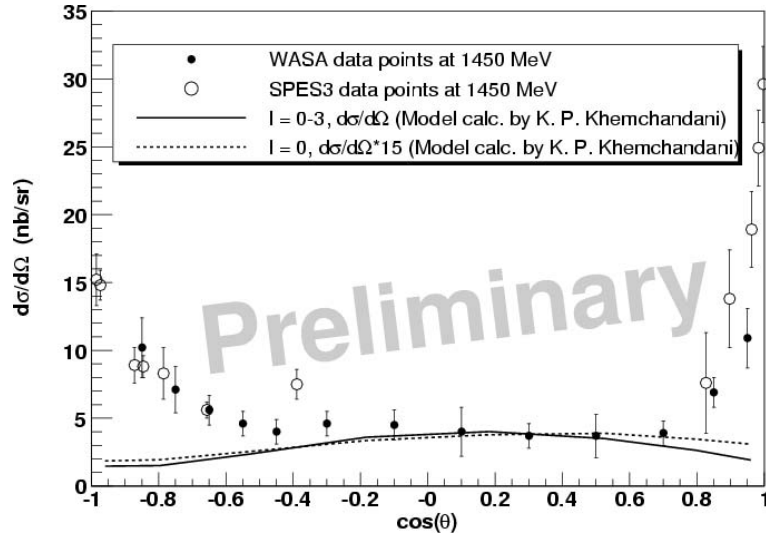


Figure 3: The WASA data points at $T_p = 1450$ MeV (black), the SPES3 data (white) from [2] and the model calculations given in Section 3. The error bars represent statistical and systematic uncertainties.

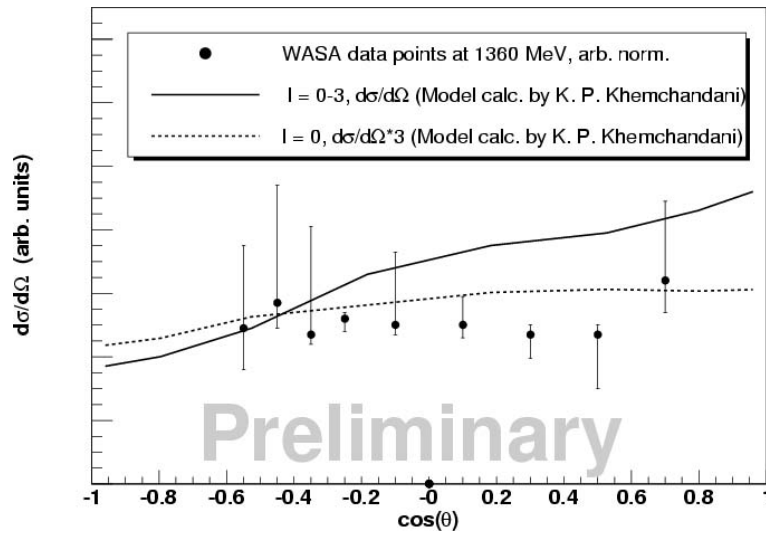


Figure 4: The new WASA data points at $T_p = 1360$ MeV, arbitrarily normalized, along with the model calculations described in Section 3.

References

- [1] F. Plouin in *Production and Decay of Light Mesons*, ed. P. Fleury (World Scientific, Singapore, 1988), p. 114.
- [2] T. Kirchner, Ph. D. thesis. (IPN Orsay, France, 1993).
- [3] R. Wurzinger *et al.*, *Phys. Rev. C* **51**, R443 (1995).
- [4] C. Hanhart and A. Kudryavtsev *Eur. Phys. J A* **6**, p. 325 (1999).
- [5] G. Fäldt and C. Wilkin, *Phys. Lett. B* **354**, p. 20 (1995).
- [6] L.A. Kondratyuk *et al.* *Acta Phys. Pol. B* **27**, p. 2977 (1996).
- [7] J. Zabierowski *et al.*, *Physica Scripta T* **99**, p. 159 (2002).
- [8] C. Ekström *et al.*, *Physica Scripta T* **99**, p. 169 (2002).
- [9] K. Schönning *et al.*, *Acta Phys. Slov.* **56-3**, p. 299 (2006).
- [10] K. Schönning *et al.* in *Proc. from the 2nd Int. η MesonNet Workshop* eds. M. Jacewicz and B. Höistad, 0710.1809v1[nucl-ex](2007).
- [11] K. Schönning *et al.*, *Nucl. Phys. A* **790**, p. 319c (2007).
- [12] K. P. Khemchandani in *Proc. from the 2nd Int. η MesonNet Workshop* eds. M. Jacewicz and B. Höistad, 0710.1809v1[nucl-ex] (2007).
- [13] K. P. Khemchandani, N. G. Kelkar and B. K. Jain, *Nucl. Phys. A* **708**, p. 312 (2002); *ibid Phys. Rev. C* **68**, p. 064610.
- [14] V. Shklyar *et al.* *Phys. Rev. C* **71**, p. 055206 (2005).

HYPERON PRODUCTION in the channel $pp \rightarrow K^+ \Lambda p$ at COSY-TOF

*W. Schroeder*¹ for the COSY-TOF Collaboration
Physikalisches Institut²
University of Erlangen - Nuremberg
Erlangen, D-91058

Abstract

The strangeness production program at the COSY-TOF experiment is discussed. The apparatus is shown emphasizing the technique to measure delayed decays. Results obtained for the reactions $pp \rightarrow K^+ \Lambda p$ are discussed.

1 Introduction

The main interest in the investigation of the associated strangeness production in elementary reactions close to threshold is to get insight into the dynamics of the production. The questions especially concern the role of N^* -resonances and the hyperon-nucleon final-state interaction which is known to be of special importance close to threshold. To get to conclusive results precise observables are needed, concentrating on exclusive data, covering the full phase space.

2 Experimental Setup

The external experiment COSY-TOF [1] is a wide angle, non-magnetic spectrometer. A few millimeters behind the very small liquid hydrogen target the start (inner) detector system, which is optimized for strangeness production measurements, is installed. The stop detector with a length of about 3 m consists of various scintillator detectors (quirl, ring and barrel). Except for small beam holes, the inner detector system, as well as the outer detector system covers the full angular range of the reaction products for the channel $pp \rightarrow K^+ \Lambda p$. This allows a complete reconstruction of the events, including a precise measurement of the delayed decay of the Λ -hyperon and especially the analysis of the Dalitz plots, which is a main topic of this contribution.

¹schroeder@physik.uni-erlangen.de

²Erwin-Rommel-Str 1, 91058 Erlangen, Germany

3 Results

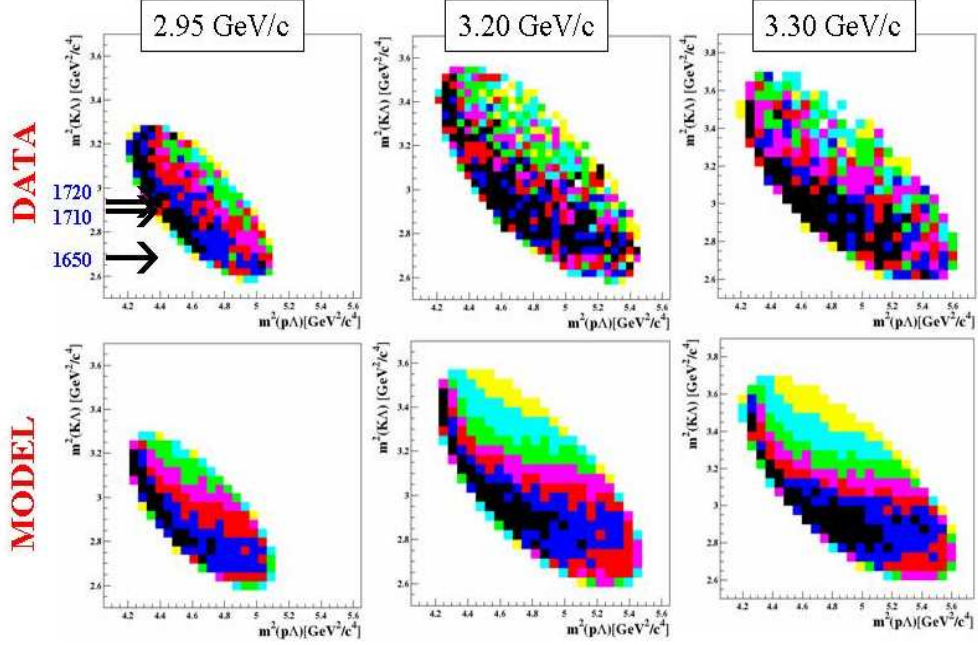


Figure 1: Dalitz plots of the reaction $pp \rightarrow K^+\Lambda p$; data (upper) compared to model-fits (lower).

In Fig. 1 (upper part) Dalitz plots for experimental data at beam momenta of $2.95 \text{ GeV}/c$, $3.20 \text{ GeV}/c$ and $3.30 \text{ GeV}/c$, respectively are shown. They obviously show strong deviations from phase space. Monte Carlo simulations show that higher partial waves influence the Dalitz plot distributions only in a minor way. The strength coefficients of these partial waves have been extracted from the experimental angular distributions, which show some anisotropy for all three ejectiles. From theoretical work and our previous investigations [4], it is most likely that the observed anisotropy has its origin in the influence of the $p\Lambda$ -final-state interaction and/or N^* -resonances. To obtain more insight into the various contributions, the data were compared with a model parametrization prepared by A. Sibirtsev [6], which includes the $N^*(1650, 1710, 1720)$ -resonances, a non-resonant term and the $p\Lambda$ -final state interaction on the amplitude base (see Eq. 1).

$$\frac{d^2\sigma}{dm_{K\Lambda}^2 dm_{p\Lambda}^2} = fl \cdot \Phi \left| \left(\sum_R (C_R \cdot A_R) + C_N \right) \cdot (1 + C_{FSI} \cdot A_{FSI}) \right|^2 \quad (1)$$

The quantity fl gives the normalization to the total cross-section, Φ is a phase-space factor. The third factor gives the deviation from an equally distributed Dalitz plot. A_R are the amplitudes of the Breit-Wigner-shapes of the three considered N^* -resonances. A_{FSI} denotes the amplitude of the $p\Lambda$ -final state interaction as given by the Jülich YN -model [7]. The strength of the individual resonances C_R , of the non-resonant contribution C_N (which includes the kaon exchange) and of the $p\Lambda$ -final state C_{FSI} can be adjusted individually. The strengths of the various contributions were adjusted to achieve a best fit for the various Dalitz plots. The results are shown in Fig. 1 (lower part). The data are well described by the model fits. The obtained reduced χ^2 -values are between 1.4 and 2.0. The most interesting result is that the strength of the contribution of the $N^*(1650)$ resonance compared to the sum of the contributions of the $N^*(1710)$ and $N^*(1720)$ changes dramatically with the beam momentum.

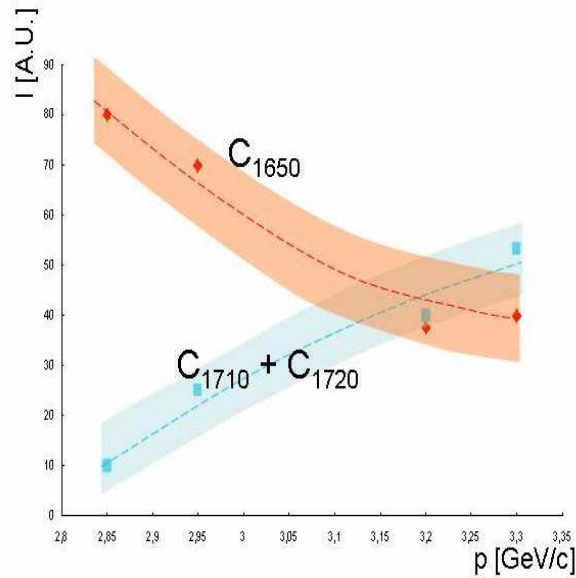


Figure 2: Contribution of $N^*(1650)$ compared to the sum of $N^*(1710) + N^*(1720)$ as a function of the beam momentum.

This is shown in Fig. 2. The given bands correspond to a 3σ -error interval of the extracted strengths of the resonances. The amplitude of the non-resonant contribution is smaller by a factor of about ten compared to the sum of the three contributing resonances. The influence of the $p\Lambda$ -final state interaction is significant even for the highest momentum; within errors the corresponding amplitude is independent of the beam momentum. From

these results it has to be concluded that there is a dominant exchange of non-strange mesons. Only these are able to contribute to the observed leading mechanism via N^* -resonances.

4 Summary and outlook

The COSY-TOF experiment is well suited for hyperon production experiments. For the reaction channel $pp \rightarrow K^+\Lambda p$ a strong influence of N^* -resonances was observed. Data with much larger event samples, which are under investigation, will allow to study the resonance parameters in detail and to search for unknown resonances. In this context the inclusion of other reaction channels accessible through np -reactions by the use of a deuterium target will be of special importance. The use of a polarized beam, which has already been used, will give access to polarization observables as analysing power and spin-transfer-coefficient.

Acknowledgments

We would like to thank very much the COSY accelerator team for the preparation of the excellent proton beam and for the good cooperation. COSY-TOF is supported by German BMBF and FZ Jülich.

5 References

References

- [1] http://www.fz-juelich.de/ikp/COSY-TOF/index_e.html
- [2] LEPS Coll., T. Nakano et al. Phys. Rev. Lett. 91 (2003) 012002
- [3] COSY-TOF coll., Phys. Lett. **B** 595 (2004) 127
- [4] COSY-TOF coll., Phys. Lett. **B** 420 (1998) 217
- [5] COSY-TOF coll., Phys. Lett. **B** 632 (2006) 27
- [6] A. Sibirtsev, private communication, 2002, 2005
- [7] A.Reuber, K.Holinde, J. Speth, Nucl. Phys. **A** 570 (1994) 543

MENU 2007
11th International Conference
on Meson-Nucleon Physics and
the Structure of the Nucleon
September 10-14, 2007
IKP, Forschungszentrum Jülich, Germany

IMPROVED STUDY OF A POSSIBLE Θ^+ PRODUCTION IN THE $pp \rightarrow pK^0\Sigma^+$ REACTION WITH THE COSY-TOF SPECTROMETER

*W. Schroeder*¹ for the COSY-TOF Collaboration
Physikalisches Institut²
University of Erlangen - Nuremberg
Erlangen, D-91058

Abstract

The $pp \rightarrow pK^0\Sigma^+$ reaction was investigated with the COSY-TOF spectrometer. The main objective was to clarify whether or not a narrow exotic $S = +1$ resonance, the Θ^+ pentaquark, is populated at $1.53 \text{ GeV}/c^2$ in the pK^0 subsystem. A data sample of much higher statistical significance compared to the previously reported data in this channel [1], has been achieved. The analysis of these data does not confirm the existence of the Θ^+ pentaquark. This is expressed as an upper limit for the cross section $\sigma(pp \rightarrow \Sigma^+\Theta^+) < 0.15 \mu\text{b}$ at the 95% confidence level.

1 Introduction

QCD does not exclude the existence of other color singlet objects, then quark-antiquark pairs or three quark systems. Within a chiral soliton model Diakonov [2] predicted the existence of an anti-decuplet of baryonic states with $J^P = 1/2^+$ consisting of four quarks and one anti-quark. Three members of this anti-decuplet are manifestly exotic, having combinations of strangeness and isospin not allowed for three-quark systems. The lightest of these exotic states is the Θ^+ pentaquark with a quark content of $uudd\bar{s}$ and thus strangeness $S = +1$. In this article the results of an experiment studying the $pp \rightarrow pK^0\Sigma^+$ reaction with the COSY-TOF spectrometer with substantially improved statistical accuracy and extended detection capability are reported.

¹schroeder@physik.uni-erlangen.de

²Erwin-Rommel-Str 1, 91058 Erlangen, Germany

2 Experimental Setup

The external experiment COSY-TOF is a wide angle, non-magnetic spectrometer, which covers, except for small beam holes, the full angular range of the reaction products for the channel $pp \rightarrow pK^0\Sigma^+$. This allows a complete reconstruction of the events, including a precise measurement of the delayed decay of the K_s^0 meson. For detailed information see [3].

3 Analysis

The analysis was carried out with three independent analysis programs, with different algorithms and event selection methods. but with a common calibration of all detector components. A $pK^0\Sigma^+$ event is identified by its topology, that is a prompt track emerging from the target (proton), a delayed decay (K^0) and optionally a kink in a charged track (Σ^+). Due to the different strategies of the analysis the overlap of found event in the different is very small. But in total more than 12.000 independent $pK^0\Sigma^+$ events were reconstructed. The resolution in the invariant mass distribution of the pK^0 subsystem is between $\sigma = 5 - 6$ MeV/ c^2 .

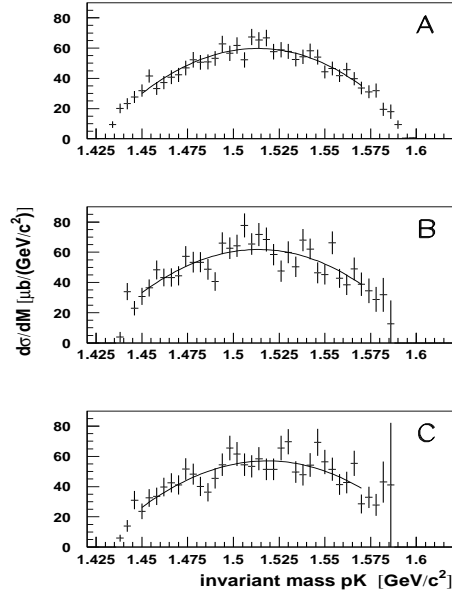


Figure 1: The invariant masses of the pK^0 subsystem for the three analyses together with a 3rd order polynomial parameterization.

4 Results

The pK^0 mass spectra are presented in Fig.1 together with a 3rd order polynomial parameterization in the mass region of $1.45 \text{ GeV}/c^2 < M_{pK^0} < 1.57 \text{ GeV}/c^2$. They were analyzed in order to determine the statistical significance with which a narrow structure might be present. A narrow structure was added to the polynomial described above. The shape of this narrow structure has been taken from Monte Carlo simulations of a resonance with a width negligible compared to the detector resolution. The mass of the resonance was varied in $1 \text{ MeV}/c^2$ steps over the M_{pK^0} range from $1.50 \text{ GeV}/c^2 - 1.55 \text{ GeV}/c^2$. The strength of the structure for each setting was varied between $-1 \mu\text{b} < \sigma_{\text{tot},X} < +1 \mu\text{b}$. These results are summarized in Fig.2,

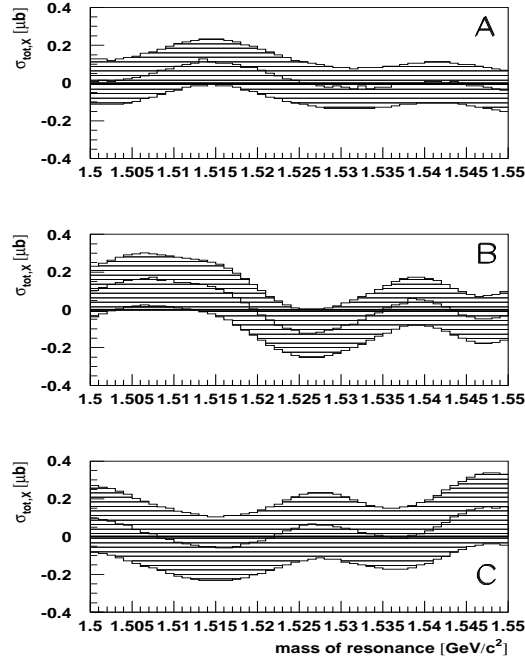


Figure 2: 95% confidence range for the cross section of a narrow resonance as a function of M_{pK^0} for the three analyses. The central lines of each band present the contribution of a hypothetical narrow resonance with the lowest χ^2 value.

where the value of $\sigma_{\text{tot},X}$ corresponding to the minimal value of χ^2 is represented by the central line of the band as a function of M_{pK^0} . The 95% confidence interval for an enhancement or suppression of the measured M_{pK^0}

differential cross section is indicated by the width of the band. The results indicate that over the full M_{pK^0} range investigated here the parameterization assuming $\sigma_{tot,X} = 0 \mu\text{b}$ is consistent with the measured data within the 95% confidence level. In particular, this new, higher statistics data do not contain positive evidence for a narrow structure at $M_{pK^0} = 1.530 \text{ GeV}/c^2$. The fluctuation of the central value of the 95% confidence intervals are not correlated between the different analyses. Based upon the smallest upper limit of the three 95% confidence intervals the maximum cross section for a narrow resonance $\sigma_{tot,X} < 0.15 \mu\text{b}$ has been deduced over the full mass range. Further details of the new measurement are given in Ref [4].

5 Summary

The reaction $pp \rightarrow pK^0\Sigma^+$ was studied in an exclusive measurement at a beam momentum of 3.059 GeV/c with complete phase space coverage. The extracted pK^0 spectra do not show evidence for a narrow resonance in the mass region of 1.50 GeV/c² - 1.55 GeV/c² in any of the three independent analyses. The data are consistent with a cross section of $\sigma_{tot,X} = 0 \mu\text{b}$ and an upper limit of 0.15 μb is derived with a confidence level of 95%. The evidence for a Θ^+ , reported in a first measurement [1], is not confirmed.

Acknowledgments

We would like to thank very much the COSY accelerator team for the preparation of the excellent proton beam and for the good cooperation. COSY-TOF is supported by German BMBF and FZ Juelich.

References

- [1] COSY-TOF Collaboration: M. Abdel-Bary *et al.*, Phys. Lett. **B** 595 (2004) 127.
- [2] D. Diakonov, V. Petrov and M. Polyakov, Z. Phys. **A** 359 (1997) 305.
- [3] http://www.fz-juelich.de/ikp/COSY-TOF/index_e.html
- [4] COSY-TOF Collaboration: M. Abdel-Bary *et al.*, Phys. Lett. **B** 649 (2007) 252

CHIRAL SYMMETRY RESTORATION IN EXCITED MESONS

J. Segovia^{*,1}, D. R. Entem^{*}, F. Fernández^{*}

^{*}Departamento de Física Fundamental y IUFFYM, University of
Salamanca, Salamanca, Spain

Abstract

Recently the Crystal Barrel Collaboration has found many new states in the excited light meson spectrum analyzing the experimental data on proton-antiproton annihilation in the range $1.9 - 2.4 \text{ GeV}$. A large degeneracy on these states has been found and interpreted by some authors as a signal of chiral symmetry restoration. In this work we show how this large degeneracy can be reproduced in the framework of a constituent quark model with a screened confinement potential. Observables that could discriminate our model from those which explicitly restore the chiral symmetry are proposed.

Chiral symmetry and confinement are two of the most important properties of QCD to describe the hadron spectra. The absence of chiral multiplets in the low-lying hadron spectrum is a signal that chiral symmetry is spontaneously broken. In recent years it has been suggested that the physics of the excited part of the meson spectrum seems to be quite different. The partial wave analysis of the proton-antiproton annihilation into mesons at LEAR in the range $1.9-2.4 \text{ GeV}$ has shown a large degeneracy on the spectra of the angularly and radially excited resonances [1,2]. The new results along with the well established states from the PDG [3] are shown in Fig. 1(a). One can see that as far as we move to higher excitation energy the different states become more and more degenerated. This phenomena has been shown to be compatible with a chiral symmetry restoration scenario and for some authors is a signal that chiral symmetry is effectively restored in high excited states. The spectrum has also been analyzed within a nonrelativistic description based on the relation $M^2 \sim L + n$ and can also be understood in this scenario, although different predictions for missing states from the chiral symmetry restoration scenario are found [4].

The present calculation has been performed in the framework of the constituent quark model of Ref. [5] where an extensive study of the meson spectra

¹E-mail address: segonza@usal.es

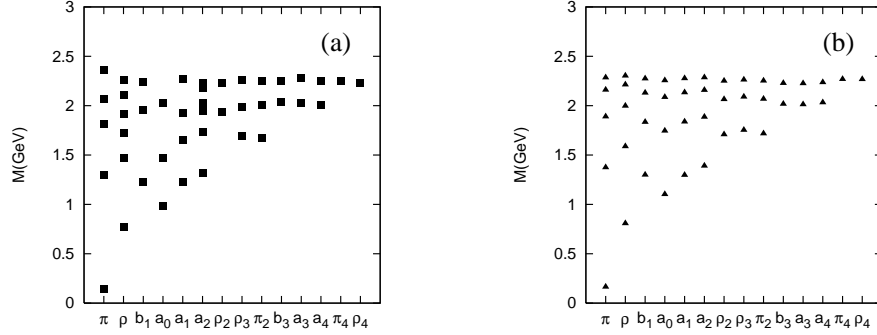


Figure 1: Light meson experimental (a) and theoretical (b) spectrum.

has been done. As a consequence of the spontaneous breaking of the original QCD $SU(3)_L \otimes SU(3)_R$ chiral symmetry, quarks acquire a dynamical mass and interact through Goldstone modes. For higher momenta perturbative QCD effects are present and we assume that quarks interact through gluon exchanges.

Lattice calculations in the quenched approximation and for heavy quarks derived a confining interaction linearly dependent on the interquark distance [6]. The consideration of sea quarks apart from valence quarks (unquenched approximation) suggests a screening effect on the potential when increasing the interquark distance. String breaking has been recently confirmed in a $n_f = 2$ lattice QCD calculation [7]. The color screening can be parametrized by the potential [8]

$$V_{CON}(\mathbf{r}_{ij}) = \{-a_c(1 - e^{-\mu_c r_{ij}}) + \Delta\}(\lambda_i^c \cdot \lambda_j^c) \quad (1)$$

At short distances this potential presents a linear behavior with an effective confinement strength $a = -a_c \mu_c (\lambda_i^c \cdot \lambda_j^c)$ while it becomes constant at large distances.

Table 1: Contribution in MeV to the mass of the high excited states from the different potential pieces.

	$\pi_0(4S)$	$\rho_1(4S)$	$\pi_4(1F)$	$\rho_4(1F)$
Goldstone bosons	-7.23	-1.29	0.16	0.50
Confinement	-416.70	-330.61	-370.02	-368.76

We have taken the parameters for the quark-quark interaction from [5] except those corresponding to the confinement potential which has been fine

tuned to obtain the experimental threshold. The product μa_c has not been modified to guarantee the good description of the low lying spectrum. In Fig. 1 we compare our calculation (b) with the excited state meson spectrum with isospin $I = 1$. One can see that the pattern of the degeneracy is very well reproduced using the values $a_c = 498.9 \text{ MeV}$ and $\mu = 0.603 \text{ fm}^{-1}$.

Although chiral symmetry is still broken, since no changes in the dynamical quark mass has been made, it is irrelevant on the dynamics since, as seen in Table 1, the contribution of the Goldstone bosons is almost negligible compared with those from the confinement potential.

Models in the Chiral Symmetry Restoration scenario are based on the assumption that increasing the excitation energy of an hadron one also increases the typical momentum of the valence quarks. Therefore the quark wave function is shifted to the high momentum region [9]. In our approach degeneracy comes about from the gradual decreases of the confinement potential slope and so the wave function range in coordinate space increases as the excitation energy increases.

We calculate the leptonic widths using the Van Royen-Weisskopf formula with the QCD corrections taken into account [10]. The width is proportional to the wave function (w.f.) at the origin $|R_n(0)|^2$. If the typical momentum of quarks increase above the chiral symmetry breaking scale one should expect that the w.f at the origin should also increase, getting much higher leptonic widths for excited mesons.

Table 2: The leptonic widths (in keV) of highly excited states in charmonium and light mesons. Experimental data are from Ref. [3] ($\psi(2S)$) and Ref. [12].

		$\psi(nS)$		
		$2S$	$3S$	$4S$
Theory		1.71	1.07	0.74
Exp		2.10 ± 0.15	0.89 ± 0.08	0.71 ± 0.10

		$\pi(nS)$			$\rho(nS)$		
		$2S$	$3S$	$4S$	$2S$	$3S$	$4S$
Theory		0.984	0.269	0.104	0.081	0.030	0.012

In our model the behavior of the wave function at the origin is just the opposite and the leptonic widths will decrease as the excitation energy increases. This behavior is observed in the leptonic widths of heavy quarkonia and explained by the flattening of the confinement potential at distances

$r \geq 1, 2fm$. [11]. In Table 2 we show the agreement of our results for the charmonium electronic widths with the experimental data. In this Table we also give our predictions for the high excitations of light mesons. The measurement of these widths in the new PANDA experiment at FAIR may give definitive arguments about the possible restoration of chiral symmetry on the high excited meson spectrum.

Acknowledgments

This work has been partially funded by Ministerio de Ciencia y Tecnología under Contract No. FPA2004-05616, and by Junta de Castilla y León under Contract No. SA-016A07

References

- [1] D.V. Bugg, Phys. Rept. **397**, 257 (2004).
- [2] S.S. Afonin, Phys. Lett. B **639**, 258 (2006).
- [3] W.-M. Yao et al., J. Phys. G **33**, 1 (2006).
- [4] S.S. Afonin, hep-ph/0707.0824.
- [5] J. Vijande, F. Fernandez, A.Valcarce, J. Phys. G: Nucl. Part. Phys **31**, 481 (2005).
- [6] G.S. Bali, Phys. Rep. **343**, 1 (2001).
- [7] G.S. Bali, H. Neff, T. Düssel, T. Lippert, K. Schilling, Phys. Rev. D **71**, 114513 (2005).
- [8] K.D. Born *et al.*, Phys. Rev. D **40**, 1653 (1989).
- [9] R.F. Wagenbrunn, L.Ya Glozman, Phys. Rev. D **75**, 036007 (2007).
- [10] R. Barbieri *et al.*, Nucl. Phys. B **154**, 535 (1979).
- [11] A.M. Badalian, A.I. Veselov, B.L.G. Bakker, J. Phys. G: Nucl. Part. Phys **31**, 417 (2005).
- [12] Kamal K. Seth, hep-ex/0405007.

BOOTSTRAP METHOD FOR THE PHYSICAL VALUES OF πN RESONANCE PARAMETERS

Kirill Semenov-Tian-Shansky^{*,#,1}, Alexander Vereshagin[%], Vladimir Vereshagin[#]

^{*}Institut für Theoretische Physik II, Ruhr-Universität Bochum, Bochum, Germany

[%]Department of Physics and Technology, University of Bergen, Bergen, Norway

[#]Department of High Energy Physics, Saint-Petersburg State University, Saint-Petersburg, Russia

Abstract

We argue how it is possible to apply the general scheme of the effective scattering theory (EST) to the description of the hadronic processes. The results of the numerical tests of sum rules for πN spectrum parameters that follow from the bootstrap system allow us to claim the consistency of the predictions obtained in the framework of our approach with the known experimental data.

1 Introduction

The essence of our work is an attempt to develop a self consistent Dyson perturbation technique for the infinite component effective scattering theory of strong interaction. It is quite reasonable to start from the definition of such a theory. We use a slightly modified version of the definition first given in [1]. The field theory is called effective if the quantum interaction Hamiltonian (in the interaction picture) contains all the monomials consistent with a given algebraic (linear) symmetry. The effective theories are as renormalizable as the ordinary renormalizable ones. The only difference is that one needs to formulate an infinite number of renormalization prescriptions (RPs) fixing the finite part of counterterms. Effective theories are intrinsically quantum constructions since we rely upon Weinberg scheme of constructing QFT

¹E-mail address: kirill.semenov@tp2.ruhr-uni-bochum.de

(see e.g. [2]). This approach is adjusted for S -matrix calculations. We call a theory constructed with the use of this scheme as effective scattering theory (EST).

In our approach we deal only with a very narrow class of localizable effective scattering theories and introduce the notion of extended perturbative scheme (see the discussion in [3, 5]). The hypothetical localizable effective theory of strong interaction requires an infinite extension of perturbative scheme by introduction of an infinite tower of baryon and meson resonances of arbitrary high spin and mass. When dealing with such a theory one has first to point out a way to assign meaning to the perturbation series. The second problem is to somehow reduce the number of independent parameters for which it is necessary to formulate RPs fixing the physical contents of the theory. In Refs. [3–5] we propose a way to construct the meaningful perturbative scheme for such a theory.

2 Construction of the Cauchy Forms

The amplitude $M_{a\alpha}^{b\beta}$ of πN binary scattering can be presented in the following form (isotopic invariance is taken to be the exact symmetry of strong interaction):

$$M_{a\alpha}^{b\beta} = \delta_{ba}\delta_{\beta\alpha}M^+ + i\varepsilon_{bac}(\sigma_c)_{\beta\alpha}M^-, \quad (1)$$

where

$$M^\pm = \bar{u}(p', \lambda') \left\{ A^\pm + \left(\frac{\tilde{k} + \tilde{k}'}{2} \right) B^\pm \right\} u(p, \lambda) . \quad (2)$$

The invariant amplitudes A^\pm , B^\pm are certain functions of Mandelstam variables s , t , u .

The tree-level binary πN scattering amplitude calculated in the framework of our effective theory approach is the sum of all possible s -, t - and u - channel resonance exchanges plus the sum of contributions of all possible $\pi\pi N\bar{N}$ vertices. To assign meaning to this sum (which is certainly a formal one) one has to switch to minimal parametrization (see [4, 5]) and to use the method of Cauchy forms ([3] and Refs. therein). The transition to the minimal parametrization helps to get rid of those combinations of Hamiltonian couplings which appear only in off-shell matrix elements and hence does not require the formulation of RPs since we are only interested in the calculation of the S -matrix.

To construct the Cauchy forms one needs to fix the values of the residues at the relevant poles and to choose properly the bounding polynomial degree. Residues at poles of tree-level amplitudes are just the on-shell spin sums

dotted by the minimal triple coupling constants. It is at this step that we take the main advantage of minimal parametrization since there is only a finite number of minimal triple vertices for each resonance with given quantum numbers. The bounding polynomial degrees are chosen in accordance with the known values of corresponding Regge intercepts.

This results in uniformly converging series of singular terms defining tree-level amplitude as the polynomially bounded meromorphic function in three mutually intersecting layers B_x : ($x \in \mathbb{R}$, $x \sim 0$; $\nu_x \in \mathbb{C}$), where $x = s, t, u$ and ν_x , $x (x = s, t, u)$: $\nu_s = u - t$, $\nu_t = s - u$, $\nu_u = t - s$, fixing the invariant amplitudes in the layers up to few unknown functions.

One of the principal results of [5] states that if one relays upon the renormalized perturbation theory scheme with on-shell renormalization point it is sufficient to formulate RPs only for minimal triple couplings and (real) resonance masses. The next step is to show that although the number of RPs fixing the physical contents of EST is still infinite these RPs are not independent.

3 Bootstrap System

Bootstrap system arise as the natural requirement that the Cauchy forms (different in different layers) should coincide in the domains of intersection of layers. This system constrains the allowed values of fundamental observables of the theory (triple minimal couplings and mass parameters). Besides it completely determines the allowed form of the four-leg pointlike vertex contributions and in this way helps to fix completely the binary scattering amplitude.

For example the set of bootstrap constrains for A^- in $B_t \cap B_u$ domain reads:

$$\Psi_s(A^-) \equiv [\text{Cauchy form in } B_u] - [\text{Cauchy form in } B_t] = 0 \text{ for } t, u \sim 0. \quad (3)$$

Expanding the bootstrap equation in powers of kinematical variables t, u in the vicinity of ($t = 0, u = 0$) one obtains an infinite set of sum rules for minimal (resultant) triple couplings and resonance masse parameters. These constrains ($m, n = 0, 1, \dots$) read as:

$$\sum_{\substack{N, \Delta \\ \text{baryons}}} g_{RB\pi N}^2 V_{m,n}(M_{RB}, J, \mathcal{N}, I) - \sum_{\substack{\text{Mesons with} \\ I=1, \text{ odd } J, P=-1}} g_{R_M\pi\pi} \cdot g_{R_M N \bar{N}} W_{m,n}(M_{R_M}, J) = 0. \quad (4)$$

Here $g_{RB\pi N}$ ($g_{R_M\pi\pi}$, $g_{R_M N \bar{N}}$) stand for minimal triple couplings of baryon (meson resonances) with pions and nucleons. $V_{m,n}$ and $W_{m,n}$ are certain

known functions depending on resonance quantum numbers (mass parameter, spin, normality and isospin). Bootstrap constrains are renorm-invariant in the sense that they are the equations for physical renormalization prescriptions (RPs): triple couplings and mass parameters.

Since bootstrap constrains connect physical quantities the sum rules (4) can be checked with help of experimental data. The numerical check (see [6]) demonstrates a good fit thus supporting the system of postulates we use in our EST approach.

4 Conclusions

We develop the logically complete scheme of EST suitable for the description of hadronic scattering processes. Numerical test of sum rules for πN (and also $\pi\pi$ and KN) resonance parameters show that the system of postulates forming the basis our approach is consistent with the presently known phenomenology. We also argue that the sum rules derived from the bootstrap system can be used as a powerful tool to study hadron spectrum.

References

- [1] S. Weinberg, *Physica A* **96**, 327 (1979).
- [2] S. Weinberg, *The Quantum Theory of Fields* (Cambridge University Press, Cambridge, 1999), vv. 1 – 2.
- [3] A. Vereshagin, V. Vereshagin, and K. Semenov-Tian-Shansky, *J. Math. Sci.* **125**, 144 (2005).
- [4] A. Vereshagin and V. Vereshagin, *Phys. Rev. D* **69**, 025002 (2004).
- [5] K. Semenov-Tian-Shansky, A. Vereshagin, and V. Vereshagin, *Phys. Rev. D* **73**, 025020 (2006).
- [6] K. Semenov-Tian-Shansky, A. Vereshagin, V. Vereshagin, arXiv:0706.3672 [hep-ph]. For the preliminary results see also A. Vereshagin and V. Vereshagin, *πN Newsletter* **15**, 288 (1999); A. Vereshagin, *πN Newsletter* **16**, 426 (2002).

η -MESON PRODUCTION IN THE COUPLED-CHANNEL EFFECTIVE LAGRANGIAN APPROACH

V. Shklyar^{*,1}, H. Lenske^{*,†}, and U. Mosel^{*}

^{*}Institut für Theoretische Physik, Universität Giessen, Giessen, Germany

[†]GSI, Darmstadt, Germany

Abstract

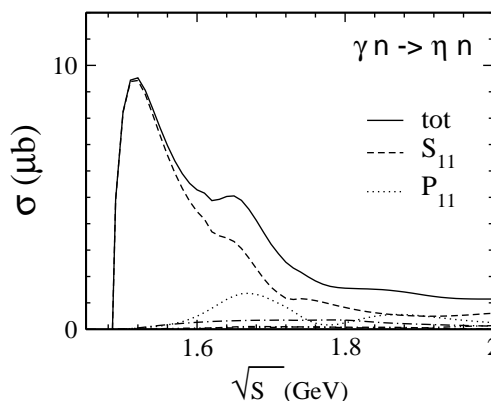
Pion- and photon-induced reactions are analyzed within the coupled-channel effective Lagrangian Giessen model for the baryon resonance analysis. Last results for the eta-meson productions both in pion and photon induced reactions are presented.

1 Introduction

The properties of most resonances have been obtained from pion-nucleon elastic scattering. Despite of extensive efforts made in the past two main problems are still encountered by any baryon resonance analyses. First, the parameters of many well established states remain uncertain. The second problem is related to 'missing' or 'unresolved' states which are supposed to exist on the basis of quark model calculations but are weakly coupled to the pion-nucleon channel.

The solution of these problems requires a coupled-channel treatment of the scattering process. First, the inclusion of as many experimental data as possible into each channel constrains free parameters and other ambiguities of the model, helping to draw a solid conclusion on the resonance parameters. Secondly, a multi-channel treatment allows to link different reaction channels as required by unitarity. Keeping that in mind we have developed an unitary coupled-channel effective Lagrangian model [1–3] for a study of pion- and photon-induced reactions in the nucleon resonance energy region. The properties of nucleon resonances are constrained by a direct comparison to the experimental data. In this contribution we report on our last results on the study of the eta-meson production mechanisms both in the pion- and photon-nucleon scattering.

¹The work is supported by Forschungszentrum Jülich and DFG.

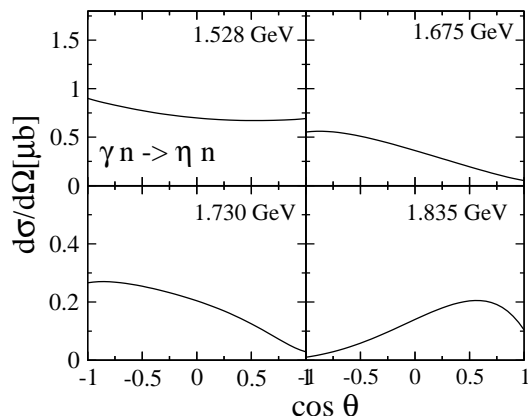
Figure 1: $\gamma n \rightarrow \eta n$ total and partial wave cross sections.

2 Results and discussion

The details of the Giessen Model can be found in [2, 3]. Here we briefly outline the main ingredients relevant for the present discussion. The Bethe-Salpeter equation (BSE) is solved in the ladder approximation to obtain a scattering amplitude. The interaction potential $[V]_{ij}$ is built up as a sum of tree-level Feynman diagrams and generally contains resonance and background terms (s - and u -, t -channels correspondingly). The contributions from the corresponding diagrams are calculated using effective interaction Lagrangians [2, 3]. Performing a partial wave decomposition and using a K -matrix approximation the Bether-Salpeter equation can be reduced to a set of algebraic equations for the scattering partial wave amplitudes. Such a formulation of the problem allows to include as many open channels as possible. In previous works, $(\pi/\gamma)N \rightarrow \gamma N$, πN , $2\pi N$, ηN , ωN , $K\Lambda$, $K\Sigma$ reactions were analysed. The obtained resonance parameters are summarized in [3, 4].

Recently, an experimental program on studies of eta-photoproduction on neutron target has been started. The first preliminary data from V. Kuznetsov *et al.* reveal an excess in the differential cross section of eta-neutron photoproduction at c.m. energies around 1.67 GeV [5]. A similar effect has been also found by the CB-ELSA collaboration. These observations rise questions about the reaction mechanisms which might be responsible for the observed phenomena. Besides prediction of a narrow state more 'conventional' effects coming from excitations of $S_{11}(1650)$ and $P_{11}(1710)$ must be explored as an alternative scenario.

In [6] the coupled-channel Giessen Model was applied to study the effect

Figure 2: $\gamma n \rightarrow \eta n$ differential cross section.

of these two state in $\gamma n \rightarrow \eta n$ reaction. The obtained properties of $S_{11}(1535)$ and $S_{11}(1650)$ are very close to the average PDG values [7]. The third resonance $P_{11}(1710)$ is rated three stars by PDG and its parameters are still under debate. We obtain a rather strong coupling of $P_{11}(1710)$ to the final eta-nucleon channel which is close to the upper bound given by PDG.

The calculated total and partial wave cross sections are presented in Fig. 1. We find a positive interference pattern between $S_{11}(1535)$ and $S_{11}(1650)$ states which indeed leads to an enhancement in the S_{11} partial wave cross section at 1.67 GeV. Note, that the above effect is not a result of a simple interference between two S_{11} resonance like it might be thought in terms of Breit-Wigner parameterization. Due to unitarization the scattering amplitude depends strongly on rescattering effects in a number of channels like πN , $2\pi N$, ηN and the decomposition into individual resonance contributions is not straightforward. Hence, the observed interference is a higher order effect coming from the resummation of the perturbation series within the ladder approximation to the BSE. A similar effect is found in the P_{11} partial wave where an excitation of $P_{11}(1710)$ also leads to an increase in the corresponding cross section at 1.67 GeV.

In Fig. 2 the predicted differential cross sections of the eta photoproduction on the neutron are shown. The contribution from the S_{11} partial wave dominates the $\gamma n \rightarrow \eta n$ reaction up to 1.6 GeV, resulting in a smooth angular dependence of the differential cross section. At 1.66 GeV the $S_{11}(1650)$ and $P_{11}(1710)$ resonances start to play a role producing an enhancement in the differential cross section at backward angles. At higher energies $\sqrt{s} \geq 1.8$ GeV the effect from these states vanishes and the calculated angular distributions become very similar to that of $\gamma p \rightarrow \eta p$. We conclude that the resonance-like

structure observed in $\gamma n \rightarrow \eta n$ reaction around 1.67 GeV can be explained by the excitation of the $S_{11}(1650)$ and $P_{11}(1710)$ resonance alone, without further need for a new resonance. We emphasize that these states contribute indirectly through higher-order interference effects as discussed above.

3 Summary

Coupled-channel calculations of pion- and photon-induced reactions have been used to constrain properties of nucleon resonances. The latest results on the eta-meson production in the nucleon resonance energy region are presented.

We have shown that the enhancement observed in the experimental data for the $\gamma n \rightarrow \eta n$ differential cross section can be explained in terms of interference effects in S_{11} and P_{11} partial waves coming from $S_{11}(1650)$ and $P_{11}(1710)$ resonance contributions respectively. At the 1.67 GeV c.m. energy the predicted differential cross section has a pronounced maximum at backward angles. Note, that experimental data on the $\gamma n \rightarrow \eta n$ cross section are usually extracted from photon-deuteron scattering data. Hence, an extended analysis taking into account the deuteron wave function explicitly is necessary for the comparison with the experimental data.

References

- [1] T. Feuster and U. Mosel, Phys. Rev. **C58**, 457 (1998), nucl-th/9708051.
- [2] G. Penner and U. Mosel, Phys. Rev. **C66**, 055211 (2002), nucl-th/0207066.
- [3] V. Shklyar, H. Lenske, U. Mosel, and G. Penner, Phys. Rev. **C71**, 055206 (2005), nucl-th/0412029.
- [4] V. Shklyar, H. Lenske, and U. Mosel, Phys. Rev. **C72**, 015210 (2005), nucl-th/0505010.
- [5] GRAAL, V. Kuznetsov, Phys. Lett. **B647**, 23 (2007), hep-ex/0606065.
- [6] V. Shklyar, H. Lenske, and U. Mosel, Phys. Lett. **B650**, 172 (2007), nucl-th/0611036.
- [7] Particle Data Group, K. Hagiwara *et al.*, Phys. Rev. **D66**, 010001 (2002).

HIGH MASS BARYONS IN PION PHOTOPRODUCTION

*A. Sibirtsev*¹

Helmholtz-Institut für Strahlen- und Kernphysik (Theorie)
Universität Bonn
Nußallee 14-16, D-53115 Bonn, Germany

Abstract

A Regge model was employed in a global analysis of the world data on π^+ and π^- photoproduction at photon energies from 3 to 8 GeV. In this energy region the resonance contributions are expected to be negligible so that the available experimental results allow to determine the non-resonant part of the reaction amplitude reliably. This amplitude is then used to predict observables for photon energies below 3 GeV. Differences between the predictions and data in this energy region are systematically examined as possible signals for the presence of high mass baryons. The analysis of differential cross section for negative pion photoproduction, obtained recently at JLab, indicates resonance structures above an invariant energy of 2 GeV.

A rough inspection of the excited baryon spectrum given by the Particle Data Group [1] suggests an impressive regularity for nucleon and Delta states with the masses above $\simeq 1.8$ GeV. The states with the same spin but opposite parity are almost degenerate. At the same time, a parity doubling was not observed for the well established low lying baryons.

One can ask why parity doubling was not discovered for low mass baryons and what is the QCD symmetry behind this phenomenon? It was proposed [2–5] that parity doubling might reflect the restoration of spontaneously broken chiral symmetry of QCD. These considerations are not the only way to explain the apparent doubling phenomenon. It was shown in the framework of a covariant constituent quark model [6], that the instanton induced multi-fermion interaction leads to a lowering of selected states that accidentally become degenerate with their parity partners.

Unfortunately some of the doublet partners for the baryons with masses above 2 GeV have not been detected yet. Therefore the crucial question of whether the parity doubling of the high mass baryons has systematic nature

¹a.sibirtsev@fz-juelich.de

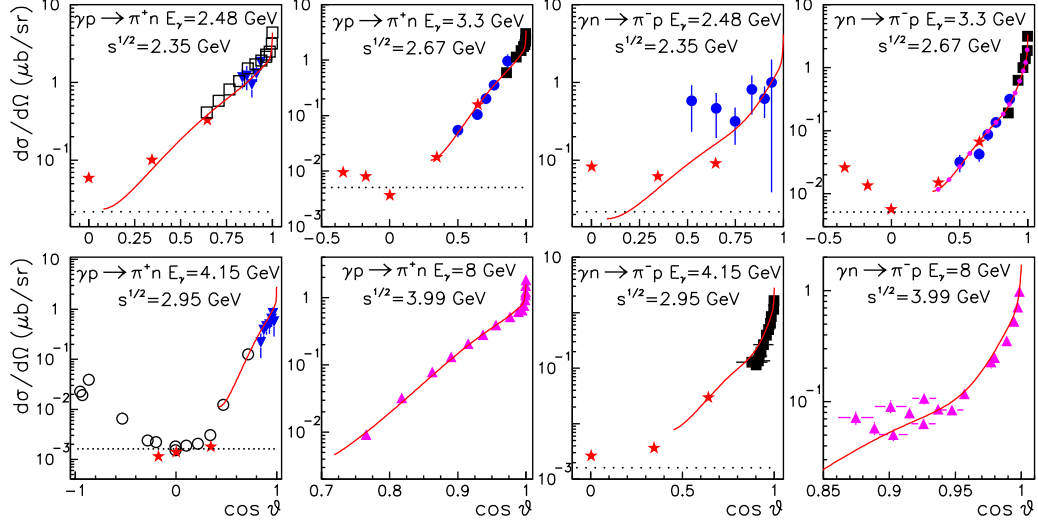


Figure 1: Angular spectra for π^+ and π^- photoproduction at different photon energies E_γ and invariant collision energies \sqrt{s} . The symbols show the data compiled in Ref. [7]. The stars are results from JLab Hall A Collaboration [8, 9]. The solid lines show the Regge calculations [7], while the dashed lines are the results obtained with the dimensional counting rule [10].

remains open. Indeed, the generation of the excited baryon spectrum is one of the unsolved puzzles of QCD that explicitly involves such fundamental properties as chiral symmetry and confinement.

The spectroscopy of high lying baryons is a non-trivial problem. In this energy region the background contribution dominates the reaction, which substantially complicates data evaluation and extraction of the resonance properties. To resolve the problem it was proposed [7] to construct the non-resonant part of the reaction amplitude and to fix it at high energies. Here the resonance contributions are expected to be negligible so that the available experimental results on differential cross sections and polarization observables allows to determine the non-resonant amplitude reliably. This amplitude is then used to predict observables at lower energies. The method was applied in the analysis of πN scattering and π photoproduction.

The analysis of the π^+ and π^- photoproduction indicates some surprising results that are presented here. In order to fix the non-resonance part of the reaction amplitude the Regge model with absorptive corrections was employed in a global evaluation of the world data available at photon energies

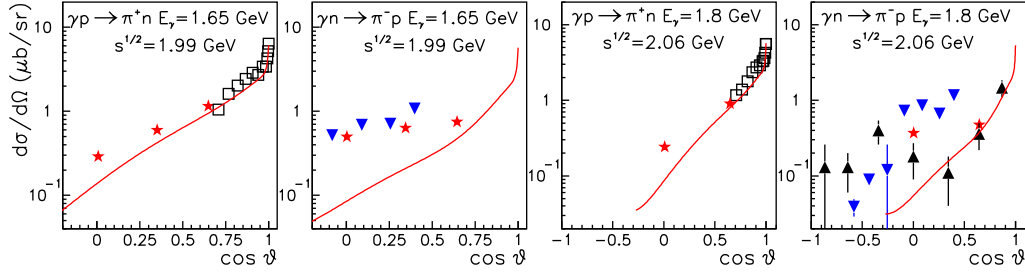


Figure 2: Angular spectra for π^+ and π^- -photoproduction at different photon energies E_γ and invariant collision energies \sqrt{s} . The symbols show the data compiled in Ref. [7]. The stars are results from JLab Hall A Collaboration [8, 9]. The solid lines show the Regge calculations from Ref. [7].

from 3 to 8 GeV. The details of the calculations and systematic comparison with data are given in Ref. [7].

The solid lines in Fig.1 show the results obtained with the Regge calculations [7]. Note that in general the model is applicable at squared four momentum transfer $|t| < 2 \text{ GeV}^2$ and the solid lines are shown for that range of t . It is clear that the calculations well reproduce differential cross sections at forward angles. Here the stars are most recent results from JLab Hall A Collaboration [8, 9]. It is important that JLab measurements cover large range of angles and overlap with the data available previously. These new results are in reasonable agreement with Regge calculations at forward angles and indicate some additional contribution at large angles.

Part of such additional contribution at large $|t| > 2 \text{ GeV}^2$ or large angles might come from the direct interaction of photon with the quark of the nucleon. The main feature of this direct interaction is that the reaction amplitude is almost independent of t and the energy dependence of the reaction cross sections is driven by the total number of elementary fields in the initial and final states. The interaction can be modeled by perturbative QCD and the dashed lines in Fig.1 show the results obtained with the Dimensional Counting Rule [10].

Fig.1 illustrates that at invariant energies $\sqrt{s} < 3 \text{ GeV}$ the differential cross sections, especially for π^- photoproduction, variate with angle and thus disagree with DCR expectations. Such angular dependence is typical for the excited baryon contribution. However to identify resonance excitation it is necessary to measure the spectra within the full angular range.

Now the non-resonant amplitude fixed at high energies can be used to predict observables for photon energies below 3 GeV. The differences between the predictions and data in this energy region might indicate the presence of excited baryons. Fig.2 shows angular spectra for π^+ and π^- -photoproduction at invariant collision energies $\sqrt{s}\simeq 2$ GeV. While the positive pion data are reasonably described by Regge calculations, the π^- photoproduction results are in strong disagreement with the predictions. Note that old as well as new JLab negative pion data indicate likewise the presence of resonance structures.

Obviously further evaluation of high lying excited baryons requires the precise measurements on differential cross sections and polarization observables that cover full angular range and scan the photon energy above $\simeq 1.6$ GeV. Presented analysis [7] illustrates that single pion photoproduction is crucial tool to study the excited baryon spectrum. And finally to resolve the current puzzle of QCD.

Acknowledgments

It is a great pleasure to thanks my collaborators, J. Haidenbauer, S. Krewald, T.-S.H. Lee, Ulf.-G. Meißner and A.W. Thomas. I appreciate discussions with I. Aznauryan, H. Gao, J. Goity, Ch. Hanhart, J.M. Laget, V. Mokeev and M. Vanderhaeghen. I acknowledge support by the JLab grant SURA-06-C0452 and the COSY FFE grant No. 41760632 (COSY-085).

References

- [1] W.-M. Yao *et al.*, *J. P hys.* **G33**, 1 (2006).
- [2] L.Ya. Glozman, *Phys. Rept.* **444**, 1 (2007).
- [3] D. Jido, M. Oka and A.Hosaka, *Prog. Theor. Phys.* **106**, 873 (2001).
- [4] T.D. Cohen and L.Ya. Glozman, *Int. J. Mod. Phys.* **A17**, 016006 (2002).
- [5] R.L. Jaffe, D. Pirjol and A. Scardicchio, *Phys. Rept.* **435**, 157 (2006).
- [6] U. Löring, B. C. Metsch and H. R. Petry, *Eur. Phys. J.* **A10**, 395 (2001).
- [7] A. Sibirtsev, J. Haidenbauer, S. Krewald, T.S.H. Lee, Ulf-G. Meißner and A.W. Thomas, *Eur. Phys. J.* **A34**, 49 (2007).
- [8] L. Y. Zhu *et al.*, *Phys. Rev. Lett.* **91**, 022003 (2003).

[9] L.Y. Zhu *et al.* [JLab Hall A Collab.], *Phys. Rev.* **C71**, 044603 (2005).

[10] S. J. Brodsky and G. R. Farrar, *Phys. Rev. Lett.* **31**, 1153 (1973).

ROPER RESONANCE EXCITATION IN NN-COLLISIONS WITH SINGLE- AND DOUBLE-PION PRODUCTION

T. Skorodko^{*,1}, C. Bargholtz[%], M. Bashkanov^{*}, D. Bogoslawsky[#], H. Calen[⊥], F. Cappellaro[§], H. Clement^{*}, L. Demiroers⁺, E. Doroshkevich^{*}, D. Duniec[§], C. Ekström[⊥], K. Franssen[⊥], L. Geren[%], L. Gustafsson[§], B. Höistad[§], G. Ivanov[#], M. Jacewicz[§], E. Jiganov[#], T. Johansson[§], O. Khakimova^{*}, M. Kaskulov^{*}, S. Keleta[§], I. Koch[§], F. Kren^{*}, S. Kullander[§], A. Kupś[⊥], A. Kuznetsov[#], K. Lindberg[%], P. Marciniewski[⊥], R. Meier^{*}, B. Morosov[#], C. Pauly[÷], H. Pettersson[§], Y. Petukhov[#], A. Povtorejko[#], A. Pricking^{*}, K. Schönning[§], W. Scobel⁺, B. Schwartz[±], V. Sopov[∓], J. Stepieniak[∠], P.-E. Tegner[%], P. Thörngren-Engblom[§], V. Tikhomirov[#], G. J. Wagner^{*}, M. Wolke[÷], A. Yamamoto[□], J. Zabierowski[▷], I. Zartova[%], J. Złomanczuk[§]

(*CELSIUS – WASA Collaboration*)

^{*}Physikalisches Institut der Universität Tübingen, D-72076 Tübingen, Germany

[%]Department of Physics, Stockholm University, Stockholm, Sweden

[#]Joint Institute for Nuclear Research, Dubna, Russia

[⊥]The Svedberg Laboratory, Uppsala, Sweden

[§]Uppsala University, Uppsala, Sweden

⁺Hamburg University, Hamburg, Germany

[±]Budker Institute of Nuclear Physics, Novosibirsk, Russia

[∓]Institute of Theoretical and Experimental Physics, Moscow, Russia

[÷]Forschungszentrum Jülich, Germany

[□]High Energy Accelerator Research Organization, Tsukuba, Japan

[∠]Soltan Institute of Nuclear Studies, Warsaw, Poland

[▷]Soltan Institute of Nuclear Studies, Lodz, Poland

¹E-mail address: skorodko@pit.physik.uni-tuebingen.de

Abstract

Whereas in most investigations the Roper resonance is sensed only very indirectly via complex partial wave analyses, we find indications for its excitation in the $pp \rightarrow np\pi^+$ reaction, where some resonance-like structure is observed in the invariant $n\pi^+$ mass spectrum at $M \approx 1360$ MeV with a width of 150 MeV. The values fit very favorably to the most recent phase shift results as well as to the observations at BES. In near-threshold two-pion production $pp \rightarrow pp\pi^0\pi^0$, where the Roper excitation and its subsequent decay into $N\pi\pi$ is the only dominant process, we find its decay into the $N\sigma$ channel as the prevailing decay process - in favor of Roper's nature as a monopole excitation

1 Introduction

The Roper resonance has been a puzzle ever since its detection in πN phase shifts [1]. In most investigations no apparent resonance signatures could be found in the observables. Not only its nature has been a matter of permanent debate, also its resonance parameters show a big scatter in their values [2].

New phase shift evaluations [3, 4] of πN and γN data show the pole of the Roper resonance to be nearly 100 MeV below its canonical value of 1440 MeV with a width not much different from that of neighboring baryon states. After the pioneering αp scattering experiment at Saclay [5], where for the first time direct evidence for the Roper resonance has been found in the missing mass spectrum, also new BES data [6] on $J/\Psi \rightarrow \bar{N}N^*$ show a clear structure in the $M_{p\pi^-}$ invariant mass spectrum at $M \approx 1358$ MeV and a width of $\Gamma \approx 179$ MeV. Note that with the pole position being roughly 80 MeV below the previously adopted value of the $N^*(1440)$, also its decay branchings (taken at the pole position) change dramatically.

2 Experiment and Results

In order to shed more light on this issue exclusive measurements of the reactions $pp \rightarrow NN\pi$ and $pp \rightarrow NN\pi\pi$ have been carried out at several energies from 650 - 1450 MeV at the CELSIUS storage ring using the 4π WASA detector setup including the pellet target system.

The $pp \rightarrow np\pi^+$ measurement at $T_p = 1.3$ GeV shows in the $M_{p\pi^+}$ spectrum the expected strong Δ^{++} excitation. The $M_{n\pi^+}$ spectrum, however, exhibits only a small structure around the position of the Δ^+ due to the isospin suppression of the latter. Towards higher $M_{n\pi^+}$ masses we find a

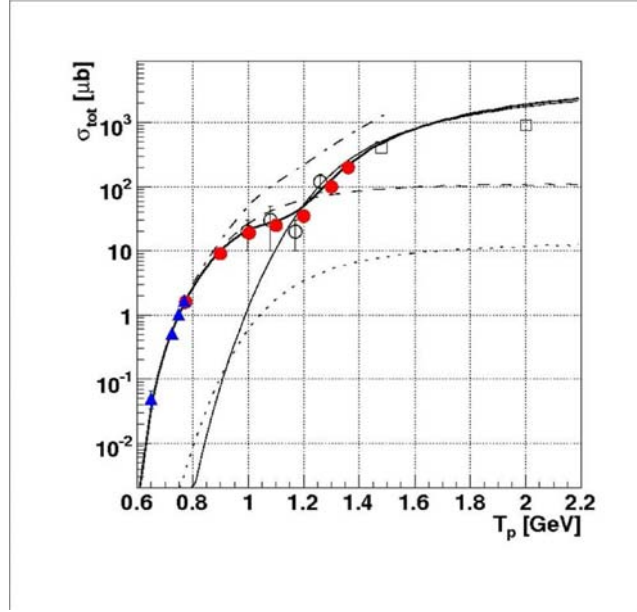


Figure 1: Energy dependence of the $pp \rightarrow pp\pi^0\pi^0$ reaction (thick solid line) together with calculations for the Roper excitation with successive decay into $N\sigma$ (dashed) and $\Delta\pi$ (dotted) channels as well as for $\Delta\Delta$ excitation (thin solid). The prediction of Ref. [9] is indicated by the dash-dotted curve. Solid dots denote results of this work, solid triangles are PROMICE/WASA results [10]. Open circles and squares show bubble chamber results of Refs. [11–13].

structure around 1360 MeV with a width of about 150 MeV, which we associate with the Roper excitation. At present the details of this structure still have to be worked out.

In Fig. 1 the energy dependence of the $pp \rightarrow pp\pi^0\pi^0$ reaction is shown, which separates into a clear Roper excitation region near threshold and a high-energy region governed by $\Delta\Delta$ excitation.

In the analysis of near-threshold $\pi^+\pi^-$ production the unique sensitivity of this reaction to the two-pion decay of the Roper resonance has been demonstrated [7, 8]. The $\pi^0\pi^0$ channel selects specifically only the isoscalar part of the Roper decay into the $\pi\pi$ channel. Analysis of these data provides a ratio of approximately 4:1 for the decay branching into $N\sigma$ and $\Delta\pi$ channels at a pole mass of 1360 MeV - in favor of a monopole mode interpretation of the Roper excitation. Note that though the branching ratios at the pole position reflect the physics of the decay of a resonance, in the PDG convention the branching ratios are quoted at the Breit-Wigner mass. Usually this

distinction is not very significant, however, the Roper resonance is one of the big exceptions, since its Breit-Wigner mass of 1440 MeV is as far as 80 MeV above the pole position. In the PDG convention our branching ratio reads 1:1 in very good agreement with the values quoted in Ref. [4]. Note that this branching ratio is a factor of 4 smaller than the one quoted in PDG [2].

Acknowledgments

We acknowledge valuable discussions with E. Oset, L. Alvarez-Ruso, A. Kaidalov, L. Dakhno, A. and V. Anisovich and A. Sarantsev on this issue. This work has been supported by BMBF (06TU201, 06TU261), COSY-FFE, DFG (Europ. Graduiertenkolleg 683), Landesforschungsschwerpunkt Baden-Württemberg and the Swedish Research Council. We also acknowledge the support from the European Community-Research Infrastructure Activity under FP6 "Structuring the European Research Area" programme (Hadron Physics, contract number RII3-CT-2004-506078).

References

- [1] L. D. Roper, Phys. Rev. Lett. **12** (1964) 340
- [2] Particle Data Group, J. Phys. **G33** (2006) 1
- [3] R. A. Arndt *et al.*, Phys. Rev. **C69** (2004) 035213 and nucl-th/0605082
- [4] A. V. Sarantsev *et al.*, arXiv:0707.3591 [hep-ph]
- [5] H. P. Morsch *et al.*, Phys. Rev. Lett. **69** (1992) 1336
- [6] M. Ablikim *et al.*, Phys. Rev. Lett. **97** (2006) 062001
- [7] W. Brodowski *et al.*, Phys. Rev. Lett. **88** (2002) 192301
- [8] F. Pätzold *et al.*, Phys. Rev. **C67** (2003) 052202R
- [9] L. Alvarez-Ruso, E. Oset, E. Hernandez, Nucl. Phys. **A633** (1998) 519
- [10] J. Johanson *et al.*, Nucl. Phys. **A712** (2002) 75
- [11] F. Shimizu *et al.*, Nucl. Phys. **A386** (1982) 571
- [12] A. M. Eisner *et al.*, Phys. Rev. **138** (1965) B670
- [13] E. Pickup, D.K. Robinson, E. O. Salant, Phys. Rev. **125** (1962) 2091

PIONIC DEUTERIUM

Th. Strauch^{*,1}, F.D. Amaro[#], D.F. Anagnostopoulos[%], P. Bühler[§],
D.S. Covita^{#,•}, H. Gorke^{*}, D. Gotta^{*}, A. Gruber[§], A. Hirtl[§], P. Indelicato[&],
E.-O. Le Bigot[&], J. Marton[§], M. Nikipelov^{*}, J.M.F. dos Santos[#],
Ph. Schmid[§], S. Schlessler[&], L.M. Simons^{•,#}, J.F.C.A. Veloso[#], J. Zmeskal[§]

*Institut für Kernphysik, FZ Jülich, D-52425 Jülich, Germany

%Dept. of Mat. Sci. and Engineering, Univ. Ioannina, GR-45110, Greece

#Dept. of Physics, Coimbra University, P-3000 Coimbra, Portugal

§Stefan Meyer Inst., Austrian Acad. of Sci., A-1090 Vienna, Austria

&Lab. Kastler-Brossel, UPMC-Paris VI, Case 74, 4 place Jussieu, F-75252
Paris, Cedex 05, France

•Paul Scherrer Institut, Villigen PSI, CH-5232 Villigen, Switzerland

Abstract

Data taking of the PIONIC HYDROGEN project has been completed with a high statistics study of the strong–interaction effects in πD by measuring the $K\beta$ X–radiation. The πD hadronic shift will provide a constraint for the πN isospin scattering lengths extracted from the πH measurement. The hadronic width is directly related to pion production at threshold.

1 Introduction

Quantum Chromodynamics (QCD) is today's fundamental microscopic theory of strong interaction. Based on QCD a new framework - Chiral Perturbation Theory (χPT) - gives a theoretical description of the interaction of hadrons at low energies in terms of an expansion in momenta, fine structure constant α and current quark masses [1, 2]. Because relative energies are restricted to the keV range in exotic atoms, they provide an ideal laboratory to study the low-energy meson-baryon interaction without the need of any extrapolation to threshold. The strong pion-nucleus s-wave interaction

¹E-mail address: t.strauch@fz-juelich.de

is observed by measuring K X-radiation in pionic atoms as a level shift ϵ_{1s} and broadening Γ_{1s} of the atomic ground state.

Pions and nucleons combine to isospin 1/2 or 3/2 systems. At threshold the πN interaction is then completely described by two amplitudes reducing to two real numbers identified with the s-wave scattering lengths. One may choose the isoscalar and isovector scattering lengths a^+ and a^- . In pionic hydrogen the hadronic shift is in leading order related by Deser-type formula proportional to the sum of the scattering lengths a^+ and a^- and the broadening to a^- [3,4]. These values have been quantified by the pionic hydrogen experiment [5]. Within the framework of χPT , the corrections to the Deser formula are calculated and in next to leading order of the chiral expansion further low-energy constants appear which are c_1 , f_1 and f_2 .

The hadronic shift in pionic deuterium [5], when determined to a precision similar to that obtained in pionic hydrogen will provide a constraint for the isoscalar and isovector scattering lengths a^+ and a^- . In addition it allows for the determination of the low-energy constant f_1 for which only dimensional estimates exist. As an outstanding case for charged pion-nucleon interactions, the shift is very sensitive to isospin-breaking corrections owing to the almost complete cancellation of the pion-proton and pion-neutron scattering lengths [6]. Furthermore, the hadronic width is directly related to pion production at threshold. The production reaction $pp \rightarrow d\pi^+$ is connected to absorption $d\pi^+ \rightarrow pp$ by detailed balance, which in the case of charge symmetry is equal to $d\pi^- \rightarrow nn$. These processes will become calculable at the percent level within the framework of χPT in the near future [7].

2 Experimental Approach

The experiment is set up at the high-intensity low-energy pion beam $\pi E5$ at the Paul-Scherrer Institut [8]. It consists of the cyclotron trap II, a cryogenic target, a reflection-type crystal spectrometer equipped with spherically bent crystals and a large-area two-dimensional position-sensitive detector built up from an array of six Charge-Coupled devices (CCDs) for X-ray detection.

After pion injection into the trap the beam is degraded in order to spiral in the magnetic field into a gas-filled target cell. In this way a few % of the incoming pions are stopped forming a concentrated X-ray source. X-rays emitted from the target gas are diffracted by a silicon crystal of 10 cm diameter and 3 m curvature radius. The spherical bending leads to a partial vertical focussing, which increases the count rate. Each CCD has 600 x 600 pixels of 40 μm x 40 μm . The efficiency is maximal around 3.5 keV ($\approx 80\%$) and, therefore, ideally suited for low energy X-rays.

The energy calibration of the πD ($3p-1s$) transition (Fig.1) is performed with the precisely known $K\alpha$ fluorescence radiation of gallium [9], which was excited by means of an X-ray tube. The response function of the spectrometer needed to extract the hadronic broadening was measured with X-rays from He-like Argon (Ar^{16+}) produced in an Electron Cyclotron Resonance Ion Trap (ECRIT) [10].

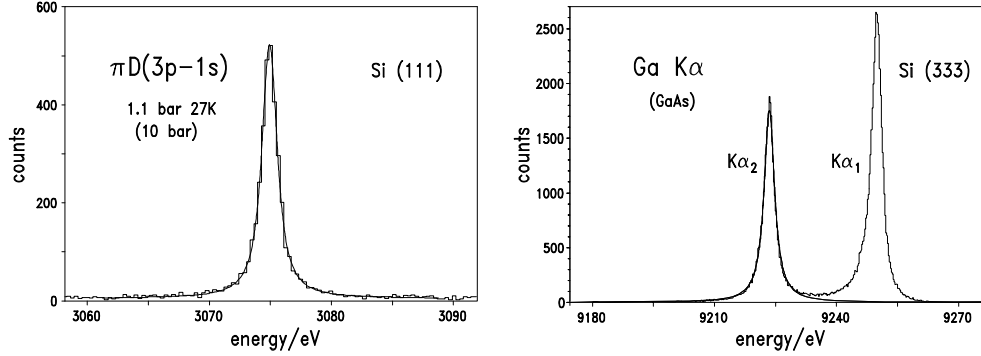


Figure 1: *left: The spectrum of $K\beta$ transition in πD measured with a Si Bragg crystal in first order at a target density equivalent to 10 bar. right: Ga $K\alpha$ doublet measured in third order used for the energy calibration.*

When extracting the hadronic effects, complications arise from processes during the atomic de-excitation cascade, in particular molecular formation [11] and Coulomb de-excitation [12]. In the case of molecular formation like $(\pi D)_{nl} + D_2 \rightarrow [(\pi dd)d]ee$ possible radiative de-excitation out of such complexes leads to an energy shift which alters the extracted hadronic shift. While not observed in πH [8], it is predicted for πD , that the fraction of X-ray emissions increases [11]. If a density dependence is observed, the pure hadronic shift must be obtained from extrapolation to density zero. In the case of Coulomb de-excitation, the energy release for the de-excitation step is converted to kinetic energy: $(\pi^- D)_n + D_2 \rightarrow (\pi^- D)_{n-1} + D + D + \textit{kinetic energy}$, leading to a Doppler broadening of the line width. Both, molecular formation and Coulomb de-excitation, are scattering processes and depend on the collision rate, i.e., on density. Consequently, the strategy of the experiment was to study the X-ray transitions at different densities.

3 First Results

The actual status of the analysis of the πH data yields the preliminary values $\epsilon_{1s} = +7.120 \pm 0.011 \text{ eV}$, $\Gamma_{1s} \approx 823 \pm 19 \text{ meV}$ [8].

The πD measurement ended up with nearly 10000 events measured at three different target densities equivalent to 3.5, 10 and 28 bar to be sensitive to effects during the atomic cascade mentioned above.

The most precise experimental values for the strong interaction shift and width in pionic deuterium are reported to be [13] $\epsilon_{1s} = -2468 \pm 55 \text{ meV} (\pm 2.2\%)$ and $\Gamma_{1s} = 1193 \pm 129 \text{ meV} (\pm 11\%)$. The preanalysis of the new data shows, that it will be possible to extract the hadronic shift and width with an uncertainty of about 0.5% and 4%, respectively, or better.

References

- [1] G.Ecker, *Prog. Part. Nucl. Phys.* **35**, 1 (1995), and ref. therein.
- [2] V.Bernard, N.Kaiser, U.-G.Meissner, *Int. J. Mod. Phys. E* **4**, 193 (1995).
- [3] J.Gasser et al., *Eur. Phys. J. C* **26**, 13 (2002).
- [4] P.Zemp, in *Proc of Chiral Dynamics 2003*, p.128, Bonn, Germany.
- [5] PSI experiments R-98.01 and R-06.03,
<http://www.fz-juelich.de/ikp/exotic-atoms>
- [6] U.-G.Meissner, U.Raha and A.Rusetski, *Phys.Lett.B* **639**, 478 (2006).
- [7] V.Lensky et al., *Eur. Phys. J. A*, **27**, 37 (2006).
- [8] D.Gotta et al., *Lect. Notes Phys.* **745**, 165 (2008).
- [9] R.Deslattes et al. *Rev. Mod. Phys.* **75**, 35 (2003).
- [10] D.F.Anagnostopoulos et al. *Nucl. Instr. Meth. A* **545**, 217 (2005).
- [11] S.Kilic, J.-P.Karr, L.Hilico, *Phys. Rev. A* **70**, 052506 (2004).
- [12] T.S.Jensen and V.E.Markushin, *Eur. Phys. J D* **19**, 165 (2002).
- [13] P.Hauser et al., *Phys. Rev. C* **58**, R1869 (1998).

PARAMETERS A AND R MEASUREMENTS IN THE RESONANCE REGION OF THE PION-NUCLEON ELASTIC SCATTERING: RECENT RESULTS AND SUBSEQUENT INVESTIGATIONS.

V. V. Sumachev^{*,1}, I. G. Alekseev[%], N. A. Bazhanov[#], V. S. Bekrenev^{*}
Yu. A. Beloglazov^{*}, P. E. Budkovsky[%], E. I. Bunyatova[#], E. A. Filimonov^{*},
V. P. Kanavets[%], L. I. Koroleva[%], A. I. Kovalev^{*}, N. G. Kozlenko^{*}, S. P.
Kruglov^{*}, A. A. Kulbardin^{*}, I. V. Lopatin^{*}, B. V. Morozov[%], V. M.
Nesterov[%], D. V. Novinsky^{*}, V. V. Ryltsov[%], V. A. Shchedrov^{*}, A. D.
Sulimov[%], D. N. Svirida[%], V. Yu. Trautman^{*},

^{*}Petersburg Nuclear Physics Institute, Gatchina, Leningrad district, Russia

[%]Institute for Theoretical and Experimental Physics, Moscow, Russia

[#]Joint Institute for Nuclear Research, Dubna, Moscow district, Russia

1 Introduction

The existing models usually predicted considerably more resonances (twice or more in number) than were found in elastic πN - scattering. This problem is known as the problem of "missing" resonances.

The recent partial wave analysis (PWA) SP06 [1] that was made at George Washington University (2006) and included the modern experimental data revealed considerably fewer (approximately half) the N^* - and Δ - resonances than those presented in the Review of Particle Physics (RPP) tables (2006) [2]. This disagreement invites further experimental investigation of the pion-nucleon interactions.

Recent spin rotation parameter A and R measurements of the PNPI and PNPI-ITEP collaborations resolved a part of the twofold ambiguities of the PWA's. These results were used in the last PWA of the George Washington University (GWU) groups. The proposal for the additional measurements of the spin-rotation parameters R and A in the resonance region of the πN interactions is motivated. Such additional experiments are necessary to complete monosemantic PWA of the πN elastic scattering.

¹E-mail address: sumachev@pnpi.spb.ru

2 Baryonic multiplets in the harmonic quark shell model.(according to R. H. Dalitz)

A hadronic system of finite size can be expected to have at least two types of excited states [3]:

- (a) rotational excitations (or Regge recurrences, in field theoretical language)
- (b) radial vibrations (pulsations)

Following Greenberg's early shell-model proposal, the harmonic oscillator $SU(6) \times O(3)$ quark model has had much success in accounting for the low-lying multiplets observed for baryonic resonance states.

The $SU(6)$ multiplets are best characterized by giving symmetry of the representation with respect to permutations of the labels of the three quarks. The 56 representation has complete symmetry (S), the 70 representation has mixed symmetry (M), and the 20 representation is antisymmetric (A). Taking together the $SU(6)$ wave function and the internal space wave function, the excited $SU(6) \times O(3)$ supermultiplets may be specified by the notation $(a, LP)N$, where a denotes the $SU(6)$ representation. It would must be 630 baryon resonance, if all revealed 70-multiplets and 56-multiplets were filled in (see Table 1.). In the PDG 2006 Baryon summary table [2] there are in general (N^* , Δ , Λ , Σ and others) 132 baryons.

3 About program of A and R parameters measurements.

The specific feature of measurements of the spin rotation parameters is such, that it is not necessary to make measurements in the full energy and angle ranges. It is enough to measure these parameters in some limited intervals of kinematical variables that can be determined beforehand on the base of existing PWAs in order to eliminate the problem of PWA ambiguities. It is enough to obtain new experimental data in the range of pion beam momentum and angles where the largest disagreement between predictions of the existing PWA's is observed;

After such measurements it will be possible to prove the choice of the transverse amplitude zero trajectory (solution branch);

The corresponding kinematical intervals can be determined by analyzing zero trajectories of πN transverse amplitudes obtained for four existing global PWAs: KA84 [4], CMB [5], VPI-GWU solutions FA02 [6] and SP06 [1]. Close inspection of the zero trajectories of the πN transverse amplitudes shows the

SU(6)LP	Resonance from KH78	Σ
(56, 0 ⁺)	P11(938), P33(1233)	2
(56, 2 ⁺)	P13(1710), F15(1684), P31(1888), P33(1868), F35(1905), F37(1913)	6
(56, 4 ⁺)	F17(2005), H19(2205), F35(-), F37(2425), H39(2217), H3,11(2416)	6
(70, 1 ⁻)	S11(1526), D13(1519), S11(1670), D13(1731), D15(1679), S31(1610), D33(1680)	7
(70, 3 ⁻)	D15(-), G17(2140), D13(2081), D15(2228), G17(-), G19(2268), D35(2305), G37(2215)	8
(70, 5 ⁻)	G19(-), I 1,11(-), G17(-), G19(2792), I1,11(2577), I1,13(-), G39(2468), I3,11(-)	8
(70, 7 ⁻)	I1,13(-), L1,15(-), I1,11(-), I1,13(-), L1,15(-), L1,17(-), I3,13(2794), L3,15(-)	8
(70, 2 ⁺)	P13(-), F15(-), P11(1723), P13(-), F15(1882), F17(-), P33(-), F35(-)	8
(56, 6 ⁺)	H 1,11(-), K1,13(2612), H39(-), H3,11(-), K3,13(-), K3,15(2990)	6
(56, 1 ⁻)	S11(1880), D13(1920), S31(1908), D33(2070), D35(1901)	5
$\Sigma=630$	$\Sigma = 39$ (64)	$\Sigma=64$

Table 1: SU(6) \times O(3) classification of nucleon resonance by G.Hoeler et al. (from KH78).

N	P-region (MeV/c)	Θ -region c.m.s.(deg.)	$d\sigma/d\Omega$ (mb/sr)
1	700 - 900	90 - 110	0.03 - 0.18
2	800 - 1000	155 - 175	0.08 - 0.60
3	800 - 1200	80 - 100	0.13 - 0.27
4	1600 - 1900	50 - 70	0.08 - 0.30
5	1800 - 2100	130 - 150	0.03 - 0.13

Table 2: Elastic $\pi^+p\text{-}\pi^+p$ scattering (Regions with presumed existence of discrete ambiguities).

N	P-region (MeV/c)	Θ -region c.m.s.(deg.)	$d\sigma/d\Omega$ (mb/sr)
1	600 - 800	60 - 80	0.06 - 0.20
2	600 - 800	100 - 120	1.0 - 1.4
3	1200 - 1400	150 - 170	0.30 - 0.53
4	1200 - 1500	60 - 80	0.05 - 0.23
5	1200 - 1500	90 - 110	0.25 - 0.40
6	1800 - 2100	140 - 150	0.002 - 0.010
7	2000 - 2100	130 - 150	0.001 - 0.003

Table 3: Elastic $\pi^-p\text{-}\pi^-p$ scattering (Regions with presumed existence of discrete ambiguities).

unexplored regions of discrete ambiguities. They are collected in the tables 2 and 3.

Spin rotation parameters in elastic scattering are determined by the measurement of the polarization of recoiled protons produced by pions on a proton target polarized in the scattering plane [7], [8]. Polarization of the recoiled protons is measured through the measurement of the asymmetry of their secondary scattering on the carbon.

References

- [1] R.A. Arndt, *et al.*, nucl-th/0605082.
- [2] W.-M.Yao *et al.*, *Journ.Phys.* **G33**, 1(2006).
- [3] R.H.Dalitz *et al.*, *Proceedings of the Hadron Structure'77*

- [4] G. Hoehler *et al.*, *πN -Newsletters* **9**, 1(1993).
- [5] R.E. Cutcosky, *et al.*, *Phys.Rev.* **D20**, 2839(1979).
- [6] R.A. Arndt *et al.*, *Phys.Rev.* **C69**, 035213(2004).
- [7] I.V. Lopatin *et al.*, *Nucl.Phys.* **A567**, 882(1994).
- [8] I.G.Alekseev *et al.*, *Phys. Lett.* **B485**, 32(2000).

RHO-LIKE-MESON FAMILY IN THE PION-PION SCATTERING

Yu.S. Surovtsev^{*}, P. Bydžovský[#]

^{*}Joint Institute for Nuclear Research, Dubna 141 980, Russia

[#]Nuclear Physics Institute, 25068 Řež, Czech Republic

Abstract

Experimental data on the isovector P -wave of $\pi\pi$ scattering have been analyzed to study ρ -like mesons. The analysis, performed in the model-independent and Breit–Wigner approaches, indicates evidently a presence of three ρ -like mesons: $\rho(1250)$, $\rho(1450)$ and $\rho(1600)$ in the 1200-1800-MeV region. The obtained P -wave $\pi\pi$ scattering length agrees mostly with the result of the local Nambu–Jona-Lasinio model.

1 The model-independent analysis

Initially we outline the application of the model-independent approach (MIA) [1] to studying the 2-channel $\pi\pi$ scattering. Let the $\pi\pi$ -scattering S -matrix be determined on the 4-sheeted Riemann surface with the right branch-points at $s = 4m_{\pi^0}^2$ and $(m_\omega + m_{\pi^0})^2$ and with the left one at $s = 0$. The surface sheets are numbered according to the signs of analytic continuations of the channel momenta $k_1 = [s - 4m_{\pi^0}^2]^{1/2}/2$ and $k_2 = [s - (m_\omega + m_{\pi^0})^2]^{1/2}/2$ as follows: signs($\text{Im}k_1, \text{Im}k_2$) = ++, +-, --, and +- correspond to sheets I, II, III, and IV, respectively. An explicit allowance for the $(m_\omega + m_{\pi^0})^2$ branch point permit us to describe transitions between the $\pi\pi$ and $\omega\pi$ initial and final states using only the Jost matrix determinant $d(k_1, k_2)$ in the Le Couteur–Newton relations (CNR) [2]. The 2-channel resonances are represented by the three possible types of pole clusters (poles and zeros on the Riemann surface) [1] **(a)**, **(b)** and **(c)**: **(a)** the resonance is described by a pair of complex-conjugate poles in the S -matrix element on sheet II and by a pair of conjugate shifted poles on sheet III; **(b)** by a pair of conjugate poles on sheet IV and by a pair of conjugate shifted poles on sheet III; **(c)** by a pair of conjugate poles on sheet II and by other on sheet IV, and by two pairs of conjugate poles on sheet III. Due to unitarity, the zeros on sheets I, IV, and III are situated in the same energy points as the corresponding poles on sheets II, III, and IV, respectively.

The considered Riemann surface is mapped by the uniformizing variable $v = [(m_\omega + m_{\pi^0})k_1 + 2m_{\pi^0}k_2]/[s((m_\omega + m_{\pi^0})/2)^2 - m_{\pi^0}^2]^{1/2}$ onto the v -plane [3]. In the S -matrix, taken as $S = S_{res}S_{bg}$, the resonance part is $S_{res} = d(-v^{-1})/d(v)$, where $d = v^{-M} \prod_{n=1}^M (1 - v_n^*v)(1 + v_nv)$ with M the number of pairs of the conjugate resonance zeros. The background part is $S_{bg} = \exp[2i(2k_1/\sqrt{s})^3(\alpha_1 + \alpha_2\theta(s-s_1)(s-s_1)/s + \alpha_3\theta(s-s_2)(s-s_2)/s)]$ where $\alpha_i = a_i + ib_i$, and s_1 and s_2 are the thresholds of the 4π and $\rho 2\pi$ channels, respectively. Due to allowing for the left branch-point in the variable v , $a_1 = b_1 = 0$. From the experimental data $b_2 = 0$.

In our analysis of data [4, 5] for η and δ ($S(\pi\pi \rightarrow \pi\pi) = \eta \exp(2i\delta)$), different number of resonances was considered: three ($\rho(770)$, $\rho(1250-1580)$, and $\rho(1550-1780)$); four (the previous three and $\rho(1860-1910)$); and five (the previous four and $\rho(1450)$). Satisfactory description of data was obtained. The values of χ^2/NDF and the constant systematic error of δ in data [5] (see [3] for discussion) are, respectively, 1.72 and -1.885° for three, 1.68 and -1.897° for four, 1.65 and -1.876° for five resonances. The analyses prefer the case in which $\rho(770)$ is described by the cluster of type **(a)** and the others by type **(b)**. The cluster poles for the 5-resonance description, located on the lower \sqrt{s} -half-plane, are (in MeV) $765.8 - i73.3$ (sheet II) and $778.2 - i68.9$ (sheet III) for $\rho(770)$, $1250 - i131.4$ (sheet III) and $1249.4 - i130.7$ (sheet IV) for $\rho(1250)$, $1469.2 - i89.3$ (sheet III) and $1465.4 - i100.4$ (sheet IV) for $\rho(1450)$, $1634.8 - i145.9$ (sheet III) and $1593.4 - i72.9$ (sheet IV) for $\rho(1600)$, and $1883 - i106.5$ (sheet III) and $1893.4 - i87.6$ (sheet IV) for $\rho(1900)$. The background parameters are: $a_2 = 0.0248$, $a_3 = 0.0841$ and $b_3 = 0.0019$. The pole clusters and background parameters for the 3- and 4-resonance descriptions are given in [3]. Though the description is practically the same in all three cases, careful consideration of the obtained parameters and energy dependence of the fitted quantities suggests that $\rho(1900)$ is strongly desired and that $\rho(1450)$ should be also present improving slightly the description.

Masses and total widths, calculated from the poles on sheet II for the type-**(a)** resonances and on sheet IV for the type-**(b)** ones, using the resonance part of the amplitude in the form $T^{res} = \sqrt{s} \Gamma_{el}/(m_{res}^2 - s - i\sqrt{s} \Gamma_{tot})$, are, respectively (in MeV): 769.3 and 146.6 for $\rho(770)$, 1256.2 and 261.4 for $\rho(1250)$, 1468.8 and 200.8 for $\rho(1450)$, 1595.1 and 145.8 for $\rho(1600)$, and 1895.4 and 175.2 for $\rho(1900)$.

2 The Breit–Wigner analysis

. It was shown in [6], that the ρ -like resonances possess also other important decay channels in addition to those considered above. The $\rho(1450)$ and/or a possible $\rho(1250)$ can decay also to $\eta\rho^0$, 4π and $\phi\pi$. The $\rho(1700)$ has a large branching to the 4π , $\rho 2\pi$ and $\eta\rho^0$ channels. To obtain information about couplings with some selected channels from analysis of the $\pi\pi$ -scattering data, we used the 5-channel Breit–Wigner (BW) forms in constructing the $d(k_1, \dots, k_5)$ -function in CNR: $S_{res} = d(-k_1, \dots, k_5)/d(k_1, \dots, k_5)$, where k_1, k_2, k_3, k_4 and k_5 are the $\pi\pi^-$, $\pi^+\pi^-2\pi^0$ -, $2(\pi^+\pi^-)$ -, $\eta 2\pi^-$ and $\omega\pi^0$ -channel momenta, respectively. The d -function is $d = d_{res}d_{bg}$ with $d_{res}(s) = \prod_r [M_r^2 - s - i \sum_{j=1}^5 \rho_{rj}^3 R_{rj} f_{rj}^2]$, where $\rho_{rj} = k_i(s)/k_i(M_r^2)$, f_{rj}^2/M_r is the partial width of resonance, $R_{rj}(s, s_j, r_{rj}, M_r)$ is a Blatt–Weisskopf barrier factor [7] with s_j the j -channel threshold and radii $r_{rj} = 0.7035$ fm for all resonances in all channels. We have assumed that $f_{r2} = f_{r3}/\sqrt{2}$. The background part $d_{bg} = \exp[-i(2k_1/\sqrt{s})^3(\alpha_1 + \alpha_2\theta(s - s_1)(s - s_1)/s)]$, where $\alpha_i = a_i + ib_i$ ($b_1 = 0$) and s_1 is the $\rho 2\pi$ channel threshold.

The data were analyzed as in MIA considering three, four and five resonances. A reasonable description of all three cases was obtained: $\chi^2/\text{NDF} = 1.87$ for three, 1.92 for four and 1.91 for five resonances. The resonance parameters for the last case are shown in Table 1. The systematic error of data [5] is -1.987° . The background parameters are: $a_1 = -0.00121 \pm 0.0018$, $a_2 = -0.1005 \pm 0.011$, and $b_2 = 0.0012 \pm 0.006$.

Table 1: The ρ -like resonance parameters (in MeV).

State	$\rho(770)$	$\rho(1250)$	$\rho(1450)$	$\rho(1600)$	$\rho(1900)$
M	777.69 ± 0.32	1249.8 ± 15.6	1449.9 ± 12.2	1587.3 ± 4.5	1897.8 ± 38
f_{r1}	343.8 ± 0.73	87.7 ± 7.4	56.9 ± 5.4	248.2 ± 5.2	47.3 ± 12
f_{r2}	24.6 ± 5.8	186.3 ± 39.9	100.1 ± 18.7	240.2 ± 8.6	73.7
f_{r3}	34.8 ± 8.2	263.5 ± 56.5	141.6 ± 26.5	339.7 ± 12.5	104.3
f_{r4}		231.8 ± 111	141.2 ± 98	141.8 ± 33	9
f_{r5}		231 ± 115	150 ± 95	108.6 ± 40.4	10
Γ_{tot}	≈ 154.3	> 175	> 52	> 168	> 10

We have calculated also the isovector P -wave length of $\pi\pi$ scattering: $a_1^1 = 33.9 \pm 2.02[10^3 m_{\pi^+}^{-3}]$. It can be compared with values evaluated by using the local [8] (34) and non-local [9] (37) Nambu–Jona-Lasinio (NJL) model and Roy's equations: [10] (38.4 ± 0.8), [11] (37.9 ± 0.5), and [12] (39.6 ± 2.4).

3 Summary

The reasonable description of the accessible experimental data on the isovector P -wave of $\pi\pi$ scattering [4, 5] has been obtained up to 1.88 GeV in MIA ($\chi^2/\text{NDF} = 1.654$) and applying the BW forms ($\chi^2/\text{NDF} = 1.906$).

For $\rho(770)$, the mass is a little smaller in MIA (769.3 MeV) and a little bigger in the BW analysis (777.69 ± 0.32 MeV) than the averaged mass (775.5 ± 0.4 MeV) in the PDG tables [6]. The total width in MIA (146.6 MeV) coincides with the PDG one (146.4 ± 1.1 MeV) but the width in the BW analysis is a little bit larger (≈ 154.3 MeV).

The 2nd ρ -like meson has the mass 1256.2 MeV in MIA and 1249.8 ± 15.6 MeV in the BW analysis. This differs significantly from the PDG value (1459 ± 11 MeV) [6]. The $\rho(1250)$ meson was discussed some time ago and it was confirmed relatively recently in some analyses [13]. If $\rho(1250)$ is the 1st radial excitation of the 1^+1^{--} -state, then it lies down well on the corresponding linear trajectory on the (n, M^2) -plane [14] (n is the radial quantum number of the $q\bar{q}$ state).

It was shown [15] that the 1600-MeV region contains in fact two ρ -like mesons. Then there are three ρ -like mesons in the 1200-1800-MeV region, the 3rd meson having the mass about 1450 MeV. This does not contradict the data. In MIA, the description is even slightly improved if this state is included.

The 4th ρ -like meson turns out to have the mass 1590 MeV rather than 1720 MeV cited in the PDG tables, though in some analyses, the resonance with the mass near 1590 MeV was also found [6]. Note that a rather large coupling of these ρ -like mesons with the 4π channels was obtained.

In the case of $\rho(1900)$, there are practically no data in this energy region. Whereas MIA testifies in favor of existence of this state, the BW analysis gives equivalent results with and without the $\rho(1900)$.

The P -wave $\pi\pi$ -scattering length, $a_1^1 = 33.9 \pm 2.02[10^3 m_{\pi^+}^{-3}]$, obtained in the BW analysis, mostly matches the result of the local NJL model [8].

Yu.S. acknowledges support provided by the Votruba-Blokhintsev Program. P.B. thanks the Grant Agency of the Czech Republic, Grant No.202/05/2142.

References

- [1] D. Krupa *et al.*, *Nuovo Cim. A* **A109**, 281 (1996); Yu.S. Surovtsev *et al.*, *Eur.Phys.J.* **A15**, 409 (2002).
- [2] K.J. Le Couteur, *Proc.Roy.Soc.* **A256**, 115 (1960); R.G. Newton, *J.Math.Phys.* **2**, 188 (1961).
- [3] Yu.S. Surovtsev and P. Bydžovský, *E-Print Archive*: hep-ph/0701274.

- [4] S.D. Protopopescu *et al.*, *Phys.Rev.* **D7**, 1279 (1973); B. Hyams *et al.*, *Nucl.Phys.* **B64**, 134 (1973).
- [5] P. Estabrooks and A.D. Martin, *Nucl.Phys.* **B79**, 301 (1974).
- [6] W.-M. Yao *et al.*[PDG], *J.Phys.* **G33**, 1 (2006).
- [7] J. Blatt and V. Weisskopf, *Theoretical nuclear physics*, (Wiley, New York, 1952).
- [8] V. Bernard *et al.*, *Phys. Lett.* **B285**, 119 (1992).
- [9] A.A. Osipov *et al.*, *E-Print Archive*: hep-ph/0603130.
- [10] J.R. Peláez and F.J. Ynduráin, *Phys.Rev.* **D71**, 074016 (2005); I. Carpini *et al.*, *Phys.Rev.* **D68**, 074006 (2003); R. Kaminski *et al.*, *Phys.Rev.* **D74**, 014001 (2006).
- [11] I. Carpini *et al.*, *Int.J.Mod.Phys.* **A21**, 954 (2006).
- [12] R. Kamiński *et al.*, *Phys.Lett.* **B551**, 241 (2003).
- [13] N.M. Budnev *et al.*, *Phys.Lett.* **B70**, 365 (1977); S.B. Gerasimov and A.B. Govorkov, *Z.Phys.* **C13**, 43 (1982); D. Aston *et al.*[LASS Collab.], *Nucl.Phys.Proc.Suppl.* **B21**, 105 (1991); T.S. Belozeroва and V.K. Henner, *Phys.Elem.Part.Atom.Nucl.* **29**, part 1, 148 (1998).
- [14] A.V. Anisovich *et al.*, *Phys.Rev.* **D62**, 051502 (2000).
- [15] C. Erkal and M.G. Olsson, *Z.Phys.* **C31**, 615 (1986); A. Donnachie and H. Mirzaie, *Z.Phys.* **C33**, 407 (1987).

ON NATURE OF THE f_0 AND f_2 MESONS

Yu.S. Surovtsev*, R. Kamiński#

*Joint Institute for Nuclear Research, Dubna 141 980, Russia

#Institute of Nuclear Physics, Polish Academy of Sciences, Cracow, Poland

Abstract

In approach, based on analyticity and unitarity, experimental data on the isoscalar S - and D -waves of $\pi\pi \rightarrow \pi\pi, K\bar{K}, \eta\eta, \eta\eta'$ have been analyzed jointly for studying the f_0 - and f_2 -mesons. Assignment of scalar and tensor mesons to lower nonets is proposed. The $f_0(1500)$ and $f_2(2000)$ are interpreted as glueballs.

1 Analysis of the isoscalar-scalar sector

First we analyze the S -waves of $\pi\pi \rightarrow \pi\pi, K\bar{K}, \eta\eta, \eta\eta'$ by the uniformizing variable method [1] applicable only in the 2- and 3-channel cases. Therefore, we have carried out two variants of the 3-channel analysis: (I) the one of $\pi\pi \rightarrow \pi\pi, K\bar{K}, \eta\eta$, and (II) of $\pi\pi \rightarrow \pi\pi, K\bar{K}, \eta\eta'$.

The 3-channel S -matrix is determined on the 8-sheeted Riemann surface with the right cuts, starting with $4m_\pi^2$, $4m_K^2$, and $4m_\eta^2$ (or $(m_\eta + m_{\eta'})^2$), and the left cuts. In the elements $S_{\alpha\beta}$, $\alpha, \beta = 1(\pi\pi), 2(K\bar{K}), 3(\eta\eta \text{ or } \eta\eta')$. The surface sheets are numbered according to the signs of analytic continuations of $k_1 = (s/4 - m_\pi^2)^{1/2}$, $k_2 = (s/4 - m_K^2)^{1/2}$, $k_3 = (s/4 - m_\eta^2)^{1/2}$ (or $k'_3 = (s - (m_\eta + m_{\eta'})^2)^{1/2}/2$) as follows: signs $(\text{Im}k_1, \text{Im}k_2, \text{Im}k_3) = ++, +, -++ , --+, +-+, +--, ---, -+-, +- -$ correspond to sheets I, II, \dots , VIII, respectively. (All, related to variant II, is denoted by prime.) The 3-channel resonances are described by seven types of pole clusters (of poles and zeros on the Riemann surface) [1] according to seven possible cases when there are resonance zeros on sheet I only in (a) S_{11} , (b) S_{22} , (c) S_{33} , (d) S_{11} and S_{22} , (e) S_{22} and S_{33} , (f) S_{11} and S_{33} , and (g) S_{11} , S_{22} and S_{33} . The cluster kind is related to the nature of state.

We use the Le Couteur–Newton relations (CNR) [2] which express the S -matrix elements of all coupled processes in terms of the Jost matrix determinant $d(k_1, \dots, k_n)$ that is a real analytic function with the only branch-points at $k_i = 0$. The branch points are taken into account in an uniformizing

variable. Neglecting the $\pi\pi$ threshold, it is [1] $w = (k_2 + k_3)/[m_\eta^2 - m_K^2]^{1/2}$ for variant I, and $w' = (k'_2 + k'_3)/[(m_\eta + m_{\eta'})^2/4 - m_K^2]^{1/2}$ for variant II. CNR on the w -plane are given in Ref. [1]. In $d(w) = d_B d_{res}$ the resonance part is $d_{res} = w^{-\frac{M}{2}} \prod_{r=1}^M (w + w_r^*)$ with M the number of resonance zeros; the background part in variant I is $d_B = \exp[-i \sum_{n=1}^3 (k_n/m_n)(\alpha_n + i\beta_n)]$, where $\alpha_n = a_{n1} + a_{n\sigma} (s - s_\sigma)/s_\sigma \theta(s - s_\sigma) + a_{nv} (s - s_v)/s_v \theta(s - s_v)$ and $\beta_n = b_{n1} + b_{n\sigma} (s - s_\sigma)/s_\sigma \theta(s - s_\sigma) + b_{nv} (s - s_v)/s_v \theta(s - s_v)$ with s_σ the $\sigma\sigma$ threshold, s_v the combined threshold of the $\eta\eta'$ -, $\rho\rho$ -, $\omega\omega$ -channels.

In variant II, we add to α'_n and β'_n the terms $(s - 4m_\eta^2)/4m_\eta^2 a'_{n\eta} \theta(s - 4m_\eta^2)$ and $(s - 4m_\eta^2)/4m_\eta^2 b'_{n\eta} \theta(s - 4m_\eta^2)$, allowing for influence of the $\eta\eta$ -channel.

References to sources of data, in variant I, can be found in [1]. In variant II, the data on $\pi\pi \rightarrow \eta\eta'$ are taken from [3]. In variant I, the analysis prefers the case when the $f_0(600)$ is described by the (**a**) cluster with poles on the complex energy plane \sqrt{s} (in MeV) 683.5 – $i589$ on sheet II, 673.3 – $i589$ on sheet III, 593.5 – $i589$ on sheet VI, 603.7 – $i589$ on sheet VII; $f_0(1370)$ – (**c**) with poles 1398.3 – $i287.5$ on sheet V, 1398.3 – $i270.5$ on sheet VI, 1398.3 – $i154.9$ on sheet VII, 1398.3 – $i171.9$ on sheet VIII; $f_0(1500)$ – (**g**) with poles 1502.6 – $i357.1$ on sheet II, 1479.1 – $i140.2$ on sheet III, 1502.6 – $i238.7$ on sheet IV, 1497 – $i139.8$ on sheet V, 1497.5 – $i191.8$ on sheet VI, 1496.7 – $i87.35$ on sheet VII, 1502.6 – $i356.5$ on sheet VIII; $f_0(1710)$ – (**b**) with poles 1708.3 – $i142.3$ on sheet III, 1708.3 – $i160.3$ on sheet IV, 1708.3 – $i323.1$ on sheet V, 1708.3 – $i305.1$ on sheet VI; the $f_0(980)$ is represented only by poles 1013.4 – $i32.8$ on sheet II and 984.1 – $i57.5$ on sheet III. The poles on sheets IV, VI, VIII and V, related to the $f_0(1500)$, are of the 2nd and 3rd order, respectively. A satisfactory description is obtained: the total χ^2/NDF for all three processes is 1.36. The background parameters are: $a_{11} = 0.2006$, $a_{1\sigma} = 0.0141$, $a_{1v} = 0$, $b_{11} = 0$, $b_{1\sigma} = -0.01025$, $b_{1v} = 0.04898$, $a_{21} = -0.7039$, $a_{2\sigma} = -1.4213$, $a_{2v} = -5.951$, $b_{21} = 0.0447$, $b_{2\sigma} = 0$, $b_{2v} = 6.787$, $b_{31} = 0.6456$, $b_{3\sigma} = 0.3348$, $b_{3v} = 0$; $s_\sigma = 1.638 \text{ GeV}^2$, $s_v = 2.084 \text{ GeV}^2$.

In variant II, the $f_0(600)$ is described by the (**a'**) cluster with poles 655.94 – $i606$ on sheet II, 651.9 – $i606$ on sheet III, 594.46 – $i606$ on sheet VI, 598.5 – $i606$ on sheet VII; $f_0(1370)$ – (**b'**) with poles 1391.2 – $i246.3$ on sheet III, 1391.2 – $i263.7$ on sheet IV, 1411.2 – $i263.7$ on sheet V, 1411.2 – $i246.3$ on sheet VI; $f_0(1500)$ – (**d'**) with poles 1504.1 – $i198.7$ on sheet II, 1499 – $i239$ on sheet III, 1504.1 – $i193.3$ on sheet IV, 1504.1 – $i199$ on sheet V, 1493.8 – $i193.8$ on sheet VI, 1504.1 – $i193.3$ on sheet VII; $f_0(1710)$ – (**c'**) with poles 1721.2 – $i142.3$ on sheet V, 1721.2 – $i109.3$ on sheet VI, 1721.2 – $i82.3$ on sheet VII, 1721.2 – $i115.3$ on sheet VIII; the $f_0(980)$ is represented by poles 1012.8 – $i31.82$ on sheet II and 986.3 – $i57.7$ on sheet III. The poles on sheets

IV and V, related to the $f_0(1500)$, are of the 2nd order. The total χ^2/NDF is ≈ 1.18 . The background parameters are: $a'_{11} = 0.02411$, $a'_{1\eta} = -0.0638$, $a'_{1\sigma} = 0$, $a'_{1v} = 0.0916$, $b'_{11} = b'_{1\eta} = b'_{1\sigma} = 0$, $b'_{1v} = 0.0388$, $a'_{21} = -3.4384$, $a'_{2\eta} = -0.5377$, $a'_{2\sigma} = 1.695$, $a'_{2v} = -4.953$, $b'_{21} = 0.1193$, $b'_{2\eta} = -0.7953$, $b'_{2\sigma} = 2.5315$, $b'_{2v} = 2.925$, $b'_{31} = 0.6731$, $s_\sigma = 1.638 \text{ GeV}^2$, $s_v = 2.126 \text{ GeV}^2$.

These types of clusters and coupling constants from our 2-channel analysis [1], suggest that $f_0(1370)$ and $f_0(1710)$ have a dominant $s\bar{s}$ component; $f_0(1500)$, the dominant glueball one. The $f_0(980)$ is described by a pole on sheet II and shifted pole on sheet III under the $\eta\eta$ threshold without the corresponding poles on sheets VI and VII, as it was expected for standard clusters. This corresponds to the description of the $\eta\eta$ bound state [1].

Masses and total widths, calculated from the pole positions, are, respectively (in MeV): 869 and 1178 for $f_0(600)$, 1013.4 and 65.6 for $f_0(980)$, 1408.8 and 344 for $f_0(1370)$, 1544 and 713 for $f_0(1500)$, 1714.2 and 285 for $f_0(1710)$.

2 Analysis of the isoscalar-tensor sector

Analyzing data [4] on the isoscalar D-waves of $\pi\pi \rightarrow \pi\pi, K\bar{K}, \eta\eta$ with an allowance also for channel $(2\pi)(2\pi)$ ($i = 4$), we used the Breit–Wigner forms in CNR. In $d(k_1, k_2, k_3, k_4) = d_B d_{res}$, $d_{res}(s) = \prod_r [M_r^2 - s - i \sum_{j=1}^4 \rho_{rj}^5 R_{rj} f_{rj}^2]$ with $\rho_{rj} = 2k_j / (M_r^2 - 4m_j^2)^{1/2}$ and f_{rj}^2 / M_r the partial width. $R_{rj}(s, M_r, s_j, r_{rj})$ is a Blatt–Weisskopf barrier factor [5] with s_j the channel threshold, and with radii $r_{rj} = 0.943 \text{ fm}$ for all resonances in all channels, except for $f_2(1270)$ and $f_2(1960)$ for which they are: for $f_2(1270)$, 1.498, 0.708 and 0.606 fm respectively in channels $\pi\pi$, $K\bar{K}$ and $\eta\eta$, and for $f_2(1960)$, 0.296 fm in channel $K\bar{K}$. The background part is $d_B = \exp[-i \sum_{n=1}^3 (2k_n / \sqrt{s})^5 (a_n + ib_n)]$, where $a_1 = \alpha_{11} + (s - 4m_K^2)/s$, $\alpha_{12} \theta(s - 4m_K^2) + (s - s_v)/s$, $\alpha_{10} \theta(s - s_v)$ and $b_n = \beta_n + (s - s_v)/s$, $\gamma_n \theta(s - s_v)$ ($n = 1, 2, 3$) with $s_v \approx 2.274 \text{ GeV}^2$ the combined threshold of channels $\eta\eta'$, $\rho\rho$, $\omega\omega$.

We obtain a satisfactory description (the total $\chi^2/\text{NDF} \approx 1.56$) already with ten resonance $f_2(1270)$, $f_2(1430)$, $f_2'(1525)$, $f_2(1580)$, $f_2(1730)$, $f_2(1810)$, $f_2(1960)$, $f_2(2000)$, $f_2(2240)$ and $f_2(2410)$ [7]. Since the analysis of $p\bar{p} \rightarrow \pi\pi, \eta\eta, \eta\eta'$ [6] requires one more resonance ($f_2(2020)$), we have made also the analysis considering it. Description is the same one as in the previous case: the total $\chi^2/\text{NDF} \approx 1.58$. The resonance parameters are shown in Table 1. The background parameters are $\alpha_{11} = -0.0755$, $\alpha_{12} = 0.0225$, $\alpha_{10} = -0.2344$, $\beta_1 = -0.0782$, $\gamma_1 = -0.05215$, $\beta_2 = -0.985$, $\gamma_2 = 0.7494$, $\beta_3 = -0.5162$, $\gamma_3 = 0.786$.

Table 1: The f_2 -resonance parameters (in MeV).

State	M	f_{r1}	f_{r2}	f_{r3}	f_{r4}	Γ_{tot}
$f_2(1270)$	1276.3±1.8	468.9±5.5	201.6±11.6	89.9±4.79	7.2±4.6	≈210.5
$f_2(1430)$	1450.5±18.8	128.3±45.9	562.3±144	32.7±18.6	8.2±63	>230
$f_2'(1525)$	1534.7±8.6	28.5±8.5	253.9±79	89.5±12.5	51.6±155	>49.5
$f_2(1565)$	1601.5±27.9	75.5±19.6	315±50.6	388.9±28.6	127±190	>170
$f_2(1730)$	1719.8±6.2	78.8±43	289.5±62.6	460.3±545.	108.6±76.	>182.4
$f_2(1810)$	1760±17.6	129.5±14.8	259±32.	469.7±25.2	90.3±89.5	>177.6
$f_2(1960)$	1962.2±29.8	132.6±23.3	331±61.5	319±42.8	62.4±91.3	>118.6
$f_2(2000)$	2006±22.7	155.7±24.4	169.5±95.3	60.4±26.7	574.8±211	>193
$f_2(2020)$	2027±25.6	50.4±24.8	441±196.7	58±50.8	128±190	>107
$f_2(2240)$	2202±45.4	133.4±32.6	545±150.4	381±116	168.8±103	>222
$f_2(2410)$	2387±33.3	175±48.3	395±197.7	24.5±68.5	462.8±211	>168

3 Summary

A confirmation of the σ -meson with the mass 869 MeV is obtained in the model-independent analysis of data on $\pi\pi \rightarrow \pi\pi, K\bar{K}, \eta\eta, \eta\eta'$.

Indication for $f_0(980)$ to be the $\eta\eta$ bound state is obtained.

The $f_0(1370)$ and $f_0(1710)$ have the dominant $s\bar{s}$ component.

The $f_0(1500)$ is supposed to be practically the 8th component of octet mixed with a glueball being dominant in this state.

We propose a following assignment of scalar mesons to lower nonets, excluding $f_0(980)$ as the $\eta\eta$ bound state. The lowest nonet: $a_0(980)$, $K_0^*(900)$, and $f_0(600)$ and $f_0(1370)$. The Gell-Mann–Okubo (GM-O) formula $3m_{f_8}^2 = 4m_{K_0^*}^2 - m_{a_0}^2$ gives $m_{f_8} = 880$ MeV. Our result: $m_\sigma = 869 \pm 14$ MeV. In relation for masses of nonet $m_\sigma + m_{f_0(1370)} = 2m_{K_0^*}$, the left side is about 26 % bigger than the right one.

For the next nonet we find: $a_0(1450)$, $K_0^*(1450)$, and $f_0(1500)$ and $f_0(1710)$. From the GM-O formula, $m_{f_8} \approx 1450$ MeV. In formula $m_{f_0(1500)} + m_{f_0(1710)} = 2m_{K_0^*(1450)}$, the left side is about 12 % bigger than the right one.

This assignment moves a number of questions, stood earlier, and does not put the new ones.

In the tensor sector, we performed two analysis – without and with the $f_2(2020)$. We do not obtain $f_2(1640)$, $f_2(1910)$, $f_2(2150)$ and $f_2(2010)$, however, we see $f_2(1450)$ and $f_2(1730)$.

Usually one assigns to the ground tensor nonet the $f_2(1270)$ and $f_2'(1525)$. To the 2nd nonet, one could assign $f_2(1600)$ and $f_2(1767)$ though the isodoublet member yet is not discovered. If $a_2(1730)$ is the isovector of this octet and if $f_2(1601)$ is almost its 8th component, then, from the GM-O formula, we expect this isodoublet mass at about 1635 MeV. Then the relation for masses of nonet would be well fulfilled. In the experiment [8] one had observed the strange isodoublet with the mass 1629 ± 7 MeV. This state might be the tensor isodoublet of the 2nd nonet.

The $f_2(1963)$ and $f_2(2207)$ together with the $K_2^*(1980)$ could be put into the 3rd nonet. In the relation $M_{f_2(1963)} + M_{f_2(2207)} = 2M_{K_2^*(1980)}$, the left

side is only 5.3 % bigger than the right one. If $f_2(1963)$ is the 8th component of octet, then the GM-O formula $M_{a_2} = 4M_{K_2^*(1980)} - 3M_{f_2(1963)}$ gives $M_{a_2} = 2031$ MeV. This value coincides with the one (2030 MeV) for a_2 -meson obtained in the analysis [9].

As to $f_2(2000)$, in the analysis with ten resonances, the ratio of its $\pi\pi$ and $\eta\eta$ widths is in the limits obtained in Ref. [6] for the tensor glueball. However, its $K\bar{K}$ width is too large for the glueball. At practically the same description with the consideration of eleven resonances as in the case of ten, their parameters have varied not much, except for the ones of $f_2(2000)$ and $f_2(2410)$. The mass of the latter has decreased by about 40 MeV. As to $f_2(2000)$, now all the obtained ratios of the partial widths are in the limits corresponding to the glueball.

Yu.S. and R.K. acknowledge support provided by the Bogoliubov–Infeld Program.

References

- [1] D. Krupa *et al.*, *Nuovo Cim.* **A109**, 281 (1996); Yu.S. Surovtsev *et al.*, *Eur.Phys.J.* **A15**, 409 (2002); *Int.J.Mod.Phys.* **A20**, 561 (2005).
- [2] K.J. Le Couteur, *Proc.Roy.Soc.* **A256**, 115 (1960); R.G. Newton, *J.Math.Phys.* **2**, 188 (1961).
- [3] F. Binon *et al.*, *Nuovo Cim.* **A80**, 363 (1984).
- [4] B. Hyams *et al.*, *Nucl.Phys.* **B64**, 134 (1973); S.J. Lindenbaum and R.S. Longacre, *Phys.Lett.* **B274**, 492 (1992).
- [5] J. Blatt and V. Weisskopf, *Theoretical nuclear physics*, (Wiley, New York, 1952).
- [6] V.V. Anisovich *et al.*, *Int.J.Mod.Phys.* **A20**, 6327 (2005).
- [7] Yu.S. Surovtsev *et al.*, *E-Print Archive*: hep-ph/0606252.
- [8] V.M. Karnaukhov *et al.*, *Yad.Fiz.* **63**, 652 (2000).
- [9] A.V. Anisovich *et al.*, *Phys.Lett.* **B517**, 261 (2001).

RESONANCE POLE BY SPEED PLOT AND TIME DELAY

N. Suzuki^{a,1}, T. Sato^a, T.-S. H. Lee^b

^aDepartment of Physics, Osaka University, Toyonaka, Osaka 560-0043,
Japan

^bPhysics Division, Argonne National Laboratory, Argonne, IL 60439, USA

Abstract

The speed plot and the time delay methods are examined using a two-channel Breit-Wigner formula. We show that the pole of the S-matrix given by using Speed plot is on the nearest unphysical Riemann sheet, while the pole given by the time delay is on the 2nd or 4th Riemann sheet. The validity of those methods is also discussed.

1 Introduction

It is an important issue how to determine the mass and the width of the nucleon resonance from the meson-baryon scattering amplitudes. The 'Speed plot' (SP) proposed by Höhler [1] and time delay methods using 'time delay' (TD) introduced by Eisenbud and Wigner [2] are frequently used to find poles of the S-matrix from the empirical partial wave amplitudes. The time delay method of Ref. [3] is not the 'eigen phase' of the coupled channel S-matrix as pointed out in Ref. [4]. Unfortunately, only the amplitude of the elastic scattering is empirically determined in most of the case and the S-matrix elements of the other open channels are not available. There can be poles on various Riemann sheets associated with a resonance when several reaction channels are open. It is interesting to study a possibility to probe poles on the various Riemann sheets. In this work, we examine the speed plot and the time delay methods using simple two-channel Breit-Wigner amplitudes to clarify the nature of the resonance information provided from those methods and the validity of those methods. We applied those methods to the πN scattering amplitudes of SAID [5].

¹E-mail address: suzuki@kern.phys.sci.osaka-u.ac.jp

2 Speed plot and time delay

The time delay associated to the scattering process has been introduced by Eisenbud and Wigner [2] by using wave-packet analysis. For the coupled-channels case, the time delay is related to the following complex number

$$\Delta t_{ij} = -i \frac{1}{S_{ij}} \frac{dS_{ij}}{dE}, \quad (1)$$

where S_{ij} is the S-matrix element for channels i, j and E is the scattering energy. Taking the real part of Δt_{ii} for elastic scattering, the time delay (TD) is defined in Ref. [3] as the energy derivative of the phase shift δ

$$TD = \text{Re}(\Delta t_{ii}) = 2 \frac{d\delta}{dE}, \quad (2)$$

where we parametrized the S-matrix using phase shift δ and inelasticity η as $S = \eta e^{2i\delta}$. In the time delay method, the resonance position is extracted from the stationary point of the time delay TD . The speed (SP) is defined from the energy derivative of the T-matrix as

$$SP = \left| \frac{dT_{ii}}{dW} \right| = \frac{1}{2} \left| \frac{dS_{ii}}{dW} \right| = \left| \eta \frac{d\delta}{dW} + \frac{1}{2i} \frac{d\eta}{dW} \right|, \quad (3)$$

where $T_{ii} = (S_{ii} - 1)/2i$. The resonance position is determined at the maximum of the speed SP . From Eqs. (2) and (3), the speed plot and the time delay method may give different resonance energy when the inelastic reaction takes place.

To understand the meaning of this difference, we studied the two-channel Breit-Wigner formula

$$T_{11} = \frac{-\gamma_1 p_1}{E - M + i\gamma_1 p_1 + i\gamma_2 p_2}. \quad (4)$$

Here p_1, p_2 are the on-shell momenta defined by $E = p_1^2/2\mu_1 = p_2^2/2\mu_2 + \Delta$. γ_1, γ_2 are constants related to the partial width. Here we take a simple example with $\Delta = 0$, $\mu_1 = \mu_2 = \mu$.

The analytic structure of the two particles scattering in two channels can be studied in four Riemann sheets. The 1st, 2nd, 3rd and 4th sheets correspond to [tt], [bt], [bb] and [tb] sheets, respectively. Here [t] and [b] represents top (physical) and bottom (unphysical) sheets for each channel. For the two-channel resonance, two poles can exist on the different Riemann sheets at the same time. One is a resonance pole on the 3rd sheet and the other one is a shadow pole [6] on the 2nd or 4th sheet.

The explicit expression of the poles of the two-channel Breit-Wigner formula can be obtained as follows. The pole on the 3rd sheet is given as

$$E = M - \mu\Gamma^2 - i\sqrt{\mu\Gamma^2(2M - \mu\Gamma^2)} \quad (5)$$

with $\Gamma = \gamma_1 + \gamma_2$. We can also find the 'shadow pole' on the 2nd or the 4th Riemann sheet depending on the sign of $\gamma = \gamma_1 - \gamma_2$ as

$$E = M - \mu\gamma^2 - i\sqrt{\mu\gamma^2(2M - \mu\gamma^2)}. \quad (6)$$

Now we can apply the speed plot and time delay methods to the above two-channel Breit-Wigner formula. The speed plot method gives the following resonance pole

$$E_{SP} = M - (\mu\Gamma^2 + i\sqrt{\mu\Gamma^2(2M - \mu\Gamma^2)})(1 + O(\mu\Gamma^2/M)). \quad (7)$$

Therefore the speed plot gives the approximate resonance pole on the 3rd sheet. The same exercise for the time delay method gives

$$E_{TD} = M - \left(\frac{1}{1-x+x^2}\mu\gamma^2 + i\sqrt{\mu\gamma^2(2M - \mu\gamma^2)}\right)(1 + O(\mu\gamma^2/M)), \quad (8)$$

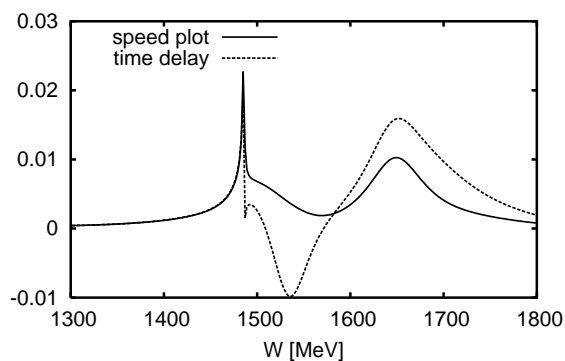
with $x = \gamma/\Gamma$. The time delay method gives the approximate pole position on the 2nd or 4th sheet.

3 Application for πN scattering amplitudes

We apply the speed plot and the time delay for the S_{11} πN amplitude of SAID analysis [5]. In PDG, two resonances $N^*(1535)$ and $N^*(1650)$ are listed and their mass and the width are given in Table 1. The results of the SP and TD are also shown in Table 1. We could not find a pole corresponding to $N^*(1535)$ from SP. This might be due to the fact that $N^*(1535)$ is too close to the ηN threshold. Therefore the condition discussed in the previous section is not satisfied. The TD has a minimum at $W = 1535\text{MeV}$, which suggests the pole is on the 4th sheet but not on the 2nd sheet. The pole of $N^*(1650)$ appears both in the SP and the TD. The SP gives a resonance pole on the 3rd sheet and TD gives a shadow pole probably on the 2nd sheet, which corresponds to the zero of the S-matrix on the physical sheet.

In summary, the SP and the TD are both approximate methods to probe the pole of the resonance. We find the speed plot gives the position of the resonance pole and time delay leads to the shadow pole/or zero of the S-matrix.

Partial wave	PDG	Speed plot	Time delay
S11(1535)	1490 to 1530 -i 45 to 125		1535 -i 33
S11(1650)	1640 to 1670 -i 75 to 90	1649 -i 65	1651 -i 51

Table 1: Pole given by the SP and the TD for the S_{11} πN partial wave.Figure 1: The SP and the TD for S_{11} partial wave of πN elastic scattering.

References

- [1] G. Höhler and A. Schulte, *πN Newsletter* **7**, 94 (1992).
- [2] L. Eisenbud, Ph. D. Dissertation, *unpublished* (Princeton, 1948); E. P. Wigner, *Phys. Rev.* **98**, 145 (1955)
- [3] N. G. Kelkar, *Jour. Phys.* **G29**, L1 (2003).
- [4] H. Haberzettl and R. Workman, arXiv:0708.3989 [nucl-th].
- [5] R. A. Arndt, I. I. Strakovsky, R. L. Workman, *Phys. Rev.* **C53**, 430 (1996); *Int. J. Mod. Phys.* **A18**, 449 (2003).
- [6] R. J. Eden and J. R. Taylor, *Phys. Rev.* **133**, B1575 (1964).

EXCLUSIVE PRODUCTION OF QUARKONIA IN pp AND $p\bar{p}$ COLLISIONS FAR FROM THE THRESHOLD

A. Szczurek
Institute of Nuclear Physics
PL-31-342 Kraków, ul. Radzikowskiego 152,
Rzeszów University, PL-35-959 Rzeszów, ul Rejtana 16A

Abstract

I discuss exclusive production of the η' , J/ψ , and $\chi_c(0^+)$ mesons in pp and $p\bar{p}$ collisions at high energies. QCD diffractive mechanisms as well as non-diffractive mechanisms are discussed. Different unintegrated gluon distribution functions (UGDF) are used. Some differential distributions are shown and discussed.

1 Introduction

The search for Higgs boson is the primary task for the LHC collider being now constructed at CERN. Although the predicted cross section is not small it may not be easy to discover Higgs in inclusive reaction due to large background in each of the final channel considered. An alternative way is to search for Higgs in exclusive or semi-exclusive reactions with large rapidity gaps. Kaidalov, Khoze, Martin and Ryskin proposed to calculate diffractive double elastic (both protons survive the collision) production of Higgs boson in terms of UGDFs [1]. Here I shall present some application of this formalism to the production of η' and $\chi_c(0^+)$ mesons. More details can be found in Refs. [2, 3].

At present, there is ongoing investigations at Tevatron aiming at measuring the exclusive production of both vector and scalar quarkonia, but no result is yet publicly available.

Recently the J/ψ exclusive production in proton-proton and proton-antiproton collisions was suggested as a candidate in searches for odderon exchange [4]. In order to identify the odderon exchange one has to consider all other possible processes leading to the same final channel. One of such processes, probably dominant, is pomeron-photon or photon-pomeron fusion [5].

2 Diffractive production of mesons

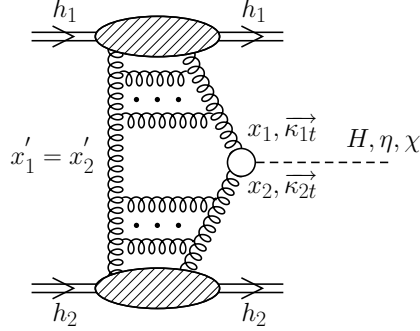


Figure 1: The sketch of the bare QCD mechanism. The kinematical variables are shown in addition.

Following the formalism for the diffractive double-elastic production of the Higgs boson one can write the amplitude from Fig.1 as

$$\mathcal{M}_{pp \rightarrow pMp}^{g^*g^* \rightarrow M} = i \pi^2 \int d^2 k_{0,t} V(k_1, k_2, P_M) \frac{f_{g,1}^{off}(x_1, x'_1, k_{0,t}^2, k_{1,t}^2, t_1) f_{g,2}^{off}(x_2, x'_2, k_{0,t}^2, k_{2,t}^2, t_2)}{k_{0,t}^2 k_{1,t}^2 k_{2,t}^2}, \quad (1)$$

where f 's are skewed unintegrated gluon distributions. For more details see [2].

As an example in Fig. 2 I show the results of calculations obtained for $M = \eta'$ with several models of UGDF (for details see [2]) for relatively low energy $W = 29.1$ GeV. For comparison I show also the contribution of the $\gamma^*\gamma^*$ fusion mechanism. The contribution of the last mechanism is much smaller than the contribution of the diffractive QCD mechanism.

In Fig.3 I show rapidity distribution of scalar $\chi_c(0^+)$ meson for different UGDFs. Similarly as for the η' production a strong dependence on UGDFs can be observed. ¹ A slightly less dependence on UGDFs can be expected for diffractive Higgs production.

3 Photoproduction of J/ψ

The basic mechanisms leading to the exclusive production of J/ψ are shown in Fig.4. The amplitude for the corresponding $2 \rightarrow 3$ process can be written

¹In Ref. [3] we discuss many more uncertainties in theoretical predictions of exclusive diffractive production.

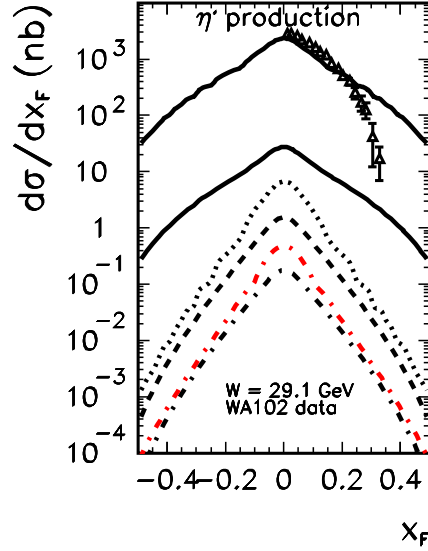


Figure 2: $d\sigma/dx_F$ as a function of Feynman x_F for $W = 29.1$ GeV and for different UGDFs. The $\gamma^*\gamma^*$ fusion contribution is shown by the dash-dotted (red) line (second from the bottom). The experimental data of the WA102 collaboration [6] are shown for comparison. The dashed line corresponds to the KL distribution, dotted line to the GBW distribution and the dash-dotted to the BFKL distribution. The two solid lines correspond to the Gaussian distribution with details explained in the original paper. No absorption corrections were included here.

as

$$\begin{aligned}
& \mathcal{M}_{h_1 h_2 \rightarrow h_1 h_2 V}^{\lambda_1 \lambda_2 \rightarrow \lambda'_1 \lambda'_2 \lambda_V}(s, s_1, s_2, t_1, t_2) \\
& \quad = \mathcal{M}_{\gamma IP} + \mathcal{M}_{IP\gamma} \\
& \quad = \langle p'_1, \lambda'_1 | J_\mu | p_1, \lambda_1 \rangle \epsilon_\mu^*(q_1, \lambda_V) \frac{\sqrt{4\pi\alpha_{em}}}{t_1} \mathcal{M}_{\gamma^* h_2 \rightarrow V h_2}^{\lambda_{\gamma^*} \lambda_2 \rightarrow \lambda_V \lambda_2}(s_2, t_2, Q_1^2) \\
& \quad \quad + \langle p'_2, \lambda'_2 | J_\mu | p_2, \lambda_2 \rangle \epsilon_\mu^*(q_2, \lambda_V) \frac{\sqrt{4\pi\alpha_{em}}}{t_2} \mathcal{M}_{\gamma^* h_1 \rightarrow V h_1}^{\lambda_{\gamma^*} \lambda_1 \rightarrow \lambda_V \lambda_1}(s_1, t_1, Q_2^2). \quad (2)
\end{aligned}$$

The amplitude of the $\gamma^* p \rightarrow J/\psi p$ was parametrized to describe data measured recently at HERA [7, 8].

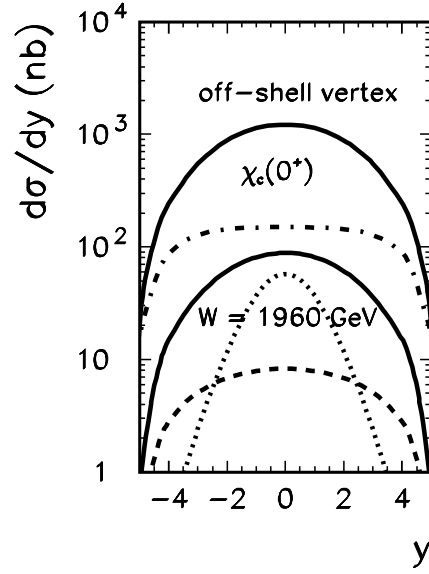


Figure 3: $d\sigma/dy$ as a function of rapidity for $W = 1960$ GeV and for different UGDs. The dashed line corresponds to the KL distribution, dotted line to the GBW distribution and the dash-dotted to the BFKL distribution. The two solid lines correspond to the KMR distributions with details explained in the original paper. No absorption corrections were included here.

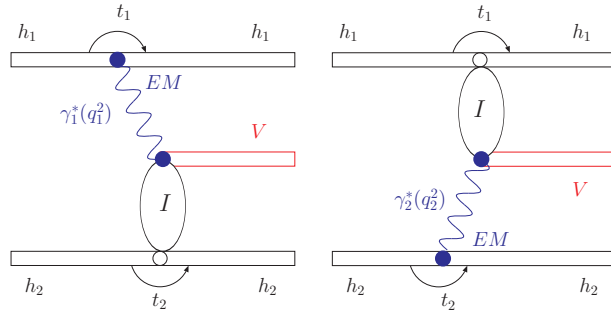


Figure 4: The sketch of the two mechanisms considered: photon-pomeron (left) and pomeron-photon (right). Some kinematical variables are shown in addition.

The differential cross section is calculated as

$$d\sigma = \frac{1}{512\pi^4 s^2} |\mathcal{M}|^2 dy dt_1 dt_2 d\phi, \quad (3)$$

where y is the rapidity of the vector meson, and ϕ is the angle between outgoing protons. Notice that the interference between the two mechanisms γIP and $IP\gamma$ is proportional to $e_1 e_2$ and introduces a charge asymmetry.

In Fig.5 I collect rapidity distributions for different energies relevant at RHIC, Tevatron and LHC. One observes an occurrence of a small dip in the distribution at midrapidity at LHC energy. One should remember, however, that the distribution for the LHC energy is long-distance extrapolation of the $\gamma^* p \rightarrow J/\psi p$ amplitude (or cross section) to unexplored yet experimentally energies. Therefore a real experiment at Tevatron and LHC would help to constrain cross sections for $\gamma p \rightarrow J/\psi p$ process.

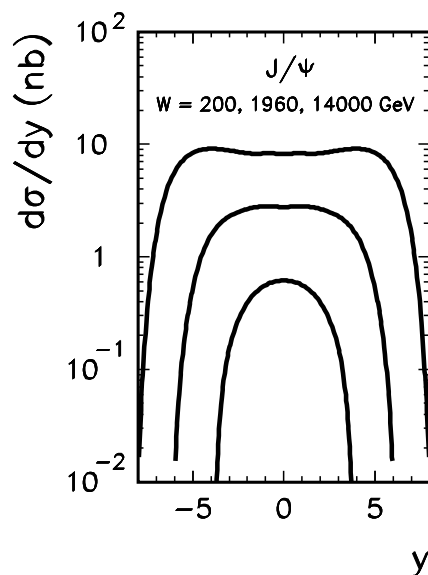


Figure 5: $d\sigma/dy$ for exclusive J/ψ production as a function of y for RHIC, Tevatron and LHC energies. No absorption corrections were included here.

The parametrization of the $\gamma^* p \rightarrow Vp$ amplitude which describes corresponding experimental data (see [5]) includes effectively absorption effects due to final state Vp interactions. In the $pp \rightarrow ppJ/\psi$ ($p\bar{p} \rightarrow p\bar{p}J/\psi$) reaction the situation is more complicated as here pp (or $p\bar{p}$) strong rescatterings occur in addition. In Ref. [5] we have included only elastic rescatterings shown schematically in Fig.6.

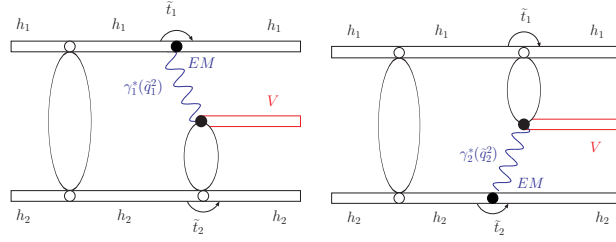


Figure 6: The sketch of the elastic rescattering amplitudes. Some kinematical variables are shown in addition.

4 Summary

In contrast to diffractive Higgs production, in the case of meson production the main contribution to the diffractive amplitude comes from the region of very small gluon transverse momenta and very small longitudinal momentum fractions. In this case application of Khoze-Martin-Ryskin UGDFs seems not justified and we have to rely on UGDFs constructed for this region.

The existing models of UGDFs predict cross section much smaller than the one obtained by the WA102 collaboration at the center-of-mass energy $W = 29.1$ GeV. This may signal presence of subleading reggeons at the energy of the WA102 experiment or suggest a modification of UGDFs in the nonperturbative region of very small transverse momenta.

The $\gamma^*\gamma^*$ fusion may be of some importance only at extremely small four-momentum transfers squared for the η' production and is practically negligible for the $\chi_c(0^+)$ production.

It was shown in [5] that at the Tevatron energy one can study the exclusive production of J/ψ at the photon-proton center-of-mass energies $70 \text{ GeV} < W_{\gamma p} < 1500 \text{ GeV}$, i.e. in the unmeasured region of energies, much larger than at HERA. At LHC this would be correspondingly $200 \text{ GeV} < W_{\gamma p} < 8000 \text{ GeV}$. At very forward/backward rapidities this is an order of magnitude more than possible with presently available machines.

An interesting azimuthal-angle correlation pattern has been obtained due to the interference of photon-pomeron and pomeron-photon helicity-preserving terms.

We have estimated also absorption effects. In some selected configurations the absorption effects may lead to the occurrence of diffractive minima. The exact occurrence of diffractive minima depends on the values of the model parameters. Such minima are washed out when integrated over the phase space or even its part.

5 Acknowledgements

I thank organizers of MENU2007 for very efficient organization of the conference and hospitality. The collaboration with Roman Pasechnik, Oleg Teryaev and Wolfgang Schäfer on the issues presented here is acknowledged. A partial support by the MEiN research grant 1 P03B 028 28 (2005-08).

References

- [1] V.A. Khoze, A.D. Martin and M.G. Ryskin, *Phys. Lett. B* **401**, 330 (1997);
V.A. Khoze, A.D. Martin and M.G. Ryskin, *Eur. Phys. J. C* **23**, 311 (2002);
A.B. Kaidalov, V.A. Khoze, A.D. Martin and M.G. Ryskin, *Eur. Phys. J. C* **31**, 387 (2003) [arXiv:hep-ph/0307064];
A.B. Kaidalov, V.A. Khoze, A.D. Martin and M.G. Ryskin, *Eur. Phys. J. C* **33**, 261 (2004);
V.A. Khoze, A.D. Martin, M.G. Ryskin and W.J. Stirling, *Eur. Phys. J. C* **35**, 211 (2004).
- [2] A. Szczurek, R. S. Pasechnik and O. V. Teryaev, *Phys. Rev. D* **75**, 054021 (2007) [arXiv:hep-ph/0608302].
- [3] R. S. Pasechnik, A. Szczurek and O. V. Teryaev, [arXiv:0709.0857].
- [4] A. Bzdak, L. Motyka, L. Szymanowski and J.-R. Cudell, arXiv: hep-ph/0702134.
- [5] W. Schäfer and A. Szczurek, arXiv:0705.2887, *Phys. Rev. D* **76**, 094014.
- [6] D. Barberis *et al.* (WA102 collaboration), *Phys. Lett.* **B422**, 399 (1998).
- [7] S. Chekanov *et al.* [ZEUS Collaboration], *Eur. Phys. J. C* **24**, 345 (2002).
- [8] A. Aktas *et al.* [H1 Collaboration], *Eur. Phys. J. C* **46**, 585 (2006).

THE RULE OF OAM AND POLARIZED VALON MODEL

F. Taghavi Shahri¹

Iran University Of Science and Technology- Tehran- Iran

F. Arash

Tafresh University-Tafresh-Iran

Abstract

In this paper, we study the rule of orbital angular momentum into the spin of proton with using the polarized Valon model. Each valence quark plus its associated sea quarks and gluons describe a valon in the dressing process of QCD. These valons have the quantum numbers of the valence quarks. In valon model we can write the Parton distributions into the hadron as a convolution of two parts: parton distribution in a valon, and valon distribution in hadron. To extract PPDFs in the proton, we have to know these function in each valon. So we need to solve the DGLAP equations into the valon. We use a simple approach to the polarized valon model and use certain criterion to initial input densities to solve the DGLAP equations in valon framework then calculate PPDFs into the proton. After calculating the first moment of each polarized parton distribution, we extract the rule of angular momentum into the valon and proton.

1 Polarized valon model

In the valon model, the structure of any hadron is obtained by convolution of two distribution: The valon distribution in the hadron and the structure function to each valon. Then polarized hadron structure in the valon model is:

$$g_1^p(x, Q^2) = \sum_v \int_x^1 \frac{dy}{y} \delta G_{v/p}(y) \mathcal{G}_1^v\left(\frac{x}{y}, Q^2\right), \quad (1)$$

Here, $\delta G_{v/p}(y)$, is the polarized valon distribution function. It refers to the probability of finding the ν valon to have momentum fraction y in the hadron

¹E-mail address: f-taghavi@iust.ac.ir

with spin aligned/ani-aligned to the spin of the proton. The polarized parton distribution function are given by:

$$\delta q_{\frac{i}{h}}(x, Q^2) = \sum_v \int_x^1 \frac{dy}{y} \delta G_{v/p}(y) \delta q_{\frac{i}{v}}\left(\frac{x}{y}, Q^2\right), \quad (2)$$

We can calculate polarized parton distribution functions from solving the DGLAP equations. At first, let us to introduce mellin transformation for function $f(x, Q^2)$ as:

$$\delta f^n(Q^2) = \int_0^1 x^{n-1} \delta f(x, Q^2) dx, \quad (3)$$

then the first moment of ppdf is :

$$\delta q^{n=1}(Q^2) \equiv \Delta q(Q^2) = \int_0^1 \delta q(x, Q^2) dx, \quad (4)$$

This quantity measures the spin contribution of parton q to the spin of proton. Now, DGLAP equations in n-moment space give us these two equations for extracting PPDFs : The non-singlet (NS) moments evolve according to:

$$\begin{aligned} & \delta q_{NS\pm}^n(Q^2) \\ = & \left(1 - \frac{\alpha_s(Q^2) - \alpha_s(Q_0^2)}{2\pi} \left(\frac{-2}{\beta_0}\right) (\delta P_{NS\pm}^{(1)n} - \frac{\beta_1}{\beta_0} \delta P_{qq}^{(0)n}) \right) L^{\left(\frac{-2}{\beta_0}\right) \delta P_{qq}^{(0)n}} \delta q_{NS\pm}^n(Q_0^2), \end{aligned} \quad (5)$$

and The evolution in the flavor singlet and the gluon sector of the moments are governed by a 2×2 splitting function matrix, with the following explicit solution:

$$\begin{aligned} & \begin{pmatrix} \delta \Sigma^n(Q^2) \\ \delta g^n(Q^2) \end{pmatrix} \\ = & \left(L^{\left(\frac{-2}{\beta_0}\right) \delta \hat{P}^{(0)n}} + \frac{\alpha_s(Q^2)}{2\pi} \hat{U} L^{\left(\frac{-2}{\beta_0}\right) \delta \hat{P}^{(0)n}} - \frac{\alpha_s(Q_0^2)}{2\pi} L^{\left(\frac{-2}{\beta_0}\right) \delta \hat{P}^{(0)n}} \hat{U} \right) \begin{pmatrix} \delta \Sigma^n(Q_0^2) \\ \delta g^n(Q_0^2) \end{pmatrix}, \end{aligned} \quad (6)$$

where $\delta g^n(Q^2)$ indicates the spin dependent quark-to-gluon evolution function. $\delta q_{NS\pm}^n$ correspond to the NS combinations: $\delta u - \delta \bar{u} \equiv \delta u_v$; $\delta d - \delta \bar{d} \equiv \delta d_v$ and $\delta \Sigma \equiv \sum (\delta q - \delta \bar{q})$. All the associated functions in the above equations have been defined in [1]. To solve the DGLAP equations, we have to know ppdfs at the initial input scale of Q_0^2 . It is assumed that the internal structure of the valon cannot be resolved at the initial scale of Q_0^2 and the proton behaves as a bound state of three constituents. It means the photon can only realize

the valence quark in the valon. So, in moment space, our initial input densities are: $\delta q_{NS}^n(Q_0^2) = \delta \Sigma^n(Q_0^2) = \int_0^1 z^{n-1} \delta(z-1) dx = 1$ and $\delta g^n(Q_0^2) = 0$ [2]. Our choice for Q_0^2 is $Q_0^2 = 0.283 \text{Gev}^2$ [3] and it can compare with the GRSV group choice: $Q_0^2 = 0.34 \text{Gev}^2$ [1]. Also, in this work, we turn out sea quark polarization. We work with perturbative QCD. In such processes with massless quarks, helicity is conserved and therefore the hard gluons cannot produce sea quark polarization perturbatively. This fact that sea quark polarization is consistent with zero, is in good agreement with HERMES data [4, 5].

2 Calculating the first moment of PPDFs in the Valon and proton

Now, we calculate the first moment of PPDFs in the valon using the DGLAP equations. They are related to the total z component of quark and gluon spins, thus:

$$\langle S_z \rangle_q = \frac{1}{2} \Delta \Sigma, \quad \langle S_z \rangle_g = \Delta g \quad (7)$$

We have this spin sum rule :

$$\frac{1}{2} = \frac{1}{2} \Delta \Sigma + \Delta g + L_z \quad (8)$$

where, L_z is the orbital angular momentum carried by the sea partons ($q - \bar{q}$ pairs and gluons) within the valon. The size of this orbital angular momentum turns out to be large and negative, mainly canceling out the gluon contribution. Ratcliffe [6] was the first to point out the necessity of including orbital angular momentum dependence of the evolution equation and predicted a negative value for $\langle L \rangle_z$ of the sea partons in the proton. In Fig.1 and Fig.2 the evolution of PPDFs and $\langle L \rangle_z$ in Valon and proton are plot (with using the polarized valon distributions [2] and using the evolution integrate in eq.2).

So, the role of Orbital angular momentum, L_z in a valon is to cancel out the gluon polarization completely, but this cancelation in proton is partial. Therefore, it is reasonable to speculate that about 60% of the spin of proton comes from gluon. It should be mentioned that the value of polarized gluon in our model is smaller than the value that the other theoretical models obtained [7–9]. Our value is $\Delta g(Q^2 = 3 \text{Gev}^2) = 0.47$ and it is close to recently COMPASS result: $\Delta g(Q^2 = 3 \text{Gev}^2) = 0.3$ [10].

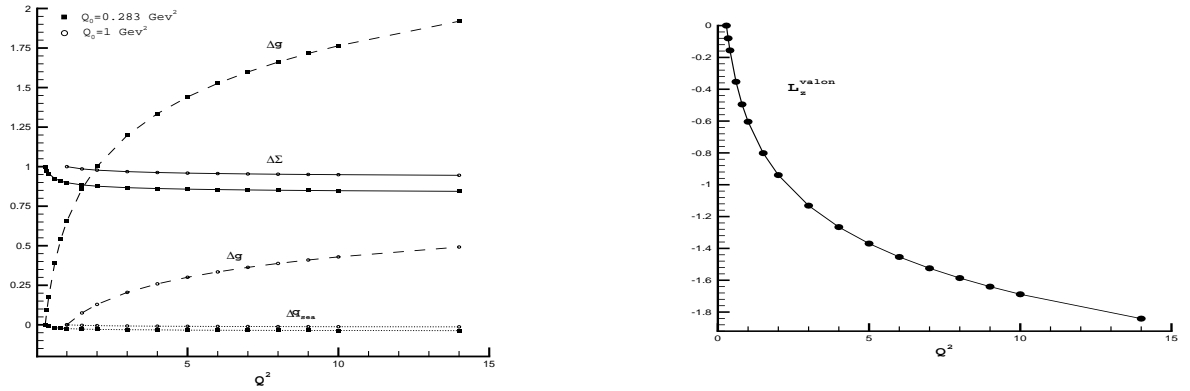


Figure 1: The evolution of PPDFs in the Valon .(Left) The evolution of L_z in the Valon($Q_0^2 = 0.283 \text{ GeV}^2$). (Right)

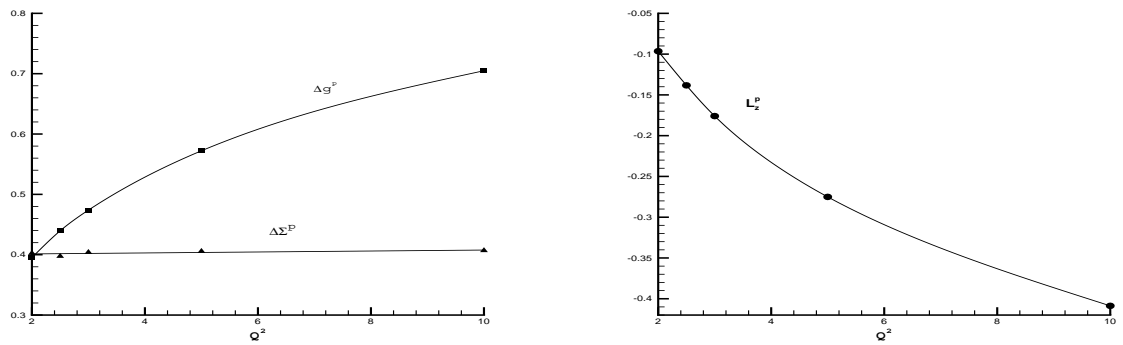


Figure 2: The evolution of PPDFs in the Proton (Left). The evolution of L_z in the Proton.(Right)

References

- [1] Bodo Lampe and Ewald reya, Phys. Rep. **332** (2000) 1.
- [2] F.Arash and F.Taghavi Shahri, JHEP. **07** (2007) 071.
- [3] F. Arash, A. N. Khorramian, Phys. Rev. C **67** (2003) 045201.
- [4] A. Airapetian,*et al.* (HERMES Coll.), Phys. Rev. Lett. **92**:012005, 2004.
- [5] A. Airapetian,*et al.* (HERMES Coll.), Phys. Rev. D**71**: 012003, 2005.
- [6] P.G. Ratcliffe, Phys. Lett. B **192** 1980.
- [7] J. Blumlein and H. Bottcher, Nucl. Phys. B **636**, (2002)225.
- [8] M.Gluck, E. Reya, M. Stratmann, and W. Vogelsang, Phys. Rev. D **63**, (2001) 094005.
- [9] Asymmetry Analysis Coll. (AAC), Y. Goto *et al.*, Phys. Rev. D **62**, (2000) 034017; *ibid* D **69**, (2004) 054021.
- [10] G. Brona *et al.* (COMPASS Coll.),hep-ex:0705.2372v1.

Q^2 -DEPENDENT OF PPDFS IN VALON MODEL

F. Taghavi Shahri¹

Iran University Of Science and Technology- Tehran- Iran

it F. Arash

Tafresh University-Tafresh-Iran

Abstract

In this paper, we want to calculate Q^2 -dependent of polarized parton distribution functions in the valon framework using the appropriate initial input densities to solve the DGLAP equations. A valon is characterized by its valence quark and its associated sea quarks and gluons. The structure of a valon arises from the perturbative dressing of the valence quark in QCD. We find Q^2 -dependent of these functions and reproduce PPDFS in the range of $1\text{GeV}^2 < Q^2 < 10^6\text{GeV}^2$. This procedure helps us to understand the validity of valon model for studying the hadron structure. It means we can use valon model as a valid model for calculating PPDFS as other theoretical models such as AAC, BB and GRSV. The results with using this model are in good agreement with the experimental data and other theoretical models.

1 Polarized valon model

In the valon model, the structure of any hadron is obtained by convolution of two distributions: The valon distribution in the hadron and the structure function to each valon. Then polarized hadron structure in the valon model is:

$$g_1^p(x, Q^2) = \sum_v \int_x^1 \frac{dy}{y} \delta G_{v/p}(y) \mathcal{G}_1^v\left(\frac{x}{y}, Q^2\right), \quad (1)$$

Here, $\delta G_{v/p}(y)$, is the polarized valon distribution function. It refers to the probability of finding the ν valon to have momentum fraction y in the hadron with spin aligned/anti-aligned to the spin of the proton. The polarized parton distribution functions are given by:

$$\delta q_{\frac{i}{h}}(x, Q^2) = \sum_v \int_x^1 \frac{dy}{y} \delta G_{v/p}(y) \delta q_{\frac{i}{v}}\left(\frac{x}{y}, Q^2\right), \quad (2)$$

¹E-mail address: f-taghavi@iust.ac.ir

We can calculate polarized parton distribution functions from solving the DGLAP equations. At first, let us introduce the Mellin transformation for the function $f(x, Q^2)$ as:

$$\delta f^n(Q^2) = \int_0^1 x^{n-1} \delta f(x, Q^2) dx. \quad (3)$$

Now, DGLAP equations in n -moment space give us these two equations for extracting PPDFs: The non-singlet (NS) moments evolve according to:

$$\delta q_{NS\pm}^n(Q^2) = \left(1 - \frac{\alpha_s(Q^2) - \alpha_s(Q_0^2)}{2\pi} \left(\frac{-2}{\beta_0} \right) (\delta P_{NS\pm}^{(1)n} - \frac{\beta_1}{\beta_0} \delta P_{qq}^{(0)n}) \right) L^{(\frac{-2}{\beta_0})\delta P_{qq}^{(0)n}} \delta q_{NS\pm}^n(Q_0^2), \quad (4)$$

and the evolution in the flavor singlet and the gluon sector of the moments are governed by a 2×2 splitting function matrix, with the following explicit solution:

$$\begin{pmatrix} \delta \Sigma^n(Q^2) \\ \delta g^n(Q^2) \end{pmatrix} = \begin{pmatrix} L^{(\frac{-2}{\beta_0})\delta \hat{P}^{(0)n}} + \frac{\alpha_s(Q^2)}{2\pi} \hat{U} L^{(\frac{-2}{\beta_0})\delta \hat{P}^{(0)n}} - \frac{\alpha_s(Q_0^2)}{2\pi} L^{(\frac{-2}{\beta_0})\delta \hat{P}^{(0)n}} \hat{U} \end{pmatrix} \begin{pmatrix} \delta \Sigma^n(Q_0^2) \\ \delta g^n(Q_0^2) \end{pmatrix}, \quad (5)$$

where $\delta g^n(Q^2)$ indicates the spin dependent quark-to-gluon evolution function. $\delta q_{NS\pm}^n$ correspond to the NS combinations: $\delta u - \delta \bar{u} \equiv \delta u_v$; $\delta d - \delta \bar{d} \equiv \delta d_v$ and $\delta \Sigma \equiv \sum(\delta q - \delta \bar{q})$. All the associated functions in the above equations have been defined in [1]. To solve the DGLAP equations, we have to know ppdfs at the initial input scale of Q_0^2 . In this work, we turn out sea quark polarization. We work with perturbative QCD. In such processes with massless quarks, helicity is conserved and therefore the hard gluons cannot produce sea quark polarization perturbatively. This fact that sea quark polarization is consistent with zero, is in good agreement with HERMES data [2, 3].

1.1 Determination of the initial input densities in valon model to solve the DGLAP equations

Valon is a cluster of valence quark and its associated sea quarks and gluons. It is assumed that the internal structure of the valon cannot be resolved at the initial scale of Q_0^2 and the proton behaves as a bound state of three constituents. It means the photon can only realize the valence quark in the valon. As Q^2 increases, other partonic components in the valon can be resolved then $\delta q_{NS}(z = \frac{x}{y}, Q_0^2) = \delta \Sigma(z = \frac{x}{y}, Q_0^2) = \delta(z - 1)$. We absolutely can find only a valence quark at $Q^2 = Q_0^2$ and no other things. So, in moment space, we obtain $\delta q_{NS}^n(Q_0^2) = \delta \Sigma^n(Q_0^2) = \int_0^1 z^{n-1} \delta(z - 1) dx = 1$ and $\delta g^n(Q_0^2) = 0$ [4], because there is no gluon at $Q^2 = Q_0^2$. Our choice for Q_0^2 is $Q_0^2 = 0.283 \text{ GeV}^2$ [5] and it can compare with the GRSV group choice: $Q_0^2 = 0.34 \text{ GeV}^2$ [1].

1.2 Calculating the valon distribution function

we choose a general form for polarized valon distribution function as:

$$\delta G^\nu(y) = \delta f^\nu(y)G^\nu(y) \quad (6)$$

Where ν refers to U and D valons and $G^\nu(y)$ is the unpolarized valon distribution function for each valon [6,7]. $\delta f^\nu(y)$ is a function with free parameters that should be determined for U and D valons:

$$\delta f^\nu(y) = ay^b(1-y)^c(1+dy^{0.5}+ey+fy^{1.5}+gy^2) \quad (7)$$

We extract the free parameters a,b,...through fitting the valence distribution in our model with the valence distribution of GRSV at the same Q^2 .

ν	a_ν	b_ν	c_ν	d_ν	e_ν	f_ν	g_ν
U	3.4443	0.33905	3.5814	-2.476	5.0713	-1.8598	2.7805
D	-0.5680	-0.3740	4.1419	-2.844	11.695	-10.096	14.469

Table I. Numerical values of fitting parameters in Eq.(7).

2 Q^2 -dependent of PPDFs

Q^2 -dependent of spin densities in valon model calculated and are given by the following functions as a function of $t = Ln[Q^2]$. These partonic evolution functions give PPDFs in the range of $1Gev^2 < Q^2 < 10^6Gev^2$.

As mentioned before each type of PPDFs can parameterized as :

$$x\delta q(x, Q^2) = a(Q^2)x^{b(Q^2)}(1-x)^{c(Q^2)}(1+d(Q^2)x+e(Q^2)x^{0.5}+f(Q^2)x^2) \quad (8)$$

where q refers to polarized valence distributions for u and d type of partons and polarized gluon distribution in the proton. We calculated the evolution of each parameter in the above equation and show that with using these evolution functions we can calculate PPDFs in the range of $1Gev^2 < Q^2 < 10^6Gev^2$ very good.

3 Results

In this part we show the results of PPDFs and proton structure functions with using the evolution functions. We compare our results with other theoretical models [8–10] and they are in good agreement with them.

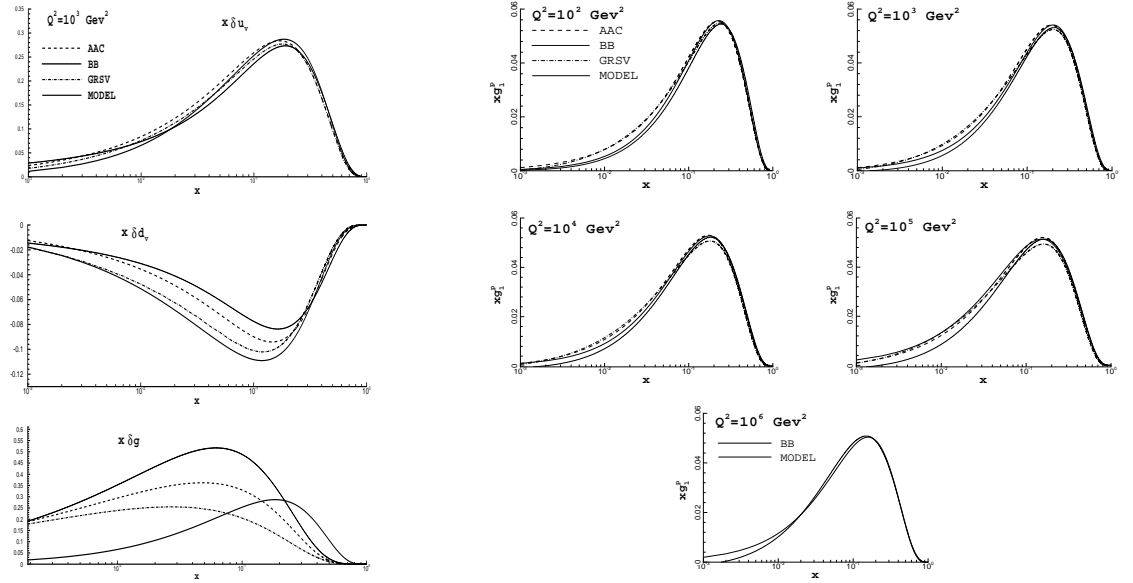


Figure 1: PPDFs for $Q^2 = 10^3 \text{ GeV}^2$ (Left) .Proton structure function for some Q^2 s .(Right)

References

- [1] Bodo Lampe and Ewald Reya, Phys. Rep. **332** (2000) 1.
- [2] A. Airapetian, *et al.* (HERMES Coll.), Phys. Rev. Lett. **92**:012005, 2004.
- [3] A. Airapetian, *et al.* (HERMES Coll.), Phys. Rev. D **71**: 012003, 2005.
- [4] F.Arash and F.Taghavi Shahri, JHEP. **07** (2007) 071.
- [5] F. Arash, A. N. Khorramian, Phys. Rev. C **67** (2003) 045201.
- [6] R. C. Hwa and M. S. Zahir, Phys. Rev. D **23**, (1981) 2539.
- [7] R. C. Hwa and C. B. Yang, Phys. Rev. C **66** (2002) 025204; R. C. Hwa and C. B. Yang, Phys. Rev. C **66** (2002) 025205.
- [8] J. Blumlein and H. Bottcher, Nucl. Phys. B **636**, (2002)225.
- [9] M.Gluck, E. Reya, M. Stratmann, and W. Vogelsang, Phys. Rev. D **63**, (2001) 094005.
- [10] Asymmetry Analysis Coll. (AAC), Y. Goto *et al.*, Phys. Rev. D **62**, (2000) 034017; *ibid* D **69**, (2004) 054021.

LATTICE QCD STUDY OF $g_A^{N^*N^*}$ WITH TWO FLAVORS OF DYNAMICAL QUARKS

T. T. Takahashi and T. Kunihiro
Yukawa Institute for Theoretical Physics
Kyoto University
Kitashirakawa-Oiwakecho, Sakyo, Kyoto 606-8502, Japan

Abstract

We report the first lattice QCD result of the axial charge of N(1535), $g_A^{N^*N^*}$. The measurement is performed with two flavors of dynamical quarks employing the renormalization-group improved gauge action at $\beta=1.95$ and the mean-field improved clover quark action with the hopping parameters, $\kappa=0.1375, 0.1390$ and 0.1400 . In order to avoid the signal contaminations by N(1650) lying just 100 MeV above N(1535), we construct 2×2 correlation matrices and diagonalize them so that clear signal separation can be found. The wraparound contributions in the correlator, which can be another source of signal contamination, are eliminated by imposing the Dirichlet boundary condition in the temporal direction. We find that the axial charge of N(1535) takes small values as $g_A^{N^*N^*} \sim 0.2$, independent of quark masses, in the pion-mass range of 0.7 to 1.1 GeV.

1 Introduction

Chiral symmetry is an approximate global symmetry in Quantum Chromodynamics (QCD), and the symmetry and its spontaneous breaking is one of the key ingredients in the low-energy hadron physics. For instance, all the hadrons can be classified into representations of $SU(N_f)_L \times SU(N_f)_R$. Once we fix the representations, it gives strong constraints to low-energy effective lagrangians and possible terms are uniquely determined besides overall constants. To embody chiral symmetry in effective lagrangians, we have two famous ways; the linear and the non-linear representations. The non-linear representation has been well studied and successful especially in the context of the chiral perturbation theory. The linear representation with scalar

mesons as chiral partners of Nambu-Goldstone bosons would be important around the chiral restoration point at high temperature/density.

As for the realization of chiral representations in the baryon sector in the linear representation, there could be naively two ways [1,2]. One is the naive assignment and the other is the so-called mirror assignment introduced by DeTar and Kunihiro [1]. We can find several important differences between these two assignments in the couplings or in the nucleon masses. For example, the nucleon and its parity partner belong to the same chiral multiplet and there can exist chirally-invariant mass terms of nucleons in the mirror assignment [1]. Due to the mass terms, nucleons can be massive even when the chiral condensate takes a small value or zero, whereas nucleon masses are simply proportional to the chiral condensate in the naive assignment [1, 2], which would be the most important difference between the naive and mirror cases. Such differences play crucial roles at finite temperature/density systems and it should be revealed directly from QCD. In order to clarify which assignment is natural, it would be advantageous to measure the axial charge of N(1535), which we assume as the chiral partner of N(940), because the axial charges of N(940) and N(1535) are sensitive to the chiral structure of baryons [1, 2] and have the same (different) signs in the naive (mirror) assignments.

In this report, we show the first unquenched lattice QCD study of $g_A^{N^*N^*}$ as well as g_A^{NN} . (For the details, see [3].) We employ $16^3 \times 32$ lattice with two flavors of dynamical quarks, generated [4] with the renormalization-group improved gauge action at $\beta = 1.95$ and the mean field improved clover quark action with the clover coefficient $c_{\text{SW}} = 1.530$. The calculations are done with the hopping parameters, $\kappa_{\text{sea}}, \kappa_{\text{val}} = 0.1375, 0.1390$ and 0.1400 .

2 Lattice QCD formulations and results

N(1535) is the ground-state nucleon in $\frac{1}{2}^-$ channel. Though a ground state signal can be in principle isolated using a large Euclidean time separation between the source and the sink points in correlators, we could suffer from the signal contamination by N(1650) lying just 100 MeV above. With the aim to separate the signals in a proper way and to optimize operators, we diagonalize correlation matrices constructed with two independent operators; $N_1(x) \equiv \varepsilon_{abc} u^a(x)(u^b(x)C\gamma_5 d^c(x))$, $N_2(x) \equiv \varepsilon_{abc} \gamma_5 u^a(x)(u^b(x)Cd^c(x))$. Here, $u(x)$ and $d(x)$ are the Dirac spinors for u- and d- quarks, respectively, and a,b,c denote the color indices. We eliminate wraparound effects, which could be another possible sources of contamination, imposing the Dirichlet boundary condition in the temporal direction.

With the optimized operators $\mathcal{N}(x)$, we can obtain vector(axial) charges $g_V(g_A)$ as follows.

$$g_V \rightarrow \frac{\text{tr}\gamma_4\Gamma\langle\mathcal{N}(t_{\text{snk}})V_4(t)\overline{\mathcal{N}}(t_{\text{src}})\rangle}{\text{tr}\Gamma\langle\mathcal{N}(t_{\text{snk}})\overline{\mathcal{N}}(t_{\text{src}})\rangle} \quad (t_{\text{snk}} \gg t \gg t_{\text{src}}) \quad (1)$$

and

$$g_A \rightarrow \frac{\text{tr}\gamma_5\gamma_3\Gamma\langle\mathcal{N}(t_{\text{snk}})A_3(t)\overline{\mathcal{N}}(t_{\text{src}})\rangle}{\text{tr}\Gamma\langle\mathcal{N}(t_{\text{snk}})\overline{\mathcal{N}}(t_{\text{src}})\rangle} \quad (t_{\text{snk}} \gg t \gg t_{\text{src}}), \quad (2)$$

with $\Gamma \equiv \frac{1+\gamma_4}{2}$. Here, $A_\mu(t) \equiv \sum_{\mathbf{x}} \bar{u}(x)\gamma_\mu\gamma_5u(x) - \bar{d}(x)\gamma_\mu\gamma_5d(x)$ and $V_\mu(t) \equiv \sum_{\mathbf{x}} \bar{u}(x)\gamma_\mu u(x) - \bar{d}(x)\gamma_\mu d(x)$ are the zero-momentum projected axial and vector currents, and the traces are taken over spinor indices. All the unwanted quantities, such as the normalization factors, are all canceled out between the denominator and the numerator.

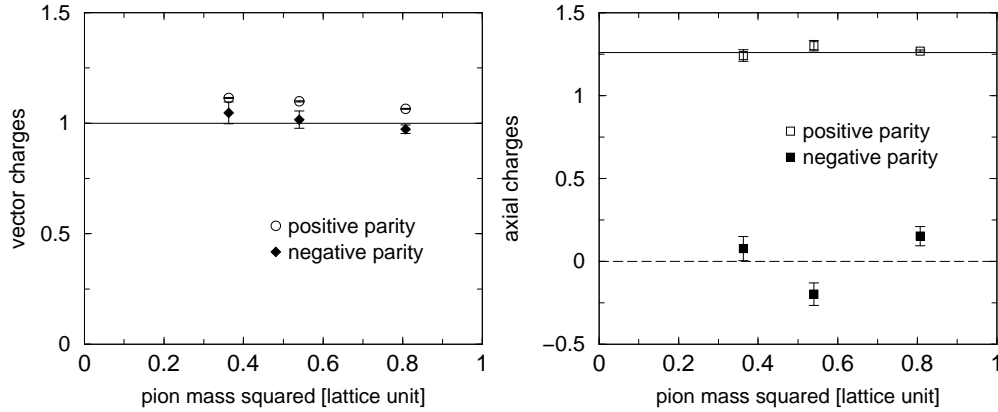


Figure 1: The renormalized vector and axial charges of the positive- and the negative-parity nucleons are plotted as the function of the squared pion mass m_π^2 . The left panel shows the results of the vector charges and the right panel the results of the axial charges. In the left panel, the solid line is drawn at $g_V = 1$ for reference. In the right panel, the solid line is drawn at $g_A = 1.26$ and the dashed line is drawn at $g_A = 0$.

The renormalization factors for bilinear operators are determined with the constants listed in Ref. [4]. We plot in the left panel in Fig. 1 the vector charges of the positive- and the negative-parity nucleons, which should be unity. The open (filled) symbols denote the vector charges of the positive- (negative-) parity nucleon at each hopping parameter. We can find about

10% deviations from unity, which can be considered to come from the systematic errors in the renormalization factors. We should then take into account at least 10% systematic errors in our results. The axial charges of the positive-parity nucleon at each hopping parameter are plotted in the right panel. They are shown as the open symbols. One can find the good agreement between the lattice data and 1.26, the experimental value.

We finally show the axial charges of the negative-parity nucleon in the right panel. One finds at a glance that they take quite small values, as $g_A^{N^*N^*} \sim 0.2$ and that even the sign is quark-mass dependent. While the wavy behavior might come from the sensitiveness of $g_A^{N^*N^*}$ to quark masses, this behavior may indicate that $g_A^{N^*N^*}$ is rather consistent with zero. The small $g_A^{N^*N^*}$ reflects the interesting chiral structure of baryons [1, 2, 5–7].

The present quark masses are unfortunately so heavy that their related pion masses are $700\text{MeV} \sim 1.1\text{GeV}$. In order to reveal the chiral structure, much lighter u,d quarks are indispensable. The study of the axial charge of Roper or N(1650) as well as the inclusion of strange sea quarks could also cast light on the low-energy chiral structure of baryons. They are left for further study.

Acknowledgments

All the numerical calculations were performed with NEC SX-8 at CMC, Osaka university and at YITP, Kyoto university. The unquenched gauge configurations employed in our analysis were all generated by CP-PACS collaboration [4].

References

- [1] C. DeTar and T. Kunihiro, Phys. Rev. D **39**, 2805 (1989).
- [2] D. Jido *et al.* Nucl. Phys. A **671**, 471 (2000)
- [3] T. T. Takahashi and T. Kunihiro, in preparation.
- [4] A. Ali Khan *et al.* [CP-PACS Collaboration], Phys. Rev. D **65**, 054505 (2002) [Erratum-ibid. D **67**, 059901 (2003)]
- [5] D. Jido, T. Hatsuda and T. Kunihiro, Phys. Rev. Lett. **84**, 3252 (2000)
- [6] R. L. Jaffe, D. Pirjol and A. Scardicchio, Phys. Rept. **435**, 157 (2006)
- [7] L. Y. Glozman, Phys. Rept. **444**, 1 (2007)

$\Lambda(1405)$ AS A RESONANCE IN THE BARYON-MESON SCATTERING COUPLED TO THE q^3 STATE IN A QUARK MODEL

Sachiko Takeuchi and Kiyotaka Shimizu^A
Japan College of Social Work,
Kiyose, Tokyo 204-8555, Japan
^ADepartment of Physics, Sophia University,
Chiyoda-ku, Tokyo 102-8554, Japan

Abstract

To describe $\Lambda(1405)$ as a resonance in the baryon-meson scattering by a quark model, we have investigated q^3 - $q\bar{q}$ scattering systems with the flavor-singlet q^3 $(0s)^2(0p)$ state, which is treated as a bound state embedded in the continuum. We found that the peak appears below the $N\bar{K}$ threshold in the spin $\frac{1}{2}$, isospin 0 channel with an appropriate width. We also compare the mechanism to form such a resonance with that of the chiral-unitary-type model.

1 Introduction

Constituent quark models are known to reproduce most of the observed low-energy features of baryons. The picture that the baryon mass comes mainly from the masses of the three constituent quarks, which interact with each other by exchanging gluons and/or Goldstone bosons, seems appropriate [1, 2]. There, however, are some exceptions. For example, such quark models cannot give the observed light mass of $\Lambda(1405)$ nor the large mass difference between $\Lambda(1405, \frac{1}{2}^-)$ and $\Lambda(1520, \frac{3}{2}^-)$. In the conventional constituent quark model, each of these baryons is treated as a system of three quarks in the flavor-singlet $(0s)^2(0p)$ state. Then, the hyperfine interaction only gives a part (~ 150 MeV) of the observed mass difference between the flavor-singlet and the flavor-octet spin- $\frac{1}{2}$ baryons, ~ 200 MeV. Moreover, in order to give the large mass difference between $\Lambda(1405)$ and $\Lambda(1520)$, one has to assume a strong spin-orbit force between quarks, which is absent in other negative-parity baryons.

$\Lambda(1405)$ is a meson-baryon resonance found in the $\Sigma\pi$ scattering state. To investigate this baryon as a negative-parity baryon embedded in the $\Sigma\pi$ continuum is most appropriate. In ref [3], the idea that $\Lambda(1405)$ can be a $N\bar{K}$ bound state has been presented. A more systematic treatment may be found in the chiral unitary approach [4].

In the present work [5], we perform the $\Sigma\pi$ - $N\bar{K}$ - $\Lambda\eta_{ud}$ coupled channel scattering calculation by the quark cluster model (QCM). Each baryon is treated as a $q^3(0s)^3$ state, and the meson is assumed to be a $q\bar{q}(0s)$ state. Moreover, we have introduced the conventional Λ^1 , the flavor-singlet $q^3(0s)^2 0p$ state, as a bound state embedded in the continuum (the Λ^1 pole).

2 Model

In QCM, the wave function of a baryon-meson system is written as a product of the single baryon and meson wave functions, ϕ_B and ϕ_M , and the relative wave function between these two clusters, $\chi(\mathbf{R}_{BM})$:

$$\Psi = \mathcal{A}_q[\phi_B \phi_M \chi(\mathbf{R}_{BM})]. \quad (1)$$

A baryon consists of three quarks and a meson consists of quark and an antiquark; \mathcal{A}_q in eq. (1) is an antisymmetrization operator among these four quarks. By integrating out the internal coordinates, we obtain the following RGM equation to determine the relative wave function:

$$\int [H_{RGM}(\mathbf{R}, \mathbf{R}') - EN_{RGM}(\mathbf{R}, \mathbf{R}')] \chi(\mathbf{R}') d\mathbf{R}' = 0, \quad (2)$$

where $H [N]$ is the hamiltonian [norm] kernel.

The hamiltonian kernel can be obtained from the hamiltonian for quarks, H_q , which consists of the kinetic term, the one-gluon-exchange term (OGE), the confinement term (Conf), the collective term (Coll), and the instanton-induced interaction term (INS) [5]:

$$H_q = \sum_i \left(\frac{p_i^2}{2m_i} + V_0 \right) - K_G + V_{\text{Conf}} + V_{\text{OGE}} + V_{\text{Coll}} + V_{\text{INS}}. \quad (3)$$

In the present work, we assume that the coupling between the scattering state and the Λ^1 pole comes from OGE, which can be written as:

$$\langle V_{3q-5q} \rangle = 6 \langle B^*(q^3)_{123} | V_{3;4\bar{5}} \frac{1}{\sqrt{4}} (1 - 2P_{24} - P_{34}) | B(q^3)_{123} M(q_4\bar{q}_5) \rangle \quad (4)$$

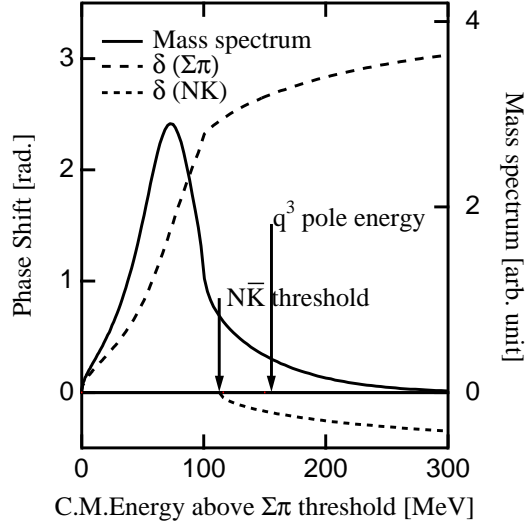


Figure 1: Mass spectrum and the phase shift (δ) of the $\Sigma\pi$ and $N\bar{K}$ coupled channel QCM.

with

$$V_{i;j\bar{k}} = \lambda_i \cdot \lambda_{\bar{k}j} \frac{\alpha_s \pi}{4 m_a^2} \left\{ \left(\frac{\mathbf{k}}{2m_a} - \frac{\mathbf{p}_i + \mathbf{p}'_i + i\boldsymbol{\sigma}_i \times \mathbf{k}}{2m_i} \right) \cdot \boldsymbol{\sigma}_{\bar{k}j} \right\} \delta_{\bar{k}j}^f, \quad (5)$$

where m_a is the quark mass in the annihilating $q_j\bar{q}_{\bar{k}}$ pair, m_i is the mass of the i -th quark, and $\mathbf{k} = \mathbf{p}_j + \mathbf{p}_{\bar{k}}$.

3 Results

When the $\langle V_{3q-5q} \rangle$ term is switched off, there is no structure in the $\Sigma\pi$ phase shift below the $N\bar{K}$ threshold in the $T=0$ nor in the $T=1$ channels. It is because the kinetic energy of the system is large due to the light pion mass. It cancels the short-ranged attraction of OGE in the $\Sigma\pi$ channel.

A resonance, however, appears when the conventional Λ^1 , the $q^3(0s)^20p$ state, is introduced into the system as a pole in the scattering. The energy of this Λ^1 pole is assumed to be 160 MeV above $\Sigma\pi$ threshold without the coupling. When the coupling is switched on, the pole energy is reduced by about 85 MeV, which corresponds to 1404 MeV; it becomes a resonance below the $N\bar{K}$ threshold (Fig. 1). The width of the peak in the mass spectrum is about 55 MeV, which also agrees reasonably with the observed one. The $N\bar{K}$ phase shift goes to negative: the scattering length is $-0.75 + i0.38$ fm,

Table 1: Matrix elements of the flavor-type operator, $-\langle \sum (F_i \cdot F_j) \rangle$, and the color-spin-type operator, $-\langle \sum (\lambda_i \cdot \lambda_j)(\sigma_i \cdot \sigma_j) \rangle$ for $T = 0$.

	flavor-type					color-spin-type			
	$\Sigma\pi$	$N\bar{K}$	$\Lambda\eta$	ΞK		$\Sigma\pi$	$N\bar{K}$	$\Lambda\eta$	ΞK
$\Sigma\pi$	-8	$\sqrt{6}$	0	$-\sqrt{6}$	$\Sigma\pi$	$-\frac{16}{3}$	$\frac{116\sqrt{7}}{21}$	$-\frac{16\sqrt{105}}{105}$	0
$N\bar{K}$		-6	$3\sqrt{2}$	0	$N\bar{K}$		0	$\frac{28\sqrt{15}}{15}$	0
$\Lambda\eta$			0	$-3\sqrt{2}$	$\Lambda\eta$			$\frac{112}{15}$	$-\frac{40\sqrt{70}}{21}$
ΞK				-6	ΞK				$-\frac{160}{21}$

which, as a simple model, agrees with the experimental value, $(-1.70 \pm 0.07) + i(0.68 \pm 0.04)$ fm [6], reasonably well.

In the baryon-meson picture where the flavor-flavor type interaction, $-F \cdot F$, is employed, the peak appears because of the attraction in the $N\bar{K}$ channel [7]. (See Table 1.) In the present scheme of the color-spin interaction, where the hyperfine interaction is proportional to $-(\lambda \cdot \lambda)(\sigma \cdot \sigma)$, there is no such an attraction in the $N\bar{K}$ channel. Thus, introducing the Λ^1 pole is necessary to reproduce the resonance. Actually, in the present case, the Λ^1 component of the wave function at the resonance is by about 2.8 larger than the $N\bar{K}$ component.

In summary, our results show that (1) there is a strong attraction in the $\Sigma\pi$ channel but not in the $N\bar{K}$ channel, (2) no peak is found in the $\Sigma\pi$ - $N\bar{K}$ - $\Lambda\eta_{ud}$ coupled channel QCM calculation if we employ the realistic reduced mass for the kinetic energy, and (3) a reasonable peak appears if the Λ^1 pole is included above the $N\bar{K}$ threshold.

Acknowledgments

This work is supported in part by a Grant-in-Aid for Scientific Research from JSPS (Nos. 15540289, 17540264, and 18042007).

References

- [1] N. Isgur and G. Karl, Phys. Rev. D **18**, 4187 (1978).
- [2] M. Furuichi, K. Shimizu, and S. Takeuchi, Phys. Rev. **C68**, 034001 (2003)

- [3] Y. Akaishi and T. Yamazaki, Phys. Rev. C **65**, 044005 (2002).
- [4] V. K. Magas, *et al.*, Phys. Rev. C **74**, 025206 (2006)
- [5] S. Takeuchi and K. Shimizu, Phys. Rev. C **76**, 035204 (2007)
- [6] A. D. Martin, Nucl. Phys. B **179**, 33 (1981).
- [7] E. Oset and A. Ramos, Nucl. Phys. A **635**, 99 (1998)

THE MASSLESS LINEAR SIGMA MODEL FOR FINITE NUCLEI AND AT FINITE TEMPERATURE

S. Tamenaga¹, H. Toki, A. Hoga, and Y. Ogawa

RCNP, Osaka University, Ibaraki, Osaka 567-0047, Japan

Abstract

We study the effect of one-loop corrections from nucleon together with those from boson in the massless linear sigma model, where we perform the Coleman-Weinberg (CW) renormalization procedure [1, 2]. As a next step, we apply the massless linear sigma model to finite nuclei and finite temperature system.

1 Introduction

A model with the good properties of the chiral symmetry is the linear sigma model which has been used in the low energy phenomenology of hadron dynamics. This model has the renormalizabilities for both boson and fermion loop. However, there are long-standing problems for renormalization with chiral symmetry. It is well known that chirally symmetric renormalization for the nucleon loop in the conventional way gives unstable effective potential and too large non-linear interactions.

2 Lagrangian and renormalization procedure

We begin with the linear sigma model with fermion:

$$\begin{aligned}\mathcal{L}^{\text{LSM}} &= \bar{\Psi} [i\gamma_\mu \partial^\mu - g_\sigma(\phi + i\gamma_5 \boldsymbol{\tau} \cdot \boldsymbol{\pi})] \Psi \\ &+ \frac{1}{2} (\partial_\mu \phi \partial^\mu \phi + \partial_\mu \boldsymbol{\pi} \cdot \partial^\mu \boldsymbol{\pi}) - \frac{\lambda}{4} (\phi^2 + \boldsymbol{\pi}^2)^2 + \varepsilon \phi \\ &- \delta\mathcal{L}_{\text{CTC}},\end{aligned}\tag{1}$$

where Ψ , ϕ , and $\boldsymbol{\pi}$ are fermion field, sigma meson field, and pi meson field, respectively. $\varepsilon\phi$ is an explicit chiral symmetry breaking term. The last term $\delta\mathcal{L}_{\text{CTC}}$ is the counterterm Lagrangian, which is necessary to renormalize the fermion and boson loops.

¹E-mail address: stame@rcnp.osaka-u.ac.jp

2.1 Loop corrections with chiral symmetry

The effective action of Eq. (1) at the one boson-loop level can be written as

$$\begin{aligned}\Gamma_B^\chi &= \int d^4x \left[\frac{i}{2} \ln \det \left(-\frac{\delta^2 \mathcal{L}}{\delta b \delta b} \right) - \text{VEV} - \delta \mathcal{L}_{\text{CTC}}^B \right] \\ &= \int d^4x \left[-V_B^R(\phi, \boldsymbol{\pi}) + \frac{1}{2} Z_{\sigma\pi}^B (\partial_\mu \phi \partial^\mu \phi + \partial_\mu \boldsymbol{\pi} \cdot \partial^\mu \boldsymbol{\pi}) + \dots \right],\end{aligned}\quad (2)$$

where \mathcal{L} includes the tree contribution and $\delta \mathcal{L}_{\text{CTC}}^B$ is the counterterms for the boson loop. We take the renormalization conditions for mass, coupling constant, and derivative term to Eq. (2) as

$$\left. \frac{\partial^2 V_B^R}{\partial \phi^2} \right|_{\phi^2=0, \boldsymbol{\pi}^2=0} = 0, \quad \left. \frac{\partial^4 V_B^R}{\partial \phi^4} \right|_{\phi^2=m^2, \boldsymbol{\pi}^2=0} = 0, \quad Z_{\sigma\pi}^B \Big|_{\phi^2=m^2, \boldsymbol{\pi}^2=0} = 0. \quad (3)$$

where we introduce the renormalization scale m to Eq. (3) in order to avoid the logarithmic singularity at the origin of the effective potential [3]. Finally the renormalized potential of boson with the chiral symmetry becomes

$$V_B^R = \frac{3\lambda^2}{16\pi^2} (\phi^2 + \boldsymbol{\pi}^2)^2 \left[\ln \left(\frac{\phi^2 + \boldsymbol{\pi}^2}{m^2} \right) - \frac{25}{6} \right]. \quad (4)$$

In the same way as the boson loop, we obtain the renormalized potential of fermion loop as

$$V_F^R = -\frac{g_\sigma^4}{8\pi^2} (\phi^2 + \boldsymbol{\pi}^2)^2 \left[\ln \left(\frac{\phi^2 + \boldsymbol{\pi}^2}{m^2} \right) - \frac{25}{6} \right]. \quad (5)$$

2.2 Effective potential and parameters

Here, we have defined a non-trivial local minimum away from the origin which determines the coupling constant λ which is dependent on the renormalization scale m ,

$$\frac{3}{2\pi^2} \left[\ln \left(\frac{f_\pi}{m} \right) - \frac{11}{6} \right] \lambda^2 + \lambda - \frac{g_\sigma^4}{\pi^2} \left[\ln \left(\frac{f_\pi}{m} \right) - \frac{11}{6} \right] - \frac{\varepsilon}{f_\pi^3} = 0. \quad (6)$$

Equation (6) has two solutions as a function of m and we choose the positive coupling constant λ as the natural choice. Both the boson and the nucleon loops are too large as compared with the tree contributions. However, the total loop potential is a reasonable and negative one due to cancellation between the large positive potential from the nucleon loop and the

Table 1: **Parameter sets through the relationships using $m = f_\pi$.**

M [MeV]	m_π [MeV]	f_π [MeV]	g_σ	λ	m_σ [MeV]
939	139	93	10.09	85.0	669.7

large negative one from the boson loop. As a result, the total renormalized loop potential plays an important role as the negative mass term of the linear sigma model. Thus the spontaneous chiral symmetry breaking occurs through the loop corrections. The parameters can be determined from experimental values and chiral symmetry in Table 1. The spontaneous chiral symmetry breaking makes fermion and sigma meson massive. Only the pion mass is generated from the explicitly chiral symmetry breaking term. Using all of the parameters, then, the renormalized effective potential consistent with chiral symmetry becomes stable around the new origin by using the CW renormalization procedure for the first time [1,2].

3 Finite system

In this section, we apply this model to finite nuclei and finite temperature. The massless chiral sigma model also has the same properties as those of the chiral sigma model [2] which includes the ω meson in order to generate an appropriate repulsive effect to obtain a stable nucleus. The difference between the chiral sigma model and the massless chiral sigma model is the loop corrections. In particular the renormalization of wave function is important for the finite system with the surface. Left hand side of Fig. 1 shows the baryon density distribution in ^{16}O with the massless chiral sigma model. The baryon density distribution becomes more smooth in spite of the large incompressibility. The effect of Dirac sea changes the density distribution in the interior region and surface region.

We also would like to see the hadron properties of the massless linear sigma model at finite temperature. In this calculation we include both Hartree and Fock terms. The stationary point, f_π , is obtained at any temperature by local minimum condition. Through this condensation, f_π , the masses of all the particles can be given. Right hand side of Fig. 1 shows the masses of mesons and nucleon as function of temperature. This behavior of the nucleon mass is almost the same as the quark-meson coupling model with the self-consistent approach. Moreover the differences between the mass parameters of σ and π mesons produce the crossover curve of the masses around the critical temperature.

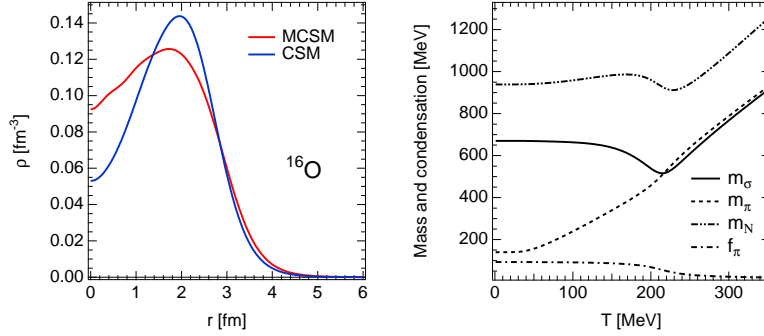


Figure 1: (LHS) The baryon density without pion mean field in ^{16}O with the chiral sigma model (CSM) in the mean field approximation and with the massless chiral sigma model (MCSM) in the relativistic Hartree approximation. (RHS) The behavior of mass and condensation dependent on temperature with the CW scheme in the case of broken chiral symmetry $\varepsilon \neq 0$.

4 Summary

We have studied the renormalization of the chiral model for the study of finite nuclei and hadron properties at finite temperature. By introducing the CW renormalization scheme we have been able to resolve the problem of the instability of the effective potential in the chiral model for the first time. We have found that the renormalization of wave function provide the smooth density distribution. We have also found the dependence of hadron masses on temperature with the boson and nucleon loops for the first time.

Acknowledgements

This work is supported by Research Fellowships of the Japan Society for the Promotion of Science (No. 18-09058).

References

- [1] S. Tamenaga, H. Toki, A. Haga and Y. Ogawa, nucl-th/0604013.
- [2] H. Toki, Y. Ogawa, S. Tamenaga and A. Haga, Phys. Part. Nucl. Phys. **59**, 209 (2007).
- [3] S. R. Coleman and E. Weinberg, Phys. Rev. **D7**, 1888 (1973).

PREPARATIONS FOR PELLET TRACKING SYSTEM

T. Tolba¹ and J. Ritman
Institut für Kernphysik
Forschungszentrum Jülich
52425 Jülich, Germany

Abstract

A Pellet Tracking System (PTS) for WASA at COSY is proposed in order to determine the interaction point (the primary interaction vertex) for each event between the COSY beam and the target pellets. The knowledge of this interaction vertex helps to reconstruct the paths of the different decay products and thus to improve the momentum resolution of the events. Furthermore, the PTS gives information about the position distribution of the pellets, thereby allowing the geometrical alignment of the system to be improved. Several measurements were done in order to test and optimize the equipment's capabilities.

1 Method

The main idea to determine the interaction point is to measure the x and z position of a pellet before and after the interaction point. That can be done by using a laser beam to light up the pellet and photographing it (using the scattered laser light from the pellet) by pairs of fast CCD line scan cameras, below and above the vertex point (see Fig. 1). The cameras are arranged at 90° relative to each other. Then the pellet trajectories can be tracked from the position information from each plane and the relative timing.

In previous work on the pellet tracker at Uppsala University a setup with one camera and one laser was used to study hair, wires as pellet simulator and pellets from a pellet test station. A one-dimensional distribution of the pellets was measured, and found to be consistent with the expectations from the geometry of the system [1–3].

¹e-mail: t.tolba@fz-juelich.de

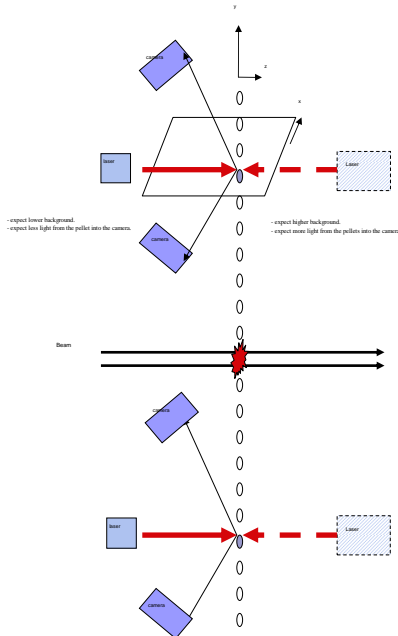


Figure 1: Proposed system to determine the x and z position of the individual pellets.

2 Results

2.1 Lens-target distance optimization

A strand of hair was photographed and its thickness (as FWHM) was measured at different distances between the lens of the camera and the hair. The relation between them is plotted in Fig. 2. The optimum measured distance was found to be $D = 173$ mm (while the calculated distance is 175 mm).

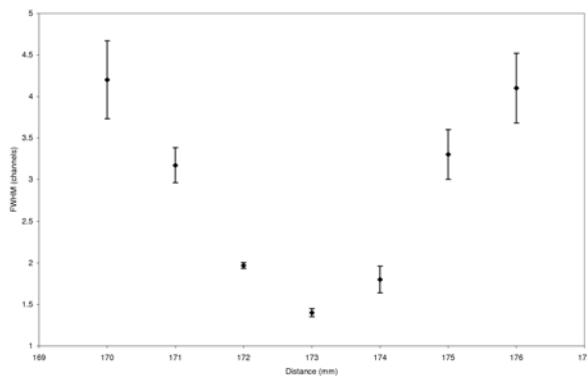


Figure 2: Measured width (FWHM) of the image of a hair as a function of the lens-target distance.

2.2 Pixel size calibration

At distance of 173 mm from the lens, an image of a grating with pitch (2.00 ± 0.03) mm was taken, (see Fig. 3). For the camera operating parameters (512 pixels of $14 \mu\text{m} \times 14 \mu\text{m}$, $D = 173$ mm and lens focal length $l = 50$ mm), the calculated magnification factor is $M = (40 \pm 3)\%$, in comparison to the measured magnification factor $M = (39.2 \pm 1)\%$ (i.e. $1 \text{ pixel} = (35 \pm 1.8) \mu\text{m}$).

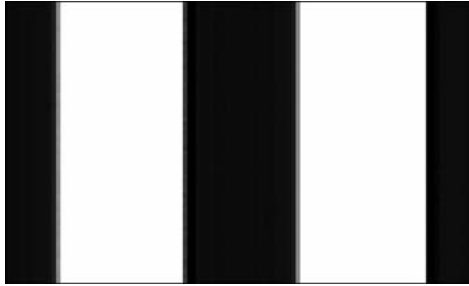


Figure 3: Pixel image for a grating of 2 mm pitch.

2.3 Hair thickness measurement

A strand of hair was fixed at the optimum distance $D = 173$ mm from the lens. At this distance the lens has a magnification factor of $(40 \pm 3)\%$. As shown in Fig. 4a,b. The FWHM of the measured light distribution was found to be (1.8 ± 0.06) channels. Using the pixel size of $14 \mu\text{m}$ [4] and the magnification factor $M = (39.2 \pm 1)\%$, the calculated thickness of the hair is found to be $(63.3 \pm 2) \mu\text{m}$, in agreement with the value $(70 \pm 5) \mu\text{m}$ measured directly with a micrometer.

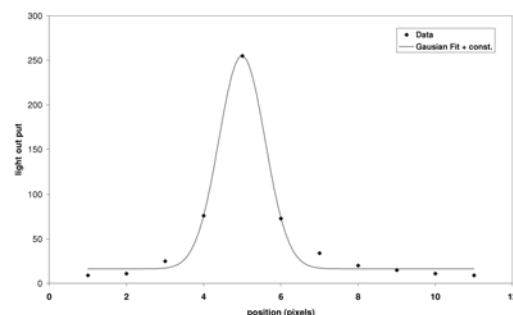
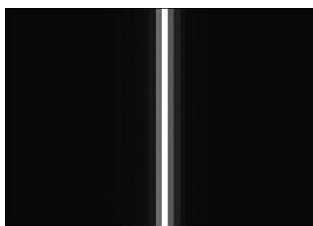


Figure 4: (a)(upper) Pixel image of the hair, (b)(lower) Gauss fit of the measured light intensity in the camera to the scattered light from a hair

2.4 Time calibration

By taking 70000 line pictures of a rotating object with (138 ± 3) kHz, using $1 \mu\text{s}$ integration time, the line rate frequency is measured to be (97.8 ± 1.7) kHz, corresponding to a time resolution of $10.2 \mu\text{s}$ (Fig. 5).

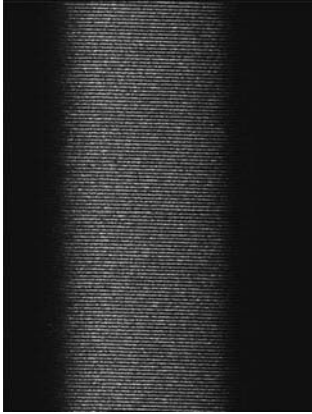


Figure 5: 70000 line pictures of a rotating source.

3 Conclusion

The optimum distance between the lens and the object measured and found to be $D = 173$ mm. At this distance the magnification factor is $M = (39.2 \pm 1)\%$, (i.e., $1 \text{ pixel} = 35 \mu\text{m}$, which is in the range of the pellet size ($25 - 40 \mu\text{m}$)). With this magnification and at this distance the thickness of a hair was measured and found to be consistent with the directly measured thickness. The maximum line rate frequency of the line scan camera found to be $(97.8 \pm 1.7)\text{kHz}$.

References

- [1] Ö. Nordhage *et al.*, *Nucl. Instrum. Meth.* **A 568**, 561 (2006).
- [2] Jonas Lith, *Development of a Tracking System for Hydrogen Pellet Targets Utilizing a Line-Scan Camera*, Master thesis, Uppsala University (2006).
- [3] Matthias Schult, *Development of a Pellet Tracking System. Project work*, Master thesis, Uppsala University (2005).
- [4] ATMEL. AVIIVATM M2 Cl CameralinkTM Line Scan Camera, (2006), Data sheet.

D AND \bar{D} MESONS IN HOT AND DENSE MATTER

L. Tolós^{*} ¹, *A. Ramos*[†] and *T. Mizutani*[§]

^{*}FIAS. J.W.Goethe-Universität.
Ruth-Moufang-Str. 1, 60438 Frankfurt (M), Germany

[†]Dept. d'Estructura i Constituents de la Matèria. Universitat de Barcelona.
Diagonal 647, 08028 Barcelona, Spain

[§]Department of Physics, Virginia Polytechnic Institute and State University.
Blacksburg, VA 24061, USA

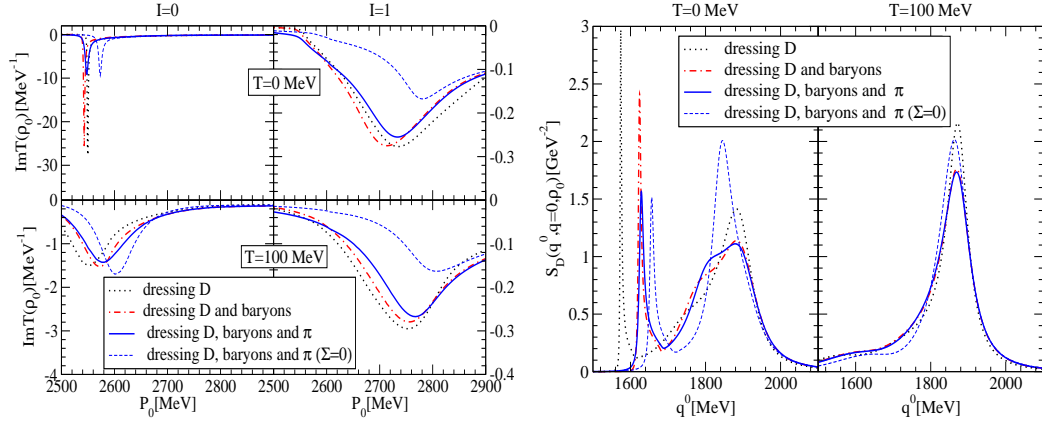
Abstract

The D and \bar{D} mesons are studied in hot dense matter within a self-consistent coupled-channel approach taking, as bare interaction, a broken $SU(4)$ s -wave Tomozawa-Weinberg interaction supplemented by an attractive isoscalar-scalar term. The in-medium solution at finite temperature incorporates Pauli blocking effects, baryon mean-field bindings, and π and open-charm meson self-energies. In the DN sector, the Λ_c and Σ_c resonances remain close to their free-space position while acquiring a remarkable width. As a result, the D meson spectral density shows a single pronounced peak close to the free mass that broadens with increasing density specially towards lower energies. The low-density theorem is not a good approximation for the repulsive \bar{D} self-energy close to saturation density. We discuss the implications for the J/Ψ suppression at CBM (FAIR).

The future CBM (Compressed Baryon Matter) experiment of the FAIR project at GSI aims at investigating, among others, the possible modifications of the properties of open (D and \bar{D}) and hidden (e.g. J/Ψ) charmed mesons in a hot and dense baryonic environment.

The in-medium modification of the $D(\bar{D})$ mesons may explain the J/Ψ suppression [1] in an hadronic environment, based on the mass reduction of $D(\bar{D})$ in the nuclear medium [2]. However, a coupled-channel meson-baryon scattering in nuclear medium is needed due to the strong coupling among the DN and other meson-baryon channels [3–6]. In the present article, we pursue a coupled-channel study on the spectral properties of D and \bar{D} mesons in

¹tolos@fias.uni-frankfurt.de

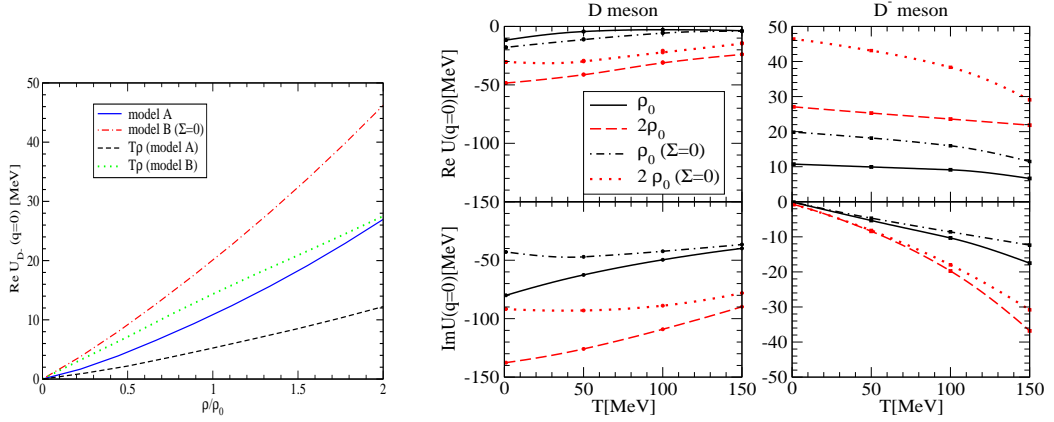
Figure 1: Λ_c and Σ_c resonances, and the D meson spectral function

nuclear matter at finite temperatures by extending the result of Ref. [3] in order to examine the possible implications in the J/Ψ suppression at FAIR. The D and \bar{D} self-energies at finite temperature are obtained by performing a self-consistent coupled-channel calculation taking, as bare interaction, a type of broken $SU(4)$ s -wave Tomozawa-Weinberg (TW) interaction supplemented by an attractive isoscalar-scalar term (Σ_{DN}). The multi-channel transition matrix T is solved using a cutoff regularization, which is fixed by reproducing the position and the width of the $I = 0$ $\Lambda_c(2593)$ resonance while a new resonance in $I = 1$ channel $\Sigma_c(2880)$ is generated [3].

The in-medium solution at finite temperature incorporates Pauli blocking effects, baryon mean-field bindings via a temperature-dependent $\sigma - \omega$ model, and π and open-charm meson self-energies in the intermediate propagators (see [7]). The in-medium self-energy and corresponding spectral density are obtained self-consistently summing T_{DN} over the nucleon Fermi distribution.

The behavior of the $I = 0$ Λ_c and $I = 1$ Σ_c resonances in hot dense matter is shown in the l.h.s. of Fig. 1 for three different self-consistent calculations: (i) including only the self-consistent dressing of the D meson, (ii) adding the mean-field binding of baryons (MFB) and (iii) including MFB and the pion self-energy (PD). The thick lines correspond to model A (viz. $\Sigma_{DN} \neq 0$) while the thin-dashed lines refer to Case (iii) within model B ($\Sigma_{DN} = 0$).

Medium effects at $T = 0$ lower the position of the Λ_c and Σ_c resonances with respect to their free values, in particular with the inclusion of MFB. Their width values, which increase due to $\tilde{Y}_c N \rightarrow \pi N \Lambda_c, \pi N \Sigma_c$ processes, differ according to the phase space available. The PD induces a small effect in the resonances because of charm-exchange channels being suppressed, while models A and B are qualitatively similar. Finite temperature results in the

Figure 2: \bar{D} mass shift as well as $T\rho$, and the D and \bar{D} potentials.

reduction of the Pauli blocking effects due to the smearing of the Fermi surface with temperature. Both resonances move up in energy closer to their free position while they are smoothen out, as in [5].

In the r.h.s of Fig. 1 we display the D meson spectral function for (i) to (iii) (thick lines) for model A and case (iii) for model B (thin line). At $T = 0$ the spectral function presents two peaks: $\tilde{\Lambda}_c N^{-1}$ excitation at a lower energy whereas the second one at higher energy is the quasi(D)-particle peak mixed with the $\tilde{\Sigma}_c N^{-1}$ state. Once MFB is included, the lower peak built up by the $\tilde{\Lambda}_c N^{-1}$ mode goes up by about 50 MeV relative to (i) since the meson requires to carry more energy to compensate for the attraction felt by the nucleon. The same characteristic feature is seen for the $\tilde{\Sigma}_c N^{-1}$ configuration that mixes with the quasiparticle peak. The PD does not alter much the position of $\tilde{\Lambda}_c N^{-1}$ excitation or the quasiparticle peak. For model B ((iii) only), the absence of the Σ_{DN} term moves the $\tilde{\Lambda}_c N^{-1}$ excitation closer to the quasiparticle peak, while the latter fully mixes with the $\tilde{\Sigma}_c N^{-1}$ excitation. When finite temperature effects are included, those structures get diluted with increasing temperature while the quasiparticle peak gets closer to its free value and it becomes narrower, because the self-energy receives contributions from higher momentum DN pairs where the interaction is weaker.

In the $\bar{D}N$ sector, the scattering lengths for model A (B) are $a^{I=0} = 0.61$ (0) fm and $a^{I=1} = -0.26$ (-0.29) fm. While our repulsive $I = 1$ is in good agreement with [6], the finite value for the $I = 0$ scattering length found in this latter reference is in contrast to the zero value found here for model B due to the vanishing $I = 0$ coupling coefficient of the corresponding pure TW $\bar{D}N$ interaction. Our results are, however, consistent with a recent calculation [8]. For model A, we obtain a non-zero value of the $I = 0$ scat-

tering length, due to the magnitude of the Σ_{DN} term. As seen in the l.h.s of Fig. 2, the \bar{D} mass shift in cold nuclear matter is repulsive and, in spite of the absence of resonances close to threshold, the low-density approximation or $T\rho$ breaks down at relatively low densities.

Finally, in the r.h.s of Fig. 2 we compare the D and \bar{D} optical potentials. For model A (B) at $T = 0$, we obtain an attractive potential of -12 (-18) MeV for D meson while the repulsion for \bar{D} is 11 (20) MeV. A similar shift in the mass for D mesons is obtained in Ref. [5]. The temperature dependence of the repulsive real part of the \bar{D} optical potential is very weak, while the imaginary part increases steadily due to the increase of collisional width. The picture is somewhat different for the D meson due to the overlap of the quasiparticle peak with the $\tilde{\Sigma}_c N^{-1}$ mode. The $\tilde{\Sigma}_c N^{-1}$ mode also alters the effect of the Σ_{DN} term on the potential.

With regard to the J/Ψ suppression, the in-medium \bar{D} mass is seen to increase by about $10 - 20$ MeV whereas the tail of the quasiparticle peak of the D spectral function extends to lower "mass" due to the thermally spread $\tilde{Y}_c N^{-1}$. But it is unlikely that this lower tail extends as far down by 600 MeV with sufficient strength. So the only way for the J/Ψ suppression to take place is by cutting its supply from the excited charmonia: $\chi_{c\ell}(1P)$ or Ψ' by their hadronic collisions, which appears fairly likely kinematically even at finite temperature in the present study.

References

- [1] T. Matsui and H. Satz, *Phys. Lett.* **B178**, 416 (1986).
- [2] K. Tsushima, D. H. Lu, A. W. Thomas, K. Saito and R. H. Landau, *Phys. Rev.* **C59**, 2824 (1999); A. Sibirtsev, K. Tsushima and A. W. Thomas, *Eur. Phys. J.* **A6**, 351 (1999); A. Hayashigaki, *Phys. Lett.* **B487**, 96 (2000); A. Mishra, E. L. Bratkovskaya, J. Schaffner-Bielich, S. Schramm and H. Stöcker, *Phys. Rev.* **C70**, 044904 (2004).
- [3] T. Mizutani and A. Ramos, *Phys. Rev* **C74**, 065201 (2006).
- [4] L. Tolos, J. Schaffner-Bielich and A. Mishra, *Phys. Rev.* **C70**, 025203 (2004).
- [5] L. Tolos, J. Schaffner-Bielich and H. Stöcker, *Phys. Lett.* **B635**, 85 (2006).
- [6] M. F. M. Lutz and C. L. Korpa, *Phys. Lett.* **B633**, 43 (2006).
- [7] L. Tolos, A. Ramos and T. Mizutani, *Phys. Rev.* **C77**, 015207 (2008).

- [8] J. Haidenbauer, G. Krein, U. G. Meissner and A. Sibirtsev, *Eur. Phys. J.* **A33**, 107 (2007).

REACTION DYNAMICS OF ω MESON PRODUCTION IN pp COLLISIONS

W. Ullrich*¹, K.-Th. Brinkmann*, J. Dietrich*, S. Dshemuchadse*, H. Freiesleben*, J. Gottwald*, R. Jäkel*, L. Karsch*, E. Kuhlmann*, M. Schulte-Wissermann*, S. Reimann*, R. Wenzel*,
for the COSY-TOF Collaboration

* Institut für Kern- und Teilchenphysik,
Technische Universität Dresden, D-01062 Dresden, Germany

Abstract

The A_y for in proton-proton collisions ($pp \rightarrow pp\omega$) has been measured at COSY with the TOF spectrometer. In the experiment a transversely polarized proton beam was used with a beam momentum of $p_{Beam} = 3065$ MeV/c, corresponding to an excess energy of $\epsilon = 129$ MeV. The result, a vanishing analyzing power, is a further step towards the determination of the leading partial waves in this reaction channel.

1 Introduction

The reaction $pp \rightarrow pp\omega$ has been studied near threshold and at moderate excess energies up to $\epsilon = 320$ MeV ($\epsilon = \sqrt{s} - \sqrt{s_0}$, $\sqrt{s_0}$: threshold energy) by means of electronic detector systems since the late 1990ies [1–4]. The energy dependence of the measured total cross sections is reproduced well by several theoretical models describing the ω production via one pion exchange [5], nucleon resonances [6] or nucleonic and mesonic currents [7]. In order to discriminate between the different theoretical approaches and to improve the understanding of the reaction dynamics involved, angular distributions have been measured as well [2–4, 8]. However, the available data do not allow to determine the energy dependent contribution of different partial waves. For this objective the measurement of polarization observables is very helpful, since they are particularly sensitive to the contributing partial waves. So far no data exist for polarization observables in this channel.

The analyzing power A_y was determined in an experiment utilizing a polarized proton beam incident on an unpolarized proton target ($pp \rightarrow pp\omega$).

¹E-mail address: W.Ullrich@physik.tu-dresden.de

2 Experiment and Results

The data were taken with the TOF spectrometer located at the COoler SYnchrotron COSY (Jülich). COSY provided a transversally polarized proton beam and the orientation of the beam polarization was flipped each operating cycle of the accelerator where each cycle took about 120 s. The beam polarization was determined to be $P_{Beam} = 0.32 \pm 0.03$ by the analysis of proton proton elastic scattering. The integrated luminosities for the resulting data sets for the two orientations of the beam polarization were determined to coincide within an uncertainty of 0.3%.

The TOF detector stands out for its large geometric acceptance ($1^\circ < \theta_{lab} < 60^\circ$, $0^\circ \leq \phi < 360^\circ$) in combination with a high detector efficiency ($> 95\%$) for the detection of charged particles. This allows the unambiguous and simultaneous identification of different reaction channels (e.g., $pp \rightarrow pp$, $d\pi^+$, $pK^+\Lambda$, $pK^+\Sigma^0$, $pp\omega$) by examining their event topology. The reaction $pp \rightarrow pp\omega$ was preselected via the main decay channel of the ω meson ($\omega \rightarrow \pi^+\pi^-\pi^0$, $\mathcal{BR} \approx 89.1\%$) which leads to four charged particles measured in the detector and one unobserved neutral pion. The outgoing protons and the charged pions, due to their large mass difference, are clearly separated in a velocity vs. polar angle representation [8]. This separation was used to assign masses to the measured velocity vectors in order to calculate the corresponding four-momenta. The main sources of background are the non-resonant and resonant two-pion production channels. Their contribution was reduced by a constraint for the acoplanarity of the pion candidates with the reconstructed meson since for an ω decaying into three pions the plane defined by the two observed pions does in general not contain the direction of the meson (for details see [8]). The analysis only considers events where the sum of momenta of the two protons points into the backward hemisphere of the CMS, since in these cases the protons are slower in the laboratory frame and the momentum resolution achieved is therefore significantly better. Hence, the determination of $A_y(\theta_\omega^*)$ is restricted to $0 < \cos\theta_\omega^* < 1$. Using the four-momenta of the two protons the missing mass is calculated.

In order to obtain differential observables, missing mass spectra have to be produced for different intervals of the observable under study. For the determination of the analyzing power A_y , missing mass spectra were created for five bins in polar and eight in azimuthal angle of the ω in the CMS and for two spin orientations of the proton beam (altogether 80 spectra). For all these spectra the number of ω events has to be determined individually. An example for one pair of missing mass spectra for one solid angular bin and both spin orientations is shown in the left frame of Fig. 1. No dependence of the background on the beam polarization was observed for any of

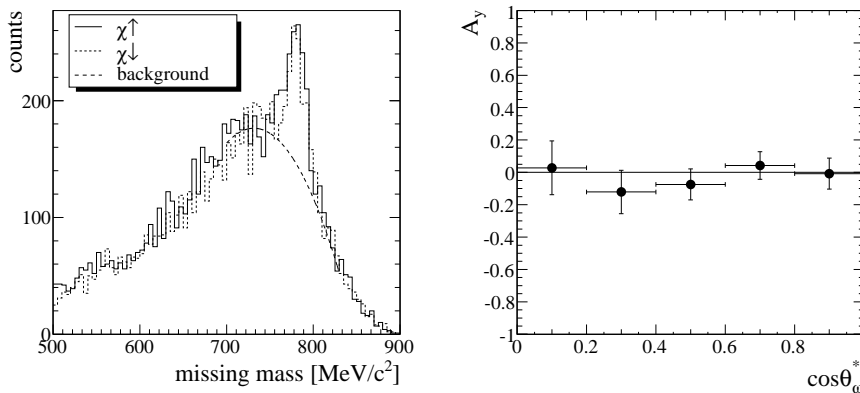


Figure 1: Left: Missing-mass spectra for the interval $0.6 < \cos\theta_\omega^* < 0.8$ and $-22.5^\circ < \phi_\omega < 22.5^\circ$ for the two orientations of the beam polarization. The dashed line represents the average background.

Right: Analyzing power for the $pp \rightarrow pp\omega$ reaction. All values agree with zero within the quoted uncertainties.

the angular bins. Therefore, an average background shape was determined and the number of ω events is the number of counts in the ω peak above this background. With these numbers the asymmetry between the two spin orientations is determined. This was done over the whole azimuthal angular range for five bins in the polar angle. From the amplitude of a cosine fit to the distribution of the asymmetry over the azimuthal angle and with the known beam polarization the analyzing power A_y was determined for the different polar angular bins. The result is shown in the right frame of Fig. 1.

3 Discussion

In the following we use the notation $(^{2S+1}L_J)_i \rightarrow (^{2S+1}L_J)_f l_\omega$ for the description of the partial waves, where the angular momentum of the proton-proton system is denoted by L , the spin by S and the total angular momentum by J . Subscripts i and f signify initial and final state, respectively, l_ω denotes the angular momentum of the ω meson relative to the proton-proton system. Directly at threshold only S-waves contribute to the exit channel. Then the partial wave is $^3P_1 \rightarrow ^1S_0 s$ with the amplitude f_1 . Due to the excess energy of $\epsilon = 129$ MeV and the observation of anisotropic angular distributions at lower excess energy [8] higher partial waves must be present. The next higher partial waves possibly contributing to A_y are $^1S_0 \rightarrow ^1S_0 p$ and $^1D_2 \rightarrow ^1S_0 p$

with the amplitudes f_2 and f_3 respectively. Considering all three partial waves, the analyzing power follows [9]

$$A_y \propto \text{Im}(f_1^*(f_2 - 1/3f_3)) k \sin\theta_\omega^* \cos\phi_\omega, \quad (1)$$

here k denotes the absolute value of the ω momentum in the CMS. That means our finding $f_1^*(f_2 - 1/3f_3) \approx 0$ indicates $f_1 \approx 0$ or $f_2 \approx 3f_3$ or $f_2 \approx f_3 \approx 0$ or $f_1^* \perp f_2$ and $f_1^* \perp f_3$. Obviously this result does not rule out a non-vanishing analyzing power below or above the excess energy of $\epsilon = 129$ MeV.

Acknowledgments

This work was supported by BMBF and FZ-Jülich.

References

- [1] F. Hibou *et al.*, Phys. Rev. Lett. **83** 492 (1999).
- [2] The DISTO collaboration, F. Balestra *et al.*, Phys. Rev. C **63** 024004 (2001).
- [3] The COSY-TOF collaboration, S. Abd El-Samad *et al.*, Phys. Lett. B **522**, 16 (2001).
- [4] S. Barsov *et al.*, Eur. Phys. J. A **31**, 95 (2007).
- [5] A.A. Sibirtsev, Nucl. Phys. A **604**, 455 (1996).
- [6] C. Fuchs *et al.*, Phys. Rev. C **67**, 025202 (2003).
- [7] K. Nakayama *et al.*, Phys. Rev. C **57**, 1580 (1998).
- [8] The COSY-TOF collaboration, M. Abdel-Bary *et al.*, Phys. Lett. B **647**, 351 (2007).
- [9] C. Hanhart, Phys. Rep. **397** 155-256 (2004) and private communications.

STUDY OF THE $p^6Li \rightarrow \eta^7Be$ REACTION

N. J. Upadhyay^{#1}, N. G. Kelkar[♣], K. P. Khemchandani[★], B. K. Jain[#]

[#]Department of Physics, University of Mumbai, Mumbai - 400 098, India.

[♣]Departamento de Física, Universidad de los Andes, Colombia.

[★]Departamento de Física Teórica and IFIC, Valencia, Spain.

Abstract

We present here the calculation on η production near threshold in the fusion of proton and 6Li producing 7Be . Considering 7Be as a ($^3He + ^4He$) cluster, we aim to study $\eta - ^7Be$ final state interaction (FSI) by solving few body equations for $\eta - ^3He - ^4He$ system. The input $\eta - ^3He$ and $\eta - ^4He$ t -matrices are themselves obtained by solving few body equations, where the scattering in presence of the nuclear medium is taken into account.

1 Introduction

The $\eta - N$ interaction dominated by S_{11} (1535) resonance, is strong and attractive in nature [1]. This has motivated search for bound and quasi-bound η -mesic nuclei in η producing reactions near threshold. The $p^6Li \rightarrow \eta^7Be$ is one such reaction, for which in 1993, the Turin group performed measurements at the incident beam energy, T_p , of 683 MeV [2] and a theoretical study of the same [3] concluded that the experimental findings did not indicate formation of $\eta - ^7Be$ quasi-bound states. However, the interest in this reaction has been regenerated by recent study of this reaction at COSY at $T_p = 673$ MeV [4], whose analysis is in process. We study the $p^6Li \rightarrow \eta^7Be$ reaction with main focus on the $\eta - ^7Be$ final state interaction.

2 The Formalism

Considering the 6Li and the 7Be nuclei as $^4He - d$ and $^4He - ^3He$ clusters, the production mechanism is assumed to proceed through a collision of the beam proton with the deuteron in 6Li -nucleus to produce η and 3He as in [3] (see Fig.1). The T-matrix including the $\eta - ^7Be$ interaction can be expressed

¹neelam@physbu.mu.ac.in

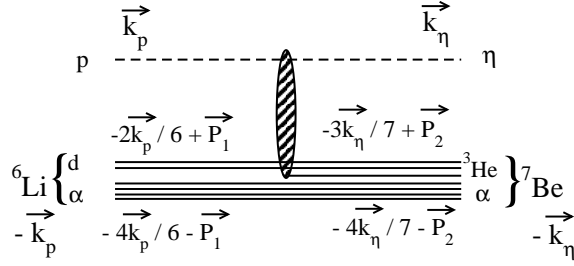


Figure 1: The reaction mechanism for $p^6Li \rightarrow \eta^7Be$ reaction.

as,

$$T = \langle \mathbf{k}_\eta, m_7 | T_{p^6Li \rightarrow \eta^7Be} | \mathbf{k}_p; m_p, m_6 \rangle \quad (1)$$

$$+ \sum_{m'_7} \int \frac{d\mathbf{q}}{(2\pi)^3} \frac{\langle \mathbf{k}_\eta; m_7 | T_{\eta^7Be} | \mathbf{q}; m'_7 \rangle}{E(k_\eta) - E(q) + i\epsilon} \langle \mathbf{q}; m'_7 | T_{p^6Li \rightarrow \eta^7Be} | \mathbf{k}_p; m_p, m_6 \rangle.$$

where the spin projections for the proton, 6Li and 7Be have been labeled as m_p, m_6 and m_7 respectively. The production matrix is written as,

$$\langle \mathbf{q} | T_{p^6Li \rightarrow \eta^7Be} | \mathbf{k}_p \rangle = i^{(L+1)} \sqrt{4\pi} \sum_{M\mu} Y_{LM}^*(\hat{Q}) F_L(Q) \langle \frac{1}{2}, L; \mu, M_L | J, m_7 \rangle$$

$$\times \langle \frac{1}{2}, \mu | T_{pd \rightarrow ^3He\eta} | \frac{1}{2}, m_p; 1, m_6 \rangle \quad (2)$$

where, μ is the spin projection of the 3He , $F_L(Q) = \int_0^\infty r^2 dr (\psi_{\alpha^3He}^{*L}(r) j_L(Qr) \times \psi_{\alpha d}^0(r))$ is the transition form factor for $^6Li \rightarrow ^7Be$, with $\mathbf{Q} = \frac{4}{7}\mathbf{q} - \frac{2}{3}\mathbf{k}_p$. Here, $\psi_{\alpha d}^0(r)$ and $\psi_{\alpha^3He}^{*L}(r)$ are the radial wave functions for 6Li and 7Be respectively. The elementary production T-matrix, $\langle |T_{pd \rightarrow ^3He\eta}| \rangle$ is written following our earlier work [5] in two-step model. To begin with, we do the calculations by neglecting the effect of Fermi motion on $\langle |T_{pd \rightarrow \eta^3He}| \rangle$.

The $\eta - ^7Be$ interaction is incorporated through a half-off-shell $\eta - ^7Be$ T-matrix,

$$T_{\eta^7Be}(k', k, z) = \int d\mathbf{x}_1 |\psi_{\alpha^3He}(x_1)|^2 \{ T_3(k', k, a_1 x_1 z) + T_\alpha(k', k, a_2 x_1 z) \}$$

where, $T_3(k', k, a_1 x_1 z)$ and $T_\alpha(k', k, a_2 x_1 z)$ represent $\eta - ^3He$ and $\eta - ^4He$ scattering matrices, respectively. They are written as,

$$T_3(k', k, a_1 x_1, z) = t_3(k', k, a_1 x_1, z) + \frac{1}{2\pi^2} \int_0^\infty q^2 dq \frac{t_3(k', q, a_1 x_1, z)}{(z - \frac{q^2}{2\mu})}$$

$$\times T_\alpha(q, k, a_2 x_1, z), \quad (3)$$

$$T_\alpha(k', k, a_2x_1, z) = t_\alpha(k', k, a_2x_1, z) + \frac{1}{2\pi^2} \int_0^\infty q^2 dq \frac{t_\alpha(k', q, a_2x_1, z)}{(z - \frac{q^2}{2\mu})} \times T_3(q, k, a_1x_1, z) \quad (4)$$

where, x_1 is the internal Jacobi co-ordinate such that the position vector, $\mathbf{r}_i = a_i \mathbf{x}_1$, of the nuclei (${}^3He/{}^4He$) in the ${}^3He - {}^4He - \eta$ center of mass system and $z = E - |\epsilon_o| + i0$ with $|\epsilon_o|$ being the energy required for the break up of 7Be into 3He and 4He .

The $t_3(k', k, a_1x_1, z)$ and $t_\alpha(k', k, a_2x_1, z)$ -matrices have been calculated as in [6].

We have used two prescriptions for $\psi_{{}^4He d}^0$ and $\psi_{{}^4He {}^3He}^{*L}$ cluster wave functions; (1) generated using Wood-Saxon potential [3, 7, 8] and (2) Green's function Monte Carlo (GFMC) Variational wave function generated using Urbana potential [9].

3 Results and Discussion

In Fig.2, we show the total cross section as a function of Q , calculated in the plane wave approximation, and those including the FSI calculated by using an ηN t -matrix corresponding to $a_{\eta N} = 0.88 + i0.41$ fm. The results here are shown for two different wave functions used for the 6Li and 7Be nuclei as discussed above. The effect of inclusion of the final state interaction seems to change the shape of the total cross section curve as a function of excess energy drastically.

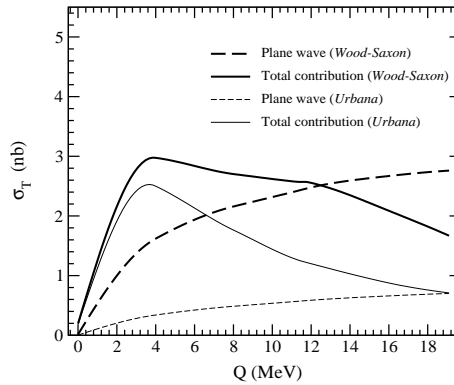


Figure 2: Total cross section as a function of Q for $a_{\eta N} = 0.88 + i0.41$ fm. The results are shown for two different prescriptions of cluster wave functions.

The results seems to be sensitive to the choice of the wave functions for

^6Li and ^7Be nuclei. In order to understand the origin of this difference, we show the sensitivity of the form factor, $F_L(Q)$, to different cluster wave functions in Fig.3.

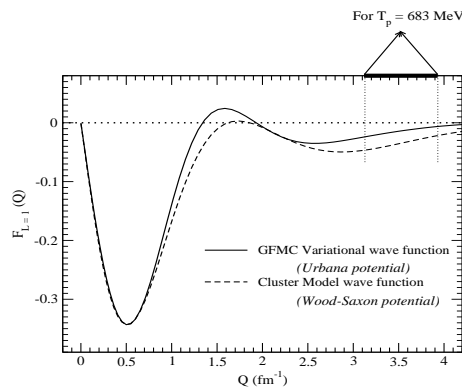


Figure 3: Sensitivity of the form factor to different cluster wave functions.

The angular distributions have also been calculated which are isotropic in nature even at the largest energy at which the calculation were carried out. At $T_p = 683$ MeV, the differential cross section is ~ 0.23 nb/sr in comparison with the experimental one [2], i.e., 4.6 ± 3.8 nb/sr.

References

- [1] R. S. Bhalerao and L. C. Liu, *Phys. Rev. Lett.* **54**, 865 (1985).
- [2] Scomparin E. *et al.*, *J. Phys. G: Nucl. Part. Phys.* **19**, L15 (1993).
- [3] J. S. Al-Khalili *et al.*, *J. Phys. G: Nucl. Part. Phys.* **19**, 403 (1993).
- [4] H. Machner *et al.*, COSY Proposal 88 (1999) and COSY Beam request 88.1-88.3 (1999).
- [5] K. P. Khemchandani *et al.*, *Nucl. Phys.* **A708**, 312 (2002).
- [6] N. G. Kelkar *et al.*, *J. Phys. G: Nucl. Part. Phys.* **32**, L19 (2006); *ibid.*, *J. Phys. G: Nucl. Part. Phys.* **32**, 1157 (2006).
- [7] B. Buck *et al.*, *J. Phys. G: Nucl. Part. Phys.* **14**, L211 (1988).
- [8] V. I. Kukulin *et al.*, *Nucl. Phys. A245*, 429 (1975).
- [9] J. L. Forest *et al.*, *Phys. Rev.* **C54**, 646 (1996).

SCALING ONSET IN THE REACTIONS $dd \rightarrow p^3H$ AND $pd \rightarrow pd$ IN THE GEV REGION

*Yu. N. Uzikov*¹

Dzhelepov Laboratory of Nuclear Problems
Joint Institute for Nuclear Research
Dubna, Moscow region, Russia, 141980

Abstract

Constituent Counting Rules (CCR) can give a definite signal for transition from meson-baryon to valence quarks level in nuclear structure. The CCR behaviour of the reactions $\gamma d \rightarrow pn$, $dd \rightarrow {}^3Hp$ and $pd \rightarrow pd$ is considered.

1 Introduction

The main goal of many experiments on deep inelastic nuclear reactions at high transferred momenta was to search for dense fluctuations of nuclear matter (multi-quark configurations). Very interesting features were observed in inclusive spectra of these reactions which can be interpreted as a manifestation of “drops” of the quark phase in nuclei (see for review Ref. [1]). However, a quantitative theory of this phenomena is still not available and, therefore, other independent signals for the transition region are necessary.

A definite signature for transition to the valence quark region is given by the constituent counting rules (CCR) [2, 3]. According to the dimensional scaling [2, 3] the differential cross section of a binary reaction $AB \rightarrow CD$ at high enough energy \sqrt{s} and transferred momentum $|t|$ can be parameterized for a given c.m.s. scattering angle θ_{cm} as

$$\frac{d\sigma}{dt}(AB \rightarrow CD) = \frac{f(t/s)}{s^{n-2}}, \quad (1)$$

where $n = N_A + N_B + N_C + N_D$ and N_i is the minimum number of point-like constituents in the i -th hadron (for a lepton and gamma one has $N_l = 1$), $f(s/t)$ is a function of θ_{cm} . The CCR follows from a self-similarity hypothesis [2] and perturbative QCD (pQCD) [3].

¹Joint Institute for Nuclear Research, Dubna, Moscow region, Russia, 141980

2 Existing CCR Data on Nuclear Reactions

High energy data for many hard processes with free baryons and mesons appear to be consistent with the CCR [4]. CCR properties were also observed in electromagnetic interactions with the deuteron. So, the reaction $\gamma d \rightarrow pn$ follows the s^{-11} scaling behaviour at photon energies $E_\gamma = 1 - 4$ GeV and high transversal momenta $p_T > 1.1$ GeV/c corresponding to large scattering angles $\theta_{cm} \sim 90^\circ$ (see Refs. [5, 6] and references therein). Meson-exchange models fail to explain the $\gamma d \rightarrow pn$ data at $E_\gamma > 1$ GeV, and therefore several nonperturbative theoretical models were suggested (see Ref. [7] and references therein).

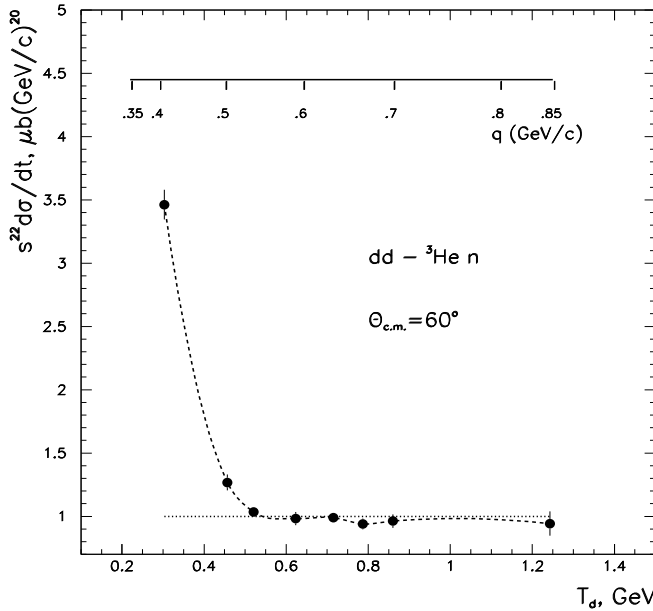


Figure 1: The cross section of the reaction $dd \rightarrow {}^3Hp$ [9] multiplied by s^{22} versus the beam energy (T_d) and internal momentum in the deuteron (q).

During last two decades, in a nuclei sector only electromagnetic processes and only on the deuteron were considered to be compatible with the CCR. However, recently it was shown [8] that the cross section of the reaction $dd \rightarrow {}^3Hp$ (and $dd \rightarrow {}^3Hen$), measured at SATURNE in 80's [9], also perfectly follows the scaling behaviour at transversal momenta $p_T \sim 0.6 - 0.9$ GeV/c (Fig.1). At the beam energy $T_d = 0.5 - 1.25$ GeV the differential cross section $d\sigma/dt$ for the maximum measured scattering angles $\theta_{cm} = 50^\circ - 60^\circ$ demonstrates the s^{-22} dependence with $\chi_{n.d.f.}^2 = 1.18$. In this reaction $n =$

$6 + 6 + 9 + 3 = 24$. Up to now, the reaction $dd \rightarrow {}^3Hen$ (3Hp) is the only pure hadronic process which involves the deuteron and 3He (3H) nuclei and found to follow the CCR. As shown in [8], the cross section of the reaction $dp \rightarrow dp$ also demonstrates the CCR behaviour $\sim s^{-16}$ at $T_d = 2T_p = 1 - 5$ GeV and $\theta_{cm} = 120^\circ - 130^\circ$, however the χ^2 -value is not good in this case, perhaps, due to different sets of the data included into analysis [8]. For other reactions with the lightest nuclei, as $dd \rightarrow dd$, $dd \rightarrow {}^4Hen\eta$, $d{}^3He \rightarrow {}^4Hep$ and $pd \rightarrow {}^3H\pi^+$, systematic experimental data at beam energies above 1 GeV and large scattering angles are absent.

3 Models

Presumably, the observed in the GeV region scaling is non-perturbative by its origin. Indeed, the pQCD is expected to be valid at very high transferred momenta and energies about hundreds GeV [10]. Furthermore, the hadron helicity conservation predicted by the pQCD was not confirmed experimentally in the scaling region of the reaction $\gamma d \rightarrow pn$ [11]. On the other hand, in these reactions the 3-momentum transfer $Q > 1$ GeV/c is large enough to probe very short distances between nucleons in nuclei, $r_{NN} \sim 1/Q$. So, one can find within the impulse approximation that at $E_\gamma = 1$ GeV and $\theta_{cm} = 90^\circ$, i.e. in the scaling onset region, the internal momentum of the nucleon in the deuteron is $q \sim 1$ GeV/c. This is very high momentum corresponding to the relative distance between nucleons $r_{NN} \sim 0.2$ fm. In the reaction $dd \rightarrow {}^3Hp$ at $T_d = 0.5 - 1.2$ GeV and $\theta_{cm} = 90^\circ$ one has $q = 0.7 - 1.1$ GeV/c. Nucleons can lose their separate identity in this overlapping region and form multi-quark configurations, which can reveal itself in the CCR scaling.

Within the constituent quark model, the observed s^{-22} behaviour shows that all constituent quarks in the initial and final state are active in the reaction $dd \rightarrow {}^3Hp$. Indeed, the nuclear matter density in the short-range configurations with high internal momenta of nucleons $q \sim 1$ GeV/c probed in this reaction, is close to the critical one, $\varepsilon_c \sim 1$ GeV/fm³, that corresponds to the phase transition [12]. On the whole, interpretation of such phenomena can be associated with the *quark-hadron duality*. So, the most accurate phenomenological description of the $\gamma d \rightarrow pn$ data was achieved within the Quark-Gluon String model formulated in terms of the Reggeon exchanges [7]. In Ref. [8] the Reggeon model [7] with some modifications was also used to describe the $dd \rightarrow {}^3Hen$ and $dp \rightarrow dp$ reactions.

One should note that the scaling behaviour s^{-11} in the reaction $\gamma d \rightarrow pn$ starts at $p_T > 1.1$ GeV/c [6], whereas the data [13] on reaction $pp \rightarrow d\pi^+$ do not follow to the expected CCR scaling regime s^{-12} at almost the same p_T

(1.0–1.4 GeV/c) at beam energy 2 - 4 GeV. The reason for absence of scaling in the reaction $pp \rightarrow d\pi^+$ can be excitation of baryon resonances in πN -interaction [14]. On the other hand, in the meson-less reaction $dd \rightarrow {}^3\text{H}p$ the s^{-22} behaviour is appeared [8] at lower p_T , 0.6 – 0.9 GeV/c.

In conclusion, the dimensional scaling is observed in several binary reactions in the few GeV region. Most likely, this behaviour is not related to the pQCD. However, this interesting phenomenon occurs at high p_T and, therefore, is certainly related to the short-range structure of the lightest nuclei. New systematic data on exclusive reactions with the lightest nuclei are required to get more insight on the origin of this scaling.

References

- [1] G.A. Leksin, *Yad. Fiz.* **65**, 2042 (2002).
- [2] V.A. Matveev, R.M. Muradyan and A.N. Tavkhelidze, *Lett. Nuovo Cim.* **7**, 719 (1973).
- [3] S.J. Brodsky and G.R. Farrar, *Phys. Rev. Lett.* **31**, 1153 (1973).
- [4] C. White et al., *Phys. Rev.* **D 49**, 59 (1994).
- [5] J. Napolitano, et al., *Phys. Rev. Lett.* **61**, 2530 (1988).
- [6] P. Rossi, et al., *Phys. Rev. Lett.* **94**, 012301 (2005);
- [7] V.Yu. Grishina et al., *Eur. Phys. J.* **A19**, 117 (2004).
- [8] Yu.N. Uzikov, *JETP Lett.* **87**, 387 (2005).
- [9] G. Bizard et al., *Phys. Rev.* **C 22**, 1632 (1980).
- [10] N. Isgur and C.H. Llewellyn Smith, *Phys. Rev. Lett.* **52**, 1080 (1984); *Phys. Lett.* **B217**, 535 (1989).
- [11] K. Wijesooriya et al., *Phys. Rev. Lett.* **86**, 2975 (2001).
- [12] F. Karsch, arXiv: hep-lat/0601013, hep-ph/0701210; V.M. Emelianov, S.L. Timoshenko, M.N. Strikhanov, *Introduction into Relativistic Nuclear Physics*, (Fizmatlit, Moskwa, 2004) (in Russian).
- [13] H.L. Andersen et al., *Phys. Rev.* **D 9**, 580 (1974).
- [14] K.A. Jenkins et al., *Phys. Rev.* **D 21**, 2445 (1980).

STUDY OF η -MESON PRODUCTION IN $dd \rightarrow {}^4He\eta$ REACTION

G.Vankova^{•,1}, M. Abdel-Bary^{*}, S. Abdel-Samad^{*}, A. Budzanowski[#], A. Chatterjee[§], J. Ernst[&], P. Hawranek⁺, F. Hinterberger[&], V. Jha[§], K. Kilian^{*}, S. Kliczewski[#], D. Kirillov[°], D. Kolev[•], M. Kravcikova[‡], M. Lesiak⁺, J. Lieb[‡], H. Machner^{*}, A. Magiera⁺, R. Maier^{*}, G. Martinska[‡], S. Nedev[∪], N. Piskunov[°], D. Prasuhn^{*}, D. Protić^{*}, J. Ritman^{*}, P. von Rossen^{*}, B. J. Roy[§], I. Sitnik[°], R. Siudak^{30#}, R. Tsenov[•], M. Ulicny[‡], J. Urban[&], C. Wilkin[×]

^{*}Institut für Kernphysik, Forschungszentrum Jülich, Jülich, Germany

[#]Institute of Nuclear Physics, Krakow, Poland

[§]Nuclear Physics Division, BARC, Bombay, India

[&]Institut für Strahlen- und Kernphysik der Universität Bonn, Bonn, Germany

⁺Institute of Physics, Jagellonian University, Krakow, Poland

[°]Laboratory for High Energies, JINR Dubna, Russia

[•]Physics Faculty, University of Sofia, Sofia, Bulgaria

[‡]Technical University, Kosice, Kosice, Slovakia

[‡]Physics Department, George Mason University, Fairfax, Virginia, USA

[‡]P. J. Safarik University, Kosice, Slovakia

[∪]University of Chemical Technology and Metallurgy, Sofia, Bulgaria

[×]Department of Physics & Astronomy, UCL, London, U.K.

Abstract The $dd \rightarrow {}^4He\eta$ reaction has been investigated at 2.39 GeV/c beam momentum. The total cross sections for polarized and unpolarized beam have been measured as well as the differential cross sections for $\cos\theta_{cm} > 0$. The cross-sections reveal strong anisotropy indicating excitation of higher partial waves at this energy.

1 Physics Motivation

Over the last years production of η meson in nucleon-nucleon interactions at energies close to threshold has been extensively investigated [1]. Extension

¹E-mail address: galia@phys.uni-sofia.bg

of the measurements to meson production in proton-deuteron and deuteron-deuteron scattering has offered a good opportunity to study the possible multi step production processes [2, 3] as well as the possible existence of eta-nucleus quasi-bound states. Data on $pd \rightarrow {}^3He\eta$ [4–6] and $dd \rightarrow {}^4He\eta$ reactions obtained in several laboratories could be interpreted as suggesting existence of bound states in eta-helium system [7–9]. The goal of $dd \rightarrow {}^4He\eta$ reaction investigation at $2.39 GeV/c$ beam momentum (reaction excess energy in the center-of-mass system $Q = 17.5 MeV$) is to provide the absent measurements at energies well above the threshold and at different polarization modes of the beam. The polarized beams allow determination of the angular distributions of respective analyzing powers and relative magnitudes of higher partial waves admixtures to the production dynamics.

2 Experiment

The measurement of reaction $dd \rightarrow {}^4He\eta$, has been performed with polarized deuteron beam delivered by the COSY accelerator in Forschungszentrum Jülich, Germany with deuteron beam momentum $2390 MeV/c$ (deuteron kinetic energy $T_d = 1160 MeV$, excess energy in the center-of-mass system $Q = 17.5 MeV$, eta c.m. momentum $(p_\eta)_{cm} = 134 MeV/c$). Available polarization states during this first measurement were: unpolarized beam and polarized one with polarization states: $P_z = -1/3$ and $P_{zz} = \pm 1$. In a Cartesian coordinate system, vector and tensor polarizations are defined as: $P_z = (N_+ - N_-)/(N_+ + N_0 + N_-)$ and $P_{zz} = (N_+ - 2N_0 + N_-)/(N_+ + N_0 + N_-)$, where N_+ , N_- and N_0 denote the number of deuterons with spin projection $+1$, -1 and 0 , respectively. The axis of polarization is perpendicular to the accelerator ring. The vector polarization of the deuteron beam has been measured with a low energy polarimeter in the injection beam line utilizing elastic scattering from a carbon target and obtained values are: $P_z = -0.32 \pm 0.02$ for the case of $P_{zz} = +1$, and $P_z = -0.33 \pm 0.02$ for $P_{zz} = -1$. The tensor polarization has been determined in this experiment measuring of the $d\mathbf{p}$ backward elastic scattering reaction at $\theta_{cm} = 180^\circ$ [10]. Outgoing deuterons have been identified by energy losses and time-of-flight measurements in the focal plane of the Big Karl magnetic spectrometer. The P_{zz} has been obtained using our value for the above cross-section, and the value of tensor analyzing power T_{20} measured at 180° in broad energy interval including our energy. The measurement [10] has given the following values for the tensor polarization: $P_{zz} = -0.60 \pm 0.11 \pm 0.01$ for nominal tensor polarization -1 and $P_{zz} = 0.81 \pm 0.14 \pm 0.01$ for tensor polarization $+1$. Here the first error is statistical one and the second one accounts for systematics.

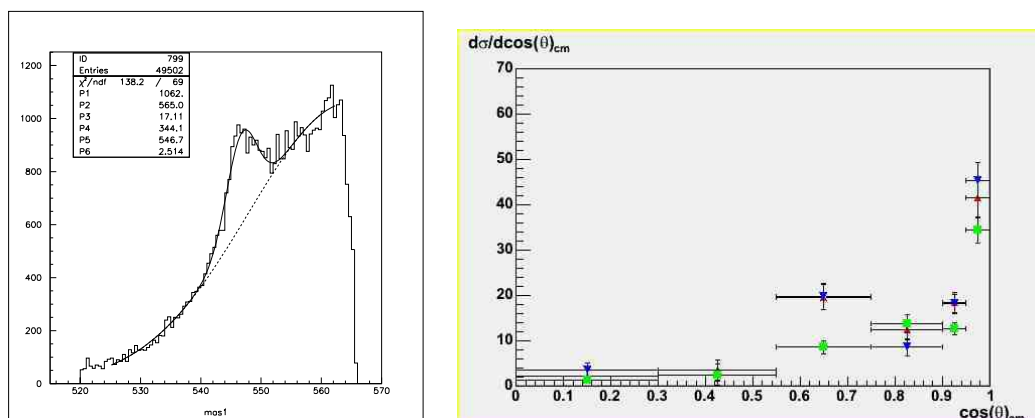


Figure 1: *Left panel:* Missing mass distribution for $P_{zz} = +1$. *Right panel:* Differential cross-sections for unpolarized and $P_{zz} = \pm 1$ beam. The blue down and red up triangles denote the differential cross-sections for tensor polarization -1 and +1 and the green squares denote the unpolarized differential cross-sections.

Helium nuclei from the reaction $dd \rightarrow {}^4He\eta$ have been detected with Big Karl magnetic spectrometer [11]. Its momentum acceptance is $\pm 4.5\%$ of the central value and for this experiment the central value has been chosen in such a way that particles with $\cos\theta_{cm} > 0$ are registered. Particle tracks are measured with two packs of multi-wire drift chambers allowing precise determination of their positions and angles in the focal plane. Two scintillator hodoscope layers located behind the focal plane, 3.8 m apart of each other, provide energy loss and time-of-flight measurement, as well as a start signal for the drift chambers. After selection of tracks belonging to alpha particles we have reconstructed their four-vectors at the target. Small correction, of about 2 MeV in average, for energy losses in the 4 mm thick liquid deuterium target has been applied, too. η - mesons in the final state have been identified by missing mass technique. An example is the spectrum on the left panel of Fig. 1, where the distribution of events over the missing mass to the 4He nucleus is shown. The peak is fitted with Gaussian and the background with a polynomial. Missing mass resolution is around 2.7 MeV, in agreement with our earlier experiments [13]. Particle flux on the target has been measured by luminosity monitors, independently for each polarization state and with systematic uncertainty of about 5–8%. For the unpolarized beam the total flux was 3.25×10^{13} particles and for $P_{zz} = +1$ and $P_{zz} = -1$ it was 2.25×10^{13} and 2.19×10^{13} particles, respectively. In order to find the angular distributions of the helium particles from the investigated reaction, we have divided the $\cos\theta_{cm}$ interval $[0 - 1]$ into 6 angular bins for each polarization

state of the beam. In each bin a spectrum similar to that on the left panel of Fig. 1 has been constructed. Then we have fitted the spectrum by a Gaussian and polynomial background. Obtained this way number of η -mesons in each angular bin was used to evaluate respective differential cross-section.

According to the theory of observables in reactions with polarized particles the differential cross section of a reaction induced by polarized deuterons is:

$$\frac{d\sigma}{d\Omega}(\theta, \varphi) = \frac{d\sigma}{d\Omega}(\theta)_{unpol.} \times \left[1 - \frac{1}{2}\tau_{20}T_{20}(\theta) + \sqrt{2}\tau_{10}iT_{11}(\theta)\cos\varphi - \sqrt{\frac{3}{2}}\tau_{20}T_{22}(\theta)\cos 2\varphi \right] \quad (1)$$

where τ_{10} and τ_{20} are the vector and tensor polarization of the beam in irreducible tensor representation, T_{20} , T_{11} , T_{22} are the respective analyzing powers in the same representation. If we assume that close to threshold only S and P waves contribute to the reaction amplitude the analyzing powers can be expressed as:

$$\begin{aligned} T_{11}(\theta) &= \frac{3}{2\sqrt{10}}\text{Im}(a_0a_1^*)\sin\theta, \\ T_{20}(\theta) &= \frac{1}{3}a_0 - \frac{9}{10}a_1^2\sin^2\theta, \\ T_{22}(\theta) &= \frac{9\sqrt{3}}{40}a_1^2\sin^2\theta, \end{aligned}$$

where a_0 and a_1 denote amplitudes for S and P wave, respectively. Measuring the differential and total cross-sections one can extract T_{11} , T_{20} and T_{22} , partial wave amplitudes and, therefore, the scattering length of the reaction.

3 Results

We have obtained the following total cross-sections:

$$\begin{aligned} \sigma_{tot}(unpol) &= 14.32 \pm 1.18 \text{ nb}, \\ \sigma_{tot}(P_{zz} = +1) &= 20.79 \pm 2.05 \text{ nb}, \\ \sigma_{tot}(P_{zz} = -1) &= 20.32 \pm 1.96 \text{ nb}. \end{aligned}$$

Errors are statistical only The systematic error is estimated to be of about 15%. Differential cross sections are plotted on Fig. 1

Apart from this measurement there are only three other measurements of $d + d \rightarrow {}^4He + \eta$ reaction available [7–9]. Two of them have been performed with unpolarized beam [7, 9] and one with polarized one [8]. In the SPES3 experiment [8] it is assumed that only S-wave is excited and the unpolarized cross section is 2/3 of the polarized one. However, the angular distribution obtained by ANKE group suggests the presence of higher partial waves [9].

The strong rise of measured differential cross sections with $\cos\theta_{cm}$ seen in Fig. 1(right panel) also indicates an influence of higher partial waves. At our energy point which is 9.2 MeV above the last point of SPES3 measurement [8] the value of the polarized cross section we got is consistent with the value of 22.4 ± 1.6 nb measured by that group.

References

- [1] J.Bijens, G.Fäldt, B.Nefkens: *Physica Scripta T99* (2002).
- [2] K.Kilian, H.Nann, E.J.Stephenson : *AIP Conf.Proc. N.221* (1990).
- [3] G.Fäldt, C.Wilkin: *Nucl. Phys.A* **587**, 769 (1995).
- [4] J.Berger et al. : *Phys. Rev.Lett.*, **61**, 919 (1988).
- [5] B.Mayer et al. : *Phys. Rev.C* **53**, 2068 (1996).
- [6] S.P.Berthet et al. : *Nucl. Phys.A* **443**, 589 (1985).
- [7] R.Frascaria et al.: *Phys. Rev. C* **50** R 537 (1994).
- [8] N.Willis et al.: *Phys. Lett. B* **406** 143 (1997).
- [9] A. Wronska et al: *Eur.Phys.J.A* **26421** (2005).
- [10] M.Lesiak et al. : *hep-ex/0512033v1*
- [11] M. Drochner et al. : *Nucl.Phys. A* 643 (1998).
- [12] G.Fäldt, C.Wilkin: *Nucl. Phys. A* **596**, 488 (1996).
- [13] M. Abdel-Barry et al. : *Phys.Rev. C*63 0440011 (2001).

SOLITON MODEL APPROACH TO KAON-NUCLEON SCATTERING IN THE PENTAQUARK CHANNEL

H. Weigel
Fachbereich Physik
Siegen University
D-57068 Siegen

Abstract

In soliton models for baryons the congruous description of hadronic decays of baryon resonances that are described as collective excitations has been a long standing problem. Here I present a solution to this problem for the pentaquark channel in the Skyrme model. The resulting kaon-nucleon scattering amplitude satisfies large N_C consistency conditions and falsifies estimates of tiny pentaquark widths that are based on axial current matrix elements. Rather this specific soliton model predicts the width to be about 50MeV and a mass of about 1800MeV, which are typical hadronic scales.

1 Introduction

Soliton models for baryons are based on action functionals of meson fields, $\Gamma = \Gamma[\Phi]$. These action functionals contain classical (static) soliton solutions, Φ_{cl} , that are identified as baryons. Their interaction with mesons is described by the (small) meson fluctuations about the soliton: $\Phi = \Phi_{\text{cl}} + \phi$. By pure definition, the expansion of $\Gamma[\Phi]$ about Φ_{cl} does not contain a term that is linear in ϕ to be interpreted as Yukawa interaction. As in experiment, resonance properties must be extracted from meson baryon scattering amplitudes. Two-meson processes acquire contributions from $\Gamma^{(2)}$, the $\mathcal{O}(\phi^2)$ piece in the expansion of $\Gamma[\Phi]$ about Φ_{cl} . It simultaneously represents the systematic (but not accurate) expansion in N_C , the number of color degrees of freedom: $\Gamma = \mathcal{O}(N_C)$, $\Gamma^{(2)} = \mathcal{O}(N_C^0)$ while terms $\mathcal{O}(\phi^3)$ vanish as $N_C \rightarrow \infty$. Hence $\Gamma^{(2)}$ contains all large- N_C information about hadronic decays of resonances. Conversely, this sheds light on *ad hoc* computations of hadronic decay widths in soliton models: The large- N_C limit of their results *must* be identical to those obtained from $\Gamma^{(2)}$. Unfortunately, the most prominent baryon resonance, the Δ , is stable for $N_C \rightarrow \infty$ and its decay is not subject

to this litmus-test. Soliton models in flavor $SU(3)$ are more challenging: In the so-called *rigid rotator approach* (RRA) resonances emerge that dwell in the anti-decuplet representation of flavor $SU(3)$. The most discussed (and disputed) such state is the Θ^+ pentaquark with zero isospin and strangeness $S = +1$. The decay properties of anti-decuplet states are indeed $\mathcal{O}(N_C^0)$. For $S = -1$ the equations of motion for ϕ yield a P -wave bound state that serves to describe the ordinary hyperons, whence the notion *bound state approach* (BSA). The litmus-test requires that the BSA and RRA give identical results for the Θ^+ properties as $N_C \rightarrow \infty$. This did not seem true and it was prematurely argued that pentaquarks were a mere artifact of the RRA [1]. Hence the comparison between the BSA and RRA serves (i) to verify that the pentaquark is a genuine prediction of soliton models and (ii) to provide an unambiguous computation of pentaquark widths. Details of these Skyrme model studies are reported in ref. [2]. Ref. [3] may be consulted for a review on $SU(3)$ soliton models.

2 Rotation–Vibration Approach & Θ^+ width

Restricting the P -wave fluctuations to the modes spanned by rigid rotations yields two bound states of strangeness $S = \pm 1$ with energies

$$\omega_{\pm} = \frac{1}{2} \left[\sqrt{\omega_0^2 + \frac{3\Gamma}{2\Theta_K} \pm \omega_0} \right] \quad \text{where} \quad \omega_0 = \frac{N_C}{4\Theta_K}. \quad (1)$$

Here Θ_K is the moment of inertia for the rotation of the soliton into strangeness direction and Γ is the functional that measures flavor symmetry breaking. Both functionals are $\mathcal{O}(N_C)$ so that $\omega_{\pm} = \mathcal{O}(N_C^0)$. While ω_- is the energy of the above mentioned bound state describing ordinary hyperons, ω_+ is eventually utilized to construct pentaquark states. When the restriction that BSA modes η are spanned by the rigid rotation is waived, $\omega_- < m_K$ corresponds to a true bound state but ω_+ turns into a continuum state. Thus, a pronounced resonance structure would be expected around $\omega = \omega_+$. Unfortunately, this is not the case, as is seen from fig. 1 [1].

In the RRA the collective coordinates $A(t) \in SU(3)$ that parameterize the flavor orientation of the soliton are canonically quantized. The resulting Hamiltonian is exactly diagonalized for arbitrary (odd) N_C [2] and symmetry breaking [4]. The resulting mass difference between the states that for $N_C = 3$ correspond to the Λ (Θ^+) and the nucleon, approaches ω_- (ω_+) as $N_C \rightarrow \infty$.

The ultimate comparison requires to generalize the RRA to the *rotation–vibration approach* (RVA)

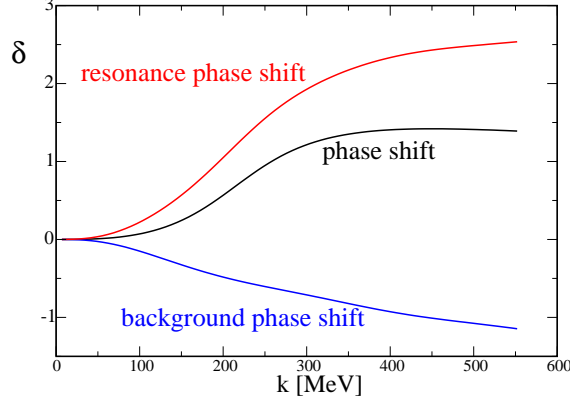


Figure 1: Phase shift in the BSA (middle, black line) and the resonance phase (top, red line) shift after removal of the background (bottom, blue line) contribution in the RVA that emerges from the constraint $\langle \eta|z \rangle = 0$.

$$U(\mathbf{x}, t) = A(t)\xi_0(\mathbf{x}) \exp \left[\frac{i}{f_\pi} \sum_{\alpha=4}^7 \lambda_\alpha \tilde{\eta}_\alpha(\mathbf{x}, t) \right] \xi_0(\mathbf{x}) A^\dagger(t), \quad (2)$$

where $\xi_0(\mathbf{x}) = \exp[i\hat{\mathbf{x}} \cdot \tau F(|\mathbf{x}|)/2]$ is the chiral field representation of the soliton (Φ_{cl}). Avoidance of double counting enforces the constraint $\langle \tilde{\eta}|z \rangle \stackrel{!}{=} 0$, where $z \sim \sin(F/2)$ is the collective mode wave–function. Eq. (2) generates a term in $\Gamma^{(2)}$ that is linear in both $\tilde{\eta}$ and the collective modes, parameterized by $A(t)$. This contribution corresponds to Yukawa exchanges and induces a separable potential V_Y for $\tilde{\eta}$. In ref. [2] we have shown that in the limit $N_C \rightarrow \infty$ the resulting equation of motion is solved by $\tilde{\eta} = \eta - \langle z|\eta \rangle z$.

Thus the BSA and RVA are indeed equivalent in the large N_C limit since the phase shifts extracted from η and $\tilde{\eta}$ are identical as $z(|\mathbf{x}|)$ is localized in space. Furthermore, the RVA provides a distinction between resonance and background contributions. Applying the R –matrix formalism shows that for $N_C \rightarrow \infty$ V_Y *exactly* contributes the resonance phase shift shown in fig. 1. Thus pentaquarks are also predicted by the BSA; just well hidden. Yet, collective coordinates are mandatory to obtain finite N_C corrections: *e. g.*, for $m_K = m_\pi$ the mass difference $M(\Theta) - M(N)$ increases by a factor two from ω_0 to $(N_C + 3)/4\Theta_K$. Skyrme model calculations indicate that $M(\Theta) - M(N)$ might be as large as 900MeV [2]. The R –matrix formalism

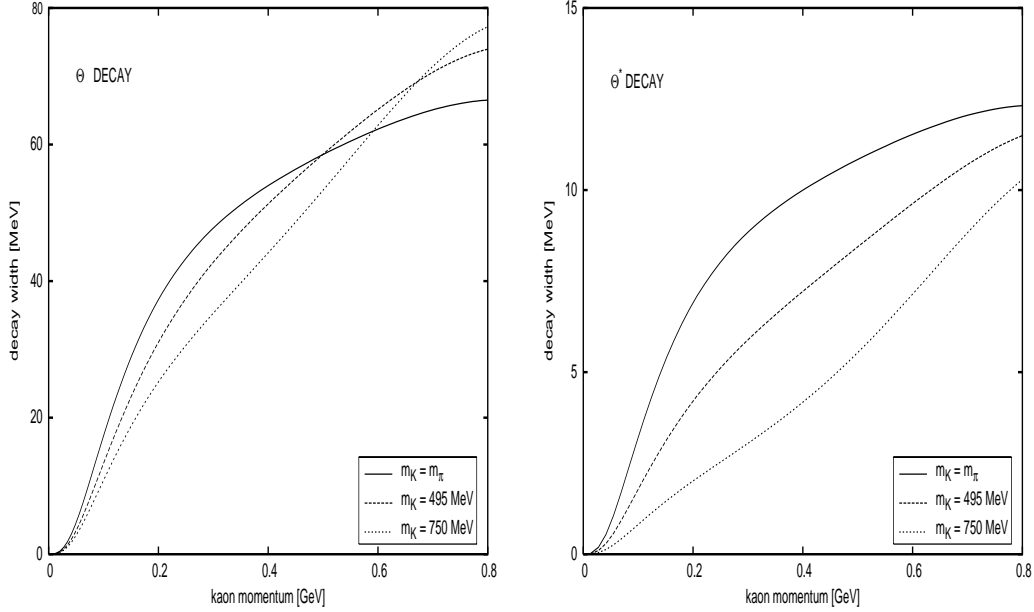


Figure 2: Skyrme model prediction for the decay width, $\Gamma(\omega)$ of Θ^+ and its iso-partner Θ^{*+} for $N_C = 3$ as function of the kaon momentum $k = \sqrt{\omega^2 - m_K^2}$, cf. eq. (3).

finally yields the Θ^+ width as a function of the kaon momentum [2]

$$\Gamma(k) = 2k\omega_0 \left| X_\Theta \int_0^\infty r^2 dr z(r) 2\lambda(r) \bar{\eta}_{\omega_k}(r) \right|^2 + \mathcal{O}(m_K^2 - m_\pi^2). \quad (3)$$

Here $\bar{\eta}_{\omega_k}(|\mathbf{x}|)$ is the P-wave background wave-function ($\bar{\eta} \hat{=} \tilde{\eta}$ for $V_Y \equiv 0$) with energy $\omega_k = \sqrt{k^2 + m_K^2}$, $\lambda(|\mathbf{x}|)$ is a radial function that stems from the Wess-Zumino term and X_Θ is the nucleon- Θ^+ transition matrix element of a collective coordinate operator. The resulting width is shown for $N_C = 3$ in fig. 2. Typical – though model dependent – results yield a Θ^+ width of around 50MeV [2]. Remarkably, the width of the Θ^{*+} , the $I = 1$ partner of Θ^+ , turns out smaller. In any event, it seems very unlikely that chiral soliton models predict a light long-living pentaquark.

3 Conclusion

Here I have compared the BSA and RRA to chiral soliton models. While the former gives the exact model results in the large N_C limit and thus serves as a litmus-test, the latter incorporates substantial finite N_C corrections. This comparison requires the consideration of harmonic oscillations in the

RRA as well. They are incorporated via the RVA which clearly shows that pentaquarks are genuine resonances within chiral soliton models.

In the flavor symmetric case the interaction Hamiltonian contains only a *single* structure (X_Θ in eq. (3)) of $SU(3)$ matrix elements for the $\Theta^+ \rightarrow KN$ transition. This proves earlier soliton model approaches [5] incorrect that adopted any possible structure that could contribute and fitted coefficients from a variety of hadronic decays under the assumption of $SU(3)$ relations.

Since the presented analysis merely concerns the treatment of kaon degrees of freedom, the qualitative results are valid for *any* chiral soliton model. In essence, these models do not predict very light and very narrow pentaquark resonances.

Acknowledgments

This presentation is based on a collaboration with H. Walliser whose contribution is gratefully acknowledged. This work is supported in parts by DFG under contract We 1254/13-1.

References

- [1] N. Itzhaki *et al.*, Nucl. Phys. **B684** (2004) 264; T. D. Cohen, Phys. Lett. **B581** (2004) 175; Phys. Rev. **D70** (2004) 014011; A. Cherman *et al.*, Phys. Rev. **D72** (2005) 094015.
- [2] H. Walliser, H. Weigel, Eur. Phys. J. A **26** (2005) 361; H. Weigel, Eur. Phys. J. **A31** (2007) 495; arXiv:0704.2281 [hep-ph]; Phys. Rev. **D75** (2007) 114018.
- [3] H. Weigel, Int. J. Mod. Phys. **A11**, 2419 (1996); H. Weigel, *Chiral Soliton Models for Baryons*, Springer Lecture Notes in Physics **743**.
- [4] H. Yabu, K. Ando, Nucl. Phys. **B301** (1988) 601.
- [5] D. Diakonov, V. Petrov, M. Polyakov, Z. Phys. **A359** (1997) 305; J. R. Ellis, M. Karliner, M. Praszalowicz, JHEP **05** (2004) 002; M. Praszalowicz, Acta Phys. Polon. **B35** (2004) 1625; M. Praszalowicz, K. Goeke, Acta Phys. Polon. **B36** (2005) 2255; G. S. Yang, H. C. Kim, K. Goeke, Phys. Rev. **D75** (2007) 094004.

SIMULATION OF THE $\bar{\text{P}}\text{ANDA}$ EXPERIMENT WITH PANDAROOT

Aleksandra Wrońska¹ for the $\bar{\text{P}}\text{ANDA}$ Collaboration

Institute of Physics
Jagiellonian University, Cracow
Reymonta 4,
30-059 Cracow, Poland

Abstract

$\bar{\text{P}}\text{ANDA}$ is a future experiment designed to study fundamental questions of hadron and nuclear physics. This requires capability to measure rare processes, *i.e.* excellent understanding and optimization of the detector system. Thus, extensive simulations are a must.

In autumn 2006 the $\bar{\text{P}}\text{ANDA}$ collaboration decided to migrate to a new simulation framework, called PandaRoot. The code is based upon the FairRoot project, which is strongly supported at GSI. Here, basic features of PandaRoot are discussed, *i.e.* its structure, supported platforms, event generators, transport codes, reconstruction and analysis. Examples of results from the complete simulation chain for a selected detector are presented.

1 The $\bar{\text{P}}\text{ANDA}$ experiment

Within the next few years, a new international facility FAIR (Facility for Antiproton and Ion Research) will be built in GSI–Darmstadt. One of its components is the High Energy Storage Ring (HESR) providing high-quality beams of antiprotons with momenta up to 15 GeV/c. $\bar{\text{P}}\text{ANDA}$ is a future large-scale detector system, located on the internal target station, which will exploit this beam.

The physics program of the $\bar{\text{P}}\text{ANDA}$ project is focused on studying the non-perturbative regime of QCD and is discussed in Ref. [1].

Planned measurements impose stringent requirements on the detector system. For example, it provides an almost full coverage of the solid angle,

¹E-mail address: wronska@if.uj.edu.pl

good particle identification in a large momentum range, good vertex and momentum resolution along with high count-rate capability. Current status of the detector design is presented in Ref. [2].

2 The PandaRoot Framework

PandaRoot is a next-generation computing framework being developed by the $\overline{\text{PANDA}}$ collaboration in synergy with other FAIR-related software activities within the joint FairRoot project. The framework serves both simulation and analysis, and will be described in the following subsections.

2.1 Objectives

The simulation studies of $\overline{\text{PANDA}}$ are detector- and physics-related.

To the first group belong simulations aiming to improve the detector setup by optimizing the acceptances and resolutions. The discrimination power of the particle identification detectors is also of vital importance. In view of the very high interaction rate of the order of 10^7 s^{-1} , simulations are helpful in choosing the appropriate granularity and provide hints that for certain regions a different detector type should be considered. Moreover, for $\overline{\text{PANDA}}$ the triggerless data acquisition system is foreseen [3]. Its proper design requires a good knowledge of total data rates of the overall detection system as well as of the individual components. Also, strategies to reduce the online data stream from about 100 GB/s to 100 MB/s are being developed and verified by simulations.

The other group of activities focuses on tests of physics-related detector performances. For this purpose, the strategies of the analysis of simulated and experimental data are being developed and tested via feasibility studies for several benchmark channels. A list of benchmark channels is given in Ref. [4].

2.2 Main Features

The main features characterizing the PandaRoot computing framework are the following:

- it serves simulations as well as data analysis;
- it is fully ROOT-based [5], which ensures good support, easy maintenance and – of crucial importance for the environment with a continuous human-power flow – a low threshold for newcomers;
- it is prepared to run on the Grid network;

- it is portable: it compiles on several different Linux flavors with many compiler versions. This feature is continuously monitored via the Quality Assurance Dashboard system, which collects compilation statistics from all sites hosting PandaRoot.

2.3 Structure of the Framework

The structure of the framework is presented schematically in Fig. 1 and described in more detail in Ref. [6]. The heart of the design is the Run Manager,

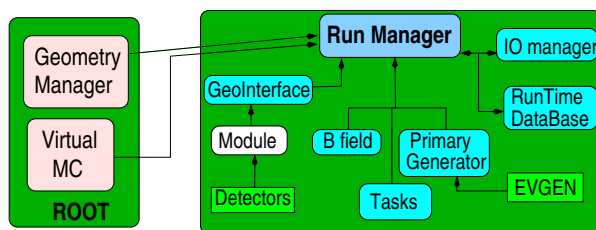


Figure 1: Schematic representation of the design of PandaRoot.

which manages the overall program flow and the communication between the different modules, namely Geometry Interface, Event Generator, IO Manager and Virtual Monte Carlo. The latter is based on a particularly interesting concept offering a possibility to switch between different transport codes (currently available are Geant3, Geant4 and Fluka) without recompilation of the code. Different analyses or operations performed on a certain set of data are plugged in to the Run Manager as Tasks, thus ensuring modularity. Moreover, tasks can be organized in a hierarchy, thereby, allowing complicated and user-defined analysis schemes.

Several event generators have been integrated into PandaRoot: Dual Parton Model [7], EvtGen [9], Pluto++ [8] and UrQMD [10]. These generators provide a model for the total $\bar{p}p$ cross-section, resonance decay trees, hadronic processes and nuclear reactions $\bar{p}A$, respectively.

Currently the \bar{P} ANDA computing group is finishing the implementation of the individual detectors in the framework. For most of the detectors, the digitization part has been implemented as well. Various reconstruction algorithms and advanced analysis tools, such as a Kalman filter and channel composition tools, are being developed in parallel.

2.4 Example of Use

Already within the present simulation framework it is possible to perform advanced physics simulations for some detectors. As an illustration, the

reconstruction of J/ψ mass from the following process: $\bar{p}p \rightarrow Y(4260) \rightarrow J/\psi \pi^+\pi^- \rightarrow e^+e^-\pi^+\pi^-$ is shown in Fig. 2. The simulation chain comprises

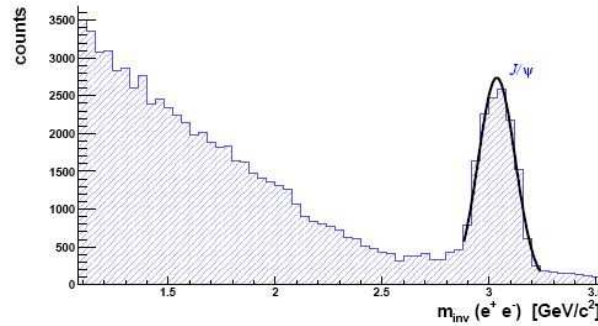


Figure 2: The reconstructed e^+e^- invariant mass for the decay of J/ψ .

event generation, simulation, track reconstruction and combinatorial analysis, for which the electron mass was assigned to all tracks.

3 Summary

PandaRoot is a versatile and a portable framework for simulation and analysis of the \bar{P} ANDA experiment. The implementation of the individual detector components is nearly finished. Furthermore, the development of advanced tools for reconstruction and analysis is in progress. The framework has already been used to optimize detector components. The first physics analyses have been performed as well.

Acknowledgments

We acknowledge the support of the European Community under the FP6 Design Study program - DIRAC Secondary Beams (grant 515873(RIDS)) and of the Polish Ministry of Science and Higher Education (grant 65/6.PR UE/2006/7).

References

- [1] J. Messchendorp, contribution to these proceedings.
- [2] K. Föhl, contribution to these proceedings.
- [3] L. Schmitt *et al.*, Modelling of the architectural studies for the PANDA DAT system, in *Proc. 15th IEEE Real Time Conference 2007*.
- [4] \bar{P} ANDA collaboration, *Technical Progress Report*, February 2005, www-panda.gsi/archive/public/panda_tpr.pdf
- [5] <http://root.cern.ch>

- [6] M. Al-Turany *et al.* in GSI Scientific Report 2004, FAIR-EXP-07,
M. Al-Turany, D. Bertini in GSI Sci. Rep. 2005, FAIR-QCD-CBM-10,
PANDA Computing Group in GSI Sci. Rep. 2006, FAIR-EXPERIMENTS-02.
- [7] V. V. Uzhinsky and A. S. Galoyan, hep-ph/0212369
- [8] <https://www-hades.gsi.de/computing/pluto/html/PlutoIndex.html>
- [9] <http://www.slac.stanford.edu/~lange/EvtGen>
- [10] <http://th.physik.uni-frankfurt.de/~urqmd/>

MEASUREMENT OF THE REACTION $dd \rightarrow \alpha K^+ K^-$ WITH ANKE/COSY

X. Yuan^{*§#1}, A. Dzyuba^{#%} and M. Büscher[#]
for the ANKE Collaboration

^{*}Institute of Modern Physics, Chinese Academy of Sciences, Lanzhou,
P.R. China

[§]Graduate University, Chinese Academy of Sciences, Beijing, P.R. China

[#]Institut für Kernphysik, Forschungszentrum Jülich, Germany

[%]High Energy Physics Department, Petersburg Nuclear Physics Institute,
Gatchina, Russia

Abstract

High resolution studies of $a_0/f_0(980)$ decays into channels involving open strangeness are currently being performed at COSY-Jülich. Here we report about a measurement of the $dd \rightarrow \alpha K^+ K^-$ reaction with the magnetic ANKE spectrometer. This reaction can be used as a “filter” for isospin-zero intermediate states, *i.e.* to selectively produce the $f_0(980)$ resonance.

1 Introduction

Quantum-chromodynamics (QCD) is the theory of strong interactions. The properties of QCD at low energies or small momentum transfers (“strong QCD”) are yet poorly known and are among the few uncharted territories of the Standard Model.

A better understanding of strong QCD can be achieved from the investigation of its symmetries and their breaking as well as the spectroscopy of strongly bound quark states (hadrons).

Precise knowledge of the $a_0(980)$ and $f_0(980)$ coupling constants to kaons would allow one to determine the $K\bar{K}$ content of the a_0/f_0 . However, the values for $g_{a_0 K\bar{K}}$ and $g_{f_0 K\bar{K}}$ are still poorly known. The isospin-violating (IV) a_0/f_0 mixing amplitude is in leading order proportional to the product of $g_{a_0 K\bar{K}}$ and $g_{f_0 K\bar{K}}$ [1,2]. Since the a_0 and the f_0 are rather narrow overlapping

¹E-mail address: x.yuan@fz-juelich.de

resonances, a_0 - f_0 mixing should give the dominant contribution to the IV effect via the reaction chain $dd \rightarrow \alpha f_0(I=0) \rightarrow \alpha a_0^0(I=1) \rightarrow \alpha(\pi^0\eta)$ [2, 3]. Any observation of $\pi^0\eta$ production in the $dd \rightarrow \alpha X$ reaction would be a direct indication of IV.

An experiment on the IV reaction $dd \rightarrow \alpha(\pi^0\eta)$ is under preparation for WASA-at-COSY. As a first step, we aim at the determination of the isospin-conserving $dd \rightarrow \alpha f_0$ cross section via a measurement of the $dd \rightarrow \alpha f_0 \rightarrow \alpha K^+ K^-$ process.

2 Event identification

In order to identify the rare $dd \rightarrow \alpha K^+ K^-$ events, two charged particles, K^+ and α , have been detected in coincidence at ANKE during an experiment in April 2006.

Positively charged Kaons can be identified in the side detection system(SD) [4,5] of ANKE by a time-of-flight (TOF) measurement (see Fig. 1), by energy-loss cuts, and by measuring the delayed decay $K^+ \rightarrow \mu^+ X$. The latter criterion allows for a very clean K^+ identification, however at reduced detection efficiency. The $dd \rightarrow \alpha K^+ K^-$ events presented here have been obtained with that criterion, for the final analysis we are aiming at a softer K^+ selection and, thus, increased statistics.

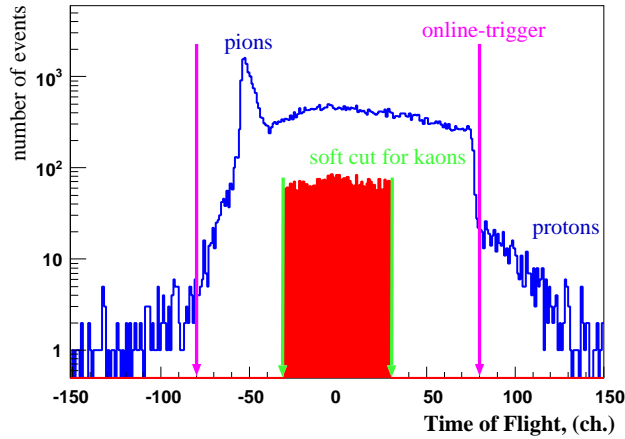


Figure 1: The TOF distribution of positively charged particles. The shaded area shows the TOF cut of kaons after background suppression via track selection and vertical angle cuts.

The TOF start counters, consisting of one layer of 23 scintillation counters, have been mounted next to the large exit window of the vacuum chamber

inside the D2 magnet of ANKE. Kaons from f_0 decay have been stopped in range telescopes that comprise the TOF stop counters. Two multi-wire proportional chambers (MWPCs) positioned between the TOF start and stop counters allow one to deduce the ejectile momenta and to suppress background from secondary scattering [6, 7].

Fast particles produced in coincidence with the K^+ candidates as well as elastically scattered deuterons have been detected in the ANKE forward-detection system (FD) [8] which contains two layers of scintillation counters for TOF and δE measurements. In addition there are three MWPCs, each with two sensitive planes, which have been exploited for momentum reconstruction and background suppression [4, 7]. Using a cut on time difference between the fast forward-going particles and K^+ , two bands of protons and deuterons are distinguished and some hints on α 's can be seen in Fig. 2.

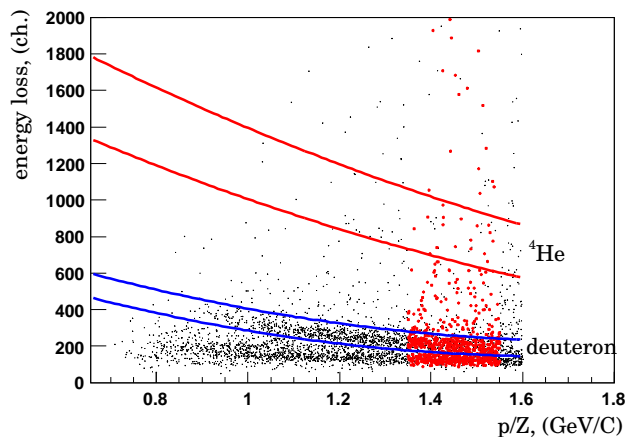


Figure 2: Energy loss in the first layer of the hodoscope *vs.* the rigidity of particles in FD. According to the phase space of the reaction $dd \rightarrow \alpha K^+ K^-$ the rigidity of α should be between 1.3 and 1.6 GeV/C.

In the missing-mass distribution of the $dd \rightarrow \alpha K^+ X$ events, some K^- candidates can be seen in the red area of Fig. 3.

3 Result and Outlook

An attempt to measure the $dd \rightarrow \alpha K^+ K^-$ reaction has been made at the ANKE spectrometer. About 10 $dd \rightarrow \alpha K^+ K^-$ candidates have been identified in a preliminary analysis. The cross section of the $dd \rightarrow \alpha f_0 \rightarrow \alpha K^+ K^-$ process will be deduced from an ongoing analysis from which an increased

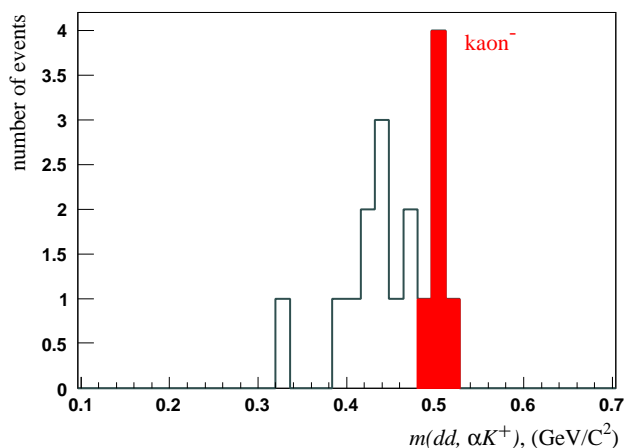


Figure 3: Missing-mass $m(dd, \alpha K^+)$ distribution of the $dd \rightarrow \alpha K^+ X$ events. The shaded area indicates the K^- candidates.

number of events is expected. A new proposal for the final experiment $dd \rightarrow \alpha(\pi^0\eta)$ with WASA-at-COSY is under preparation.

References

- [1] N. N. Achasov et al., *Phys. Lett.* **B 88**, 367 (1979).
- [2] C. Hanhart et al., *Phys. Rept.* **397**, 155 (2004) [arXiv:hep-ph/0311341].
- [3] V. Y. Grishina et al., *Phys. Lett.* **B 521**, 217 (2001).
- [4] S. Barsov et al., *Nucl. Instrum. Methods Phys. Res.* **A 462**, 364 (2001).
- [5] M. Büsche et al., *Nucl. Instrum. Methods Phys. Res.* **A 481**, 378 (2002).
- [6] V. Kleber, et al., *Phys. Rev. Lett.* **36**, 172304 (2003).
- [7] P. Fedorets, et al., *Phys. At. Nucl. (Yad. Fiz.)* **69**, 306 (2006).
- [8] S. Dymov, et al. *Phys. Lett.* **B 635**, 270 (2006).

%

CASCADE RESONANCE PROPERTIES FROM CHARM BARYON DECAYS AT *BABAR*

V. Ziegler

Stanford Linear Accelerator Center
Menlo Park, CA 94025
U.S.A.

Abstract

We present studies of hyperon and hyperon resonance production in charm baryon decays at *BABAR*. Two-body decay spin formalisms are extended to three-body final states and are used to study $\Xi(1530)^0$ production in Λ_c^+ decay. Similarly, the properties of the $\Xi(1690)^0$ are extracted from a detailed isobar model analysis of the $\Lambda_c^+ \rightarrow \Lambda K_S K^+$ Dalitz plot.

1 Introduction

Although considerable advances have been made in baryon spectroscopy over the past decade, there has been very little improvement in our knowledge of cascade resonances since 1988 [2]. The $\Xi(1690)$ has been observed in the $\Lambda\bar{K}$, $\Sigma\bar{K}$ and $\Xi\pi$ final states with various degrees of certainty. Its quantum numbers have not yet been measured. The $\Xi(1530)$ has primarily been seen via its decay to $\Xi\pi$, however its spin-parity remains uncertain.

2 The $\Xi(1530)^0$ from $\Lambda_c^+ \rightarrow \Xi^-\pi^+K^+$ Decay

The $\Xi(1530)^0$ resonance is observed in the $\Xi^-\pi^+$ system produced in the decay $\Lambda_c^+ \rightarrow (\Xi^-\pi^+)K^+$. The data sample analyzed corresponds to a total integrated luminosity of $\sim 230 \text{ fb}^{-1}$ [3, 4].

The Dalitz plot for $\Lambda_c^+ \rightarrow \Xi^-\pi^+K^+$ is dominated by the contribution from $\Lambda_c^+ \rightarrow \Xi(1530)^0K^+$. The efficiency-corrected projection of the $\Xi^-\pi^+$ invariant mass for the Λ_c^+ signal region is shown in Fig. 1(a). The Dalitz plot (Fig. 1(d)) shows evidence for only one resonant structure. A clear band can be seen at the nominal mass squared of the $\Xi(1530)^0 \rightarrow \Xi^-\pi^+$.

Spin information for the $\Xi(1530)$ is obtained using Legendre polynomial moments ($P_L(\cos\theta_{\Xi^-})$, where $\cos\theta_{\Xi^-}$ is the Ξ^- helicity cosine). The $\sqrt{10}P_2(\cos\theta_{\Xi^-})$ moment of the $(\Xi^- \pi^+)$ system invariant mass distribution for the Λ_c^+ signal region indicates that spin 3/2 is clearly favored (see Fig. 1(b)), whereas the $7/\sqrt{2}P_4(\cos\theta_{\Xi^-})$ moment is consistent with being flat (Fig. 1(c)) implying that spin 5/2 is ruled out. Schlein *et al.* [5] showed that $J^P = 3/2^+$ or $J^P = 5/2^-$ and claimed $J > 3/2$ not required, thereby concluding that $J^P = 3/2^+$ was favored by their data. The present analysis by establishing $J = 3/2$ also establishes positive parity by implication.

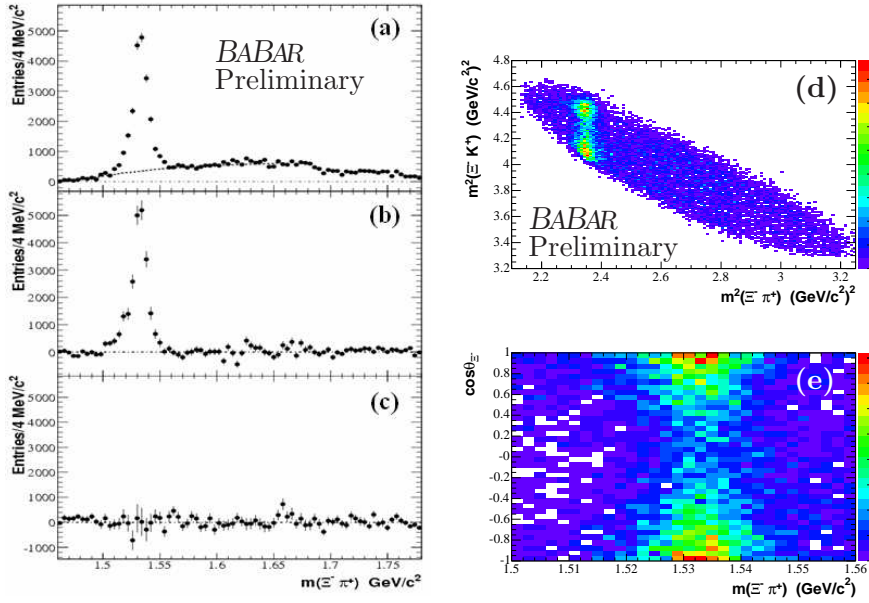


Figure 1: The Λ_c^+ -mass-sideband-subtracted (a) $m(\Xi^- \pi^+)$ projection, (b) $\sqrt{10}P_2(\cos\theta_{\Xi^-})$ and (c) $7/\sqrt{2}P_4(\cos\theta_{\Xi^-})$ moments of the $\Xi^- \pi^+$ system invariant mass distribution, for the Λ_c^+ signal region, after efficiency correction. In (a) the dashed curve represents the estimated background contribution in the $\Xi(1530)$ region. (d) The Dalitz plot of $m^2(\Xi^- K^+)$ versus $m^2(\Xi^- \pi^+)$ for the Λ_c^+ signal region. (e) The corresponding rectangular Dalitz plot for the $\Xi(1530)^0$ mass region.

3 The $\Xi(1690)^0$ from $\Lambda_c^+ \rightarrow (\Lambda \bar{K}^0) K^+$ Decay

The $\Xi(1690)^0$ is observed in the $\Lambda \bar{K}^0$ system produced in the decay $\Lambda_c^+ \rightarrow (\Lambda \bar{K}^0) K^+$, where the \bar{K}^0 is reconstructed via $K_S \rightarrow \pi^+ \pi^-$.

The data sample analyzed corresponds to a total integrated luminosity of $\sim 200 \text{ fb}^{-1}$ [3,4]. The invariant mass spectrum of the resulting Λ_c^+ candidates

before efficiency-correction and the $\Lambda\bar{K}^0$ mass distribution corresponding to the Λ_c^+ signal region are shown in Fig. 2(a) and (b), respectively. A clear peak is seen in the vicinity of the $\Xi(1690)^0$; it should be noted that this signal is skewed significantly toward high mass.

The second and fourth order Legendre polynomial moments as a function of the mass of the (ΛK_S) system display no peaking structure at the position of the $\Xi(1690)^0$, which suggests that the $\Xi(1690)^0$ spin is probably 1/2. However, the Λ helicity cosine ($\cos\theta_\Lambda$) distribution is not flat in contrast to the expectation for a spin 1/2 to 1/2 transition. The Dalitz plot of $\Lambda_c^+ \rightarrow \Lambda\bar{K}^0 K^+$ signal candidates is shown, without efficiency-correction, in Fig. 3(a). A clear band is observed in the mass-squared region of the $\Xi(1690)^0$, together with an accumulation of events in the $\bar{K}^0 K^+$ threshold region; the latter is consistent with a contribution to the Dalitz plot due to the $a_0(980)^+$ resonance. In contrast, the Dalitz plots corresponding to the Λ_c^+ mass-sideband regions exhibit no structure [3].

The Dalitz plot of Fig. 3(b) is described in terms of an isobar model consisting of the coherent superposition of amplitudes characterizing $(\Lambda a_0(980)^+)$ and $(\Xi(1690)^0 K^+)$ decay of the Λ_c^+ . The $a_0(980)$ is known to couple to both $\eta\pi$ and $\bar{K}K$ and is characterized by the Flatté parametrization [6], while a Breit-Wigner function is used to describe the amplitude for the $\Xi(1690)^0$.

The intensity distribution at a point on the Dalitz plot is described by the squared modulus of the coherent superposition of these two amplitudes, assuming that the $\Xi(1690)^0$ has spin 1/2, since the moment projections favor this choice. Fits to the Dalitz plot assuming spin 3/2 and 5/2 are poorer than for spin 1/2, and yield systematic failures in the description of the resulting $\cos\theta_\Lambda$ and $m(\Lambda K_S)$ projections [3]. The skewing of the ΛK_S invariant mass projection results from the interference between the $a_0(980)^+$ and the $\Xi(1690)^0$. The actual $\Xi(1690)^0$ signal is symmetric and smaller than the observed signal, because of significant interference effect [3].

4 Conclusions

The properties of the $\Xi(1530)^0$ are studied using the decay $\Lambda_c^+ \rightarrow \Xi^-\pi^+K^+$. The spin of the $\Xi(1530)$ is established as 3/2. The properties of the $\Xi(1690)^0$ are extracted from fits to the $\Lambda_c^+ \rightarrow \Lambda K_S K^+$ Dalitz plot. The hypothesis that the $\Xi(1690)$ has spin 1/2 yields an excellent description of the data, whereas spin values of 3/2 and 5/2 result in poorer fit probabilities, and fail to reproduce the observed skewed $\Xi(1690)$ lineshape.

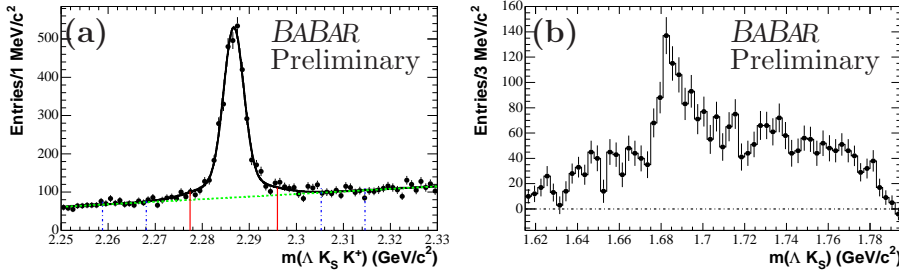


Figure 2: (a) The invariant mass distribution of uncorrected $\Lambda_c^+ K_S K^+$ candidates in data. (b) The Λ_c^+ mass-sideband-subtracted $\Lambda_c^+ K_S$ invariant mass projection of uncorrected $\Lambda_c^+ K_S K^+$ candidates.

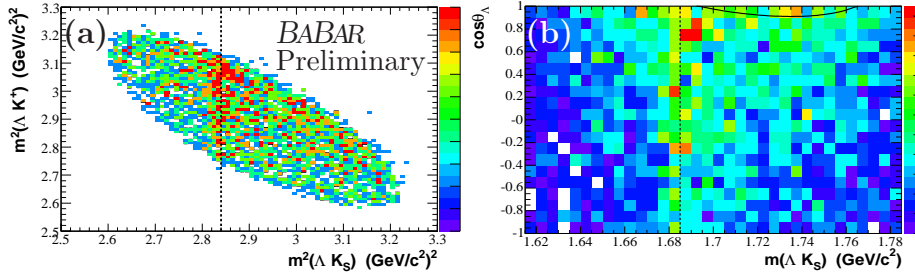


Figure 3: (a) The Dalitz plot for $\Lambda_c^+ \rightarrow \Lambda \bar{K}^0 K^+$ corresponding to the Λ_c^+ signal region indicated in Fig. 2. The dashed line indicates the nominal mass-squared region of the $\Xi(1690)^0$. (b) The rectangular Dalitz plot for $\Lambda_c^+ \rightarrow \Lambda \bar{K}^0 K^+$ corresponding to the Λ_c^+ signal region indicated in Fig. 2. The black curve corresponds to the $a_0(980)^+$ pole position.

References

- [1] B. Aubert *et al.*, Nucl. Instr. Meth. **A479**, 1 (2002).
- [2] W.-M. Yao *et al.* (PDG2006), J.Phys. G:Nucl.Part.Phys. **33**, 1 (2006).
- [3] Veronique Ziegler, *Ph.D. Thesis*, SLAC-R-868 (2007).
- [4] The use of charge conjugate states is implied throughout.
- [5] P. E. Schlein *et al.*, Phys. Rev. Lett. **11**, 167 (1963); J. Button-Schafer *et al.*, Phys. Rev. **B142**, 883 (1966).
- [6] S. M. Flatté, Phys. Lett. **B63**, 224 (1976).

STUDIES OF THE $\Lambda(1405)$ IN PROTON-PROTON COLLISIONS WITH ANKE AT COSY-JÜLICH

I. Zychor

The Andrzej Sołtan Institute for Nuclear Studies
05-400 Świerk, Poland

Abstract

The lineage of the $\Lambda(1405)$ was studied in the $pp \rightarrow pK^+Y^0$ reaction at a beam momentum of 3.65 GeV/c at COSY-Jülich. The ANKE spectrometer was used to identify two protons, one positively charged kaon, and one negatively charged pion in the final state. Invariant-mass and missing-mass techniques were applied to separate two neighbouring neutral excited hyperon resonances, the $\Sigma^0(1385)$ and $\Lambda(1405)$. Both the shape and the position of the $\Lambda(1405)$ distribution are similar to those measured in other reactions and this information contributes to the ongoing debate regarding the structure of this resonance.

1 Introduction

The $\Lambda(1405)$ is a well established four-star resonance [1] but it is still not well understood as a baryonic state; it does not fit in easily within the simple quark picture [2]. The $\Lambda(1405)$ might be the spin-multiplet partner of the $J^P = \frac{3}{2}^- \Lambda(1520)$, a meson-baryon resonance, a $\bar{K}N$ quasi-bound state [3], or a $q^4\bar{q}$ pentaquark state [4]. Recent theoretical investigations based on chiral dynamics predict the existence of two poles in the vicinity of the $\Lambda(1405)$ [5–7] with a decay spectrum that depends upon the production process. In any event, the $\Lambda(1405)$ does not have a Breit-Wigner shape because of the opening at 1432 MeV/c² of the decay mode $\bar{K}N$ [8–10]. Independent of the model, if the $\Lambda(1405)$ were a single quantum state, its lineage should be independent of the method of production.

The $\Sigma^0(1385)$ and $\Lambda(1405)$ resonances overlap significantly because their widths of 36 MeV/c² and 50 MeV/c², respectively, are much larger than the mass difference of ~ 20 MeV/c². This is the main experimental difficulty in investigating the $\Lambda(1405)$ nature *via* the $\Sigma^+\pi^-$ and $\Sigma^-\pi^+$ decay modes since

these are also possible final states for the $\Sigma^0(1385)$ disintegration. However, the $\Lambda(1405) \rightarrow \Sigma^0\pi^0$ decay can be used to identify this resonance unambiguously because isospin forbids this mode for the $\Sigma^0(1385)$.

In Fig. 1 the simplified decay scheme of excited neutral resonances with masses below $1432 \text{ MeV}/c^2$ demonstrates the differences between $\Sigma^0(1385)$ and $\Lambda(1405)$ utilised in the present analysis.

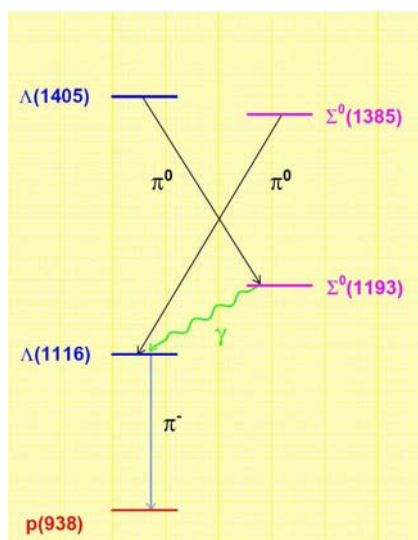


Figure 1: Simplified decay scheme for the $\Lambda(1405)$ and $\Sigma^0(1385)$ hyperon resonances

2 Experiment, analysis and simulations

The experiment was performed at the Cooler Synchrotron COSY, a medium energy accelerator and storage ring for protons and deuterons, which is operated at the Research Center Jülich (Germany) [?]. COSY supplied a stored proton beam with a momentum of $3.65 \text{ GeV}/c$ at a revolution frequency of $\sim 10^6 \text{ s}^{-1}$. Using a hydrogen cluster-jet target, the average luminosity during the measurements was $L = (55 \pm 8) \text{ pb}^{-1}$.

The ANKE spectrometer [12] used in the experiments consists of three dipole magnets that guide the circulating COSY beam through a chicane. The central C-shaped spectrometer dipole D2, placed downstream of the target, separates the reaction products from the beam. The ANKE detection system, comprising range telescopes, scintillation counters and multi-

wire proportional chambers, registers simultaneously positively and negatively charged particles and measures their momenta [13].

The following configuration of detectors was used to measure particles over a particular momentum range:

1. forward (Fd) and side-wall (Sd) counters for protons between 0.75 GeV/c and the kinematic limit,
2. telescopes and side-wall scintillators for K^+ between 0.2 and 0.9 GeV/c,
3. scintillators for π^- between 0.2 and 1.0 GeV/c.

The angular acceptance of the spectrometer dipole D2 is $|\vartheta_H| \lesssim 12^\circ$ horizontally and $|\vartheta_V| \lesssim 5^\circ$ vertically. Momenta, reconstructed from tracks in multi-wire proportional chambers, allow the masses of particles to be determined to within $\sim 10 \text{ MeV}/c^2$.

A multiparticle final state, containing two protons, a positively charged kaon, a negatively charged pion and an unidentified residue X^0 selected the $pp \rightarrow pK^+p\pi^-X^0$ reaction. In the $\Sigma^0(1385) \rightarrow \Lambda\pi^0$ decay the X^0 residue is a π^0 while, for the $\Lambda(1405) \rightarrow \Sigma^0\pi^0$ decay, $X^0 = \pi^0\gamma$ (see Fig. 1).

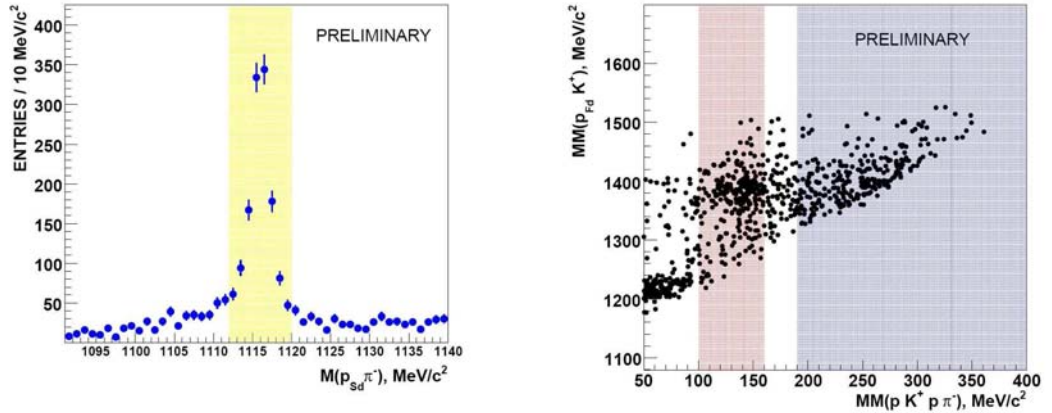


Figure 2: *Left:* Invariant mass $M(p_{Sd}\pi^-)$ measured in the 3.65 GeV/c $pp \rightarrow pK^+Y^0$ reaction. The yellow horizontal box shows the band used to select the Λ . *Right:* Missing mass $MM(p_{Fd}K^+)$ versus the missing mass $MM(pK^+\pi^-p)$. The left (red) vertical box covers the π^0 region and the right (blue) one has $MM(pK^+\pi^-p) > 190 \text{ MeV}/c^2 \gg m(\pi^0)$.

The following method was used to separate the $\Lambda(1405)$ from the $\Sigma^0(1385)$:

1. identify four particles: p_{Fd} , p_{Sd} , K^+ and π^- ,

2. analysed events with the invariant mass of the $p_{Sd}\pi^-$ pair equal to the mass of the Λ ,
3. select events with the missing mass of $(p_{Fd}, p_{Sd}, K^+, \pi^-)$ equal to a π^0 mass to isolate the $\Sigma^0(1385)$ and much higher than the π^0 mass to identify the $\Lambda(1405)$.

In the left part of Fig. 2 the invariant mass $M(p_{Sd}\pi^-)$ of the $p_{Sd}\pi^-$ pairs is shown, where the protons were registered in the side-detector counters. In the mass region around $1116 \text{ MeV}/c^2$ a peak with a FWHM of $\sim 5 \text{ MeV}/c^2$ is visible on a background that is mostly combinatorial in nature. The vertical box marks invariant-masses between 1112 and $1120 \text{ MeV}/c^2$. Events within this box are plotted in the right panel of Fig. 2 in a distribution of $MM(p_{Fd}K^+)$ versus $MM(pK^+\pi^-p)$. The two vertical bands show the four-particle missing-mass $MM(pK^+\pi^-p)$ criteria used to separate the $\Sigma^0(1385)$ candidates from those of the $\Lambda(1405)$. The left band is optimized to identify a π^0 whereas the right one selects masses significantly greater than $m(\pi^0)$. The deviation of $\sim 8 \text{ MeV}/c^2$ from the nominal pion mass of $135 \text{ MeV}/c^2$ is not unexpected in a mass reconstruction involving four particles.

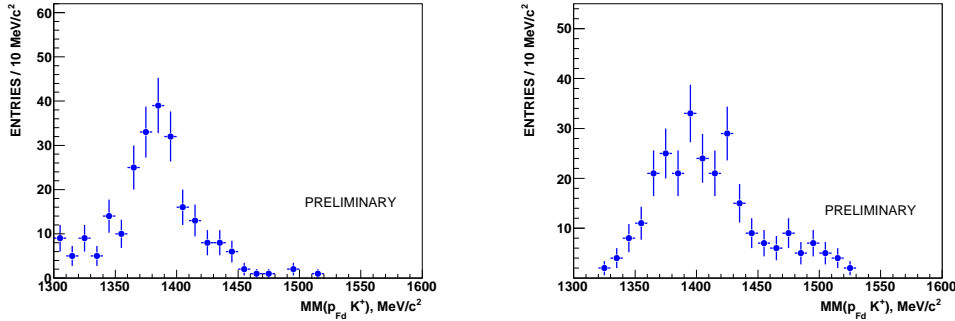


Figure 3: Missing-mass $MM(p_{Fd}K^+)$ distribution for the $pp \rightarrow pK^+p\pi^-X^0$ reaction for events with $M(p_{Sd}\pi^-) \approx m(\Lambda)$. The distribution obtained for $MM(pK^+\pi^-p) \approx m(\pi^0)$ is presented in the left panel and for $MM(pK^+\pi^-p) > 190 \text{ MeV}/c^2$ in the right one.

In the left part of Fig. 3 the missing-mass $MM(p_{Fd}K^+)$ distribution is shown for $MM(pK^+\pi^-p) \approx m(\pi^0)$. A peak around a mass of $1385 \text{ MeV}/c^2$ and a width of $\sim 50 \text{ MeV}/c^2$ is seen on a rather small background. In the right part of Fig. 3 the distribution, obtained for $MM(pK^+\pi^-p) > 190 \text{ MeV}/c^2$, has a peak near $1400 \text{ MeV}/c^2$ and a tail on the high missing-mass side.

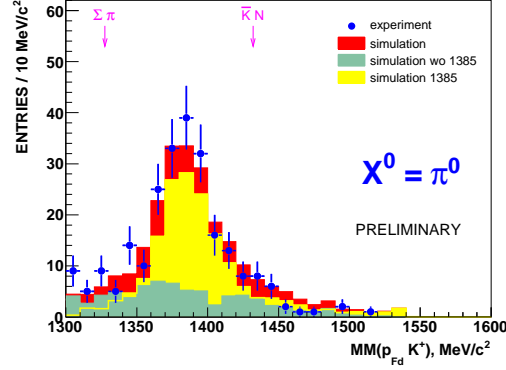


Figure 4: Missing-mass $MM(p_{Fd}K^+)$ distribution for the $pp \rightarrow pK^+p\pi^-X^0$ reaction for events with $M(p_{Sd}\pi^-) \approx m(\Lambda)$ and $MM(pK^+\pi^-p) \approx m(\pi^0)$. Experimental points with statistical errors are compared to the red histogram of the fitted overall Monte Carlo simulations. The simulation includes resonant contributions (yellow) and non-resonant phase-space production (green). Arrows indicate the $\Sigma\pi$ and $\bar{K}N$ thresholds.

In order to explain the measured spectra, Monte Carlo simulations were performed to estimate backgrounds from non-resonant and resonant reactions. The following non-resonant processes have been included:

1. $pp \rightarrow NK^+\pi X(\gamma)$
2. $pp \rightarrow NK^+\pi\pi X(\gamma)$

with X representing any allowed Λ or Σ hyperon. The second group consists of the following exclusive hyperon production reactions:

1. $pp \rightarrow pK^+\Sigma^0(1385)$
2. $pp \rightarrow pK^+\Lambda(1405)$
3. $pp \rightarrow pK^+\Lambda(1520)$

The simulations, based on the GEANT3 package, were performed in a similar manner to those in Ref. [14].

In the study of $\Sigma^0(1385)$ production and its backgrounds, events were generated according to phase space using a relativistic Breit-Wigner parameterizations for the known hyperon resonance [1]. The relative contributions

of the resonant and non-resonant reactions were deduced by fitting the experimental data to the simulated spectra. In Fig. 4 the histograms show the resonant contribution from the $pp \rightarrow pK^+\Sigma^0(1385)$ reaction (solid-yellow) and the sum of non-resonant contributions (solid-green). The result of the overall simulations is shown as a red histogram.

Turning now to the $\Lambda(1405)$, simulations show that the $\Sigma^0(1385)$ does not contaminate the missing-mass $MM(pK^+\pi^-p)$ range above $190 \text{ MeV}/c^2$ (see Fig. 5). This point is crucial since it allows us to obtain a clean separation of the $\Sigma^0(1385)$ from the $\Lambda(1405)$.

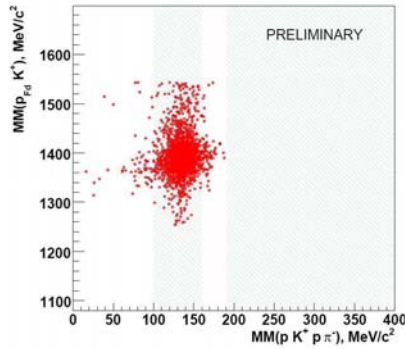


Figure 5: Simulated distribution of events with missing mass $MM(p_{Fd}K^+)$ versus $MM(pK^+\pi^-p)$. The left shaded vertical box covers the π^0 region and the right one has $MM(pK^+\pi^-p) > 190 \text{ MeV}/c^2 \gg m(\pi^0)$. Notice an absence of events in the right box.

In order to extract the $\Lambda(1405)$ distribution from the measured $\Sigma^0\pi^0$ decay, the non-resonant contributions have first been fitted to the experimental data. The resulting non-resonant background is indicated by the shaded histogram in the left panel of Fig. 6. When this is subtracted from the data, we obtain the distribution shown as experimental points in the right panel of Fig. 6.

3 Results

In Table 1 the information that is relevant for the evaluation of the total cross section is given. For both the hyperons measured this is of the order of a few μb .

The $(\Sigma\pi)^0$ invariant-mass distributions have been previously studied in two hydrogen bubble chamber experiments. Thomas *et al.* [10] found ~ 400

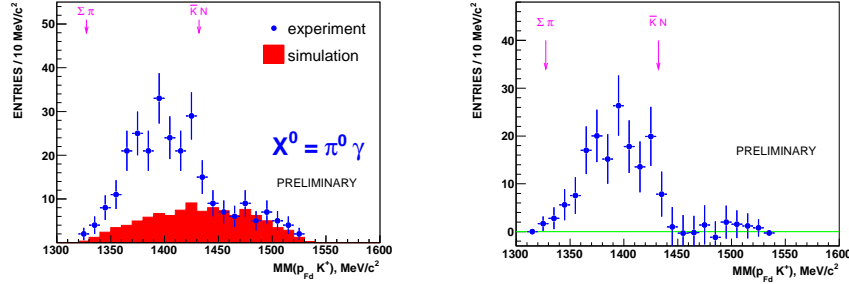


Figure 6: *Left:* Experimental missing-mass $MM(p_{F_d}K^+)$ distribution for the $pp \rightarrow p\bar{K}^+p\pi^-X^0$ reaction for events with $M(p_{S_d}\pi^-) \approx m(\Lambda)$ and $MM(pK^+\pi^-p) > 190 \text{ MeV}/c^2$ compared to the shaded histogram of the fitted non-resonant Monte Carlo simulation. *Right:* The background-subtracted lineage of the $\Lambda(1405)$ decaying into $\Sigma^0\pi^0$.

$\Sigma^+\pi^-$ or $\Sigma^-\pi^+$ events corresponding to the $\pi^-p \rightarrow K^0\Lambda(1405) \rightarrow K^0(\Sigma\pi)^0$ reaction at a beam momentum of $1.69 \text{ GeV}/c$. Hemingway [8] used a $4.2 \text{ GeV}/c$ kaon beam to investigate $K^-p \rightarrow \Sigma^+(1660)\pi^- \rightarrow \Lambda(1405)\pi^+\pi^- \rightarrow (\Sigma^+\pi^-)\pi^+\pi^-$ and measured 1106 events [8].

In Fig. 7 our experimental points are compared to the results of Thomas and Hemingway, which have been normalised by scaling their values down by factors of ~ 3 and ~ 7 , respectively. The effect of the $\bar{K}N$ threshold is quite obvious in these data, with the $\Lambda(1405)$ mass distribution being strongly distorted by the opening of this channel. Despite the very different production mechanisms, the three distributions have consistent shapes.

This might suggest that, if there are two states present in this region, then the reaction mechanisms in the three cases are preferentially populating the

Table 1: Total cross section for the production of the $\Sigma^0(1385)$ and $\Lambda(1405)$ resonances in the $3.65 \text{ GeV}/c$ $pp \rightarrow pK^+Y^0$ reaction

	$\Sigma^0(1385)$	$\Lambda(1405)$
number of events	170 ± 26	156 ± 23
acceptance	2.0×10^{-6}	4.4×10^{-6}
combined BR (%)	56	21
luminosity (pb^{-1})	55 ± 8	55 ± 8
detection efficiency (%)	55 ± 11	55 ± 11
cross section (μb)	$5.0 \pm 1.2_{\text{stat}} \pm 2.0_{\text{syst}}$	$5.6 \pm 0.8_{\text{stat}} \pm 2.2_{\text{syst}}$

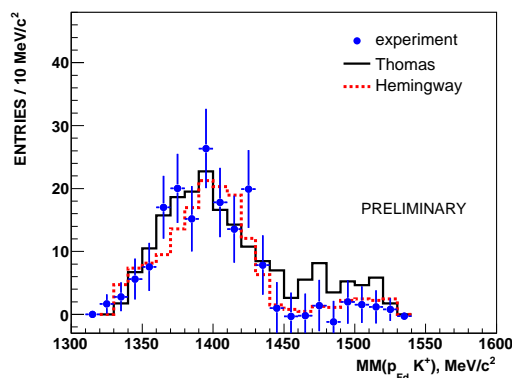


Figure 7: The background-subtracted line shape of the $\Lambda(1405)$ decaying into $\Sigma^0\pi^0$ (points) compared to $\pi^-p \rightarrow K^0(\Sigma\pi)^0$ [10] (black-solid line) and $K^-p \rightarrow \pi^+\pi^-\Sigma^+\pi^-$ [8] (red-dotted line) data.

same one. It should, however, be noted that by identifying a particular reaction mechanism, the proponents of the two-state solution can describe the shape of the distribution that we have found [7].

4 Outlook

The decay of excited hyperons Y^{0*} via $\Lambda\pi^0$ and $\Sigma^0\pi^0 \rightarrow \Lambda\gamma\pi^0$ can be detected directly in electromagnetic calorimeters by registering neutral particles, *i.e.* γ and/or π^0 . Measurements of such channels are underway in γp reactions (CB/TAPS at ELSA [15], SPring-8/LEPS [16]) and are also planned in pp collisions with WASA at COSY [17].

Acknowledgments

The results presented constitute the common effort of many members of the ANKE collaboration (www.fz-juelich.de/ikp/anke) and the COSY accelerator group, as described in Ref. [18]. This work has been supported by COSY-FFE Grant, BMBF, DFG and Russian Academy of Sciences.

References

- [1] W.-M. Yao *et al.*, J. Phys. G **33**, 1 (2006), but see also the mini review in D.E. Groom *et al.*, Eur. Phys. J. C **15**, 1 (2000).
- [2] N. Isgur and G. Karl, Phys. Rev. D **18**, 4187 (1978).
- [3] R.H. Dalitz and S.F. Tuan, Ann. Phys. (N.Y.) **10**, 307 (1960).
- [4] T. Inoue, arXiv:0708.2339 [hep-ph].
- [5] D. Jido *et al.*, Nucl. Phys. A **725**, 181 (2003).
- [6] V.K. Magas, E. Oset and A. Ramos, Phys. Rev. Lett. **95**, 052301 (2005).
- [7] L.S. Geng and E. Oset, arXiv:0707.3343 [hep-ph].
- [8] R.J. Hemingway, Nucl. Phys. B **253**, 742 (1984).
- [9] R.H. Dalitz and A. Deloff, J. Phys. G **17**, 289 (1991).
- [10] D.W. Thomas, *et al.*, Nucl. Phys. B **56**, 15 (1973).
- [11] R. Maier, Nucl. Instr. Meth. A **390**, 1 (1997)
- [12] S. Barsov *et al.*, Nucl. Instr. Meth. A **462**, 364 (2001).
- [13] M. Büscher *et al.*, Nucl. Instr. Methods A **481**, 378 (2002)
- [14] I. Zychor *et al.*, Phys. Rev. Lett. **96**, 012002 (2006).
- [15] H. Schmieden, ELSA Letter of Intent ELSA/4-2003.
- [16] H. Fujimura, AIP Conf. Proc. **915**, 737 (2007).
- [17] H.-H. Adam *et al.*, nucl-ex/0411038.
- [18] I. Zychor *et al.*, arXiv:0705.1039 [nucl-ex]

Participants

Patrick Achenbach	Johannes Gutenberg-Universität Mainz
Sergey Afonin	St. Petersburg State University
Miguel Albaladejo	Universidad de Murcia
Hamoud Alharbi	National Center for Mathematics and Physics at KACST
Mauro Anselmino	University and INFN, Torino
David Armstrong	College of William and Mary
Shahin Atashbar Tehrani	Persian Gulf University
Urnaa Badarch	University Giessen
Gunnar Bali	Universität Regensburg
Fouad Ballout	FZ Jülich
Luca Barion	FZ Jülich
Sergey Barsov	FZ Jülich
Vadim Baru	Institute for Theoretical and Experimental Physics, Moscow, Russia
Mikhail Bashkanov	Univ. Tübingen
Gerhard Baur	FZ Jülich
Silas Beane	University of New Hampshire
Ulf Bechstedt	FZ Jülich
Matthias Behler	Mainz University
Falco Beijer	Pfeiffer Vacuum GmbH
Himani Bhatt	Indian Institute of Technology, Bombay
Pedro Bicudo	IST, Lisboa
Ikaros Bigi	University of Notre Dame
Roelof Bijker	Instituto de Ciencias Nucleares
Johan Bijnens	Lund University, Lund, Sweden
Cesare Bini	Sapienza Università' di Roma and INFN Roma
Michael Birse	University of Manchester
Andrea Bizzeti	Università' di Modena e Reggio Emilia and INFN Sezione di Firenze
Jan Blomgren	Uppsala University, Dept of Neutron Research
Harald Bongen	FZ Jülich
Norbert Bongers	FZ Jülich
Bugra Borasoy	Bonn University
Ekaterina Borodina	FZ Jülich
Robert Bradford	University of Rochester
Ronald Brings	FZ Jülich
Kai Brinkmann	IKTP, TU Dresden
William Briscoe	The George Washington University
Markus Büscher	FZ Jülich
Maxim Bychkov	University of Virginia
Hans Calen	Uppsala University
Kavita Chandwani	Indian Institute of Technology Bombay
Wen-Chen Chang	Institute of Physics, Academia Sinica, Taiwan

David Chiladze	FZ Jülich
Rsulan Chistov	ITEP Moscow
Ales Cieply	Institute of Nuclear Physics, Rez near Pragü, Czechia
Heinz Clement	Univ. Tübingen
Tom Cohen	University of Maryland
Marialaura Colantoni	Universita' del Piemonte Orientale e INFN-Torino
Catalina Curceanu	Laboratori Nazionali di Frascati dell'INFN
Rafal Czyzykiewicz	Jagellonian University, Cracow and FZ Jülich
Rita De Masi	Institut de Physique Nucleaire Orsay
Jean-Pierre Didelez	Institut de Physique Nucleaire Orsay
Jürgen Dietrich	FZ Jülich
Michael Doering	University of Valencia
Heinz Dohmen	Oerlikon Leybold Vacuum GmbH
Frank Dohrmann	FZ Dresden-Rossendorf
Alessandro Drago	University of Ferrara
Michael Dugger	Arizona State University
Alexey Dzyuba	FZ Jülich
Bruno El-Bennich	LPNHE Univ. Pierre et Marie Curie, Paris
Sergey Eliseev	Laboratory of Theoretical Physics, R, Dubna
Ralf Engels	FZ Jülich
Evgeny Epelbaum	FZ Jülich and Bonn University
Franz-Josef Etzkorn	FZ Jülich
Riccardo Fabbri	DESY-ZEUTHEN
Amir Fariborz	SUNY Institute of Technology
Pavel Fedorets	ITEP Moscow
Olaf Felden	FZ Jülich
Robert Fersch	College of William and Mary
Detlef Filges	FZ Jülich
Christian Fischer	Institut für Kernphysik, TU Darmstadt
Klaus Foehl	University of Edinburgh
Antonio Fonseca	Centro Fisica Nuclear da Universidade Lisboa
Aida Galoyan	LPP JINR, Dubna
Gurjav Ganbold	JINR, Dubna and Institute of Physics and Technology, Ulaanbaatar
Haiyan Gao	Duke University and TUNL
Anders Gardestig	University of South Carolina
Archil Garishvili	FZ Jülich
Jürg Gasser	Univ. Bern
Werner Gast	FZ Jülich
Daniel Gazda	Institute of Nuclear Physics, Rez near Prague
Ralf Gebel	FZ Jülich
Albrecht Gillitzer	FZ Jülich
Derek Glazier	University of Edinburgh
Leonid Glozman	University of Graz

Alexander Glushkov	Odessa University
Frank Goldenbaum	FZ Jülich
Detlev Gotta	FZ Jülich
Harald Griefhammer	George Washington University
Kirill Grigoriev	FZ Jülich
Vera Grishina	FZ Jülich
Frank Grümmer	FZ Jülich
Peter Grünschloss	Calplus GmbH
Dieter Grzonka	FZ Jülich
Ali Murat Guler	Middle East Technical University
Helmut Haberzettl	George Washington University
Dietrich Habs	LMU Garching
Johann Haidenbauer	FZ Jülich
Rene Halver	FZ Jülich
Guido Hamacher	Pfeiffer Vacuum GmbH
Hans-Werner Hammer	Bonn University
Christoph Hanhart	FZ Jülich
Fred Harris	University Hawaii
Michael Hartmann	FZ Jülich
Hassan Hassanabadi	Shahrood University of Technology
Martin Hausner	FZ Jülich
Jun He	CEA-Saclay
Volker Hejny	FZ Jülich
Thomas Hemmert	Physik Dep. T39, TU München
Kurt Henn	FZ Jülich
Frank Hinterberger	Bonn University
Aye Thandar Htay	FZ Jülich
Jie Hu	Duke University
Fei Huang	China Center of Advanced Science and Technology
Fabian Hügging	FZ Jülich
Tetsuo Hyodo	Yukawa Institute for Theoretical Physics, Kyoto
Yoichi Ikeda	Department of Physics, Osaka University
Takashi Inoue	Dept. Phys. Sophia University, Tokyo
Tomoichi Ishiwatari	Stefan Meyer Institut für subatomare Physik, Wien
Sergiy Ivashyn	National Science Center, Kharkov
Herbert Jäger	FZ Jülich
Marco Jagodzinska	FZ Jülich
Brajesh K. Jain	Mumbai University
Harald Janssen	Calplus GmbH
Michal Janusz	FZ Jülich and Jagiellonian University, Krakow
Benedykt R. Jany	FZ Jülich and Nuclear Physics Department, Jagiellonian University, Krakow
Vishwajeet Jha	Nuclear Physics Division, BARC, Mumbai
Bruno Julia-Diaz	University of Barcelona

Stefan Jurk	iseg Spezialelektronik GmbH
Andro Kacharava	Erlangen University
Mardy Karnadi	FZ Jülich
Irakli Keshelashvili	FZ Jülich
Olena Khakimova	Univ. Tübingen
Dimitry Khaneft	FZ Jülich
Olga Khetselius	Nucl.Spectr.Lab., Odessa University
Alfons Khoukaz	IKP, Universität Münster
Anatoly Khrykin	JINR, Dubna
Kurt Kilian	FZ Jülich
Daniil Kirillov	FZ Jülich
Matthias Kirsch	Struck Innovative Systeme GmbH
Daniela Kiselev	Paul Scherrer Institut
Stanislaw Kistryn	Jagiellonian University, Krakow
Pawel Klaja	FZ Jülich
Vera Kleber	Bonn University
Eberhard Klempt	Bonn University
Rüdiger Koch	FZ Jülich
Stefan Kölling	FZ Jülich
Evgeni Kolomeitsev	GSI Darmstadt
Polina Kravchenko	PNPI, S.Petersburg
Gastao Krein	Instituto de Fisica Teorica
Siegfried Krewald	FZ Jülich
Bernd Krusche	Basel University
Bastian Kubis	HISKP (Theorie), Bonn University
Eberhard Kuhlmann	Institut für Kern- und Teilchenphysik, TU Dresden
Roland Kuhn	Technische Universität München, Physik Department
Pawel Kulesa	FZ Jülich and Institute of Nuclear Physics Cracow
Viacheslav Kulikov	ITEP, Moscow
Andrzej Kupsc	Department of Nuclear And Particle Physics, Uppsala University
Alexander Kvinikhidze	Razmadze Mathematical Institute, Tbilisi
Valentyn Kyryanchuk	FZ Jülich
Timo Lahde	Department of Physics, University of Washington, Seattle, WA
Jens Soeren Lange	Universität Giessen
Inti Lehmann	University of Glasgow
Andreas Lehrach	FZ Jülich
Paolo Lenisa	Universita' di Ferrara and INFN - Ferrara
Horst Lenske	U. Giessen
Vadim Lensky	FZ Jülich
Vladimir Leontyev	FZ Jülich
Felipe Llanes Estrada	Depto. Fisica Teorica I, Universidad Complutense Madrid
Markus Lochno	Tektronix GmbH
Bernd Lorentz	FZ Jülich

Alfredo Luccio	Brookhaven National Laboratory
Matthias F.M. Lutz	GSI Darmstadt
Valery Lyubovitskij	Institute of Theoretical Physics, University of Tübingen
Nikolay Lyutorovich	St. Petersburg State University
Frank Maas	CNRS/IN2P3/Institut de Physique Nucleaire Orsay
Alexander Machavariani	JINR Dubna and HEPI Tbilisi
Hartmut Machner	FZ Jülich
Andrzej Magiera	Institute of Physics, Jagiellonian University
Rudolf Maier	FZ Jülich
Alberto Martinez Torres	IFIC-Universidad de Valencia
Sergio Mauro	WIENER, Plein & Baus GmbH
Judith McGovern	University of Manchester
Bryan McKinnon	University of Glasgow
Craig McNeile	University of Glasgow
Ulf-G. Meißner	FZ Jülich and Bonn University
Wally Melnitchouk	Jefferson Lab
Marius Mertens	FZ Jülich
Johan Messchendorp	KVI/RuG, Groningen
Pekko Metsae	University of Helsinki
Bernard Metsch	Bonn University
Malte Mielke	IKP, Universität Münster
Maxim Mikirtychyants	Petersburg Nuclear Physics Institute and FZ Jülich
David Minossi	FZ Jülich
Hans-Peter Morsch	Soltan Institute for Nuclear Studies, Warsaw
Ulrich Mosel	University of Giessen
Pawel Moskal	Jagellonian University and FZ Jülich
Fred Myhrer	University of South Carolina
Satoshi Nakamura	TRIUMF
Takashi Nakano	RCNP, Osaka University
Kanzo Nakayama	University of Georgia
Mariana Novoa	University of Giessen
Alexey Nefediev	ITEP Moscow
Ben Nefkens	University California Los Angeles
Mikhail Nekipelov	FZ Jülich
Dominik Nickel	Technische Universität Darmstadt
Nikolai Nikolaev	L.D.Landau Institute for Theoretical Physics and FZ Jülich
Victor Nikonov	HISKP Bonn, PNPI Gatchina
Mikheil Niroadze	High Energy Physics Institute of Tbilisi State University
Tetsuo Nishikawa	Tokyo Institute of Technology
Jouni Niskanen	University of Helsinki
Andreas Nogga	FZ Jülich
Walter Oelert	FZ Jülich
Dieter Oellers	FZ Jülich

Henner Ohm	FZ Jülich
Hiroaki Ohnishi	RIKEN
Vitaly Okorokov	MEPhI - Moscow Engineering Physics Institute
Jose A. Oller	Universidad de Murcia
Eulogio Oset	University of Valencia
Simone Pacetti	LNF-INFN Frascati and CSR Enrico Fermi, Roma
Michael Papenbrock	IKP, Universität Münster
Mark W. Paris	EBAC @ Jefferson Lab
Vladimir Pascalutsa	ECT* Trento
Christian Pauly	FZ Jülich
Fedor Pavlov	FZ Jülich
Jose R. Pelaez	University Complutense de Madrid
Mario Pelliccioni	Universita' degli Studi di Torino, INFN
Michael Pennington	IPPP, Durham University
Henrik Pettersson	IKP, Uppsala University
Daniel Phillips	Ohio University
Jerzy Pietraszko	GSI Darmstadt
Stephane Platchkov	CEA Saclay
Henk Polinder	FZ Jülich
Maxim Polyakov	Ruhr-University Bochum
Sergey Prakhov	University California Los Angeles
Dieter Prasuhn	FZ Jülich
Elisabetta Prencipe	University of Ferrara and INFN
Annette Pricking	Univ. Tübingen
Joanna Przerwa	FZ Jülich
Piotr Raczka	University of Warsaw
Ali A. Rajabi	Shahrood University of Technology
Frank Rathmann	FZ Jülich
Christoph Redmer	FZ Jülich
David Richards	Jefferson Laboratory
James Ritman	FZ Jülich
Craig Roberts	Argonne National Laboratory
Eduard Roderburg	FZ Jülich
David Rodriguez Entem	University of Salamanca and IUFFyM
Günther Rosner	University of Glasgow
Anatoli Rouba	Research Institute for Nuclear Problems, Minsk
Ankhi Roy	IIT Bombay
Enriqü Ruiz Arriola	Universidad de Granada
Akaki Rusetsky	HISKP, Bonn University
Michael Sadler	Abilene Christian University
Mikko Sainio	Helsinki Institute of Physics
Naohito Saito	KEK
Elena Santopinto	INFN

Andrei Sarantsev	Bonn University
Pavel Saviankou	FZ Jülich
Susan Schadmand	FZ Jülich
Andreas Schäfer	University of Regensburg
Wo. Schäfer	FZ Jülich
D. Schoenfelder	FZ Jülich
Joseph Schechter	Physics Department, Syracuse University
Ralf Schleichert	FZ Jülich
Herbert Schneider	FZ Jülich
Karin Schoenning	Uppsala University
Wolfgang Schroeder	FZ Jülich and Erlangen University
Otto Schult	FZ Jülich
Martin Schulte-Wissermann	TU Dresden
Thomas Sefzick	FZ Jülich
Kimiko Sekiguchi	RIKEN
Marc Sellschopp	Pfeiffer Vacuum GmbH
Kirill Semenov-Tian-Shansky	Ruhr Universität Bochum and St. Petersburg State University
Valeriy Serdyuk	FZ Jülich
Hellmut Seyfarth	FZ Jülich
Neha Shah	Indian Institute of Technology Bombay
Kiyotaka Shimizu	Department of Physics, Sophia University
Vitaly Shklyar	Inst. für Theor. Physik I, Universität Giessen
Mohammad R. S. K. Sofla	Shahrood University of Technology
Alexander Sibirtsev	HISKP, Universität Bonn
Regina Siudak	Institute of Nuclear Physics, Cracow,
Tatiana Skorodko	Uni. Tübingen
Tytus Smolinski	FZ Jülich and Jagiellonian University, Cracow
Andrey Sokolov	FZ Jülich
Josef Speth	FZ Jülich
Dirk Spoelgen	FZ Jülich
Roxanne Springer	Duke University
Jugoslav Stahov	University of Tuzla
Florica Stancu	University of Liege
Aleksandr Starostin	University of California Los Angeles
Rolf Stassen	FZ Jülich
Hans-Joachim Stein	FZ Jülich
Joanna Stepaniak	Institute for Nuclear Studies, Warsaw
Günter Sterzenbach	FZ Jülich
Hans Stockhorst	FZ Jülich
Tobias Stockmanns	FZ Jülich
Igor Strakovsky	The George Washington University
Thomas Strauch	FZ Jülich
Hans Stroehrer	FZ Jülich

Viktorin Sumachev	Petersburg Nuclear Physics Institute
Mizuki Sumihama	Osaka University RCNP
Yury Surovtsev	Bogoliubov Laboratory of Theoretical Physics, JINR, Dubna
Nobuhiko Suzuki	Department of Physics, Osaka University
Takatoshi Suzuki	RIKEN
Alfred Svarc	Rudjer Boskovic Institute
Antoni Szczurek	Institute of Physics and University of Rzeszow
Berhan Taddesse	Jacobs University Bremen
Fatemeh Taghavi Shahri	IUST
Toru Takahashi	Yukawa Institute for Theoretical Physics, Kyoto University
Sachiko Takeuchi	Japan College of Social Work
Makoto Takizawa	Showa Pharmaceutical University
Setsuo Tamenaga	RCNP, Osaka University
Ulrike Thoma	Bonn University
Anthony Thomas	Jefferson Lab
Raimund Tölle	FZ Jülich
Walter Toki	Colorado State University
Tamer Tolba	FZ Jülich
Laura Tolos	FIAS. University of Frankfurt
Sergey Trusov	FZ Jülich
Antonios Tsapalis	University of Athens
Kay Ulbrich	Bonn University
Wolfgang Ullrich	TU Dresden
Maurizio Ungaro	Jefferson Lab
Yury Valdau	FZ Jülich
Eef van Beveren	Coimbra University
Brandon Van der Ventel	Stellenbosch University
David van Niekerk	Stellenbosch University
Willem van Oers	University of Manitoba, Winnipeg
Galina Vankova-Kirilova	Sofia University
Tsvetanova Raghava Varma	Indian Institute of Technology Bombay
Peter Vlasov	FZ Jülich
Mikhail Voloshin	FTPI, University of Minnesota
Michael von Düring	CAEN GmbH
Fan Wang	Nanjing University
Rainer Wanke	Mainz University
Wojciech Węglorz	FZ Jülich
Christian Weidemann	FZ Jülich
Herbert Weigel	Fachbereich Physik, Siegen University
Dominic Welsch	FZ Jülich
Eberhard Widmann	Stefan Meyer Institute for Subatomic Physics, Vienna
Uwe-Jens Wiese	Institute for Theoretical Physics, Bern University
Alexander Winnemöller	IKP, Universität Münster

Peter Wintz	FZ Jülich
Andreas Wirzba	FZ Jülich
Magnus Wolke	FZ Jülich
Aleksandra Wronska	Jagiellonian University, Cracow
Xiaohua Yuan	FZ Jülich
Leonid Yurev	FZ Jülich
Zhongdong Zhang	FZ Jülich
Qiang Zhao	IHEP Beijing
Veronique Ziegler	SLAC
Bing-song Zou	IHEP Beijing
Pawel Zupranski	The Andrzej Soltan Institute for Nuclear Studies
Izabella Zychor	IPJ Swierk

Program

Registration		
<i>Plenary Session Monday, Sep. 10, 2007 9:00 - 12:30</i>		
<i>chair: S. Krewald</i>		
Welcome (<i>H. Machner</i>)		
Welcome to the Research Center (<i>U. Samm</i>)		
W. van Oers	Department of Physics and Astronomy University of Manitoba	Opening Remarks (IUPAP)
J. Gasser	Univ. Bern, Switzerland	Chiral Effective Field Theory
C. Curceanu	Laboratori Nazionali di Frascati dell'INFN	Kaonic Atoms Experimental Studies at DAPHNE
<i>chair: J. Ritman</i>		
R. Wanke	Mainz University	Wigner-Cusp in Kaon Decays and Determination of $\pi\pi$ Scattering Lengths
J. Bijnens	Lund University, Lund, Sweden	Eta and Eta' Physics
M. Wolke	FZ Juelich	Eta Meson Decays with WASA-at-COSY
<i>Parallel Sessions 1-5 - Monday, Sep. 10, 2007 14:30 - 16:10</i>		
<i>Session 1: πN Interaction I</i>		
<i>chair: B. Nefkens</i>		
T. D. Cohen	University of Maryland	Interplay of the Chiral and Large $N(c)$ Limits in πN Scattering
T. Inoue	Dept. Phys. Sophia University, Tokyo	Pion-Nucleon P_{33} and P_{11} Scatterings in the Lippmann-Schwinger Approach
P. Metsd	University of Helsinki	Pion-Nucleon Partial Wave Analysis with Fixed- t Analyticity Constraints
M.E. Sainio	Helsinki Institute of Physics	The GMO Sum Rule Revisited
J. He	CEA-Saclay	πN to ηN Process in a Chiral Quark Model Approach
<i>Session 2 : Scalar Mesons I</i>		
<i>chair: E. van Beveren</i>		
J.R. Pelaez	University Complutense de Madrid	Scalar Mesons from Unitarized Chiral Perturbation Theory
J. Oller	Universidad de Murcia	Topics on Scalar Meson Dynamics
M. Bashkanov	Univ. Tuebingen	σ -Channel Low-Mass Enhancement in Double-Pionic Fusion
A.V. Nefediev	ITEP	The Nature of the Light Scalar Mesons from their Radiative Decays
A. Fariborz	SUNY Institute of Technology	Scalar Mesons: A Chiral Lagrangian Study of their Mixing and Substructure

<i>Session 3: Meson Production I</i>		<i>chair: W. Briscoe</i>
K. Nakayama	University of Georgia	Meson Production in NN Collisions
H. Haberzettl	George Washington University	Photoproduction of Pseudoscalar Mesons
A. Dzyuba	FZ Juelich	Kaon-Pair Production in Hadron-Induced Reactions at ANKE
W.-C. Chang	Institute of Physics, Academia Sinica, Taiwan	Explore Pomeron Trajectory at Low Energies - Measurement of ϕ -Meson Photoproduction from Protons and Deuterons Near Threshold by LEPS/SPring-8 Experiment
<i>Session 4: Baryon Spectroscopy I</i>		<i>chair: E. Oset</i>
M. Doering	University of Valencia	The Nature of the $N^*(1535)$
T. Skorodko	Uni. Tuebingen	Excitation of the Roper Resonance in Single and Double-Pion Production
I. Zychor	IPJ Swierk	Studies of $\Lambda(1405)$ in pp Collisions with ANKE at COSY-Juelich
S. Takeuchi	Japan College of Social Work	$\Lambda(1405)$ as a Resonance in the Baryon-Meson Scattering Coupled to the q^3 State in a Quark Model
<i>Session 5: Electron Scattering</i>		<i>chair: A. Szczurek</i>
I. Lehmann	University of Glasgow	HERMES Results on Hard-Exclusive Processes
R. De Masi	IPN Orsay	Generalized parton distributions and deeply virtual Compton scattering at CLAS
W. Melnitchouk	Jefferson Lab	Quark Hadron Duality in Electron Scattering
P. Kravchenko	PNPI, S.Petersburg	Latest HERMES Results on Quark Helicity Distribution from Semi-Inclusive Deep-Inelastic Scattering
<i>Parallel Sessions 6-10 - Monday, Sep. 10, 2007 16:50 - 18:30</i>		
<i>Session 6: πN Interaction II</i>		<i>chair: H. Lenske</i>
A.Kudryavtsev (V. Baru)	Institute for Theoretical and Experimental Physics, Moscow, Russia	Pion-Deuteron Scattering Length in Chiral Perturbation Theory up to Order $\chi^3/2$
J. Stahov	University of Tuzla	Evaluation of the πN sigma Term Using Dispersion Relations - Present Status
T. Strauch	FZ Juelich	Pionic Deuterium

V. Sumachev	Petersburg Nuclear Physics Institute	Parameters A and R Measurements in the Resonance Region of the Pion-Nucleon Elastic Scattering: Recent Results and Subsequent Investigations
K. Semenov	Ruhr Universitaet Bochum, St. Petersburg State University	Bootstrap for Physical Values of π N Resonance Parameters
Poster Session		
Session 7: Scalar Mesons II		<i>chair: G. Krein</i>
E. van Beveren	Coimbra University	How We Discovered the Nonet of Light Scalar Mesons
S.A. Ivashyn	National Science Center "Kharkov Institute for Physics and Technology", Institute for Theoretical Physics, Ukraine	Light Scalar Meson Decays and Mixing in ChPT
M. Albaladejo	Universidad de Murcia	S-Wave Meson Scattering in Unitary Chiral Perturbation Theory
Yu.S. Surovtsev	Bogoliubov Laboratory of Theoretical Physics, Joint Institute for Nuclear Research	On the Nature of the f_0 - and f_2 -Mesons
X. Yuan	FZ Juelich	Measurement of the reaction $dd \rightarrow \alpha K^+ K^-$ with ANKE/COSY
Poster Session		
Session 8: Meson Decays		<i>chair: F. Harris</i>
B. Borasoy	Bonn University	Decays of Eta and Eta' Mesons
A. Kupsc	Department of Nuclear And Particle Physics, Uppsala University	Multiple Meson Production in pp Interactions as a Background for eta and eta' Decay Studies
A. Bizzeti	Universita' di Modena e Reggio Emilia and INFN Sezione di Firenze	Highlights on Radiative Kaon and Hyperon Decays from NA48/2
S. Prakhov	University California Los Angeles	New Results on Measurement of Rare Decay $\eta \rightarrow \pi^0 \gamma \gamma$
A. Roy	IIT Bombay	Branching Ratio for $\eta \rightarrow \pi^0 \gamma \gamma$ with CBELSA/TAPS
Poster Session		
Session 9: Symmetries		<i>chair: W. van Oers</i>
A. Magiera	Institute of Physics, Jagiellonian University	Studies of Charge Symmetry Breaking Reactions at COSY
B. Kubis	Helmholtz-Institut fuer Strahlen- und Kernphysik (Theorie), Universitaet Bonn	Isospin Violating Nucleon Form Factors

D.S. Armstrong	College of William and Mary	Strangeness Content of the Nucleon via Parity Violating Asymmetries in Polarized Electron Scattering
F. Maas	CNRS/IN2P3/IPN Orsay	Parity Violating Electron Scattering: The Role of Strange Quarks at Small Momentum Transfer
M. Behler	Mainz University	Symmetry Tests in NA48 with Kaons
Poster Session		
Session 10: Instrumentation		<i>chair: J. Niskanen</i>
K. Foehl	University of Edinburgh	The PANDA Detector at FAIR
A. Wronska	Jagiellonian University, Cracow	Simulation of the PANDA Experiment with PandaRoot
R. Schleichert	FZ Juelich	Silicon Detectors for Internal Target Experiments
L. Barion	University of Ferrara and INFN / FZ Juelich	The PAX Experiment at FAIR
A. Lehrach	FZ Juelich	High-Energy Storage Ring (HESR)
Poster Session		
Welcome Dinner Seekasino		
Plenary Session Tuesday, Sep. 11, 2007 8:30 - 12:30		
<i>chair: A. Schaefer</i>		
C. Bini	Sapienza Universita' di Roma and INFN Roma	KLOE Results on Hadron Physics
M.R. Pennington	IPPP, Durham University	Structure of Light Scalar Mesons
J. Schechter	Physics Department, Syracuse University	Scalar Mesons from an Effective Lagrangian Approach
K.-T. Brinkmann	IKTP, TU Dresden	Physics Program at COSY
<i>chair: H. Gao</i>		
S. Beane	University of New Hampshire	Hadron, Hadron-Hadron and Hadron-Hadron Properties from Lattice QCD
U.-J. Wiese	Institute for Theoretical Physics, Bern University	Chiral Symmetry on the Lattice
A. Schaefer	University of Regensburg	Hadron Structure from Lattice QCD
Parallel Sessions 11-15 - Tuesday, Sep. 11, 2007 14:30 - 16:10		
Session 11: Spin Physics		<i>chair: W. Melnitchouk</i>
R. Fersch	College of William and Mary	Spin Physics with CLAS
St. Platchkov	CEA Saclay	The COMPASS Experiment at CERN: New Results and Forthcoming Studies
A. Fabbri	DESY-ZEUTHEN	Latest HERMES Results on Transverse Spin in Hadron Structure and Formation

F. Rathmann (A. Kacharava)	Erlangen University	Spin Physics from COSY to FAIR
A. Drago	University of Ferrara	Spin Physics with Antiprotons
<i>Session 12: Scalar Mesons III</i>		<i>chair: J. Schechter</i>
T. Lahde	Department of Physics, University of Washington, Seattle, WA	Scalar Pion Form Factor from J/psi Decays
D. Rodriguez Entem	University of Salamanca and IUFFyM	Chiral Symmetry Restoration in Excited Mesons
G. Ganbold	Joint Institute for Nuclear Research, Dubna and Institute of Physics and Technology, Ulaanbaatar	Mesons and Glueballs: A Quantum Field Approach
A. Khrykin	JINR	On a Possible Origin of a Resonance-Like Structure in the Two-Photon Invariant Mass Spectrum of the Reaction $pp \rightarrow pp \gamma \gamma$
<i>Session 13: Meson Production II</i>		<i>chair: H. Clement</i>
J. Pietraszko (I. Froehlich)	GSI Darmstadt	PP Collisions with HADES
W. Ullrich	TU Dresden	Reaction Dynamics of omega Meson Production in $\vec{p}p$ Collisions
K. Schoenning	Uppsala University, Sweden	Production of omega in pd to $3He$ omega with CELSIUS/WASA
O. Khakimova	Univ. Tuebingen	Measurement of the ABC-Effect in the Most Basic Double-Pionic Fusion Process
G. Vankova	University of Sofia	Study of eta-Meson Production in the $\vec{d}d$ to α eta Reaction
<i>Session 14: Baryon Spectroscopy II</i>		<i>chair: B. Metsch</i>
B. McKinnon	University of Glasgow	Baryon Spectroscopy at CLAS (Pentaquark Review)
M. Nanova	University of Giessen	$\gamma p \rightarrow p \pi^0 \eta$ and Related Reactions Studied with CBELSA/TAPS
V. Shklyar	Inst. fuer Theor. Physik I, Universitaet Giessen	eta-Photoproduction on the Nucleon in the Resonance Energy Region
D.I. Glazier	University of Edinburgh	Recoil Polarisation Observables in pion and eta Photoproduction with the CB@MAMI

H. Hassanabadi	Shahrood University of Technology	Determination of the potential coefficients of the Baryons & the effect of spin & isospin potential on their energy
<i>Session 15: Hadrons in Medium I</i> <i>Magiera</i>		<i>chair: A.</i>
B.K. Jain	Mumbai University	Study of the p 6Li to eta 7Be reaction
V. Jha	Nuclear Physics Division, BARC, Mumbai	Search for eta-Nucleus Bound States
M. Papenbrock	IKP, Universitaet Muenster	Investigation of the dp to 3HeX (X=eta,pi0,pipi) Reactions at ANKE
A. Galoyan	LPP JINR	Monte Carlo Simulation of Meson-Nucleon and Meson-Nucleus Interactions at High Energies
<i>Parallel Sessions 16-20 - Tuesday, Sep. 11, 2007 16:50 - 18:30</i>		
<i>Session 16: KN Interaction</i>		<i>chair: A. Gardestig</i>
A. Rusetsky	HISKP, University of Bonn	Kaon-Nucleon Scattering Lengths from Experiment on Kaonic Deuterium
F. Huang	China Center of Advanced Science and Technology	Kaon Nucleon and Anti-Kaon Nucleon Interactions in a Chiral Constituent Quark Model
A. Cieply	Institute of Nuclear Physics, Rez near Prague, Czechia	Multichannel Chiral Approach for Kaonic Hydrogen
T. Ishiwatari	Stefan Meyer Institut fuer subatomare Physik	Precise Determination of Kaonic 4He X-ray Energy
<i>Session 17: Meson Production III</i>		<i>chair: H. Haberzettl</i>
M. Dugger	Arizona State University	Photoproduction of Eta and Eta' Mesons from the Proton
P. Klaja	FZ Juelich	Comparative Study of proton-eta and proton-eta' Interaction via pp and p-meson Invariant Mass Distributions
J. Przerwa	FZ Juelich	Isospin Dependence of the Eta' Meson Production in Nucleon-Nucleon Collisions
H. Pettersson	IKP, Uppsala University	High Statistics Measurements of eta-Production in Proton-Proton Collisions
C. Pauly	FZ Juelich	3pi0 Final States with WASA at CELSIUS and COSY
<i>Session 18: High Energy Processes I</i>		<i>chair: A. Drago</i>
R. Bijker	Instituto de Ciencias Nucleares	The Gottfried Sum Rule in an Unquenched Quark Model

Ch. Fischer	Institut fuer Kernphysik, TU Darmstadt	Meson Properties from Non-perturbative Quark-Gluon Dynamics
R. Kuhn	Technische Universitaet Muenchen, Department Physik	Measurements of the Gluon Polarization in the Nucleon
P. Fedorets	ITEP Moscow	A Frozen Pellet Target for PANDA
<i>Session 19: Heavy Mesons I</i>		<i>chair: H.-W. Hammer</i>
R.P. Springer	Duke University	Positive and Negative Parity Charmed Mesons in Heavy Quark Effective Field Theory
F.A. Harris	University Hawaii	Recent BES Results and the BESIII Upgrade
B. El-Bennich	LPNHE Univ. Pierre et Marie Curie, Paris	B Meson Decays into Pion Pion and Kaon: CP Violation and Pseudoscalar Meson Interactions
G. Krein	Instituto de Fisica Teorica	Dbar -Nucleon Interaction from Meson-Exchange and Quark-Gluon Dynamics
<i>Session 20: Baryon Spectroscopy III</i>		<i>chair: F. Stancu</i>
L.Ya.Glozman	University of Graz	QCD Symmetries in Excited Hadrons
M. Sumihama	Osaka University, RCNP	K+ Photoproduction by Linearly Polarized Photons at SPring-8/LEPS
R. Bradford	University of Rochester	Studies of Kaon Photoproduction from the Proton Using CLAS at Jefferson Lab
T. Hyodo	Yukawa Institute for Theoretical Physics, Kyoto	Exotic Hadrons in s-Wave Chiral Dynamics
A. Martinez Torres	IFIC-Universidad de Valencia	Dynamically Generated Resonances in the Two Mesons - One Baryon Systems
<i>Plenary Session Wednesday, Sep. 12, 2007 8:30 - 12:30</i>		
<i>chair: H. Stroeher</i>		
M. Lutz	GSI Darmstadt	Structure of Baryons
P. Achenbach	Institut fuer Kernphysik, Johannes Gutenberg-Universitaet Mainz	Physics Program at MAMI-C
U. Thoma	Bonn University	Baryon Spectroscopy - Recent results from the Crystal Barrel Experiment at ELSA -
B.S. Zou	IHEP Beijing	Baryon Resonances Observed at BES
<i>chair: J. Gasser</i>		
T. Nakano	RCNP, Osaka University	Evidence for Theta+ Photo-Production at LEPS

A. Starostin	University of California Los Angeles	Baryon Spectroscopy with Inelastic Channels: Crystal Ball Experience
H. Gao	Duke University and TUNL	Scaling in Charged Pion Photoproduction From Nucleon
<i>Parallel Sessions 21-25 - Wednesday, Sep. 12, 2007 14:30 - 16:10</i>		
<i>Session 21: Exotics</i>		<i>chair: R. Bijker</i>
E. Santopinto	INFN	Tetraquark Spectroscopy
F. Wang	Nanjing University	Systematic Study of Multi Quark States
H. Weigel	Fachbereich Physik, Siegen University	Soliton Model Approach to Kaon Nucleon Scattering in the Pentaquark Channel
Y. Azimov	Petersburg Nucl. Phys. Inst.	How Is Exotics Produced? Where to Search for It?
F. Taghavi Shahri	IUST	The Rule of Orbital Angular Momentum and Polarized Valon Model
<i>Session 22: NN Interaction</i>		<i>chair: J.-P. Didelez</i>
E. Ruiz Arriola	Universidad de Granada	Renormalizing the Schroedinger Equation for NN Scattering
A.E. Gardestig	University of South Carolina	Extraction of the neutron-neutron scattering length from $\pi^- d \rightarrow nn \gamma$ using χ PT
V. Lensky	FZ Juelich	Neutron-neutron scattering length from the reaction $\gamma d \rightarrow \pi^+ nn$
D. Chiladze	FZ Juelich	np-Amplitude Studies at ANKE
S. Kvinikhidze	Razmadze Mathematical Institute, Tbilisi	A Possible Renormalization Group Approach to Nuclear Current Operators
<i>Session 23: Baryon Spectroscopy IV</i>		<i>chair: U. Thoma</i>
B. Metsch	Bonn University	The Relativistic Quark Model
F. Stancu	University of Liege	Quark Models: Recent Results
A. Svarc	Rudjer Bovslovic Institute	On Ambiguities and Uncertainties in PWA
A. Sibirtsev	HISKP, Universitaet Bonn	High Mass Baryons in Single Pion Photoproduction
N. Suzuki	Department of Physics, Osaka University	Resonance Pole by Speed Plot and Time Delay
<i>Session 24: Hadrons in Medium II</i>		<i>chair: B.K. Jain</i>
E. Oset	University of Valencia	Photoproduction of Omega and Omega in the Nuclear Medium
F. Dohrmann	FZ Dresden-Rossendorf	Inclusive dielectron production in C+C collisions with HADES

S. Eliseev	Bogoliubov Laboratory of Theoretical Physics, Joint Institute for Nuclear Research, Dubna	In Pursuit of New Physics with K^+ Scattering on Nuclei at Intermediate Energy
D. Gazda	Institute of Nuclear Physics, Rez near Prague	Dynamics of K bar Nuclear States
Session 25: Meson Production IV		<i>chair: M. Sadler</i>
V. Baru	<i>Institute for Theoretical and Experimental Physics, Moscow, Russia</i>	<i>Progress in $NN \rightarrow NN \pi$</i>
F. Myhrer	<i>University of South Carolina</i>	<i>Two Pion Exchange Effects in pp to $pp \pi^0$</i>
A. Machavariani	<i>JINR Dubna, HEPI Tbilisi</i>	<i>Screening in the Bremsstrahlung Reactions and Magnetic Moment of the Delta Resonance</i>
D.G. Richards	<i>Jefferson Laboratory</i>	<i>Excited States of Charmonium from Lattice QCD</i>
Guided Tour COSY		
Guided Tour Aachen		
Plenary Session Thursday, Sep. 13, 2007 8:30 - 12:30		
<i>chair: B.S. Zou</i>		
M.B. Voloshin	FTPI, University of Minnesota	Decay of Open Charm Hadrons
R. Chistov	ITEP Moscow	Charmed Hadrons from B-Decay
W. Toki	Colorado State University	Hadronic B-Decays
I. Bigi	University of Notre Dame	On the Brink of Major Discoveries in Weak Charm Decays - a Bismarckian Chance to Make History
<i>chair: T. Nakano</i>		
S. Kistryn	Jagiellonian University, Krakow	Three-Nucleon System Dynamics Studied via d-p Breakup
K. Sekiguchi	RIKEN	Three Nucleon Scattering Experiments from RIKEN
D.R. Phillips	Ohio University	Chiral Effective Theory Calculations of Electron and Photon Scattering from Light Nuclei
Parallel Sessions 26-30 - Thursday, Sep. 13, 2007 14:30 - 16:10		
Session 26: Strange Few Nucleon Systems		<i>chair: E. Widmann</i>
H. Ohnishi	RIKEN	Search for Deeply Bound Kaonic State
P. Bicudo	IST, Lisboa	The Hexaquark-Flavoured AntiK-N-N state Computed Microscopically with a Clusterized Octoquark

Y. Ikeda	Department of Physics, Osaka University	Three-Body Resonance Pole of Strange Dibaryon in the $\bar{K}NN - \pi YN$ Coupled System
T. Suzuki	RIKEN	An Experimental Search for Strange Multi-Baryonic Systems in $4\text{He}(\text{stopped}\bar{K}, YN)$ Reaction
T. Nishikawa	Tokyo Institute of Technology	Bound Kaon Approach for the $pp\bar{K}^0$ - System in the Skyrme Model
<i>Session 27: Few Body I</i>		<i>chair: H. Griesshammer</i>
J. Blomgren	Uppsala University, Dept of Neutron Research	Three Body Force Effects in Neutron-Deuteron Scattering at 95 MeV
E. Epelbaum	FZ Juelich, Universitaet Bonn	Delta-Resonance Contributions to the Nuclear Force
A. Fonseca	Centro Fmsica Nuclear da Universidade Lisboa	Coulomb Effects in Few Nucleon Systems abstract talk
D. Kiselev	Paul Scherrer Institut	Vector and Tensor Analyzing Power of the $H(\text{vec}(d), \gamma)3\text{He}$ Capture Reaction
S. Nakamura	TRIUMF	Bridging over π -Production and Weak Processes in Few-Nucleon Systems with Chiral Perturbation Theory
<i>Session 28: Form Factors</i>		<i>chair: C. Roberts</i>
V. Pascalutsa	ECT* Trento, Italy	Delta-N Transition Form Factors
F.J. Llanes Estrada	Depto. Fisica Teorica I, Universidad Complutense Madrid	The $1/x$ Form Factor of the Nucleon
M. Ungaro	Jefferson Lab	Baryon Resonance Form Factor at CLAS
M. Colantoni	Universita' del Piemonte Orientale e INFN-Torino	First Results on Pion Polarizabilities @ COMPASS
M. Bychkov	University of Virginia	High Precision Measurement of the Pion Form Factors via Radiative Pion Decay $\pi \rightarrow e \nu \gamma$
<i>Session 29: Baryon Spectroscopy V</i> <i>Shimizu</i>		<i>chair: K.</i>
I. Strakovsky	The George Washington University	Partial-Wave Analysis and Spectroscopy. From Pion-Nucleon Scattering to Pion Electroproduction up to $W = 2.5$ GeV

B. Julia-Diaz	University of Barcelona	Dynamical Coupled-Channel Model Analysis of pi-N Scattering and Electromagnetic Pion Production Reactions
V. Nikonov	HISKP Bonn, PNPI Gatchina	First Results from Analysis of pp->p K Lambda Reaction
M. Paris	EBAC @ Jefferson Lab	Dynamical Coupled-Channel Approach to omega-Meson Production with Pions and Photons
E. Prencipe	University of Ferrara and INFN	Charm and Charmonium Spectroscopy at BaBar
<i>Session 30: Hadrons in Medium III</i>		<i>chair: F. Myhrer</i>
A.M. Gueler	Middle East Technical University	Measurement of Charged-Particle Multiplets in (Anti-)Neutrino-Nucleus Interactions
D.D. van Niekerk	Stellenbosch University	Neutrino-induced Kaon Production
<i>Parallel Sessions 31-35 - Thursday, Sep. 13, 2007 16:50 - 18:30</i>		
<i>Session 31: Lattice Calculations</i>		<i>chair: R. Springer</i>
C. McNeile	University of Glasgow	Lattice Approach to Light Scalars
G. Bali	Universitaet Regensburg	Lattice Approach to Charmed States
A. Tsapalis	University of Athens, Institute of Accelerating Systems and Applications	Nucleon and pion-nucleon form factors from Lattice QCD
T.T. Takahashi	Yukawa Institute for Theoretical Physics, Kyoto University	Lattice QCD Study of $g_A^{N^*N^*}$ with Two-Flavors of Dynamical Quarks
J. Hu	Duke University	Pion Physics from Lattice QCD
<i>Session 32: Few Body II</i>		<i>chair: A. Fonseca</i>
H. Griesshammer	Center for Nuclear Studies, The George Washington University	Compton Scattering off the Deuteron and the Nucleon Polarizabilities
A. Rouba	Research Institute for Nuclear Problems, Minsk	Deuteron Spin Dichroism in Carbon Target
Y. Uzikov (V. Serdyuk)	JINR Dubna	Scaling Behavior of the Reactions dd to p3H and pd to pd in the GeV Region
V.V. Kulikov	ITEP, Moscow	Quasielastic Deuteron and Triton Knockout from Light Nuclei by Intermediate Energy Pions

<i>Session 33: High Energy Processes II</i>			<i>chair: W. Toki</i>
A. Szczurek	Institute of Physics and University of Rzeszow	Exclusive Production of Quarkonia in pp and p \bar{p} Collisions Far from the Threshold	
D. Nickel	Technische Universitaet Darmstadt	Studying Unquenching Effects in the Quark Propagator	
S. Atashbar Tehrani	Persian Gulf University	QCD analysis for nuclear parton distributions at next to leading order	
M. Nekipelov	FZ Juelich	Present Understanding of Spin-Filtering Experiments	
<i>Session 34: Heavy Mesons II</i>			<i>chair: I. Bigi</i>
V. Lyubovitskij	Institute of Theoretical Physics, University of Tuebingen	Strong and Radiative Decays of New Heavy Mesons Containing Strange Quarks and Hadronic Molecules	
V. Ziegler	SLAC	Cascade Resonance Properties from Charm Baryon Decays at BaBar	
S. Pacetti	LNF-INFN Frascati / Centro Studi e Ricerche Enrico Fermi, Roma	Extraction of Form Factors in ISR Processes at BaBar	
M. Pelliccioni	Universita' degli Studi di Torino, INFN	Charm Dalitz Analysis at BaBar	
Q. Zhao	Institute of High Energie Physics, Chinese Academy of Sciences	The Role of Electromagnetic Transitions in V to VP	
<i>Session 35: Hadrons in Medium IV</i>			<i>chair: M.B. Voloshin</i>
L. Tolos	FIAS. University of Frankfurt	Open-charm mesons in hot and dense nuclear matter	
S.S. Afonin	St. Petersburg State University	Spontaneous P-parity Violation in Dense Baryon Matter	
M. Takizawa	Showa Pharmaceutical University	Restoration of U _A (1) Symmetry and eta' Meson at Finite Density	
S. Tamenaga	RCNP Osaka University	The Massless Linear Sigma Model for Finite Nuclei and at Finite Temperature	
Conference Dinner Burg Baesweiler, Dinner Talk by D.Habs (LMU München)			
<i>Plenary Session Friday, Sep. 14, 2007 8:30 - 12:30</i>			
<i>chair: A. Thomas</i>			
N. Saito	KEK	The Japanese Proton Accelerator Facility	
B. Krusche (cancelled)	Basel University	Photoproduction of Eta-Mesons off Nuclei	

U. Mosel	University of Giessen	Hadrons in Medium - Theory Meets Experiment
P. Lenisa	Universita' di Ferrara and INFN - Ferrara	Towards Polarized Antiprotons at FAIR
<i>chair: U. Mosel</i>		
J.G. Messchedorp	KVI/RuG	Hadron Physics with Anti-Protons
G. Rosner	University of Glasgow	Overview of CLAS Physics
A.W. Thomas	Jefferson Lab	Future Scientific Opportunities at Jefferson Lab
<i>chair: R. Maier</i>		
C. Roberts	Argonne National Lab	Dynamics, Symmetries and Hadron Properties
M. Anselmino	University and INFN, Torino	The Transverse Partonic Structure of the Proton
B.M.K. Nefkens	UCLA	Concluding Remarks
Tour COSY , Farewell Coffee		

	Poster	
A.V.Glushkov	Odessa University	EPPP and Resonance Phenomena in Heavy Nuclei Collisions and Structurization of the Positron Spectrum. Compound Nucleus in Extreme External Electric Field
A.V.Glushkov	Odessa University	A Discharge of Meta-Stable Nuclei During Negative Muon Capture: Energy Approach
O. Khetselius	Nucl.Spectr.Lab., Odessa University	Nuclear Electric Quadrupole Moments and HFS Parameters for Heavy Isotopes: Nuclear Effects Contributions
O. Khetselius	Nucl.Spectr.Lab., Odessa University	Generalized Multi-Configuration Model of Decay of the Multipole Giant Resonances Applied to Aanalysis of Reaction mu-n on the Nucleus 40Ca
A. Machavariani	JINR Dubna, HEPI Tbilisi	Field-Theoretical Two-Body and Three-Body Equations for the Multichannel Reactions with the Intermediate Delta-Resonance and Quark-Gluon Degrees of Freedom
A. Machavariani	JINR Dubna, HEPI Tbilisi	Experimental test of the proton a structure effects in the polarized pp or pd elastic scattering experiments
H.P. Morsch	Soltan Institute for Nuclear Studies, Warsaw	Relation of nucleon resonances to the gluon structure of QCD
S. Nakamura	TRIUMF	Renormalization Group Analysis of the Chiral NLO Pion Production Operator
M. Mikirtychians	PNPI Gatchina	The Polarized Internal Target at ANKE
Y. Surovtsev	Bogoliubov Laboratory of Theoretical Physics, Joint Institute for Nuclear Research	Rho-like-meson family in the pion-pion scattering
F.J. Llanes Estrada	Depto. Fisica Teorica I, Universidad Complutense Madrid	The J=0 Fixed Pole in Deeply Virtual Compton Scattering - New Perspectives
F. Taghavi Shahri	IUST	Q ² -Dependence of Polarized Parton Distribution Functions in the Valon Model
H. Alharbi	National Center for Mathematics and Physics at KACST	Poincaré Invariant Coupled Channel model for the Pion-Nucleon System: Instant Form Model
U. Badarch	University Giessen	In-Medium Nucleon-Nucleon Interaction Nuclear EOS

A. Galoyan	LPP JINR	Multiplicity Fluctuations in Interactions of Light Nucleus with Carbon Nuclei at Mometum of 4.2 GeV/c/nucleon and their Theoretical Interpretation
W.J. Briscoe	The George Washington University	Near Threshold Pion Production at MAXLAB
J. Stepaniak	Institute for Nuclear Studies, Warsaw	New eta Rare Decay Results from CELSIUS/WASA Experiment
M. Sadler	Abilene Christian University	Pion-Nucleon Scattering in the N*(1440) Resonance Region
S. Ivashyn	National Science Center "Kharkov Institute for Physics and Technology", Institute for Theoretical Physics, Ukraine	Application of chiPT with Vector Mesons: Kaon Electromagnetic Form Factors and KbarK Contribution to Muon Anomalous Magnetic Moment
W. Schroeder	University of Erlangen-Nuremberg	Improved Study of Possible Theta+ Production in the pp to pK0 Sigma+ Reaction with the COSY-TOF Experiment
W. Schroeder	University of Erlangen-Nuremberg	Hyperon Production in the Channel pp to K+ Lambda p at COSY-TOF
C. Pauly	FZ Juelich	WASA-at-COSY
B. Taddesse	Jacobs University Bremen	
D. Duniec	Dept. of Nuclear and Particle Physics, Uppsala University	eta' Decays with WASA-at-COSY
B.R. Jany	Nuclear Physics Department Jagiellonian University / FZ Juelich	
C.F. Redmer	FZ Juelich	In Search of the Box Anomaly with the WASA-at-COSY Facility
M. Janusz	FZ Juelich and Jagiellonian University, Krakow	From Charged Tracks to ChPT Anomalies (WASA-at-COSY)
L. Yurev	FZ Juelich	
T. Tolba	FZ Juelich	A Pellet Tracking System for WASA-at-COSY
T. Stockmanns	FZ Juelich	A High Rate and High Resolution Micro-Vertex-Detector for the PANDA-Experiment at FAIR

M. Mertens	FZ Juelich	Development of a Versatile Readout System for High Rate Detector Electronics
P. Klaja	Jagellonian University and FZ Juelich	Proton-Proton Correlation Function for the pp to pp eta Reaction Measured with COSY-11
P. Moskal		
R. Czyzykiewicz	Jagellonian University and FZ Juelich	Studies of the eta Meson Production with a Polarized Proton beam at COSY-11
P. Moskal		

Author Index

- Abdel-Bary, M., 469
Abdel-Samad, S., 469
Abramov, B. M., 1
Adrianov V.A., 6
Adrianov, A.A., 6
Afonin S.S., 6
Agakishiev, G., 71, 105
Agodi, C., 71, 105
Albaladejo, M., 11
Aleksseev, I. G., 400
Alharbi H. H., 15
Alkofer, R., 97
Amaro, F. D., 396
Anagnostopoulos, D. F., 396
Arash, F., 426, 431
Atashbar Tehrani, S., 20
Author, T., 314
Author, Y., 314
Azimov, Ya., 24
- Bühler, P., 396
Böhmer, M., 71, 105
Büscher, M., 484
Bacelar, J. C. S., 297
Balanda, A., 71, 105
Bantes, B., 297
Bargholtz, C., 207, 392
Barion, L., 28
Bartholomy, O., 297
Baru, V., 261
Baryshevsky, V., 32
Bashkanov, M., 207, 392
Bayadilov, D., 297
Bazhanov, N. A., 400
Beck, R., 297
Beer, G., 182
Behler, M., 36
Bekrenev, V. S., 400
- Bellia, B., 71, 105
Beloglazov, Y. A., 297
Beloglazov, Yu. A., 400
Belver, D., 105
Belyaev, A., 71, 105
Bhang, H., 182
Bijker R., 40
Bizzeti, A., 44
Blanco, A., 71, 105
Blankleider, B., 257
Bogoslawsky, D., 207, 392
Borodin, Yu. A., 1
Boyard, J. L., 105
Braun-Munzinger, P., 71, 105
Brinkmann, K.-Th., 457
Budkovsky, P. E., 400
Budzanowski, A., 202, 469
Bulychjov, S. A., 1
Bunyatova, E. I., 400
Bychkov, M., 48
Bydžovský, P., 405
- Cabanelas, P., 71, 105
Calen, H., 207, 392
Cappellaro, F., 207, 392
Cargnelli, M., 182
Castelijns, R., 297
Castro, E., 71, 105
Chang W.C., 52
Chatterjee, A., 202, 469
Chernenko, S., 71, 105
Chiba, J., 182
Choi, S., 182
Christ. T., 71, 105
Cieplý, A., 57
Clement, H., 207, 392
Colantoni, M., 62
COMPASS collaboration, 248

Covita, D. S., 396
 Crede, V., 297
 Curceanu, C., 182
 Czyżykiewicz, R., 66
 Díaz, J., 71, 105
 Demiroers, L., 207, 392
 Destefanis, M., 71, 105
 Dietrich, J., 457
 Dohrmann, F., 71, 105
 Doroshkevich, E., 207, 392
 Dshemuchadse, S., 457
 Dudek, J., 76
 Dukhovskoy, I. A., 1
 Duniec, D., 198, 207, 392
 Dutz, H., 297
 Dybczak, A., 71, 105
 Dzyuba, A., 484
 Eberl, T., 71, 105
 Ehmanns, A., 297
 Ekström, C., 392
 Ekström, C., 207
 El-Bennich, B., 80
 Eliseev, S.M., 85
 Elsner, D., 297
 Entem, D. R., 375
 Epelbaum, E., 261
 Ernst, J., 469
 Espriu D., 6
 Essig, K., 297
 Ewald, R., 297
 Föhl, K., 101
 Fabbietti, L., 71, 105
 Fabbri, R., 89
 Fabry, I., 297
 Faessler, A., 266
 Fariborz, A. H., 93
 Fateev, O., 71, 105
 Fernández, F., 375
 Filimonov, E. A., 400
 Finocchiaro, P., 71, 105
 Fischer, C. S., 306
 Fischer, C.S., 97
 Flemming, H., 297
 Fonte, P., 71, 105
 Fröhlich, I., 71, 105
 Franssen, K., 207, 392
 Freiesleben, H., 457
 Friedman, E., 124
 Friese, J., 71, 105
 Fuchs, K., 297
 Fukuda, Y., 182
 Funke, Ch., 297
 Furman, A., 80
 Güler, A. M., 144
 Gal, A., 124
 Galatyuk, T., 71, 105
 Galoyab, A., 115
 Galoyan, A., 111
 Ganbold, G., 119
 Garzón, J.A., 71, 105
 Gazda, D., 124
 Gerasimov, S. B., 224
 Geren, L., 207, 392
 Gernhäuser, R., 71, 105
 Gilardi, C., 71, 105
 Glazier, D. I., 128
 Glushkov, A. V., 132, 139, 211
 Goeke K., 24
 Golubeva, M., 71, 105
 González-Díaz, D., 71, 105
 Gorke, H., 396
 Goslawski, P., 323
 Gothe, R., 297
 Gotta, D., 396
 Gottwald, J., 457
 Gregor, R., 297
 Gridnev, A. B., 297
 Grosse, E., 71, 105
 Gruber, A., 396

Guber, F., 71, 105
 Gustafsson, L., 207, 392
 Gutsche, T., 266
 Gutz, E., 297
 Gårdestig, A., 293

 Höffgen, S., 297
 Höistad, B., 207, 392
 Hügging, F., 279
 Hadzimehmedovic, M., 149
 Haga, A., 444
 Haidenbauer, J., 244, 261
 Hanaki, T., 182
 Hanhart, C., 261
 Hassanabadi, H., 153
 Hawranek, P., 202, 469
 Hayano, R. S., 182
 He, J., 161
 Heilmann, M., 71, 105
 Hennino, T., 71, 105
 Hinterberger, F., 469
 Hirtl, A., 396
 Hoffmeister, P., 297
 Holzmann, R., 71, 105
 Horn, I., 297
 Hosaka, A., 170
 Hu, J., 165
 Hyodo, T., 170

 Ierusalimov, A., 71, 105
 Iio, M., 182
 Ikeda, Y., 174
 Indelicato, P., 396
 Inoue, T., 178
 Iori, I., 71, 105
 Ishikawa, T., 182
 Ishimoto, S., 182
 Ishiwatari, T., 182
 Itahashi, K., 182
 Ivanov, G., 207, 392
 Ivashkin, A., 71, 105

 Ivashyn, S., 186, 190
 Iwai, M., 182
 Iwasaki, M., 182

 Jäkel, R., 457
 Jacewicz, M., 207, 392
 Jaegle, I., 297
 Jahn, R., 202
 Jain, B. K., 461
 Janusz, M., 194
 Jany, B. R., 198
 Jha, V., 202, 469
 Jiang, F.-J., 165
 Jido, D., 170
 Jiganov, E., 207, 392
 Johansson, T., 207, 392
 Juhász, B., 182
 Junkersfeld, J., 297
 Jurkovic, M., 71, 105

 Kämpfer, B., 71, 105
 Köse, U., 144
 Kühn, W., 71, 105
 Kailas, S., 202
 Kalinowsky, H., 297
 Kamiński, R., 410
 Kammer, S., 297
 Kanaki, K., 71, 105
 Kanavets, V. P., 400
 Karavicheva, T., 71, 105
 Karsch, K., 457
 Kaskulov, M., 207, 392
 Keleta, S., 207, 392
 Kelkar, N. G., 461
 Khakimova, O., 207, 392
 Khanov, A. I., 1
 Khemchandani, K. P., 362, 461
 Khetselius, O. Yu., 139, 211, 217
 Khorramian, A. I., 20
 Khoukaz, A., 323
 Khrykin, A. S., 224

Kienle, P., 182
 Kilian, K., 202, 469
 Kirillov, Da., 202, 469
 Kirillov, Di., 202, 469
 Kirschner, D., 71, 105
 Kladnickaya, E. N., 115
 Klaja, P., 229, 234
 Kleber, V., 297
 Klein, Frank, 297
 Klein, Friedrich, 297
 Klempt, E., 297
 Kliczewski, S., 202, 469
 Koch, H., 297
 Koch, I., 207, 392
 Koenig, I., 71, 105
 Koenig, W., 71, 105
 Kolb, B.W., 71, 105
 Kolev, D., 202, 469
 Konrad, M., 297
 Kopf, B., 297
 Korchin, A., 186, 190
 Koroleva, L. I., 400
 Kotte, R., 71, 105
 Kotulla, M., 297
 Kovalev, A. I., 400
 Kozlenko, N. G., 400
 Kozuch, A., 71, 105
 Krücken, R., 71, 105
 Kravchenko, P., 239
 Kravcikova, M., 202, 469
 Krein, G., 244
 Kren, F., 207, 392
 Krizek, F., 71, 105
 Kruglov, S. P., 400
 Krusche, B., 297
 Krutenkova, A. P., 1
 Kudryavtsev, A., 261
 Kugler, A., 71, 105
 Kuhlmann, E., 457
 Kuhn, R., 248
 Kulbardis, A. A., 400
 Kulikov, V. V., 1
 Kullander, S., 207, 392
 Kunihiro, T., 435
 Kupść, A., 207, 392
 Kupsc, A., 252
 Kurepin, A., 71, 105
 Kutsarova, T., 202
 Kuznetsov, A., 207, 392
 Kvinikhidze, A. N., 257
 Löhner, H., 297
 Lamas-Valverde, J., 71, 105
 Lang, M., 297
 Lang, S., 71, 105
 Lange, J.S., 71, 105
 Langheinrich, J., 297
 Le Bigot, E.-O., 396
 Lenske, H., 383
 Lensky, V., 261
 Lesiak, L., 202
 Lesiak, M., 469
 Lieb, J., 202, 469
 Lindberg, K., 207, 392
 Liu, L. C., 202
 Llanes-Estrada, F.J., 97
 Loboda, A. V., 139, 211
 Loiseau, B., 80
 Lopatin, I. V., 297, 400
 Lopes, L., 71, 105
 Lotz, J., 297
 Lugert, S., 297
 Lyubovitskij, V. E., 266
 M. Pant, L. M., 297
 Müntz, C., 71, 105
 Machavariani, 270
 Machner, H., 202, 469
 Magiera, A., 202, 469
 Maier, L., 71, 105
 Maier, R., 202, 469
 Malinovskaya, S. V., 139

Mangiarotti, A., 71, 105
 Marín, J., 71, 105
 Marciniewski, P., 207, 392
 Mareš, J., 124
 Markert, J., 71, 105
 Martemianov, M. A., 1
 Martinska, G., 202, 469
 Marton, J., 182, 396
 Mathur, N., 76
 Matsuda, Y., 182
 Matsyuk, M. A., 1
 Matthäy, H., 297
 Meier, R., 207, 392
 Meißner, U.-G., 244, 261
 Menze, D., 297
 Mersmann, T., 323
 Mertens, M. C., 279
 Mertens, T., 297
 Metag, V., 71, 105, 297
 Metsä, P., 284
 Michalska, B., 71, 105
 Mielke, M., 323
 Mishra, D., 71, 105
 Mizutani, T., 452
 Morales, C., 297
 Morinière, E., 71, 105
 Morosov, B., 207, 392
 Morozov, B. V., 400
 Mosel, U., 383
 Moskal, P., 66, 234, 252
 Mousa, J., 71, 105
 Moussallam, B., 80

 Nakamura, S. X., 288, 293
 Nanova, M., 297
 Naumann, L., 71, 105
 Nedev, S., 202, 469
 Nekipelov, M., 302
 Nekipelov, N., 396
 Nesterov, V. M., 400
 Nickel, D., 306

 Novinski, D. V., 297
 Novinsky, D. V., 400
 Novotny, R., 71, 105, 297

 Ogawa, Y., 444
 Ohnishi, H., 182
 Okada, S., 182
 Oller, J.A., 11
 Osmanovic, H., 149
 Ostrick, M., 297
 Otwinowski, J., 71, 105
 Outa, H., 182

 Pérez Cavalcanti, T., 71, 105
 Pacetti, S., 318
 Pachmayer, Y.C., 71, 105
 Palka, M., 71, 105
 Papenbrock, M., 323
 Paris, M., 328
 Parpottas, Y., 71, 105
 Pauly, C., 207, 332, 392
 Pechenov, V., 71, 105
 Pechenova, O., 71, 105
 Pettersson, H., 207, 336, 392
 Petukhov, Y., 207, 392
 Pfeiffer, M., 297
 Pietraszko, J., 71, 105
 Piqueras, C., 11
 Piskunov, N., 202, 469
 Povtorejko, A., 207, 392
 Prasuhn D., 469
 Prencipe, E., 340
 Pricking, A., 207, 392
 Protić, D., 202, 469
 Przerwa, J., 345
 Przygoda, W., 71, 105

 Radkov, A., 297
 Rajabi, A. A., 153
 Ramos, A., 452
 Ramstein, B., 71, 105
 Rausmann, T., 323

Redmer, C. F., 350
 Reimann, S., 457
 Reshetin, A., 71, 105
 Richards, D., 76
 Ritman, J., 202, 279, 448, 469
 Rossen, P. v., 202
 Rouba, A., 32
 Roy, A., 297
 Roy, B. J., 202, 469
 Roy-Stephan, M., 71, 105
 Rustamov, A., 71, 105
 Ryltsov, V. V., 400

 S. Surovtsev, Yu. S., 405, 410
 Süle, A., 297
 Sadler, M., 354
 Sadovsky, A., 71, 105
 Saghai, B., 161
 Sailer, B., 71, 105
 Sainio, M. E., 358
 Salabura, P., 71, 105
 Santopinto E., 40
 Santos, dos J. M. F., 396
 Sato, M., 182
 Sato, T., 174, 415
 Schönning, K., 207, 362, 392
 Schadmand, S., 297
 Schlessner, S., 396
 Schmah, A., 71, 105
 Schmid, P., 182
 Schmid, Ph., 396
 Schmidt, Ch., 297
 Schmieden, H., 297
 Schoch, B., 297
 Schroeder, W., 367, 371
 Schulte-Wissermann, M., 457
 Schwenzer, K., 97
 Scobel, W., 207, 392
 Segovia, J., 375
 Semenov-Tian-Shansky, K., 379
 Shchedrov, V. A., 400

 Shende, S., 297
 Shimizu, K., 439
 Shkyar, V., 383
 Shukla, P., 202
 Shwartz, B., 207, 392
 Sibirtsev, A., 244, 387
 Simon, R., 71, 105
 Simons, L. M., 396
 Sitnik, I., 202, 469
 Siudak, R., 202, 469
 Skorodko, T., 207, 392
 Smejkal, J., 57
 Sokhoyan, V., 297
 Sopov, V., 207, 392
 Spataro, S., 71, 105
 Spruck, B., 71, 105
 Stahov, J., 149, 354
 Stepeniak, J., 207, 392
 Stockmanns, T., 279
 Ströbele, H., 71, 105
 Strakovsky, I., 24
 Strauch, Th., 396
 Stroth, J., 71, 105
 Sturm, S., 71, 105
 Sudol, M., 71, 105
 Sulimov, A. D., 400
 Sumachev, V. V., 297, 400
 Suzuki, N., 415
 Suzuki, S., 182
 Suzuki, T., 182
 Svirida, D. N., 400
 Szczepanek, T., 297
 Szczurek, A., 419

 Täschner, A., 323
 Taghavi Shahri, F., 431
 Taghavi, F., 426
 Takahashi, T. T., 435
 Takeuchi, S., 439
 Tamenaga, S., 444
 Tarantola, A., 71, 105

Tarasov, V. E., 1
 Tatsuno, H., 182
 Tegner, P.-E., 207, 392
 Teilab, K., 71, 105
 Thörngren-Engblom, P., 207, 392
 Thoma, U., 297
 Tiburzi, B. C., 165
 Tikhomirov, V., 207, 392
 Tlustý, P., 71, 105
 Toki, H., 444
 Tolós, L., 452
 Tolba, T., 448
 Tomono, D., 182
 Trautman, V. Yu., 400
 Traxler, M., 71, 105
 Trebacz, R., 71, 105
 Trnka, D., 297
 Tsenov, R., 202, 469
 Tsertos, H., 71, 105
 Turdakina, E. N., 1

 Ulicny, M., 469
 Ullrich, W., 457
 Upadhyay, N. J., 461
 Urban, J., 202, 469
 Uzhinsky, V., 111
 Uzhinsky, V. V., 115
 Uzikov, Yu. N., 465

 van der Ventel, B. I. S., 310
 van Niekerk, D. D., 310
 van Pee, H., 297
 Vankova, G., 202
 Vankova, G., 469
 Varma, R., 297
 Veloso, J. F. C. A., 396
 Vereshagin, A., 379
 Vereshagin, V., 379
 Veretenkin, I., 71, 105
 Vlasov, P., 332
 von Rossen, P., 469

 Wüstenferd, J., 105
 Wagner, G. J., 207, 392
 Wagner, V., 71, 105
 Walther, D., 297
 Wambach, J., 306
 Watson, S., 354
 Watts, D. P., 128
 Weigel, H., 474
 Weinheimer, Ch., 297
 Wen, H., 71, 105
 Wendel, Ch., 297
 Wenzel, R., 457
 Widmann, E., 182
 Wilkin, C., 469
 Wisniowski, M., 71, 105
 Wojcik, T., 71, 105
 Wolke, M., 207, 392
 Wrońska, A., 479

 Yamamoto, A., 207, 392
 Yamazaki, T., 182
 Yim, H., 182
 Yuan, X., 484
 Yurev, L., 194
 Yurevich, S., 71, 105

 Zabierowski, J., 207, 392
 Zanevsky, Y., 71, 105
 Zartova, I., 207, 392
 Zhao, Q., 161
 Zhong, X., 161
 Ziegler, V., 488
 Zieliński, M., 252
 Zmeskal, J., 182, 396
 Zumbruch, P., 71, 105
 Zychor, I., 492
 Złomanczuk, J., 207, 392